THE UNIVERSITY of TULSA

Department of Petroleum Engineering

Fluid Flow Projects

Seventy Fifth Semi-Annual Advisory Board Meeting Brochure and Presentation Slide Copy

November 3, 2010

Tulsa University Fluid Flow Projects
Seventy Fifth Semi-Annual Advisory Board Meeting Agenda
Wednesday, November 3, 2010

Tuesday, November 2, 2010

Tulsa University High-Viscosity Oil Projects
Advisory Board Meeting
University of Tulsa – Allen Chapman Activity Center - Chouteau
440 South Gary
Tulsa, Oklahoma
8:15 a.m. – Noon

Tulsa University High-Viscosity Oil Projects, Tulsa University Hydrate Flow Performance JIP and Tulsa University Fluid Flow Projects Workshop Luncheon
University of Tulsa – Allen Chapman Activity Center - Atrium
440 South Gary
Tulsa, Oklahoma
12:00 – 1:00 p.m.

Tulsa University Fluid Flow Projects Workshop
University of Tulsa – Allen Chapman Activity Center - Chouteau
440 South Gary
Tulsa, Oklahoma
1:00 – 3:00 p.m.

Tulsa University High-Viscosity Oil Projects, Tulsa University Hydrate Flow Performance JIP, Tulsa University Fluid Flow Projects and Tulsa University Paraffin Deposition Projects
Tour of Test Facilities
University of Tulsa North Campus
2450 East Marshall
Tulsa, Oklahoma
3:30 – 5:30 p.m.

Tulsa University High-Viscosity Oil Projects. Tulsa University Hydrate Flow Performance JIP and Tulsa University Fluid Flow Projects
Reception
University of Tulsa – Allen Chapman Activity Center - Chouteau
440 South Gary
Tulsa, Oklahoma
6:00 – 9:00 p.m.

Wednesday, November 3, 2010

Tulsa University Fluid Flow Projects
Advisory Board Meeting
University of Tulsa – Allen Chapman Activity Center - Chouteau
440 South Gary
Tulsa, Oklahoma
8:00 a.m. – 5:00 p.m.

Tulsa University Fluid Flow Projects and Tulsa University Paraffin Deposition Projects
Reception
University of Tulsa – Allen Chapman Activity Center - Atrium
440 South Gary
Tulsa, Oklahoma
5:30 – 9:00 p.m.

Thursday, November 4, 2010

Tulsa University Paraffin Deposition Projects
Advisory Board Meeting
University of Tulsa – Allen Chapman Activity Center - Chouteau
440 South Gary
Tulsa, Oklahoma
8:00 a.m. – 1:00 p.m.

Tulsa University Fluid Flow Projects
Seventy Fifth Semi-Annual Advisory Board Meeting Agenda
Wednesday, November 3, 2010

8:00 a.m.	**Breakfast – Allen Chapman Activity Center – Chouteau**	
8:30	**Introductory Remarks**	Cem Sarica
8:45	**TUFFP Progress Reports**	
	High Pressure - Large Diameter Multiphase Flow Loop	Scott Graham/ Cem Sarica
	Effects of High Oil Viscosity on Slug Liquid Holdup in Horizontal Pipes	Ceyda Kora
10:15	**Coffee Break**	
10:30	**TUFFP Progress Reports**	
	Wave Characteristics in Annular Gas-Liquid Flow	Abdel Alsarkhi
	Liquid Entrainment in Annular Two-Phase Flow in Inclined Pipes	Abdel Alsarkhi
	A Unified Drift Velocity for Intermittent Flow	Ben Jeyachandra
11:45 a.m.	**Lunch – Allen Chapman Activity Center - Gallery**	
1:00 p.m.	**TUFFP Progress Reports**	
	High Oil Viscosity Two-Phase Flow in Inclined Pipes	Ben Jeyachandra
	Investigation of Slug Length for High Viscosity Oil-Gas Flow	Eissa Alsafran
2:30	**Coffee Break**	
2:45	**TUFFP Progress Reports**	
	Low Liquid Loading Three-Phase Flow	Kiran Gawas
	Transient Gas/Liquid Two-Phase Modeling	Michelle Li
	Liquid Unloading from Gas Wells	Ge (Max) Yuan
4:15	**TUFFP Business Report**	Cem Sarica
4:30	**Open Discussion**	Cem Sarica
5:00	**Adjourn**	
5:30	**TUFFP/TUPDP Reception - Allen Chapman Activity Center - Atrium**	

Table of Contents

Executive Summary

Progress on each research project is given later in this Advisory Board Brochure. A brief summary of the activities is given below.

Investigation of Gas-Oil-Water Flow

Three-phase gas-oil-water flow is a common occurrence in the petroleum industry. The ultimate objective of TUFFP for gas-oil-water studies is to develop a unified model based on theoretical and experimental analyses. A three-phase model has already been developed. There are several projects underway addressing the three-phase flow.

High Viscosity Oil Two-phase Flow Behavior

Oils with viscosities as high as 10,000 cp are produced from many fields around the world. Current multiphase flow models are largely based on experimental data with low viscosity fluids. The gap between lab and field data may be three orders of magnitude or more. Therefore, current mechanistic models need to be improved with higher liquid viscosity experimental results. Modifications or new developments are necessary.

An earlier TUFFP study conducted by Gokcal (2005) showed that the performances of existing models are not sufficiently accurate for high viscosity oils with a viscosity range of 200 – 1000 cp. It was found that increasing oil viscosity had a significant effect on flow behavior. Our current efforts in this project continue at multiple fronts:

1. *Translational Velocity Study:* A unified drift velocity closure relationship for the inclination angle range of 0 - 90° is developed utilizing 2 in., 3 in. and 6 in. ID data acquired at TUFFP for viscosities ranging from 1 cp to 1,000 cp. This closure relationship can easily be used in every multiphase flow software.
2. *Slug Length Study:* Dr. Eissa Al-Safran of Kuwait University completed the investigation of the slug length for high viscosity oils which was started as his sabbatical research assignment. In an earlier study by Gokcal (2008) slug lengths were found to decrease with increasing liquid viscosity and follow a log-normal distribution.
3. *Slug Liquid Holdup Study:* One of the important closure relationships of the slug flow is the slug liquid holdup. Current experimental study focused on the investigation of the slug liquid holdup. During this period, a newly developed capacitance probe has been used. Data acquisition has been completed and a new Slug Liquid Holdup closure relationship has been developed.

Droplet Homo-phase Interaction Study

There are many cases in multiphase flow where droplets are entrained from or coalesced into a continuous homophase. For example, in annular mist flow, the liquid droplets are in dynamic equilibrium with the film on the walls, experiencing both entrainment and coalescence. Very few mechanistic models exist for entrainment rate and coalescence rate. Understanding the basic physics of these phenomena is essential to model situations of practical interest to the industry. Droplet homo-phase covers a broad range of possibilities.

A past sensitivity study of multiphase flow predictive models showed that, in stratified and annular flow, the variation of droplet entrainment fraction can significantly affect the predicted pressure gradient. Therefore, a need was identified to experimentally investigate entrainment fraction for inclined pipes. The results of the experimental study conducted by Kyle Magrini (2009) for various inclination angles showed the dependency of entrainment fraction to the inclination angle of the pipe. Currently, our efforts are focused on developing a better entrainment fraction closure relationship valid for all inclination angles. Dr. Abdel Al-Sarkhi, Research Associate Professor of Petroleum Engineering, is conducting this project.

Simplified Transient Flow Studies

The objective is to develop a simplified transient model as a screening tool. Significant progress was reported in this project at the last Advisory Board meeting. Two simplified transient models using two-fluid and drift flux approaches were developed. Model predictions are compared with the TUFFP transient flow data. Two-fluid model is found to perform well for separated flow patterns. Flow pattern independent drift flux model seems to perform quite well in intermittent flow, and reasonably well for stratified flow. A driver program based on steady state flow pattern identification is developed to select the best model.

Low Liquid Loading Gas-Oil-Water Flow in Horizontal and Near Horizontal Pipes

Low liquid loading exists widely in wet gas pipelines. These pipelines often contain water and hydrocarbon condensates. Small amounts of liquids can lead to a significant increase in pressure loss along a pipeline. Moreover, existence of water can significantly contribute to the problem of corrosion and hydrate formation problems. Therefore, understanding of flow characteristics of low liquid loading gas-oil-water flow is of great importance in transportation of wet gas.

In a previous study, large amount of data were collected on various flow parameters such as flow patterns, phase distribution, onset of droplet entrainment,

entrainment fraction, and film velocity using a model oil with a viscosity range of 25 to 10 cp. In this study, Isopar-L with similar fluid properties as wet gas condensate is used as liquid phase. Several tests have been conducted for both three-phase gas-oil-water flows for low water cuts. The initial analyses of the results indicate that as water cut increases the liquid entrainment rate decreases. Moreover, it is observed that increases in liquid superficial velocity keeping the superficial gas velocity decrease the entrainment fraction which is not observed in small diameter flow loop testing.

Up-scaling Studies

One of the most important issues that we face in multiphase flow technology development is scaling up of small diameter and low pressure results to large diameter and high pressure conditions. Studies with a large diameter facility would significantly improve our understanding of flow characteristics in actual field conditions. Therefore, our main objective in this study is to investigate the effect of pipe diameter and pressures on flow behavior using a larger diameter flow loop.

This project is one of the main activities of TUFFP, and a significant portion of the TUFFP budget is allocated to the construction of a 6" high pressure flow loop. The concrete foundation and steel supporting structures have been completed. All major equipments have been purchased. The construction of test section and the piping in the circulation area and the instrumentation/control system are almost complete. Commissioning of the gas compressor will take place in November with shakedown tests of the entire facility beginning in January. The flow loop is expected to be fully operational in March of 2011.

Liquid Unloading from Gas Wells

Liquid loading of liquid in the wellbore has been recognized as one of the most severe problems in gas production. At early times of the production, natural gas carries liquid in the form of mist since the reservoir pressure is sufficiently high. As the gas well matures, the reservoir pressure decreases reducing gas velocity. The gas velocity may go below a critical value resulting in liquid accumulation in the well. The liquid accumulation increases the bottom-hole pressure and reduces gas production rate significantly.

Although significant effort has been made to predict the liquid loading of gas wells, experimental data are very limited. The objective of this project is to better understand of the mechanisms causing the loading and develop new technologies to prevent or remediate liquid-loading problems in gas wells. This project is an experimental and modeling study. Flow characteristics will be observed and measured along the pipe. The effects of well deviation to the liquid loading will be investigated. The Turner model and its modified versions along with other models (including the TUFFP unified model) will be evaluated with experimental results. The existent models will be improved or a new model developed based on the experimental measurements and observations.

Design of the experimental facility is completed. The facility modifications will be completed during the winter months and the experimental program will be started in spring of 2011.

Unified Mechanistic Model

TUFFP maintains, and continuously improves upon the TUFFP unified model. Collaborative efforts with Schlumberger Information Systems continue to improve the speed and the performance of the software.

Current TUFFP membership stands at 14 (13 industrial companies and MMS). Efforts continue to further increase the TUFFP membership level. A detailed financial report is provided in this report. The sum of the 2010 income and the reserve account is projected to be $669,959.00. The expenses for the industrial member account are estimated to be $609,174.76 leaving a positive balance of $60,783.86.

Several related projects are underway. The related projects involve sharing of facilities and personnel with TUFFP. The Paraffin Deposition consortium, TUPDP, is into its fourth phase with 9 members a budget of $540,000/year. Tulsa University High Viscosity Oil Projects (TUHOP) Joint Industry Projects is into its third year. TUHOP currently has currently five members with recent addition of PetroChina.

A new JIP is being formed to investigate unloading of vertical gas wells using surfactants for a period of three years. The JIP is funded by Research Partnership to Secure Energy for America (RPSEA), which is an organization managing DOE funds, and various oil and gas operating and service companies. This JIP will utilize some of the TUFFP capabilities. If a member of the JIP is not a member of TUFFP, a facility utilization fee equivalent of one year TUFFP membership fee will be paid to TUFFP. Current industrial members of the JIP are Chevron, ConocoPhillips, Marathon, and Shell. All are current members of TUFFP.

Fluid Flow Projects

75th Fluid Flow Projects Advisory Board Meeting

Welcome

Safety Moment

- Emergency Exits
- Assembly Point
- Tornado Shelter
- Campus Emergency
  - Call 9-911
  - Campus Security, ext. 5555 or 918-631-5555
- Rest Rooms

Fluid Flow Projects

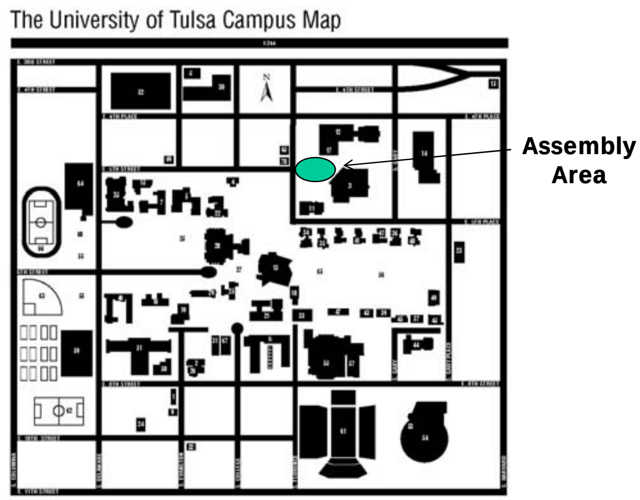

Fluid Flow Projects

Advisory Board Meeting, November 3, 2010

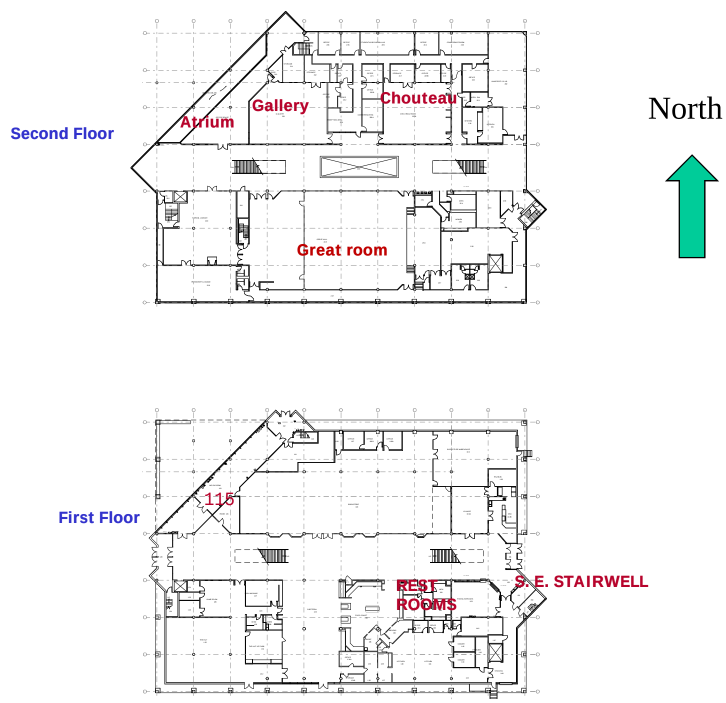

Introductory Remarks

- 75th Semi-Annual Advisory Board Meeting
- Handout
  - Combined Brochure and Slide Copy
- Sign-Up List
  - Please Leave Business Card at Registration Table

Team

- Research Associates
  - Cem Sarica (Director)
  - Holden Zhang (Associate Director)
  - Abdel Al-Sarkhi (Visiting Research Professor)
  - Mingxiu (Michelle) Li (Resigned August 2010)
  - Eissa Al-Safran (Collaborator)
- Visiting Scholar
  - Jinho Choi, SNU
  - Hoyoung Lee, SNU

Team …

- Project Coordinator
  - Linda Jones
- Project Engineer
  - Scott Graham
- Research Technicians
  - Craig Waldron
  - Brandon Kelsey
- Web Master
  - Lori Watts

Team …

- TUFFP Research Assistants
  - Rosmer Brito (MS) – Venezuela
  - Kiran Gawas (Ph.D.) – India
  - Mujgan Guner (Ph.D.) – Turkey
  - Benin (Ben) Chelinsky Jeyachandra (MS) – India
  - Ceyda Kora (MS) – Turkey
  - Ge Yuan (MS) – PRC
  - Wei Zheng (MS) – PRC

Guests

- Xiaoping Li, CUP
- Glenn R. Dissinger, Aspen Technology, Inc.
- Vikas Dhole, Aspen Technology, Inc.
- Ben Fischer, Aspen Technology, Inc.

Membership and Financial Status

- 14 Members in 2010
- Seoul National University Collaboration
  - Three Years Agreement with Possible Two Year Extension
  - TUFFP
    - Provides Guidance to Research Scholars (SNU Ph.D. Candidates) and Access to Facilities Through TUFFP Projects
    - Receives $110,000/Year
- Membership Fee Increased to $55,000

Agenda

- 8:30 Introductory Remarks
- 8:45 Progress Reports
  - High Pressure – Large Diameter Multiphase Flow Loop
  - Effects of High Oil Viscosity on Slug Liquid Holdup in Horizontal Pipes
- 10:15 Coffee Break
- 10:30 Progress Reports
  - Wave Characteristics in Annular Gas-Liquid Flow
  - Liquid Entrainment in Annular Two-Phase Flow in Inclined Pipes
  - A Unified Drift Velocity for Intermittent Flow

Fluid Flow Projects

Advisory Board Meeting, November 3, 2010

Agenda …

- 11:45 Lunch – ACAC – Gallery
- 1:00 Progress Reports
  - High Oil Viscosity Two-Phase Flow in Inclined Pipes
  - Investigation of Slug Length for High Viscosity Oil-Gas Flow
- 2:30 Coffee Break

Fluid Flow Projects

Advisory Board Meeting, November 3, 2010

Agenda …

- 2:45 Progress Reports
  - Low Liquid Loading Three-phase Flow
  - Transient Gas/Liquid Two-phase Flow Modeling
  - Liquid Unloading from Gas Wells
- 4:15 TUFFP Business Report
- 4:30 Open Discussion
- 5:00 Adjourn
- 5:30 TUFFP/TUPDP Reception
  ACAC – Atrium

Other Activities

- Nov. 2, 2010
  - TUHOP Meeting
  - TUFFP Workshop
    - Excellent Presentations
    - Beneficial for Everybody
  - Facility Tour
- Nov. 4, 2010
  - TUPDP Meeting

Fluid Flow Projects

Executive Summary of Research Activities

Cem Sarica

Advisory Board Meeting, November 3, 2010

Unified Model

- Objective
  - Develop and Maintain an Accurate and Reliable Steady State Multiphase Simulator
- Past Studies
  - Zhang *et al.* Developed "Unified Model" in 2002 for Two-phase Flow
    - Became TUFFP's Flagship Steady State Simulator
    - Applicable for All Inclination Angles
  - "Unified Model was Extended to Three-phase in 2006

Unified Model …

- Current Activities
  - Code and Software Improvement Efforts

Unified Model …

- Future Activities
  - Continue Improvements in Both Modeling and Software Development

Three-phase Flow Studies

- Significance
  - Good Understanding of Gas-Oil Flow
  - Poor Understanding of Gas-Oil-Water Flow
- Objective
  - Development of Improved Prediction Models
- Past Studies
  - Oil-Water
    - Trallero (1994), Horizontal
    - Flores (1996), Vertical and Deviated
    - Alkaya (1999), Inclined

Three-phase Flow Studies …

- Past Studies …
  - Three-phase
    - Keskin (2007), Experimental Horizontal Three-phase Study
    - Zhang and Sarica (2005), Three-phase Mechanistic Model Development
    - Gizem (2010) Slug Flow Evolution in Hilly Terrain Pipelines
    - Need to More Research on Oil-Water Flow
  - Recent Oil-Water Studies with Emphasis on Droplets
    - Vielma (2006), Horizontal Flow
    - Atmaca (2007), Inclined Flow
    - Sharma (2009), Modeling Based on Minimum Energy Concept

Three-phase Flow Studies …

- Current Activity
  - No Direct Projects Underway
  - Various Other Projects Contribute to This Project
    - Low-Liquid Loading Three-phase Flow
    - Unified Model and Software Development

Up-Scaling Studies

- Significance
  - Better Design and Operation
- Objective
  - Testing and Improvement of Existing Models for Large Diameter and Relatively High Pressures
- Past Studies
  - Low Pressure and 6-in. ID Low Liquid Loading (Fan and Dong)
  - High Pressure 2 in. ID (Manabe, 2002)

Up-Scaling Studies …

- Current Project
  - Construction of a New High Pressure, Large Diameter Facility
  - Extension of Low Liquid Loading Study to High Pressures is Envisioned as the First Study

Up-Scaling Studies …

- Status
  - Financial Shortcomings Solved
  - Equipment Purchases
    - All of the Equipment are either Purchased or Ordered
  - Significant Progress on Construction
  - Need to Firm up Instrumentation
  - On Time for Completion
    - 1st Quarter of 2011

Up-Scaling Studies …

- First Study
  - Low Liquid Loading Pressure Up-scaling

Fluid Flow Projects

High Pressure – Large Diameter Multiphase Flow Loop

Scott Graham and Cem Sarica

Outline

- Introduction
- Objectives
- Facility Design and Construction
- Capital Cost

Introduction

- Pressure and Pipe Diameter Affect Flow Behavior in Multiphase Flow Significantly
- Limited Study of Multiphase Flow in Large-Diameter Pipes at Pressure Conditions Higher than 2,000 kpa (290 psi)
- Need
  - Investigation of Diameter and Pressure Effects on Multiphase Flow
  - Experimental Data
- Requires a Proper Facility

Objectives

- Design and Construct a 6 in. ID High Pressure Multiphase Facility
- Conduct Research Projects to Better Understand Multiphase Flow
- Upscale Available Predictive Tools

Facility Design and Construction

- Design
  - Fluids
  - Operating Range
  - Facility Layout
  - Instrumentation
- Construction Activities

Fluids

- Gas Phase
  - Nitrogen
  - Natural Gas
- Oil Phase
  - Tulco Tech-80 Mineral Oil

Operating Range (Flow Pattern Map)

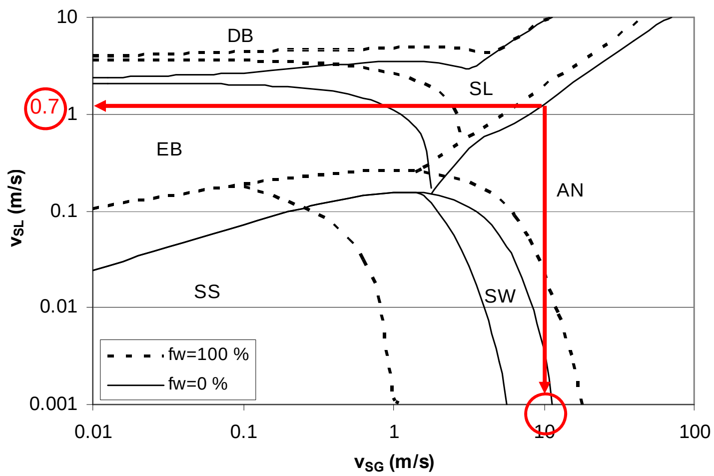

Operating Range …

- Operating Pressure = 500 psig
- $v_{SL,\ max}$=0.7 m/s; $v_{Sg,\ max}$=10 m/s
- f_w Between 0 and 100 %
- $q_{G,\ max}$ = 18 MMSCFD
- $q_{L,\ max}$ = 200 GPM
- Separator 54" x 10' @ 600 psig

Facility Diagram

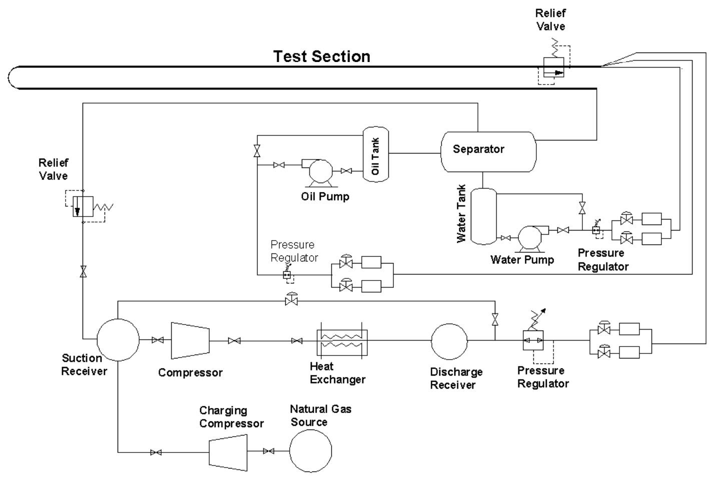

Fluid Flow Projects

Advisory Board Meeting, November 3, 2010

Facility Layout

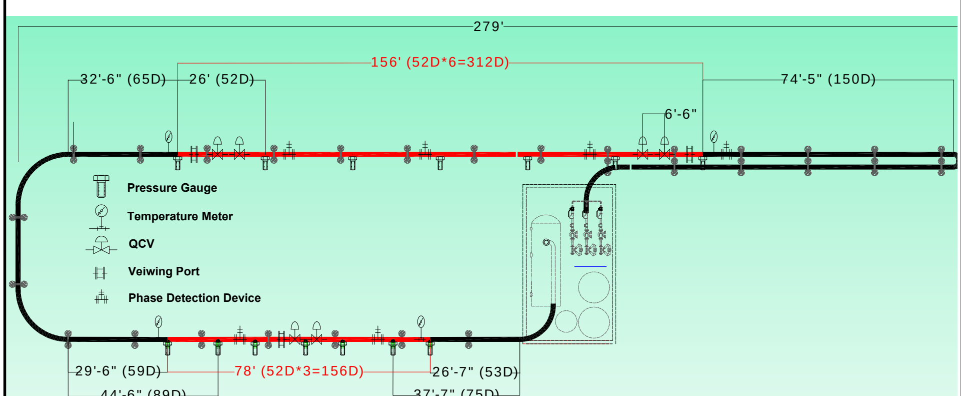

Fluid Flow Projects

Advisory Board Meeting, November 3, 2010

Facility Layout …

- 6 in. ID Stainless Steel Pipe
- Test Section-1
  - 156 ft (312D) Long and -3°<θ<+3°
- Test Section-2
  - 78 ft (156D) Long and Horizontal
- Flow Development Sections with Sufficient Lengths

Facility Layout …

- Test Section-1
  - Six 26 ft (52D) Long Pressure Drop Sections
  - Two 6.5 ft Long Trap Sections
  - Two Viewing Ports
  - Two Temperature Transducers
  - Four Phase Detection Devices (TBD)
- Test Section-2
  - Six Pressure Drop Sections
  - One 6.5 ft Trap Section
  - One Viewing Port
  - Two Phase Detection Devices (TBD)
  - Two Temperature Transducers

Basic Instrumentation

	Pressure (psig)	Capacity
Gas Flow Rate	600	18 MMSCFD
Water Flow Rate	600	200 GPM
Oil Flow Rate	600	200 GPM
Differential Pressure	500	0 – 50 in H_2O
Pressure	600	0 – 800 psi
Temperature	500	0-100 ° C
Quick Closing Valves	600	6 in. ID

Fluid Flow Projects

Advisory Board Meeting, November 3, 2010

Specific Instrumentation

- Trap Sections
  - Test Section-1
    - Located at Upstream and Downstream
  - Test Section-2
    - Located at Center

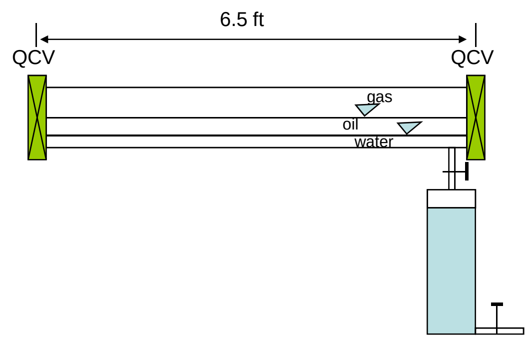

Fluid Flow Projects

Advisory Board Meeting, November 3, 2010

Special Instrumentation ..

- Whole Perimeter Viewing Section
  - Visual Flow Observation

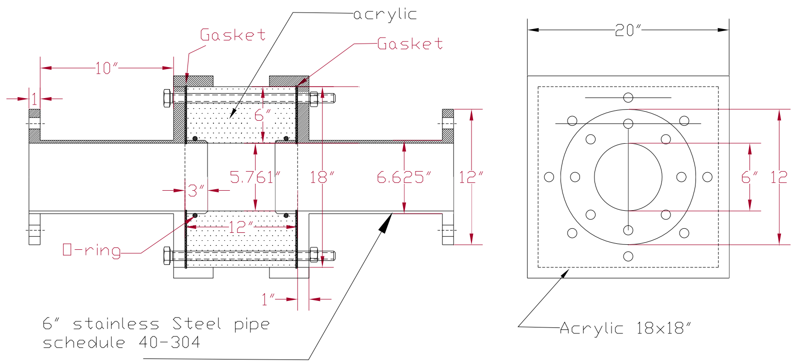

Special Instrumentation …

- Boroscope
  - Visual Flow Observation

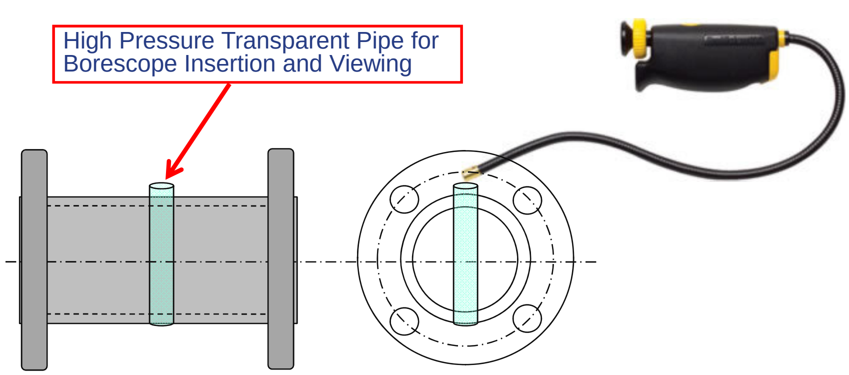

Construction Activities

- Equipment Pad
- Piers
- Structure
- Piping
- Equipment
- Vessels

Fluid Flow Projects

Advisory Board Meeting, November 3, 2010

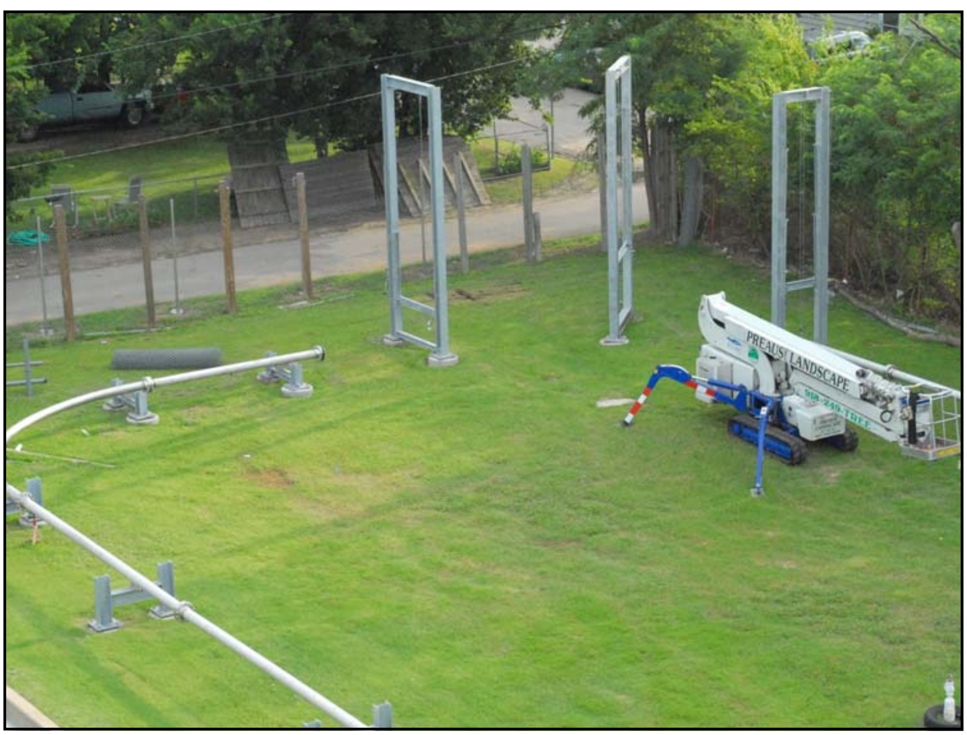
PREAUS LANDSCAPE


LANDSCAPE


PREAUS LANDSCAPE OF
ARBORISTS - LANDSCAPE CONTRACTO


BELGER
Ingersoll-Rand
Hertz

Fluid Flow Projects

Executive Summary
of Research Activities

Cem Sarica

Advisory Board Meeting, November 3, 2010

High Viscosity Multiphase Flow

- Significance
  - Discovery of High Viscosity Oil Reserves
- Objective
  - Development of Better Prediction Models
- Past Studies
  - First TUFFP Study by Gokcal (2005)
    - Existing Models Perform Poorly for Viscosities Between 200 and 1000 cp
    - Significantly Different Flow Behavior
      - Dominance of Slug Flow
  - Recent Study by Gokcal (2008)
    - New Drift Velocity and Translational Velocity Closure Models
    - New Slug Frequency Correlation

Fluid Flow Projects Advisory Board Meeting, November 3, 2010

High Viscosity Multiphase Flow …

- Current Study (Status)
  - Slug Liquid Holdup Closure Relationship Development
  - Drift Velocity Study
  - Slug Length Closure Relationship Development

High Viscosity Multiphase Flow …

- Slug Liquid Holdup
  - Study is Completed
    - Liquid Holdup Measurement Methods
      - Quick Closing Valves
      - Capacitance Sensor
    - New Holdup Correlation is Developed

High Viscosity Multiphase Flow …

- Drift Velocity Study
  - Completed
  - New Unified Drift Velocity Closure Relationship Developed
    - Using all Available Data with Various Pipe Diameters and Inclination Angles

High Viscosity Multiphase Flow …

- Slug Length Study
  - Shorter Slug Lengths are Experimentally Observed
  - Significant Progress in Probabilistic/Deterministic Modeling of Slug Length Study

High Viscosity Multiphase Flow …

- Continuation Study
  - Inclination Angle Effects
    - Underway
    - Facility is Being Modified
  - Higher Viscosity Oils (1,000 – 10,000 cp)
    - Future Work

Fluid Flow Projects

Effects of High Oil Viscosity on Slug Liquid Holdup in Horizontal Pipes

Ceyda Kora

Advisory Board Meeting, November 3, 2010

Outline

- Objectives
- Experimental Study
- Experimental Results
- Correlation and Model Evaluation
- Correlation Development
- Conclusions
- Recommendations

Objectives

- Investigate Slug Liquid Holdup for High Viscosity Oil and Gas Flow
- Develop Closure Models for Slug Liquid Holdup

Experimental Facility

Experimental Facility …

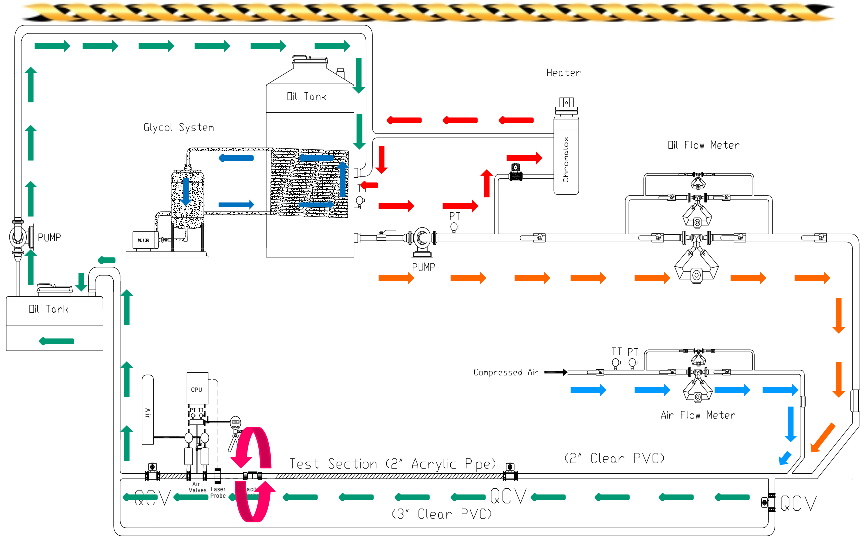

Fluid Flow Projects

Advisory Board Meeting, November 3, 2010

Test Fluids

- Citgo Sentry 220
  - Mineral Oil
  - API Gravity: 27.6 °
  - Viscosity: 0.22 Pa·s @ 40 °C
  - Specific Gravity: 0.89 @ 25 °C
- Air

Fluid Flow Projects

Advisory Board Meeting, November 3, 2010

Test Fluids …

- Citgo Sentry 220

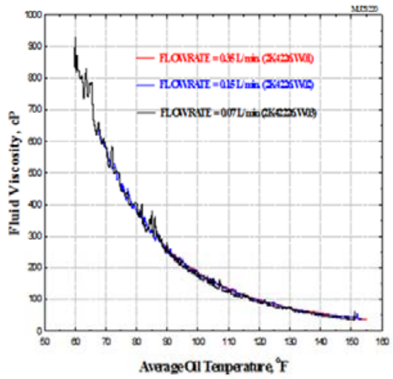

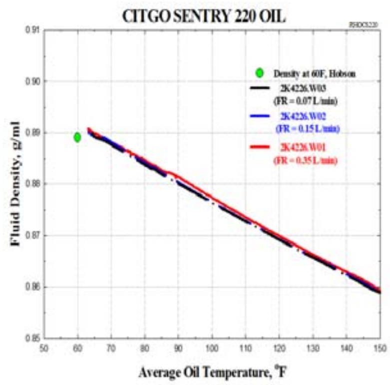

Testing Range

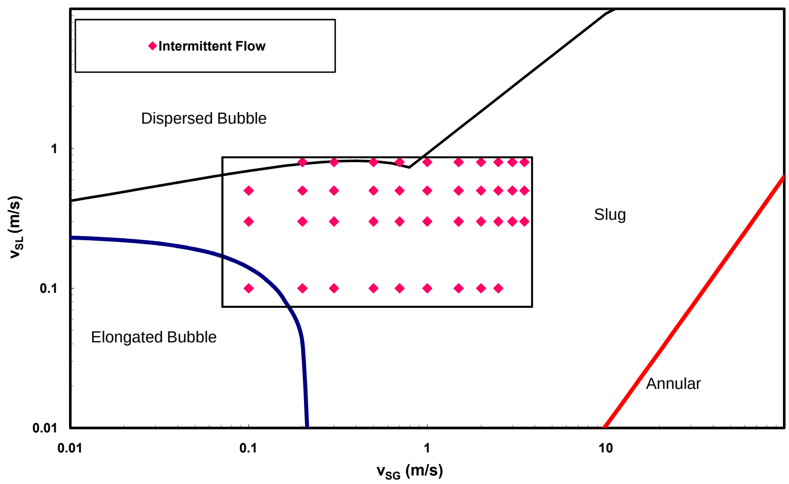

Testing Range …

- Superficial Liquid Velocity
  - 0.1 – 0.8 m/s
- Superficial Gas Velocity
  - 0.1 – 3.5 m/s
- Oil Viscosities
  - 0.587, 0.378, 0.257, 0.181 Pa·s
- Inclination
  - Horizontal

Experimental Study

- Capacitance Sensor
  - Provide Detailed Information Along Slug
    - Slug Liquid Holdup
    - Bubble Sizes
    - Large Bubble Locations
    - Liquid Film Height (h_F)

Capacitance Sensor

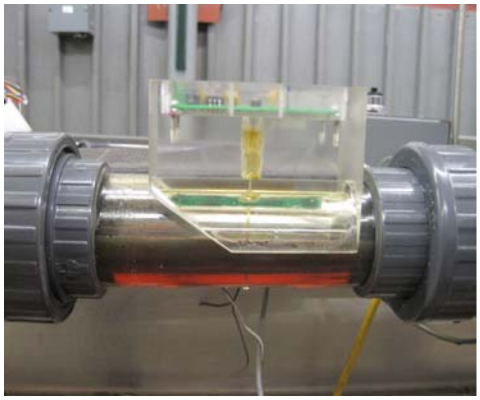

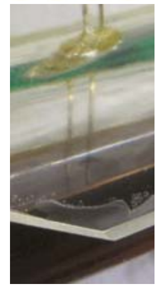

Fluid Flow Projects   Advisory Board Meeting, November 3, 2010

Capacitance Sensor …

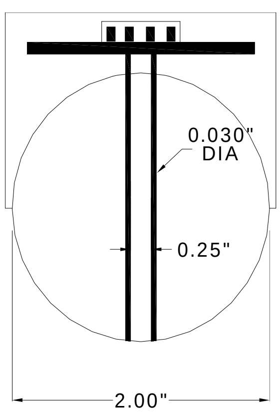

- **Dimensionless Voltage**

$$V^* = \frac{V_{read} - V_{\min}}{V_{\max} - V_{\min}}$$

- **Liquid Holdup**

$$H_{Ls} = \frac{A_{liquid}}{A_{total}}$$

Fluid Flow Projects   Advisory Board Meeting, November 3, 2010

Data Acquisition System

- Main Data Acquisition System
  - Temperature, Pressure, Flow Rates
  - Scan Rate: 10 Hz
- Portable Data Acquisition System
  - Voltage Signals from Capacitance
  - Scan Rate: 1000 Hz

Uncertainty Analysis

Measured Parameter	Instrument	Random Uncertainty	Systematic Uncertainty	Combined Uncertainty
Gas Flow Rate	Micro Motion™	±0.16%	±0.1%	±0.33%
Liquid Flow Rate	Micro Motion™	±0.17%	±0.1%	±0.35%
Temperature	RTD	±0.02°C	±0.5°C	±0.5°C
Pressure	Rosemount Pressure Transducer	±0.64%	±0.05%	±1.3%

Experimental Results

- Slug Flow Tests
  - 144 Tests Conducted with Capacitance Sensor
  - 144 Data Points Collected
  - High Speed Camera Used to Identify
    - Entrained Bubbles in Liquid Slug
    - Liquid Film Region

Experimental Results …

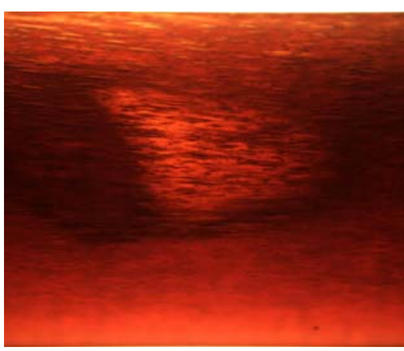

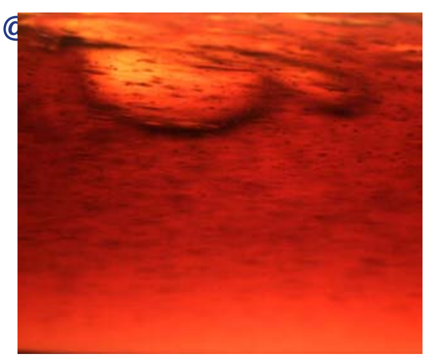

μ_O=0.181 Pa·s @ V_M=1.5 m/s

Fluid Flow Projects
Advisory Board Meeting, November 3, 2010

Slug Liquid Holdups

μ_o=0.587 Pa·s

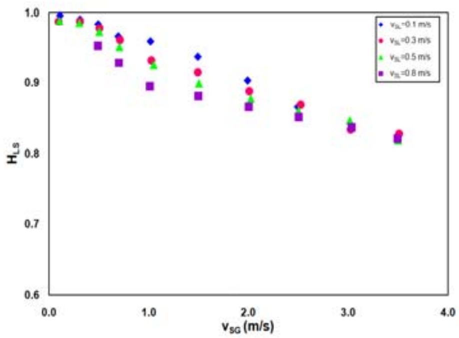

μ_o=0.378 Pa·s

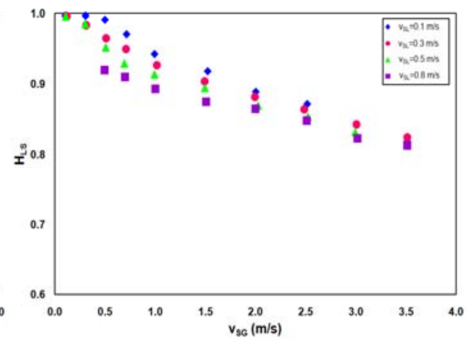

Fluid Flow Projects

Advisory Board Meeting, November 3, 2010

Slug Liquid Holdups …

μ_o=0.257 Pa·s

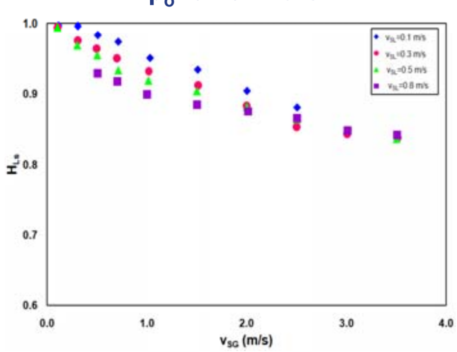

μ_o=0.181 Pa·s

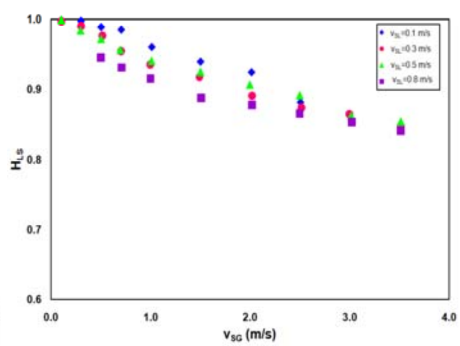

Fluid Flow Projects

Advisory Board Meeting, November 3, 2010

Slug Liquid Holdups…

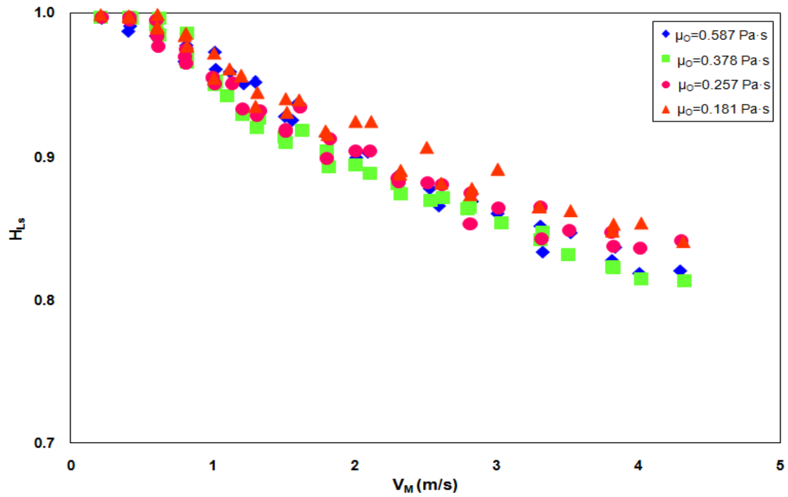

Slug Liquid Holdups …

μ_o=0.587 Pa·s, @ V_{SL}=0.8 m/s

μ_o=0.181 Pa·s, V_{SL}=0.8 m/s

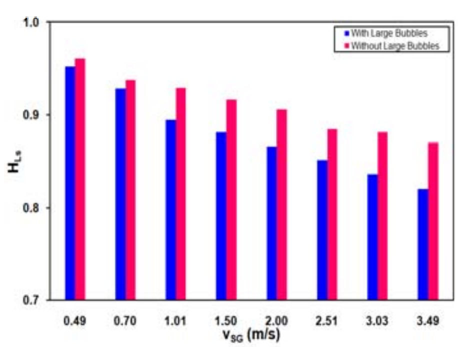

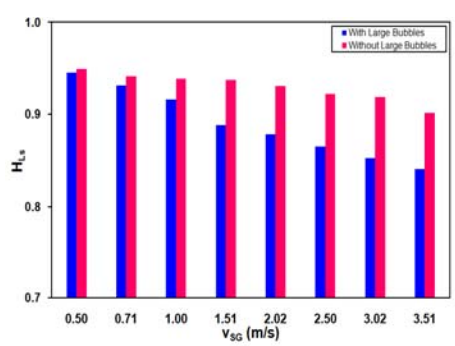

Liquid Film Heights

μ_o=0.587 Pa·s

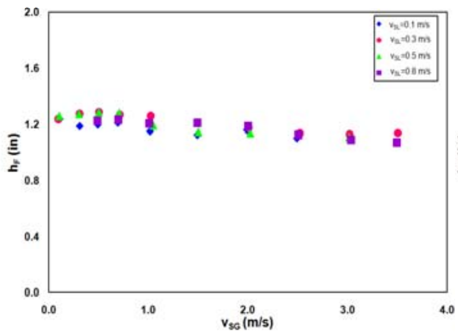

μ_o=0.378 Pa·s

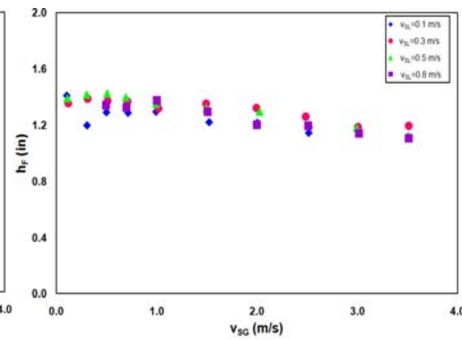

Liquid Film Heights …

μ_o=0.257 Pa·s

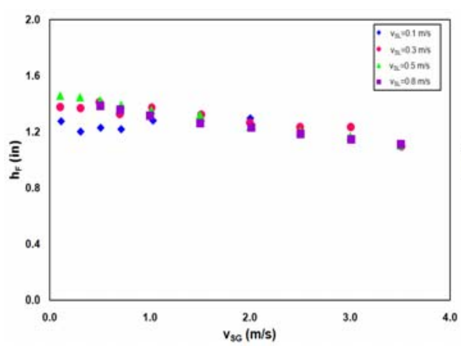

μ_o=0.181 Pa·s

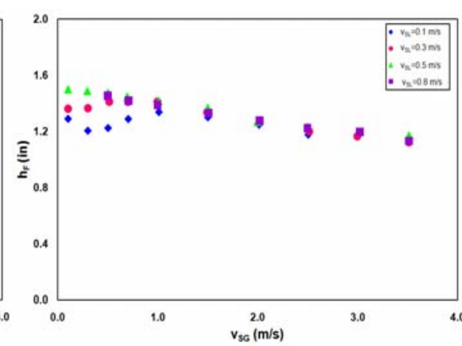

Liquid Film Heights …

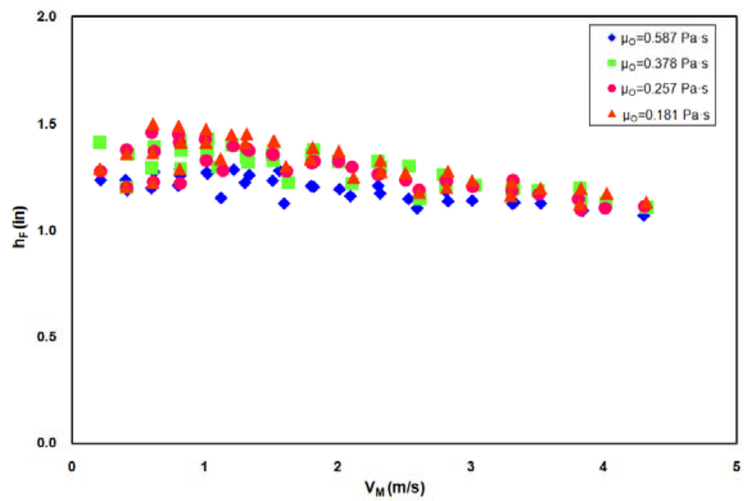

Model and Correlation Evaluation

Gregory *et al.*	$H_{Ls} = \dfrac{1}{1+\left(\dfrac{v_M}{8.66}\right)^{1.39}}$
Gomez *et al.*	$H_{Ls} = 1.0e^{-(7.85\cdot10^{-3}\theta+2.48\cdot10^{-6}N_{Re,m})}$
Abdul Majeed	$H_{Ls} = (1.009 - Cv_M)\xi$
Al-Safran	$H_{Ls} = 1.05 - \dfrac{0.0417}{\Theta - 0.123}$
Zhang *et al.*	$H_{Ls} = \dfrac{1}{1+\dfrac{T_{SM}}{3.16[(\rho_L-\rho_G)g\sigma]^{0.5}}}$

Model and Correlation Evaluation

μ_o=0.587 Pa·s

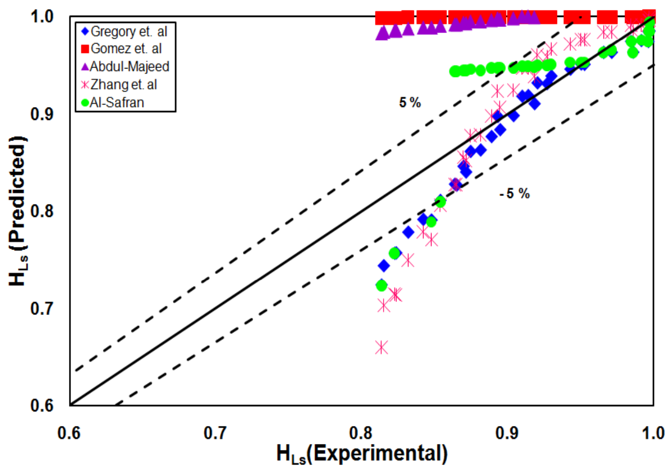

Model and Correlation Evaluation

μ_o=0.587 Pa·s

All Data Points

Correlation/Model	Statistical Parameters					
	ε_1 (%)	ε_2 (%)	ε_3 (%)	ε_4 (-)	ε_5 (-)	ε_6 (-)
Gregory *et al.*	-3.10	3.12	3.07	-0.03	0.03	0.03
Gomez *et al.*	9.69	9.69	7.00	0.08	0.08	0.06
Abdul-Majeed	9.40	9.40	6.22	0.08	0.08	0.05
Zhang *et al.*	-1.67	3.27	5.10	-0.01	0.03	0.04
Al-Safran	1.24	3.34	4.45	0.01	0.03	0.04

Data Points @ V_M<2 m/s

Correlation/Model	Statistical Parameters					
	ε_1 (%)	ε_2 (%)	ε_3 (%)	ε_4 (-)	ε_5 (-)	ε_6 (-)
Gregory *et al.*	-1.13	1.16	0.79	-0.01	0.01	0.01
Gomez *et al.*	4.62	4.62	3.49	0.04	0.04	0.03
Abdul-Majeed	4.89	4.89	3.19	0.05	0.05	0.03
Zhang *et al.*	1.33	1.33	0.97	0.01	0.01	0.01
Al-Safran	0.57	1.67	2.31	0.00	0.02	0.02

Data Points @ V_M≥2 m/s

Correlation/Model	Statistical Parameters					
	ε_1 (%)	ε_2 (%)	ε_3 (%)	ε_4 (-)	ε_5 (-)	ε_6 (-)
Gregory *et al.*	-5.72	5.72	2.78	-0.05	0.05	0.02
Gomez *et al.*	15.91	15.91	3.54	0.14	0.14	0.03
Abdul-Majeed	15.72	15.72	3.00	0.13	0.13	0.02
Zhang *et al.*	-5.86	5.99	5.59	-0.05	0.05	0.05
Al-Safran	1.90	6.33	6.96	0.02	0.05	0.06

Model and Correlation Evaluation …

μ_o=0.378 Pa·s

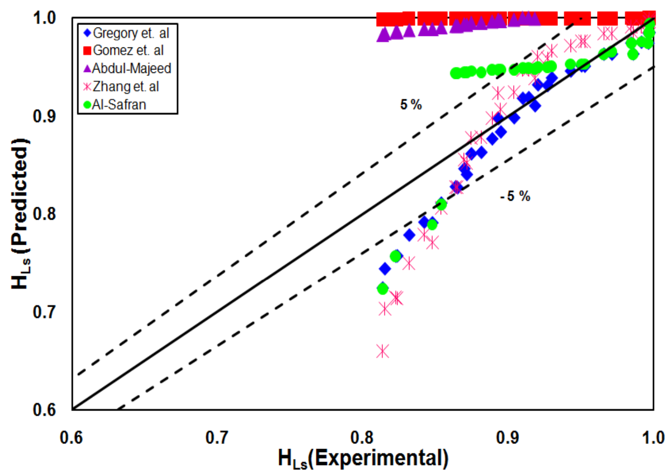

Model and Correlation Evaluation

μ_o=0.378 Pa·s

All Data Points

Correlation/Model	Statistical Parameters					
	ε_1 (%)	ε_2 (%)	ε_3 (%)	ε_4 (-)	ε_5 (-)	ε_6 (-)
Gregory *et al.*	-2.42	2.72	3.15	-0.02	0.02	0.03
Gomez *et al.*	10.46	10.46	7.14	0.09	0.09	0.06
Abdul-Majeed	10.18	10.18	6.38	0.09	0.09	0.05
Zhang *et al.*	-1.72	4.09	5.94	-0.01	0.04	0.05
Al-Safran	1.67	4.26	5.16	0.02	0.04	0.04

Data Points @ V_M<2 m/s

Correlation/Model	Statistical Parameters					
	ε_1 (%)	ε_2 (%)	ε_3 (%)	ε_4 (-)	ε_5 (-)	ε_6 (-)
Gregory *et al.*	-0.37	0.88	1.01	0.00	0.01	0.01
Gomez *et al.*	5.43	5.43	4.13	0.05	0.05	0.04
Abdul-Majeed	5.71	5.71	3.84	0.05	0.05	0.03
Zhang *et al.*	1.94	2.00	1.60	0.02	0.02	0.01
Al-Safran	1.29	2.28	2.66	0.01	0.02	0.02

Data Points @ V_M≥2 m/s

Correlation/Model	Statistical Parameters					
	ε_1 (%)	ε_2 (%)	ε_3 (%)	ε_4 (-)	ε_5 (-)	ε_6 (-)
Gregory *et al.*	-5.29	5.29	2.87	-0.04	0.04	0.02
Gomez *et al.*	17.50	17.50	3.45	0.15	0.15	0.02
Abdul-Majeed	16.44	16.44	2.95	0.14	0.14	0.02
Zhang *et al.*	-6.83	7.02	6.05	-0.06	0.06	0.05
Al-Safran	2.39	8.06	8.22	0.02	0.07	0.07

Model and Correlation Evaluation …

μ_o=0.257 Pa·s

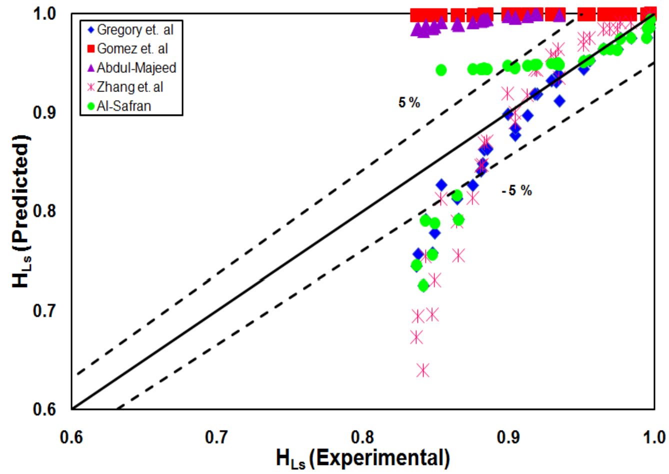

Fluid Flow Projects

Advisory Board Meeting, November 3, 2010

Model and Correlation Evaluation

μ_o=0.257 Pa·s

All Data Points →

Correlation/Model	Statistical Parameters					
	ε_1 (%)	ε_2 (%)	ε_3 (%)	ε_4 (-)	ε_5 (-)	ε_6 (-)
Gregory *et al.*	-3.12	3.18	3.77	-0.03	0.03	0.03
Gomez *et al.*	9.53	9.53	6.21	0.08	0.08	0.05
Abdul-Majeed	9.29	9.29	5.49	0.08	0.08	0.05
Zhang *et al.*	-3.32	5.02	7.37	-0.03	0.04	0.06
Al-Safran	0.21	4.25	5.72	0.00	0.04	0.05

Data Points @ V_M<2 m/s →

Correlation/Model	Statistical Parameters					
	ε_1 (%)	ε_2 (%)	ε_3 (%)	ε_4 (-)	ε_5 (-)	ε_6 (-)
Gregory *et al.*	-0.65	0.75	0.84	-0.01	0.01	0.01
Gomez *et al.*	5.09	5.09	3.54	0.05	0.05	0.03
Abdul-Majeed	5.39	5.39	3.25	0.05	0.05	0.03
Zhang *et al.*	1.42	1.50	1.21	0.01	0.01	0.01
Al-Safran	0.95	1.65	2.08	0.01	0.02	0.02

Data Points @ V_M≥2 m/s →

Correlation/Model	Statistical Parameters					
	ε_1 (%)	ε_2 (%)	ε_3 (%)	ε_4 (-)	ε_5 (-)	ε_6 (-)
Gregory *et al.*	-6.58	6.58	3.54	-0.06	0.06	0.03
Gomez *et al.*	15.75	15.75	2.77	0.14	0.14	0.02
Abdul-Majeed	14.75	14.75	2.34	0.13	0.13	0.02
Zhang *et al.*	-9.95	9.95	7.29	-0.08	0.08	0.06
Al-Safran	-0.89	8.14	8.77	-0.01	0.07	0.08

Fluid Flow Projects

Advisory Board Meeting, November 3, 2010

Model and Correlation Evaluation …

μ_o=0.181 Pa·s

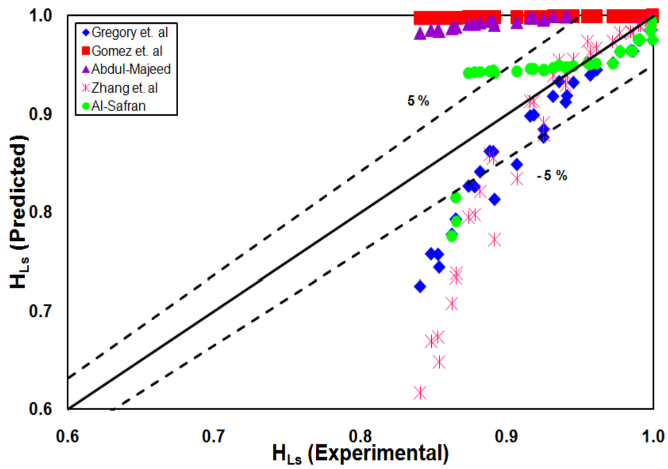

Fluid Flow Projects

Advisory Board Meeting, November 3, 2010

Model and Correlation Evaluation

μ_o=0.181 Pa·s

All Data Points

Correlation/Model	Statistical Parameters					
	ε_1 (%)	ε_2 (%)	ε_3 (%)	ε_4 (-)	ε_5 (-)	ε_6 (-)
Gregory *et al.*	-4.28	4.28	3.80	-0.04	0.04	0.03
Gomez *et al.*	8.17	8.17	5.94	0.07	0.07	0.05
Abdul-Majeed	7.95	7.95	5.23	0.07	0.07	0.04
Zhang *et al.*	-5.51	5.97	8.26	-0.05	0.05	0.07
Al-Safran	0.54	3.20	4.22	0.00	0.03	0.04

Data Points @ V_M<2 m/s

Correlation/Model	Statistical Parameters					
	ε_1 (%)	ε_2 (%)	ε_3 (%)	ε_4 (-)	ε_5 (-)	ε_6 (-)
Gregory *et al.*	-1.72	1.72	0.92	-0.02	0.02	0.01
Gomez *et al.*	3.89	3.89	3.10	0.04	0.04	0.03
Abdul-Majeed	4.20	4.20	2.83	0.04	0.04	0.03
Zhang *et al.*	0.05	0.74	1.16	0.00	0.01	0.01
Al-Safran	-0.21	1.51	1.75	0.00	0.01	0.02

Data Points @ V_M≥2 m/s

Correlation/Model	Statistical Parameters					
	ε_1 (%)	ε_2 (%)	ε_3 (%)	ε_4 (-)	ε_5 (-)	ε_6 (-)
Gregory *et al.*	-7.85	7.85	3.38	-0.07	0.07	0.03
Gomez *et al.*	14.16	14.16	2.93	0.12	0.12	0.02
Abdul-Majeed	13.21	13.21	2.51	0.12	0.12	0.02
Zhang *et al.*	-13.29	13.29	7.58	-0.11	0.11	0.06
Al-Safran	1.97	6.41	6.76	0.02	0.06	0.06

Fluid Flow Projects

Advisory Board Meeting, November 3, 2010

Correlation Development

- **Froude Number**

$$N_{F_r} = \frac{v_M}{(gd)^{0.5}} \sqrt{\frac{\rho_L}{\rho_L - \rho_G}}$$

- **Viscosity Number**

$$N_{\mu} = \frac{v_M \mu_L}{gd^2(\rho_L - \rho_G)}$$

Correlation Development …

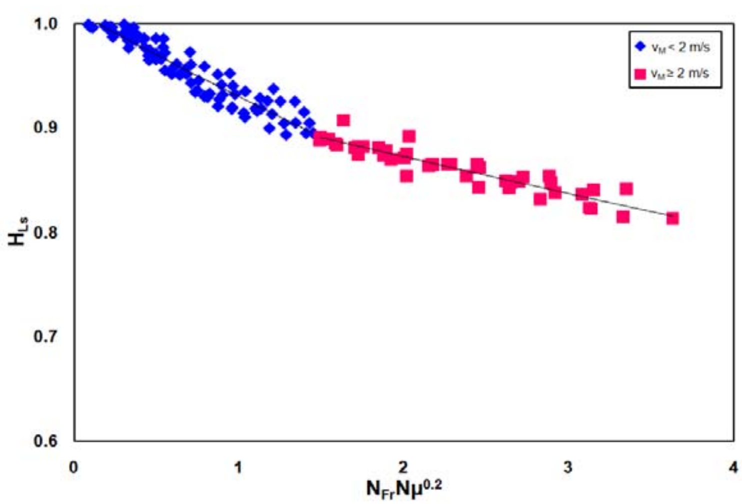

Correlation Development …

- $0.15 < N_{Fr}N_{\mu}^{0.2} < 1.5$

$$H_{Ls} = 1.012\, e^{(-0.085\, F_r N_{\mu}^{0.2})}$$

- $N_{Fr}N_{\mu}^{0.2} \geq 1.5$

$$H_{Ls} = 0.9473\, e^{(-0.041\, F_r N_{\mu}^{0.2})}$$

- $N_{Fr}N_{\mu}^{0.2} \leq 0.15$

$$H_{Ls} = 1.0$$

Correlation Development …

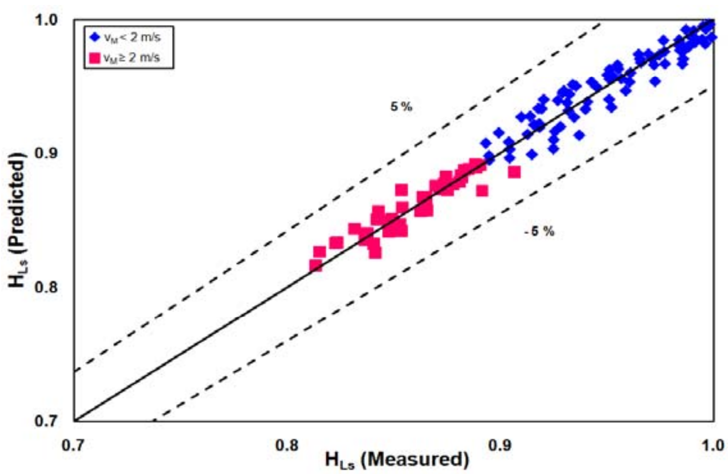

Conclusions

- Slug Liquid Holdup Decreases with Increasing Superficial Gas Velocity
- Slug Liquid Holdup Slightly Decrease with Increasing Superficial Liquid Velocity
- No Significant Change in Slug Liquid Holdup Observed with Increasing Oil Viscosity

Conclusions

- Decrease in the Amount of Small Entrained Bubbles Visually Observed with Decreasing Oil Viscosity
- No Large Bubbles Encountered at v_{SL} = 0.1 m/s
- No significant Change Observed in the Effect of Large Bubbles on Slug Liquid Holdup with Increasing Oil Viscosity

Conclusions

- Slight Increase in Liquid Film Height Observed with Decreasing Oil Viscosity
- Performance of Existing Correlations and Models Satisfactory at V_M<2 m/s
- Discrepancy between Predicted and Measured Slug Liquid Holdups Observed above $V_M \geq 2$ m/s
- New Slug Liquid Holdup Correlations Developed as a Function of Liquid Viscosity

Recommendations

- Design of Capacitance Sensor Can be Improved
- More Capacitance Sensors Can be Added to the Test Section to Investigate Phase Distribution during Slug Development
- Effect of Pipe Inclination Needs to be Investigated

Recommendations

- More Experimental Data are Required to Evaluate the Performance of Developed Correlations
- Gamma Ray Densitometer Can be Used to Compare Capacitance Sensor Results
- Effect of Top Oil Film on Slug Characteristics Needs to be Investigated

Fluid Flow Projects
Advisory Board Meeting, November 3, 2010

Questions & Comments

Fluid Flow Projects
Advisory Board Meeting, November 3, 2010

EFFECTS OF HIGH OIL VISCOSITY ON SLUG LIQUID HOLDUP IN HORIZONTAL PIPES

Ceyda Kora

Project Completion Dates

Literature Review .... Completed
Facility Modifications .... Completed
Preliminary Testing .... Completed
Testing .... Completed
Data Evaluation .... Completed
Final Report .... Completed

Objectives

The main objectives of this study are,

- Investigation of slug liquid holdup for high viscosity oil and gas flow,
- Development of closure models for slug liquid holdup.

Introduction

Heavy oils are produced and transported from many places around the world. Because of the increased consumption of hydrocarbon resources and decline in discoveries of low viscosity oils, the importance of heavy oil has increased. It is important to design a proper production system in order to eliminate operational problems for high oil viscosity fields. Available multiphase flow models are primarily developed for low viscosity liquids. TUFFP has been studying the high viscosity oil multiphase flow systematically since 2005, and has made significant progress towards the improvements in high viscosity oil multiphase flow prediction.

The first experimental study at TUFFP on high viscosity oil was completed by Gokcal (2005). The effects of high oil viscosity on oil-gas two-phase flow behavior were investigated and significant changes in flow behavior were observed. Intermitted flow (slug and elongated bubble) is the dominant flow pattern for high viscosity oil and air flow. Slug characteristics need to be examined in detail for better understanding of high liquid viscosity effect.

An experimental and theoretical investigation of slug flow for high oil viscosity in horizontal pipes was completed by Gokcal in 2008. He developed models for drift velocity, transitional velocity and slug frequency by taking into account the viscosity effect. Slug liquid holdup was not studied due to a lack of proper instrumentation. Only average liquid holdup was measured in his study. Therefore, investigation of slug liquid holdup for high viscosity oil and gas two-phase flow is the focus of this study.

The most challenging part of this study is to measure gas void fraction in liquid slugs. For the measurement of slug liquid holdup, a new capacitance sensor (CS) has been developed and experiments were conducted at 70, 80, 90, 100 °F oil temperatures corresponding 0.587 Pa·s, 0.378 Pa·s, 0.257 Pa·s and 0.181 Pa·s oil viscosities.

Experimental Study

Experimental Facility

An existing TUFFP indoor high viscosity facility has been modified for this study (Fig. 1). This facility was previously used by Gokcal (2005 and 2008) to investigate the effects of high oil viscosity on slug flow characteristics. There are four main parts of the facility: metering section, test section, heating system and cooling system. The test section was designed as an 18.9-m (62-ft) long, 50.8-mm (2-in.) ID pipe consisting of a clear PVC pipe section and a transparent acrylic pipe section. A 9.15-m (30-ft) long transparent acrylic pipe section is used to observe the flow behavior visually.

The test oil viscosity is very sensitive to temperature changes. The temperature measurements are imperative to determine the viscosity of the oil during experiments. Therefore, it is crucial to conduct experiments at a constant temperature. Existing heating and cooling systems are used to control temperature. Resistance Temperature Detector (RTD) transducers already exist in the facility to measure temperatures during experiments. Pressure transducers and differential pressure transducers are located at various points to monitor the pressure and pressure drop during experiments.

Data Acquisition System

Previously developed data acquisition program is used for the high viscosity facility. Pressure, temperature,flow rates, superficial gas and superficial liquid velocities are monitored on the PC of the facility during the experiments. In addition, the capacitance sensor is connected to a portable data acquisition system using a scan rate of 1000 Hz to measure the resulting voltage signals from the sensor. Data acquisition duration is fixed for 10 seconds. As a result 10,000 data points are collected in one test.

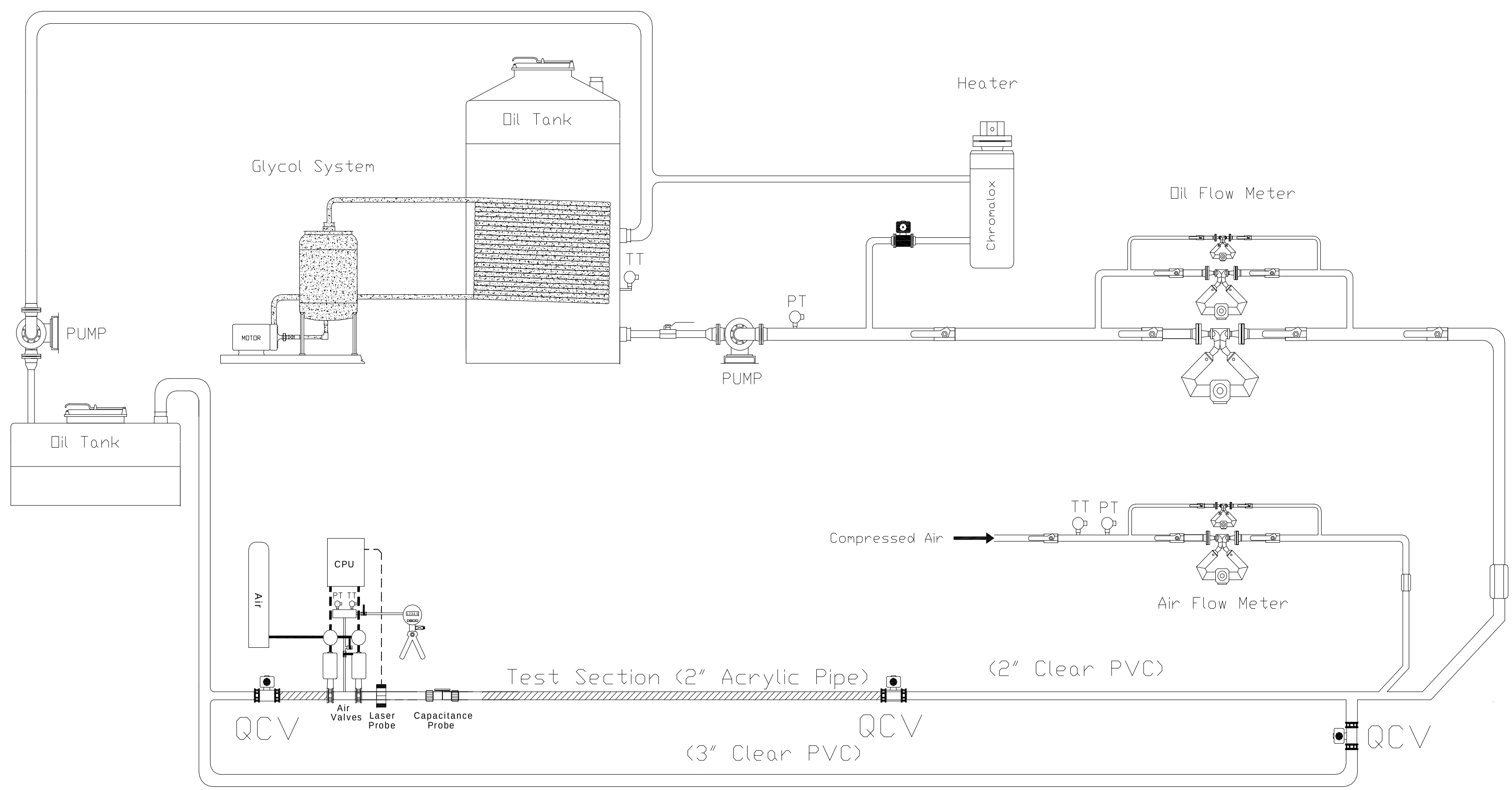

Figure 1: Schematic of High Viscosity Facility of Tulsa University Fluid Flow Projects (TUF

Test Fluids

The previously used high viscosity oil (Citgo Sentry 220) and air were selected again for this study. Following are the typical properties of the oil:

Gravity: 27.6 °API

Viscosity: 0.220 Pa·s @ 40 °C

Density: 889 kg/m^3 @ 15.6 °C

The oil viscosity vs. temperature behavior is shown in Fig. 2.

Test Range

In this study, experiments were conducted at various oil and gas velocities and different oil viscosities corresponding to different temperatures. Since the slug characteristics were examined by Gokcal (2008) in the previous project of TUFFP, his test matrix is used as the starting point of this study. Superficial oil velocities range from 0.1 m/s to 0.8 m/s. Superficial air velocities range from 0.1 to 3.5 m/s. The viscosity of Citgo Sentry 220 oil is very sensitive to temperature changes. Experiments were conducted at four different viscosities: 0.587, 0.378, 0.257, and 0.181 Pa·s, respectively. The test section was kept horizontal.

Instrumentation

Capacitance Sensor

A new capacitance sensor (CS) had been developed in-house for the measurement of slug liquid holdup and liquid film height. The principle of the capacitance method is based on the differences in the dielectric constants of the gas and liquid phases in the flow. The new design of the CS provides detailed information across the slug body. A schematic of the capacitance probe is shown in Fig. 3. The sensor consists of two parallel copper wires positioned perpendicular to the flow with a distance in between (0.25 in.), an electronic circuit to filter, amplify and convert the measured capacitance to a voltage, and the housing.

Static calibration of CS was accomplished by placing different amounts of liquid volumes in an acrylic pipe tester with the CS in the middle, and measuring the height of the fluid in the pipe, then recording the corresponding sensor output voltage. Dynamic calibration of CS was conducted using existing quick-closing valve system.

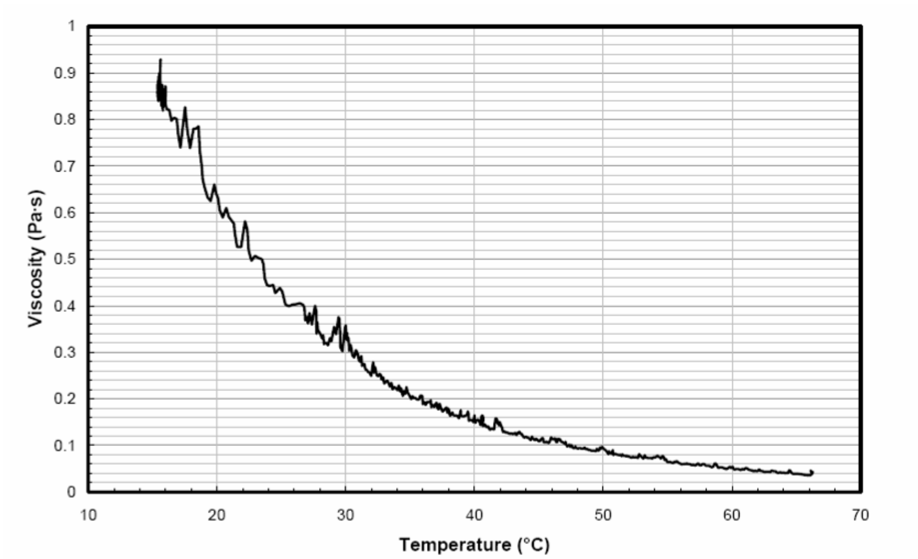

Figure 2: Viscosity vs. Temperature for Citgo Sentry 220 Oil

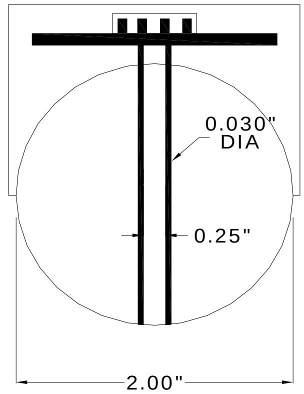

Figure 3: Schematic of New Capacitance Sensor

Uncertainty Analysis

There always exists an error in every measurement. Error is defined as the difference between true and measured values (Dieck 2002). Since the true value and thus error cannot be predicted exactly, the uncertainty analysis for every measurement needs to be conducted. This analysis provides confidence in the quality of the experimental data.

Errors are classified as random and systematic errors. A random error is naturally inherited and cannot be eliminated, yet it has to be quantified. The difference between average of measured values and true value gives the systematic errors. Systematic error remains constant for all experiments. A detailed presentation of random and systematic uncertainty and uncertainty propagation modeling in designing experiments is given by Al-Safran (2003).

Gokcal (2008) performed an uncertainty analysis for all instruments of the TUFFP high viscosity facility considering random and systematic uncertainty analysis. The calculated uncertainties are listed in Table 1.

Systematic uncertainty of quick-closing valve system was determined as ±0.005 in terms of holdup. Since quick-closing valve system is used for dynamic calibration of capacitance sensor, systematic uncertainty for slug liquid holdup measurements can be stated as ±0.005. Random uncertainty analysis cannot be performed for capacitance sensor. However, a correction factor was added to experimental data based on dynamic calibration in order to increase the confidence of data.

Table 1: Uncertainty Analysis Results for High Viscosity Facility (Gokcal 2008)

Measured Parameter	Instrument	Random Uncertainty	Systematic Uncertainty	Combined Uncertainty
Gas Flow Rate	Micro Motion™	±0.16%	±0.1%	±0.33%
Liquid Flow Rate	Micro Motion™	±0.17%	±0.1%	±0.35%
Temperature	RTD	±0.02°C	±0.5°C	±0.5°C
Pressure	Rosemount Pressure Transducer	±0.64%	±0.05%	±1.3%

Experimental Results

The effects of high oil viscosity on slug liquid holdup and liquid film height were experimentally investigated in horizontal pipes. 144 tests were conducted at 0.587 Pa·s, 0.378 Pa·s, 0.257 Pa·s and 0.181 Pa·s oil viscosities. Superficial oil velocities and superficial air velocities range from 0.1 to 0.8 m/s and 0.1 to 3.5 m/s, respectively.

Slug Liquid Holdups

High speed video camera was used to analyze the characteristics of entrained gas in the slug body. Slug flow videos were recorded at 0.587 Pa·s and 0.181 Pa·s oil viscosities for various superficial gas and liquid velocities. Large and small entrained bubbles were observed in the liquid slug as shown in Figs. 4 and 5. A decrease in the amount of small entrained bubbles was visually observed with decreasing oil viscosity. This could be due to the faster segregation of liquid and gas in low viscosity oils because of the lower drag force. The movements of entrained gas bubbles are slower in viscous oils. Large bubbles were encountered at mixture velocities from 0.6 to 3.5 m/s.

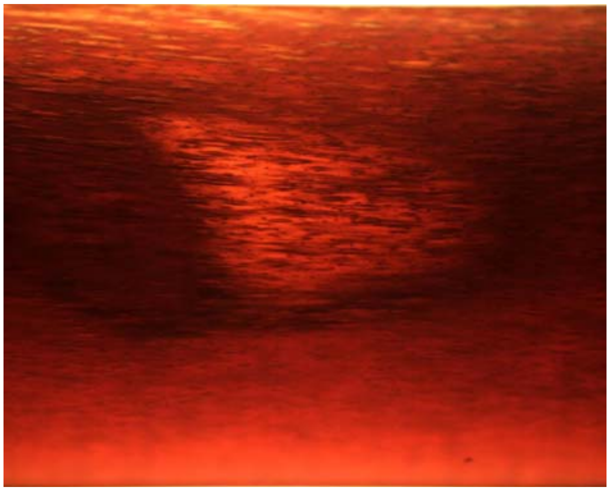

Figure 4: Liquid Slug for 0.587 Pa·s Oil Viscosity at v_M=1.5 m/s.

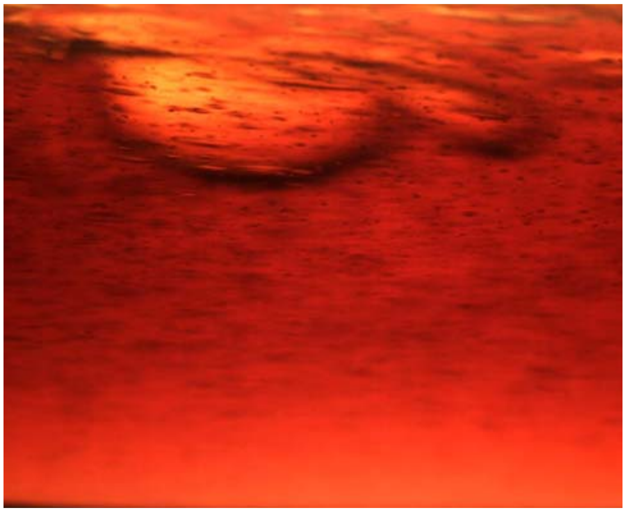

Figure 5: Liquid Slug for 0.181 Pa·s Oil Viscosity at v_M=1.5 m/s.

Figures 6 − 9 show the measured slug liquid holdups at four different oil viscosities. Results are presented for various superficial gas velocities and 0.1, 0.3, 0.5 and 0.8 m/s superficial liquid velocities. As superficial gas velocity increases, slug liquid holdup decreases at all oil viscosities. A slight decrease in slug liquid holdup was observed with increasing superficial liquid velocity. This decrease is resulted from the high gas bubble entrainment rate at slug front at higher superficial liquid velocities. This variation in liquid holdup with superficial liquid velocity diminishes as superficial gas velocity increases above 3 m/s or decreases below 0.3 m/s. This observation suggests that slug liquid holdup is sensitive to liquid flow rate over a specific range of gas flow rates. No considerable viscosity effect is observed on slug liquid holdup within 0.587 Pa·s to 0.181 Pa·s oil viscosity range shown as in Fig. 10. Nevertheless, slightly high liquid holdups were observed at high mixture velocities for the lowest oil viscosity, 0.181 Pa·s. This is caused by decrease in entrained small bubbles with decreasing oil viscosity.

In order to investigate the effect of large bubbles on slug liquid holdup, capacitance sensor readings were reevaluated after omitting the large bubbles in the slug body. Large bubbles were not encountered at v_{SL}=0.1 m/s. There is no significant change observed in the effect of large bubbles on liquid holdup with changing oil viscosity as shown in Figs. 11 and 12.

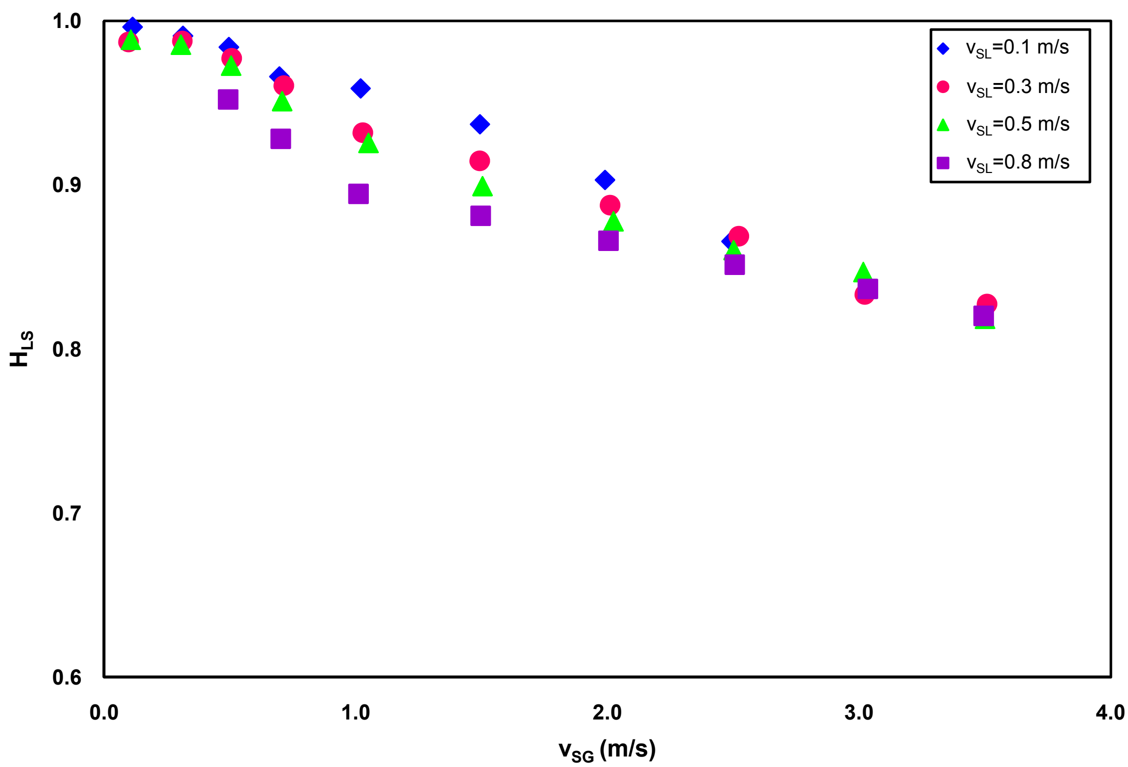

Figure 6: Slug Liquid Holdups for μ_o=0.587 Pa·s

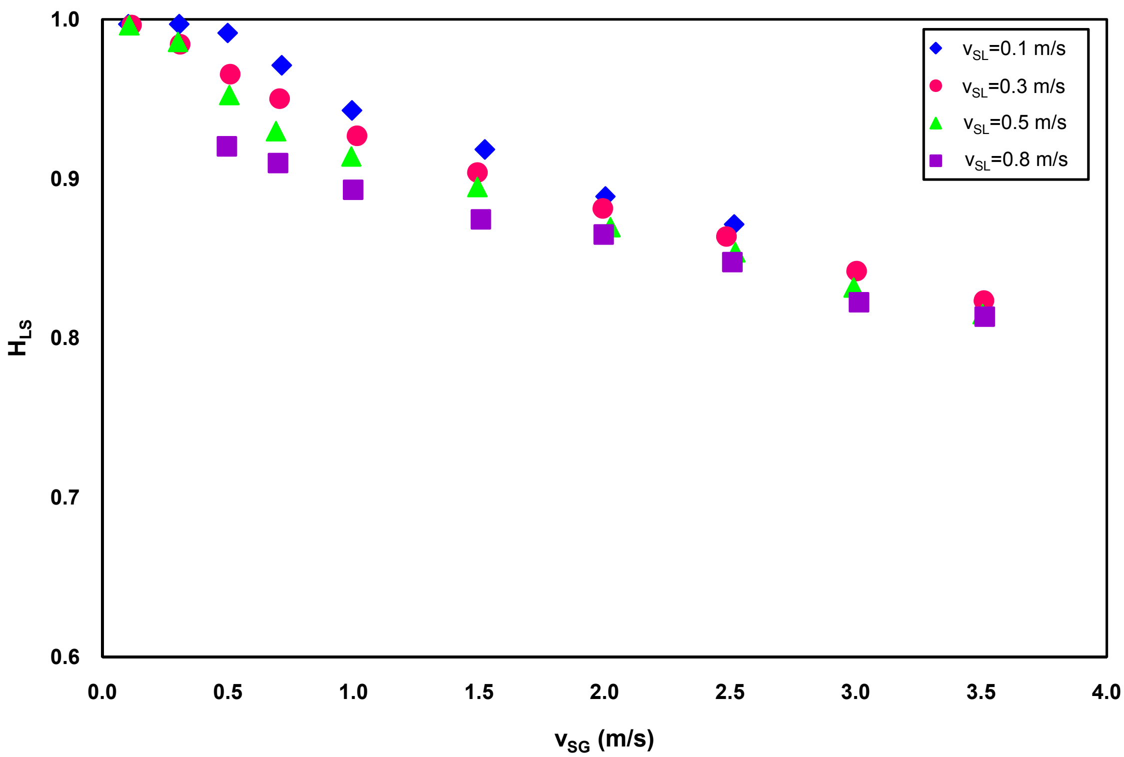

Figure 7: Slug Liquid Holdups for μ_o=0.378 Pa·s

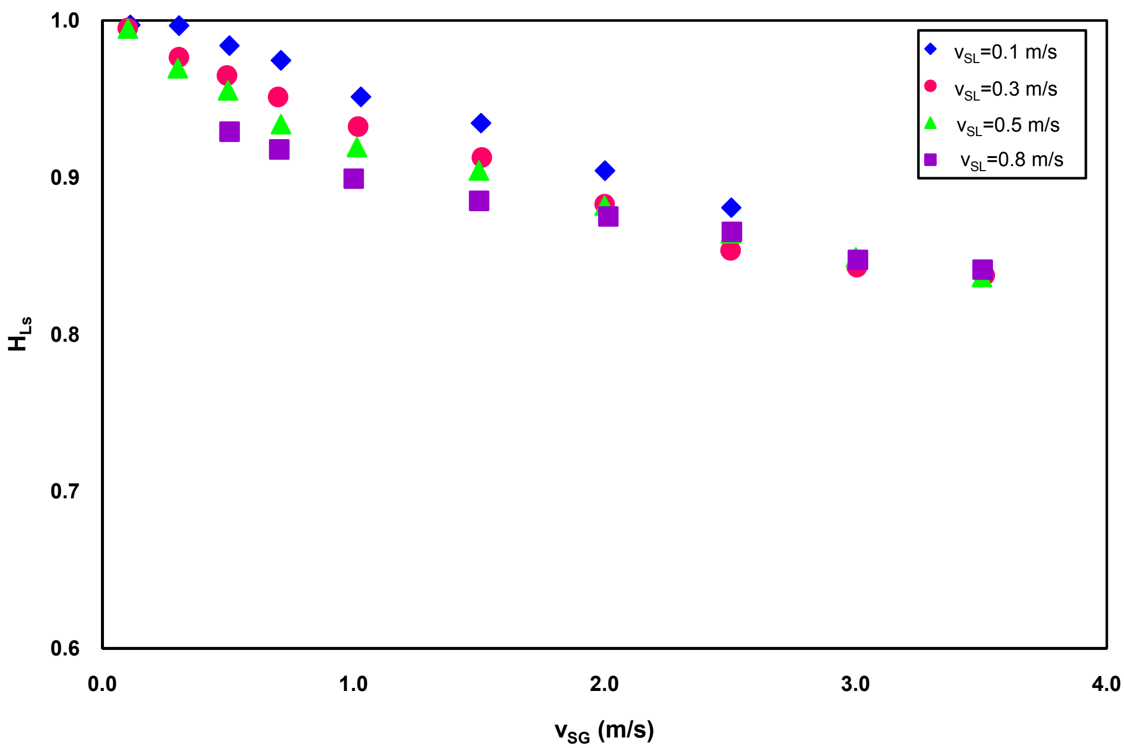

Figure 8: Slug Liquid Holdups for μ_o=0.257 Pa·s

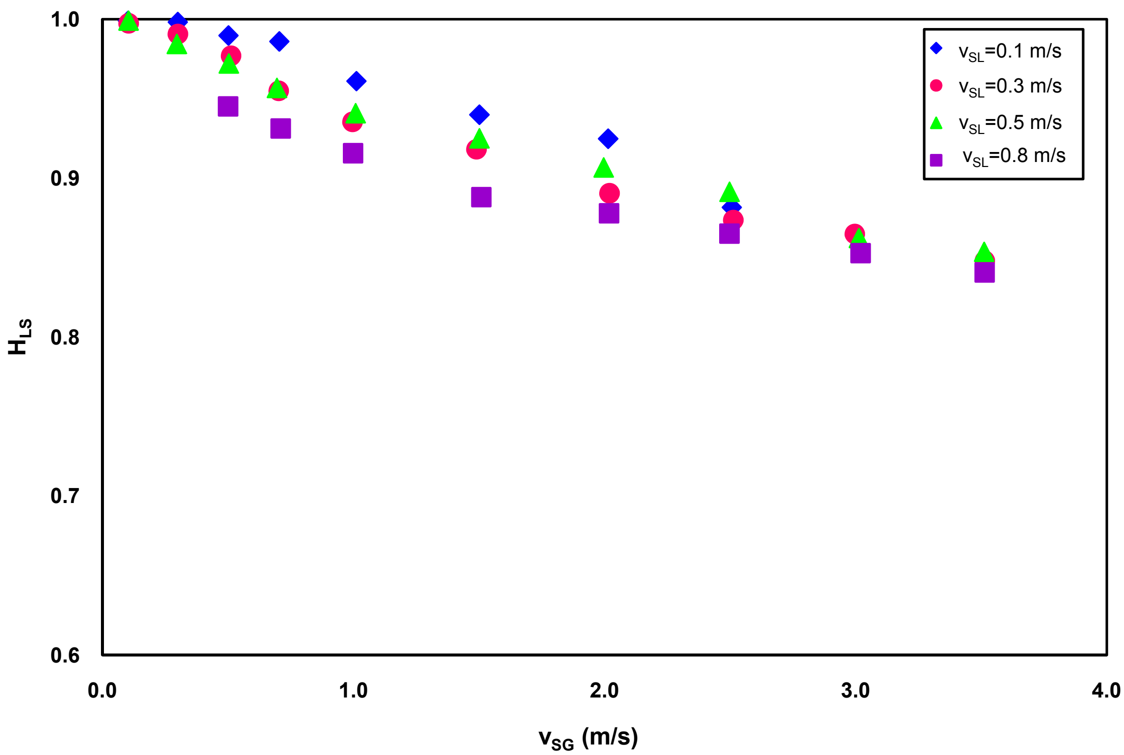

Figure 9: Slug Liquid Holdups for μ_o=0.181 Pa·s

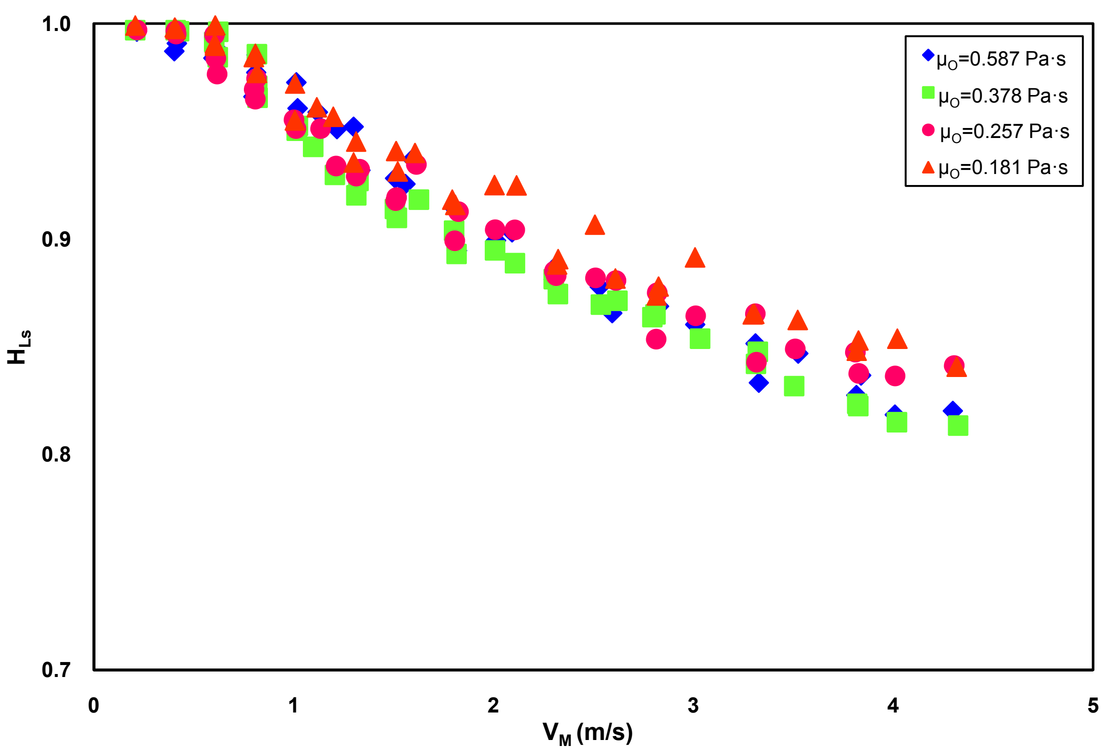

Figure 10: Slug Liquid Holdups vs. Mixture Velocity at Different Oil Viscosities

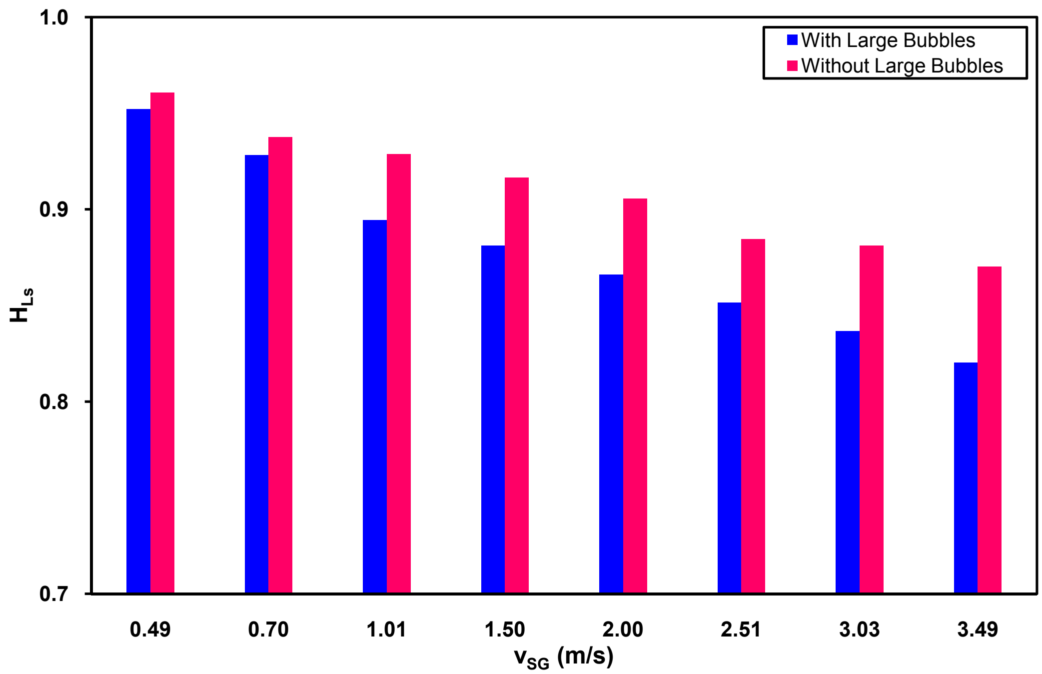

Figure 11: Comparison of Slug Liquid Holdups with Large Bubbles and without Large Bubbles for v_{SL} = 0.8 m/s at μ_o=0.587 Pa·s

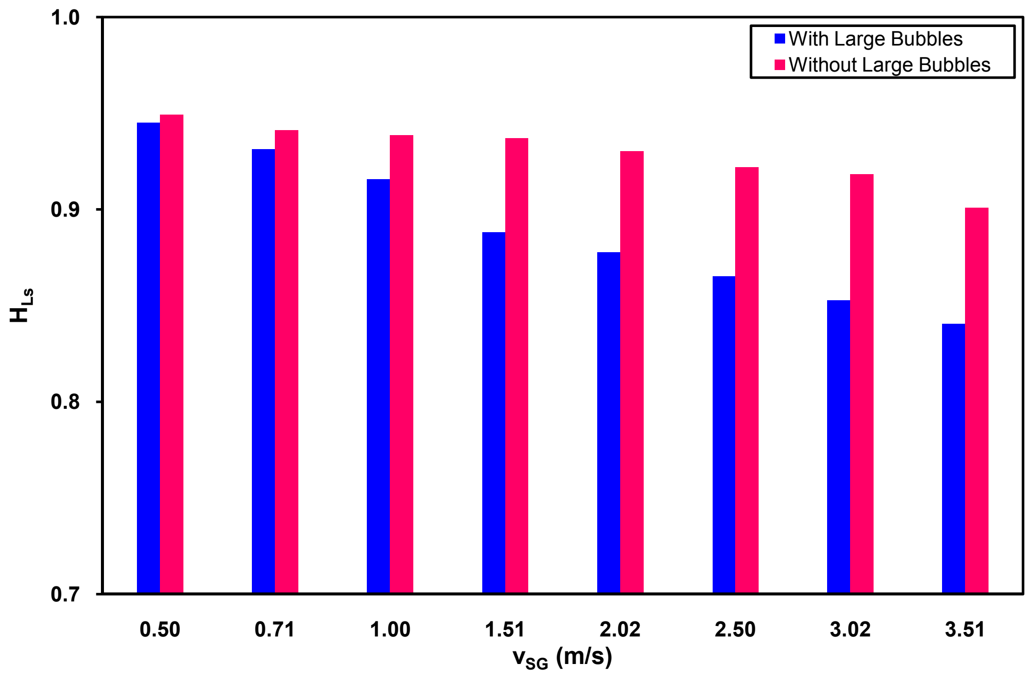

Figure 12: Comparison of Slug Liquid Holdups with Large Bubbles and without Large Bubbles for v_{SL} = 0.8 m/s at μ_o=0.181 Pa·s

Liquid Film Height

The results of the measured liquid film heights are presented in Figs. 13 – 16 at 0.587 Pa·s, 0.378 Pa·s, 0.257 Pa·s and 0.181 Pa·s oil viscosities, respectively. Superficial oil and gas velocities varied from 0.1 to 0.8 m/s and from 0.1 to 3.5 m/s, respectively. The liquid height measurement during this experimental study was a challenge because of the slow drainage of high viscosity oil, resulting in a liquid film on top of the pipe during the flow. This problem worsens under the condition of high viscosity oil due to the increase of slug frequency with increasing liquid viscosity (Gokcal, 2008). When the slug frequency decreases, the time interval between consecutive slugs becomes longer and top oil film drains more. As liquid viscosity decreases, liquid film height slightly increases due to higher drainage rate of top oil film as shown in Fig. 17. With increasing superficial gas velocity, liquid film heights approach the same trend for all viscosities.

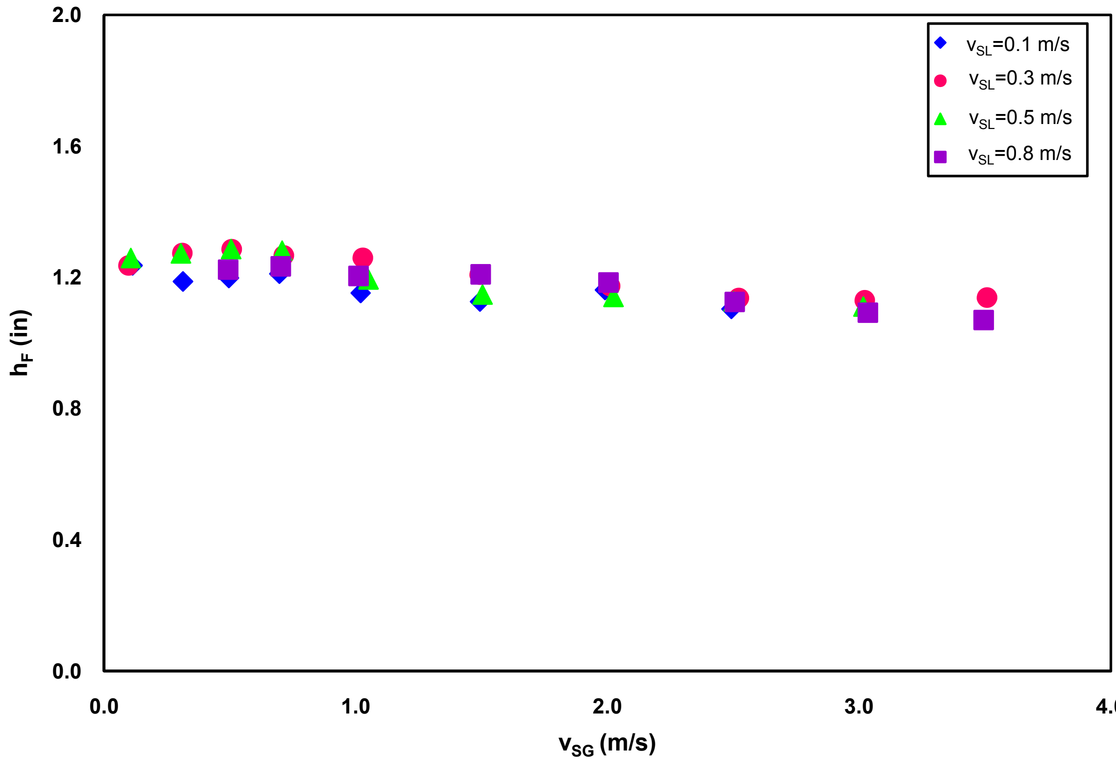

Figure 13: Liquid Film Heights for μ_o=0.587 Pa·s

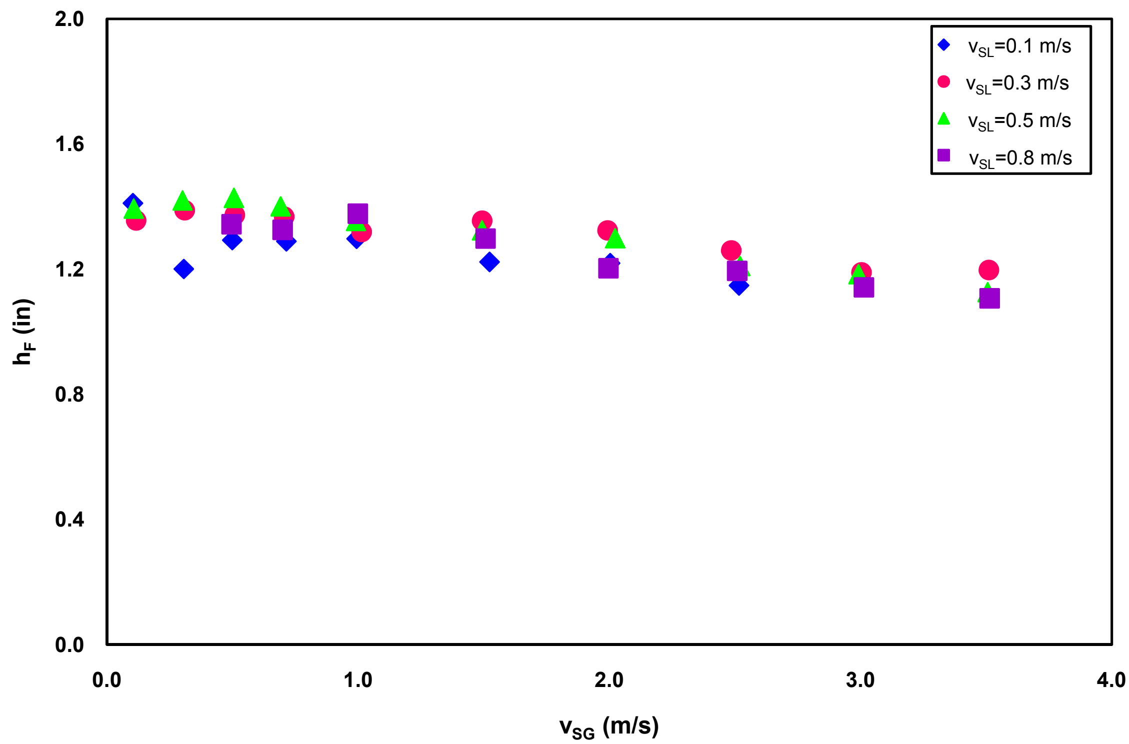

Figure 14: Liquid Film Heights for μ_o=0.378 Pa·s

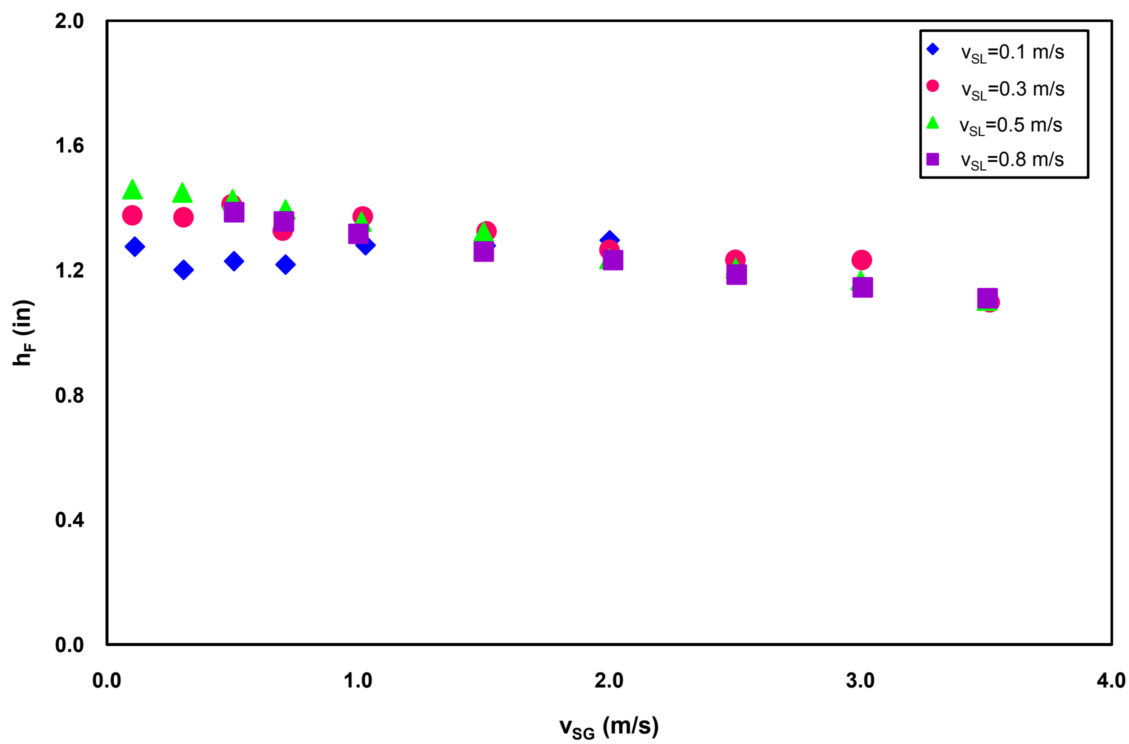

Figure 15: Liquid Film Heights for μo=0.257 Pa·s

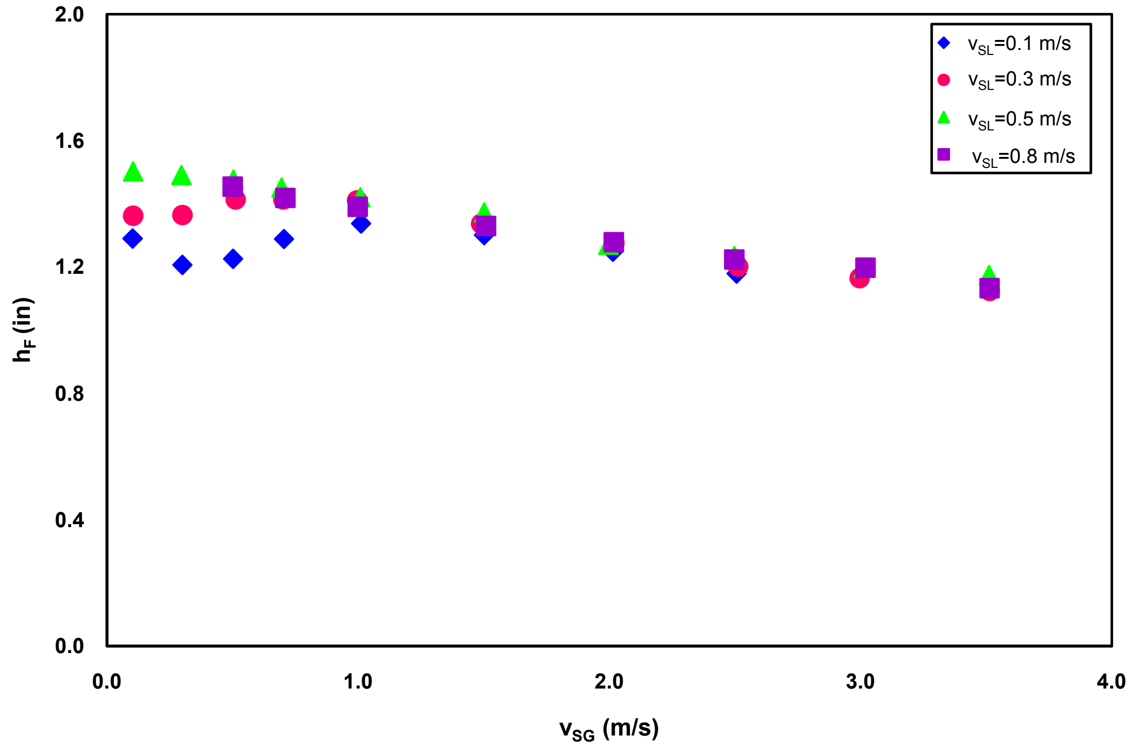

Figure 16: Liquid Film Heights for μo=0.181 Pa·s

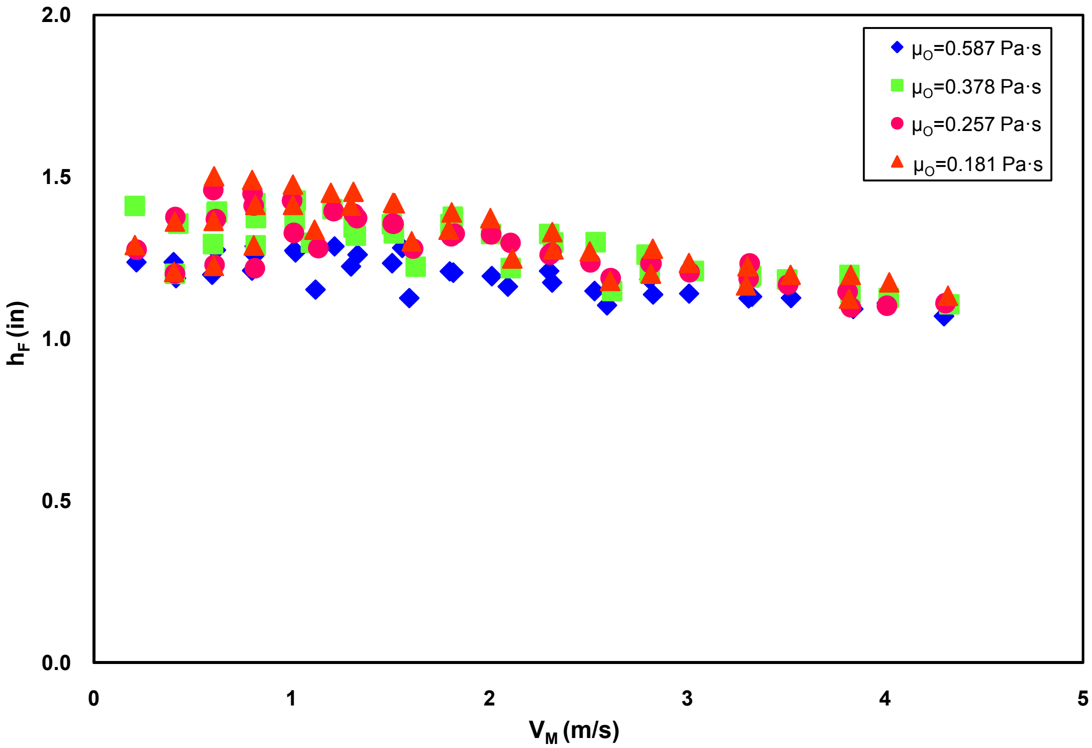

Figure 17: Liquid Film Heights vs. Mixture Velocity at Different Oil Viscosities

Model and Correlation Evaluation

Existing slug liquid holdup model and correlations are compared with the experimental data acquired in the present study. Zhang *et al.* (2003) mechanistic model and Gregory *et al.* (1978), Gomez *et al.* (2000), Abdul-Majeed (2000), Al-Safran (2009) empirical correlations were evaluated for their performance under high liquid viscosity condition. The comparison results and the performance of these methods are discussed below.

Slug Liquid Holdup Predictions

The performance of available slug liquid holdup model and correlations against the measured data are reviewed in three groups: predictions for all data points, predictions for data points with mixture velocity less than 2 m/s and predictions for data points with mixture velocity equal or higher than 2 m/s.

Predictions for All Data Points

Figures 18 − 21 display the comparison between the predictions of Zhang *et al.* (2003) mechanistic model and Gregory *et al.* (1978), Gomez *et al.* (2000), Abdul-Majeed (2000), Al-Safran (2009) correlations and entire measured slug liquid holdups at 0.587 Pa·s, 0.378 Pa·s, 0.257 Pa·s and 0.181 Pa·s oil viscosities, respectively. All methods exhibit the same trend for all viscosities. Predictions of Gomez *et al.* and Abdul-Majeed correlations are very close to each other, and they overestimate slug liquid holdups significantly. Although these empirical correlations consider the liquid viscosity, they were validated for low viscosity oils. Al-Safran correlation performs fairly accurate above slug liquid holdup value of 0.93. However, predictions of this correlation become inconsistent below slug liquid holdup of 0.93, where it over-predicts then under-predicts the liquid holdup. The reason of this behavior is the non-convergence of mechanistic model used to calculate the momentum exchange rate term especially at high superficial gas velocities. Gregory *et al.* correlation and Zhang *et al.* model perform better than the other correlations. Tables 2 − 5 show the results of the comparisons. Although Gregory *et al.* correlation and Zhang *et al.* model underestimate the liquid holdup above 2 m/s mixture velocity they still produce the best overall results based on the statistical parameters ε_2 and ε_5.

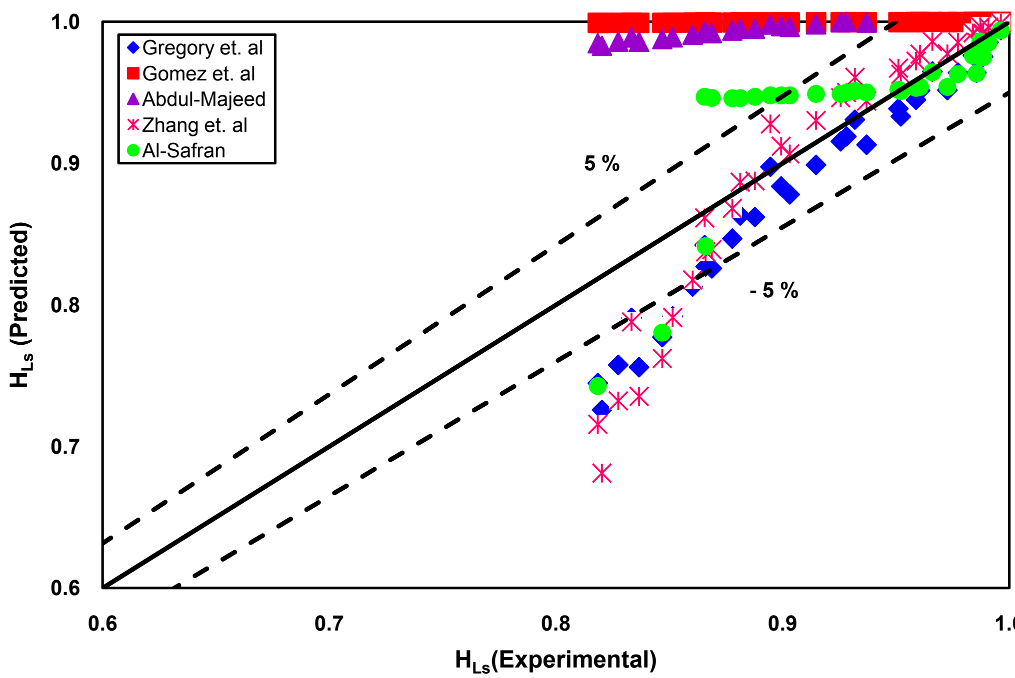

Figure 18: Performance of Correlations and Model against Measured Slug Liquid Holdups for μ_o=0.587 Pa·s

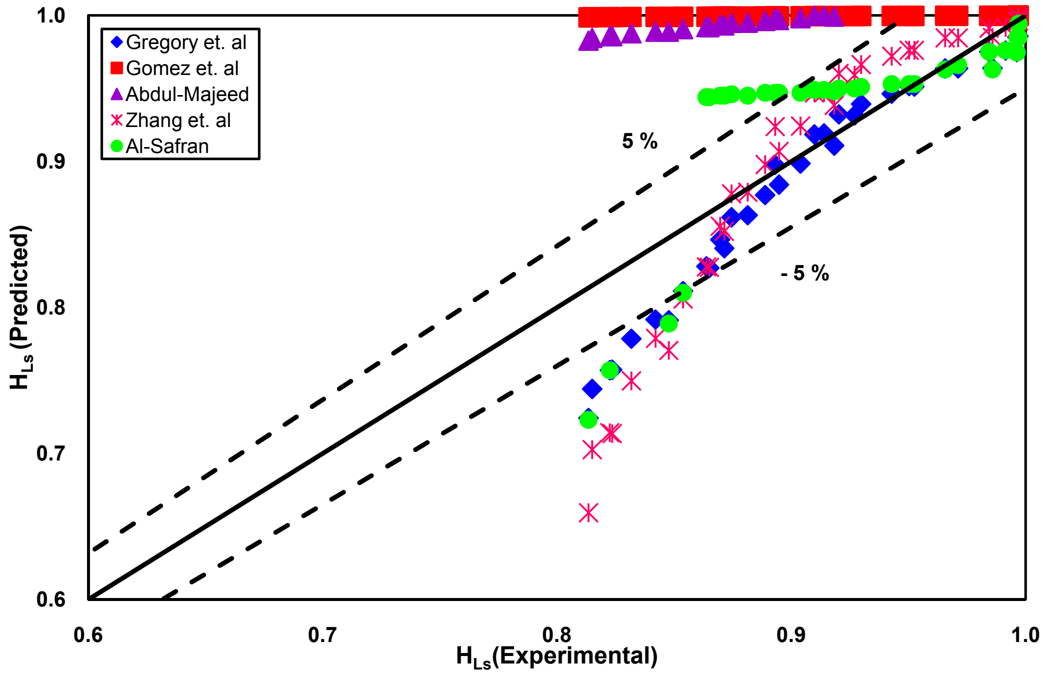

Figure 19: Performance of Correlations and Model against Measured Slug Liquid Holdups for μ_o=0.378 Pa·s

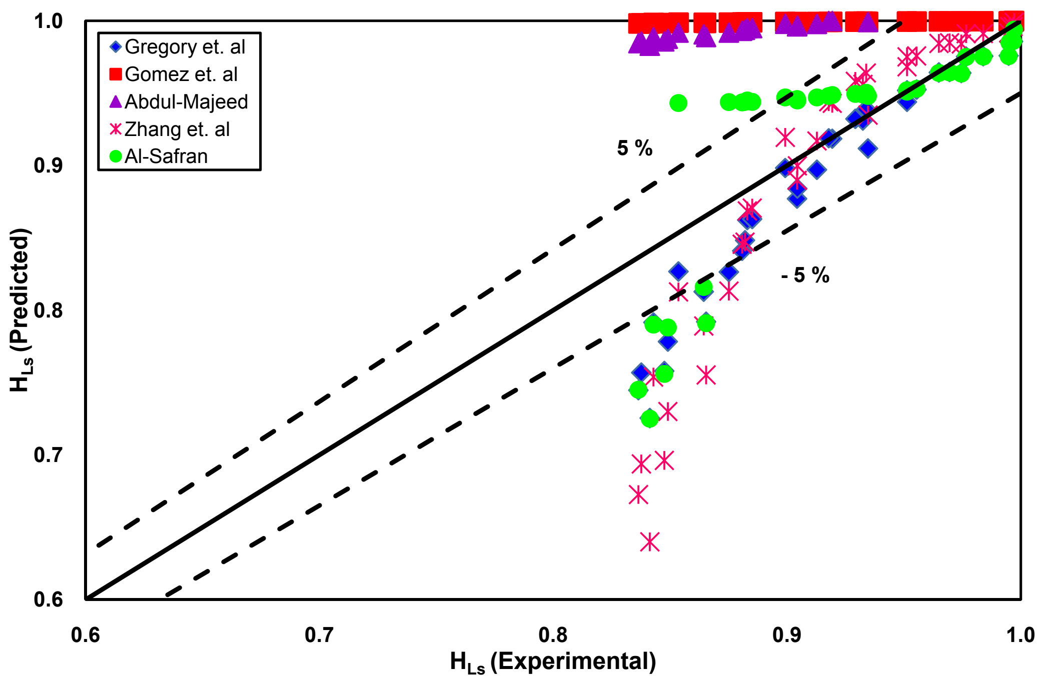

Figure 20: Performance of Correlations and Model against Measured Slug Liquid Holdups for μ_o=0.257 Pa·s

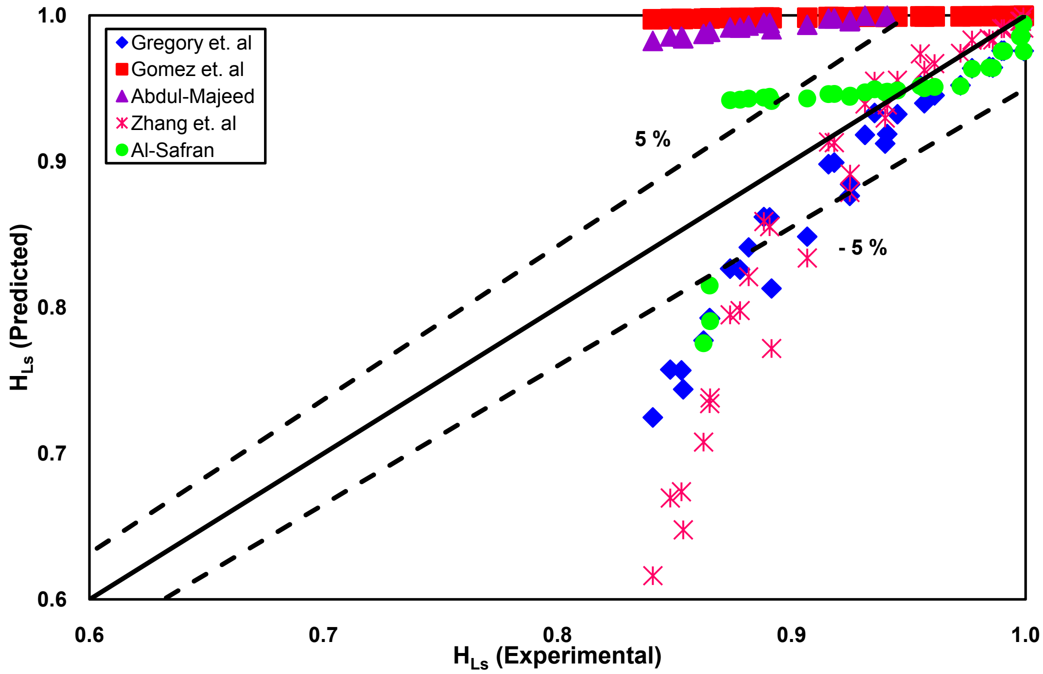

Figure 21: Performance of Correlations and Model against Measured Slug Liquid Holdups for μ_o=0.181 Pa·s

Table 2: Existing Model/Correlation Evaluation against Present Slug Liquid Holdup Data for μo=0.587 Pa·s

Correlation/Model	Statistical Parameters					
	ε_1 (%)	ε_2 (%)	ε_3 (%)	ε_4 (-)	ε_5 (-)	ε_6 (-)
Gregory *et al.*	-3.10	3.12	3.07	-0.03	0.03	0.03
Gomez *et al.*	9.69	9.69	7.00	0.08	0.08	0.06
Abdul-Majeed	9.40	9.40	6.22	0.08	0.08	0.05
Zhang *et al.*	-1.67	3.27	5.10	-0.01	0.03	0.04
Al-Safran	1.24	3.34	4.45	0.01	0.03	0.04

Table 3: Existing Model/Correlation Evaluation against Present Slug Liquid Holdup Data for μ_o=0.378 Pa·s

Correlation/Model	Statistical Parameters					
	ε_1 (%)	ε_2 (%)	ε_3 (%)	ε_4 (-)	ε_5 (-)	ε_6 (-)
Gregory *et al.*	-2.42	2.72	3.15	-0.02	0.02	0.03
Gomez *et al.*	10.46	10.46	7.14	0.09	0.09	0.06
Abdul-Majeed	10.18	10.18	6.38	0.09	0.09	0.05
Zhang *et al.*	-1.72	4.09	5.94	-0.01	0.04	0.05
Al-Safran	1.67	4.26	5.16	0.02	0.04	0.04

Table 4: Existing Model/Correlation Evaluation against Present Slug Liquid Holdup Data for μ_o=0.257 Pa·s

Correlation/Model	Statistical Parameters					
	ε_1 (%)	ε_2 (%)	ε_3 (%)	ε_4 (-)	ε_5 (-)	ε_6 (-)
Gregory *et al.*	-3.12	3.18	3.77	-0.03	0.03	0.03
Gomez *et al.*	9.53	9.53	6.21	0.08	0.08	0.05
Abdul-Majeed	9.29	9.29	5.49	0.08	0.08	0.05
Zhang *et al.*	-3.32	5.02	7.37	-0.03	0.04	0.06
Al-Safran	0.21	4.25	5.72	0.00	0.04	0.05

Table 5: Existing Model/Correlation Evaluation against Present Slug Liquid Holdup Data for μ_o=0.181 Pa·s

Correlation/Model	Statistical Parameters					
	ε_1 (%)	ε_2 (%)	ε_3 (%)	ε_4 (-)	ε_5 (-)	ε_6 (-)
Gregory *et al.*	-4.28	4.28	3.80	-0.04	0.04	0.03
Gomez *et al.*	8.17	8.17	5.94	0.07	0.07	0.05
Abdul-Majeed	7.95	7.95	5.23	0.07	0.07	0.04
Zhang *et al.*	-5.51	5.97	8.26	-0.05	0.05	0.07
Al-Safran	0.54	3.20	4.22	0.00	0.03	0.04

Predictions against Data Points at v_M <2 m/s

In this section, measured slug liquid holdups with mixture velocity less than 2 m/s were compared with predictions of correlations and the model. Tables 6 − 9 show the statistical analysis of the comparisons. Statistical parameters ε_2 and ε_5 indicate that all of the methods perform well for this group of data at all oil viscosities.

The discrepancy between predicted and measured slug liquid holdup values becomes significant above 2 m/s mixture velocity. Tables 10 – 13 denote the increase in ε_2 and ε_5 values for this data set. While Gomez *et al.* (2000) and Abdul-Majeed *et al*. (2000) correlations overestimate the slug liquid holdups, Gregory *et al.* correlation and Zhang *et al.* model underestimate the data. Al-Safran (2009) correlation mostly did not converge for the data points with superficial gas velocity higher than 2.5 m/s. Thus, those data points were not included in the evaluation.

The discrepancy between predicted and measured slug liquid holdup values becomes significant above 2 m/s mixture velocity. Tables 10 – 13 denote the increase in ε_2 and ε_5 values for this data set. While Gomez *et al.* (2000) and Abdul-Majeed *et al*. (2000) correlations overestimate the slug liquid holdups, Gregory *et al.* correlation and Zhang *et al.* model underestimate the data. Al-Safran (2009) correlation mostly did not converge for the data points with superficial gas velocity higher than 2.5 m/s. Thus, those data points were not included in the evaluation.

Table 6: Existing Model/Correlation Evaluation against Present Slug Liquid Holdup Data at v_M < 2 m/s for μ_o=0.587 Pa·s

Correlation/Model	Statistical Parameters					
	ε_1 (%)	ε_2 (%)	ε_3 (%)	ε_4 (-)	ε_5 (-)	ε_6 (-)
Gregory *et al.*	-1.13	1.16	0.79	-0.01	0.01	0.01
Gomez *et al.*	4.62	4.62	3.49	0.04	0.04	0.03
Abdul-Majeed	4.89	4.89	3.19	0.05	0.05	0.03
Zhang *et al.*	1.33	1.33	0.97	0.01	0.01	0.01
Al-Safran	0.57	1.67	2.31	0.00	0.02	0.02

Table 7: Existing Model/Correlation Evaluation against Present Slug Liquid Holdup Data at v_M < 2 m/s for μ_o=0.378 Pa·s

Correlation/Model	Statistical Parameters					
	ε_1 (%)	ε_2 (%)	ε_3 (%)	ε_4 (-)	ε_5 (-)	ε_6 (-)
Gregory *et al.*	-0.37	0.88	1.01	0.00	0.01	0.01
Gomez *et al.*	5.43	5.43	4.13	0.05	0.05	0.04
Abdul-Majeed	5.71	5.71	3.84	0.05	0.05	0.03
Zhang *et al.*	1.94	2.00	1.60	0.02	0.02	0.01
Al-Safran	1.29	2.28	2.66	0.01	0.02	0.02

Table 8: Existing Model/Correlation Evaluation against Present Slug Liquid Holdup Data at vM < 2 m/s for μ_o=0.257 Pa·s

Correlation/Model	Statistical Parameters					
	ε_1 (%)	ε_2 (%)	ε_3 (%)	ε_4 (-)	ε_5 (-)	ε_6 (-)
Gregory *et al.*	-0.65	0.75	0.84	-0.01	0.01	0.01
Gomez *et al.*	5.09	5.09	3.54	0.05	0.05	0.03
Abdul-Majeed	5.39	5.39	3.25	0.05	0.05	0.03
Zhang *et al.*	1.42	1.50	1.21	0.01	0.01	0.01
Al-Safran	0.95	1.65	2.08	0.01	0.02	0.02

Table 9: Existing Model/Correlation Evaluation against Present Slug Liquid Holdup Data at v_M < 2 m/s for μ_o=0.181 Pa·s

Correlation/Model	Statistical Parameters					
	ε_1 (%)	ε_2 (%)	ε_3 (%)	ε_4 (-)	ε_5 (-)	ε_6 (-)
Gregory *et al.*	-1.72	1.72	0.92	-0.02	0.02	0.01
Gomez *et al.*	3.89	3.89	3.10	0.04	0.04	0.03
Abdul-Majeed	4.20	4.20	2.83	0.04	0.04	0.03
Zhang *et al.*	0.05	0.74	1.16	0.00	0.01	0.01
Al-Safran	-0.21	1.51	1.75	0.00	0.01	0.02

Predictions against Data Points at $v_M \geq 2$ m/s

Table 10: Existing Model/Correlation Evaluation against Present Slug Liquid Holdup Data at $v_M \geq 2$ m/s for μ_o=0.587 Pa·s

Correlation/Model	Statistical Parameters					
	ε_1 (%)	ε_2 (%)	ε_3 (%)	ε_4 (-)	ε_5 (-)	ε_6 (-)
Gregory *et al.*	-5.72	5.72	2.78	-0.05	0.05	0.02
Gomez *et al.*	15.91	15.91	3.54	0.14	0.14	0.03
Abdul-Majeed	15.72	15.72	3.00	0.13	0.13	0.02
Zhang *et al.*	-5.86	5.99	5.59	-0.05	0.05	0.05
Al-Safran	1.90	6.33	6.96	0.02	0.05	0.06

Table 11: Existing Model/Correlation Evaluation against Present Slug Liquid Holdup Data at $v_M \geq 2$ m/s for μ_o=0.378 Pa·s

Correlation/Model	Statistical Parameters					
	ε_1 (%)	ε_2 (%)	ε_3 (%)	ε_4 (-)	ε_5 (-)	ε_6 (-)
Gregory *et al.*	-5.29	5.29	2.87	-0.04	0.04	0.02
Gomez *et al.*	17.50	17.50	3.45	0.15	0.15	0.02
Abdul-Majeed	16.44	16.44	2.95	0.14	0.14	0.02
Zhang *et al.*	-6.83	7.02	6.05	-0.06	0.06	0.05
Al-Safran	2.39	8.06	8.22	0.02	0.07	0.07

Table 12: Existing Model/Correlation Evaluation against Present Slug Liquid Holdup Data at $v_M \geq 2$ m/s for μ_o=0.257 Pa·s

Correlation/Model	Statistical Parameters					
	ε_1 (%)	ε_2 (%)	ε_3 (%)	ε_4 (-)	ε_5 (-)	ε_6 (-)
Gregory *et al.*	-6.58	6.58	3.54	-0.06	0.06	0.03
Gomez *et al.*	15.75	15.75	2.77	0.14	0.14	0.02
Abdul-Majeed	14.75	14.75	2.34	0.13	0.13	0.02
Zhang *et al.*	-9.95	9.95	7.29	-0.08	0.08	0.06
Al-Safran	-0.89	8.14	8.77	-0.01	0.07	0.08

Table 13: Existing Model/Correlation Evaluation against Present Slug Liquid Holdup Data at $v_M \geq 2$ m/s for μ_o=0.181 Pa·s

Correlation/Model	Statistical Parameters					
	ε_1 (%)	ε_2 (%)	ε_3 (%)	ε_4 (-)	ε_5 (-)	ε_6 (-)
Gregory *et al.*	-7.85	7.85	3.38	-0.07	0.07	0.03
Gomez *et al.*	14.16	14.16	2.93	0.12	0.12	0.02
Abdul-Majeed	13.21	13.21	2.51	0.12	0.12	0.02
Zhang *et al.*	-13.29	13.29	7.58	-0.11	0.11	0.06
Al-Safran	1.97	6.41	6.76	0.02	0.06	0.06

Discussion

The existing slug liquid holdup methods do not show good agreement with measurements for high viscosity liquids especially above 2 m/s mixture velocity. Laminar flow was mostly observed in the liquid phase for high viscosity oil-gas slug flow. The evaluated correlations were developed based on low viscosity liquids. For these studies, experimental results might be in laminar flow region at low flow rates. Thus, these correlations perform well against the present slug liquid holdups at low velocities. On the other hand, they might observe turbulence flow behavior at high flow rates during their experiments. This might be the reason for the disagreement between predicted and measured values at high mixture velocities.

Previously, Zhang *et al.* slug liquid holdup prediction was based on a turbulent flow assumption. The momentum term in the slug liquid holdup model was modified considering the laminar behavior of high viscosity oil flow. Although after this modification Zhang *et al.* model worked better for high viscosity oil predictions, additional improvements are still needed. Development of a new slug liquid holdup correlation depending on liquid viscosity will help to improve the performance of multiphase flow models.

Correlation Development

Available slug liquid holdup models and correlations do not sufficiently perform for viscous liquids. The comparison results are shown above. Therefore, new empirical correlations were developed to predict slug liquid holdup for high viscosity oil-gas flow in horizontal pipes.

The influence of inertia and viscosity related forces on liquid holdup was congregated with two dimensionless groups. Wallis (1969) defined the dimensionless Froude number for inertia and gravity forces, and viscosity number for viscosity and gravity forces as shown in Eqs. 5 and 6, respectively.

$$N_{F_r} = \frac{v_M}{(gd)^{0.5}}\sqrt{\frac{\rho_L}{\rho_L - \rho_G}} \ . \tag{5}$$

$$N_{\mu} = \frac{v_M \mu_L}{gd^2(\rho_L - \rho_G)} \ . \tag{6}$$

Strong relationship was observed between slug liquid holdup and mixture velocity. This is why mixture velocity is used in both dimensionless equations. The product of Froude number and viscosity number was plotted against slug liquid holdup. The powers of Froude and viscosity number were optimized to get the minimum error between the data points and the equation. All liquid holdup values fall on a line after the optimization as shown in Fig. 22. The powers of viscosity and Froude numbers were determined as 0.2 and 1, respectively.

Two different trends were observed in Fig. 22. Although all data points can be predicted with one equation, two different equations were found more efficient. 2 m/s mixture velocity or 1.5 of $N_{Fr}N_{\mu}^{0.2}$ was designated as the boundary between these two trends. In model evaluation chapter, it was also revealed that Gregory *et al.* (1978) correlation and Zhang *et al.* model (2003) show disagreement with the experimental data after 2 m/s mixture velocity. This discrepancy results from the effect of high oil viscosity on slug liquid holdup. The new correlations are expected to improve predictions of slug liquid holdup for high viscosity oil especially at high mixture velocities. Final forms of the correlations are given as:

For $0.15<N_{Fr}N\mu^{0.2}<1.5$,

$$H_{Ls} = 1.012\, e^{(-0.085\, F_r N_\mu^{0.2})} \ . \tag{7}$$

For $N_{Fr}N\mu^{0.2}\geq1.5$,

$$H_{Ls} = 0.9473\, e^{(-0.041\, F_r N_\mu^{0.2})} \ . \tag{8}$$

For $N_{Fr}N\mu^{0.2}\leq0.15$,

$$H_{Ls} = 1.0$$

The predictions of the new proposed equations were compared with the present data in Fig. 23. More experimental data are required from high viscosity liquid studies to test the performance of the proposed correlations.

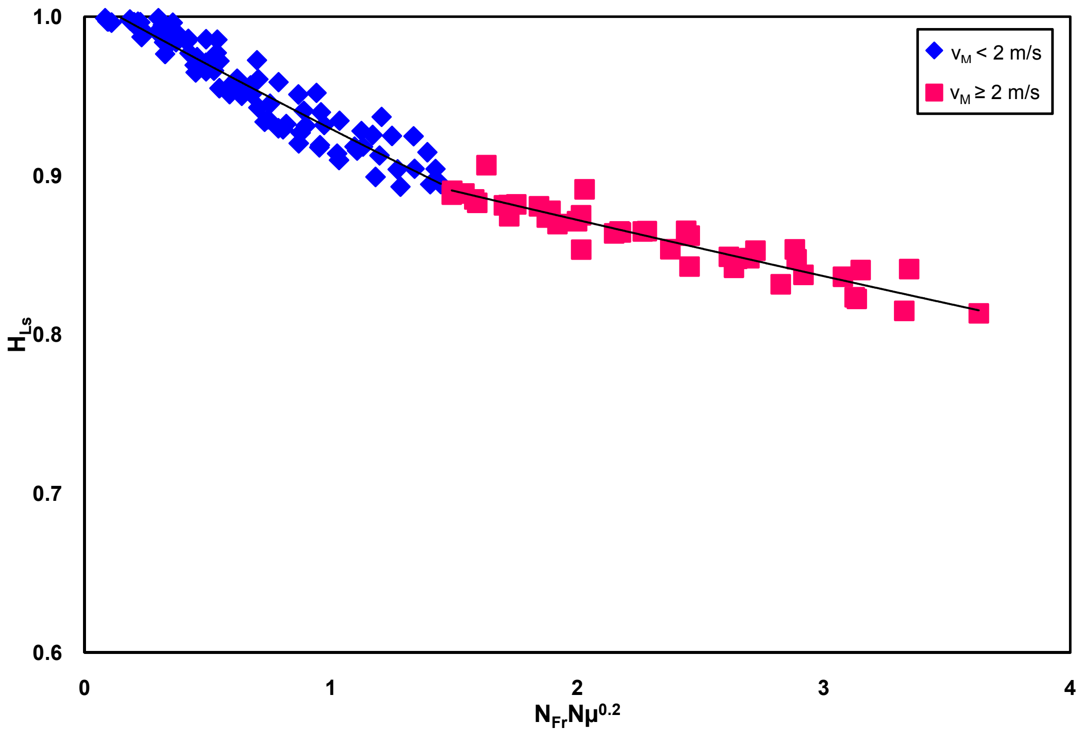

Figure 22: Liquid Holdup vs. Multiplication of Froude Number and Viscosity Number for All Data Points

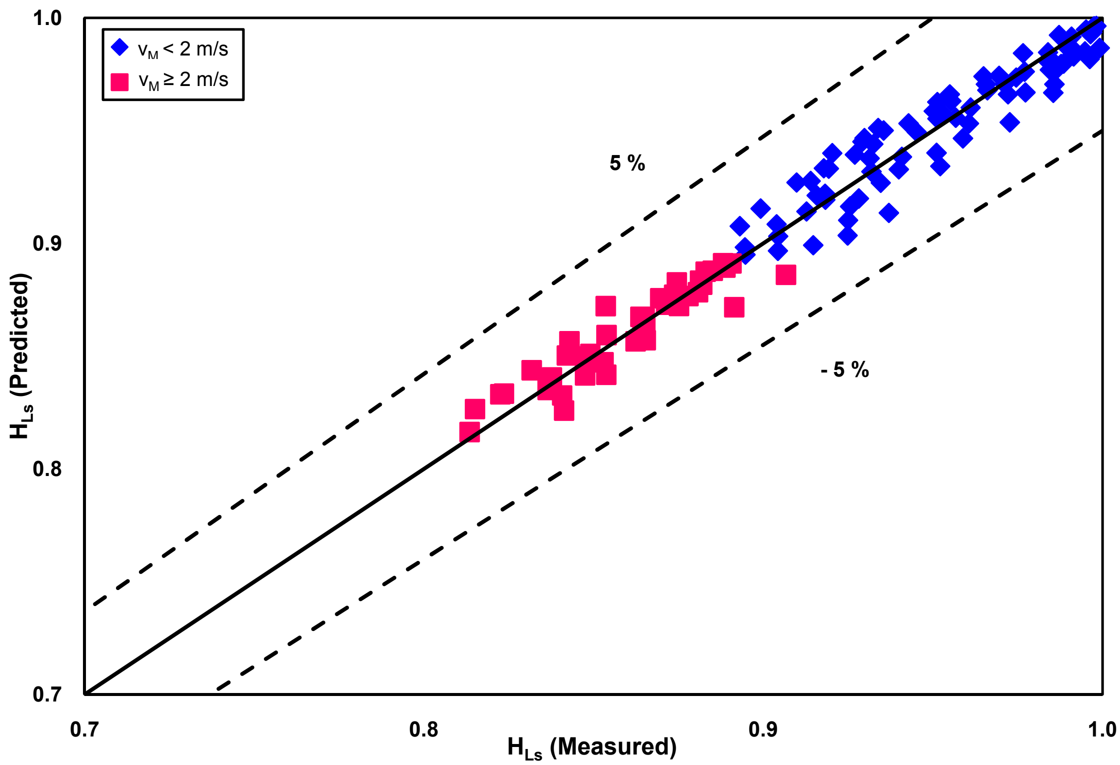

Figure 23: Performance of the Proposed Correlations

Conclusion

- Large and small entrained bubbles in the liquid slug were detected during the analysis of high speed camera videos. Large bubbles were observed at mixture velocities from 0.6 to 3.5 m/s. A decrease in the amount of small entrained bubbles was visually observed with decreasing oil viscosity.
- Slug liquid holdup decreases at all oil viscosities with increasing superficial gas velocity.
- A slight decrease in slug liquid holdup was observed as superficial liquid velocity increases. The decrease results from the high amount of entrained small bubbles in liquid slug at higher superficial liquid velocities.
- No significant change in slug liquid holdup is observed with increasing oil viscosity within 0.587 Pa·s to 0.181 Pa·s oil viscosity range. Nevertheless, slightly high liquid holdups were observed at high mixture velocities for 0.181 Pa·s oil viscosity. This may be due to the result of the decrease in entrained small bubbles at lower oil viscosities.
- The effect of large bubbles on slug liquid holdup was investigated by reevaluating liquid holdup data after omitting the large bubbles in the slug body. Large bubbles were not encountered at v_{SL} = 0.1 m/s. There is no significant change observed in the effect of large bubbles on liquid holdup as oil viscosity increases.
- At high superficial gas velocity conditions, no significant effect of oil viscosity on liquid film height is observed.
- A slight increase in liquid film height was observed with increasing liquid viscosity due to high top oil film drainage within 0.587 Pa·s to 0.181 Pa·s range. However, Nadler and Mewes (1995) stated that they observed significant increase in liquid film holdup for higher liquid viscosities. Their liquid viscosity range was from 0.001 Pa·s to 0.034 Pa·s. This discrepancy shows the importance of the oil viscosity range for the interpretation of the experimental results.
- Gregory *et al.* (1978), Gomez *et al*. (2000), Abdul-Majeed (2000), Al-Safran (2009) correlations and Zhang *et al.* (2003) mechanistic model show good agreement with the measured slug liquid holdup data for mixture velocities lower than 2 m/s. Gregory *et al.* correlation and Zhang *et al.* model give the best predictions at all viscosities. Discrepancy between slug liquid holdup predictions of evaluated methods and present study measurements becomes significant above 2 m/s mixture velocity. Therefore, new correlations as a function of liquid viscosity were developed based on experimental data of the present study.

Recommendations

- A new capacitance sensor was designed and built for this study. Although developed capacitance sensor provides detailed information along the slug, the design of the capacitance sensor can be improved for better results across the cross-sectional area of the pipe.
- More capacitance sensors can be added to the test section in order to investigate the change in phase distribution of high viscosity oil and gas between developing slugs and fully developed slugs through test section.
- High viscosity studies were mostly conducted in horizontal pipes. The effect of pipe inclination needs to be investigated for high viscosity oil and gas two-phase flow.
- Temperature control is the most challenging part of this study. Since the viscosity of Citgo Sentry 220 is adjusted by temperature changes, it is important to have automatic control on heating and cooling system. Moreover, an online viscometer may be installed to the test section for instantaneous viscosity measurements.
- It is recommended to evaluate the proposed correlations against a data bank with different fluid properties and large test matrix.
- Gamma-Ray densitometer can be used to measure slug liquid holdup and liquid film height for high viscosity oil. These results can be compared with capacitance sensor results.
- There always exists a liquid film on top of the pipe during slug flow due to low drainage of high viscosity oil. The effect of

top oil film on slug characteristics needs to be investigated.

Nomenclature

B_R	=	combined uncertainty
b_i	=	elemental systematic uncertainty
CS	=	capacitance sensor
d	=	pipe diameter
df	=	degrees of freedom
e_i	=	actual error
e_j	=	relative error
g	=	gravity acceleration
H_{Ls}	=	liquid holdup in slug body
μ_L	=	liquid viscosity
N	=	number of data points
$N\mu$	=	dimensionless viscosity number
N_{Fr}	=	Froude number
ρ_L	=	liquid density
ρ_G	=	gas density
S_X	=	standard deviation of a population
$S_{\overline{X}}$	=	standard deviation of a population average
t_{95}	=	student's t
U_{95}	=	combined uncertainty with 95% confidence
v_M	=	mixture velocity
$\overline{X}$	=	population average
x_i	=	*i*th element in the population

References

Abdul-Majeed, G.: "Liquid Slug Holdup in Horizontal and Slightly Inclined Two-Phase Slug Flow," Journal of Petroleum Science and Engineering, 27, pp. 27-32 (2000).

Al-Safran, E.: "Prediction of Slug Liquid Holdup in Horizontal Pipes," Journal of Energy Resources Technology, Volume 131, Issue 2 (2009).

Dieck, R. H.: Measurement Uncertainty: Methods and Application, Third Edition, ISA, (2002).

Gregory, G.A., Nicholson, M.K., Aziz, K.: "Correlation of the Liquid Volume Fraction in The Slug for Horizontal Gas-Liquid Slug Flow," Int. J. Multiphase Flow 4, pp. 33-39 (1978).

Gokcal, B.: "Effects of High Oil Viscosity on Two-Phase Oil-Gas Flow Behavior in Horizontal Pipes," Ms Thesis, The University of Tulsa, Tulsa, OK (2005).

Gokcal, B.: "An Experimental and Theoretical Investigation of Slug Flow for High Oil Viscosity in Horizontal Pipes," Ph.D. Dissertation, The University of Tulsa, Tulsa, OK (2008).

Gokcal, B.: "An Experimental and Theoretical Investigation of Slug Flow for High Oil Viscosity in Horizontal Pipes," TUFFP ABM (September 2008a), pp. 47-76 (2008).

Gomez, L.E., Shoham, O., Taitel, Y.: "Prediction of Slug Liquid Holdup: Horizontal to Upward Vertical Flow," Int. J. Multiphase Flow 26, 517–521 (2000).

Nadler, M., and Mewes, D.: "Effects of the Liquid Viscosity on the Phase Distributions in Horizontal Gas-Liquid Slug Flow," Int. J. Multiphase Flow, Vol. 21, No. 2, pp. 253-266 (1995).

Zhang, H.-Q., Wang, Q., Sarica, C., and Brill, J.P.: "Unified Model for Gas-Liquid Pipe Flow via Slug Dynamics - Part 1: Model Development," ASME, J. Energy Res. Tech., Vol. 125 (2003).

Fluid Flow Projects

Executive Summary of Research Activities

Cem Sarica

Droplet Homo-phase Studies

- Significance
  - Better Predictive Tools Lead to Better Design and Practices
- General Objective
  - Development of Closure Relationships
- Past Study
  - Earlier TUFFP Study Showed
    - Entrainment Fraction (FE) is Most Sensitive Closure Parameter in Annular Flow
    - Limited Data, Especially for Inclined Flow Conditions

Droplet Homo-phase Studies …

- Current Study
  - Liquid Entrainment in Annular Two-Phase Flow in Inclined Pipes
  - Objectives
    - Acquire Data for Various Inclination Angles for 3-in. ID Pipe Using Severe Slugging Facility
      - Existing Data are for 1 and 1 ½ in.
    - Develop a New Closure Relationship

Fluid Flow Projects

Advisory Board Meeting, November 3, 2010

Droplet Homo-phase Studies …

- Status
  - Experimental Study is Completed
    - Entrainment Fraction is Found to Vary with Inclination Angle
    - Performance Analysis of the Existing Correlations is Completed
  - A New Closure Relationship Development is Underway

Fluid Flow Projects

Advisory Board Meeting, November 3, 2010

Fluid Flow Projects

Inclination Effects on Wave Characteristics in Annular Gas-Liquid Flows

AbdelSalam Al-Sarkhi

Outline

- Objectives
- Introduction
- Literature Review Summary
- Experimental Facility
- Measurement Techniques
- Experimental Results
- Wave Characterization Results
- Conclusions

Objectives

- Acquire Experimental Data of Wave Characteristics in Two-phase Gas-liquid Annular Flow for Inclination Angles from 0°, to 90° from Horizontal
- Examine the Effect of Pipe Inclination and Diameter on Wave Characteristics in Annular Flow
- Improve Existing or Develop New Models/Correlation If Necessary

Introduction

- Multiphase Flow Mechanistic Models Are Tools in Multiphase Design and Applications
  - Pressure Gradient
  - Liquid Holdup
  - Temperature Gradient
  - Etc.

Introduction

- These Mechanistic Models (e.g. TUFFP Unified Model) Require Closure Relationships
  - Interfacial Friction Factor
  - Droplet Entrainment Fraction
  - Slug Translational Velocity
  - Etc.

Introduction

- Wave Characteristics Information at Different Inclinations is Critically Important in Predicting the Behavior of Annular Flow
  - Fraction of Liquid Entrainment
  - Interfacial Friction Factor
  - Annular Flow Modeling

Literature Review Summary

- Most Studies are Limited to Few Angles and Smaller Pipe
- Annular Flow Is Different for Small Diameter Pipes (Al-sarkhi & Hanratty)
- Drops in Annular Flow are Created from the Wall Film (Geraci *et al.*)
- Drops are not Created from the Entire Liquid Film Interface, But from Disturbance Waves (Geraci *et al.*)

Literature Review Summary…

- Waves are the Source of Drops (Azzopardi & Whalley (1980)
- Liquid is Transported to the Upper Part of the Pipe Against the Force of Gravity by the Disturbance Waves and not by the Secondary Gas Flow or Any Other Mechanisms (Sutharshan *et al.* (1995))
- In Horizontal Flow the Large Disturbance Waves Cover Only Lower Half of the Pipe
- At the Top There are Only Small Amplitude Ripples (Geraci *et al.* (2007b))

Literature Review Summary…

- Increasing the Pipe Inclination From The Horizontal:
  - Decreases the Amplitude of the Disturbance Waves
  - Increases the Fraction of the Pipe Circumference over Which Disturbance Waves Occurs
- At Inclinations Very Close to Vertical, Disturbance Waves are Present around the Entire Section (Geraci *et al.* (2007b))

Literature Review Summary…

- Entrainment Occurs by Breaking Up of Interfacial Disturbance Waves (Woodmansee (1968))
- Onset of Entrainment is Strongly Depends on Wave Celerity and Amplitude (Ishii & Grolmes (1975))
- Entrainment Fraction is Strongly Related to the Waves Taking Place at the Gas-liquid Interface

Experimental Facility

- 3 in. Severe Slugging Flow Loop

Fluid Flow Projects

Advisory Board Meeting, November 3, 2010

Experimental Facility …

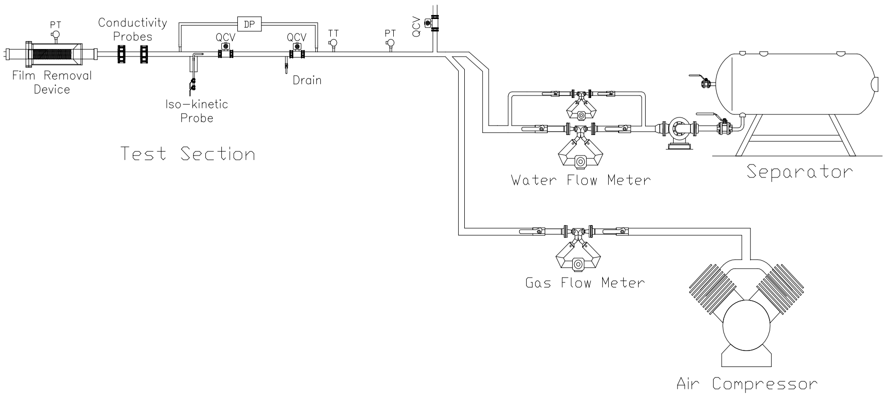

Fluid Flow Projects

Advisory Board Meeting, November 3, 2010

Test Matrix

Group	1					2					3					4				
Case	1	2	3	4	5	6	7	8	9	10	11	12	13	14	15	16	17	18	19	20
V_{SL}, m/s	0.0035	0.0035	0.0035	0.0035	0.0035	0.01	0.01	0.01	0.01	0.01	0.02	0.02	0.02	0.02	0.02	0.04	0.04	0.04	0.04	0.04
V_{SG}, m/s	40	50	60	70	80	40	50	60	70	80	40	50	60	70	80	40	50	60	70	80

- 140 Annular Two-phase Flow Tests
- Inclination Angle For Every Case
  - 0º, 10º, 20º, 45º, 60º, 75º, and 90º from Horizontal

Measurement Techniques

- Conductivity Probe
- Film Removal Device

Conductivity Probe

Conductivity Probe …

- Assembly Configuration

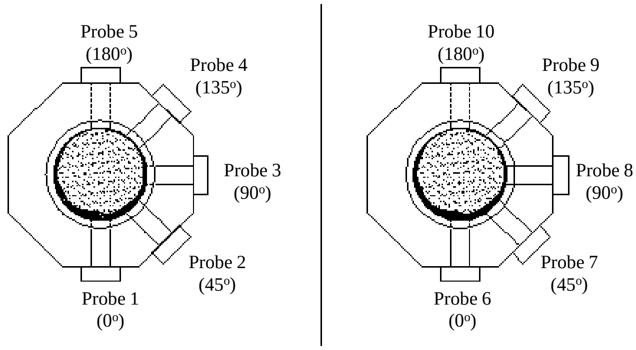

Conductivity Probe …

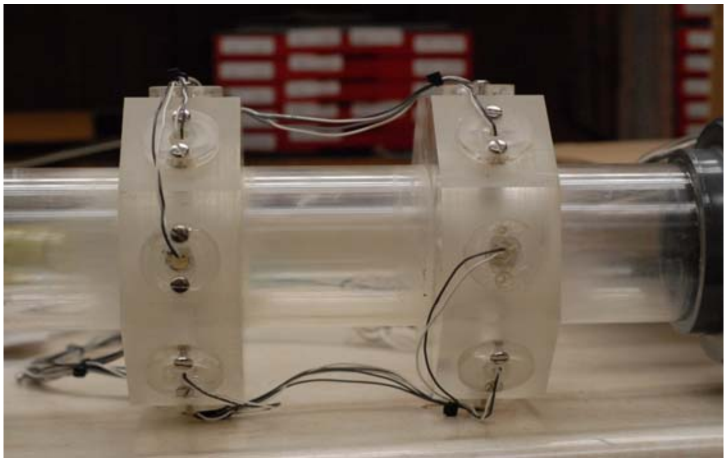

Film Removal Device

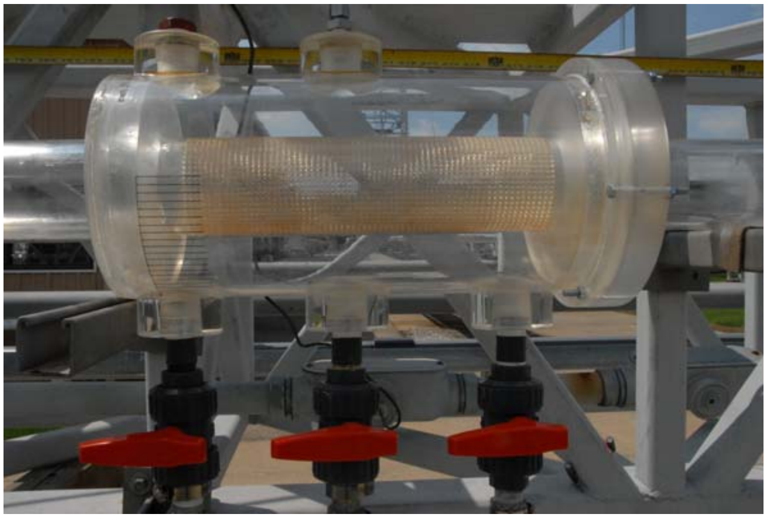

Film Removal Device …

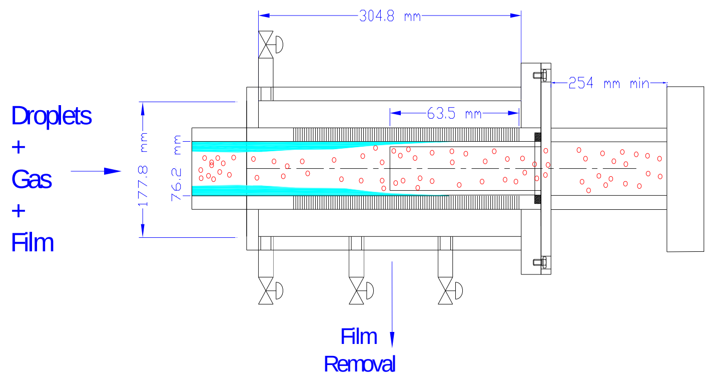

Experimental Results

- Wave Characteristics
  - Celerity
  - Frequency
  - Amplitude
  - Wavelength
- Average Film Thickness
- Entrainment Fraction
  - Film Removal Technique
- Liquid Holdup

Wave Celerity

- Wave Celerity is Calculated Using Cross-correlation Between Two Conductivity Probes
- Time Delay Between Signals is Determined Using Matlab and Confirmed With a Hand Written VBA Program in Microsoft Excel

Fluid Flow Projects

Advisory Board Meeting, November 3, 2010

Wave Frequency

- Wave Frequency is Determined Using a Combination of Power Spectrum Method In MATLAB and Manual Counting of the Waves
- Power Spectrum Gives Predominant Frequency or Range of Frequencies
- Waves are Manually Counted and Compared to the Power Spectrum Value

Fluid Flow Projects

Advisory Board Meeting, November 3, 2010

Wave Amplitude

- Wave Amplitude is Determined by Averaging Wave Heights of a Film Height Time Trace That are Larger Than the Average Film Thickness Plus 2 Standard Deviations

Wave Characterization Results

- Wave Characterization in Annular Flow
  - Wave Celerity, C,
  - Frequency, f,
  - Amplitude, $\Delta h_W(0)$
  - Liquid Film Thickness at the Bottom of the Pipe, $h_L(0)$,
  - Liquid Film Reynolds Number, Re_{LF}
  - Liquid Film Velocity, v_{LF}

Wave Celerity

v_{SL} = 0.0035, v_{Sg} 40→80

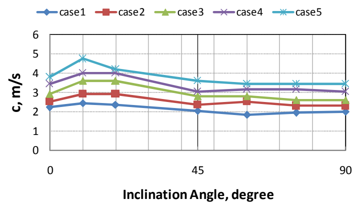

v_{SL} = 0.01, v_{Sg} 40→80

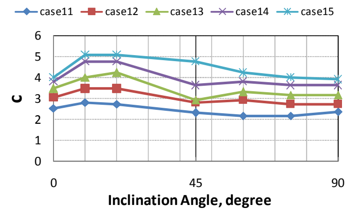

v_{SL} = 0.02, v_{Sg} 40→80

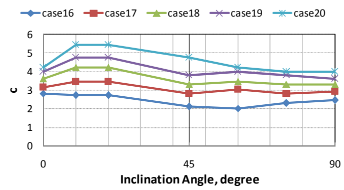

v_{SL} = 0.04, v_{Sg} 40→80

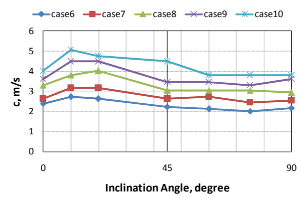

The wave celerity increases with increasing superficial gas and liquid velocities

Wave Celerity

- Wave Celerity is Strongly Dependent on Modified Lockhart-Martinelli Parameter or Froude Number Ratio, *X**

$$X^* = \sqrt{\frac{\rho_G}{\rho_L}\frac{\dot{m}_L}{\dot{m}_G}} = \sqrt{\frac{\rho_L}{\rho_G}}\frac{v_{SL}}{v_{Sg}} = \frac{Fr_{SL}}{Fr_{Sg}}$$

$$Fr_{SL} = \sqrt{\frac{\rho_L v_{SL}^{\;2}}{(\rho_L - \rho_G) g D \cos\theta}} \qquad Fr_{Sg} = \sqrt{\frac{\rho_G v_{Sg}^{\;2}}{(\rho_L - \rho_G) g D \cos\theta}}$$

Normalized Wave Celerity vs. *X** for Different Pipe Inclinations and Diameters, and Liquid Viscosity and Surface Tension

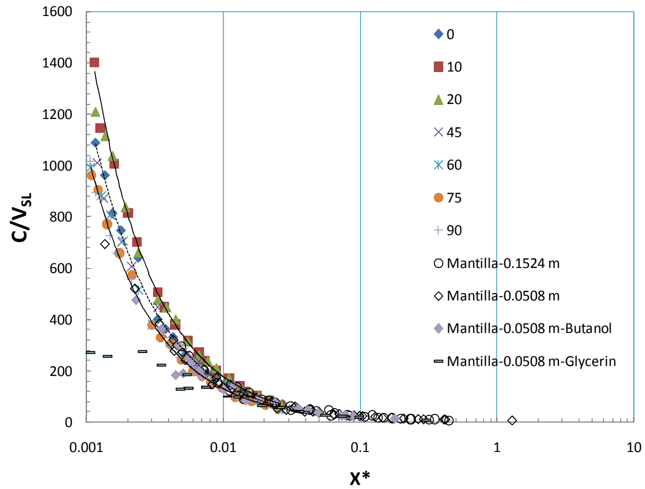

Parameter (Mantilla)	Value
Water	
Density (kg/m^3)	997
Viscosity (Pa-s)	0.00102
Surface tension (N/m)	0.073
Water – 5% Butanol	
Density (kg/m^3)	989
Viscosity (Pa-s)	0.00122
Surface tension (N/m)	0.035
Water – 47% Glycerin – Salt	
Density (kg/m^3)	1130
Viscosity (Pa-s)	0.0071
Surface tension (N/m)	0.061

Wave Celerity Correlations

- **Horizontal**

$$C / v_{SL} = 2.379 X^{*-0.9}$$

- **Inclination Angles of 10° & 20°**

$$C / v_{SL} = 2.323 X^{*-0.94}$$

- **Inclination Angles 45° - 90°**

$$C / v_{SL} = 1.942 X^{*-0.91}$$

Wave Celerity Variation with *X** in Horizontal Pipes

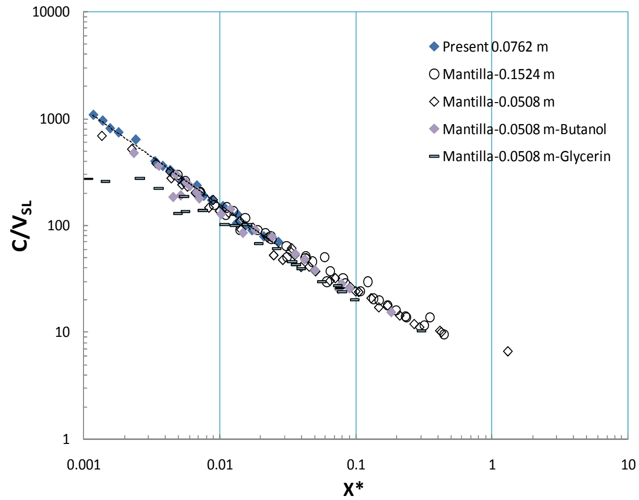

Fluid Flow Projects

Advisory Board Meeting, November 3, 2010

Wave Frequency

v_{SL} = 0.0035, v_{Sg} 40→80

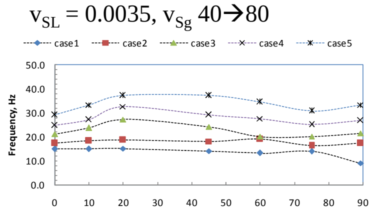

v_{SL} = 0.01, v_{Sg} 40→80

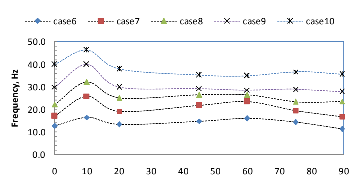

v_{SL} = 0.02, v_{Sg} 40→80

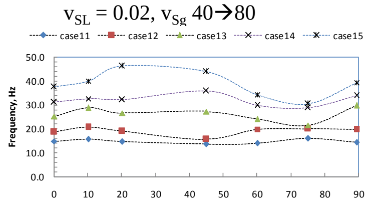

v_{SL} = 0.04, v_{Sg} 40→80

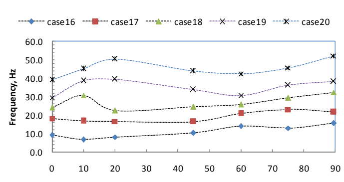

The wave frequency increases with increasing superficial gas and liquid velocities

Fluid Flow Projects

Advisory Board Meeting, November 3, 2010

Strouhal Number, St, (Dimensionless Wave Frequency)

- Proposed by Azzopardi (2006)
- Linear Relation on Log-log Scale

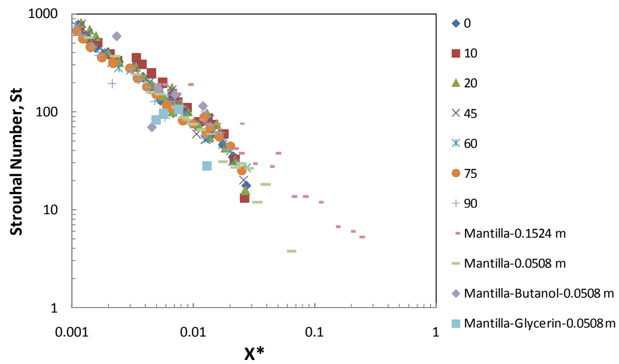

Fluid Flow Projects

Advisory Board Meeting, November 3, 2010

Strouhal Number, St, (Dimensionless Wave Frequency)

- Strouhal Number can Be Correlated Reasonably for All Inclination Angles As

$$St = 1.103 X^{*-0.93}$$

Where

$$St = fD / v_{SL}$$

f is the wave frequency in Hz
D is the pipe diameter
v_{SL} is the superficial liquid velocity

Fluid Flow Projects

Advisory Board Meeting, November 3, 2010

Wave Amplitude

- As v_{Sg} Increases, Wave Amplitude and Average Film Thickness Decreases Owing to More Even Film Distribution Around the Pipe
  - This Decreases the Average Film Thickness at the Bottom of the Pipe, $h_L(0)$, and the Wave Amplitude, $\Delta h_W(0)$

Fluid Flow Projects

Advisory Board Meeting, November 3, 2010

Wave Amplitude with Pipe Inclination Angles

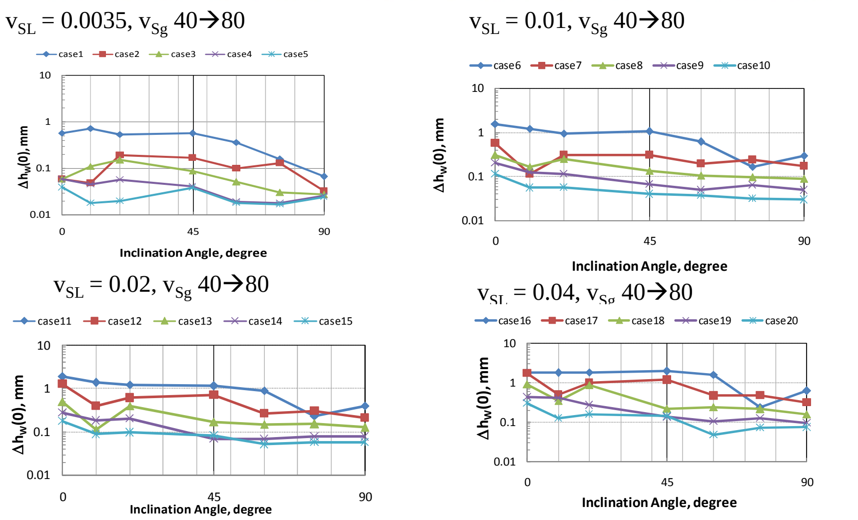

Fluid Flow Projects

Advisory Board Meeting, November 3, 2010

$h_L(0)$ vs. $\Delta h_W(0)$

- Relationship Between Wave Amplitude and Liquid Film Thickness at the Bottom of the Pipe

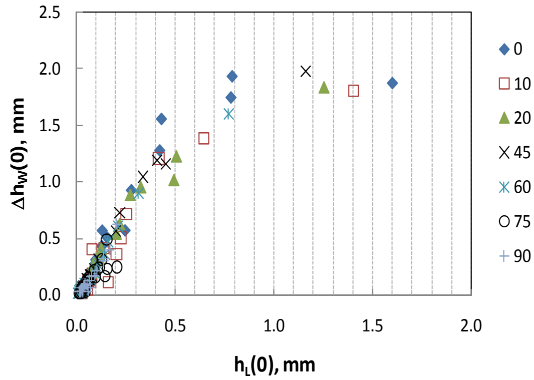

Maximum Value vs. θ

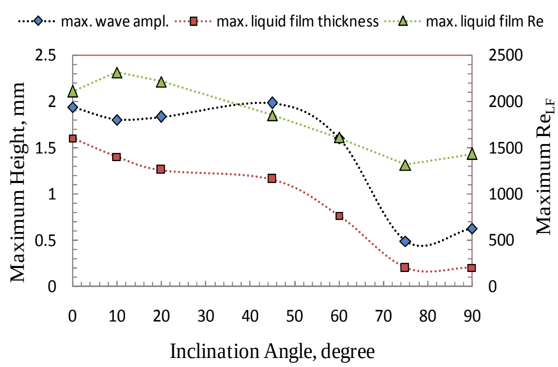

- Maximum Wave Amplitude, Liquid Film Thickness at the Bottom of the Pipe and Maximum Liquid Film Reynolds Number Variation with Pipe Inclination Angle

$h_L(0)$ vs. $\Delta h_W(0)$ Semi-Log Scale

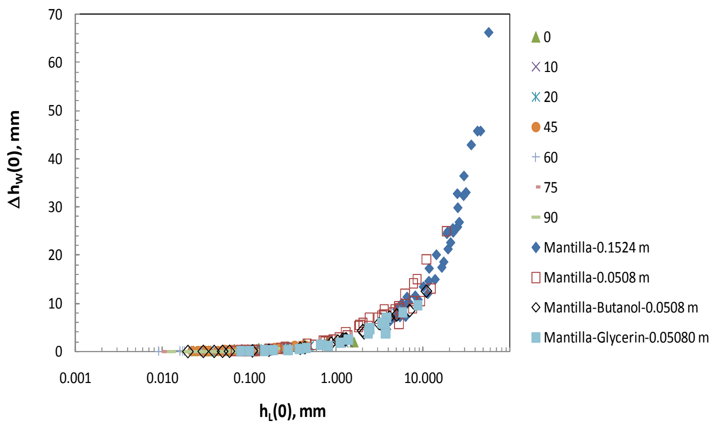

Wave Amplitude Variation with Liquid Film Thickness at the Bottom of the Pipe

$h_L(0)$ vs. $\Delta h_W(0)$ Log-Log Scale

- **Normalized Wave Amplitude Variation with the Normalized Liquid Film Thickness**

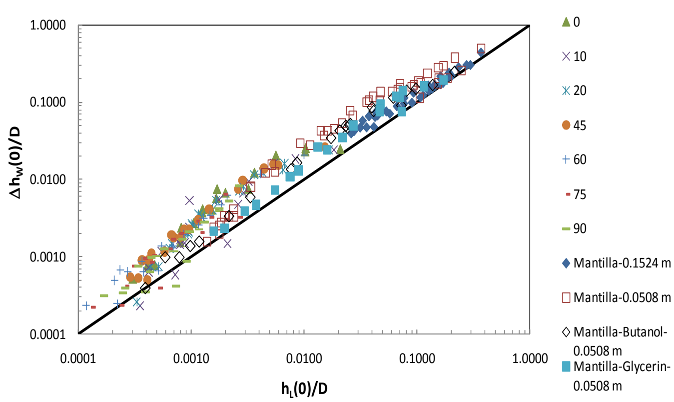

Average Liquid Film Thickness at the Bottom of the Pipe, $h_L(0)$

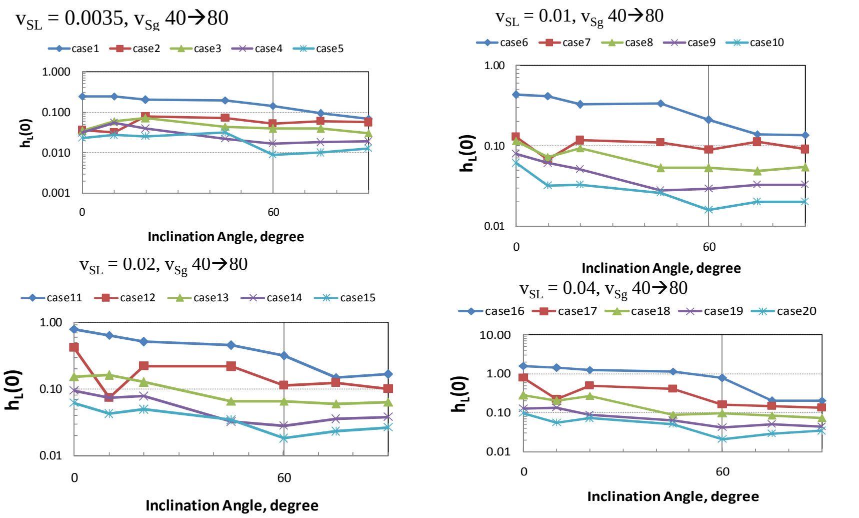

Fluid Flow Projects

Advisory Board Meeting, November 3, 2010

Average Liquid Film Thickness at the Bottom of the Pipe, $h_L(0)$

- $h_L(0)$ Decreases with Increasing Pipe Inclination Angle and with the Gas Velocity
- At Very High Gas Velocity $h_L(0)$ Does not Change Much with Pipe Inclination Especially at High Angle of Inclination (>60°)
- *$h_L(0)$* Increases with Increasing Superficial Liquid Velocity

Fluid Flow Projects

Advisory Board Meeting, November 3, 2010

Liquid Film Reynolds Number, Re_{LF}

- **Liquid Film Reynolds Number, Re_{LF}, is Important in Determination of the Liquid Film Wall Shear Stress and The Interfacial Friction Factor in Annular Flow (Henstock and Hanratty (1976))**

$$\mathrm{Re}_{LF} = \frac{4W_{LF}}{\mu_L \pi D}$$

$$W_{LF} = W_L(1 - F_E) \qquad W_L = \rho_L v_{SL} A_P$$

Where,
W_{LF} is the Liquid film mass flow rate (kg/s).
W_L is the liquid mass flow rate
F_E is the fraction of droplet entrainment ($F_E = (W_L - W_{LF})/W_L$); the liquid density and is the pipe cross sectional area.

Liquid film Reynolds Number Variation with X^* for All Inclination Angles

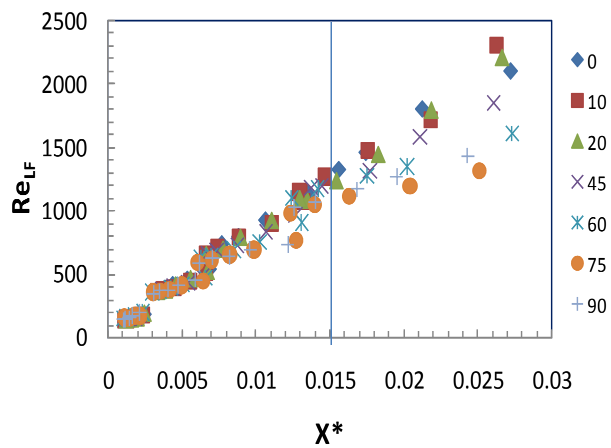

Note Inclination Angle Effect Becomes Apparent after X^*=0.015

Re_{LF} VS. *X** for Angle of Inclinations 0-45°

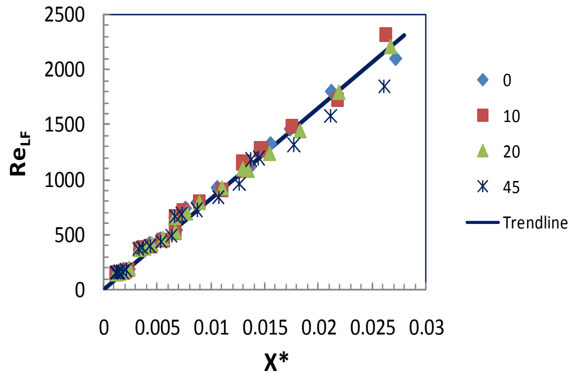

$$Re_{LF} = 82331X*$$

Fluid Flow Projects

Advisory Board Meeting, November 3, 2010

Re_{LF} vs. *X** for Angle of Inclinations 0-45°

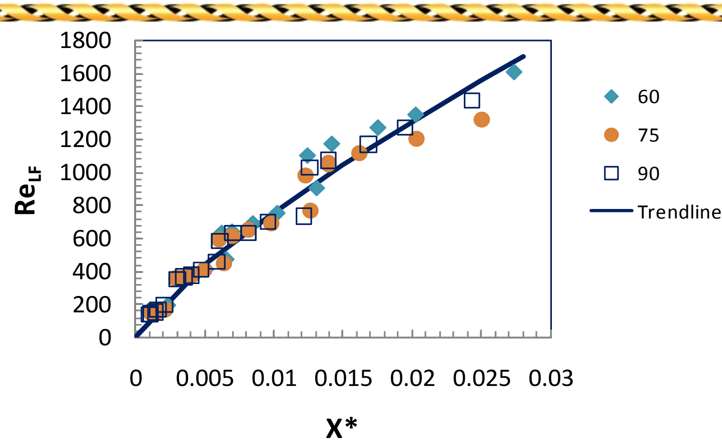

$$Re_{LF} = 28233X*^{0.785}$$

Fluid Flow Projects

Advisory Board Meeting, November 3, 2010

Variation of Re_{LF} With Pipe Inclination Angles

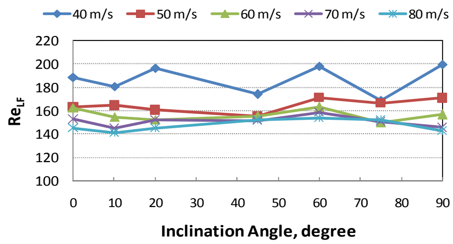

v_{SL}= 0.0035 m/s (Legends are v_{Sg} in m/s)

v_{SL}= 0.02 m/s

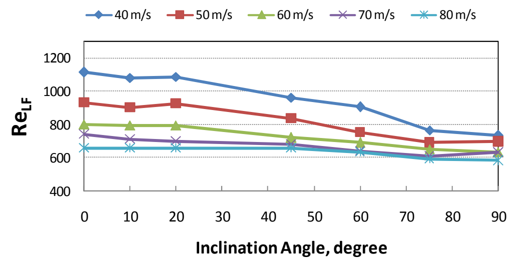

Variation of Re_{LF} With Pipe Inclination Angles

v_{SL}= 0.04 m/s

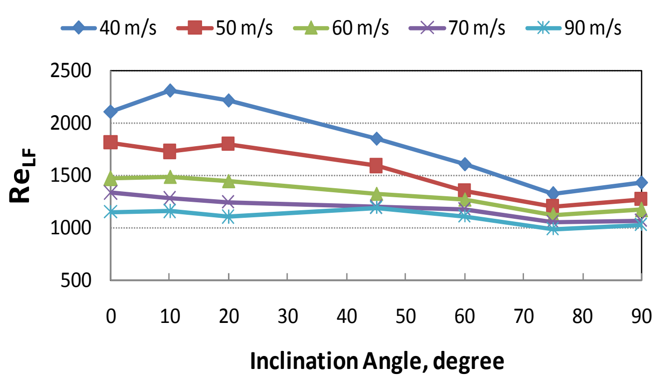

Re_{LF} vs. X^*

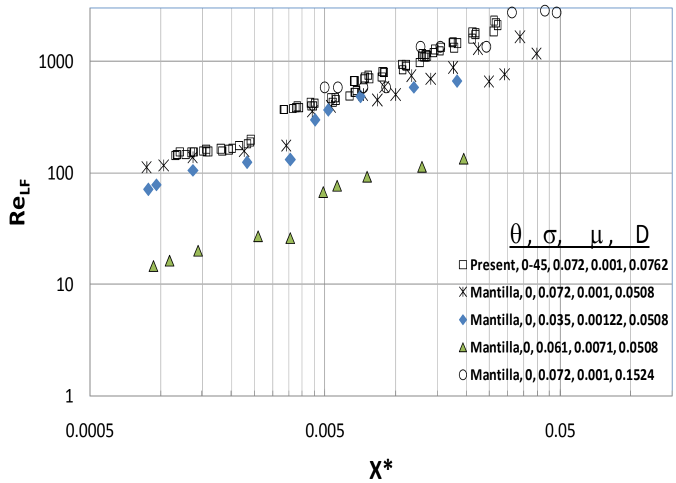

θ, in deg
σ, in N/m,
μ, in Pa-s,
D, in m

Re_{LF} vs. X^*

- Observations
  - Re_{LF} Variation with X^* is Less Sensitive to Pipe Diameter
  - Re_{LF} is Not Sensitive to Surface Tension
  - Re_{Lf} is Very Sensitive to Viscosity of Liquid
    - Low at Higher Liquid Viscosity

Liquid Film Velocity, v_{LF}

Liquid Film Measurement Locations and Distribution of the Unfolded Liquid Film Area

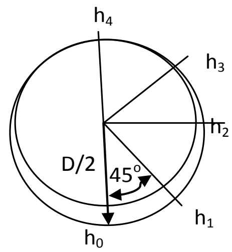

Arc Lengths at Five Locations

$$L_0 = L_1 = L_2 = L_3 = \frac{D}{2}\frac{45\pi}{180}$$

Liquid Film Internal arc Lengths $\quad l_0 \neq l_1 \neq l_2 \neq l_3$

Fluid Flow Projects

Advisory Board Meeting, November 3, 2010

Liquid Film Hydraulic Diameter and Reynolds Number

- **Geometrical Parameters**

$$\alpha_1 = \sin^{-1}\left((h_0 - h_1)/L_1\right) \qquad l_0 = L_0 \cos(\alpha_1)$$

A_0, Area of Trapezoid $\quad A_0 = (h_0 + h_1)/2 \times l_0$

Total Liquid Film Area $\quad A_{LF} = 2 \times (A_0 + A_1 + A_2 + A_3)$

Liquid Film Velocity $\quad v_{LF} = W_{LF} / (\rho_L A_{LF})$

$$D_{h_{LF}} = \frac{4A_{LF}}{\pi D} \qquad \mathrm{Re}_{LF} = \frac{\rho_L V_{LF} D_{h_{LF}}}{\mu_L}$$

Fluid Flow Projects

Advisory Board Meeting, November 3, 2010

v_{LF} Variation with Pipe Inclinations

v_{Sg} = 50 m/s

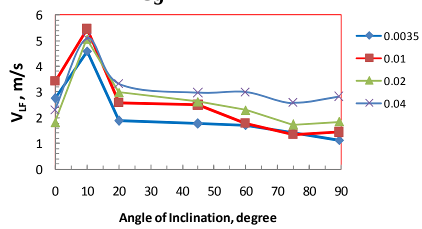

v_{Sg} = 60 m/s

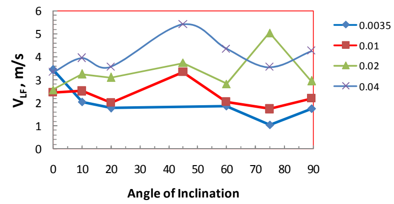

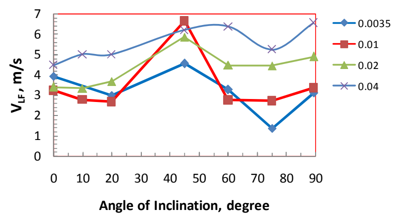

v_{Sg} = 70 m/s (Legends are v_{SL} in m/s)

v_{LF} Variation with Pipe Inclinations

- Liquid Film Velocity is Function of v_{SL}, v_{Sg} and the Pipe Inclination Angle
- v_{LF} Increases with Increasing the v_{SL} and v_{Sg}
- Peak Value for v_{LF} at Certain Angle for Certain Operating Condition
  - Peak Shifts Toward Higher Angles as v_{Sg} Increases

Conclusions

- Wave Characteristics are Very Crucial for Understanding and Modeling of Annular Flow
- Pipe Inclination Effects on Wave Characteristics is Significant
- Wave Amplitude may be Presented As a Function of Liquid Film Thickness at the Bottom of the Pipe for Any Pipe Diameter, Surface Tension and Viscosity
- Wave Amplitude Increases Sharply with Increasing the Liquid Film Thickness at the Bottom of the Pipe

Fluid Flow Projects

Advisory Board Meeting, November 3, 2010

Conclusions…

- Liquid Film Reynolds Number for Horizontal and Low Inclination Angle Cases is Strongly Depending on X^*
- Increasing X^* will Increase Re_{LF}
- Re_{LF}
  - Less Sensitive to the Change in Pipe Diameter and Surface Tension
  - Very Sensitive to the Change in Liquid Viscosity

Fluid Flow Projects

Advisory Board Meeting, November 3, 2010

Conclusions…

- Dimensionless Wave Celerity (C/v_{SL}) is Well Correlated With X^*
- Increasing X^* Will Decrease (C/v_{SL})
- Grouping of Low and High Inclination Angles Was Clearly Noticed on the Plots of (C/v_{SL}) Versus X^*
- Effect of Pipe Diameter and Surface Tension on the Behavior of (C/v_{SL}) vs. X^* was Insignificant
- Effect of Liquid Viscosity was Only Pronounced At Lower Values of X^*

Conclusions…

- Dimensionless Wave Frequency (Strouhal) Number is Well Correlated With X^*
  - Larger the X^* is, Smaller the Strouhal Number is
- Maximum Value of Liquid Film Reynolds Number and Liquid Film Thickness at the Bottom of the Pipe Decreases with Inclination Angle Increase
- Maximum Value of the Wave Amplitude Decreases Sharply With Inclination Angle Increase Only at Higher Inclination Angles (Large Than 45^o)

Questions/Comments

?

Fluid Flow Projects

Advisory Board Meeting, November 3, 2010

Inclination Effects on Wave Characteristics in Annular Gas-Liquid Flows

A. Al-Sarkhi

Abstract
Measurements of wave characteristics have been conducted in a 0.0762 m internal diameter pipe at inclinations of 0^o, 10^o, 20^o, 45^o, 60^o, 75^o, and 90^o from horizontal. Wave celerity, and frequency are very strongly dependent on modified Lockhart-Martinelli parameter, X^*, and the inclination angle. Wave celerity increases as the pipe is inclined upward and reaches a maximum point around the 10° to 20° then decreases until it reaches the minimum and approximately constant value near vertical. Wave amplitude increases with increasing liquid film thickness at the bottom of the pipe. Wave amplitude depends on liquid film thickness for any pipe diameter, surface tension and viscosity. Strouhal Number (dimensionless wave frequency) decreases with increasing X^*. Effect of pipe diameter, surface tension and liquid viscosity on the liquid film Reynolds number, Re_{LF}, was studied. Re_{LF} variation with X^* is not sensitive to the surface tension and less sensitive to the pipe diameter. However, Re_{LF} is very sensitive to the viscosity of the flowing liquid. Liquid film velocity increases with increasing the superficial liquid and gas velocities. A correlation for wave celerity, amplitude and frequency is proposed in this paper.

Introduction

An annular flow pattern can exist at high gas velocities in a pipe. In annular flow, liquid flows in a film along the pipe wall and as droplets entrained in the gas core. There is a liquid mass transfer between the film and the gas core, whereby droplets deposit at the film and are formed by atomization at the film – gas core interface. Due to gravity, the liquid film at the wall is distributed asymmetrically for all configurations except vertical. For air-water systems, the flow in the film is characterized by the intermittent appearance of disturbances, which are a group of large amplitude waves that could be considered as patches of turbulence. The irregular waves are the source of drops that enter the gas phase.

The annular flow pattern is quite different for small diameter pipes (less than 3 cm internal diameter (ID)) and large diameter pipes (larger than 5 cm ID) in that the disturbance waves for small diameter pipes are wrapped around the whole circumference. The pattern resembles what is observed in vertical pipes (Al-sarkhi and Hanratty 2001).

Geraci *et al.* (2007a) explained how the majority of drops in annular flow are created from the wall film by the action of flowing of the gas phase over it. However, drops are not created from the entire liquid film interface, but particularly they arise from disturbance waves.

Azzopardi and Whalley (1980) concluded that waves are the source of drops. This conclusion was proved through the experiment in which injecting small quantities of liquid into a film flow whose flow rate was just below the flow rate for formation of waves, they were able to create waves on demand. These experiments, which employed an axial viewing technique, gave very strong proof that drops are only created when there are waves present.

Sutharshan *et al.* (1995) measured the liquid film velocity in horizontal annular flow in a pipe with 0.0254 m internal diameter. It was concluded that the liquid is transported to the upper part of the tube against the force of gravity by the disturbance waves and not by the secondary gas flow or any other mechanisms.

Geraci *et al.* (2007b) studied the effect of inclination on the disturbance wave characteristics in 38 mm pipe diameter. It was observed that in horizontal flow the film interface is covered by large disturbance waves only over the lower half of the pipe, while at the top there are only small amplitude ripples. With increasing the inclination of the pipe upward from the horizontal, the amplitude of the disturbance waves decreases, but the fraction of the pipe circumference over which disturbance waves occurs increases. At inclinations very close to vertical, disturbance waves are present around the entire section.

The influence of entrained droplets in horizontal annular flows is more complicated than that of the vertical orientation. The wave characteristics and liquid film distribution in horizontal or slightly inclined pipes is different from that in a vertical or highly inclined pipes. The rate of droplet deposition varies with gravitational settling that causes an asymmetric distribution of droplets/film thickness and contributes directly to the local rate of deposition. The influence of gravity on deposition and the asymmetric distribution of drops increase with increasing droplet size and pipe inclination from vertical to the horizontal orientation.

Entrainment occurs by the breaking up of the interfacial waves (Woodmansee (1968)). The description of the wave characteristics, namely, celerity, wavelength, frequency, amplitude are very important for prediction and modeling the droplet entrainment. The onset of entrainment is strongly dependent on the wave celerity and amplitude (Ishii and Grolmes (1975)). Wave modeling deals with the prediction of the conditions at which waves are formed and become unstable. Several studies in the past have been obtained the wave characteristics based on the linear stability analysis (Lighthill and Whitham (1955), Wallis (1969), Andreussi *et al.* (1985), Andritsos (1986), Bruno and McCready (1988), Barnea and Taitel (1993), Uphold (1997)). Several other studies have been attempted with nonlinear analysis and shallow water theory (Hanratty and Hershman (1961), Miya *et al.* (1971), Watson (1989), Pols (1998), Johnson *et al.* (2005)).

The entrainment fraction is strongly related to the waves taking place at the gas-liquid interface. There is a large amount of data and correlations for the prediction of entrainment fraction in literature. However, the entrainment predictions vary significantly with the different correlations resulting in high uncertainties, which affect any calculation and design that include entrainment. The correlations, mostly, do not incorporate wave characteristics, which affect significantly the entrainment fraction (Mantilla 2008). In addition there is a lack of a complete mechanistic model with good confidence level for the prediction of entrainment fraction.

The focus of this study is to examine the effect of pipe inclination and diameter on wave characteristics in annular flows. This information is critically important in predicting the behavior of an annular flow and fraction of entrainment prediction in large diameter pipes.

Experimental Program

Experimental Range

140 annular two-phase flow tests were conducted for inclination angles of 0°, 10°, 20°, 45°, 60°, 75°, and 90° from horizontal. The test matrix conducted in this work is shown in Table 1. For each test, the pressure at the film removal device is held constant using the gate valve at the outlet of the pipe. In addition, both liquid and gas flow rates are held constant for each experimental run. In Table 1, every group has common superficial liquid velocity, v_{SL}; every case has the same superficial liquid and gas velocity and variable inclination angle from 0 to 90 degree.

Table 1: Test Matrix and Cases Studied

Group	1					2					3					4				
Case	1	2	3	4	5	6	7	8	9	10	11	12	13	14	15	16	17	18	19	20
v_{SL}, m/s	0.0035	0.0035	0.0035	0.0035	0.0035	0.01	0.01	0.01	0.01	0.01	0.02	0.02	0.02	0.02	0.02	0.04	0.04	0.04	0.04	0.04
v_{Sg}, m/s	40	50	60	70	80	40	50	60	70	80	40	50	60	70	80	40	50	60	70	80

Experimental Facility

A schematic of the test facility is shown in Fig. 1. The 76.2-mm ID facility is 17.5 m in length and is inclinable from 0^o to 90^o from horizontal. Air and water were used as the working fluids. At standard conditions, the water density, viscosity, and surface tension are 998 kg/m^3, 0.001 Pa·s, and 0.073 N/m. The compressed air was supplied by dry rotary screw and two-stage compressors. Both gas and liquid were metered using Coriolis type mass flow meters. The water is pumped using a progressive cavity pump. Both the air and water are relieved to atmosphere at the outlet of the pipe section to decrease the back pressure of the system and increase air velocities. A 76.2-mm gate valve is located at the outlet to control the back pressure of the system. The test section consisted of three major components: a quick-closing valve section, film removal section, and conductivity probe section.

Film Removal Section

The film removal section is located 13-m (L/d=172) downstream of the inlet. The section consists of a film removal device and film volume tank. The film removal device is used to measure the liquid film flow rate. The device utilizes a long porous section and inserted sleeve to separate the liquid film from the entrained droplets. Figure 2 is a schematic and a picture of the film removal device. The flow passes through the porous section and the liquid film, traveling at a lower velocity than the gas core, is pushed through the porous section. The high inertia of the entrained droplets, flowing close to the gas velocity, prevents them from being removed through the porous section. To ensure no droplets will escape, a long sleeve was inserted close to where the liquid film dissipates. This sleeve is able to move in and out in the pipe to make sure the liquid film passes under the sleeve and only the gas core with droplets passes through the test section. The film volume is collected in a small tank with a capacity of 22 liters. The volume of water from the liquid film and sampling time (10 minutes) is measured to determine the film flow rate. The measurement is repeated three times for each test point to ensure the accuracy of the results.

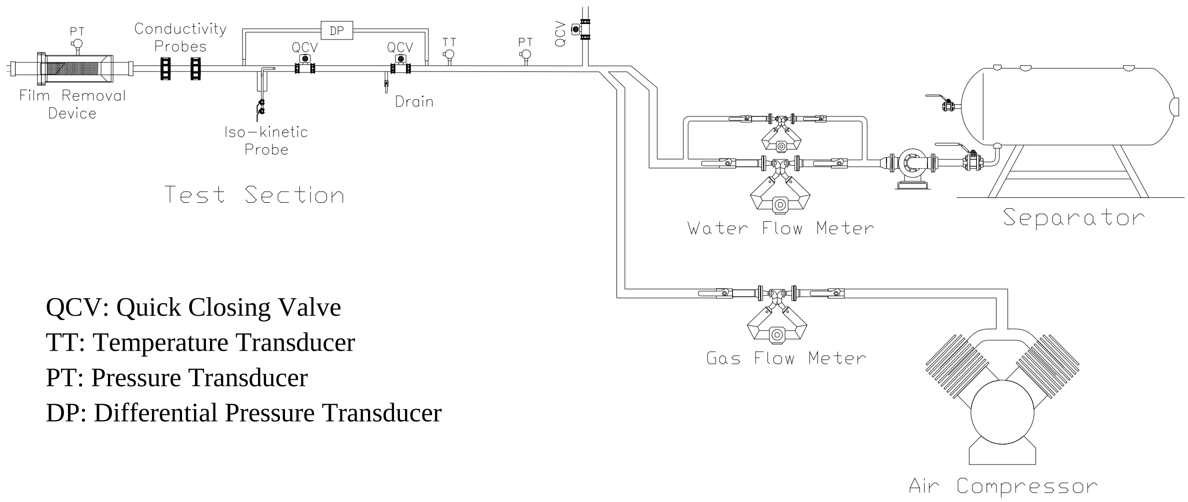

Figure 1: Schematic of the Test Facility

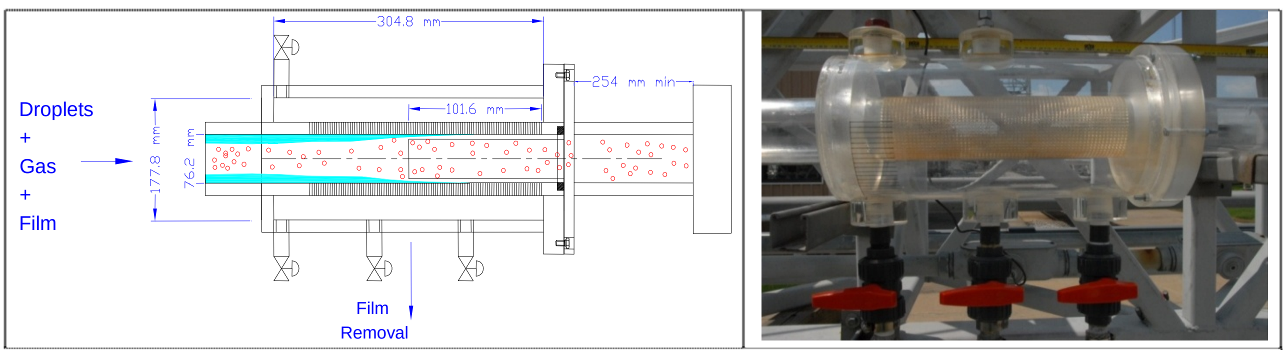

Figure 2: Film Removal Device

Conductivity Probe Section

The conductivity section is utilized to obtain average thickness and wave characteristics of the liquid film. Located 12.5-m (*L/D*=164) from the inlet, the conductivity probe section consists of two probe assemblies, flush mounted conductance probes, and a conductivity meter printed circuit board. To obtain the film height, the conductivity meter board applies a DC voltage across the probes and reads the resulting current between the two plates of the probe. This current is then converted to an analog signal. This signal is then recorded by a handheld Omega AD128 data logger at a rate of 500 Hz.

The conductance section consists of two octagonal shaped probe assemblies spaced 0.15 m apart. Each assembly contains five flush mounted probes installed from the bottom to the top of the pipe, spaced 45^{o} apart. The orientation of the probes in each assemble can be found in Fig. 3.

Flush mounted conductance probes were chosen for this study due to the thin liquid films encountered at the studied flow conditions. Liquid films from 4-mm down to 0.03-mm can be measured with this probe type. The flush mounted probes consist of two parallel plates, 1.59-mm wide and 10-mm long, spaced 1.5-mm apart. Brass is used in the construction of the probes due to its high conductivity and corrosion resistance.

The flush mounted conductance probes are calibrated dynamically to avoid any complications encountered with static calibration. Flow conditions produce a variation of thick to very thin films were selected to develop the calibration curve. A Fowler depth micrometer model Mark IV with an accuracy of 0.002-mm has been used to determine the true height of the liquid film. The micrometer is attached to a conductivity circuit with one lead in the flowing film and the micrometer tip being used as the second lead. For each superficial gas and liquid velocity, the mean film thickness is found using the micrometer, conductivity circuit, and oscilloscope, more details can be found in Magrini (2009).

Wave Measurements

Wave characteristics are recorded simultaneously with the measurement of the liquid film flow rate. Each test is recorded for 40 seconds at a rate of 500 Hz. The conductivity of the fluid is measured during each test using an YSI conductivity meter model 30.

Quick-closing valves are used to measure the liquid holdup. Due to the low volume of liquid holdup for the given slow conditions, a syringe is used to abstract the liquid holdup volume

The film thickness is measured using flush mounted conductivity probes installed from the bottom to the top of the pipe, spaced 45^o apart. The average film thickness is determined by averaging a 40 s time trace for each probe.

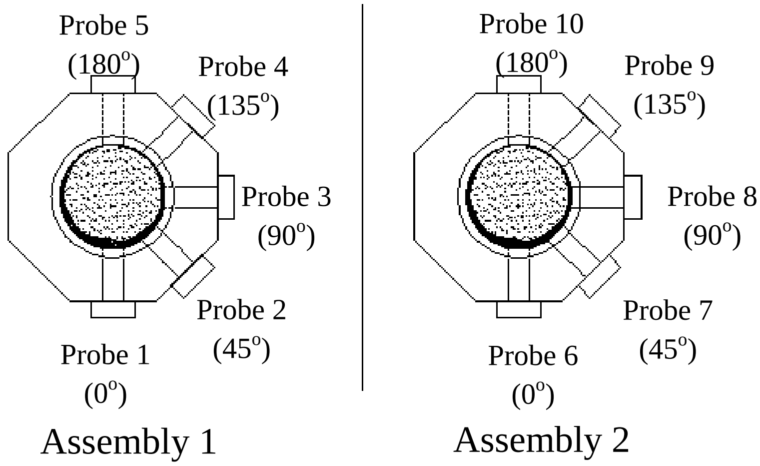

Figure 3: Conductivity Assembly Setup

Wave Celerity

The wave celerity is calculated using the cross-correlation between two conductivity probes spaced a known distance apart. The time delay between signals is determined using MATLAB and confirmed with a hand written VBA program in Microsoft Excel. An example of the cross-correlation calculation can be found in Fig. 4 for flow conditions of v_{SL} = 0.04 m/s and v_{Sg} = 80 m/s at horizontal.

Wave Frequency

The wave frequency is determined using a combination of the power spectrum method in MATLAB and manual counting of the waves. The power spectrum gives the predominant frequency or range of frequencies. The waves are then manually counted and compared to the power spectrum value. For the case of v_{SL} = 0.04 m/s and v_{Sg} = 50 m/s at horizontal, the corresponding power spectrum can be found in Fig. 5 A&B. The time trace of the film height for the same flowing conditions is shown in Fig. 5A. As can be seen in Fig. 5B, the predominant frequency is 18 Hz, which matches the number of waves in the time trace.

Wave Amplitude

The wave amplitude is determined by averaging the wave heights of a film height time trace that are larger than the average film thickness plus 2 standard deviations.

Results and Discussion

Wave characterization in an annular flow will be explained based on wave celerity, C, frequency, f, and amplitude, $\Delta h_W(0)$ and the liquid film thickness at the bottom of the pipe, $h_L(0)$, the liquid film Reynolds number, Re_{LF}, and liquid film velocity, v_{LF}.

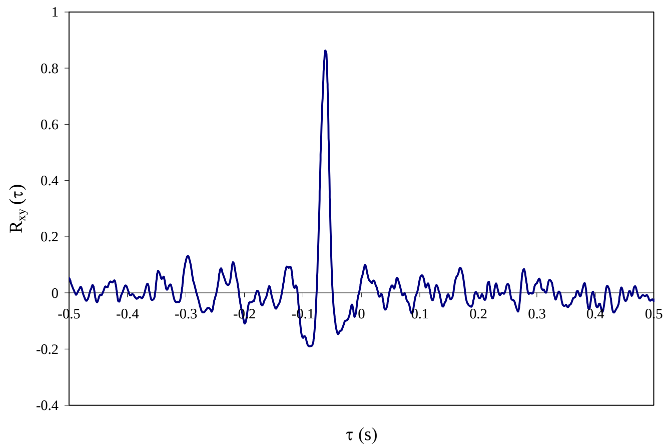

Figure 4: Cross-Correlation Result Example

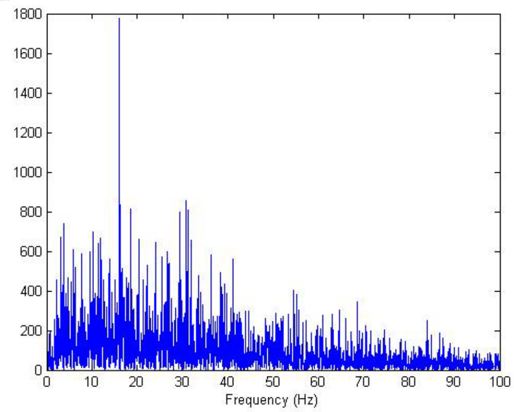

Figure 5A: MATLAB Power Spectrum

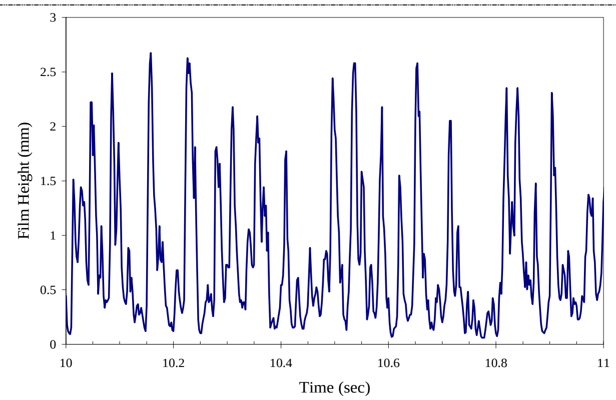

Figure 5B: Liquid Film Height Time Trace

Wave Celerity

Wave celerity, C, is a strong function of the superficial liquid, and gas velocities. The celerity is also dependent on the inclination angle. The wave celerity increases with increasing superficial gas and liquid velocities. As can be seen in Fig. 6, starting from the horizontal case, wave celerity increases as the pipe is inclined. The wave celerity reaches a maximum point between the 10° and 20° inclination angle. After this maximum, the wave celerity will decrease until it reaches the minimum and approximately constant value near vertical. For constant superficial velocities, the variation in the wave celerity is almost negligible between 70° and 90° of pipe inclination, therefore, the effect of pipe inclination on the wave celerity is substantial over the range of inclinations from 10° to 20° in the range of v_{SL} and v_{SG} of this study.

In general wave celerity and entrainment fraction are very strongly dependent on modified Lockhart-Martinelli parameter, X^*, or the Froude number ratio based on the superficial liquid and gas velocities and pipe inclination angle. X^* can be defined as:

$$X^* = \sqrt{\frac{\rho_G}{\rho_L}}\frac{\dot{m}_L}{\dot{m}_G} = \sqrt{\frac{\rho_L}{\rho_G}}\frac{v_{SL}}{v_{Sg}} = \frac{Fr_{SL}}{Fr_{Sg}}$$

$$Fr_{SL} = \sqrt{\frac{\rho_L v_{SL}^{\ 2}}{(\rho_L - \rho_G)gD\cos\theta}}$$

$$Fr_{Sg} = \sqrt{\frac{\rho_G v_{Sg}^{\ 2}}{(\rho_L - \rho_G)gD\cos\theta}} \tag{1}$$

Using X^* for the analysis will combine the superficial velocities and densities ratio of liquid and gas in a single parameter. Figure 7 shows the wave celerity normalized by the superficial liquid velocity plot against the X^*. Increasing X^*, will decrease the C/v_{SL}.

The similarity in the behavior or the grouping of low and high inclination angles can be noticed from Fig. 7. It is clearly seen that from 10° to 20° the celerities are higher than the horizontal and the rest of the inclination angles due to the changes in the wave structure within the range of the operational condition of this study. This behavior motivated us to deal with group of low and high angle of inclinations in the analysis of the characteristics of the waves.

The wave celerity can be correlated with very good accuracy for the horizontal, the inclination angles of 10° and 20°, and the inclination angles 45° and up to 90° cases, respectively, as

$$C / v_{SL} = 2.379 X^{*-0.9}, \quad (2)$$

$$C / v_{SL} = 2.323 X^{*-0.94}, \quad (3)$$

$$C / v_{SL} = 1.942 X^{*-0.91}. \quad (4)$$

Figure 8 shows the comparison for the horizontal case of the present study and Mantilla (2008). These are different results from different laboratories in different pipe diameters at different viscosity and surface tension. The last case in the legends is for Mantilla (2008) for air-water-glycerin-salt has a viscosity of 7 times higher than other cases. Almost all cases follow similar behavior except the high viscosity case at low values of X^*. The fluid properties of the fluids used in Mantilla (2008) are given in Table 2.

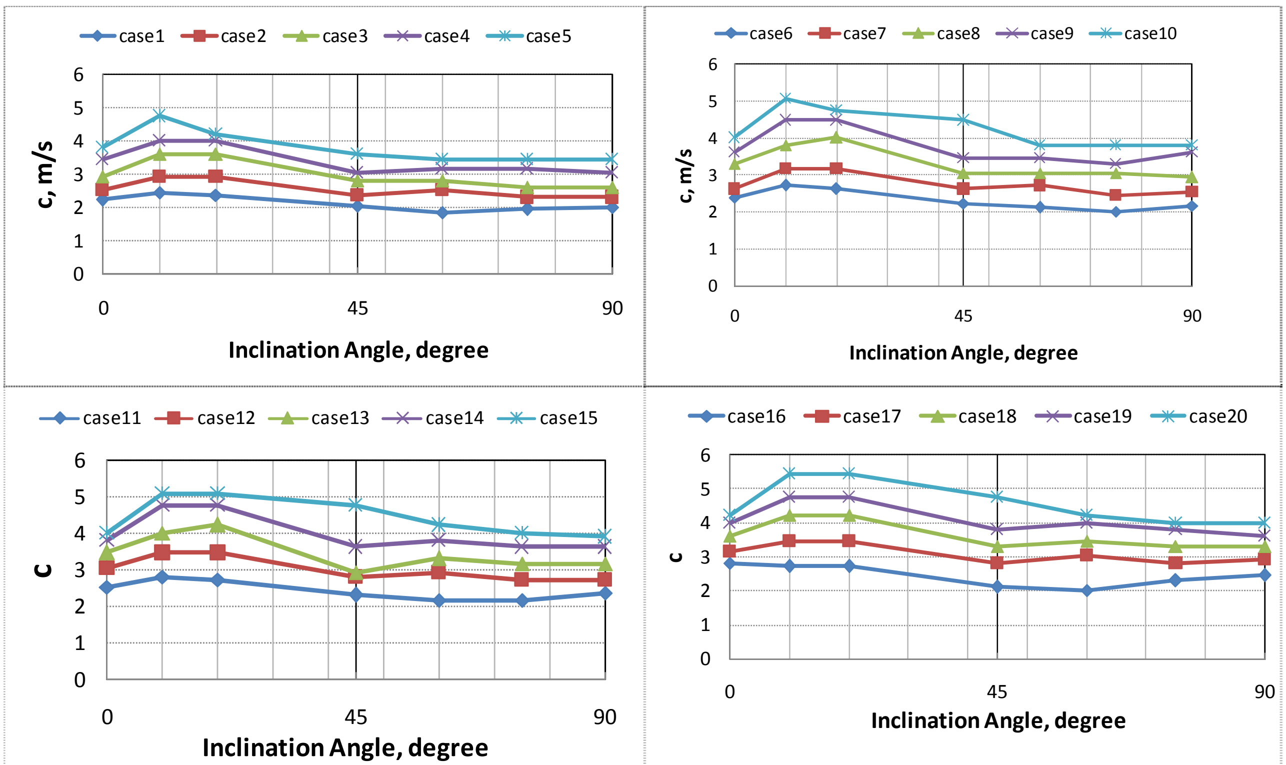

Figure 6: Wave Celerity Variation with Pipe Inclination Angle at Different Gas and Liquid Superficial Velocities (Cases are listed in Table 1, for each figure or group increasing the number of the case means increasing the vSg at same vSL).

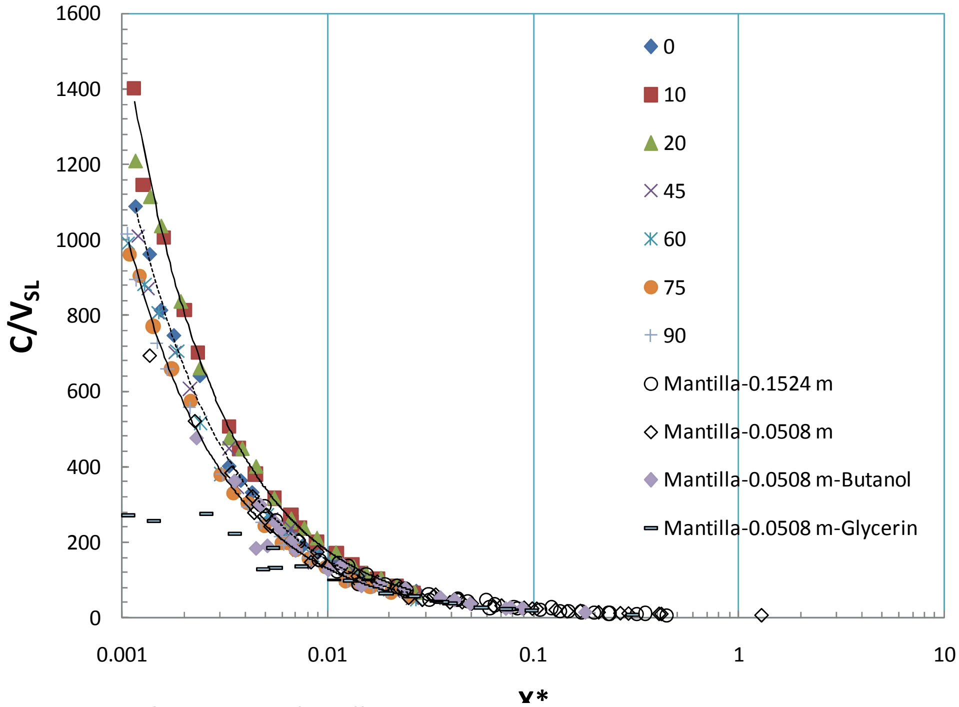

Figure 7: Normalized Wave Celerity vs. X* for Different Pipe Inclinations and Diameters, and Liquid Viscosity and Surface Tension

Table 2: Properties of Fluids Used in Mantilla (2008)

Parameter	Value
Water	
Density (kg/m^3)	997
Viscosity (Pa-s)	0.00102
Surface tension (N/m)	0.073
Water – 5% Butanol	
Density (kg/m^3)	989
Viscosity (Pa-s)	0.00122
Surface tension (N/m)	0.035
Water – 47% Glycerin – Salt	
Density (kg/m^3)	1130
Viscosity (Pa-s)	0.0071
Surface tension (N/m)	0.061

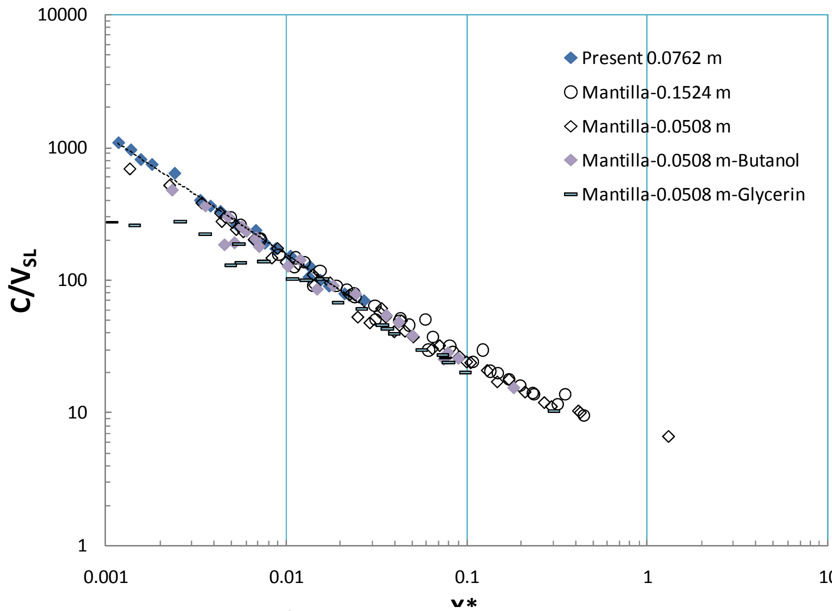

Figure 8: Wave Celerity Variation with X* in Horizontal Pipes

Thus, it can be concluded from the trends of the plots in Fig. 8 that the effect of surface tension on wave celerity (for the range of operational conditions under consideration) could not be noticed. Almost all points follow the same trend. The scattered data points are mainly for air-water-glycerin-salt which has a much higher viscosity.

Wave Frequency

Wave frequency at different pipe inclination angles is shown in Fig. 9. Wave frequency increases with increasing superficial gas velocity. The increase in the superficial liquid velocity results in an increase in the wave frequency. At low v_{SL} (case 1 to 5, v_{SL} = 0.0035m/s) there is a slight increase in the frequency at high v_{Sg} for angles between 10° and 60°. It seems that there is no inclination effect on wave frequency at low v_{Sg}.

A relationship between the Strouhal number (dimensionless wave frequency) and the Lockhart-Martinelli number, X^*, has been proposed by Azzopardi (2006) for disturbance waves. Figure 10 shows all present work data and data from Mantilla (2008). As suggested by Mantilla (2008) for his results only data for v_{Sg} > 20 m/s in the 2-inch pipe and v_{Sg} > 10 m/s in the 0.1524 m pipe were used (annular flow beyond the onset of entrainment) show a linear relationship when plotted on log-log coordinates. Most of the data have similar behavior. The scattered point are mainly for the case of air-water-glycerin-salt of Mantilla's data and points at low inclination angles (0, 10, 20^o) from the present work at X^*=0.026.

There seems to be no inclination effect on the Strouhal number except that the low inclination angles data points start to deviate from the straight line at the highest value of X^* and few points for the case of air-water-glycerin-salt data. The trend of St-X^* curve is in line with the results of Geraci *et al.* (2007b), Fukano *et al.* (1983), Jayanti *et al.* (1990) and Paras and Karabelas (1991).

The Strouhal Number can be correlated reasonably for all inclination angles as

$$St = 1.103 X^{*-0.93} . \quad (5)$$

Where Strouhal Number is defined as $St = fD / v_{SL}$. f is the wave frequency in Hz, D is the pipe diameter and v_{SL} is the superficial liquid velocity.

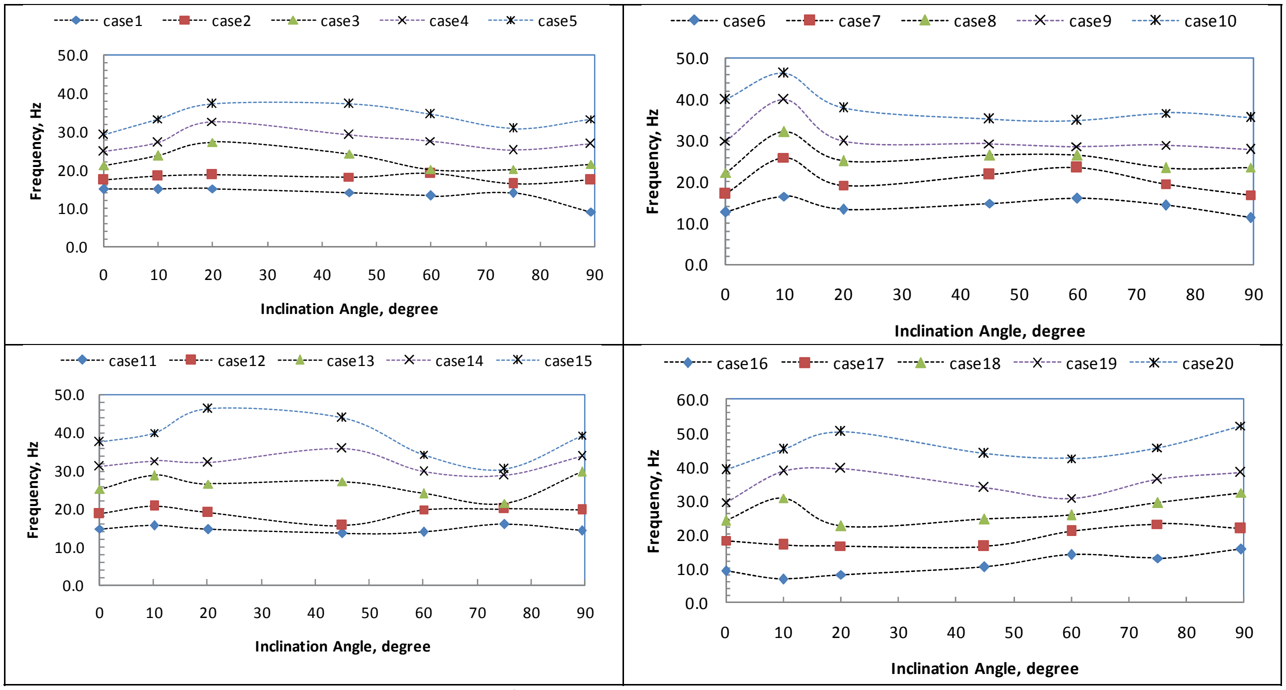

Figure 9: Wave frequency Variation with Inclination Angle

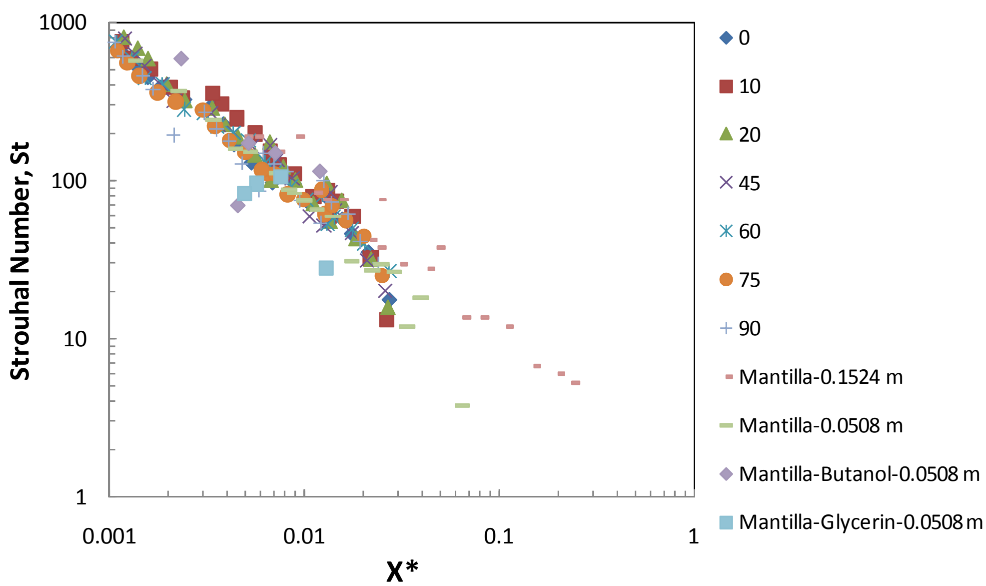

Figure 10: Strouhal Number Variation with X*

Wave Amplitude

Wave amplitude and liquid film thickness are strongly dependent parameters. The wave amplitude and liquid film thickness has an opposite behavior compared to wave celerity with respect to the superficial gas velocity. As superficial gas velocity increases, wave amplitude and average film thickness decreases as the film evenly distributes around the pipe. Similarly, increasing the inclination angle promotes the symmetry of the film, decreasing the average film thickness at the bottom of the pipe, $h_L(0)$, and the wave amplitude, $\Delta h_W(0)$ (see Fig. 11).

Figure 12 shows a very interesting relationship between wave amplitude and the liquid film thickness at the bottom of the pipe. For all operational conditions, the wave amplitude has similar behavior when plotted versus the liquid film thickness at the bottom of the pipe.

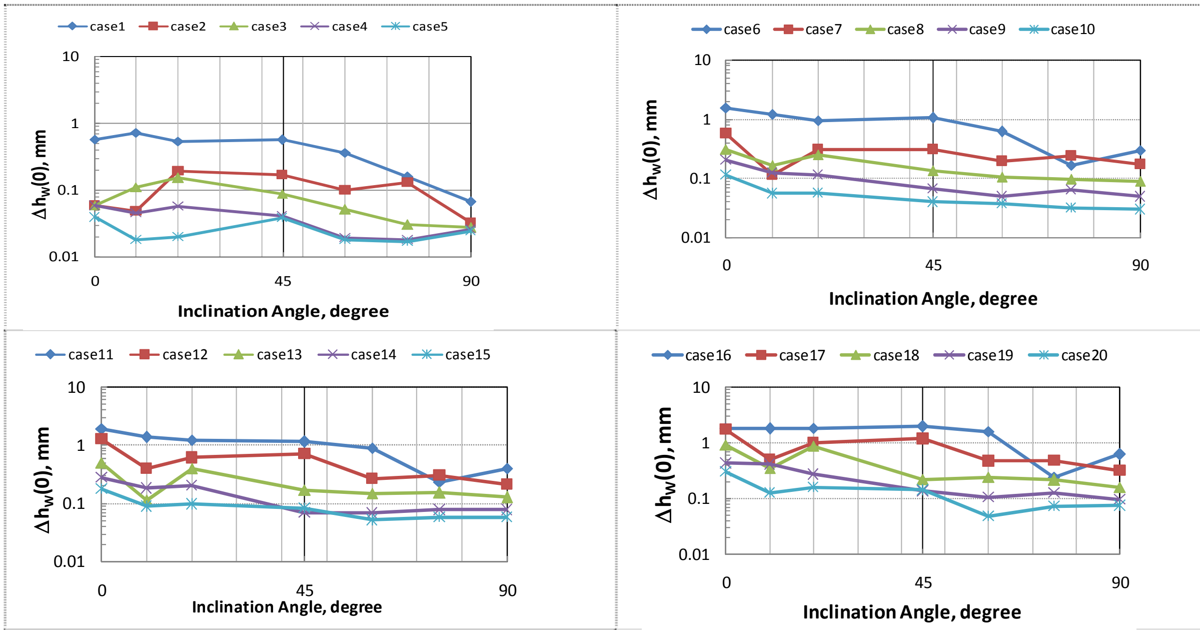

Figure 11: Variation of Wave Amplitude with Pipe Inclination Angles (Cases are shown in Table 1)

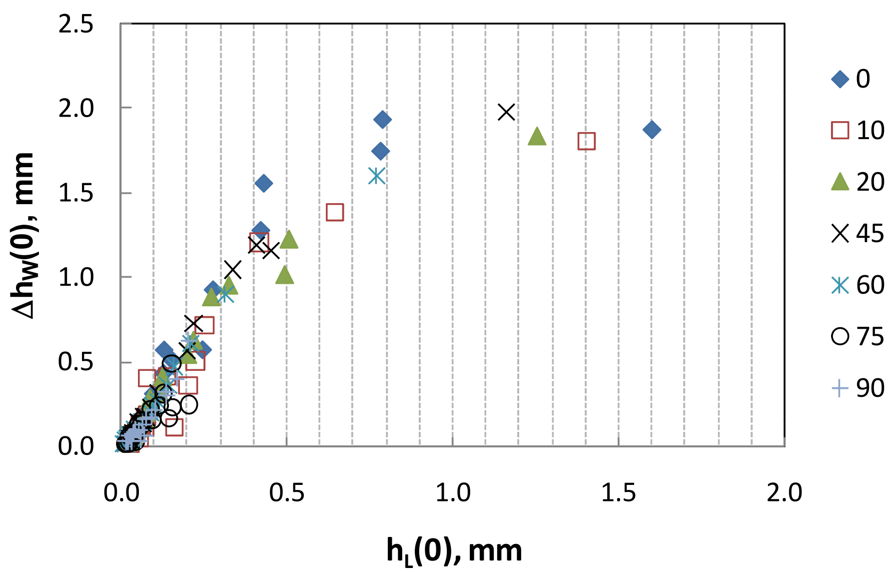

Figure 12: Wave Amplitude as a Function of Liquid Film Thickness at the Bottom of the Pipe for All Operational Conditions.

The inclination effects are clear in which the wave amplitude $\Delta h_w(0)$, for the same range of v_{SL} and v_{SG} could not match the same liquid film thickness at the bottom of the pipe, $h_L(0)$, for all angles of inclination. Wave amplitude and liquid film thickness reaches higher values at lower inclination angles than at higher inclination angles for the same operational conditions. Figure 13 shows the variations in the maximum liquid film thickness and maximum wave amplitude points with the angle of inclinations. On the same figure a plot of liquid film Reynolds number, Re_{LF}, which will be explained later, is also presented. Maximum liquid film thickness, $h_L(0)$, and Reynolds number, Re_{LF}, decreases with increasing the pipe inclination angles. The decrease in the maximum liquid film thickness, $h_L(0)$, and the maximum wave amplitude, $\Delta h_w(0)$, is steeper after 45°. However the maximum value of wave amplitude stays almost constant up to 45° then decreases sharply with increasing the inclination angle.

Figure 14 shows a comparison between the present work data and Mantilla (2008) for air and water in different pipe diameters. All plots shows similar behavior in which the wave amplitude increases with increasing the liquid film thickness at the bottom of the pipe. Figure 15 shows the same data on Fig. 14 but normalized by the pipe diameter and plotted on log-log scale.

As can be seen in Figs 14 and 15, over the studied range of operational conditions, the wave amplitude is mainly function of the film thickness at the bottom of the pipe, regardless of the pipe diameter, and fluid properties. The wave amplitude increases with increasing the average liquid film thickness.

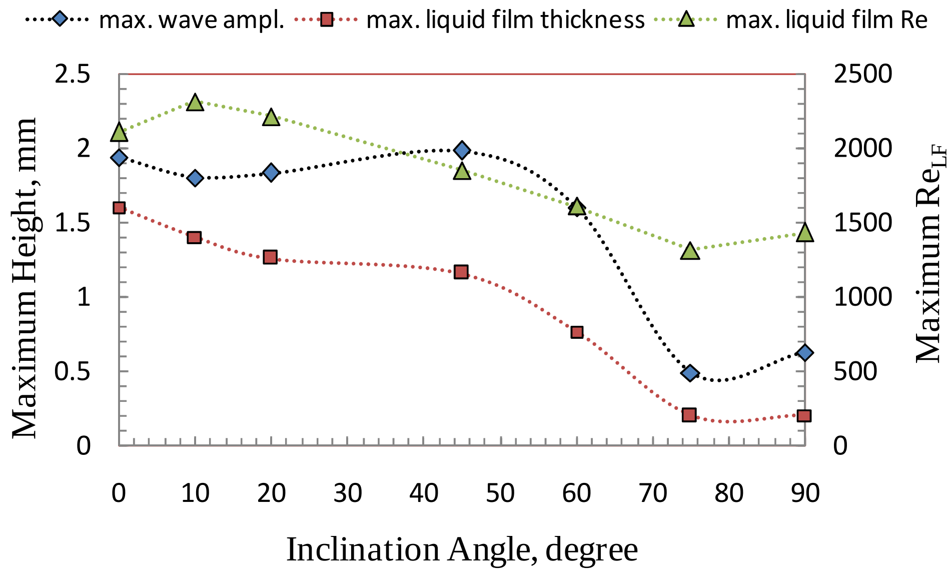

Figure 13: Maximum Wave Amplitude, Liquid Film Thickness at the Bottom of the Pipe and Maximum Liquid Film Reynolds Number Variation with Pipe Inclination Angle

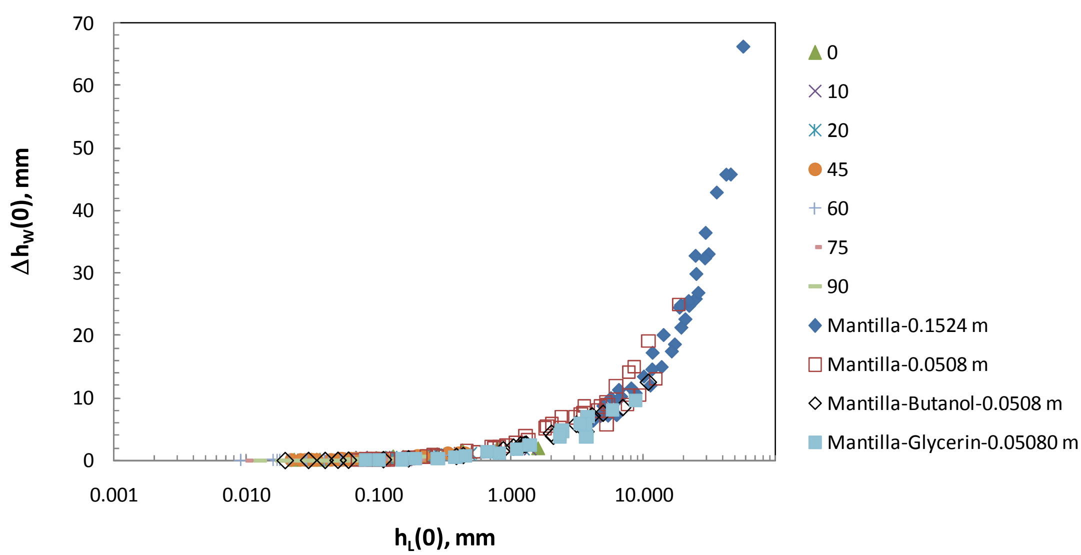

Figure 14: Wave Amplitude Variation with Liquid Film Thickness at the Bottom of the Pipe

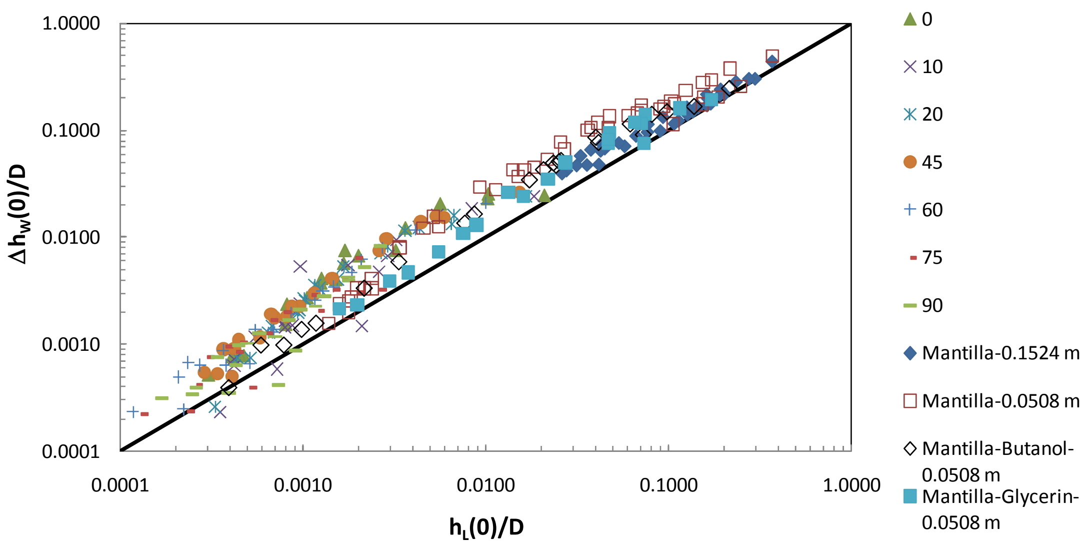

Figure 15: Normalized wave Amplitude Variation with the Normalized Liquid Film

Average Liquid Film Thickness at the Bottom of the Pipe, $h_L(0)$

As shown in Fig. 16, the average liquid film thickness decreases with increasing pipe inclination angles from horizontal and with increasing the gas velocity. At the very high gas velocity the liquid film thickness at the bottom of the pipe does not change much with pipe inclination especially at high angle of inclination (>60°). The average liquid film thickness, $h_L(0)$, increases with increasing superficial liquid velocity.

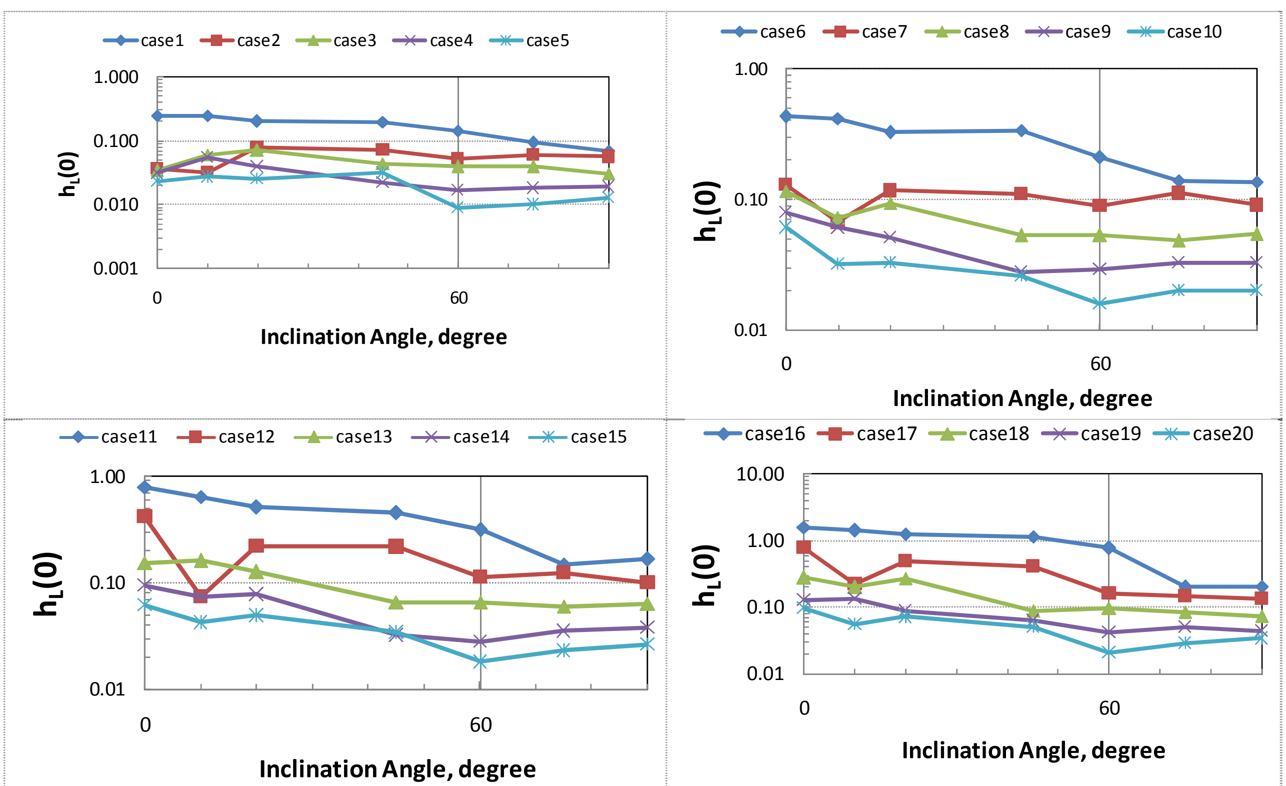

Figure 16: Average Liquid Film Thickness (in mm) at the Bottom of the Pipe Variations with Pipe Inclination Angle (Semi-log Scale)

Liquid Film Reynolds Number, Re_{LF}

Liquid film Reynolds number, Re_{LF}, is very important parameter for determining the liquid film wall shear stress and the interfacial friction factor in an annular flow (Henstock and Hanratty (1976)). Liquid film Reynolds Number can be calculated as in Eq. (6)

$$\mathrm{Re}_{LF} = 4W_{LF} / (\mu_L \pi D) . \tag{6}$$

Where, W_{LF} is the Liquid film mass flow rate (kg/s).

$$W_{LF} = W_L (1 - F_E) . \tag{7}$$

Where, W_L is the liquid mass flow rate ($W_L = \rho_L v_{SL} A_P$); F_E is the fraction of droplet entrainment $(F_E=(W_L\text{-}W_{LF})/W_L)$; ρ_L the liquid density and A_P is the pipe cross sectional area.

The liquid film Reynolds number can be correlated with X^* as shown in Fig. 17. Effects of angle of inclinations appear after 45° in form of a scattered points from a straight line and only when $X^* > 0.015$. The behavior for inclination angles of 0° to 45° is the same for all range of X^* of this study.

Figure 18 shows that the liquid film Reynolds number variation with X^* for angle of inclinations 0-45 follows a straight line. The liquid film Reynolds number for angle of inclinations from 0-45^o can be well correlated by the straight line equation shown below,

$$\mathrm{Re}_{LF} = 82331 X^* . \tag{8}$$

Re_{LF} deviates from the straight line of Eq. (8) for values of X^*> 0.015. However for the angle of inclination angles from 60° to 90° the liquid film Reynolds number variation with X^* which is shown in Fig. 19 can be well correlated by the power trend line of the form

$$\mathrm{Re}_{LF} = 28233 X^{*0.785} \tag{9}$$

Figures 20 - 22 show the variation of Re_{LF} with pipe inclination angles at certain superficial gas and liquid velocities. At low V_{SL} the variation of Re_{LF} is not significant with pipe inclination. However as the v_{SL} increases the effect of pipe inclination on the Re_{LF} is pronounced specially at low superficial gas velocities. At the highest v_{Sg}, the effect of pipe inclination on Re_{LF} is not very significant.

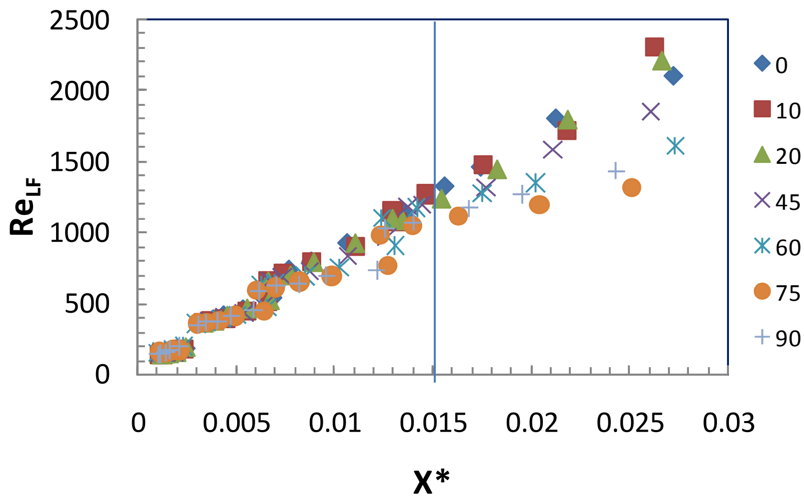

Figure 17: Liquid film Reynolds Number Variation with X* for All Inclination Angles (Note Inclination Angle Effect Becomes Apparent after X*=0.015)

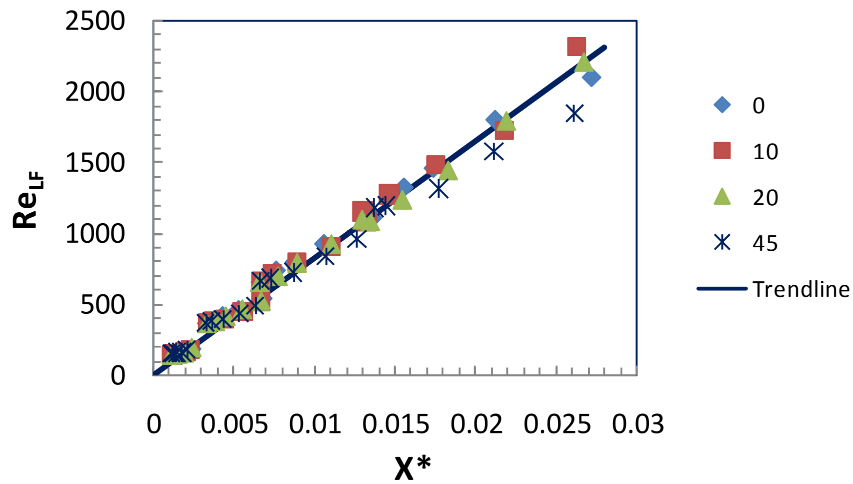

Figure 18: Liquid film Reynolds Number Variation with X* for Angle of Inclinations 0-45°

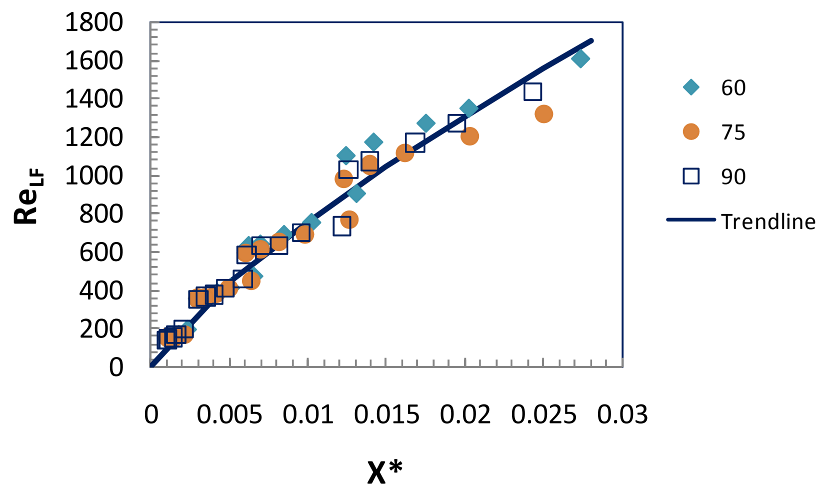

Figure 19: Liquid Film Reynolds Number Variation with X* for Angle of Inclinations 60°-90°

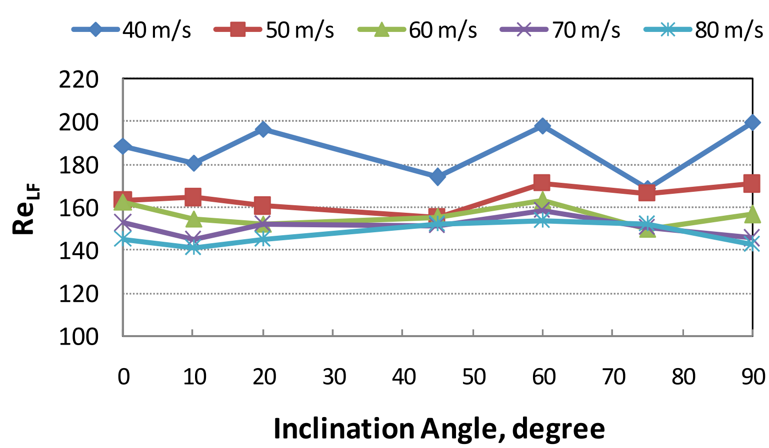

Figure 20: Liquid film Reynolds Number Variation with Pipe Inclination at vSL= 0.0035 m/s (Legends are vSg in m/s)

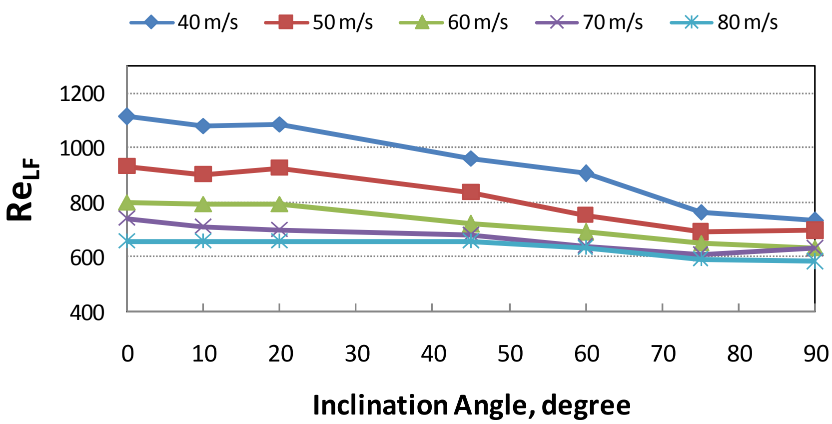

Figure 21: Liquid Film Reynolds Number Variation with Pipe Inclination at vSL= 0.02 m/s (Legends are vSg in m/s)

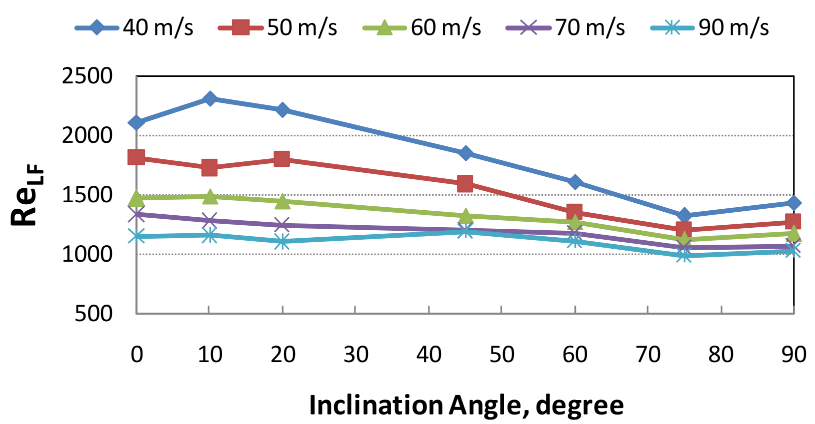

Figure 22: Liquid Film Reynolds Number Variation with Pipe Inclination at vSL= 0.04 m/s (Legends are vSg in m/s)

Figures 23 shows very interesting behavior of Re_{LF} variation with X^*. Re_{LF} variation with X^* is less sensitive to the pipe diameter. Re_{LF} is not sensitive to the surface tension. However, Re_{Lf} is very sensitive to the viscosity of the flowing liquid. The Re_{LF} is low at higher liquid viscosity.

Liquid Film Velocity, v_{LF}

Liquid film area was calculated from the measurement of the liquid film height at five locations (0, 45, 90 and 180 degrees from the bottom of the pipe) as shown in Fig. 24. The half of the film can be unfolded to form a trapezoidal shape as shown in the Fig. 24 below;

The arc length between the five measured locations is L_0, L_1, L_2, L_3 are equals and can be calculated from

$$L_0 = L_1 = L_2 = L_3 = (D/2)(45\pi/180)\,. \tag{10}$$

However, the liquid film internal side arc lengths are not necessarily equals ($l_0 \neq l_1 \neq l_2 \neq l_3$) since the inner side is not absolutely circle, Thus

$$\alpha_1 = \sin^{-1}\left((h_0 - h_1)/L_1\right). \tag{11}$$

$$l_0 = L_0 \cos(\alpha_1)\,. \tag{12}$$

Then, A_0 is the area of the trapezoid can be calculated as

$$A_0 = (h_0 + h_1)/2 \times l_0\,. \tag{13}$$

Similarly, A_1, A_2, and A_3 are obtained.

Thus, the total liquid film area will be $A_{LF} = 2\times(A_0 + A_1 + A_2 + A_3)$ and the liquid film velocity will be $V_{LF} = W_{LF}/(\rho_L A_{LF})$, The hydraulic diameter of the liquid film and Reynolds number can be calculated as

$$D_{h_{LF}} = 4A_{LF}/(\pi D)\,;\quad \mathrm{Re}_{LF} = \rho_L v_{LF} D_{h_{LF}}/\mu_L \tag{14}$$

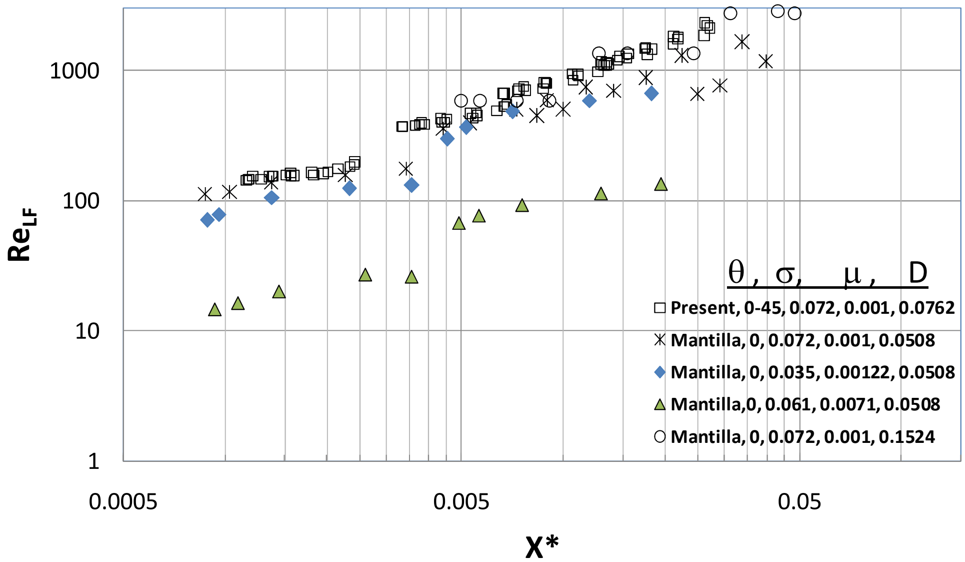

Figure 23: Variation of Liquid Film Reynolds Number with X* in Different Pipes, with Surface Tension and Viscosity. (In the legend; inclination angle, θ, in degree; surface tension, σ, in N/m, dynamic viscosity, μ, in Pa-s, and Pipe diameter, D, in m respectively).

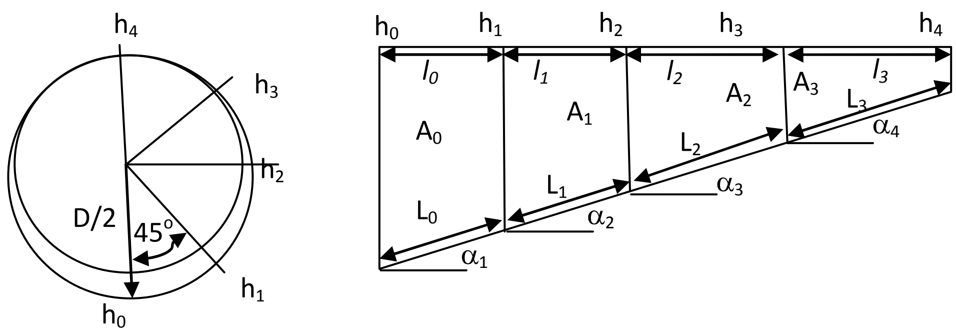

Figure 24: Liquid Film Measurement Locations and Distribution of the Unfolded Liquid Film Area

Plots of v_{LF} variation with pipe inclinations are illustrated in Figs. 25-27. Liquid Film velocity is function of the superficial liquid and gas velocities and the pipe inclination angle. v_{LF} increases with increasing the v_{SL} and v_{Sg}. The plots of the v_{LF} versus the inclination angle show a peak value for v_{LF} at certain angle for certain condition. This peak is shifted toward the higher angles as the superficial gas velocity increases.

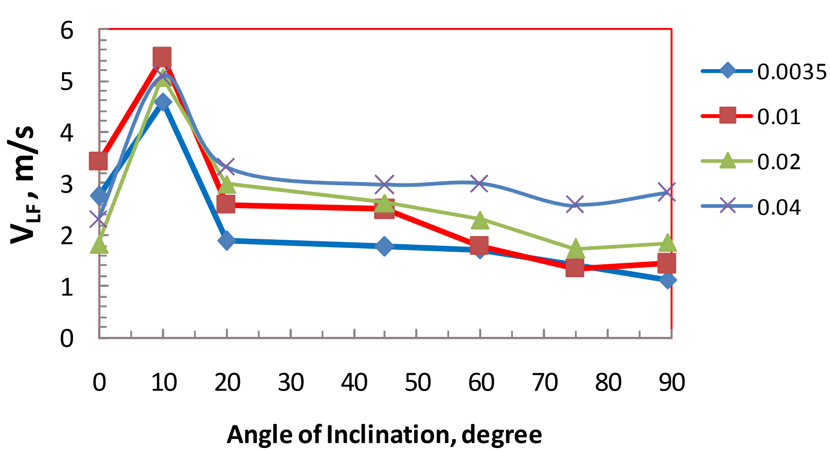

Figure 25: Variation of the Liquid Film Velocity with Inclination Angle at vSg = 50 m/s. (Legends are vSL in m/s)

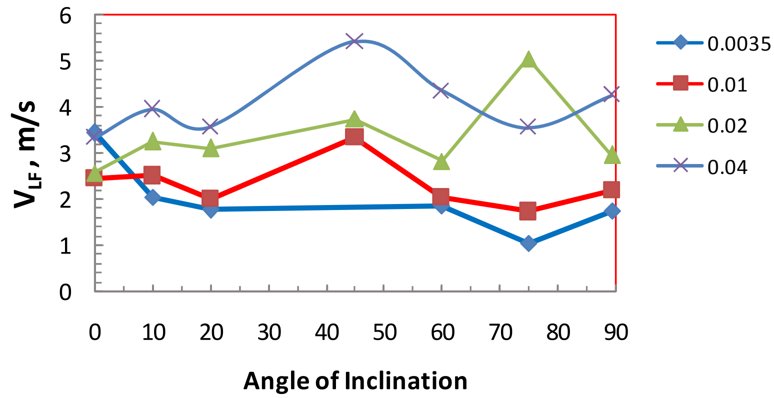

Figure 26: Liquid Film Velocity Variation with Pipe Inclination at vSg = 60 m/s (Legends are vSL in m/s)

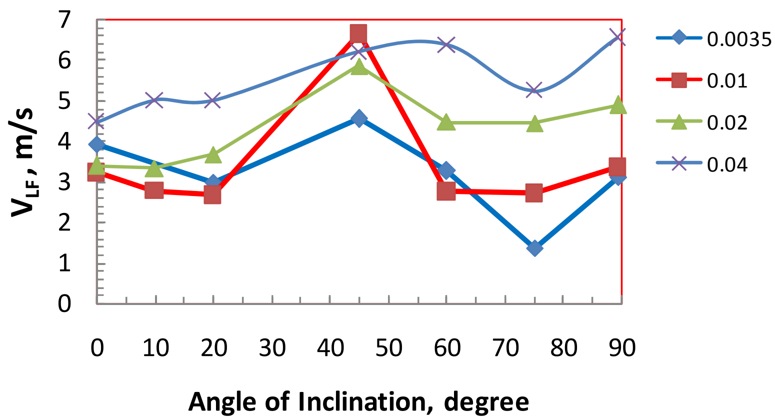

Figure 27: Liquid Film Velocity Variation at vSg = 70 m/s (Legends are vSL in m/s)

Concluding Remarks

Wave characteristics are very crucial for understanding and modeling of any annular flow. Pipe inclination effects on wave characteristics have been explained in this paper.

Most interestingly, wave amplitude may be presented as a function of liquid film thickness at the bottom of the pipe for any pipe diameter, surface tension and viscosity. Wave amplitude increases sharply with increasing the liquid film thickness at the bottom of the pipe.

Liquid film Reynolds number for horizontal and low inclination angle cases is strongly depending on the modified Lockhart-Martinelli parameter X^*. Re_{LF} for different surface tension, viscosity and pipe diameter is presented in this work as a function of X^*. Increasing X^* will increase Re_{LF}. Re_{LF} is less sensitive to the change in pipe diameter and surface tension and very sensitive to the change in liquid viscosity.

Dimensionless wave celerity (C/v_{SL}) is also well correlated with X^*. Increasing X^* will decrease the (C/v_{SL}). The grouping of low inclination and higher inclination angles was clearly noticed on the plots of (C/v_{SL}) versus X^*. The low inclination angles have higher (C/v_{SL}) than those of higher inclination angles. The effect of surface tension, viscosity and pipe diameter was presented in this work. Effect of pipe diameter of the behavior of (C/v_{SL}) versus X^* was insignificant. Effect of the surface tension was also insignificant. Effect of liquid viscosity was pronounced at lower values of X^* only. The dimensionless wave frequency (Strouhal number) is well correlated with X^*. Strouhal number for different pipe diameter, viscosity and surface tension at different inclination angles is presented in this paper as a function of X^*. The larger the X^*, the smaller the Strouhal number.

Maximum value of liquid Reynolds number and liquid film thickness at the bottom of the pipe decreases with increasing the angle of inclination. The maximum value of the wave amplitude decreases sharply with increasing the angle of inclination only at higher inclinations angle (large than 45°)

Nomenclature

Symbol	Description	Unit
A_{pipe}	*Cross sectional area of the pipe*	*m2*
c	*Celerity*	*m/s*
D	*Diameter*	*m*
F_E	*Entrainment fraction*	*/*
g	*Acceleration due to gravity*	*m/s2*
h_L	*Liquid film thickness*	*m*
H_L	*Holdup*	*/*
h_w	*Wave height*	*m*
ID	*Inner diameter of pipe*	*/*
L	*Length*	*m*
L_w	*Wave spacing*	*/*
$\left(\frac{dp}{dL}\right)$	*Total pressure gradient*	*Pa/m*
Re	*Reynolds number*	*/*
T	*Temperature*	*oC*
St	*Strouhal number (dimensionless wave frequency)*	*/*
v	*Velocity*	*m/s*
W	*Mass flow rate*	*kg/s*
We	*Weber Number*	*/*
X	*Lockhart-Martinelli parameter*	*/*
X^*	*Froude number ratio based on superficial velocities Eq. 1*	*/*
Δh_w	*Wave Amplitude*	*m*
θ	*Inclination angle*	*degree*
λ	*Wavelength*	*m*
ρ	*Density*	*kg/m3*
σ	*Surface tension*	*N/m*
μ	*Viscosity*	*Pa.s*

Subscripts

Symbol	Description	Unit
cr	*Critical*	*/*
E	*Entrained*	*/*
F	*Film*	*/*
G	*Gas*	*/*
L	*Liquid*	*/*
LE	*Liquid Entrained*	*/*
LF	*Liquid Film*	*/*
lim	*Limiting*	*/*
max	*Maximum*	*/*
Sg	*Superficial gas*	*/*
SL	*Superficial liquid*	*/*
w	*Wave*	*/*

References

Al-Sarkhi, A. and Hanratty, T. J., 2001. Effect of pipe diameter on the performance of Drag-Reducing Polymers in annular gas-liquid flows. Trans IChemE, Chemical Engineering Research and Design, 79 Part A, 402-408.

Andreussi, P., J. C. Asali and T. J. Hanratty (1985). "Initiation of Roll Waves in Gas-Liquid Flows." *AIChE Journal* 31(1): 119-126.

Andritsos, N. (1986). Effect of Pipe Diameter and Liquid Viscosity on Horizontal Stratified Flow. Ph.D. Dissertation. University of Illinois at Urbana-Champaign.

Azzopardi, B. J., Ed. (2006). Gas-Liquid Flows, Begell House.

Azzopardi B.J., Whalley P.B. (1980) Artificial waves in annular two-phase flow. ASME Winter Annual Meeting, Chicago, IL, November 16-21.

Bamea, D. and Y. Taitel (1993). "Kelvin-Helmholtz Stability Criteria for Stratified Flow: Viscous Versus Non-Viscous (Inviscid) Approaches.." *International Journal of Multiphase Flow* 19(4): 639-649.

Bruno, K. and M. J. McCready (1988). "Origin of Roll Waves in Horizontal Gas- Liquid Flows." *AIChE Journal* 34(9): 1431-1440.

Fukano, T., Ousaka, A., Morimoto, T., Sekoguchi, K., 1983. Air-annular two-phase flow in a horizontal tube. In: Second Report, Bulletin of the Japanese Society of Mechanical Engineers, vol. 26, pp. 1387–1395.

Geraci, G., B. J. Azzopardi, H.R.E. van Maanen,(2007a). Inclination Effects on Circumferential Film Flow Distribution in Annular Gas/Liquid Flows 53, No. 5, AIChE Journal

Geraci, G., B.J. Azzopardi, H.R.E. van Maanen, (2007b). Effect of inclination on circumferential film thickness variation in annular gas/liquid flow, Chemical Engineering Science 62, 3032 – 3042.

Hanratty, T. J. and A. Hershman (1961). "Initiation of Roll Waves." *AIChE Journal:* 488-497.

Henstock, W. H. and T. J. Hanratty (1976). The Interfacial Drag and the Height of the Wall Layer in Annular Flow." AIChE Journal 22(6): 990-1000.

Ishii, M. and M. A. Grolmes (1975). Inception criteria for droplet entrainment in two-phase concurrent film flow. *AlChE Journal* 21(2): 308-318.

Jayanti, S., Hewitt, G.F., White, S.P., 1990. Time dependent behaviour of the liquid film in horizontal annular flow. International Journal of Multiphase Flow 16, 1097–1116.

Johnson, G. W., J. Nossen and A. F. Bertelsen (2005). A Comparison between Experimental and Continuous Theoretical Roll Waves in Horizontal and Slightly Inclined Pipes at High Pressure. BHR Group 2005 Multiphase Production Technology, Barcelona.

Lighthill, M. J. and G. B. Whitham (1955). "On Kinematic Waves. I. Flood Movement in Long Rivers." *Proc. Roy. Soc. A* 229: 281-345.

Magrini, K, (2009). Liquid entrainment in annular gas-liquid flow in inclined pipes. M.S. Dissertation, the University of Tulsa.
Mantilla, I. (2008). Mechanistic modeling of liquid entrainment in gas in horizontal pipes, Ph.D. Dissertation, The University of Tulsa.
Miya, M., D. E. Woodmansee and T. J. Hanratty (1971). "A Model for Roll Waves in Gas-Liquid Flow." *Chemical Engineering Science* 26: 1915-1931.
Paras, S.V., Karabelas, A.J., 1991. Droplet entrainment and deposition in horizontal annular flow. International Journal of Multiphase Flow 17, 455–468.
Pols, R. M. (1998). Waves in separated two-phase flow. Ph.D. Dissertation, The University of Nottingham (United Kingdom).
Sutharshan, B. ,Kawaji, M. and Ousaka, A. (1995). Measurement of circumferential and axial liquid film velocities in horizontal annular flow, Int. J. Multiphase Flow 21 (2), 193-206.
Wallis, G. B. (1969). One Dimensional Two-Phase Flow, McGraw-Hill.
Watson, M. (1989). Wavy Stratified Flow and the Transition to Slug Flow. Proceedings of the 4th International Conference in Multi-phase Flows, Nice, France.
Woodmansee, D. E. (1968). Atomization from a flowing horizontal water film by a parallel air flow. Ph.D. Dissertation. University of Illinois at Urbana-Champaign.

Fluid Flow Projects

Inclination Angle Effects on Entrainment Fraction in Annular Gas-Liquid Flow

Abdelsalam Al-Sarkhi

Advisory Board Meeting, November 3, 2010

Outline

- Objectives
- Introduction
- Literature Review
- Sensitivity Analysis
- Closure Relation Development
- Model Evaluation
- Conclusions

Objectives

- Investigate Effects of Inclination Angle on Entrainment Fraction, F_E
- Develop Inclination Angle Dependent F_E Closure Relationship

Fluid Flow Projects

Advisory Board Meeting, November 3, 2010

Introduction

- Mechanistic Models Require Closure Relationships
  - Interfacial Friction Factor
  - Droplet Entrainment Fraction
  - Slug Translational Velocity
  - Others

Fluid Flow Projects

Advisory Board Meeting, November 3, 2010

Introduction …

- Chen (2005a) Sensitivity Study
  - Droplet Entrainment Fraction is One of the Most Sensitive Parameter Compared to Other Closure Relationships

Fluid Flow Projects

Advisory Board Meeting, November 3, 2010

Literature Review

- Annular Flow Pattern Is Quite Different for Small Diameter Pipes (Al-sarkhi & Hanratty)
- Droplets are not Created from the Entire Liquid Film Interface, But Particularly They Arise from Disturbance Waves (Geraci *et al.*)
- Increasing Upward Inclination Angle
  - Amplitude of Disturbance Waves Decreases
  - Fraction of Pipe Circumference over Which Disturbance Waves are Present Increases
  - At Inclinations Very Close to Vertical, Disturbance Waves are Present Around the Entire Section (Geraci *et al.* (2007b))

Fluid Flow Projects

Advisory Board Meeting, November 3, 2010

Literature Review

Annular flow in 2.54 cm pipe at v_{Sg} = 52 and v_{SL} = 0.02m/s

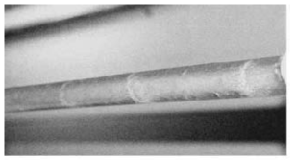

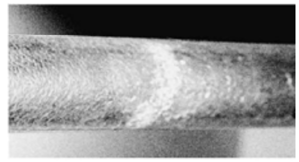

Annular flow in 9.53 cm pipe, v_{Sg} =30 m/s, v_{SL} = 0.034 m/s

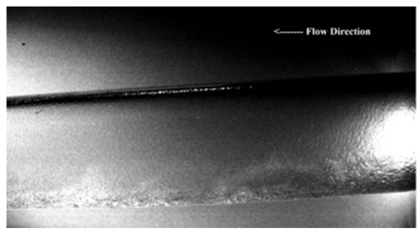

Literature Review Summary

- Most Research and Methods are for Vertical Annular Flow
- In Most Methods, Empirical Constants are Implemented Based on Experimental Data
- Few Entrainment Fraction Experimental Data Points for Inclined Flow
- Conflicting Results for Pipe Inclination Effect on Entrainment Fraction

Sensitivity Analysis

- Average Values of All Significant Parameters at All Inclination Angles are Calculated
- Percentage of Maximum Variation Above and Below the Average was Obtained
- If There is No Inclination Effect
  - Percentage Variation Over/Below the Average Value of Any Parameters) Should be the Same
  - Percentage of Variation Above And Below the Average Value Should Be Negligible or Minimum

Fluid Flow Projects

Advisory Board Meeting, November 3, 2010

Sensitivity Analysis …

- Percentage of Variation Above or/and Below the Average Value for All Important Parameters is not Negligible and in Some Cases Reaches Above 100%
- Maximum Percentage of Fluctuations of F_E Occurs at v_S=0.04 m/s (Max. Value in All Cases) and v_{Sg}=40 m/s (Min. Value in All Cases)

Fluid Flow Projects

Advisory Board Meeting, November 3, 2010

Sensitivity Analysis…

- Maximum Percent of Variation Above/below Average Value for F_E may Reach 40% Showing the Effect of Pipe Inclination
- Maximum Variation Above/Below the Average of Wave Amplitude is 130%
- Pipe Inclination Effect is a Strong Function of X*, Wave Celerity, Frequency, Amplitude and Liquid Film Thickness at the Bottom of the Pipe $H_l(0)$

$$X^* = \sqrt{\frac{\rho_G}{\rho_L}\frac{\dot{m}_L}{\dot{m}_G}} = \sqrt{\frac{\rho_L}{\rho_G}}\frac{V_{SL}}{V_{SG}} = \frac{Fr_{SL}}{Fr_{SG}}$$

Maximum Variation Below Average of All Data at All Angles

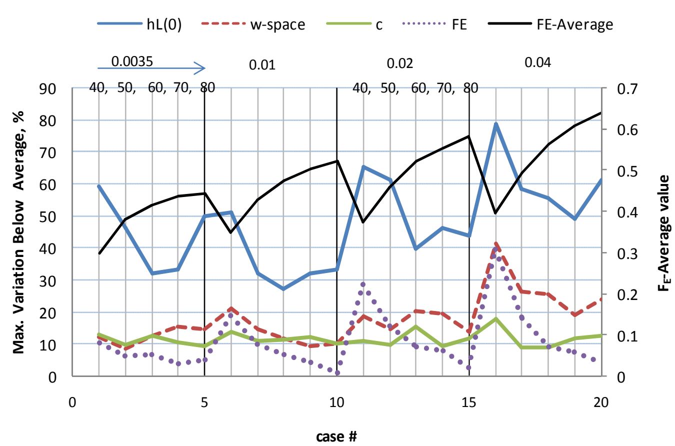

Average Value of All Parameters

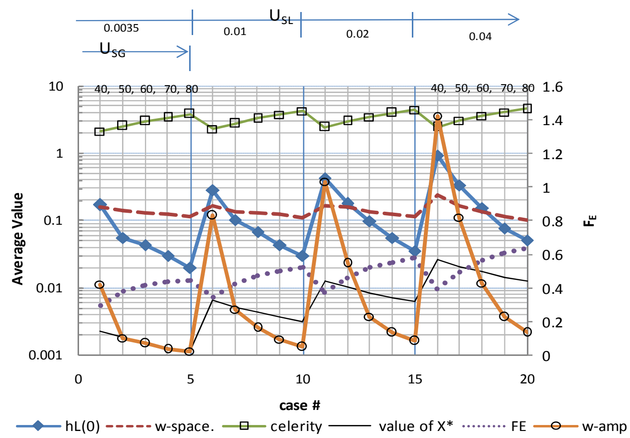

(Average Over All Angles)

Fluid Flow Projects

Advisory Board Meeting, November 3, 2010

Inclination Angle Effect - Direct Implementation Geraci *et al.* (2007)

- As Inclination Angle Increases, Liquid Film Thickness at the Bottom Decreases
- Wave Activity of Liquid Film Increases
- Combination of These Two Balance out Resulting in Near Insensitivity of F_E to Pipe Inclination
  - Not Completely Right for All Pipe Inclination Angles and for Wide Range of Superficial Liquid and Gas Velocities
  - May Be Applied only at Certain Operational Conditions
- Their Study Covered Very Narrow Range of v_{SL} (only 15 and 21.5 m/s) Resulting in Low Entrainment (Less Than 0.08)

Fluid Flow Projects

Advisory Board Meeting, November 3, 2010

Inclination Angle Effect - Direct Implementation (Magrini (2009))

$v_{SL} = 0.0035$, v_{Sg} 40→80

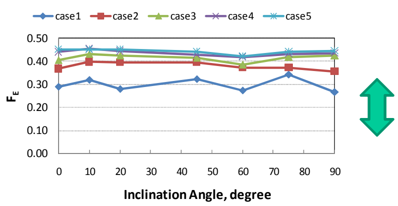

$v_{SL} = 0.01$, v_{Sg} 40→80

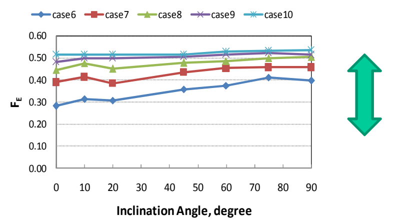

$v_{SL} = 0.02$, v_{Sg} 40→80

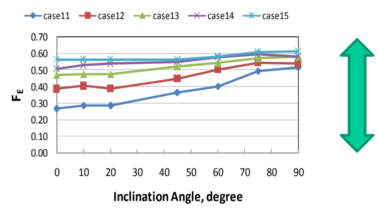

$v_{SL} = 0.04$, v_{Sg} 40→80

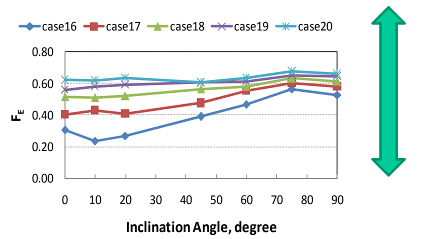

Dependency of Entrainment Fraction on X* and Re_{SL} or v_{SL}

- Magrini (2009) Entrainment Fraction Data for 0, 10, 20 and 45 Degrees Follow Same Trend

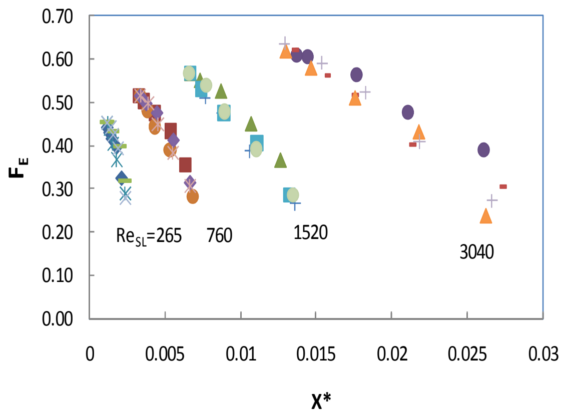

Dependency of Entrainment Fraction on X* and Re_{SL} or v_{SL}

- Magrini (2009) Entrainment Fraction Data for 60, 75, and 90 Degrees Follow Same Trend

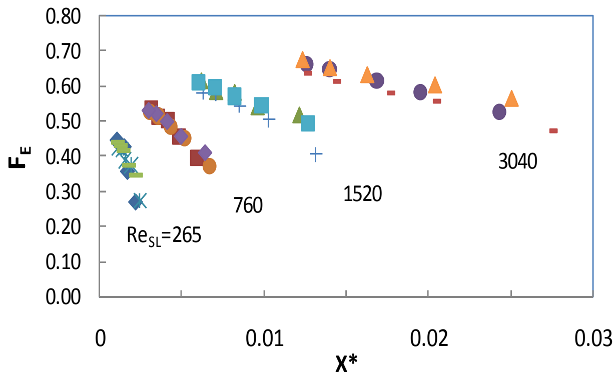

Fluid Flow Projects

Advisory Board Meeting, November 3, 2010

Entrainment Fraction Correlation Using Magrini (2009) Data

- From 0° to 45°

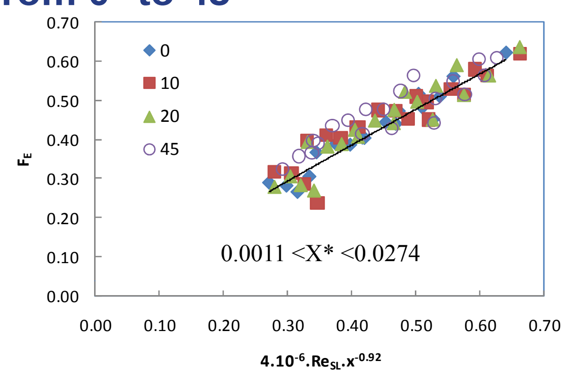

$$F_E = 0.892\left(4\times10^{-6}\,\mathrm{Re}_{SL}^{1}\,X\,*^{-0.92}\right)^{0.874}$$

Fluid Flow Projects

Advisory Board Meeting, November 3, 2010

Entrainment Fraction Correlation Using Magrini (2009) Data

- From 60° to 90°

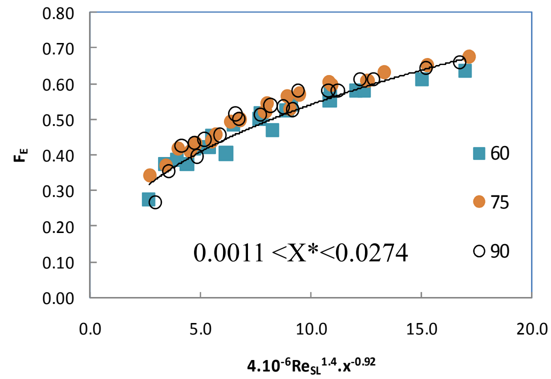

$$F_E = 0.221\left(4\times10^{-6}\,\mathrm{Re}_{SL}^{1.4}\,X*^{-0.92}\right)^{0.403}$$

Comparison of Measured Data (Magrini (2009)) With Prediction

- For Angle of Inclination Between 0°- 45°

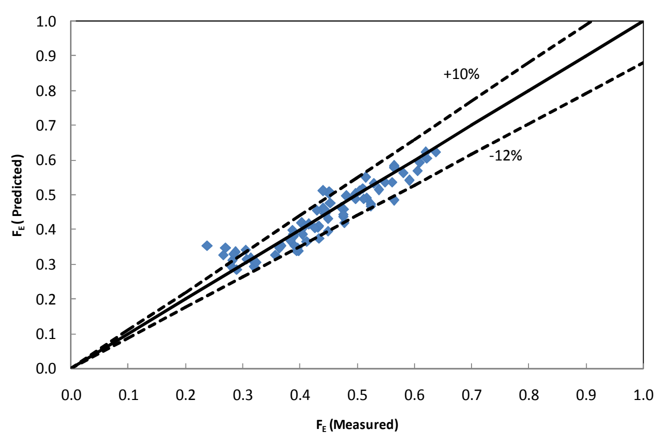

Comparison of Measured Data (Magrini (2009)) With Prediction

- For Angle of Inclination Between 60°- 90°

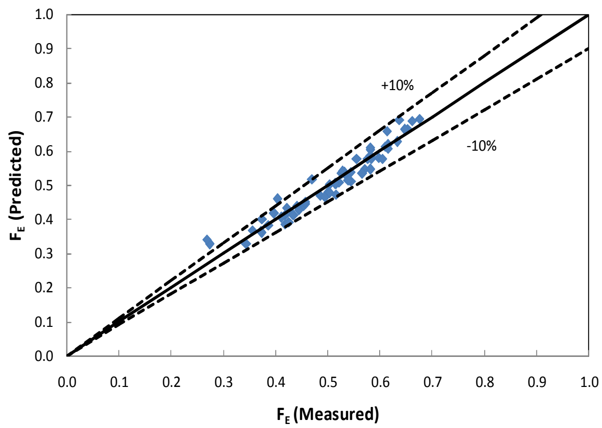

Comparisons with Other Studies

- *Ousaka et al. (1996)*
  - 0°, 30°, 45°, 60° and 75° Inclination Angles
  - 25.4 mm ID
  - v_{Sg}=15 to 40 m/s, v_{SL}= 0.06 to 0.2 m/s
  - 0.032<X*<0.375

Ousaka *et al.* (1996) …

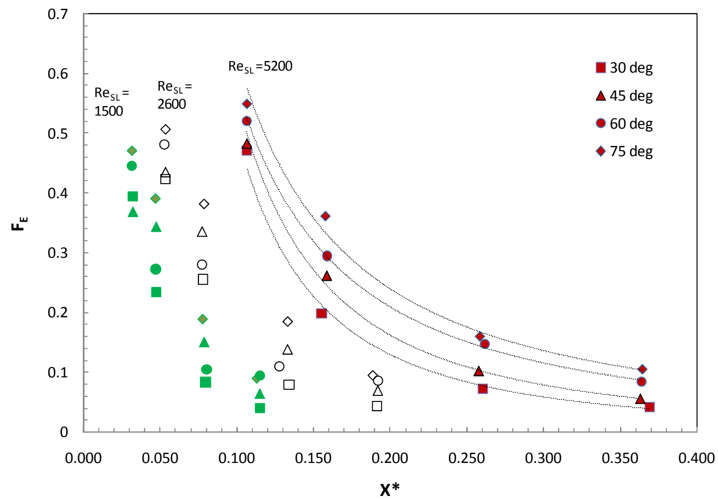

Fluid Flow Projects

Advisory Board Meeting, November 3, 2010

Ousaka *et al.* (1996) …

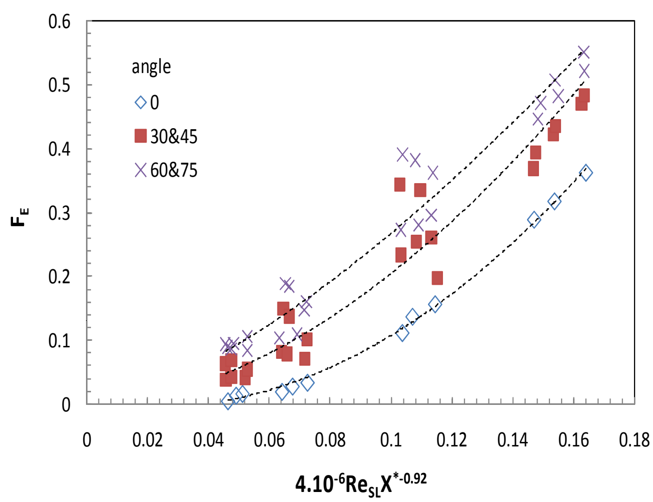

Fluid Flow Projects

Advisory Board Meeting, November 3, 2010

Owen (1985)

- Vertical Pipe
- 0.03175 m ID
- v_{Sg}=17 to 70 m/s, v_{SL}= 0.0495 to 0.4 m/s
- 0.0126<X*<0.259

Fluid Flow Projects

Advisory Board Meeting, November 3, 2010

Owen (1985) …

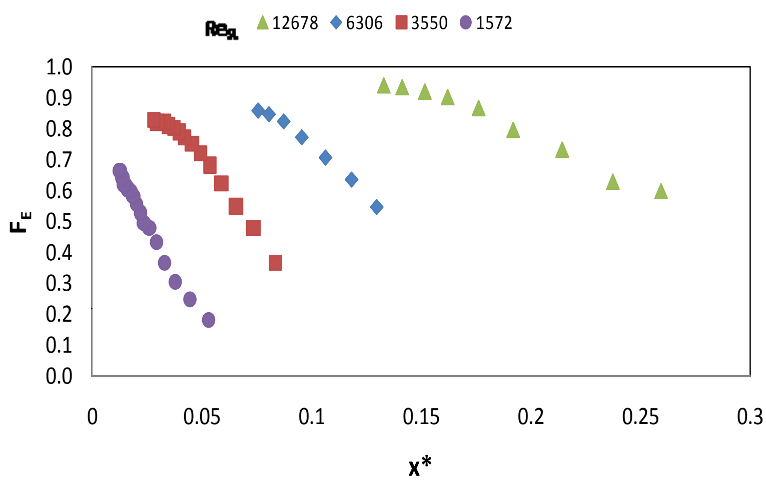

Fluid Flow Projects

Advisory Board Meeting, November 3, 2010

Owen (1985) …

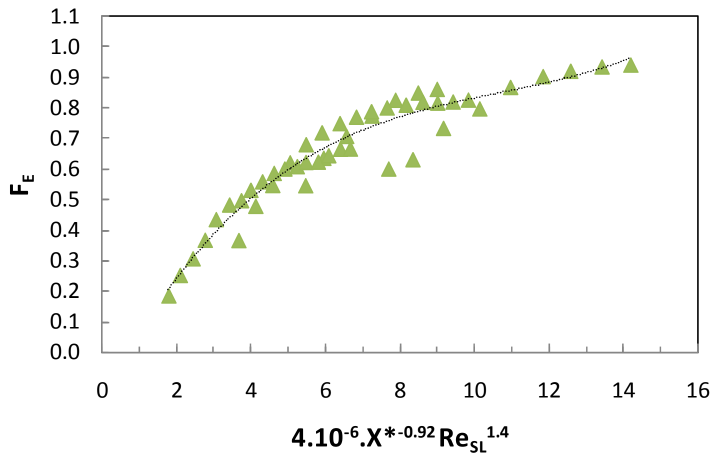

Fluid Flow Projects

Advisory Board Meeting, November 3, 2010

Shadel (1988)

- Shadel (1988)
  - Vertical Flow of Air-water in 0.0254 and 0.042 m ID, 0.005 <X*> 0.088

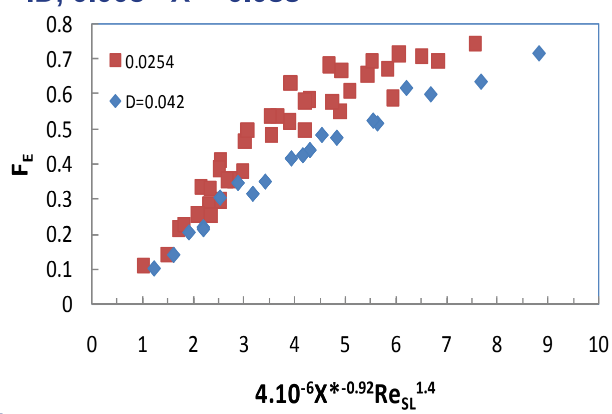

Fluid Flow Projects

Advisory Board Meeting, November 3, 2010

Mantilla (2008)

- Horizontal 0.0508 ID. Pipe
- Air-water, Air-water+Butanol and Air-water+Salt+Glycerin

Fluid	Properties	Value
Air	Density (kg/m³)	2.4
	Viscosity (Pa.s)	1.8E-5
Water	Density (kg/m³)	997
	Viscosity (Pa.s)	1.02E-3
	Surface tension (N/m)	0.073
Water-5% (V/V) Butanol	Density (kg/m³)	989
	Viscosity (Pa.s)	1.22E-3
	Surface tension (N/m)	0.035
Water-47% (V/V) Glycerin-Salt	Density (kg/m³)	1130
	Viscosity (Pa.s)	7.1E-3
	Surface tension (N/m)	0.061

Mantilla (2008) …

- Surface Tension has No Effect on F_E While Viscosity Showed Significant Effect

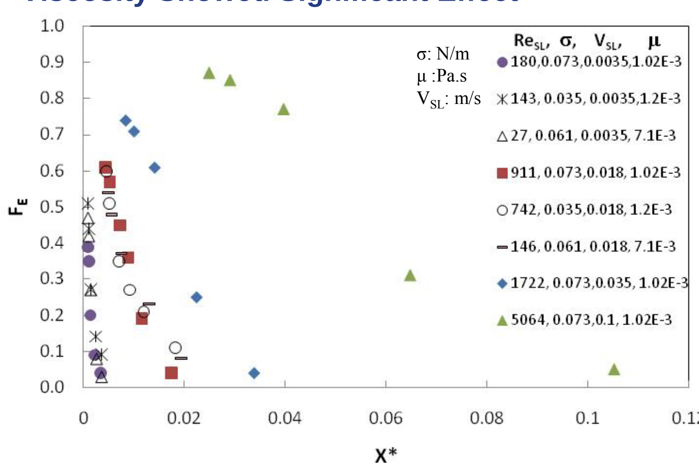

Mantilla (2008) …

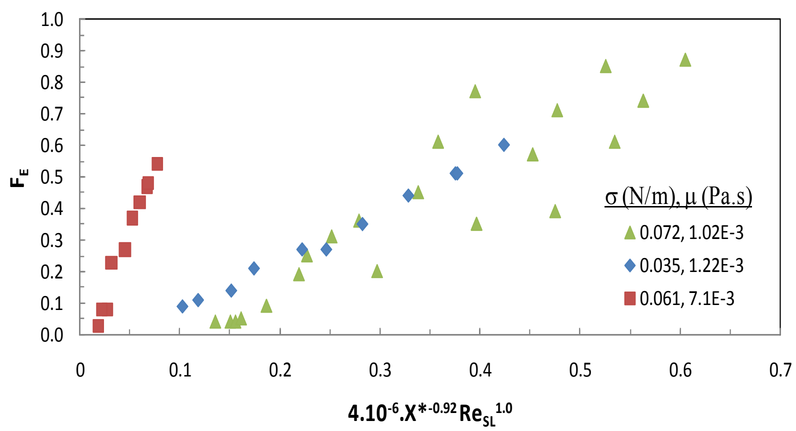

Entrainment Fraction Correlation Using All Available Data

- High Inclination Angles (No Correction for Pipe Diameter)

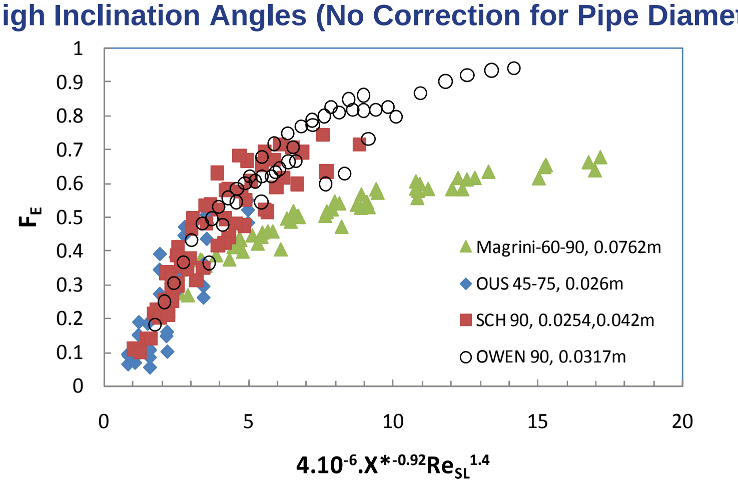

Entrainment Fraction Correlation Using All Available Data

- High Inclination Angles (With Pipe Diameter Correction)

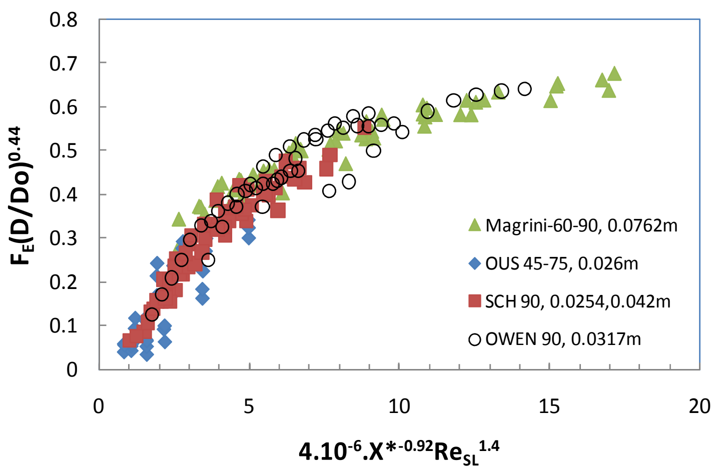

Fluid Flow Projects

Advisory Board Meeting, November 3, 2010

Entrainment Fraction Correlation Using All Available Data

$$F_E = (D/D_0)^{-0.44}\left\{0.24\ln\left(X^{*-0.92}\,\mathrm{Re}_{SL}{}^{1.4}\right) - 2.98\right\}$$

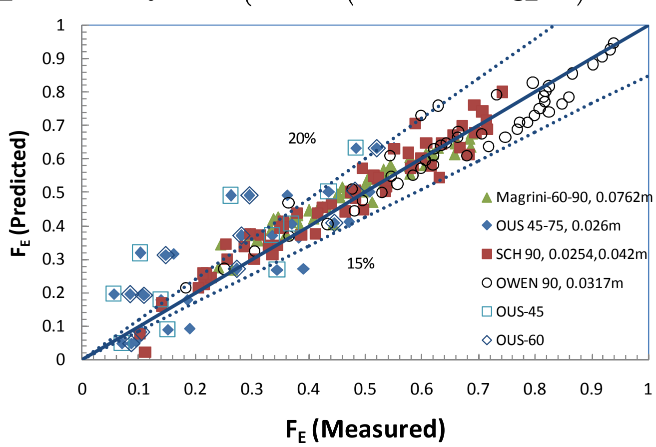

Fluid Flow Projects

Advisory Board Meeting, November 3, 2010

Entrainment Fraction Correlation Using All Available Data

- Low Inclination Angles (0 - 45°)

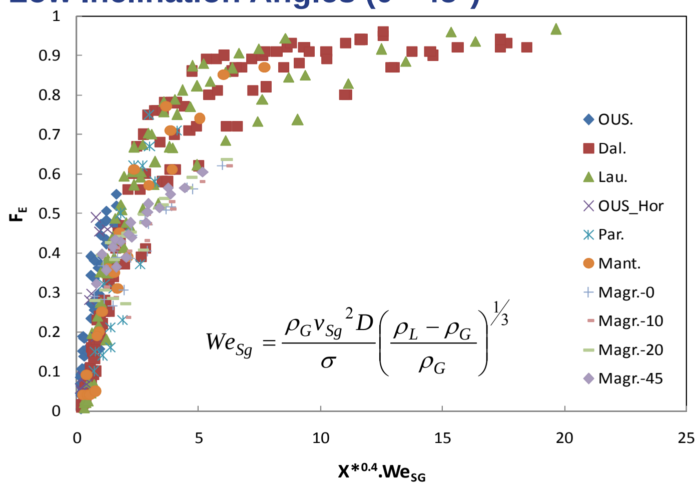

Fluid Flow Projects

Advisory Board Meeting, November 3, 2010

Entrainment Fraction Correlation Using All Available Data

- Low Inclination Angles (0-45°) Semi-log Scale

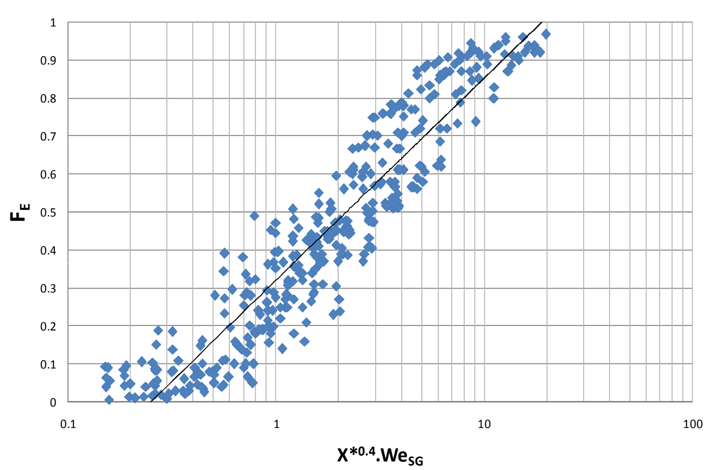

Fluid Flow Projects

Advisory Board Meeting, November 3, 2010

Problems With Some Entrainment Models

- **Sawant *et al.* (2008)**

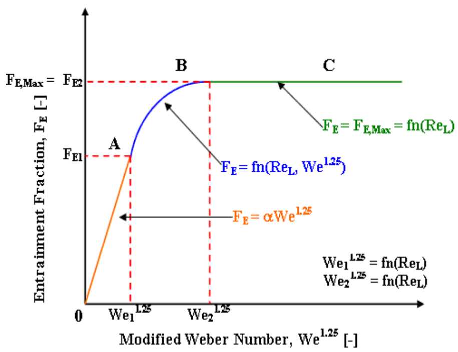

$$F_E = F_{E,\max} \tanh(\alpha We^{1.25})$$

$$F_{E,Max} = 1 - \mathrm{Re}_{F,\lim} / \mathrm{Re}_{SL}$$

$$\mathrm{Re}_{F,\lim} = 250\ln(\mathrm{Re}_{SL}) - 1265$$

$$\alpha = 2.31 \times 10^{-4} \mathrm{Re}_{SL}{}^{-0.35}$$

Most of the ranges are function of Re_{SL}

Swant *et al.* (2008)

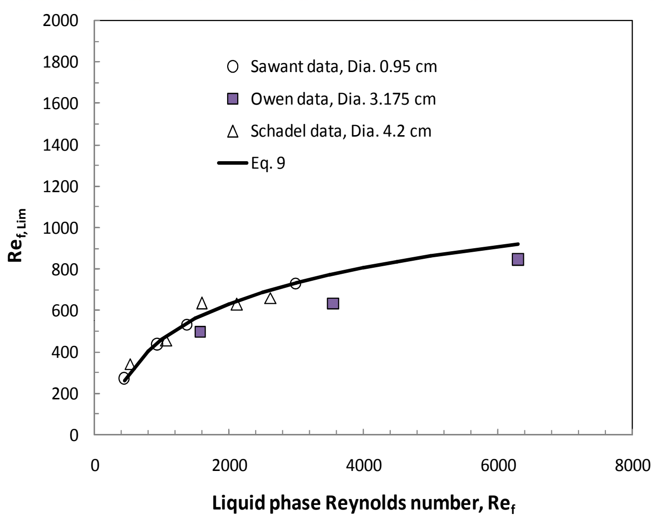

Swant *et al.* (2008) …

Extended Range

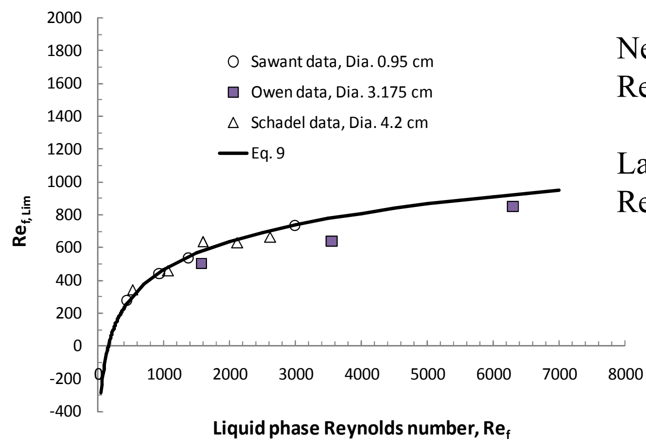

Negative Value for $Re_{f,lim}$ for Re_{SL}<157

Large Error for Re_{SL}<500

Swant *et al.* (2008) …

Extended Range

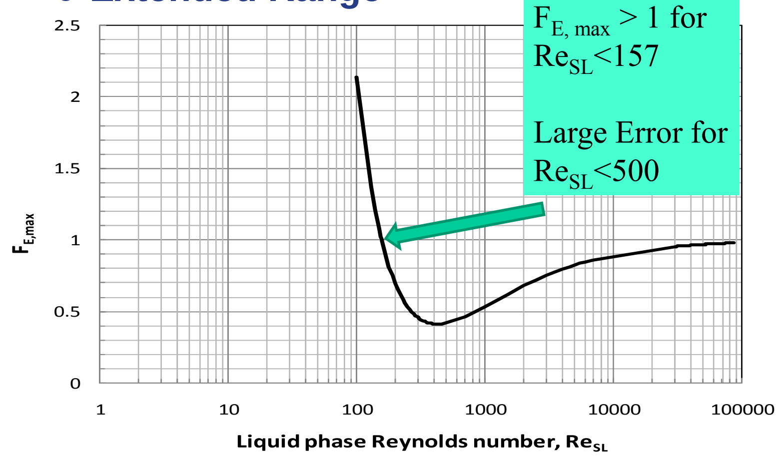

$F_{E,\ max}$ > 1 for Re_{SL}<157

Large Error for Re_{SL}<500

Swant et al. (2008) …

- Comparison Between Experimental Data and Predictions

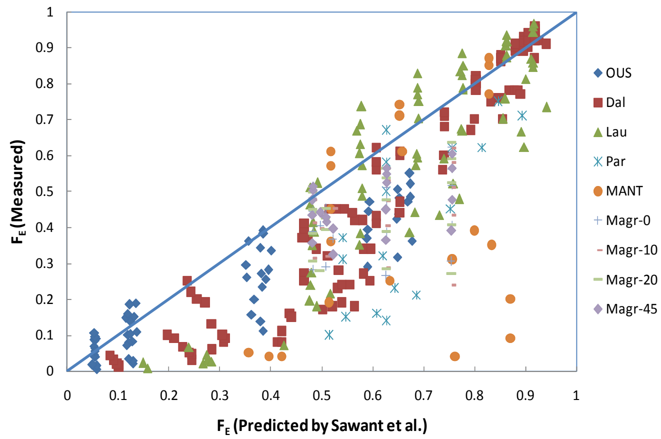

Fluid Flow Projects

Advisory Board Meeting, November 3, 2010

Swant *et al.* (2008)…

- Modified Sawant *et al.*

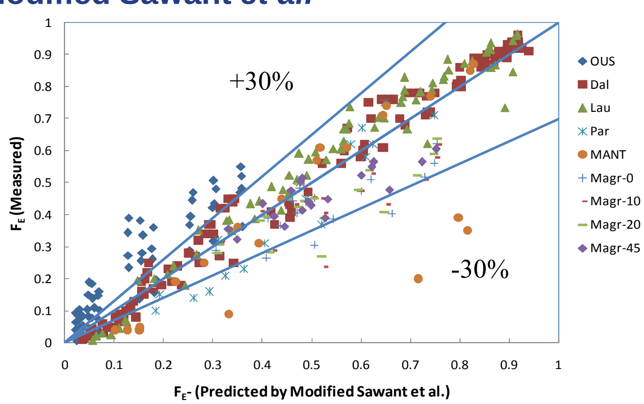

$$F_E = F_{E,\max} \tanh(X^{*0.4} \alpha We^{1.25})$$

Fluid Flow Projects

Advisory Board Meeting, November 3, 2010

Swant *et al.* (2008)…

- **Modified Sawant *et al.***
  - For Re_{SL} > 900; to Overcome the Problem of $Re_{f,lim}$

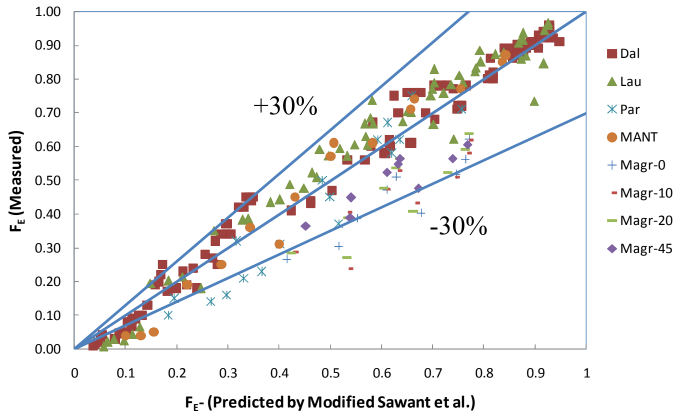

Fluid Flow Projects

Advisory Board Meeting, November 3, 2010

Problems With Some Entrainment Models…

- **Pan and Hanratty**

$$\frac{F_E / F_{E,\max}}{1 - F_E / F_{E,\max}} = 9\times 10^{-8}\left(\frac{D v_G{}^3 \sqrt{\rho_L \rho_G}}{\sigma}\right)\left(\frac{\rho_G{}^{1-m} \mu_G{}^m}{d_{32}{}^{1+m} g \rho_L}\right)^{1/(2-m)}$$

Values of 0, 0.6, 1 are used for exponent *m*

$$F_{E,\max} = 1 - W_{F,cr} / W_L$$

$$W_{F,cr} = 0.25 \mu_L \pi D \,\mathrm{Re}_{F,cr}$$ the critical liquid film flow rate

$$\mathrm{Re}_{F,cr} = 7.3(\log w)^3 + 44.2(\log w)^2 - 263 \log w + 439 \Rightarrow$$ w = 1.8 to 28

$$w = (\mu_L / \mu_G)\sqrt{\rho_G / \rho_L}$$

Fluid Flow Projects

Advisory Board Meeting, November 3, 2010

Pan & Hanratty …

- Critical Liquid Film Flow Rate, $W_{F,cr}$, at Low Re_{SL} can be Greater Than W_L,
  - Due to Re_{LFC} or W_{LFC} Being Function of W Only
  - W is Only Function of the Physical Properties of Gas and Liquid (Viscosity and Density)
- This Leads to a Negative Value for Maximum Entrainment Fraction $F_{E,\,max}$.
  - Was Tested For Air And Water Data
  - Found Negative $F_{E,max}$ for All Data With Re_{SL}< 275

Problems With Some Entrainment Models…

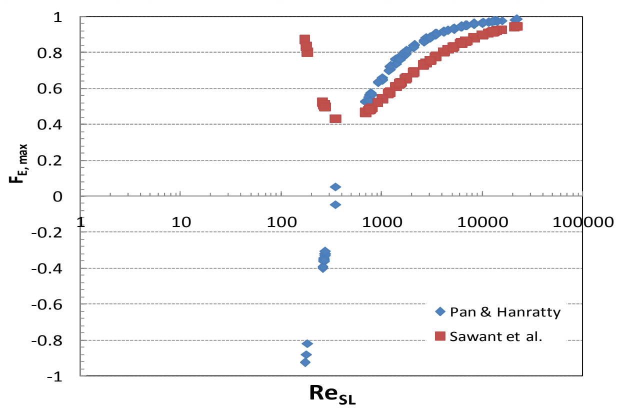

Comparison of Maximum Entrainment Fraction Modeled by Pan and Hanratty and Sawant *et al.* (Semi-log Scale)

Conclusions

- Clear Inclination Effect on Entrainment Observed
- Entrainment Fraction Increases With Inclination Angle Especially at High v_{SL} and Low v_{Sg}
- Correlations for Entrainment Fraction in terms of X* and Re_{SL} for Magrini's Data at Low and High Inclination have Been Found

Conclusions …

- Inability of Single Correlation or Model to Predict Entrainment at All Angles
- Available Correlations For Maximum Entrainment Fraction have Serious Problems at Low v_{SL} and Need to Be Modified
- Entrainment Prediction Improvement is Needed
- More Inclined Entrainment Data is Needed

Questions/Comments

?

Fluid Flow Projects

Advisory Board Meeting, November 3, 2010

Inclination Effects on Entrainment Fraction in Annular Gas-Liquid Flow

Abstract

This report presents the effects of the inclination angle on the liquid entrainment fraction of entrainment F_E. An inclination angle dependent F_E closure relationshipfor based on Magrini (2009) data has been developed. Moreover, a general correlation based on all available data is presented. Effects of other parameters, e.g. surface tension and pipe diameter, have also been explained for the available data. The major problems of the most commonly used models for F_E are also identified.

Introduction

Annular flow pattern in a pipe can exist at high gas and liquid flow rates. In annular flow, part of the liquid flows along the wall as a film and part as drops entrained in the gas. There is a liquid mass transfer between the film and the gas core, whereby droplets deposit to the film are formed by atomization of the film. Under equilibrium conditions the rate of atomization equals the rate of deposition. Due to gravity the liquid in the film is distributed asymmetrically. For air-water systems, the film flow is characterized by the intermittent appearance of disturbances, which are a group of large amplitude waves that could be considered as patches of turbulence. The irregular waves are the source of drops that enter the gas phase.

The annular flow pattern is quite different for small diameter pipes (less than 3 cm internal diameter (ID)) and large diameter pipes (larger than 5 cm ID) in that the disturbance waves for small diameter pipes are wrapped around the whole circumference. The pattern resembles what is observed in vertical pipes (Al-sarkhi and Hanratty (2001)). For low viscosity liquids, the initiation of atomization occurs when disturbance waves appear on the liquid layer (Pan, and Hanratty, (2002b))

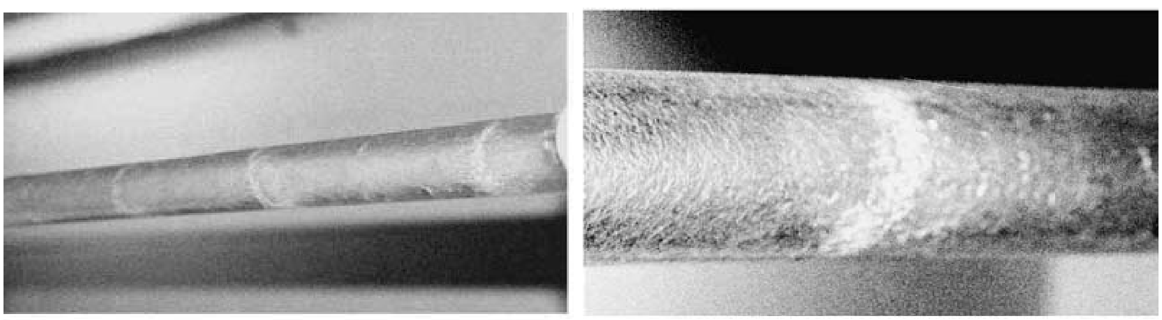

Figure 1 A: Annular flow in 2.54 cm pipe at v_{Sg} = 52 and v_{SL} = 0.02m/s (flow direction from right to left).

Geraci *et al.* (2007a) explained how the majority of drops in annular flow are created from the film by the flowing gas phase. However, drops are not created from the entire liquid film interface, but particularly they arise from disturbance waves.

Azzopardi and Whalley (1980) concluded that waves are the source of drops. This conclusion was proved through the experiment in which injecting small quantities of liquid into a film flow whose flow rate was just below the flow rate for formation of waves, they were able to create waves on demand. These experiments, which employed an axial viewing technique, gave very strong proof that drops are only created in presence of waves.

Sutharshan *et al.* (1995) measured the liquid film velocity in horizontal annular flow in a pipe with 0.0254 m internal diameter. It was concluded that the liquid is transported to the upper part of the tube against the force of gravity by the disturbance waves and not by the secondary gas flow or any other mechanisms.

Geraci *et al.* (2007b) studied the effect of inclination on the disturbance wave characteristics in 38 mm pipe diameter. It was observed that in horizontal flow the film interface is covered by large disturbance waves only over the lower half of the pipe, while at the top there are only small amplitude ripples. With increasing the inclination of the pipe upward from the horizontal, the amplitude of the disturbance waves decreases, but the fraction of the pipe circumference over which disturbance waves occurs increases. At near vertical inclinations, disturbance waves are present around the entire section.

In addition to the angle of inclination, liquid surface tension is another parameter which may affect the F_E at certain operational conditions but has to be studied systematically by fixing all other parameters and with enough data points at different flow conditions and pipe inclinations.

The focus of this study is mainly to examine the effect of pipe inclination, diameter and physical properties on entrained droplet in annular flows. The diameter and physical properties of liquid effect on F_E will be investigated for the limited cases available in literature. Such information is critically important in predicting the behavior of large diameter pipes especially with the very limited data available in literature.

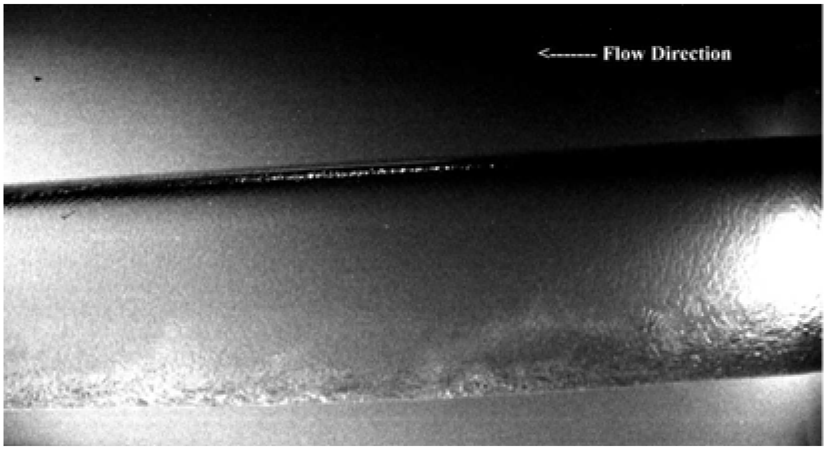

Figure 1 B: Annular flow in 9.53 cm pipe, vSg =30 m/s, vSL = 0.034 m/s

Effect of Pipe Inclination: Sensitivity Analysis

Sensitivity analysis is used to prove the effect of the pipe inclination on Fraction of liquid Entrainment F_E. The data consists of twenty cases (at different v_{SL} and v_{Sg}), and every case is for different pipe inclination from 0° to 90° (see Table 1). For every case, the only variable is the pipe inclination angles. The average values of all significant parameters at all inclination angles are calculated, and the percentage of maximum variation above and below the average was obtained and presented.

If there is no inclination effect, then at the same conditions for different angles, the results (the percentage variation over/below the average value of any parameters) should be the same, and the percentage of variation above and below the average value should be negligible or at least minimum. The average of the results was considered and the variation above and below the average was noticed. It was noticed that the percentage of variation above or/and below the average value for all important parameters is not negligible and in some cases reaches above 100%.

Maximum percentage of fluctuations of F_E occurs at v_{SL}=0.04 m/s (max. value in all cases) and v_{Sg} = 40 m/s (lowest value in all cases). This is matching the maximum value of X* (Froude number ratio as in Eq. 1) in all runs and maximum percentage of fluctuation in celerity below the average of all runs, and it is also matching the maximum percentage of variation below the average value of liquid film thickness at the bottom of the pipe.

Pipe inclination effect is a strong function of X*, wave celerity, frequency, amplitude and liquid film thickness at the bottom of the pipe, $h_L(0)$. The maximum percent of variation above/below the average value for F_E may reach 40% showing the effect of pipe inclination. The maximum variations above/below the average are around 60%, 100%, 24% for the wave spacing, liquid film thickness at the bottom of the pipe $h_L(0)$, and the wave celerity, respectively. The maximum variation above/below the average of wave amplitude is 130%.

The behavior of the average value of wave celerity, c, is similar to the behavior of the average value of entrainment fraction, F_E. This means that it is maximum at the highest superficial liquid and gas velocity and minimum at the lowest superficial liquid and gas velocities. More interesting is the behavior of the average value (not the percent of variations) of the wave amplitude for all cases. As the superficial velocity of gas increases (for the same v_{SL}), the amplitude decreases. This means that the liquid that forms the wave now is in a form of droplets entrained in the gas. At the maximum droplet entrainment, the amplitude of the wave is at its minimum, the wave celerity value is at its maximum, and the value of the liquid film at the bottom of the pipe is at its minimum. In conclusion, the average value of the wave amplitude behavior is opposite to that of the fraction of entrainment and wave celerity (see Figs. 2-5).

The average values over all inclination angles for all significant parameters are shown in Fig. 5. The average value of F_E is at its maximum in Case 20 (cases are listed in Table 1), at which maximum average of celerity, minimum average value of wave spacing and liquid film at the bottom of the pipe. Maximum average value of F_E occurs at relatively high value of X*. The fluctuations above and below the average value depends on the operation condition (v_{SL} and v_{Sg}) as well as the inclination angle.

Table 1: Sensitivity Analysis Parameters

Case #	v_{SL} m/s	v_{Sg} m/s	X*	F_E, % B-Avg	F_E, % A-Avg	$h_L(0)$ % B-avg	$h_L(0)$ % A-avg	c % B-avg	c % A-avg	L_W, % B-avg	L_W, % A-avg	Ampl. % B-aveg	Ampl. % A-avg
1	0.0035	40	0.002298	10.6	14.7	59.2	45.8	13.0	15.0	12.1	38.2	84.4	68.7
2	0.0034	50	0.001844	6.3	4.7	46.2	43.6	9.9	14.4	8.5	11.8	69.3	85.1
3	0.0036	60	0.001526	7.0	4.0	32.3	58.1	12.8	20.5	12.5	15.2	63.3	103.9
4	0.0036	70	0.001301	4.0	4.1	33.3	100.0	10.8	17.3	15.5	18.7	52.3	53.8
5	0.0035	80	0.001137	5.1	1.9	50.0	50.0	9.6	24.3	14.8	24.8	31.6	56.9
6	0.01	40	0.006507	19.1	17.7	51.0	50.5	13.7	17.1	21.0	19.2	80.1	87.0
7	0.01	50	0.005253	10.2	7.1	31.9	26.4	11.0	15.0	14.9	21.4	58.5	107.8
8	0.01	60	0.004324	6.7	5.6	27.1	75.0	11.4	20.9	11.7	22.9	45.3	85.9
9	0.01	70	0.003672	4.4	3.4	32.3	80.6	12.4	18.6	9.6	21.0	49.3	113.3
10	0.01	80	0.003223	1.3	2.6	33.3	100.0	10.4	19.5	10.1	13.7	43.1	120.1
11	0.02	40	0.012998	28.8	38.1	65.2	83.1	11.0	15.3	18.8	12.0	77.5	87.3
12	0.02	50	0.010462	15.8	18.6	61.1	133.3	10.0	14.5	14.8	14.8	60.6	134.1
13	0.02	60	0.008614	9.2	11.6	40.0	60.0	15.6	21.9	20.4	19.2	51.3	119.7
14	0.02	70	0.007327	8.0	7.6	46.2	79.5	9.4	18.9	19.5	17.9	50.5	105.9
15	0.02	80	0.006452	2.7	5.8	44.0	68.0	12.0	14.4	13.8	14.1	41.0	103.1
16	0.04	40	0.026136	39.7	43.1	78.8	70.0	18.2	15.1	41.4	61.9	82.7	39.0
17	0.04	50	0.020886	18.4	22.1	58.3	132.3	9.1	11.6	26.4	25.3	60.6	113.0
18	0.04	60	0.01738	9.3	12.3	55.5	78.2	9.0	16.2	25.5	36.8	62.4	115.4
19	0.04	70	0.01462	7.6	7.5	49.1	78.2	11.8	15.8	19.1	15.0	57.7	90.6
20	0.04	80	0.012932	4.4	6.0	61.1	94.4	12.6	18.6	24.2	19.1	63.6	131.8

Table 1 nomenclature is given below:

Average: the average value at all inclination angles (at the same operating conditions, v_{SL} and v_{SG})
Max: the maximum value at all inclinations
Min: the minimum value at all inclination at same v_{SL} and v_{SG}
B-Avg: below average
A-Avg: above average
L_W: wave spacing
$h_L(0)$: Liquid film thickness at the bottom of the pipe
Ampl.: wave amplitude ($\Delta h_W(0°)$)
C: wave celerity
X^*: Froude number ratio (Fr_{SL}/Fr_{SG})

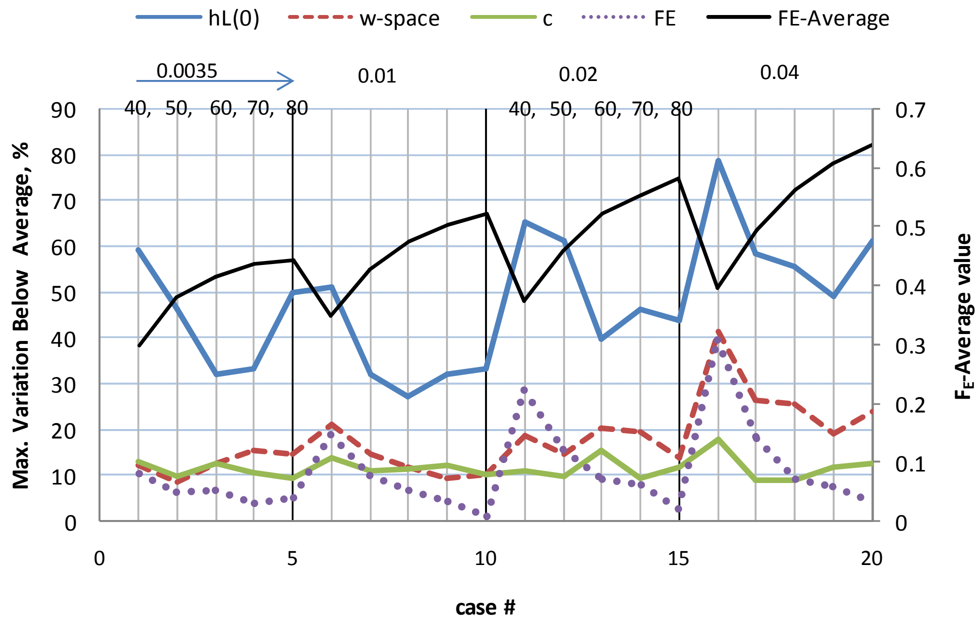

Figure 2: Maximum variation below the average of all data at all angles. The average value of FE is shown on the secondary axis (right hand side of the graph)

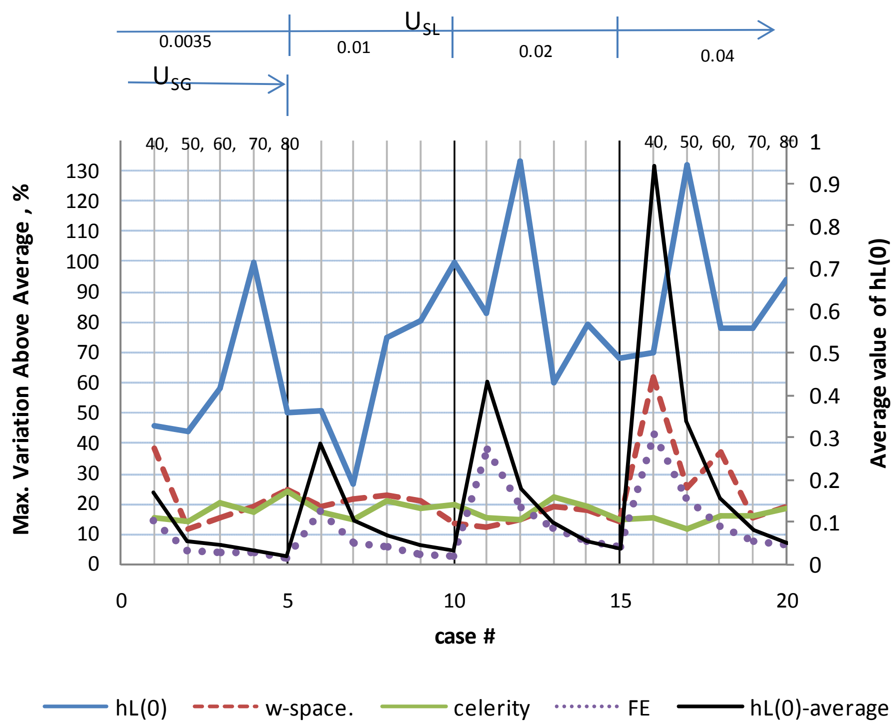

Figure 3: Maximum variation above the average of all data at all angles. The average value of hL(0o) is shown on the secondary axis (right hand side of the graph). Average value of liquid film thickness in mm

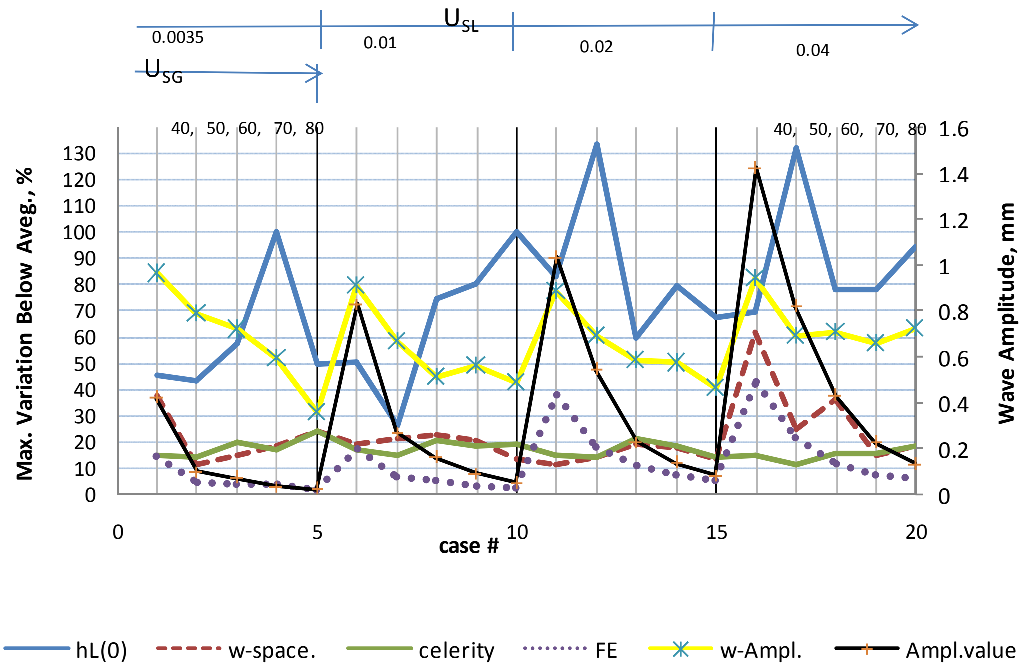

Figure 4: Maximum variation below the average of all data at all angles. The average value of ΔhW(0o) is shown on the secondary axis (right hand side of the graph)

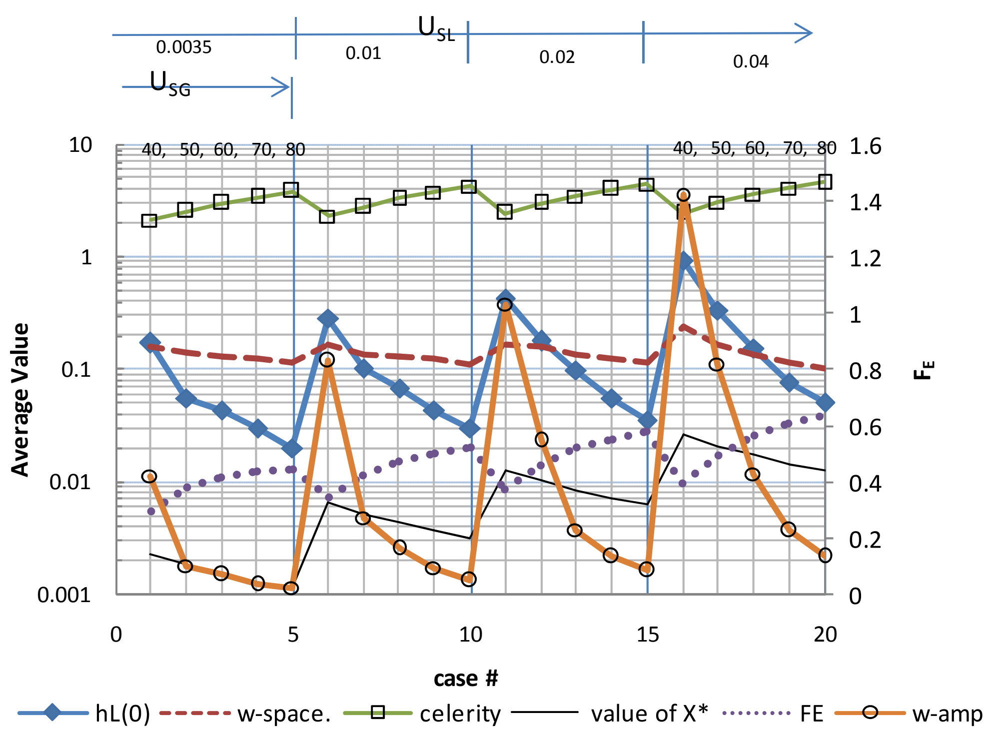

Figure 5: The average value of all parameters (average over all angles). The value of FE is shown on the secondary axis

Inclination Angle Effect - Direct implementation

Table 2 describes the cases studied.

The inclination angle effect on F_E can be characterized based on the wave celerity, the liquid film thickness, the pipe diameter and the operational conditions.

The wave celerity increases with increasing superficial gas velocity. The celerity is also dependent on the superficial liquid velocity. As the superficial liquid velocity increases, the wave celerity increases. The wave celerity increases as the pipe inclination increases. The wave celerity reaches a maximum point around the 10° to 20° inclination angle. After this maximum, the wave celerity will decrease until it reaches almost constant value between 60° and 90° inclination angles. The liquid film thickness has an opposite behavior with respect to the superficial gas velocity. As superficial gas velocity increases, average film thickness decreases since the liquid film evenly distributes around the pipe. Similarly, increasing the inclination angle promotes the symmetry of the film decreasing the average film thickness at the bottom of the pipe.

Geraci *et al.* (2007) concluded that, for the flow rates studied, the entrainment fraction was slightly influenced by pipe inclination. They proposed that, as the inclination angle increases, the film thickness at the bottom decreases, but the wave activity of the film increases. The combination of these two trends may balance out resulting in near insensitivity of entrainment fraction to pipe inclination. This conclusion is not completely right for all pipe inclination angles and for wide range of superficial liquid and gas velocities. This conclusion may be applied only at high gas velocity or at certain operational conditions and pipe inclination angles. Geraci *et al.* study covered very narrow range of superficial gas velocity (only 15 and 21.5 m/s) resulting in low entrainment fractions. less than 0.08.

F_E sensitivity to inclination angle is shown in Fig. 6. F_E is insensitive to the pipe inclination only at very high gas velocity and lowest to medium liquid superficial velocity. F_E is less sensitive to the pipe inclination angle at the highest gas velocity and low liquid velocity. F_E is very sensitive to the pipe inclination for lower gas velocities and higher liquid velocities. The higher the inclination is the larger the entrainment is. This is also observed by Ousaka (1996). Some published studies (Geraci *et al.* 2007) have not seen the effect of pipe inclination angles simply because either they did not cover a wide range of superficial liquid and gas velocities or all inclination angles from horizontal to vertical. Not seeing the effect of pipe inclinations on the entrainment fraction may also be interpreted as that the gas velocities were high enough to reach the maximum entrainment fraction which is in the present case at or above 80 m/s, and it can be seen clearly from Fig. 6 that the effect of the inclination angles in this case is minor specially at low liquid superficial velocities.

Table 2: Cases Studied

Group	1					2					3					4				
Case	1	2	3	4	5	6	7	8	9	10	11	12	13	14	15	16	17	18	19	20
v_{SL}, m/s	0.0035	0.0035	0.0035	0.0035	0.0035	0.01	0.01	0.01	0.01	0.01	0.02	0.02	0.02	0.02	0.02	0.04	0.04	0.04	0.04	0.04
v_{Sg}, m/s	40	50	60	70	80	40	50	60	70	80	40	50	60	70	80	40	50	60	70	80
Angle	0→90	0→90	0→90	0→90	0→90	0→90	0→90	0→90	0→90	0→90	0→90	0→90	0→90	0→90	0→90	0→90	0→90	0→90	0→90	0→90

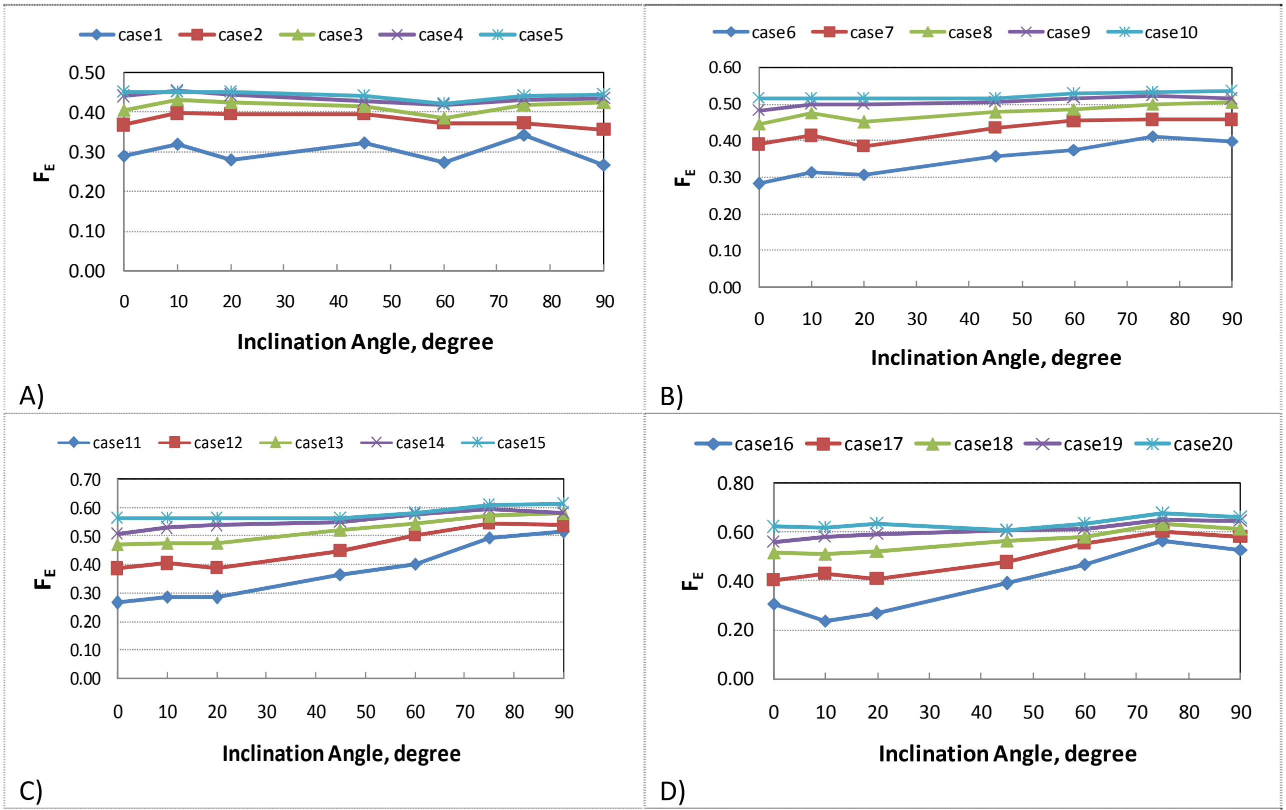

Figure 6: Variation of fraction of entrainment with angle of inclinations

Dependency of Entrainment Fraction on Dimensionless Parameters of X* and Re_{SL}

The parameters X* and Re_{SL} are defined as follows:

$$Fr_{Sg} = \sqrt{\frac{\rho_G v_{Sg}{}^2}{(\rho_L - \rho_G) g D \cos\theta}} \qquad Fr_{SL} = \sqrt{\frac{\rho_L v_{SL}{}^2}{(\rho_L - \rho_G) g D \cos\theta}}$$

$$X^* = \sqrt{\frac{\rho_G}{\rho_L}} \frac{\dot{m}_L}{\dot{m}_G} = \sqrt{\frac{\rho_L}{\rho_G}} \frac{v_{SL}}{v_{Sg}} = \frac{Fr_{SL}}{Fr_{Sg}} . \tag{1}$$

$$\mathrm{Re}_{SL} = \frac{\rho_L v_{SL} D}{\mu_L} . \tag{2}$$

Magrini (2009) entrainment fraction data are plotted in Figs. 7 and 8 as functions of X* and Re_{SL} for two different inclination angle ranges, respectively. Figure 9 shows the scatter when all the data plotted on one graph. It can be also seen in Fig. 8 that for the first group of angles of inclination (0-45^o) that at the maximum Re_{SL} the match is not as good as that at lower Re_{SL} specially at the highest value of X*. However, this is not seen in the second group of angles of inclination (60-90^o).

Entrainment Fraction Correlation

The effect of the pipe inclination angle for the range of X* studied can be correlated by two empirical relationships; one covering inclination angles from 0° to 45° and the other from 60° to 90°. Figure 10 displays the correlations. Equations 3 and 4 provide the empirical correlations for the inclination angle ranges of 0° to 45° and 60° to 90°, respectively.

$$F_E = 0.892\left(4\times10^{-6}\,\mathrm{Re}_{SL}^{1}\,X^{*-0.92}\right)^{0.874} . \tag{3}$$

$$F_E = 0.221\left(4\times10^{-6}\,\mathrm{Re}_{SL}^{1.4}\,X^{*-0.92}\right)^{0.403} . \tag{4}$$

It should be noted above correlations are developed for the range of 0.0011 <X* <0.0274.

Figure 11 shows the comparison between the measured and the predicted (Eq. 3) values of entrainment fraction for the inclination angle range from 0° to 45°. The measurements of Magrini (2009) were within ±10 % of the predicted value by Eq. 3. Figure 12 shows the comparison between the measured and the predicted (Eq. 4) values of entrainment fraction for the inclination angle range from 60° to 90°. The measurements of Magrini (2009) were within ±10 % of the predicted value by Eq. 4.

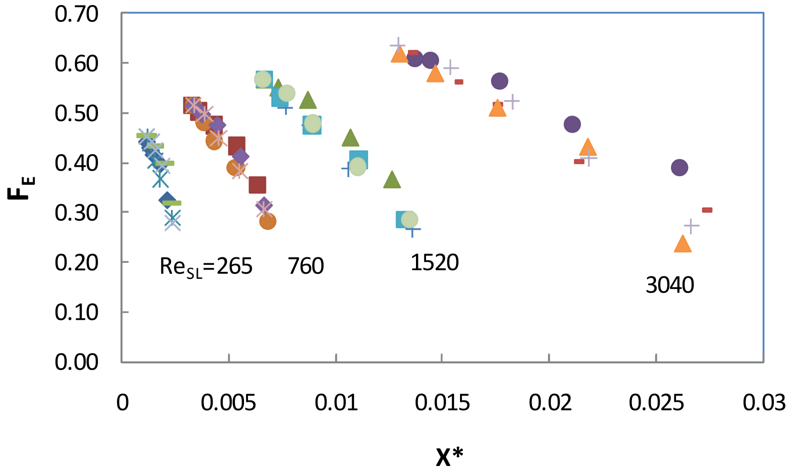

Figure 7: Entrainment Fraction vs. X* for 0, 10, 20 and 45 degrees.

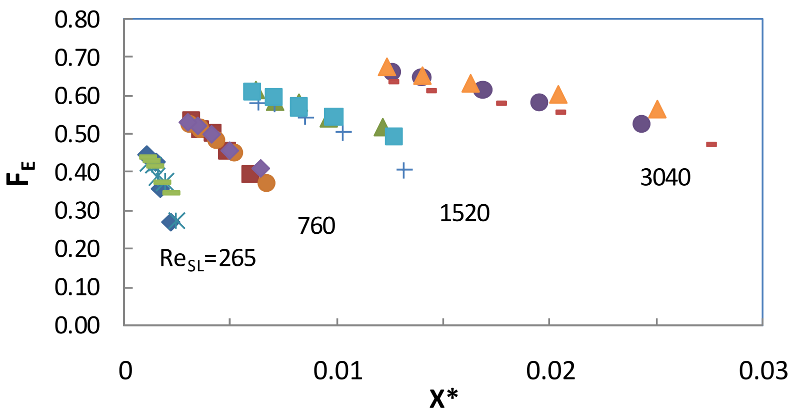

Figure 8: Entrainment Fraction vs. X* for 60, 75, and 90 degrees.

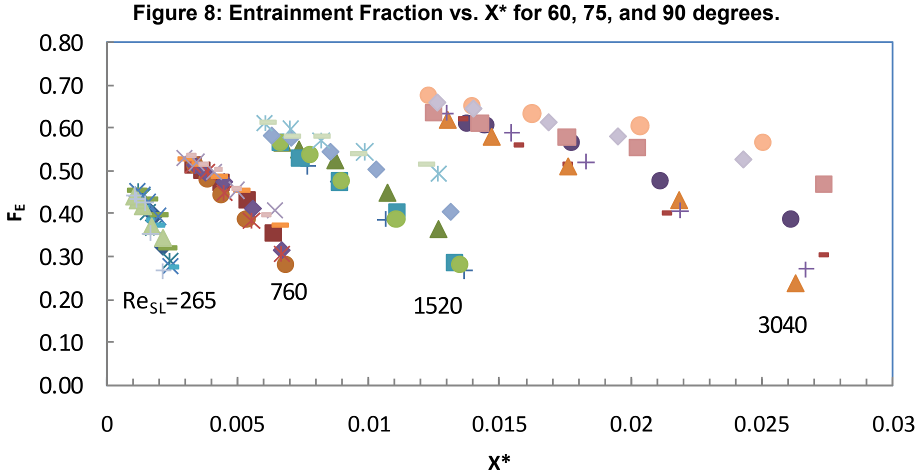

Figure 9: Entrainment Fraction vs. X* for all angles of inclination.

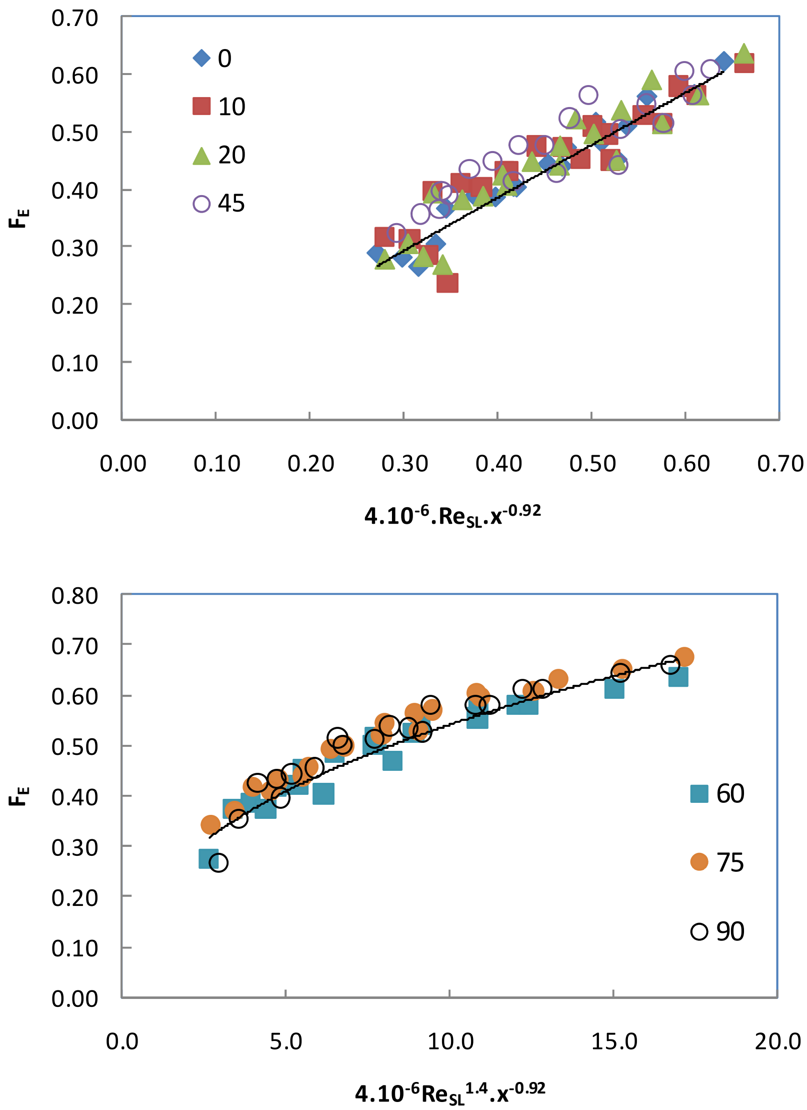

Figure 10: Fraction of entrainment correlation for Magrini (2009) data at different inclinations

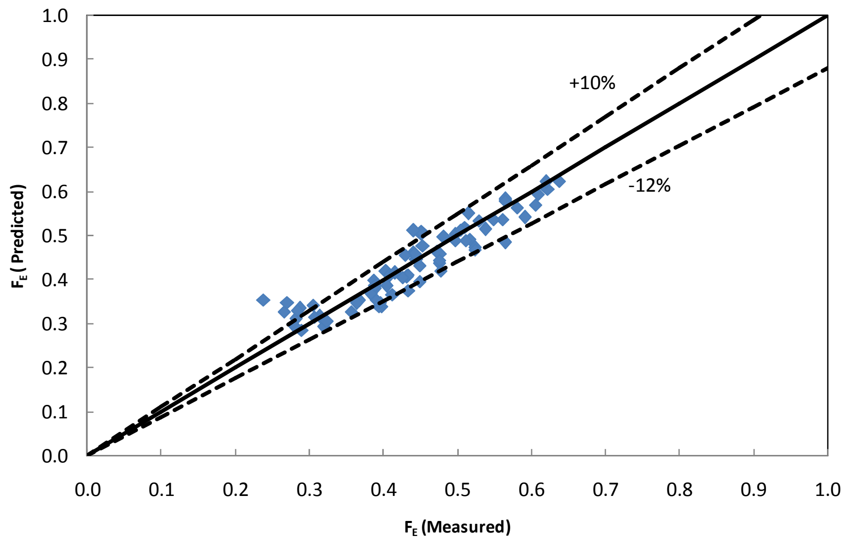

Figure 11: Comparison of the measured data (Magrini (2009)) with prediction by Eq. 3 for angle of inclination between 0° - 45°

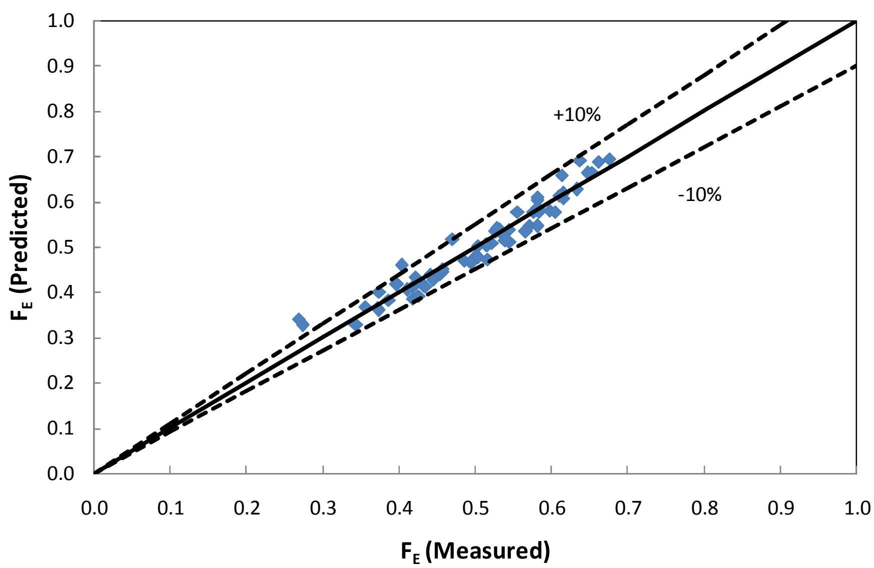

Figure 12: Comparison of the measured data (Magrini (2009)) with prediction by Eq. 4 for angle of inclination between 60° - 90° degrees.

Comparisons with Other Studies

In this section, the same parameters used in the analysis of Magrini (2009) data will be tested against other published work. It should be noted that pipe diameters and X* ranges are different in the other studies.

Ousaka et al. (1996)

Ousaka *et al.* (1996) conducted air/water annular flow experiments in a 25.4-mm (1-in.) ID pipe for superficial gas velocity range of 15 - 40 m/s, and superficial water velocity range of 0.06 - 0.2 m/s. The inclination angles were 0, 30, 45, 60 and 75 degrees. The range of X* for Ousaka data is $0.032<X^*<0.375$. This range is larger than that of Magrini (2009), which is $0.0011<X^*<0.0274$. It was concluded from their results that entrainment fraction is clearly dependent on pipe inclination.

A comparison of the above correlating parameters with Ousaka *et al.* (1996) is shown in Fig. 13. Figure 13 shows the trend of the Ousaka data. In general, Ousaka data can be classified into three groups of low, medium and high angle of inclinations. For the range of the operational conditions and angle of inclinations studied entrainment fraction increases with increasing pipe inclination and Re_{SL} $X^{*-0.92}$. Similar behavior is observed in Magrini's data.

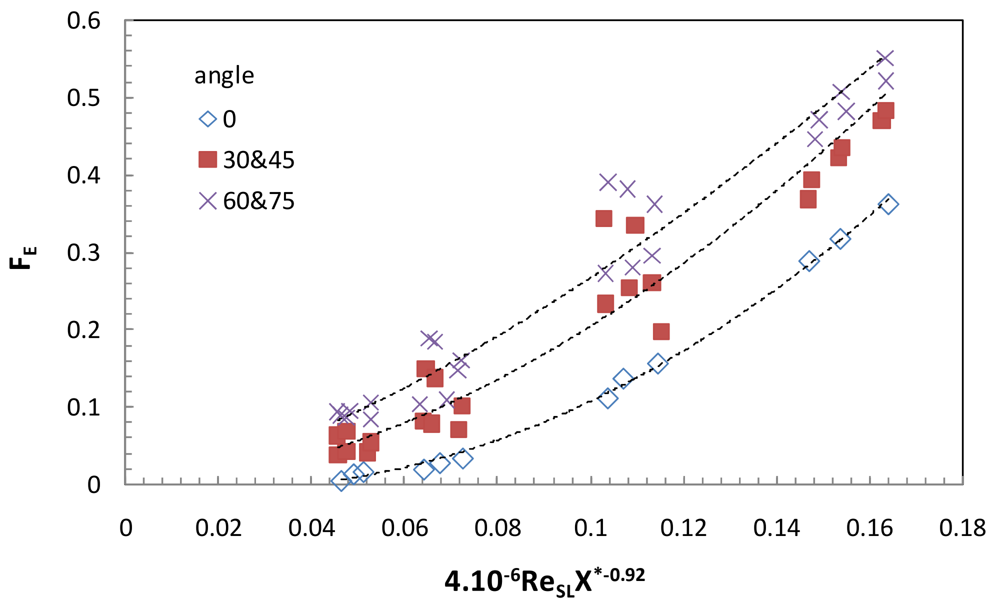

Figure 13: Entrainment Fractional at different inclination angles for Ousaka (1996) data

Figure 14 show the F_E vs. X* behavior. F_E decreases exponentially with increasing of X*. Similar behavior was noticed in Magrini (2009) data (Figs. 7 and 8). The effect of pipe inclination angle can be seen in Fig. 14. For the same X^*, the larger the angle of inclination is the higher the F_E becomes.

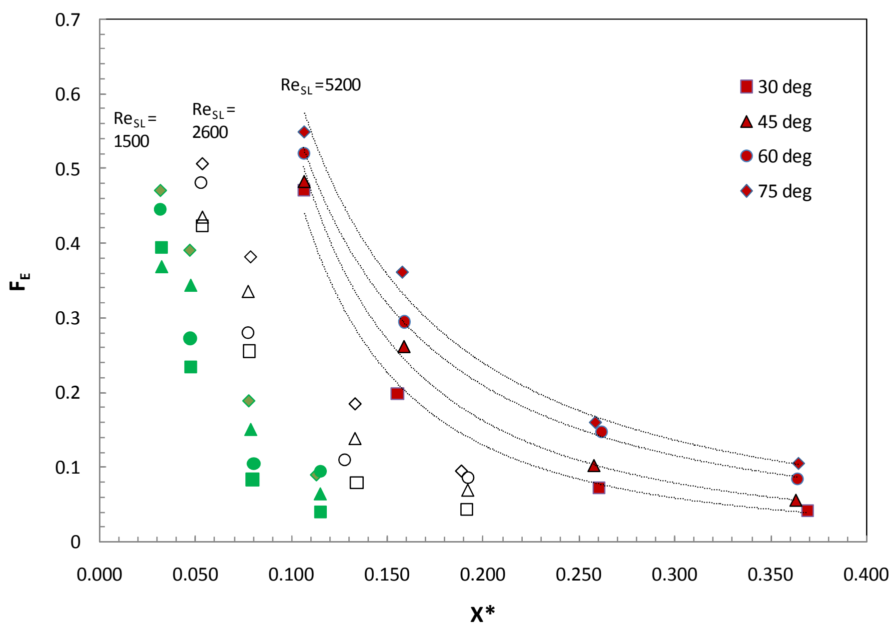

Figure 14: Entrainment Fraction vs. on X* for Ousaka (1996) for angle of 30, 45, 60 and 75 degrees.

Owen (1985)

Owen (1985) acquired entrainment data for upward vertical flow of air-water in a 0.03175 m ID. pipe. Figure 15 shows F_E vs. X* behavior. Figure 16 shows the performance of the correlating parameters proposed above using Magrini (2009) data. Owen data covers the following superficial liquid velocity, superficial gas velocity, and X* ranges, respectively: $0.0495<v_{SL}<0.4$; $17<v_{Sg}<72$; $0.0126<X^*<0.259$.

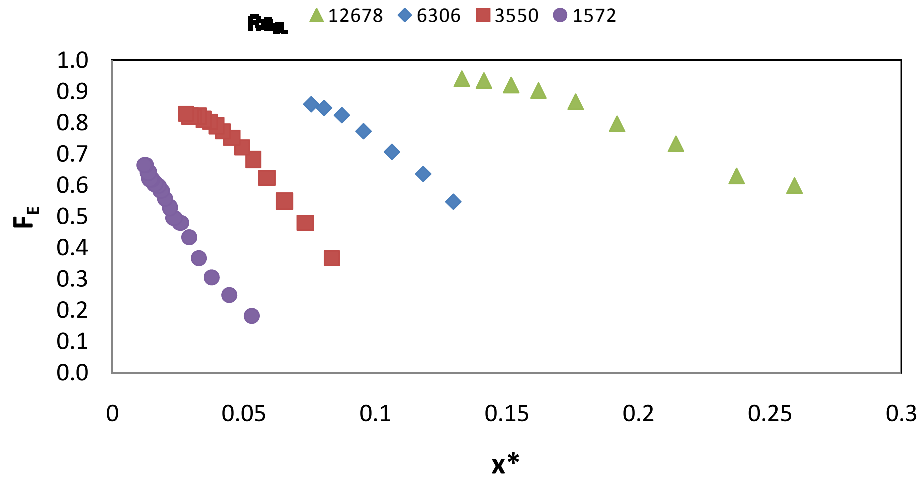

Figure 15: Dependence of Entrainment Fraction on X* for Owen (1985) data

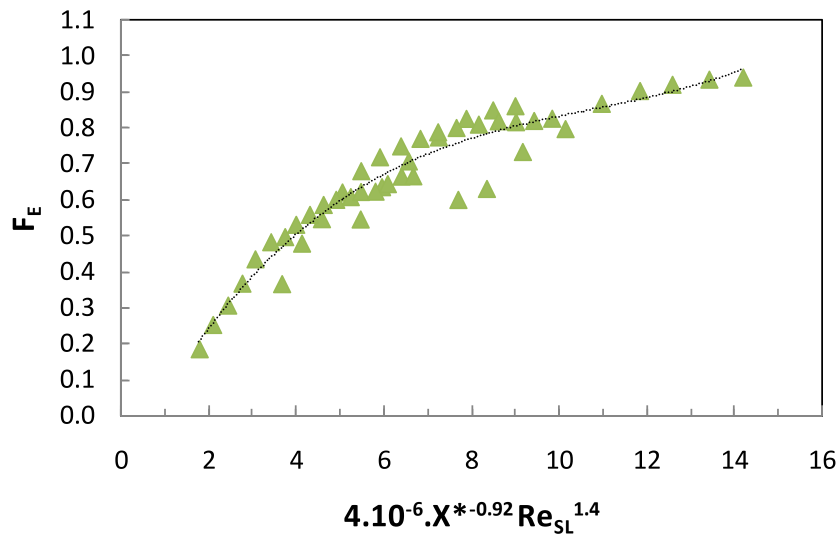

Figure 16: Performance of Entrainment Fraction Correlation Parameter for Owen (1985) Data

Shadel (1988)

Shadel (1988) acquired entrainment data for upward vertical flow of air-water in 0.0254 and 0.042 m ID. pipes. Figure 17 shows the performance of the correlating parameters proposed above using Magrini (2009) data.

In Shadel data, the X* ranges between 0.005 and 0.088. Shadel data indicates a pipe diameter effect.

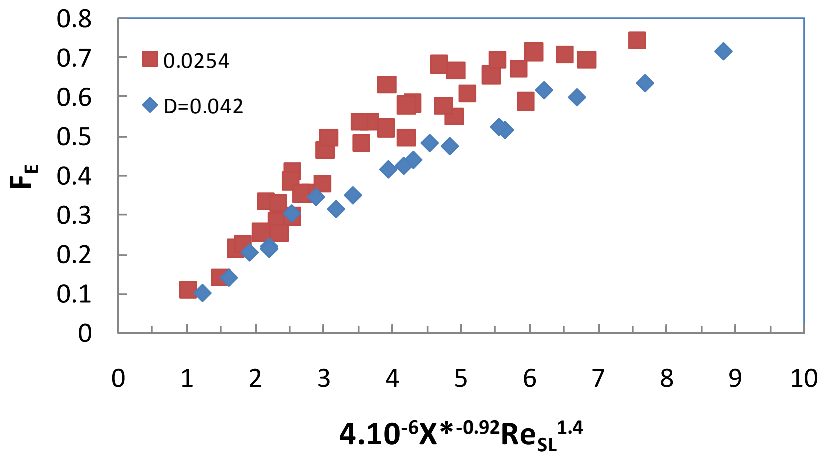

Figure 17: Performance of Entrainment Fraction Correlation Parameter for Shadel (1988) Data

Mantilla (2008)

Mantilla (2008) acquired liquid entrainment data for horizontal flow of air-water, air-water+butanol and air-water+salt+glycerin in a 0.0508 ID. pipe. The operational pressure and temperature where 206843 Pa and 21 C°. The fluid properties are shown in Table 3. Surface tension and liquid viscosity were variable in this work.

Figure 18 shows F_E vs. X* behavior. Figure 19 shows the performance of the correlating parameters proposed above using Magrini (2009) data. It is seen from Fig. 19 that for the condition studied by Mantilla, the surface tension has no effect on F_E at all while the viscosity showed significant effect.

Table 3: Fluid Properties of Mantilla (2008)

Fluid	Properties	Value
Air	Density (kg/m^3)	2.4
	Viscosity (Pa.s)	1.8E-5
Water	Density (kg/m^3)	997
	Viscosity (Pa.s)	1.02E-3
	Surface tension (N/m)	0.073
Water-5% (V/V) Butanol	Density (kg/m^3)	989
	Viscosity (Pa.s)	1.22E-3
	Surface tension (N/m)	0.035
Water-47% (V/V) Glycerin-Salt	Density (kg/m^3)	1130
	Viscosity (Pa.s)	7.1E-3
	Surface tension (N/m)	0.061

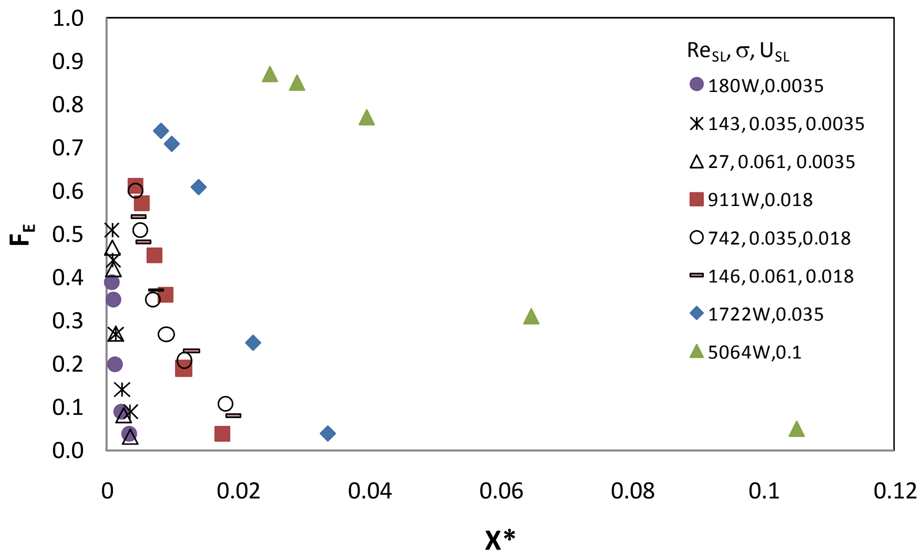

Figure 18: Entrainment Fraction vs. X* for Various Surface Tension, vSL and ReSL (Mantilla (2008) Horizontal Data)

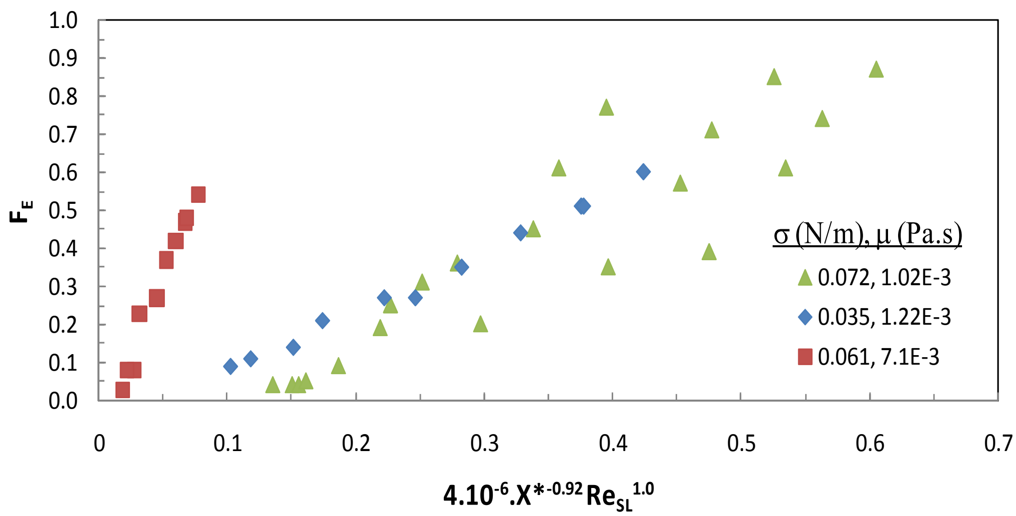

Figure 19: Entrainment Fraction Variation with Liquid Surface Tension and Viscosity

Entrainment Fraction Correlation Using All Available Data

High inclination angles

Figure 20 shows the entrainment fraction as a function of X* and Re_{SL}. At high inclination angles, wave structure and liquid film distribution are almost the same, and the only difference left is the pipe diameter. A pipe diameter effect is clearly identified from Fig. 20. A correction for the pipe diameter (Eq. 5) is needed to have similar trend for all cases which is shown in Fig. 21.

$$F_E = (D/D_0)^{-0.44}\left\{0.24LN\left(X^{*-0.92}\,\mathrm{Re}_{SL}{}^{1.4}\right) - 2.98\right\} \quad (5)$$

Where D_0 is the largest pipe diameter (0.0762 m) and D is the pipe diameter for all cases. Equation 5 well correlates the experimental data within +20% and -15% as shown in Fig. 22. It can be noticed in Fig. 22 that almost all outlier points are from one study.

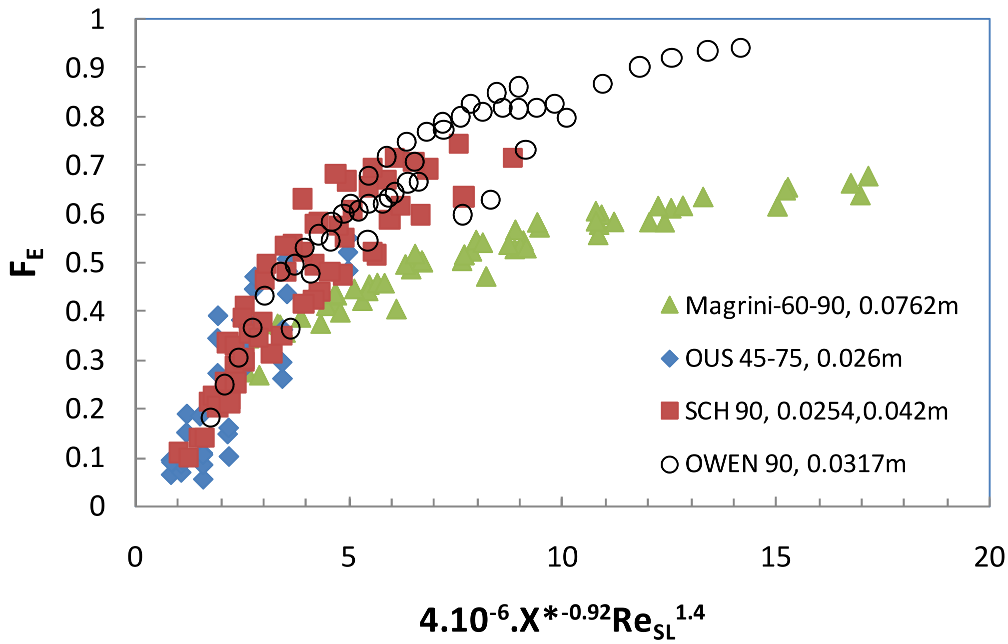

Figure 20: Entrainment fraction for high inclination angles (with no correction for pipe diameter)

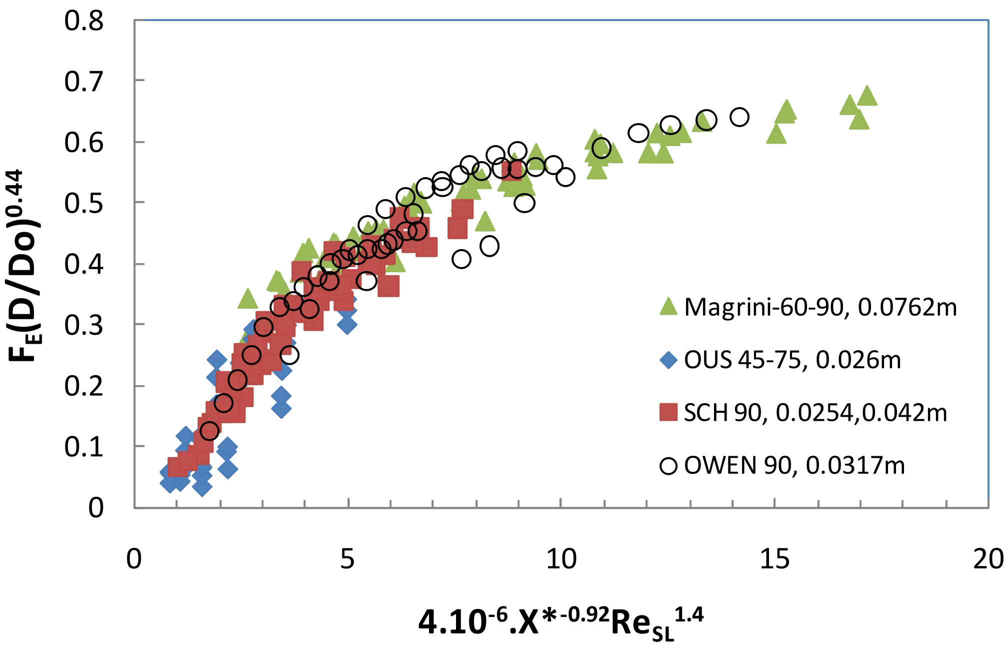

Figure 21: Entrainment fraction for high inclination angles (with correction for pipe diameter)

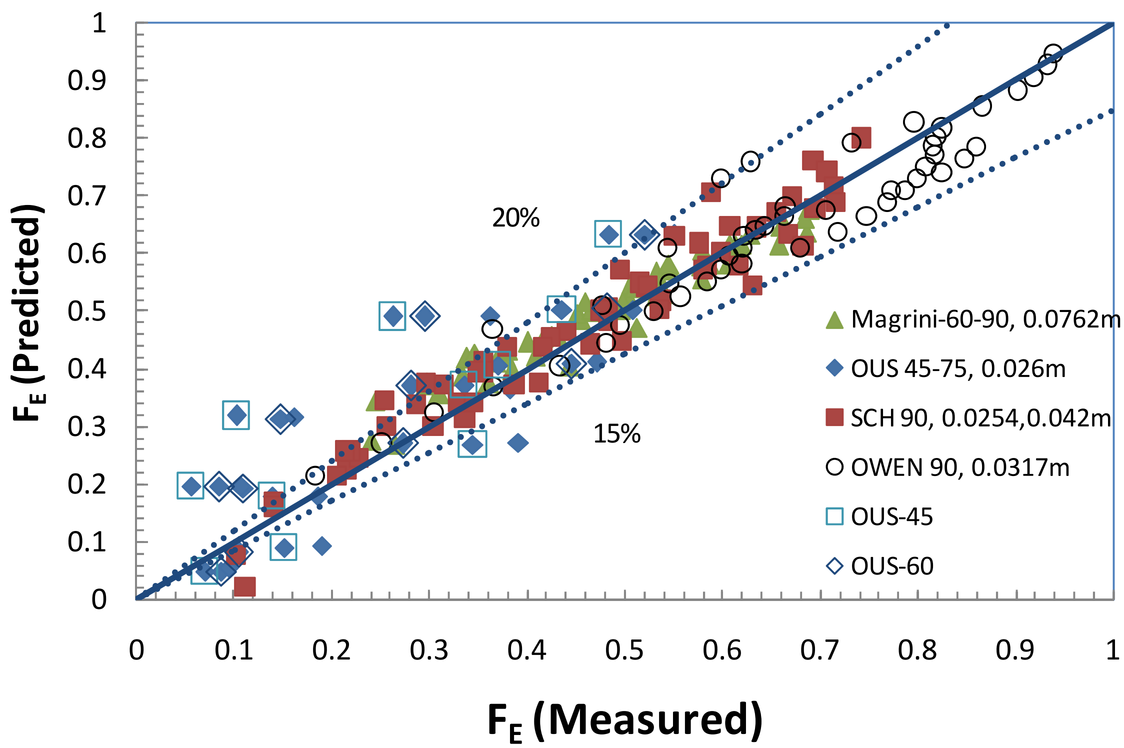

Figure 22: Comparison between measured fraction of entrainment and prediction by Eq. 4.

Low inclination angles

An attempt to correlate entrainment fraction at low inclination angles (0° - °45) is shown in Figs. 23 and 24 for the data of Ousaka, Dallman, Luarinat, Paras, Mantilla and Magrini. The correlation is based on X* and Weber number based on superficial gas velocity, We_{Sg} is defined as:

$$We_{Sg} = \frac{\rho_G {v_{Sg}}^2 D}{\sigma}\left(\frac{\rho_L - \rho_G}{\rho_G}\right)^{1/3} \qquad (6)$$

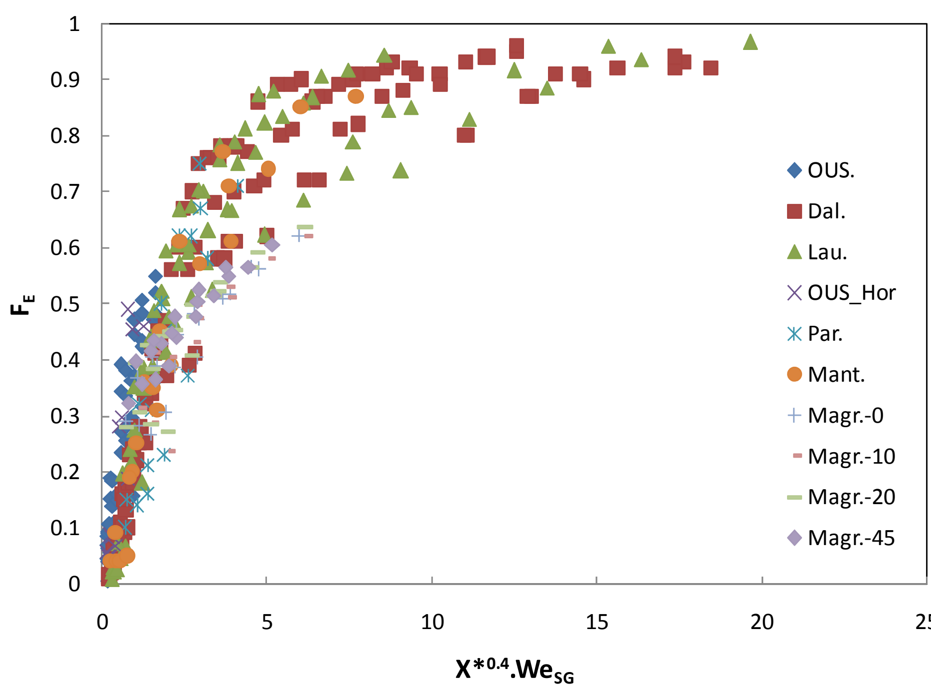

Figure 23: Entrainment fraction as a function of X* and WeSG

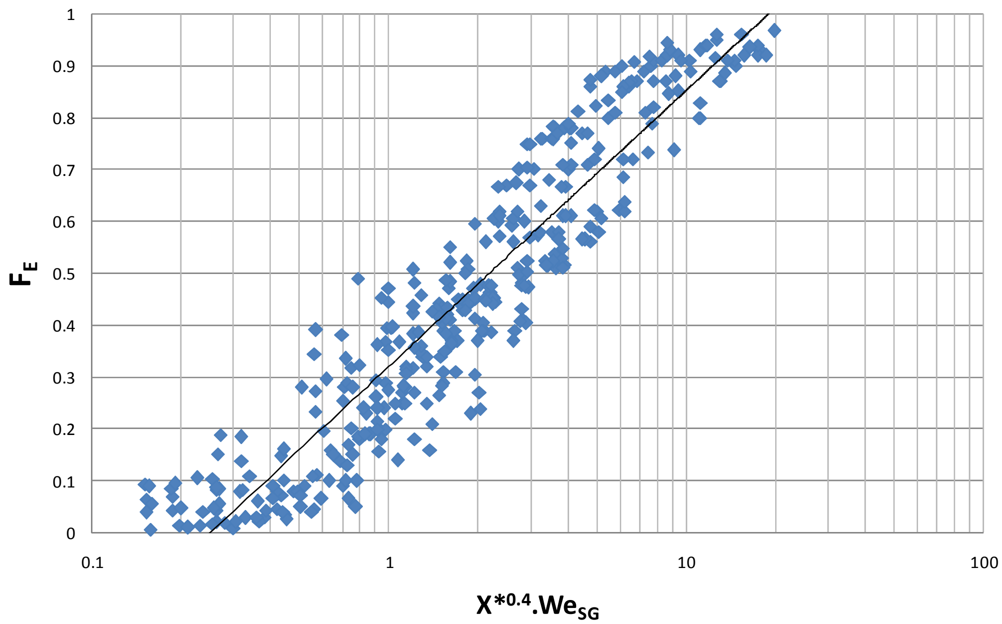

Figure 24: Entrainment fraction as a function of X* and WeSg

The effect of pipe diameter at lower pipe inclination angles is very large and strongly associated with wave structure, liquid film thickness and distribution variation with inclination. The effect of pipe diameter at high inclination angles (>°45) is less since the wave structure and the liquid film distribution variations with inclination will be less. In fact, at high inclination angle and large gas velocity, the average value of celerity and the liquid film thickness with pipe inclination is almost the same. A correlation for the combined effect of pipe diameter, wave structure and film distribution on F_E at lower inclination angles could not be found.

Problems with Some of the Entrainment Fraction Models

Sawant et al. (2008)

Sawant *et al.* (2008) developed a simple, explicit correlation based on the Weber number and liquid phase Reynolds number, as defined by Ishii and Mishima (1989). This correlation was verified with experimental data under high flow and high pressure conditions. Data was collected in a 9.4-mm (0.37-in.) ID pipe at pressures of 1.2, 4, and 6 bar, superficial gas velocities of 15 to 100 m/s, and superficial liquid velocities of 0.05 to 0.75 m/s. The methodology for the modeling of entrainment fraction proposed by Sawant *et al.* is shown in Fig. 25. The entrainment curve is divided into three regions: a Weber number dependent region O-A, a transition region A-B and a liquid phase Reynolds number dependant region B-C.

As the superficial gas velocity is increased, a higher entrainment fraction results. At point A, the first transition point, in Fig. 25, the liquid film flow rate decreases sufficiently, and the interfacial momentum transfer is affected. Thus, in this part of the curve (A-B), the entrainment fraction depends on both the liquid phase Reynolds number and the Weber number. The liquid film flow rate decreases further with the increase in the superficial gas velocity. At point B, the second transition point, there is no more interaction between the gas core and the liquid film. The liquid film in this region (B-C) gets submerged into the viscous sub-layer of the core gas flow, leading to the suppression of entrainment. In this region the further increase in the superficial gas velocity has no effect on the entrainment fraction which stays constant. The liquid film flow rate at both the transition points and at the limiting entrainment fraction region increases with the increase in the liquid phase Reynolds number.

They proposed the following correlation for the prediction of the entrainment fraction:

$$F_E = F_{E,\max} \tanh(\alpha We^{1.25}) \,. \tag{7}$$

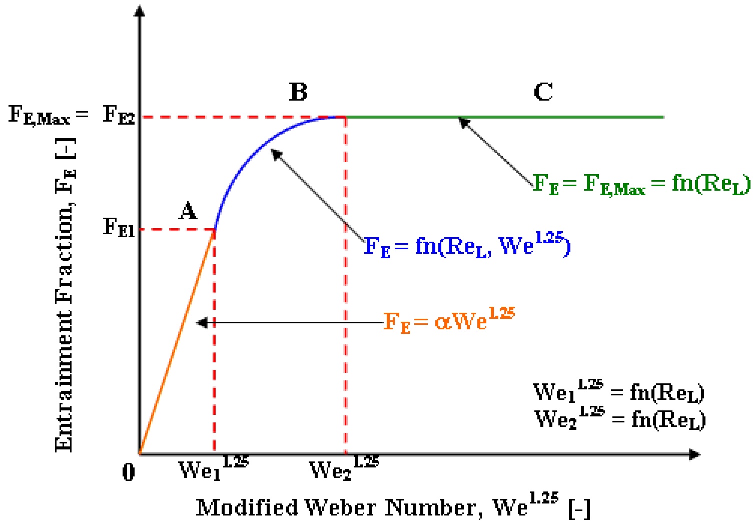

Figure 25: Sawant et al. (2008) Correlation Methodology

.

Where $F_{E,max}$ is the maximum entrainment fraction defined as a function of liquid phase Reynolds number and limiting liquid film Reynolds number. Since no satisfactory correlation is available for the prediction of limiting entrainment fraction, the following correlation for the prediction limiting liquid film Reynolds number obtained from the experimental data is proposed.

$$F_{E,Max} = 1 - \mathrm{Re}_{f,\lim} / \mathrm{Re}_{SL} , \quad (8)$$

where

$$\mathrm{Re}_{f,\lim} = 250 \ln(\mathrm{Re}_{SL}) - 1265 . \quad (9)$$

Coefficient α accounts for the dependence of the transition points A and B on liquid phase Reynolds number. Based on the experimental data, the following correlation was obtained

$$\alpha = 2.31 \times 10^{-4} \mathrm{Re}_{SL}^{-0.35} . \quad (10)$$

The limiting liquid film flow rate occurs at high gas velocity at which the suppression of entrainment takes place. In Fig. 26, $Re_{f,lim}$ measured by Owen *et al.* (1985) in 3.2 cm diameter test section and Schadel (1988) in 4.2 cm diameter test section are plotted against the liquid phase Reynolds number Re_{SL} along with Sawant *et al.* (2008) experimental data. It can be observed that the $Re_{f,lim}$ initially increases with the liquid phase Reynolds number and asymptotically approaches a constant value at higher superficial liquid Reynolds number. Very limited experimental data is available in literature on the $Re_{f,lim}$. Many researchers assumed that the limiting liquid film Reynolds number at which the suppression of entrainment takes place is same as the liquid film Reynolds number at the onset of entrainment at very high gas velocity (Asali *et al.*, 1985; Owen *et al.*, 1985 and Schadel, 1988). However, just before the onset of entrainment, there are no entrained droplets in the gas phase. Therefore, the correlations developed for the prediction of onset of entrainment are applicable when the gas phase is pure. While the mechanism of suppression of entrainment might be very similar to the onset of entrainment under high gas velocity, we need to consider the effect of entrained droplets on the gas phase turbulence while modeling the suppression of entrainment.

The correlation given with Eq. 9 results in negative values of $Re_{f,lim}$ for $Re_{SL}<157$ as shown in Fig. 26B. In addition, it displays a strange behavior for the limiting entrainment fraction $F_{E,max}$ at lower values of Re_{SL} ($Re_{SL}<500$) as shown in Fig. 27.

Figure 28 shows the poor performance of Swant et al. correlation against Magrini (2009) data. A modification is made to Sawant *et al.* model by introducing the parameter X*. The modified equation is given in Eq. 11.

$$F_E = F_{E,\max} \tanh(X^{*0.4} \alpha We^{1.25}) . \quad (11)$$

Figure 29 shows a comparison between the measured fractions of entrainment and predicted by Modified Sawant *et al.* Some of the outsider points are due to the strange behavior of the correlation equation of $Re_{f,lim}$ in Eq. 9. Fig. 30 shows the same figure (Fig. 29) but for the points with $Re_{SL}> 900$.

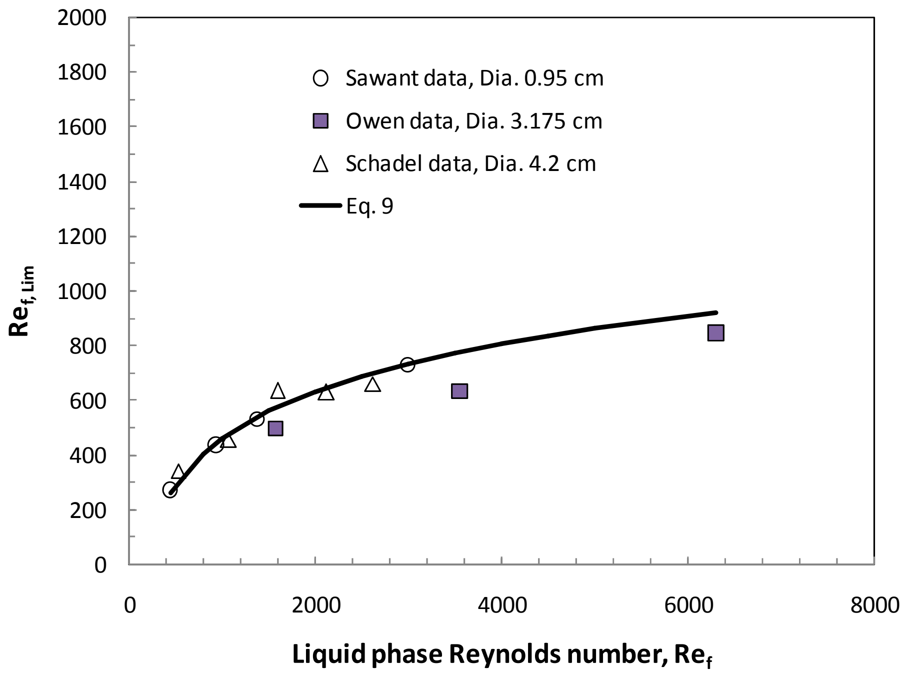

Figure 26A: Variation of limiting liquid film Reynolds number from Sawant et al. (2008)

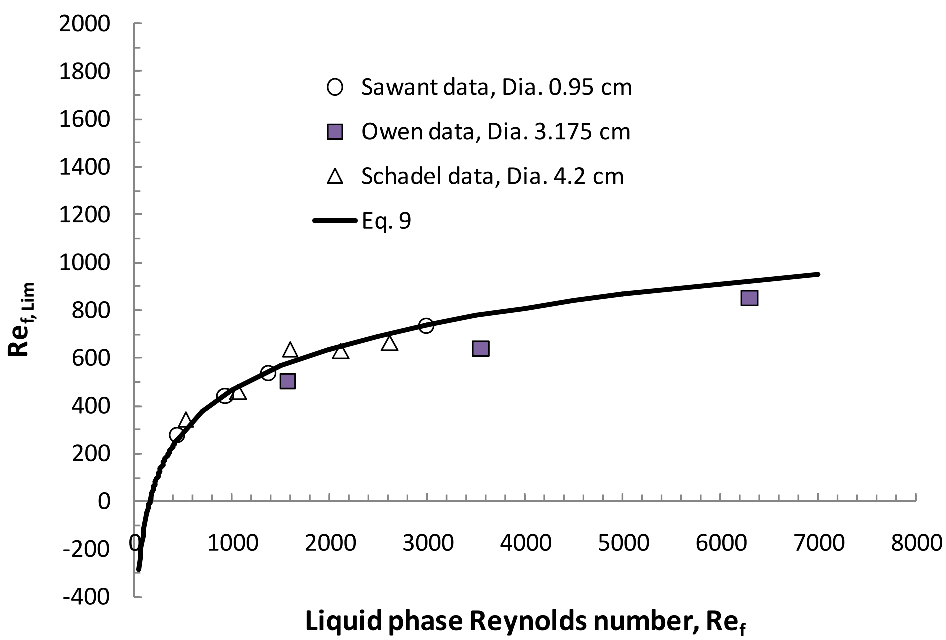

Figure 26B: Variation of limiting liquid film Reynolds number from Sawant et al. (2008) (extended range)

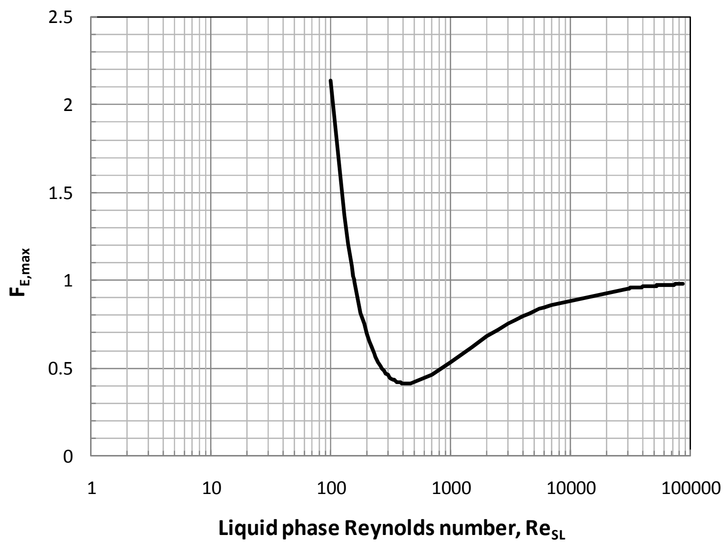

Figure 27: Variation of maximum entrainment fraction with liquid phase Reynolds number

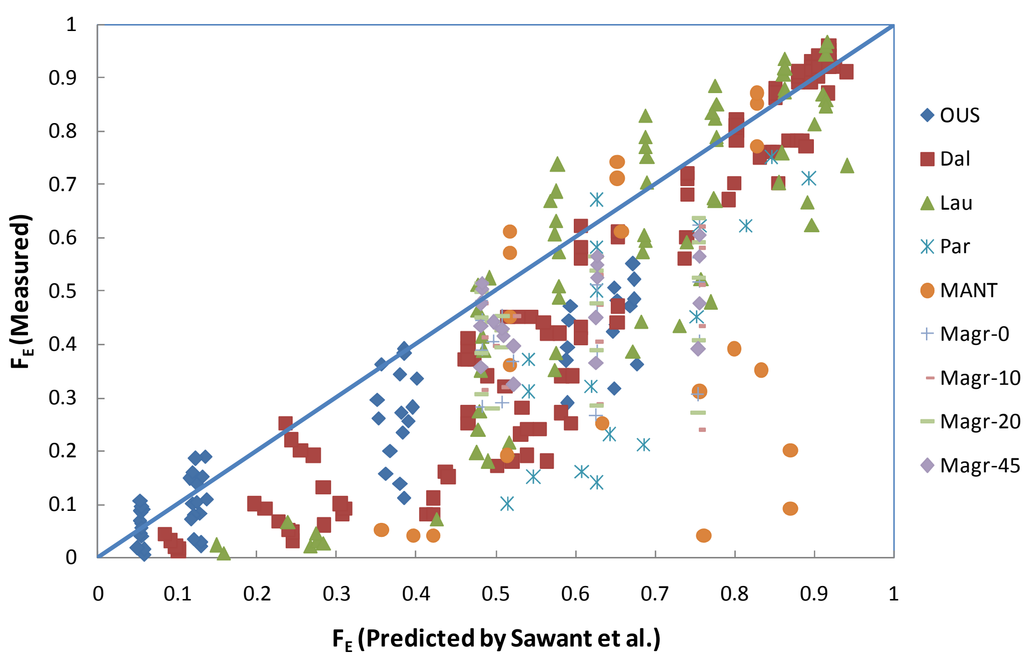

Figure 28: Comparison between the measured fraction of entrainment and predicted by Sawant et al.

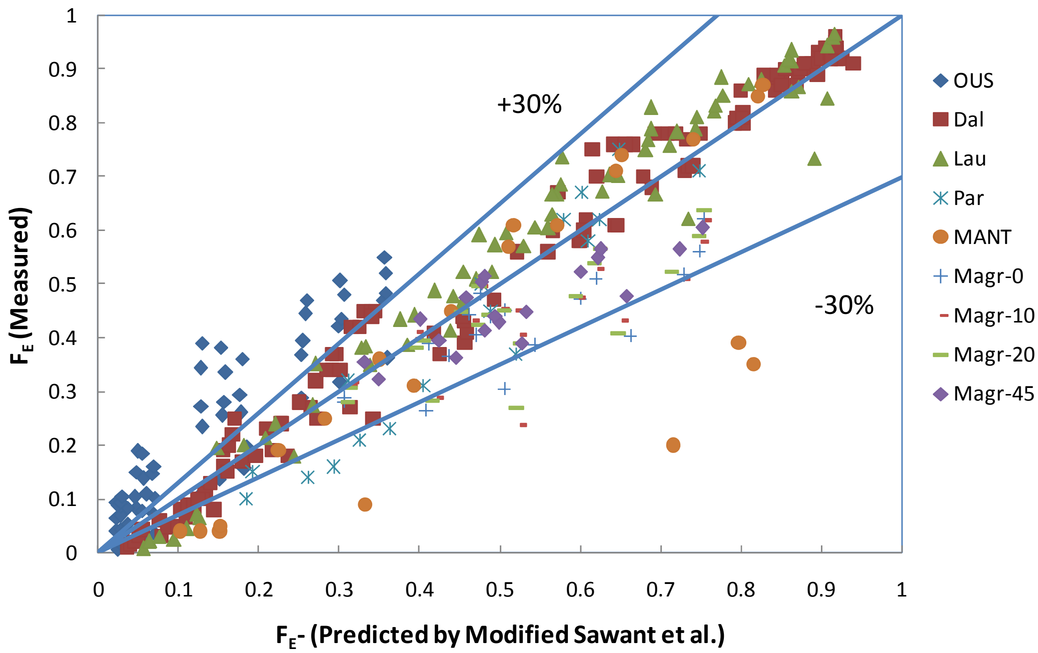

Figure 29: Comparison between the measured fraction of entrainment and predicted by Modified Sawant et al.

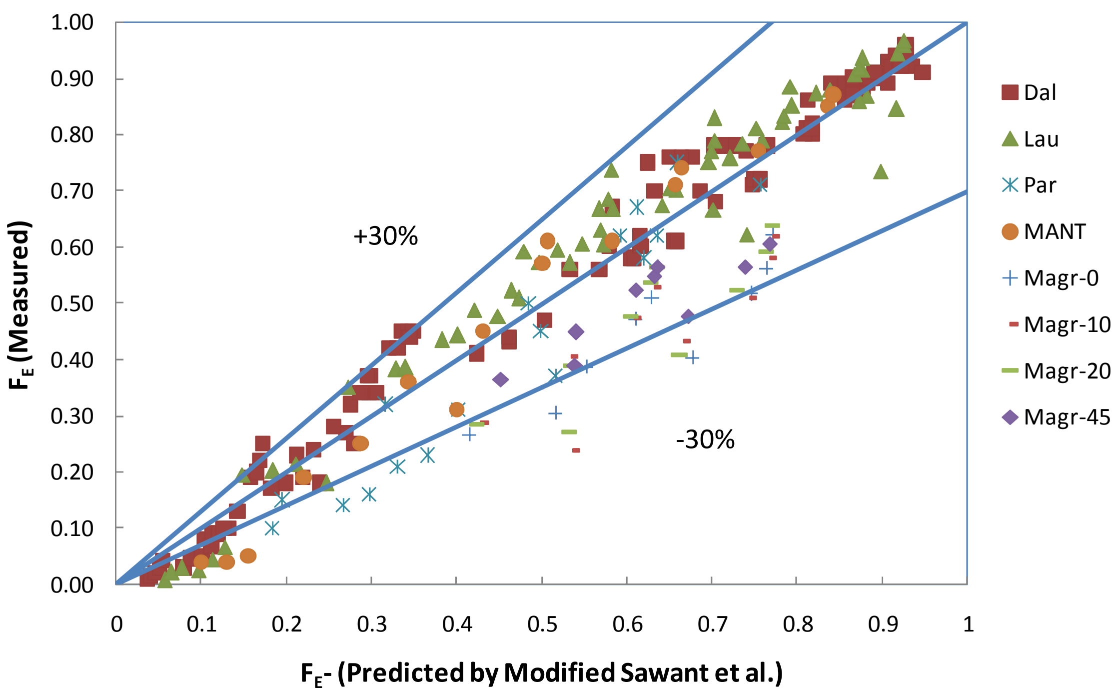

Figure 30: Comparison between the measured fraction of entrainment and predicted by Modified Sawant et al. for only ReSL> 900

Pan and Hanratty

Pan and Hanratty (2002b-horizontal)) developed an entrainment correlation for low viscous fluids based on balancing the rates of droplet deposition and atomization. For low viscosity liquids, the initiation of atomization occurs when disturbance waves appear on the liquid layer. Effects of gravity and droplet size on entrainment are considered. Pan and Hanratty correlations are the only correlations to explicitly consider a critical film flow rate in the maximum entrainment fraction calculation. The entrainment correlation is defined as

$$\frac{F_E / F_{E,\max}}{1 - F_E / F_{E,\max}} = 9\times10^{-8}\left(\frac{D v_G{}^3 \sqrt{\rho_L \rho_G}}{\sigma}\right)\left(\frac{\rho_G{}^{1-m}\mu_G{}^m}{d_{32}{}^{1+m} g \rho_L}\right)^{1/(2-m)}, \quad (12)$$

where $F_{E,max}$ is the maximum entrainment defined as

$$F_{E,\max} = 1 - W_{F,cr} / W_L \ . \quad (13)$$

$W_{F,cr}$ is the critical liquid film flow rate calculated using a correlation based on experimental work by Andreussi *et al.* (1985)

$$W_{F,cr} = 0.25 \mu_L \pi D \, \mathrm{Re}_{F,cr} \ , \quad (14)$$

where

$$\mathrm{Re}_{F,cr} = 7.3(\log w)^3 + 44.2(\log w)^2 - 263 \log w + 439 \ , \quad (15)$$

and

$$w = (\mu_L/\mu_G)\sqrt{\rho_G/\rho_L} \ . \quad (16)$$

Values of 0, 0.6, or 1 are used for exponent *m* in Eq. 12 depending on the drag coefficient calculation method of the terminal velocity of droplets. The Sauter mean diameter, d_{32}, is calculated using one of two correlations presented in the work.

Predictions of $F_E/F_{E,max}$ were compared to values obtained by Dallman (1978), Laurinat (1982), Williams (1990), and Paras and Karabelas (1991b). Results showed good agreement with data for the 23.1-mm pipe ID, under prediction for the 50.8-mm ID data, and over prediction for the 95.3-mm ID data. Equation 15 was derived from measurements for w = 1.8 to 28, and it should not be used outside this range.

The problem in this procedure is in predicting the critical liquid film flow rate, $W_{F,cr}$. Many cases with low Re_{SL} results in $W_{F,cr}$ to be greater than W_L leading to a negative value for $F_{E,\ max}$. This problem is due to the fact that the Re_{LFC} or $W_{F,cr}$ is developed as a function of w only. w is only function of the physical properties of gas and liquid (viscosity and density). This ignores the effect of the total liquid flow rate W_L on the W_{LFC} , the critical film flow rate below which atomization does not occur. In other words ignoring this dependency means the disturbance wave effects do not exist. This is certainly not correct. Pan and Hanratty's approach was tested for air and water data with range of w between 1.97 to 3.1 which is in the valid range of Equation 15 as claimed and found a negative $F_{E,max}$ for the all data with $Re_{SL} < 275$.

A test for the validity of this model is explained in this example. Consider an air-water annular flow at standard conditions in 0.072 m ID, ρ_L= 1000 kg/m^3, μ_L =0.001 Pa.s, Re_{Fcr}=370, $W_{F,cr}$ =0.022144 kg/s. Then $F_{E,max}$ will be zero if W_L=$W_{F,cr}$=0.022144 kg/s. This means all the cases with superficial liquid velocity, V_{SL}< 0.004856 m/s will have negative value of $F_{E,max}$. which is unphysical and the opposite of what was observed in Magrini (2009) and Mantilla (2008). The problem of predicting FE, max in both Pan and Hanratty and Sawant *et al.* is demonstrated in Fig. 31.

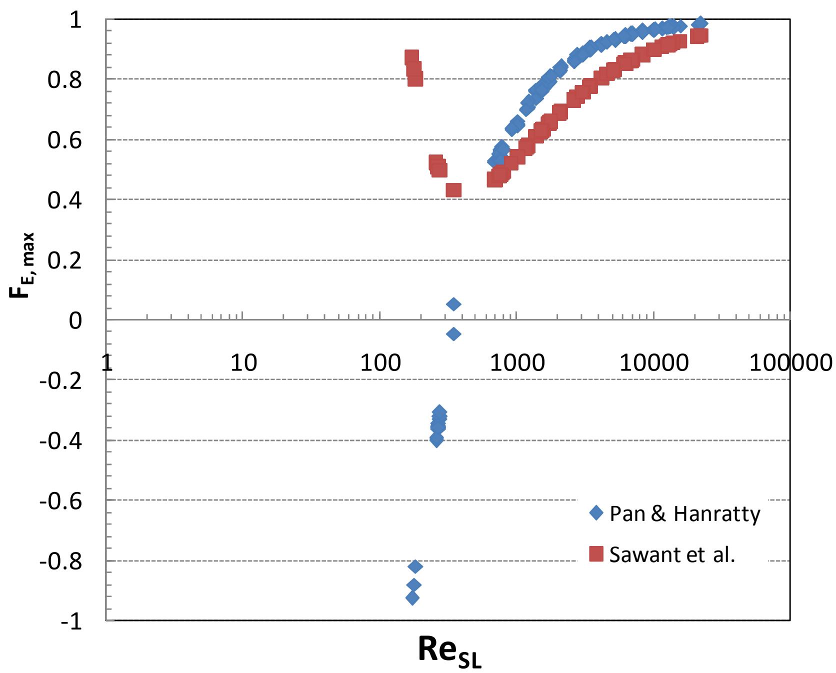

Figure 31: Comparison of maximum fraction of entrainment modeled by Pan and Hanratty and Sawant et.al. (Semi-log scale)

Summary and Conclusions

The following conclusions can be drawn from this study:

- Sensitivity analysis has been done and shown the importance of the inclination angle and the wave characteristics on the fraction of entrainment in an annular flow.
- Correlations for entrainment fraction in terms of X* and Re_{SL} for Magrini's Data at low and high inclination have been found.
- Comparison with all available data has been performed.
- Pipe inclination effect on the fraction of entrainment is pronounced at high v_{SL} and low v_{Sg}
- Entrainment fraction increases with increase in the inclination angle especially at high v_{SL} and low v_{Sg}
- The available correlations for maximum entrainment fraction have serious problems at low v_{SL} and need to be modified.

Recommendations

- Almost all available data in literature is for air-water. All available correlation was based on air-water results. The effect of surface tension can only be implemented if a complete set of data is established at variable surface tensions and for all pipe inclinations. More accurate entrainment fraction measurements are needed for all inclination angles in different pipe diameter.
- Effect of pipe inclination angles on the onset of droplet entrainment has not been studied. Inception criteria for droplet entrainment in film flow as a function of pipe inclination angles is also important for entrainment modeling.

Nomenclature

Symbol	Description	Unit
A_{pipe}	Cross sectional area of the pipe	m^2
c	Celerity	m/s
D	Diameter	m
F_E	Entrainment fraction	/
g	Acceleration due to gravity	m/s^2
h_L	Liquid film thickness	m
H_L	Holdup	/
h_w	Wave height	m
ID	Inner diameter of pipe	/
L	Length	m
L_w	Wave spacing	/
m	Exponent for Pan and Hanratty (2002b) correlation	/
$\left(\frac{dp}{dL}\right)$	Total pressure gradient	Pa/m
q	Volumetric flow rate	m^3/s
Re	Reynolds number	/
T	Temperature	^oC
v	Velocity	m/s
W	Mass flow rate	kg/s
We	Weber Number	/
X	Lockhart-Martinelli parameter	/
X^*	Froude number ratio based on superficial velocities Eq. 1	/
Δh_w	Wave Amplitude	m
ϑ	Inclination angle	degree
λ	Wavelength	m
ρ	Density	kg/m^3
σ	Surface tension	N/m
μ	Viscosity	Pa.s

Subscripts

Symbol	Description	Unit
cr	Critical	/
E	Entrained	/
F	Film	/
G	Gas	/
L	Liquid	/
LE	Liquid Entrained	/
lim	Limiting	/
max	Maximum	/
SG	Superficial gas	/
SL	Superficial liquid	/
w	Wave	/

References

Al-Sarkhi A and Hanratty TJ. Effect of pipe diameter on the performance of Drag-Reducing Polymers in annular gas-liquid flows. Trans IChemE, Chemical Engineering Research and Design. 2001; 79 Part A: 402-408.

Andreussi, P., Asali, J., Hanratty, T.J., 1985. "Initiation of roll waves in gas–liquid flows," AIChE J., 31(1), pp. 119-126.

Azzopardi BJ, Whalley PB. Artificial waves in annular two-phase flow. ASME Winter Annual Meeting, Chicago, IL, November 16-21, 1980.

Asali, J.C., Leman, G.W., Hanratty, T.J., 1985. Entrainment measurement and their use in design equations. PCH Physicochem. Hydrodyn. 6, 207–221.

Dallman, J.C., 1978. "Investigation of Separated Flow Model in Annular Gas-Liquid Two-Phase Flow," PhD Dissertation, University of Illinois at Urbana, Champaign.

Geraci G, Azzopardi BJ and van Maanen HRE. Inclination Effects on Circumferential Film Flow Distribution in Annular Gas/Liquid Flows. AIChE Journal. 2007a; 53 (5):1144-1150.

Geraci, G, Azzopardi BJ, and van Maanen HRE. Effect of inclination on circumferential film thickness variation in annular gas/liquid flow, Chemical Engineering Science. 2007b; 62: 3032 – 3042.

Ishii, M., and Mishima, K., 1989. "Droplet Entrainment Correlation in Annular Two-Phase Flow," Int. J. Heat and Mass Transfer, 32(10), pp. 1835-1846.

Laurinat, J.E., 1982. "Studies on the Effects of Pipe Size on Horizontal Annular Two-Phase Flows," PhD Dissertation, University of Illinois at Urbana, Champaign.

Magrini, K.L., 2009. "Liquid Entrainment in Annular Gas/Liquid Flow in Inclined Pipes," MS Thesis, University of Tulsa.

Mantilla, I., 2008. "Mechanistic Modeling of Liquid Entrainment in Gas in Horizontal Pipes," PhD Dissertation, University of Tulsa.

Ousaka, A., and Kariyasaki, A., 1992. "Distribution of Entrainment Flow Rate for Air-Water Annular Two-Phase Flow in a Horizontal Tube," JSME Int. J., 35(2), pp. 354-360.

Ousaka, A., Nagashima, T., and Kariyasaki, A., 1996. "Effect of Inclination on Distribution of Entrainment Flow Rate in an Inclined Upward Annular Flow," Trans. the Japan Soc. of Mech. Eng., Part B, v 62, n 600, pp. 2950-2956.

Owen, D.G., Hewitt, G.F., and Bott, T.R., 1985. "Equilibrium Annular Flows at High Mass Fluxes: Data and Interpretation," PCH PhysioChemical Hydrodynamics, 6(1/2), pp. 115-131.

Pan, L., and Hanratty, T.J., 2002b. "Correlation of Entrainment for Annular Flow in Horizontal Pipes," Int. J. Multiphase Flow, 28(3), pp. 385-408.

Paras, S.V., and Karabelas, A.J., 1991. "Droplet Entrainment and Deposition in Horizontal Annular Flow," Int. J. Multiphase Flow, 17(4), pp. 455-468.

Sawant, P., Ishii, M., and Mori, M., 2008. "Droplet Entrainment Correlation in Vertical Upward Co-Current Annular Two-Phase Flow," Nuclear Engineering and Design, 238, pp. 1342-1352.

Schadel, S.A., 1988. "Atomization and Deposition Rates in Vertical Annular Flow," PhD Dissertation, University of Illinois at Urbana, Champaign.

Sutharshan B ,Kawaji M and Ousaka A. Measurement of circumferential and axial liquid film velocities in horizontal annular flow. Int. J. Multiphase Flow. 1995; 21 (2): 193-206.

Williams, L.R., 1990. "Effect of Pipe Diameter on Horizontal Annular Two-Phase Flow," PhD Dissertation, University of Illinois at Urbana, Champaign.

Fluid Flow Projects

Unified Drift Velocity Closure Relationship for High Viscosity Oil-Gas Flow

Benin Chelinsky Jeyachandra

Dr. Abdel Al-Sarkhi

Advisory Board Meeting, November 3, 2010

Outline

- Objectives
- Introduction
- Literature Review
- Drift Velocity Correlations
  - Horizontal Flow
  - Vertical Flow
  - Inclined Flow
- Conclusions
- Future Tasks

Objectives

- Develop a Unified Drift Velocity Correlation for High Viscosity Oil-Gas Flow
- Validate Drift Velocity Correlations with Experimental Results

Introduction

- High Viscosity Oil
  - Definition
  - Significance of High Viscosity Oil
  - Observed Flow Patterns
  - Discrepancy in Modeling
- Drift Velocity
  - Definition
  - Significance of Modeling Drift Velocity

Literature Review

- Parameters Affecting Drift Velocity
- Drift Velocity
  - Horizontal Flow
  - Vertical Flow
  - Inclined Flow

Fluid Flow Projects

Advisory Board Meeting, November 3, 2010

Literature Review

- Expression for Translational Velocity and Drift Velocity
  - Nicklin *et al.* (1962)

$$v_t = C_o v_s + v_d$$

Fluid Flow Projects

Advisory Board Meeting, November 3, 2010

Literature Review …

- Parameters Affecting Drift Velocity
  - Zukoski (1966)
    - Eotvos Number

$$Eo = (\rho_L - \rho_G) g D^2 / \sigma$$

    - Inverse Viscosity Number

$$N_f = D^{3/2} \sqrt{\rho_L (\rho_L - \rho_G) g} / \mu_L$$

    - Inclination Angle

Literature Review …

- Effect of Tube Size, Rheology of Liquid
  - Shosho and Ryan (2001)
    - Experiments with Newtonian and Non-Newtonian Liquids
    - Correlated Drift Velocity with Eotvos Number, Morton Number and Froude Number

$$Mo = \frac{g\mu^4}{\rho\sigma^3}$$

Literature Review …

- Effect of Viscosity
  - Joseph (2003)
    - Model to Predict Bubble Rise Velocity of Spherical Bubbles
    - Considered Effects of Viscosity and Surface Tension
    - Viscosity Slows Bubble Rise Velocity

Literature Review …

- Drift Velocity in Horizontal Pipe
  - Benjamin (1968)

$$v_d = 0.542\sqrt{gD}$$

  - Nicholson *et al.* (1981) and Bendiksen (1984)

Literature Review …

- **Drift Velocity in Horizontal Pipe**
  - **Weber (1981)**

$$v_d / \sqrt{gD} = 0.54 - 1.76 Eo^{0.56}$$

  - **Ben-Mansour *et al.* (2010)**

$$Fr = \frac{v_d}{\sqrt{gD}} \quad N_\mu = \frac{\mu}{\rho D^{3/2} g^{1/2}} \quad Eo = \frac{\sigma}{\rho D^2 g}$$

Literature Review …

- **Drift Velocity in Vertical Pipe**
  - **Dumitrescu (1943), Davies and Taylor (1950)**

$$v_\mathrm{d} = 0.351\sqrt{gD}$$

  - **Joseph (2003)**

$$v_d = -\frac{4}{3}\frac{\mu}{\rho r} + \sqrt{\frac{4}{9} gr + \frac{16}{9}\frac{\mu^2}{(\rho r)^2}}$$

Literature Review …

- Drift Velocity in Inclined Pipe
  - Bendiksen (1984)

$$v_{\mathrm{d}} = \mathrm{v}_{\mathrm{d}}^{\mathrm{h}} \cos\theta + \mathrm{v}_{\mathrm{d}}^{\mathrm{v}} \sin\theta$$

  - Weber *et al.* (1986), Carew *et al.* (1995)
    - Increase in Drift Velocity with Increase in Inclination Peaking Around 30-50°
    - Decreases After the Peak

Fluid Flow Projects Advisory Board Meeting, November 3, 2010

Literature Review …

- Drift Velocity in Inclined Pipe
  - Bonnecaze *et al.* (1971)
    - Gravitational Potential
  - Hasan and Kabir (1986)

$$v_d = v_d^v \sqrt{\sin\theta}(1+\cos\theta)^{1.2}$$

Fluid Flow Projects Advisory Board Meeting, November 3, 2010

Test Oil Characteristics

- Test Liquid: Citgo Sentry 220 Oil
  - Gravity: 27.6 °API
  - Viscosity: 0.220 Pa·s @ 40 °C
  - Density: 889 kg/m^3 @ 15.6 °C
  - Surface Tension: 0.02976 N/m
- Test Gas: Air

Significance of Experiments

- Experiments With Single Oil-Varying Viscosities by Temperature Change
- Large Diameter Pipes Used to Conduct Experiments

Fluid Flow Projects
Advisory Board Meeting, November 3, 2010

Experiments for Horizontal Flow

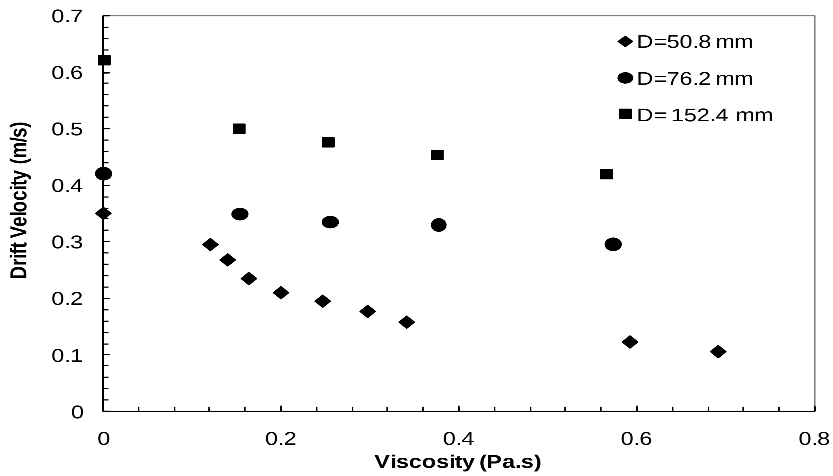

Correlation

- Horizontal Flow
  - Ben-Mansour *et al* (2010)
    - Dimensional Analysis for Correlating Froude, Viscosity and Eotvos Number

$$Fr^{h} = 0.53\,\mathrm{e}^{-13.7\,N_{\mu}^{0.46} Eo^{0.1}}$$

Fluid Flow Projects Advisory Board Meeting, November 3, 2010

Curve Fitting for Horizontal Froude Number Data

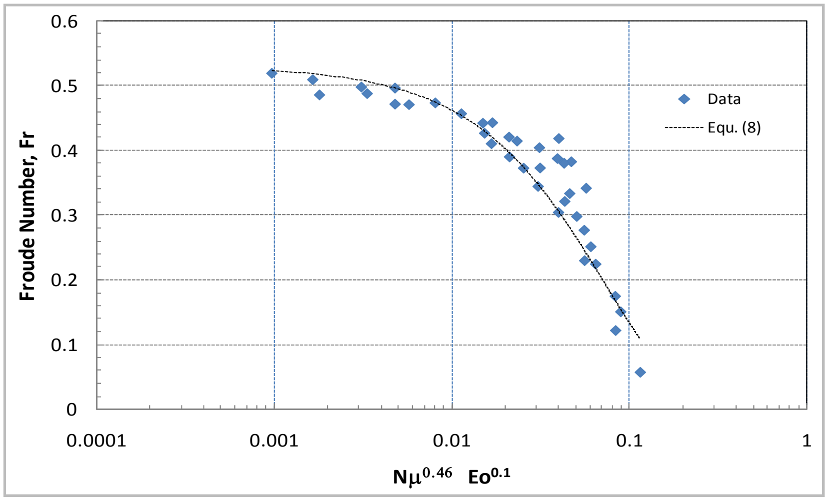

Fluid Flow Projects

Advisory Board Meeting, November 3, 2010

Predicted vs. Measured Froude Number for Horizontal Flow

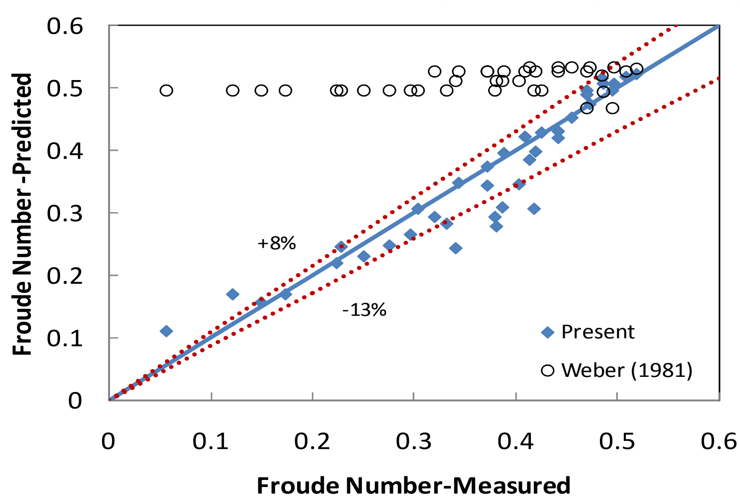

Fluid Flow Projects

Advisory Board Meeting, November 3, 2010

Drift Velocity for Vertical Flow

- Joseph (2003)

$$v_d^{\,v} = -\frac{4}{3}\frac{\mu}{\rho r} + \sqrt{\frac{4}{9} g r + \frac{16}{9}\frac{\mu^2}{(\rho r)^2}}$$

$$Fr^v = \frac{1}{\sqrt{gD}}\left(-\frac{4}{3}\frac{\mu}{\rho r} + \sqrt{\frac{4}{9} g r + \frac{16}{9}\frac{\mu^2}{(\rho r)^2}}\right)$$

Measured vs. Predicted Drift Velocity for Vertical Flow

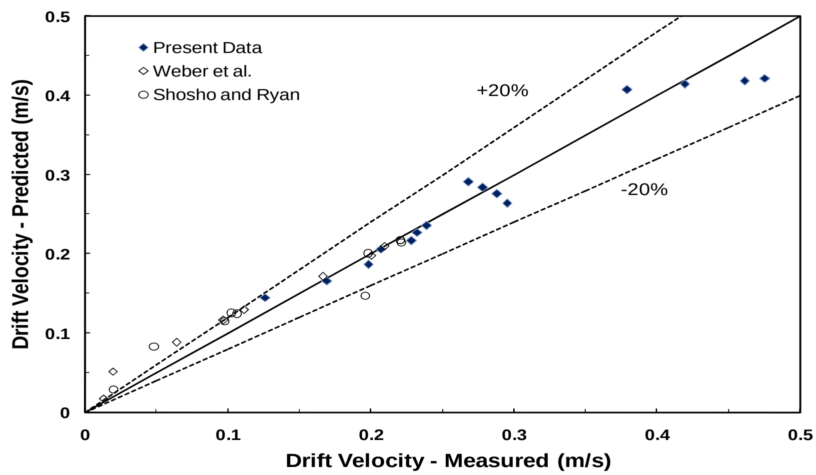

Drift Velocity in Upward Inclined pipes

- Water-Air Case
  - Experiments conducted in 2-in., 3-in., and 6-in. ID Pipes
  - Previous Experiments of Alves (1993) and Zukoski (1966)

$$F_r = -0.248\theta^2 + 0.299\theta + 0.497$$

Froude Number in Air-Water System

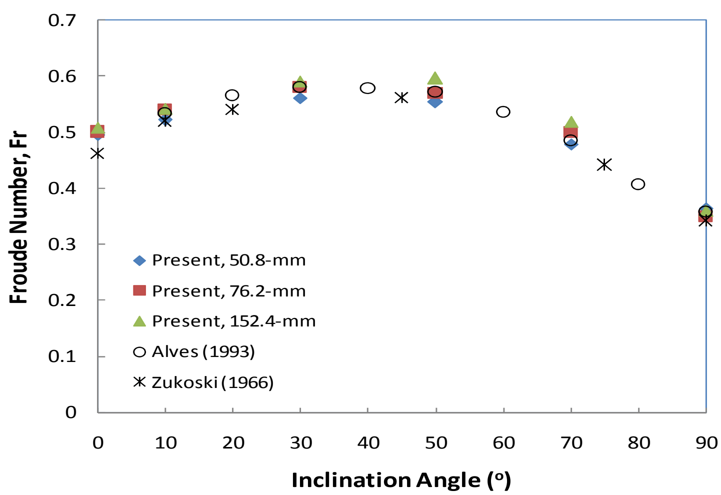

Measured vs. Predicted Froude Number for Air-Water System

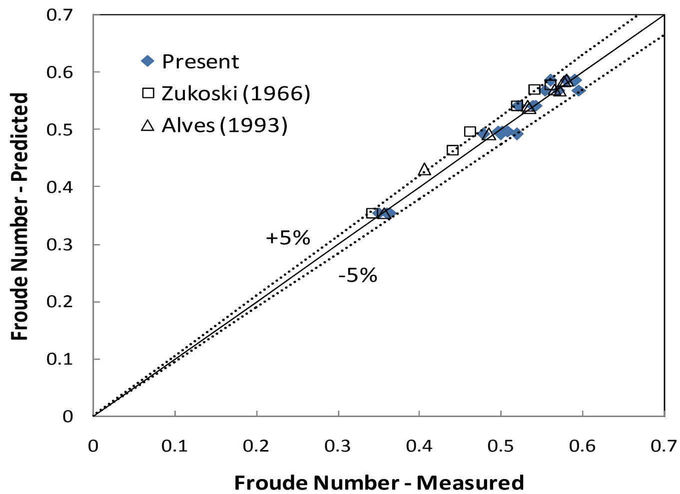

Experimental Results for Viscous Oil Flow

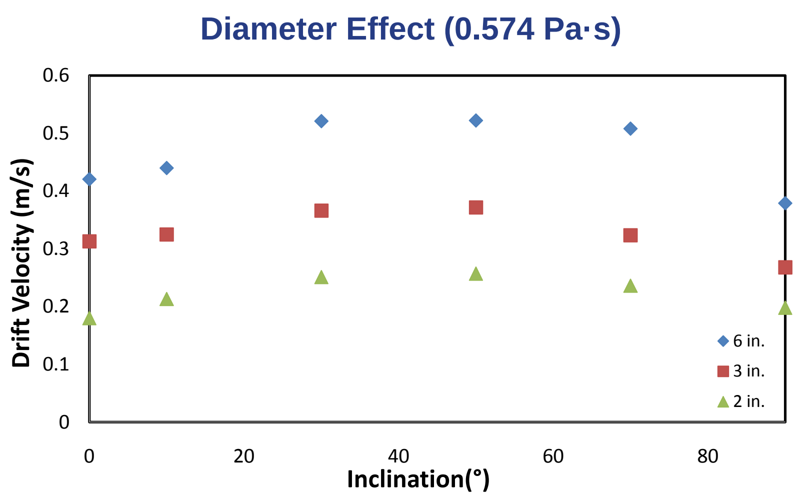

Experimental Results …

Diameter Effect (0.378 Pa·s)

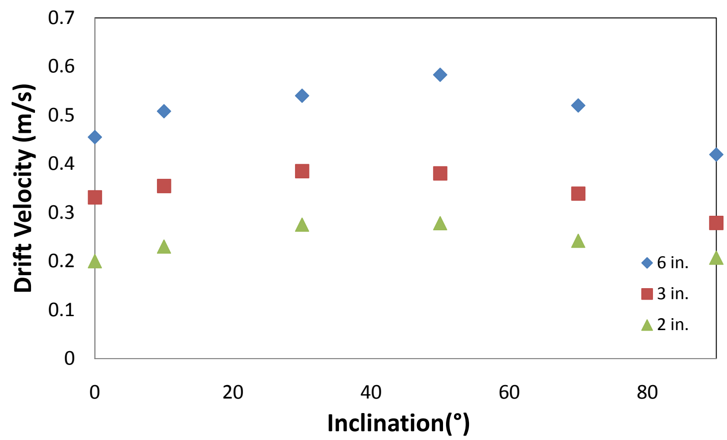

Experimental Results …

Diameter Effect (0.256 Pa·s)

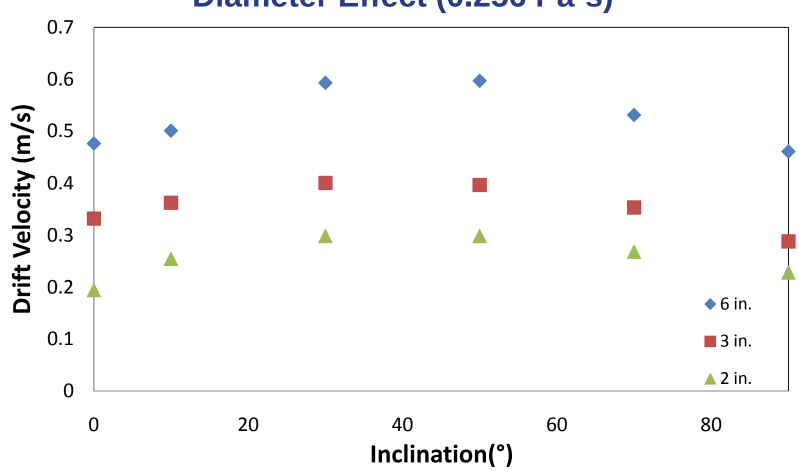

Experimental Results …

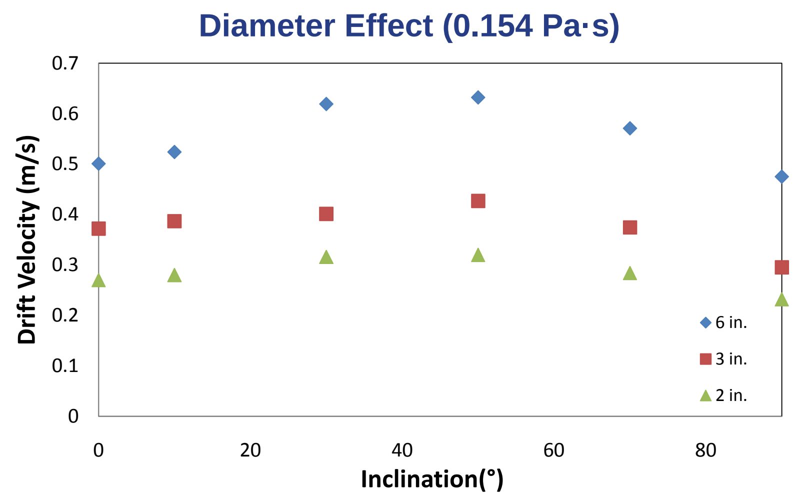

Fluid Flow Projects

Advisory Board Meeting, November 3, 2010

Drift Velocity Correlation for Inclined Flow

- Modified Bendiksen's Equation

$$Fr_\theta = Fr^h \cos\theta + Fr^v \sin\theta$$

- Horizontal and Vertical Components Calculated Taking Viscosity Into Consideration

Fluid Flow Projects

Advisory Board Meeting, November 3, 2010

Predicted vs. Measured Froude Number for Inclined Flow

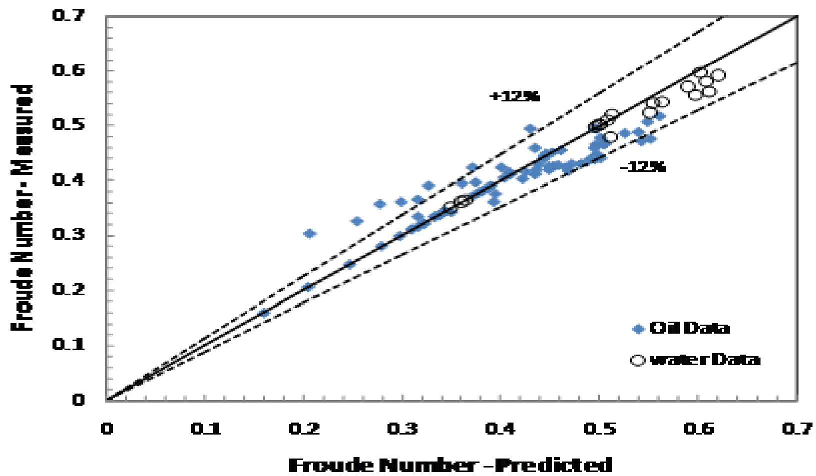

Fluid Flow Projects

Advisory Board Meeting, November 3, 2010

Conclusion

- **Horizontal Drift Velocity**

$$Fr^{h} = 0.53\, e^{-13.7\, N_{\mu}^{0.46}\, Eo^{0.1}}$$

- **Vertical Drift Velocity**

$$Fr^{v} = \frac{1}{\sqrt{gD}}\left(-\frac{4}{3}\frac{\mu}{\rho r} + \sqrt{\frac{4}{9}gr + \frac{16}{9}\frac{\mu^{2}}{(\rho r)^{2}}}\right)$$

- **Inclined Drift Velocity**

$$Fr_{\theta} = Fr^{h}\cos\theta + Fr^{v}\sin\theta$$

Fluid Flow Projects

Advisory Board Meeting, November 3, 2010

Recommended Future Tasks

- Improve Accuracy of Bubble Cap Radius, To Improve Vertical Drift Velocity Model
- Conduct Experiments with Higher Viscosity Oils

Questions/Comments

A Unified Drift Velocity Closure Relationship for Intermittent Two-Phase High Viscosity Oil Flow in Pipes

Benin Chelinsky Jeyachandra and Dr. Abdel Al-sarkhi.

Project Completion Dates

Literature Review .... December 2009
Drift Velocity Experiments .... January 2010
Model Development .... June 2010

Introduction

High viscosity oils are being produced from many oil fields around the world. Oil production systems are currently flowing oils with viscosities as high as 10 Pa·s. Current multiphase flow models are largely based on experimental data with low viscosity liquids. Commonly used laboratory liquids have viscosities less than 0.020 Pa·s. Multiphase flows are expected to exhibit significantly different behavior for higher viscosity oils.

Gokcal *et al.* (2006) experimentally observed slug flow to be the dominant flow pattern for the high viscosity oil and gas flows. The knowledge of the slug flow characteristics is crucial to design pipelines and process equipments. In order to improve the accuracy of slug characteristics for high viscosity oils, new or improved models for flow characteristics such as translational velocity is required.

Translational velocity is composed of a superposition of the bubble velocity in stagnant liquid, i.e. the drift velocity, v_d, and the maximum velocity in the slug body. The research efforts have typically been focused on the drift velocity in horizontal and upward inclined pipes.

Nicklin *et al.* (1962) proposed an equation for translational velocity as,

$$v_t = C_s v_s + v_d \ . \tag{1}$$

The parameter C_s is approximately the ratio of the maximum to the mean velocity of a fully developed velocity profile. C_s equals approximately 1.2 for turbulent flow and 2.0 for laminar flow.

Literature Review

Horizontal Flow

Zukoski (1966) experimentally investigated the effects of liquid viscosity, surface tension, pipe inclination on the motion of single elongated bubbles in stagnant liquid for different pipe diameters. He also found that the effect of viscosity is negligible on the drift velocity for $Re=v_d\rho D/\mu>200$. Wallis (1969) and Dukler and Hubbard (1975) claimed that there is no drift velocity for horizontal flow since gravity cannot act in the horizontal direction. However, Nicholson *et al.* (1981), Weber (1981), and Bendiksen (1984) showed that drift velocity exists for the horizontal case and the value of drift velocity can exceed the vertical flow value. The drift velocity is a result of hydrostatic pressure difference between the top and bottom of the bubble nose.

Benjamin calculated the value of the drift velocity coefficient by using inviscid potential flow theory which inherently neglects surface tension and viscosity. Benjamin (1968) proposed the following relationship for the drift velocity horizontal pipes,

$$v_d = 0.542\sqrt{gD} \ . \tag{2}$$

The drift velocity in horizontal slug flow is the same as the velocity of the penetration of a bubble when liquid is drained out of a horizontal pipe. Bendiksen (1984) and Zukoski (1966) supported the study of Benjamin (1968), experimentally.

Weber (1981) developed a correlation for drift velocity in horizontal pipes based on the experimental data of Zukoski (1966) for liquids of low viscosities as shown in Eq. (3)

$$v_d / \sqrt{gD} = 0.54 - 1.76Eo^{\ 0.56} , \tag{3}$$

where Eotvos number defined as $Eo = \sigma / \rho D^2 g$.

A dimensional analysis for the drift velocity in horizontal pipes was presented by Ben-Mansour *et al.* (2010). The step-by-step method was used and the following dimensionless numbers have been found.

$$Fr = \frac{v_d}{\sqrt{gD}} , \quad N_\mu = \frac{\mu}{\rho D^{3/2} g^{1/2}} , \quad Eo = \frac{\sigma}{\rho D^2 g} .$$

The first dimensionless group is the Froude number, *Fr*, the second is the viscosity number, N_μ, and the third is Eotvos number, *Eo*. It was concluded that the drift velocity in a horizontal pipe can be modeled using those three dimensionless groups.

Vertical Flow

Dumitrescu (1943) and Davies and Taylor (1950) performed a potential flow analysis to find the drift velocity for vertical flow. Both derived the same dimensionless group (Froude number), and found that

Froude number has a constant value. Davies and Taylor estimated the constant value as 0.328. Dumitrescu made more accurate calculations and theoretically determined this value as 0.351 which agreed well with the air/water experimental data of Nicklin *et al.* (1962).

$$v_d = 0.351\sqrt{gD} \quad . \tag{4}$$

For vertical flow, Joseph (2003) proposed a model for the bubble rise velocity in vertical flow and taking viscosity, surface tension and shape of the bubble nose effects into consideration. From the experimental results, it is observed that the bubble nose is almost spherical. When the bubble nose is spherical (axi-symmetric cap), the effect of the surface tension vanishes and the equation becomes only function of the fluid viscosity and the radius of the spherical cap bubble as shown in Eq. 5.

$$v_d = -\frac{4}{3}\frac{\mu}{\rho r} + \sqrt{\frac{4}{9}gr + \frac{16}{9}\frac{\mu^2}{(\rho r)^2}} \quad , \tag{5}$$

where r is the radius of cap, ρ and μ are the density and viscosity of the liquid. It was shown that the experimental data of Bhaga and Weber (1981) and the model predictions were in good agreement.

Inclined Flow

For the inclined case, Zukoski, Bendiksen, Weber *et al.* (1986), Hasan and Kabir (1986), and Carew *et al.* (1995) experimentally studied drift velocity and found that the drift velocity increases with inclination angle and then decreases to lowest value for vertical flow, reaching to maximum value at an intermediate angle of inclination around 40º to 60º from the horizontal. This fact was explained qualitatively by Bonnecaze *et al.* (1971). They discussed that the gravitational potential first increases and then decreases as the inclination angle changes from vertical to horizontal position.

Weber *et al.* experimentally studied bubble rise velocity (in relatively small pipe diameters from 0.6 to 3.7 cm) for high viscosity Newtonian liquids. Froude number, *Fr*, was correlated as a function of Eotvos number, *Eo*, the Morton number, ($M=g\mu^4/\rho\sigma^3$), and the inclination angle, θ.

Bendiksen performed an experimental study for velocities of single elongated bubbles in flowing liquids at different inclination angles. The measured velocities were plotted against the liquid velocity for each inclination angle. Then, drift velocities were found by the extrapolation of the data to zero liquid velocity. He correlated the drift velocity for inclined flow by using the drift velocities for horizontal and vertical flow:

$$v_d = v_d^h \cos\theta + v_d^v \sin\theta \quad . \tag{6}$$

Hasan and Kabir performed an experimental study in the range of 90º>Θ>30º and proposed the relation:

$$v_d = v_d^v \sqrt{\sin\theta}(1+\cos\theta)^{1.2} \quad . \tag{7}$$

Carew *et al.* (1995) studied the motion of long bubbles in inclined pipes experimentally with viscous Newtonian and non-Newtonian liquids. He proposed an empirical correlation for the drift velocity of elongated bubble in inclined pipes. The correlation depends on inclination angle and surface tension and is valid at *Re>200* and *Eo>1/60.*

Shosho and Ryan (2001) performed an experimental study to investigate the effects of tube size, fluids including Newtonian and non-Newtonian on drift velocity for vertical and inclined tubes. The drift velocity in terms of Froude number was correlated with Eotvos and Morton numbers. Froude number increased and decreased as the angle of inclination increased for both Newtonian and non-Newtonian fluids. For non-Newtonian fluids with high Morton number, Froude number was affected by both viscous forces and tube size.

From the literature review related to drift velocity for horizontal, inclined and vertical pipes, it is apparent that detailed research has been conducted on the effects of surface tension, pipe diameter on drift velocity at different inclination angles. However, for the effect of high viscosity on drift velocity, experimental and theoretical studies are scarce and conducted for relatively small pipe diameter.

Experimental Setup and Procedure:

The experimental facility consists of an oil storage tank, a 20 HP screw pump, a 3.05-m long acrylic pipe, heating and cooling loops, transfer hoses and instrumentation. Details of the experimental setup is given in Gokcal *et al.* (2008) and shown Fig. 1. Experiments were conducted on 50.8, 76.2 and 152.4 mm ID diameter pipes. The acrylic pipe is located close to the storage tank. The inclination of the pipe can be varied using a pulley arrangement. The pipe inclination can be changed from 0° to 90°.

The heating and cooling loops are used to maintain the desired temperature and thereby to control the viscosity of the oil. The oil pump supplies the pipe with oil. Then, the main inlet valve and the auxiliary inlet valve are closed. The drainage valve is opened to drain the residual oil captured and thereby create a gas pocket. Next, the drainage valve is closed and the main inlet valve is opened to release the gas bubble into the stagnant oil column. The drift velocity is measured by two lasers (for 50.8, 76.2 mm ID pipe) or optical sensors (for 152.4 mm ID pipe) separated by a distance of 0.9144 m. The optical sensors work by principle that the light intensity changes when it reflects/refracts the oil or the gas phase. This is stored as voltage readings in a data acquisition system with a frequency of 500 readings/sec. The data is analyzed in a computer and the drift velocity is calculated by dividing the distance between the two sensors with time difference between the two voltage peaks.

A facility modification was carried out for the horizontal case. The end plate of the pipe was removed, and it was replaced with a plug. This would facilitate the removal of plug after the pipe is filled and the draining of oil can be modeled as the penetration of gas bubble into the fluid.

Water and viscous oil were used as test fluids. The properties of the oil are given in Table 1. The most important characteristic of the oil is its large range of viscosity owing to strong temperature dependence.

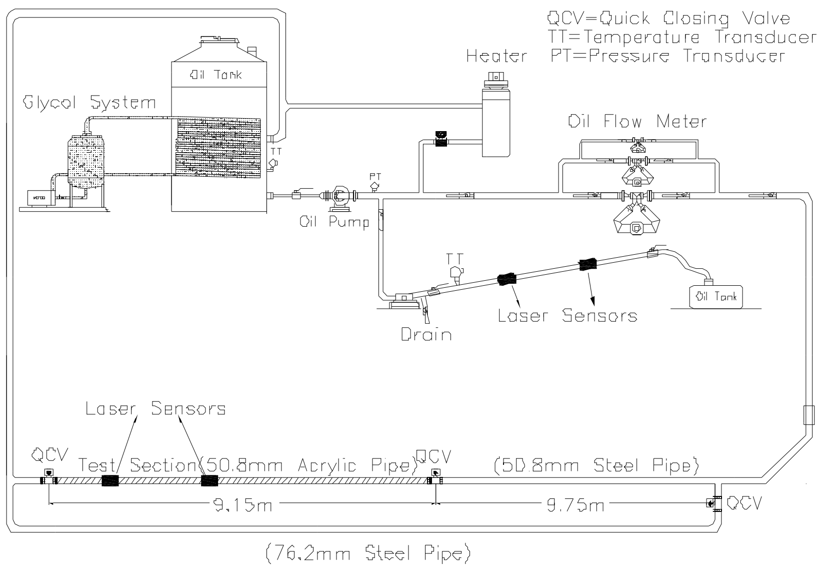

Fig. 1: Schematic of Indoor High Viscosity Test Facility

Results and Discussions

Initially, an experiment is conducted with water for horizontal pipe to prove that the system is working properly. The results for water are compared with Benjamin's model prediction. The predictions of drift velocity of the water from Benjamin's model show excellent agreement with the data. The rest of experiments conducted at different oil temperature corresponding to range of viscosities from 0.154 to 0.574 Pa·s.

Drift Velocity in Horizontal Pipes

Figure 2 shows the experimental results for drift velocity vs. viscosity for horizontal pipes of different diameters. Drift velocity decreases with increasing the viscosity. As the pipe diameter increases, the drift velocity increases. The decrease in the drift velocity with viscosity is steeped in the small pipes than in the large pipes. The plots tend to have an asymptotic level at very high viscosity which leads to a small variation in drift velocity variation with viscosity.

As shown by Ben-Mansour *et al.* (2010) the drift velocity in a horizontal pipe can be correlated using Froude, Viscosity, and Eotvos Numbers. Figure 3 shows the correlation for drift velocity in horizontal pipes at different viscosities, diameter and surface tensions. It is worth to note that data include oil at different viscosities and water in different pipe diameters. The experimental data for drift velocity in pipes of different diameters with liquid of various viscosities are well correlated by

$$Fr = 0.53\,\mathrm{e}^{-13.7\, N_{\mu}^{0.46} Eo^{0.1}} \,. \tag{8}$$

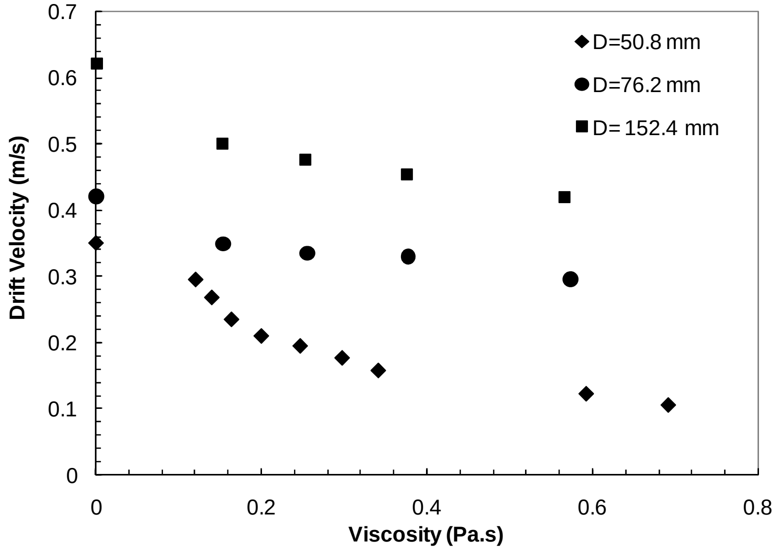

Fig. 2: Drift Velocity Variation with Viscosity

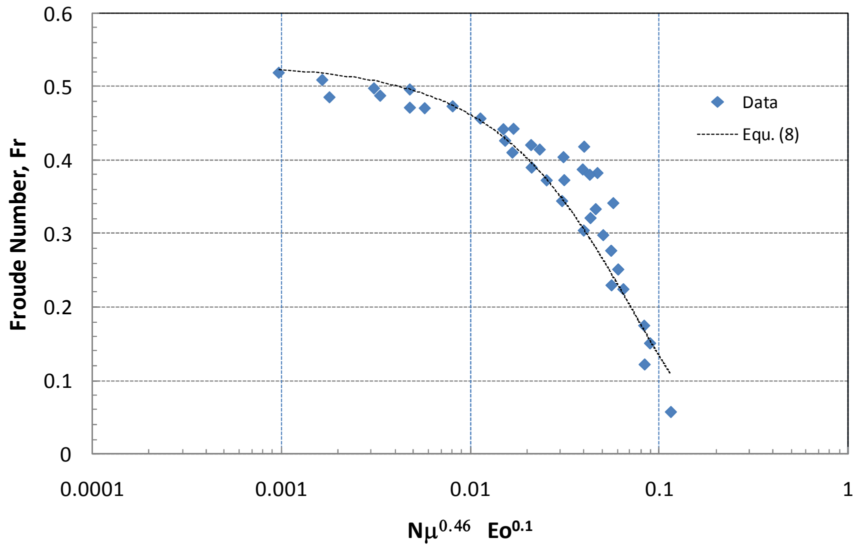

Fig. 3: Horizontal Froude Number Correlation vs. Experimental Data

Evaluation of Drift Velocity Correlation in Horizontal Pipes

Figure 4 shows the comparison between the measured data and the predicted result using Eq. 8. On the same plot the prediction of Weber (1981) for low viscosities is shown. It can be seen clearly that most of the data collapse in a range of +8% and –13%. Weber (1981) correlation matches only for points at high values of Froude numbers which is expected since the correlation was developed based on Zukoski's data in water-air system. Most of the data with Froud numbers around 0.5 are for water experiments.

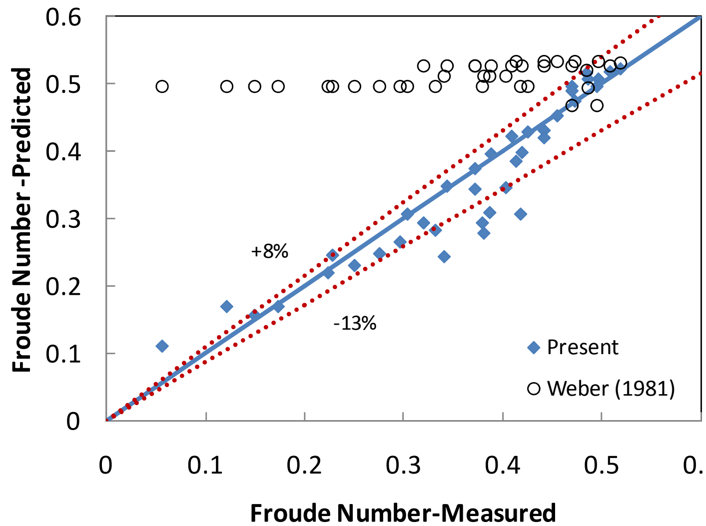

Fig. 4: Comparison of Correlation Predictions with Measured Froude Number for Horizontal Flow

Drift Velocity in Vertical pipes

Several correlations available in literature for rise velocity in stagnant fluid (Davies and Taylor (1950), White and Beardmore (1962), D. D. Joseph (2003)). Figure 5 shows the comparison of the model predictions of Joseph (2003) with experimental data from Weber *et al.* (1986), Shosho and Ryan (2001) and this study. The bubble radius and liquid viscosity must be known to calculate the drift velocity from Eq. 5. It is experimentally observed that the radius of bubble is approximately from 0.55 to 0.6 of the radius of the pipe. This value is used for the rest of calculations to compare model predictions with experimental results. Weber *et al.* (1986) performed their experiments in 37.3 mm ID pipe (relatively small) for viscosities between 0.051 and 0.183 Pa·s. Shosho and Ryan experiments were also for same diameter for viscosities between 0.003 and 0.883 Pa·s. They are the only available dataset for higher viscosity range with comparable pipe diameter in the literature. Joseph (2003) model correlated the experimental data well within ±20%. The present work experimental data agreed very well with this correlation. Better match can be obtained if the curvature of the bubble cap is included.

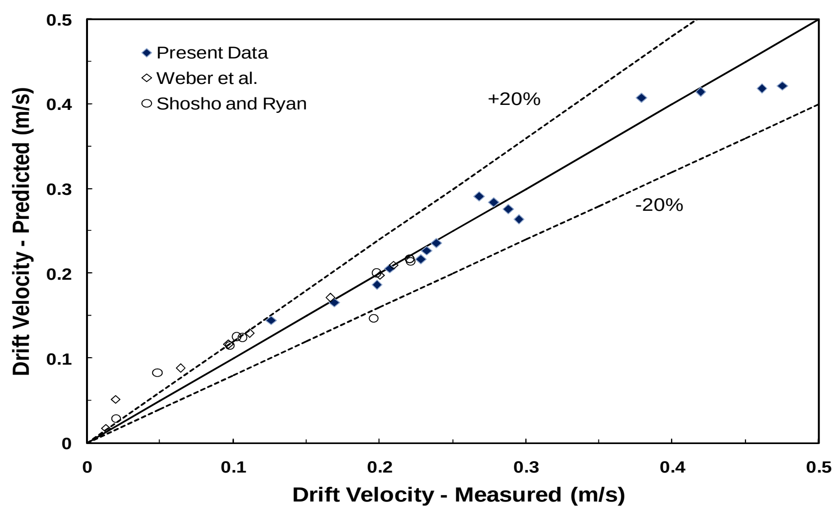

Fig. 5: Comparison of Joseph (2003) Model Predictions with Measured Drift Velocities for Vertical Case

Drift Velocity in Upward Inclined pipes

Effect of pipe diameter and inclination angle at certain oil viscosity is presented in Figs. 6-9. Effect of viscosity at certain pipe diameters is shown in Figs. 10-12

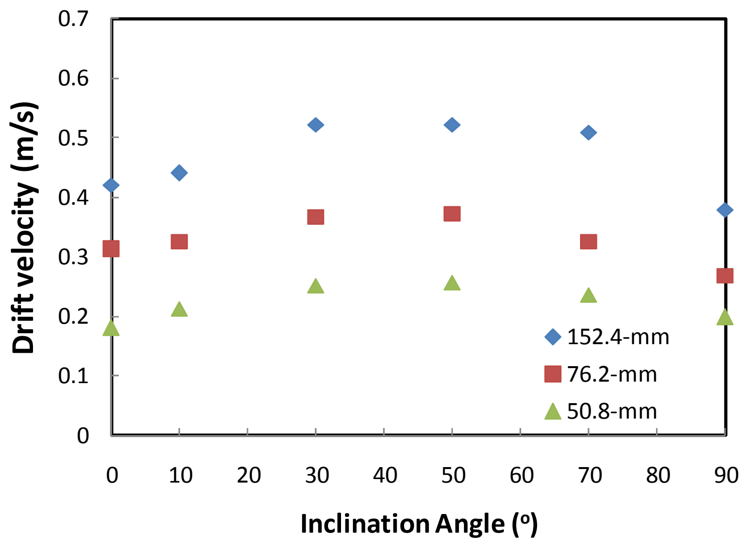

Fig. 6: Effect of Pipe Diameter on Drift Velocity for 0.574 Pa·s Viscosity Oil

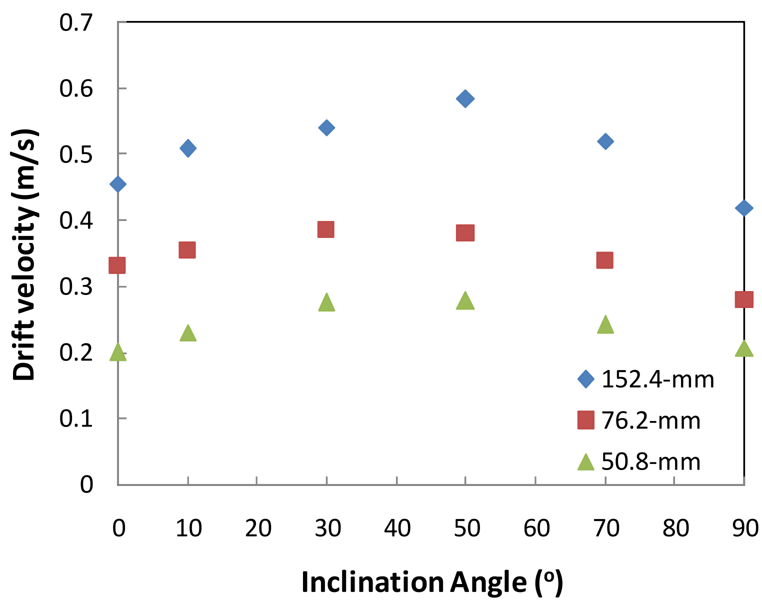

Fig. 7: Effect of Diameter on Drift Velocity for 0.378 Pa·s Viscosity Oil

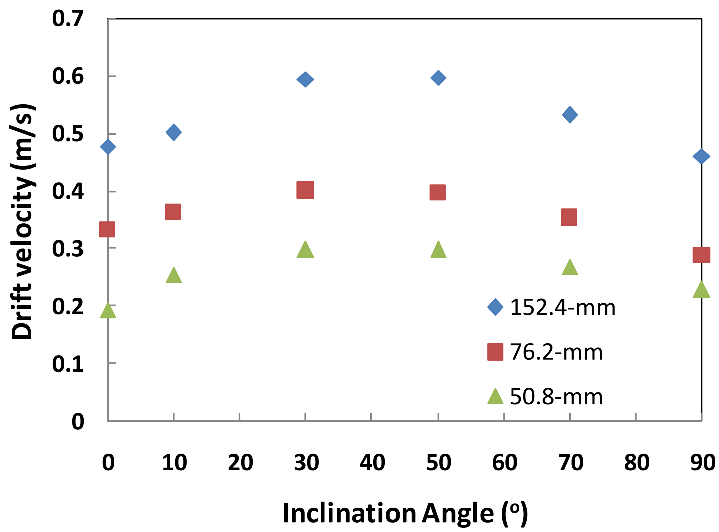

Fig. 8: Effect of Diameter on Drift Velocity for 0.256 Pa·s Viscosity Oil

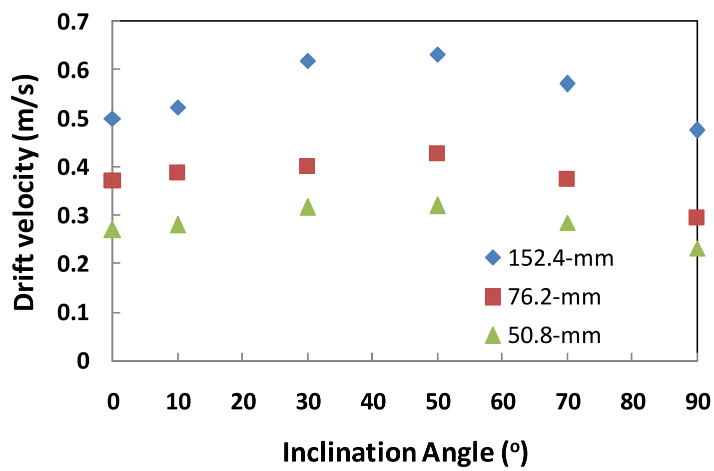

Fig. 9: Effect of Diameter on Drift Velocity for 0.154 Pa·s Viscosity Oil

From Figs. 6-9, it is observed that there is a clear effect of diameter on drift velocity. For horizontal flow, when diameter increases, the gravitational potential increases. This leads to a stronger drive for the gas bubble to penetrate into the stagnant liquid column, hence the higher drift velocity. As the inclination gradually increases, so does the drift velocity, and it peaks at an inclination around 30-50º. The gravitation potential is at its maximum at this inclination angle. As the inclination is increased further, the effect of drainage area comes into consideration. Even though the gravitational potential is high, the area available for oil to drain is low. This, in turn, creates a resistance for the air bubble to penetrate into the oil effectively reducing the drift velocity. With increasing pipe inclination, the extended air bubble location which is in contact with the upper part of the pipe (at low inclination angle) moves toward the centerline of the pipe. At right angle the extended air bubble location is in the center of the pipe.

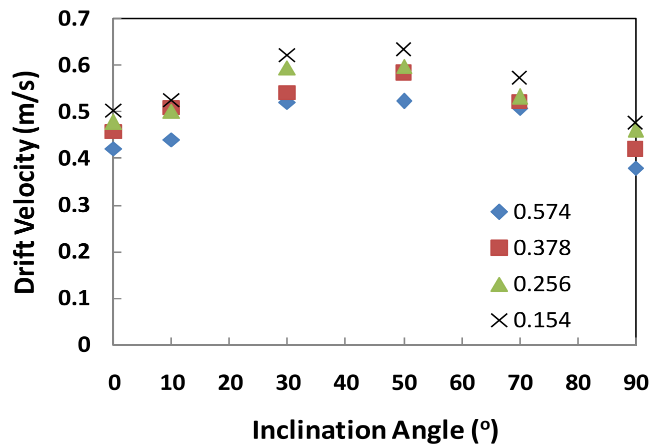

Fig. 10: Viscosity Effect on Drift Velocity for 152.4. mm Diameter Pipe (Viscosities in Pa·s)

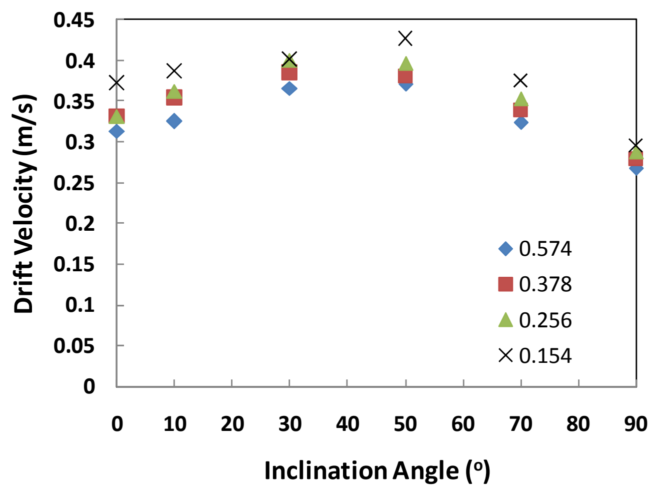

Fig. 11: Viscosity Effect on Drift Velocity for 76.2 mm Diameter Pipe

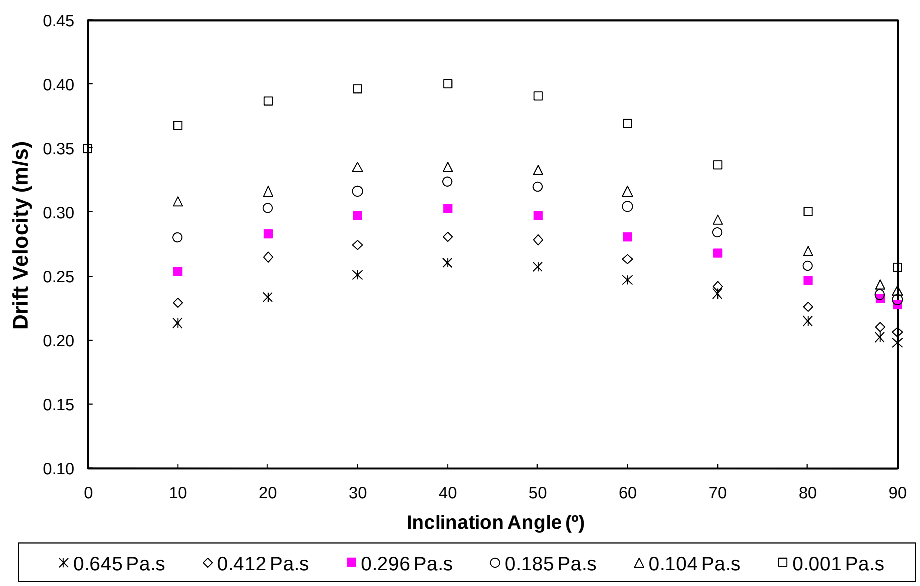

Fig. 12: Viscosity Effect on Drift Velocity for 50.8 mm Diameter Pipe

From Figs. 10-12, it is observed that as the viscosity increases, drift velocity decreases. As viscosity increases, the resistance for the gas bubbles to intrude into the stagnant column increases, thereby, it reduces the drift velocity. The same parabolic behavior of drift velocity, increasing as the inclination angle increases, reaching a maximum at 30-50º and then decreasing, is observed.

Drift Velocity Correlation in Upward Inclined Pipes

Figure 13 shows the comparison between the experimental data and the predicted result using similar approach as Bendiksen (Eq. 6). The modified Bendiksen correlation shown in Eq. 10 for all pipe inclination is just simply uses the Froude number instead of drift velocity. The horizontal and vertical component of the Froude number in the equation is obtained from the experimental values for 0º and 90º, respectively, which accounts for the effects of viscosity.

$$Fr_\theta = Fr^h \cos\theta + Fr^v \sin\theta \,. \tag{10}$$

Where, Fr_θ is the Froude number at angle of inclinations and θ is the angle of inclination and h and v are for the horizontal and vertical cases, respectively.

It can be observed that most of the data points for high viscosity oil fall within ± 12% limit. It can also be observed that all data points for water lie very close to the 45º line. These observations imply there is good match between the predicted value and the experimental data provided viscosity effects are considered.

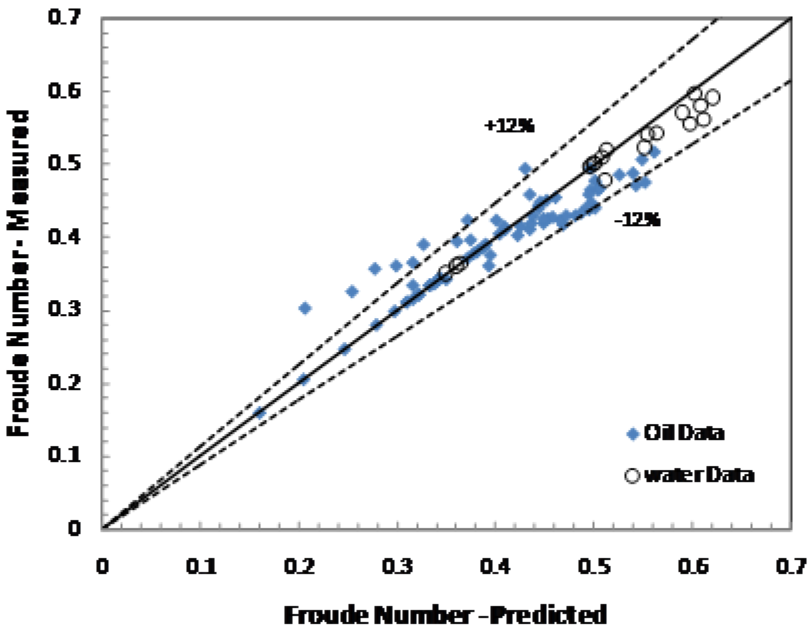

Fig. 13: Comparison of the Correlation Predictions with Measured Froude Number for Inclined Flow

Conclusions

Drift velocity experiments were conducted on high viscosity oil for varying viscosities, pipe diameters and inclination angles. It was observed that viscosity has a profound effect on drift velocity. Drift velocity increases with increasing the pipe diameter and decreases with increasing the liquid viscosity. For horizontal flow, a dimensionless analysis was performed, and a new correlation for horizontal drift velocity was developed and tested with the available data set. For the inclined case, effect of pipe inclination on drift velocity was explained. As the pipe inclination increases, the drift velocity increases and it peaks at an inclination around 30-50° then it decreases again. For the vertical case of oil-air system, the correlation developed by Joseph (2003) was tested with the data set, and a very good match was obtained. For inclined flow, it was observed that the correlation developed by Bendiksen modified by using Froude number instead of drift velocity worked well provided the viscosity effects are considered for the horizontal and vertical component. Therefore, the correlation developed for horizontal flow and Joseph (2003) correlation for vertical flow can be used in congruence with the modified Bendiksen's equation to provide accurate values for drift velocity in horizontal and upward inclined case.

References

Alves, I.N., Shoham, O., Taitel Y., 1993. Drift Velocity of Elongated Bubbles in Inclined Pipes, Chem. Eng. Sci. 48, 3063-3070.

Bendiksen, K. H., 1984. An Experimental Investigation of the Motion of Long Bubbles in Inclined Tubes, Int. J. Multiphase Flow 10, 467-483.

Ben-Mansour, A. Sharma, B. Jeyachandra, B. Gokcal, A. Al-sarkhi, C. Sarica, 2010. Effect of Pipe diameter and high oil viscosity on drift velocity for horizontal pipes, 7th North American Conference on Multiphase Technology, Banff, Canada-2nd -4th June.

Benjamin, T. B., 1968. Gravity Currents and Related Phenomena, J. Fluid. Mech. 31, Part 2, 209-248.

Bhaga, T. and Weber, M. E., 1981. Bubbles in Viscous Liquids: Shapes, Wakes, and Velocities, J. Fluid Mech. 105, 61-85.

Bonnecaze, R. H., Eriskine, W. Jr., and Greskovich, E. J., 1971. Holdup and Pressure Drop for Two-Phase Slug Flow in Inclined Pipelines, AIChe J. 17, 1109-1113.

Carew, P.S, Thomas, N. H., Johnson, A.B., 1995. A Physically Based on Correlation for the Effects of Power Law Rheology and Inclination on Slug Rise Velocity, Int. J. Multiphase Flow 21, 1091-1106.

Davies, R. M. and Taylor, G. I., 1950. The Mechanics of Large Bubbles Rising Through Liquids in Tubes, Proc. R. Soc. Lond., A 200, 375-390.

Dukler, A. E. and Hubbard, M. G., 1975. A Model for Gas-Liquid Slug Flow in Horizontal and Near-Horizontal Tubes, Ind. Eng. Chem. Fundam. 14, 337-347.

Dumitrescu, D. T., 1943. Strömung an einer Luftblase im senkrechten Rohr. Z. Angew. Mat. Mech. 23, 139-149.

Gokcal, B., Wang, Q., Zhang, H. Q., and Sarica, C., 2006. Effects of High Oil Viscosity on Oil-Gas Flow Behavior in Horizontal Pipes, SPE 102727, Presented at the 2006 SPE ATCE, San Antonio, TX, September 24 – 27.

Gokcal, B, Al-Sarkhi, A.S., and Sarica, C., 2008. Effects of High Oil Viscosity on Drift Velocity for Horizontal Pipes, Presented at BHRg Conference of Multiphase Production Technology, Banff, June 4-6.

Hasan, A.R., and Kabir, C.S., 1986. Predicting Multiphase Flow Behavior in a Deviated Well, SPE 15449, Presented at 61st ATCE, New Orleans.

Joseph, D. D., 2003. Rise velocity of a Spherical Cap Bubble, J. Fluid Mech. 488, 213-223.

Nicklin, D. J., Wilkes, J. O., Davidson, J. F., 1962. Two-Phase Flow in Vertical Tubes, Trans. Inst. Chem. Eng. 40, 61-68.

Nicholson, M.K., Aziz K., and Gregory G. A., 1981. Intermittent Two-Phase Flow in Horizontal Pipes: Predictive Models, Can. J. Chem. Eng. 56, 389-399.

Shosho, C. E. and Ryan, M. E., 2001. An Experimental Study of the Motion of Long Bubbles in Inclined Pipes, Chem. Eng. Sci., 56, 2191-2204.

Wallis, G. B., 1969. One Dimensional Two-Phase Flow, McGraw-Hill, New York.

Weber, M.E., 1981. Drift in Intermittent Two-Phase Flow in Horizontal Pipes, Can. J. Chem. Eng. 59, 398-399.

Weber, M.E., Alarie, A., and Ryan, M. E., 1986. Velocities of Extended Bubbles in Inclined Tubes," Chem. Eng. Sci. 41, 2235-2240.

White, E. T. and Beardmore R. H., 1962. the velocity of rise of single cylindrical air bubbles through liquids contained in vertical tubes, Chemical Engineering Science 17, 351-361.

Zukoski, E. E., 1966. Influence of Viscosity, Surface Tension, and Inclination Angle on Motion of Long Bubbles in Closed Tubes, J. Fluid Mech. 25, 821-837.

Fluid Flow Projects

Inclination Effects on High Viscosity Oil-Gas Two Phase Flow

Benin Chelinsky Jeyachandra

Advisory Board Meeting, November 3, 2010

Outline

- Objectives
- Introduction
- Summary of Literature Review
- Experiment Setup
- Flow Patterns
- Capacitance Sensor
- Preliminary Experiments
- Future Tasks

Objectives

- Conduct Experiments on Slightly Inclined High Viscosity Oil-Gas Two Phase Flow
- Analyze the Data and Identify Inclination Effects on Flow Characteristics of High Viscosity Oil-Gas Two Phase Flow

Introduction

- Accurate Modeling of High Viscosity Liquid Flow Behavior
- Gokcal (2005, 2008) - Modeling of Flow Characteristics for Horizontal Flow
- Kora (2010) - Liquid Holdup

Literature Review Summary

- Available Multiphase Flow Models Developed for Low Viscosity Liquids
- Few Studies Include Liquid Viscosity Effect on Slug Characteristics
- Limited Experimental Data on High Viscosity Oil Multiphase Flow

Fluid Flow Projects

Advisory Board Meeting, November 3, 2010

Test Fluid

- Test Liquid: Citgo Sentry 220 Oil
  - Gravity: 27.6 °API
  - Viscosity: 0.220 Pa·s @ 40 °C
  - Density: 889 kg/m3 @ 15.6 °C
  - Surface Tension: 0.02976 N/m
- Test Gas: Air

Fluid Flow Projects

Advisory Board Meeting, November 3, 2010

Experimental Setup

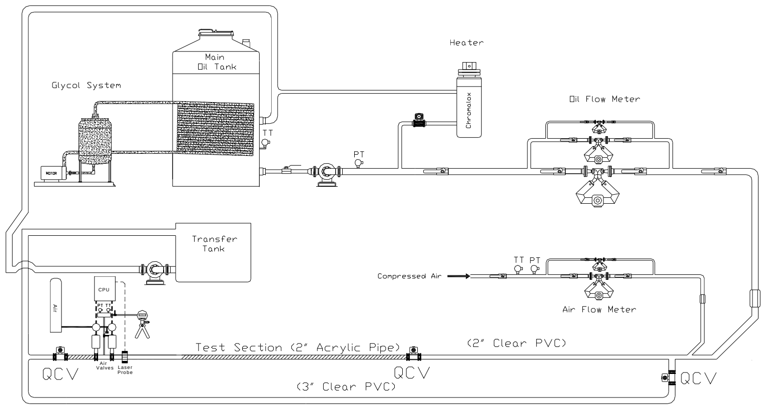

Fluid Flow Projects

Advisory Board Meeting, November 3, 2010

Experimental Parameters

- Flow Pattern
- Pressure Gradient
- Liquid Holdup
- Translational Velocity
- Slug Length
- Slug Frequency
- Film Thickness

Fluid Flow Projects

Advisory Board Meeting, November 3, 2010

Instruments

- Capacitance Sensor
- Laser Sensors
- Quick Closing Valves
- Differential Pressure Sensors
- High Speed Camera

Test Range

- Diameter of Pipe: 50.8 mm (2 inch)
- Inclination Angles: +2°, -2°
- Viscosity Range:
  - 587 cP (70 °F)
  - 378 cP (80 °F)
  - 256 cP (90 °F)
  - 181 cP (100 °F)
- Superficial Gas Velocity: 0.1 – 5 m/s
- Superficial Liquid Velocity: 0.01 – 1.75 m/s

Flow Pattern for +2° Inclination

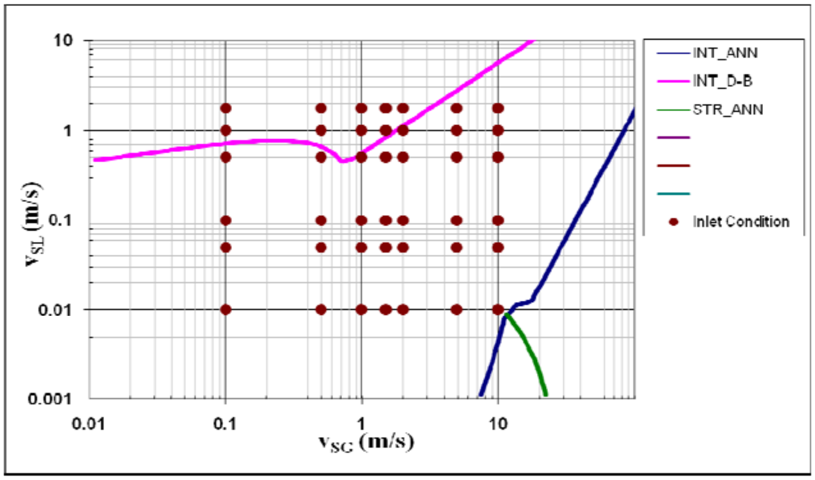

Flow Pattern for -2° Inclination

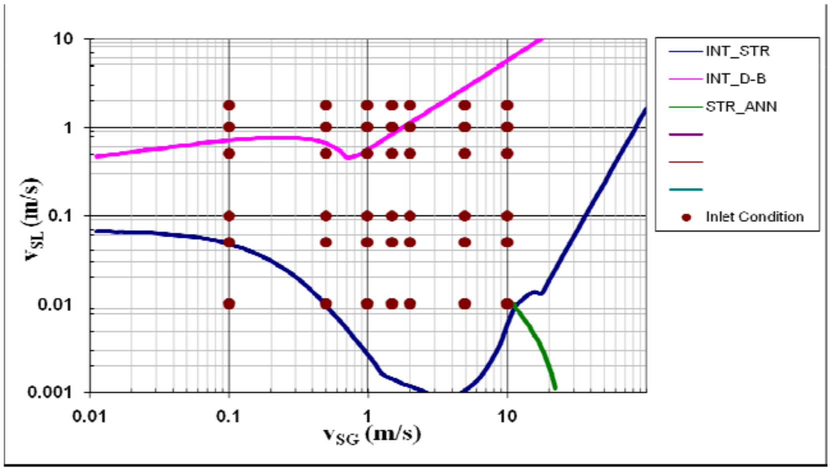

Fluid Flow Projects

Advisory Board Meeting, November 3, 2010

Progress

- New Capacitance Sensor Integrated Into the System
- Static Calibration of Capacitance Sensor Completed
- Two Laser Sensors Integrated into the System
- Inclination of Facility Completed

New Capacitance Sensor

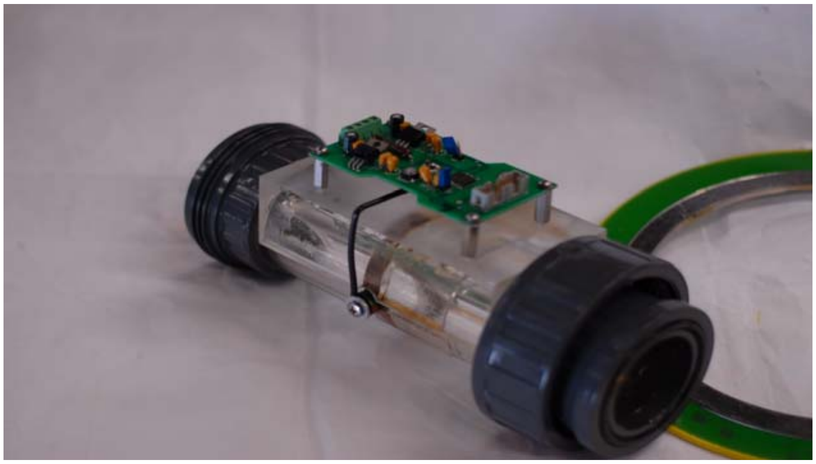

Old Capacitance Sensor

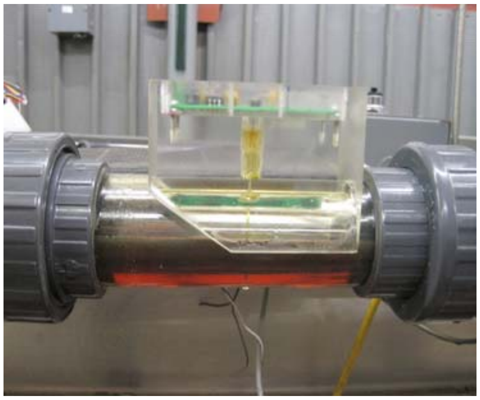

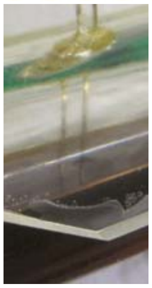

Static Calibration

- Known Volume of Oil is Injected into the Capacitance Sensor and the Voltage Response is Noted

Old Capacitance Sensor

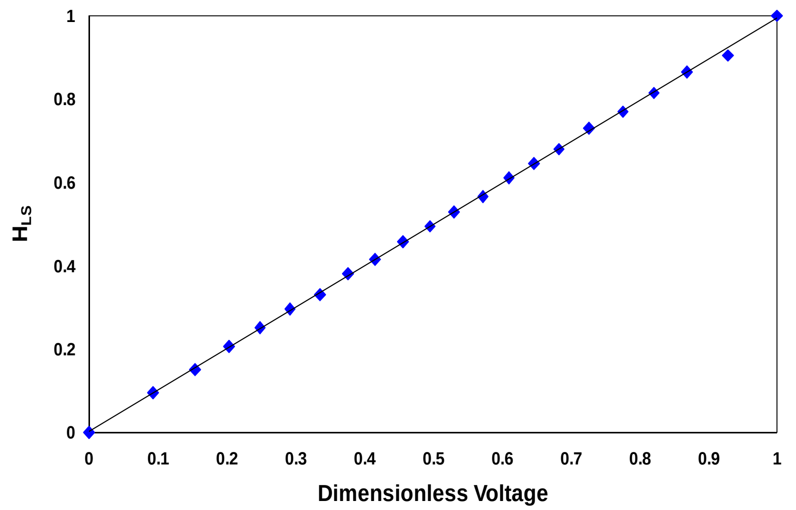

New Capacitance Sensor

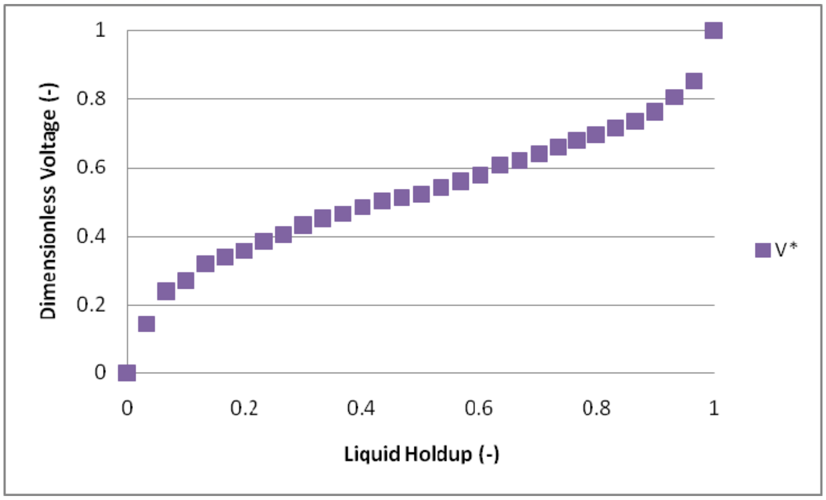

Dynamic Calibration

- Integrate the New Capacitance Sensor into the Flow Loop
- Use Existing Quick Closing Valves and High Speed Camera to Capture a Liquid Slug
- Actual Liquid Holdup vs. Calculated Liquid Holdup for Various Test Conditions

Preliminary Experiments

- v_{SL}=0.01 m/s v_{Sg}=0.1 m/s

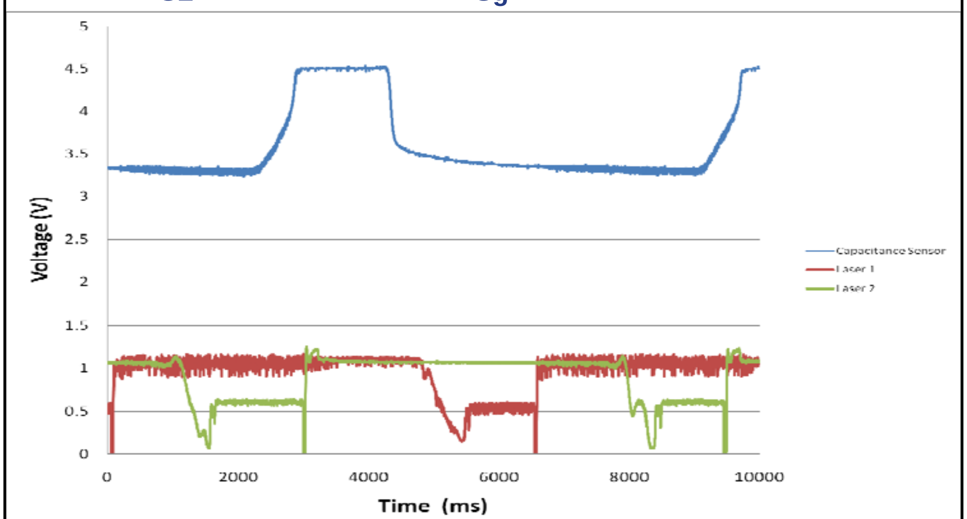

Preliminary Experiments

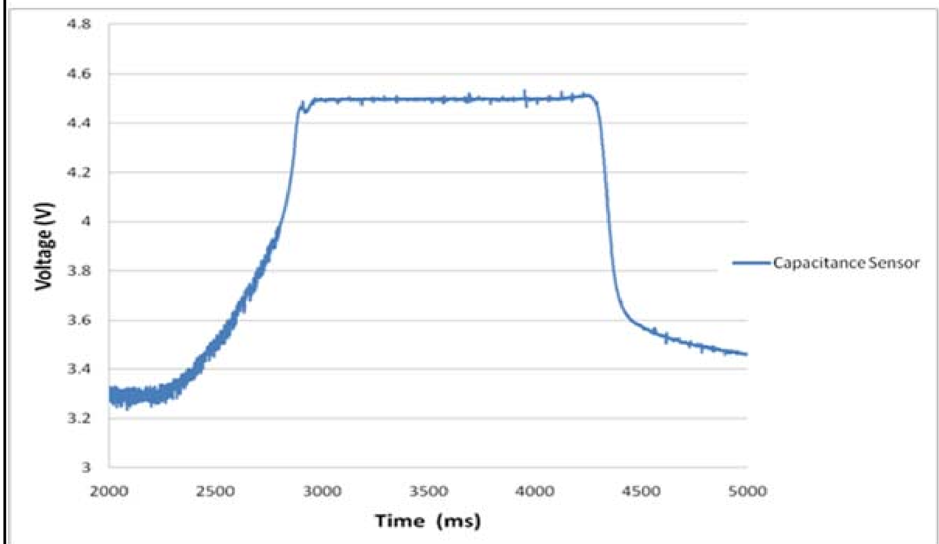

Old Capacitance Sensor

- v_{SL} = 0.1 m/s & v_{Sg} = 0.1 m/s

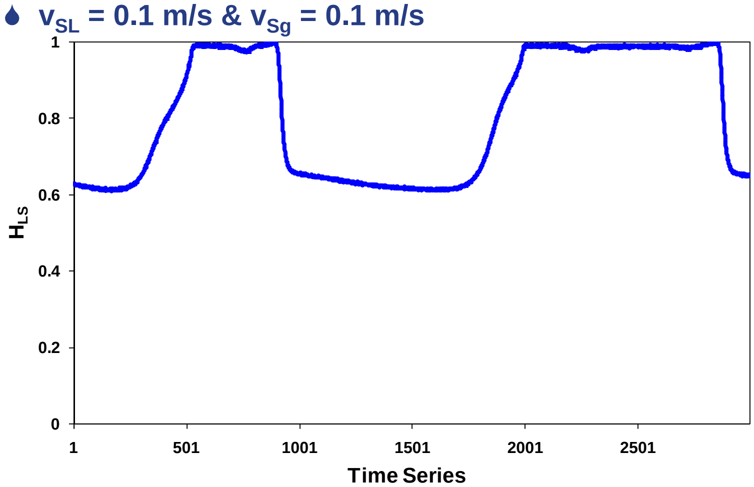

Fluid Flow Projects

Advisory Board Meeting, November 3, 2010

Preliminary Experiments

v_{SL}=0.5 m/s v_{Sg}=1 m/s

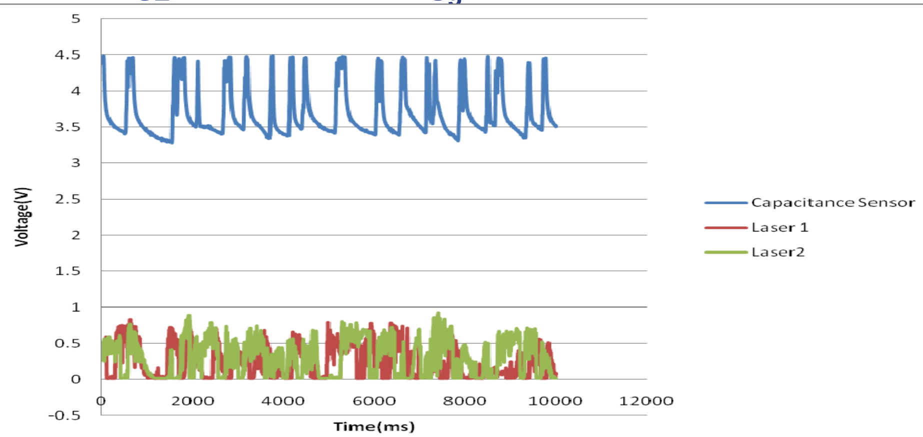

Fluid Flow Projects

Advisory Board Meeting, November 3, 2010

Preliminary Experiments

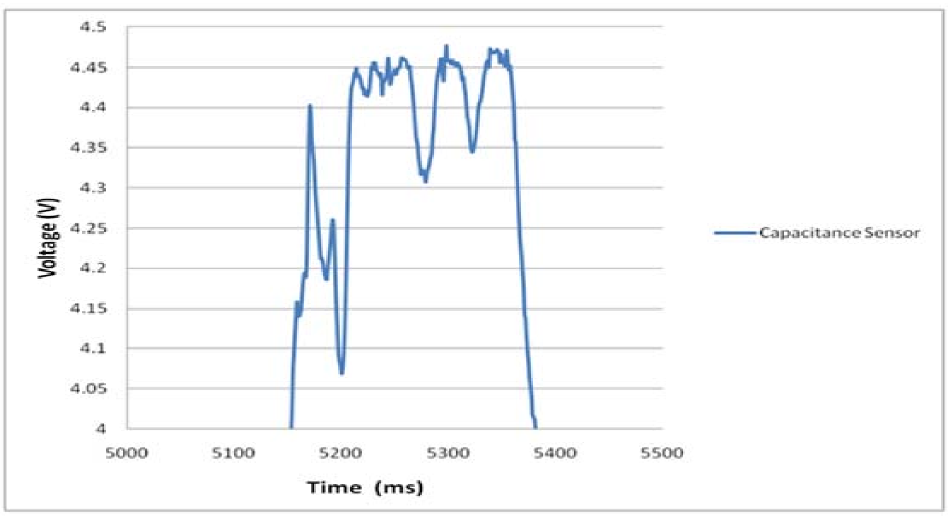

Fluid Flow Projects

Advisory Board Meeting, November 3, 2010

Old Capacitance Sensor

- v_{SL} = 0.5 m/s & v_{Sg} = 1 m/s

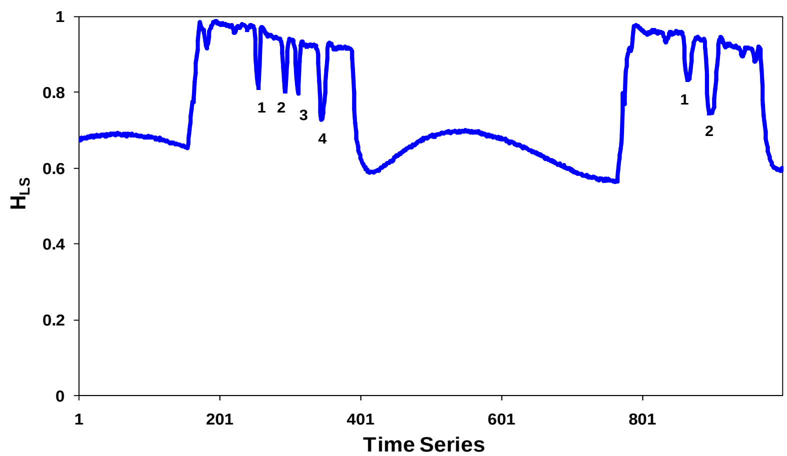

Future Tasks

- Dynamic Calibration for New Capacitance Sensor
- Record Videos with High Speed Video Camera for Each Flow Rate and Temperature
- Evaluate Data Acquired From Capacitance Sensor, Laser Sensor and Differential Pressure Sensor
- Compare Acquired Data with Predictions of Existing Correlations

Project Schedule

Literature Review	Completed
Facility Modifications	Underway
Preliminary Testing	Underway
Testing	November 2010
Data Analysis	March 2011
Final Report	May 2011

Questions

Inclination Effects on Flow Characteristics of High Viscosity Oil-Gas Two Phase Flow

Benin Chelinsky Jeyachandra

Project Completion Dates

Introduction

Nearly 70% of the oil resources available currently are high viscosity oil reserves. Depletion of lighter hydrocarbon resources has also increased the importance of high viscosity oils. A thorough knowledge on the flow behavior of high viscosity oils is required to optimize production facilities. The existing multiphase flow models were developed using the data collected from experiments on low viscosity oils. Hence these models inherently neglect the effect of viscosity on flow characteristics of multiphase flow.

Gokcal (2005) experimentally studied the effects of high viscosity on two phase oil-gas flow. There was marked difference between the experimental results and the model predictions. Intermittent slug and elongated bubble flow were observed to be the dominant flow pattern. Gokcal (2008) conducted experiments and developed correlations for two phase slug flow characteristics, taking into account, the effects of viscosity. The parameters that studied were pressure gradient drift velocity, transitional velocity, slug length and slug frequency. All tests were conducted for horizontal flow. The range of viscosities studied was from 121 cp to 1,000 cp. Kora (2010) conducted experiments and developed correlations for liquid holdup in horizontal high viscosity oil-gas flow.

The next logical step in the understanding of high viscosity oil-air two-phase flow would be to investigate the effect of inclination on the different flow parameters.

Literature Review

A detailed literature review on the effects of inclination and viscosity on multiphase flow was presented during May 2010 TUFFP Advisory Board meeting. The review revealed that the available correlations and models with the exception of drift velocity closure relationship, do not consider the combined effect of inclination angle and liquid viscosity. The inclined flow needs to be studied thoroughly from flow characterization to closure relationship development.

Experimental Study

Facility

The indoor high viscosity oil-gas facility is being modified to perform experiments to study the inclination effects. The capacity of the oil storage tank is 3.03m^3. A 20 HP screw pump is used to push the liquid through the loop. Air is delivered through a dry rotary screw type compressor. The oil and the air mix in a tee junction before proceeding to the test section.

The facility is comprised of a metering section, a test section, a heating system and a cooling system. The test section is 18.9 m (62 ft) long, 50.8 mm (2 in.) ID pipe. Nearly half of the pipe is made of a clear PVC pipe section and the rest is transparent acrylic pipe section (Fig. 1).

A 9.15-m (30 ft) long transparent acrylic pipe section is used to observe the flow behavior visually. A flexible hose connects the test section with the 76.2 mm (3 in.) ID return pipe. An oil transfer tank (1.32 m^3) is located at the end of return pipe. Return pipe is connected to this tank with a flexible hose. 3-hp progressing cavity pump is used to pump the oil from the new tank back to the main tank through the riser. The oil flow rates are measured at the inlet of the facility using Micro Motion mass flow meters (CMF025, CMF100, and CMF300). The air is measured at the inlet of the facility using Micro Motion mass flow meters (CMF025 and CMF050).

Separation is accomplished by gravity separation of air and oil. The separated air is removed through the ventilation system. The test section is supported on stands and the inclination of the test section can be set from -2° to 2° from horizontal by adjusting the heights of the stands.

The viscosity of the oil is controlled by controlling the temperature of oil at the tank. A 20 KW Chromalox heater capable of heating the heavy oil from 70°F to 140°F is used. The heating and the cooling section thus play a major part in the experiment to control the viscosities. Resistance Temperature Detector (RTD) transducers measure the temperatures during experiments. Pressure transducers and differential pressure transducers are located at different places to measure pressure and pressure drop in the loop.

Test Fluids

The high viscosity oil that would be used for this experiment is CITGO Sentry 220. The gas phase used is compressed air. Following are the typical properties of the oil:

Gravity: 27.6 °API
Viscosity: 0.220 Pa·s @ 40 °C
Density: 889 kg/m^3 @ 15.6 °C
Surface tension: 0.03 N/m @ 40 °C

Testing Range

Inclination, gas and oil flow rates, and oil temperature will be varied. Superficial liquid velocities will be varied from 0.01 m/s to 1.75 m/s and gas superficial velocity will be varied from 0 m/s to 10 m/s, respectively. The lower limits of superficial velocities are due to the accuracy limits of the Micro Motion TM flow meters. The higher limits are determined by the pressure gradient and facility limits. The experiments will be performed at temperatures of 21.1, 26.7, 32.2, and 37.8 °C (70, 80, 90, and 100 °F). The oil viscosities corresponding to the above temperatures are 0.587, 0.378, 0.257, and 0.181 Pa·s, respectively. The pipe inclination values are 2°, - 2° from horizontal. The test matrix superimposed on TUFFP unified flow pattern map for 2°, - 2°inclined flow is showed in Fig. 2 and 3, respectively.

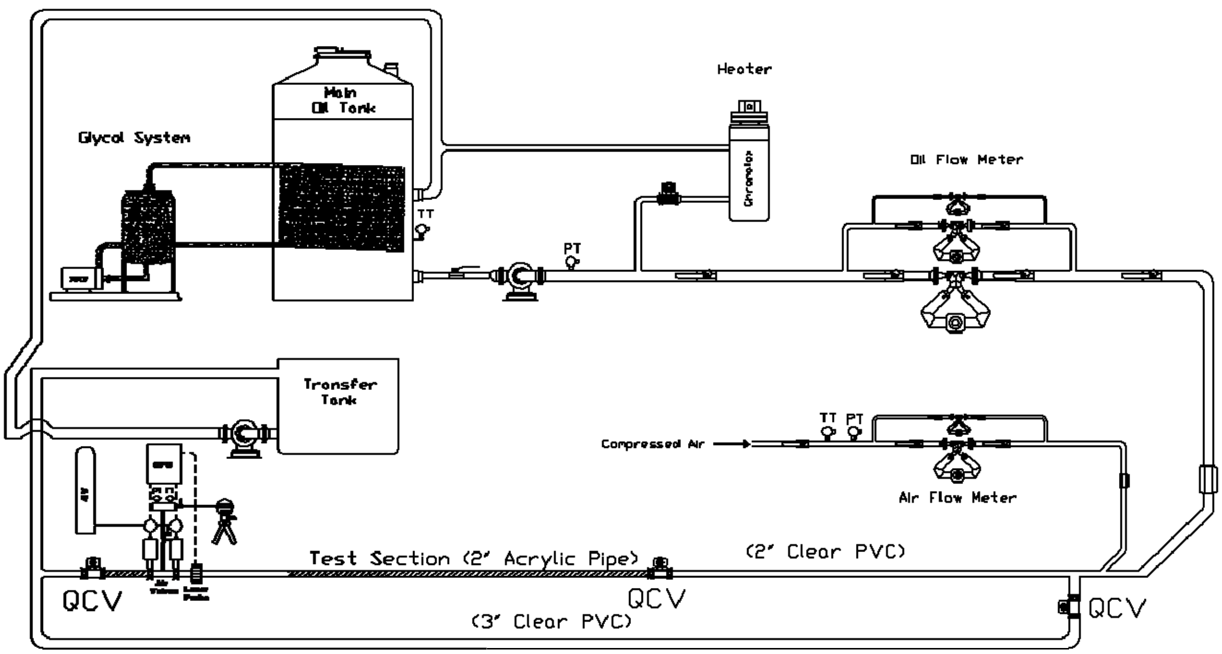

Figure 1 – High Viscosity Oil-Gas Two Phase Flow Loop.

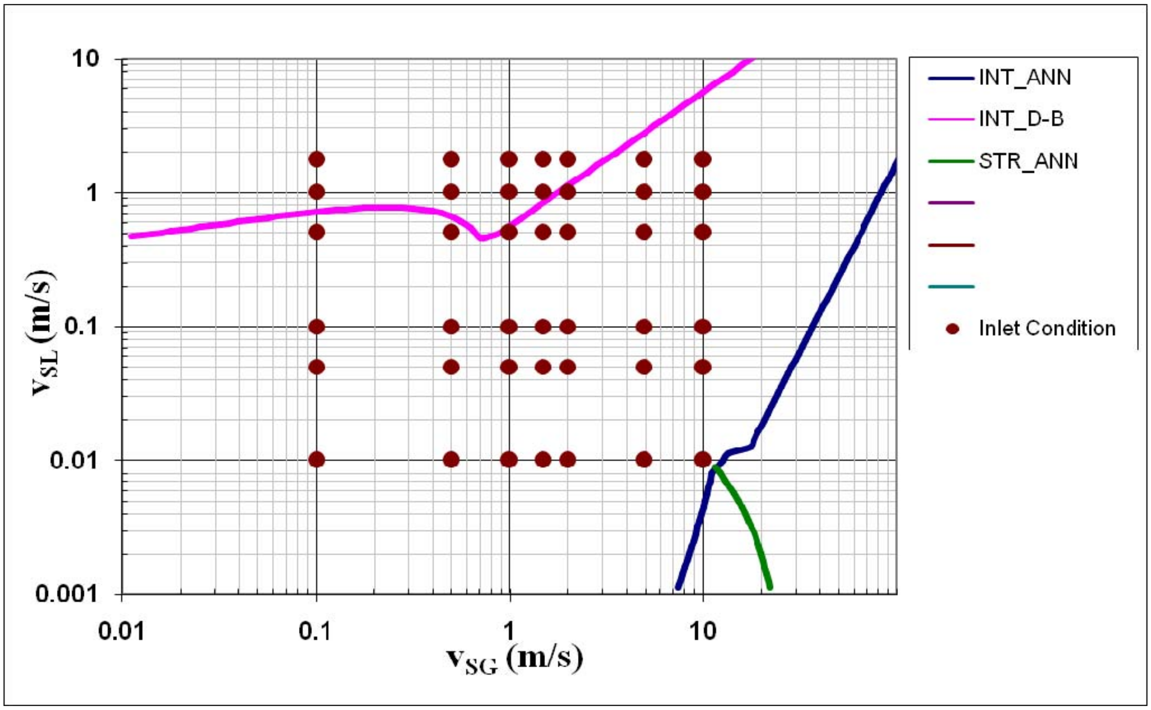

Figure 2 – TUFFP Unified Flow Pattern Map for Test Matrix of +2° Inclined Two Phase Flow.

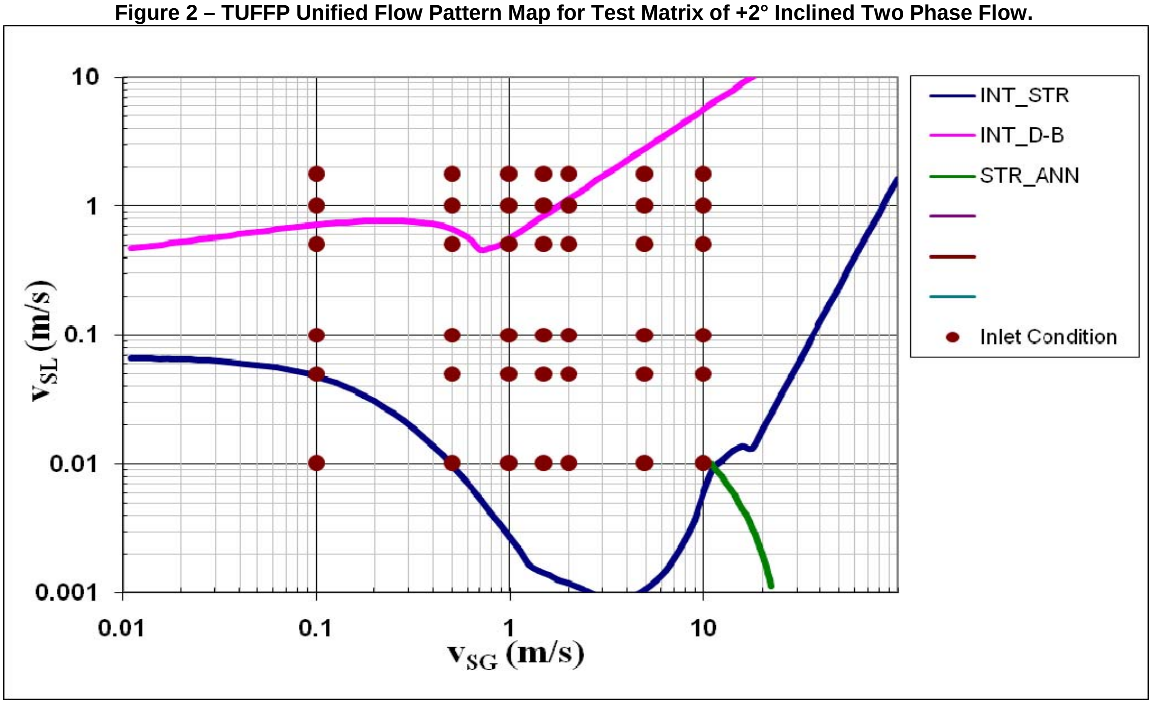

Figure 3 – TUFFP Unified Flow Pattern Map for Test Matrix of -2° Inclined Two Phase Flow.

Measurement and Instrumentation

Flow Patterns

TUFFP high speed video system will be used to identify the flow patterns. The flow patterns will be recorded using the high speed video system and the flow behavior will be analyzed.

Differential Pressure (DP) Measurement

There are 4 differential pressure transducers on the flow loop. DP1 and DP2 are located at the PVC section of the loop and are used for monitoring the development of flow. DP3 and DP4 located at the acrylic section are used for measuring the differential pressure.

Slug Length, Slug Frequency, and Translational Velocity

The acrylic section has provision for 2 laser sensors which when coupled with data acquisition system will provide the data for slug length, slug frequency and translational velocity.

Liquid Holdup

The most challenging part of this study is to measure gas void fraction in liquid slugs. For the measurement of slug liquid holdup, the existing capacitance sensor was improved upon and a new capacitance sensor (CS) has been developed. A summary of the capacitance sensor and the static calibration that was conducted is detailed below.

Capacitance Sensor

Gregory et al. (1978) used in-situ capacitance sensors, designed by Gregory and Mattar (1972) to acquire data for liquid holdup in a slug in horizontal pipes. Kouba (1986) and Felizola (1992) also measured instantaneous liquid holdup with parallel ring and helical wrap capacitance sensors. A quick-closing valve system was used for dynamic calibration of these capacitance sensors. After trapping the air-kerosene mixture, the mixture was drained and actual liquid holdup is calculated based on the drained volume for low viscosity oil.

A new capacitance sensor (CS) had been developed in-house for the measurement of slug liquid holdup.The principle of the capacitance method is based on the differences in the dielectric constants of the gas and liquid phases in the flow. Gokcal (2008) used a concave type capacitance sensor for slug length and slug frequency measurements. Previously, the concave type capacitance sensor was tested for slug liquid holdup measurements. No significant differences in the output data were observed during slug flow. This design was improved by Kora (2010) and consisted of two parallel copper wires positioned perpendicular to the flow with a distance in between (0.25 in.), an electronic circuit to filter, amplify and convert the measured capacitance to a voltage, and the housing.

To further enhance the quality of data and provide a circumferential snapshot of a slug, the design was modified by placing 2 concave C-shaped copper strips (Fig. 4) together covering the inner circumference of the pipe and plugging it to a circuit to amplify and record the data.

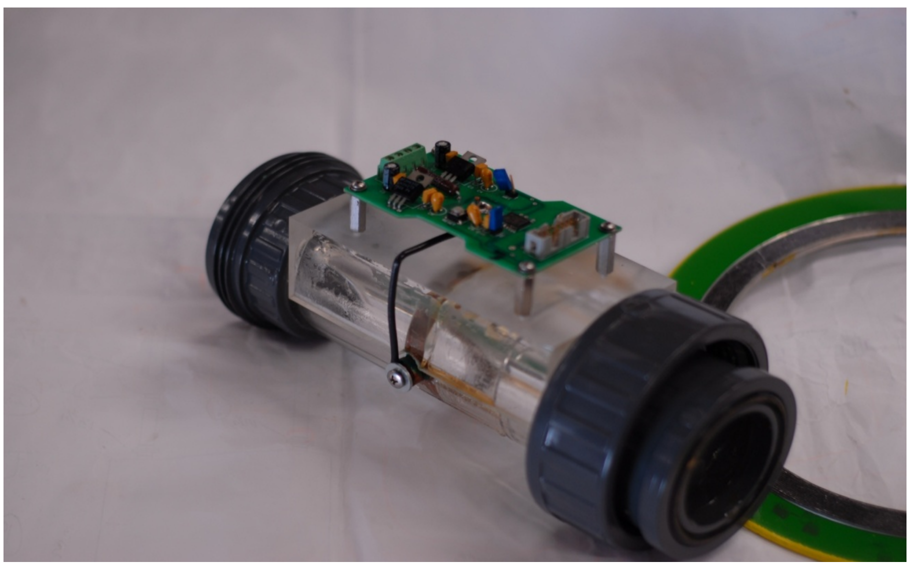

Figure 4 - New Concave Type Capacitance Sensor.

Static Calibration

Figure 5 shows the static calibration curve for the new capacitance sensor. Static calibration of CS was accomplished by placing different amounts of liquid volumes in an acrylic pipe tester with the CS in the middle, and measuring the height of the fluid in the pipe, then recording the corresponding sensor output voltage. The actual voltage reading was then converted to a dimensionless voltage.

The corresponding liquid holdup was calculated as the ratio of the volume of the liquid injected and the total volume of the tester. A graph of dimensionless voltage vs. liquid holdup was plotted and the resulting curve is the static calibration curve. The shape of the curve is S-shaped and is expected because of the shape effect of the pipe. During the initial phase and final phase of injection, oil wets the perimeter of the pipe quickly compared to the middle phase where the wetting is almost linear.

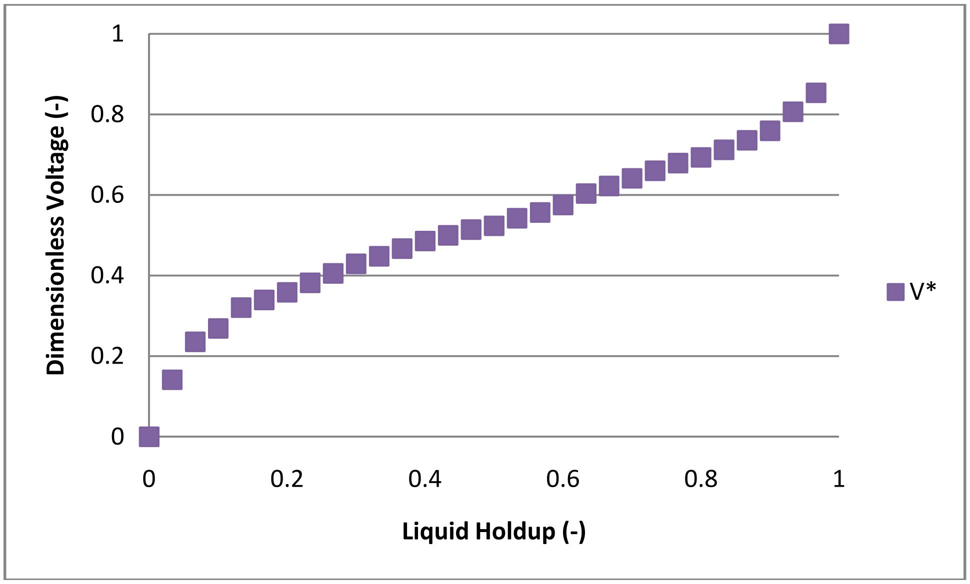

Figure 5 – Static Calibration of Capacitance Sensor.

Dynamic Calibration

Dynamic calibration of CS will be conducted using existing quick-closing valve system (QCV). CS, QCV and high speed video camera should be synchronized. CS will be placed 1.5 ft before the quick-closing valve system. Shortly before capturing the slug body with QCV, data collection process with CS will be started. High speed video camera will be used to verify the trapped part of the slug body for the analysis of the CS reading. The dynamic calibration plot should be generated by plotting the actual liquid holdup data (QCV measurement) versus the calculated liquid holdup data (capacitance sensor output) at different test conditions. Finally, in order to calculate the liquid holdup in the slug body, numerical integration is used to estimate the area under the curve, and it is divided by the area as if the liquid slug is pure oil.

Results

5 horizontal tests were conducted to verify if the output of capacitance sensor is in sync with the flow at 70 °F corresponding to 0.587 Pa·s oil viscosity. The superficial gas velocities varied from 0.01 to 1.5 m/s and superficial liquid velocities from 0.1 to 0.5 m/s. Visual observation confirmed that there was no large bubble entrained for lower superficial velocities but as the superficial velocities increase, the number of large bubbles entrained within the slug body increased. This effect leads to decrease in slug liquid holdup. It was also observed that the size of the large bubbles decreases as the superficial velocities increase.

CS provides extensive information through the slug. Even though measuring holdup with quick-closing valve system is a non-intrusive method the results are restricted by the representation of the trapped parts of the liquid slugs. Non-homogenous form of liquid slug is determined from high speed camera videos and CS readings. This is the primary reason of discrepancy between the quick-closing system and CS slug liquid holdup data. Therefore, CS will be used for the measurement of slug liquid holdup.

The data acquisition system (DAQ) is programmed to capture data for 10 seconds with a frequency of 1000 readings/second. Figure 6 shows the variation of voltage in capacitance and laser sensors, as a slug passes through. This corresponds to vSL= 0.01 m/s and vSg= 0.1 m/s. The voltage reading for 10 seconds give a single well defined slug with very less entrained gas bubbles. Figure 7 shows a magnified view of the same slug.

Figure 8 shows the voltage variations for a higher superficial velocities of v_{SL}= 0.5 m/s and v_{Sg}= 1 m/s for 10 seconds. As can be seen clearly, the number of slugs in a 10 second period has increased to11 slugs. Figure 9 which magnifies a particular slug in the capacitance series shows the presence of 4 large bubbles entrained in the slug body.

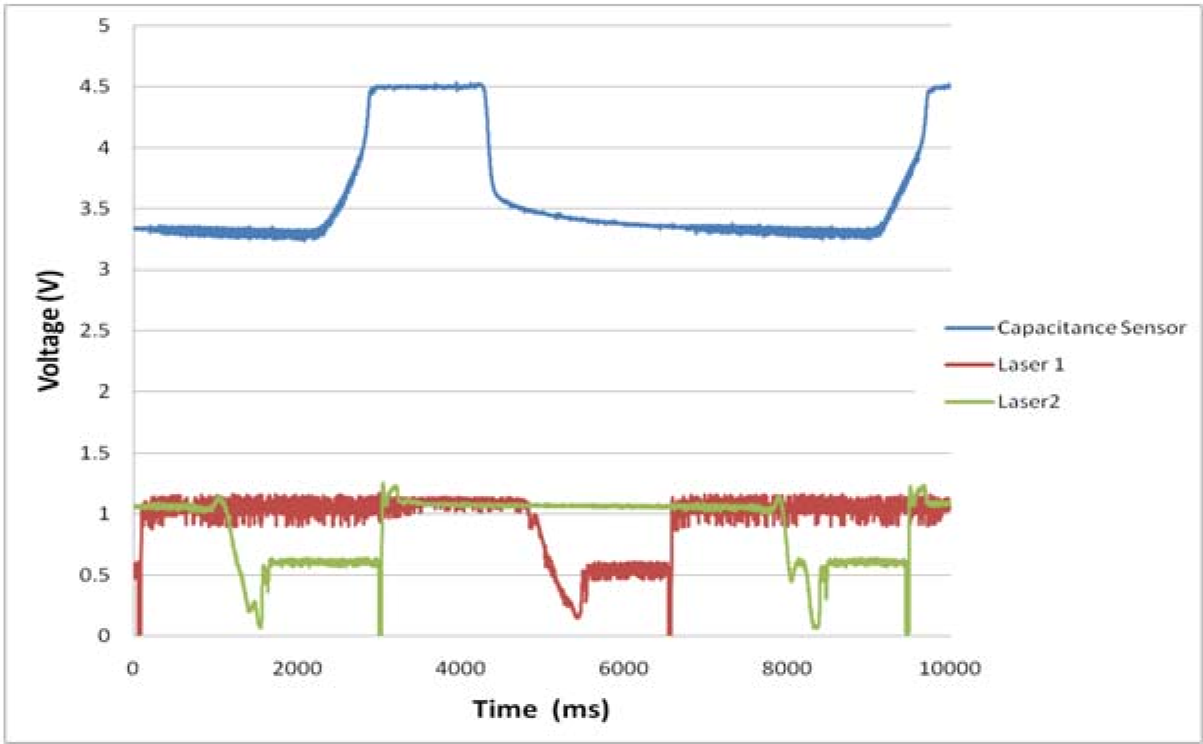

Figure 6 – Laser and Capacitance Sensor Reading for v_{SL}= 0.01 m/s and v_{Sg}= 0.1 m/s.

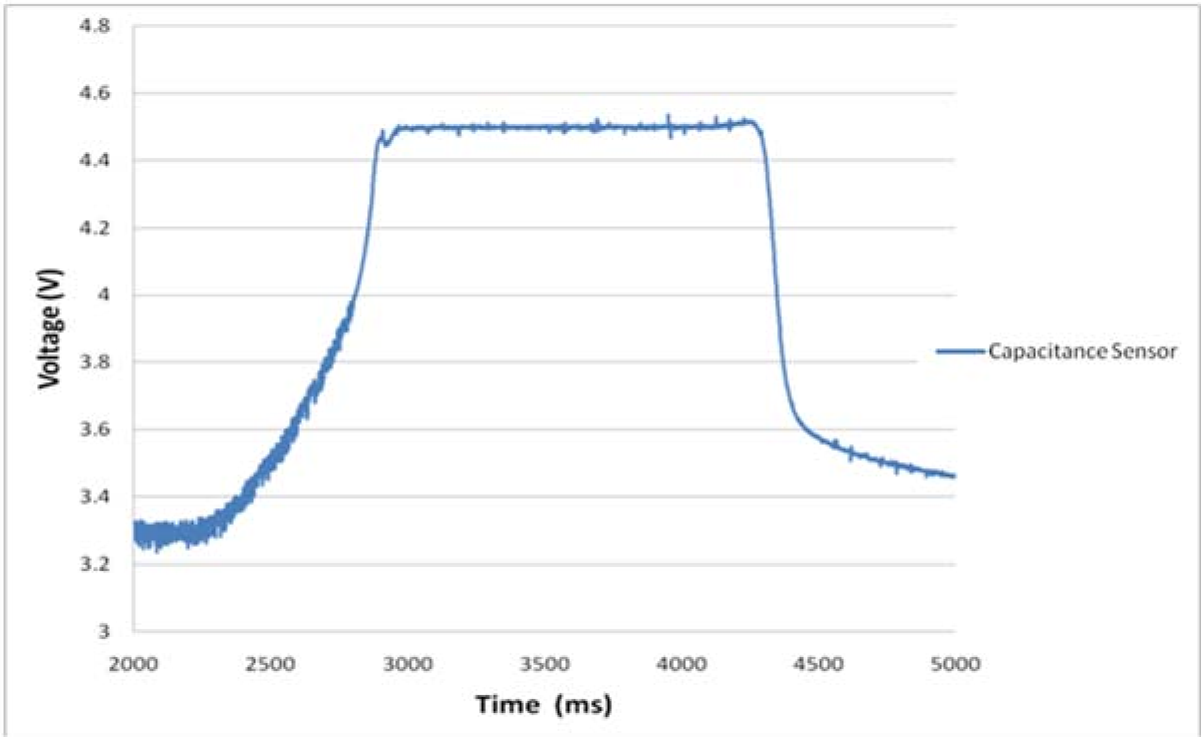

Figure 7- Magnified View of Slug Region for v_{SL}= 0.01 m/s and v_{Sg}= 0.1 m/s.

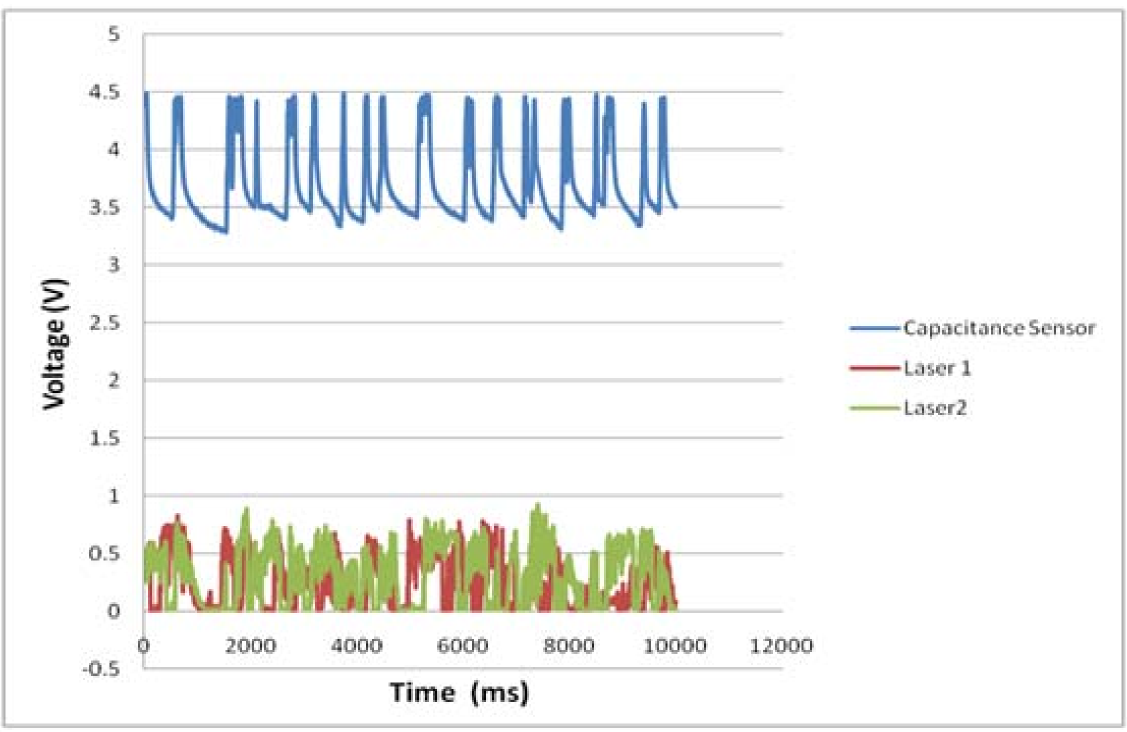

Figure 8 – Laser and Capacitance Sensor Reading for v_{SL}= 0.5 m/s and v_{Sg}= 1 m/s.

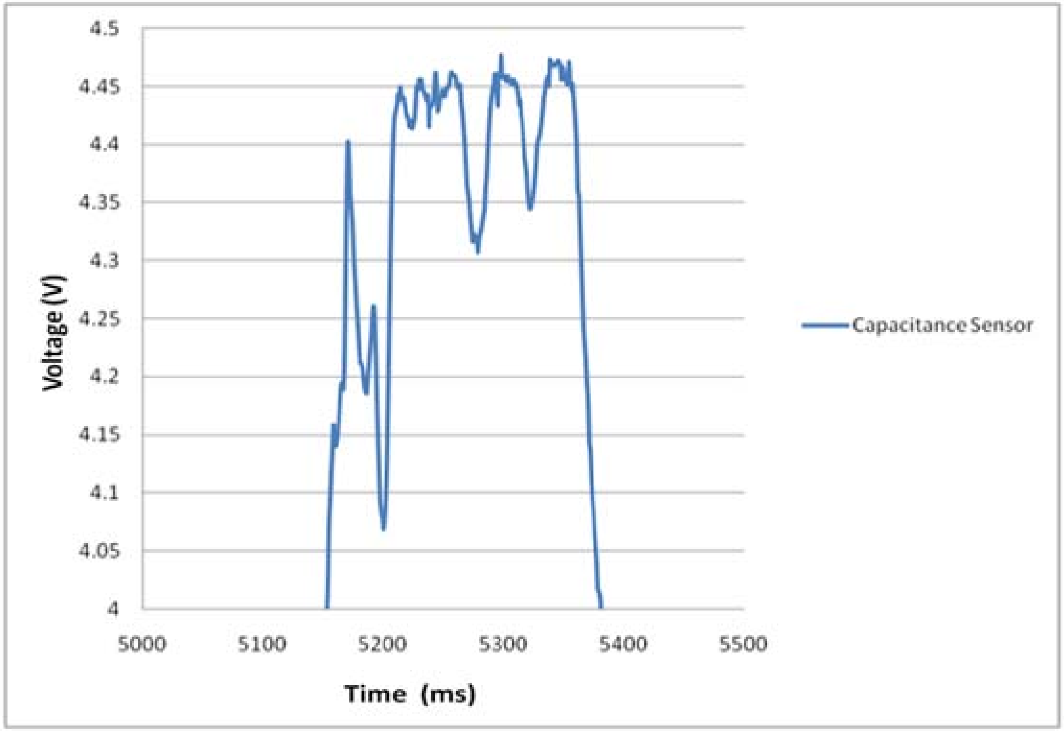

Figure 9- Magnified View of Slug Region for v_{SL}= 0.5 m/s and v_{Sg}= 1 m/s.

Facility Modifications Update

The new capacitance sensor was integrated into the loop along with the laser sensors and the circuitry. Inclination of the flow loop is completed. The first phase of testing will have an inclination angle of -2°. The loop is already inclined using a pivot arrangement. Additional supports are being provided. A new base has to be designed for the quick closing valves to adjust with inclination angles. The return pipe has to be re-routed to the auxiliary tank as the current configuration may lead to terrain slugging.

Conclusions

From the preliminary experiments it is observed that the capacitance sensor is in proper working condition and it is able to capture the movement of slug with good accuracy. Dynamic calibration of CS with quick closing valves will aid in collecting liquid holdup data. It is also observed that for low superficial velocities, the slug length is long and the slug body contains less entrained bubbles. As the superficial velocity increases, the slug length decreases and entrainment of large bubbles within the slug body.

Nomenclature

ID = internal diameter of the pipe
V = velocity [m/s]

Greek Letters

μ = viscosity [kg/ms]
ρ = density [kg/m3]
σ = surface tension [N/m]
θ = inclination angle [º]

Subscripts

G = gas phase
L = liquid phase

References

Felizola, H.: "Slug Flow in Extended Reach Directional Wells," Ms Thesis, The University of Tulsa, Tulsa, OK (1992).

Gregory, G. A, Mattar, L.: "An in-situ volume fraction sensor for two-flows of non-electrolytes." Can. J. Pet. Tec. 12–13 48–52 (1973).

Gregory, G.A., Nicholson, M.K., Aziz, K.: "Correlation of the Liquid Volume Fraction in The Slug for Horizontal Gas–Liquid Slug Flow," Int. J. Multiphase Flow 4, 33–39 (1978).

Kouba, G.: "Horizontal Slug Flow Modeling and Metering," Ph.D. Dissertation, The University of Tulsa, Tulsa, OK (1986).

Kouba, G. E., W. P. Jepson.: "The How of Slug In Horizontal, Two Phase Pipelines," Twelfth Annual Energy-Sources 'Technology Conference and Exhibition, Houston, Texas (1989).

Fluid Flow Projects

Investigation of High Viscosity Oil Two-Phase Slug Length in Horizontal Pipes

Eissa Al-safran (KU/KOC)

Outline

- Introduction
- Flow Visualization
- Data Analysis
- Physical and Theoretical Viscosity Effect
- Modeling
- Future Work

Significance

- Pipeline Design (Sizing and Routing)
  - Pressure Drop
  - Liquid Volume
- Facility/Equipment Design
  - Instantaneous Liquid Rate at Pipe Outlet is 5-20 x Average Rate
  - Slug Catchers
  - Multiphase Pumps
  - Multiphase Meters

Fluid Flow Projects Advisory Board Meeting, Nov. 3, 2010

Significance …

- Flow Assurance
  - Terrain Slugging
  - Erosion/Corrosion
- Mechanical Integrity
  - Piping System
  - System Components

Fluid Flow Projects Advisory Board Meeting, Nov. 3, 2010

Literature Review

- No Literature is Found on High Viscosity Oil Two-phase Slug Length
- Low Viscosity Oil Slug Length is Strongly Correlated to Pipe Diameter, and Insensitive to Other Parameters
- Low Viscosity Oil Slug Length
  - Smallest Near the "Center" of Slug Flow Region on Flow Pattern (FP) Map
  - L_s Increases Near Transition Boundaries

Literature Review ...

- High Viscosity Effect on Liquid Holdup in Film and Slug Regions-Direct Relationship
- High Viscosity Effect on Slug Frequency-Inverse Relationship
- Increase of Slug Frequency and Slug Liquid Holdup Results in Short Slugs

Flow Visualization

- Slug Zone (v_{SL}=0.01 m/s, v_{Sg}=1.5 m/s)
  - Slug Front

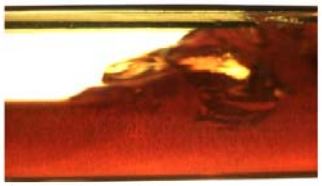

μ=0.590 Pa.s

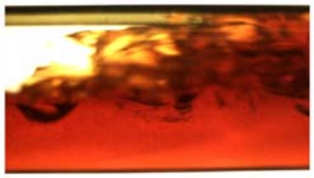

μ=0.182 Pa.s

Fluid Flow Projects

Advisory Board Meeting, Nov. 3, 2010

Flow Visualization ...

- Slug body

μ=0.590 Pa.s

μ=0.182 Pa.s

Fluid Flow Projects

Advisory Board Meeting, Nov. 3, 2010

Flow Visualization ...

➢ Slug Tail

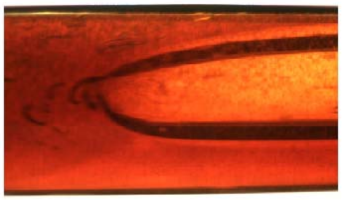

μ=0.590 Pa.s

μ=0.182 Pa.s

Fluid Flow Projects

Advisory Board Meeting, Nov. 3, 2010

Flow Visualization ...

- Film Region (v_{SL}=0.1 m/s, v_{Sg}=2 m/s, μ=0.26 Pa.s)

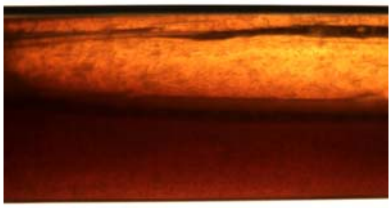

Developing film

Developed film

Fluid Flow Projects

Advisory Board Meeting, Nov. 3, 2010

Data Analysis

- Comparison (Kouba (1986), BP Loop (2001), Alsafran (2003), Gokcal (2008))

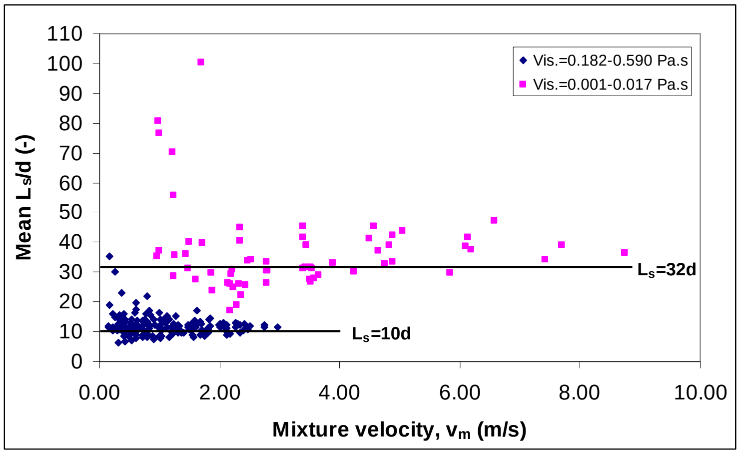

Fluid Flow Projects

Advisory Board Meeting, Nov. 3, 2010

Data Analysis ...

- Slug Length Distribution Comparison (Low Viscosity vs. Moderate vs. High Viscosity)

v_{SL}=0.3 m/s
v_{Sg}=1.5 m/s

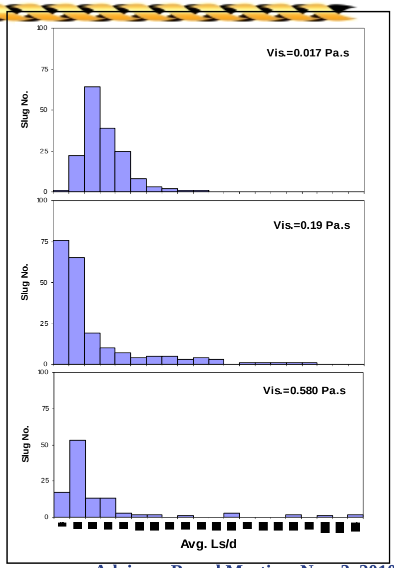

Fluid Flow Projects

Advisory Board Meeting, Nov. 3, 2010

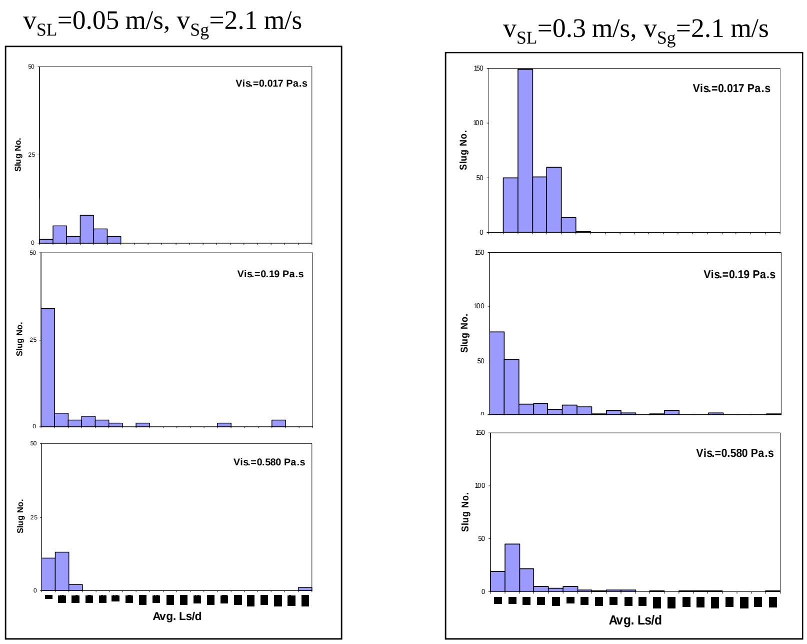

Data Analysis ...

- **Analysis of Variance (ANOVA) to Test the Following Hypothesis:**

$$H_0 : \mu_{low} = \mu_{mid} = \mu_{high}$$

  - **Calculate p-value and Set Significance Level (α=0.10), i.e. 90% Confidence**
  - **Calculated p-value<α, Thus Reject H_0**

Physical Viscosity Effect

- Dukler *et al.* (1985) Proposed Minimum Slug Length Physical Model

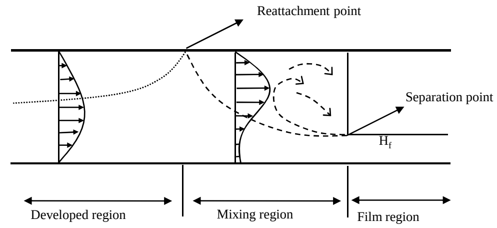

  - Sudden Expansion at Separation Point
  - New Wall Boundary at Reattachment Point
  - Downstream a Fully Developed Velocity Profile is Formed and Flow "Memory" Vanishes

Fluid Flow Projects   Advisory Board Meeting, Nov. 3, 2010

Physical Viscosity Effect ...

- Proposed High Viscosity Liquid Physical Model
  - Thick Film-Less Expansion (Jet Velocity)
  - Less (Short) Front Mixing Intensity
  - Smaller Velocity Profile and Maximum Velocity

$$v_z = \frac{\Delta P \times R^2}{4\mu L}\left[1-\left(\frac{r}{R}\right)^2\right]$$

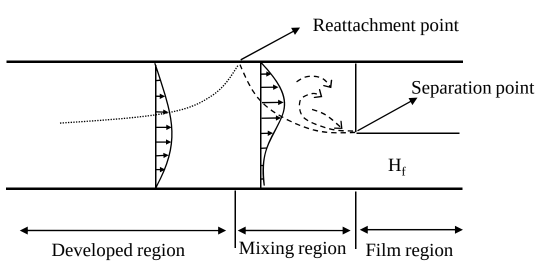

Fluid Flow Projects   Advisory Board Meeting, Nov. 3, 2010

Theoretical Viscosity Effect

$$L_s = \frac{v_s}{\upsilon_s \left(H_{LLS} - H_{LTBe}\right)}\left[\left(\frac{W_L}{\rho_L A_p v_s} - H_{LTBe}\right) + c\left(H_{LLS} - H_{LTBe}\right)\right]$$

First Term: $\left[\frac{v_s \downarrow}{\upsilon_s \uparrow \left(H_{LLS} \uparrow - H_{LTBe} \Uparrow\right)\downarrow}\right]\downarrow$

Second Term: $\left[\left(\frac{W_L \rightarrow}{\rho_L (\rightarrow) A_p (\rightarrow) v_s (\downarrow)}\right)\uparrow - H_{LTBe} \Uparrow\right]\downarrow$

Third Term: $\left[c(\rightarrow)\left(H_{LLS} \uparrow - H_{LTBe} \Uparrow\right)\right]\downarrow$

Thus, Slug Length Decreases with Increasing Liquid Viscosity

Modeling

- **Woods and Hanratty (1996) (Low Viscosity)**

$$\frac{f_s D}{v_{SL}} = 1.2\left(\frac{L_s}{d}\right)^{-1} \quad \text{.......................} \ (1)$$

- **This Study (High Viscosity)**

$$\frac{f_s d}{v_{SL}} = 1.94\left(\frac{L_s}{d}\right)^{-1} \quad \text{.......................} \ (2)$$

Modeling ...

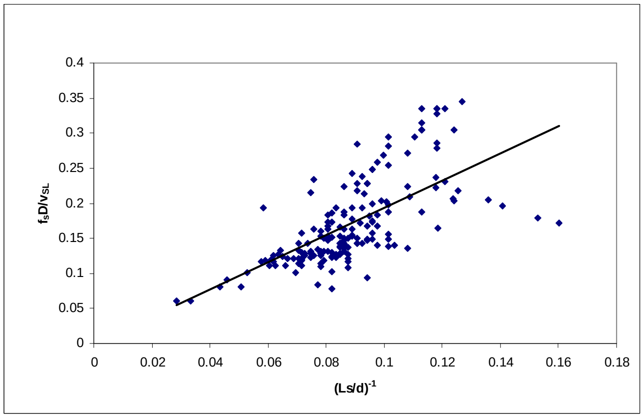

Modeling ...

- **Wallis (1969) Presented Dimensional Analysis for Inertia and Viscous Forces**

$$F_{rd} = \frac{v_d}{(gd)^{0.5}} \sqrt{\frac{\rho_L}{(\rho_L - \rho_G)}} \quad \ldots\ldots\ldots\ldots\ldots\ldots\ldots (3)$$

$$N_\mu = \frac{v_d \mu_L}{gd^2(\rho_L - \rho_G)} \quad \ldots\ldots\ldots\ldots\ldots\ldots\ldots (4)$$

Modeling ...

- Combing Froude and Viscosity Numbers

$$N_f = \frac{F_{rd}}{N_\mu} = \frac{d^{3/2}\sqrt{\rho_L(\rho_L - \rho_G)g}}{\mu_L} \quad \text{..................... (5)}$$

- Gokcal *et al.* (2009) showed

$$f_s = 2.623\left(\frac{N_f^{-0.612} v_{SL}}{d}\right) \quad \text{..................... (6)}$$

Fluid Flow Projects

Advisory Board Meeting, Nov. 3, 2010

Modeling ...

- Combing Eqs. 2, 5 and 6, and Solving for Dimensionless Slug Length

$$\frac{L_s}{d} = \beta_0 N_f^{\beta_1} \quad \text{..................... (7)}$$

- Linearizing and Fitting the Proposed Model against High Viscosity Data

$$\frac{L_s}{d} = 2.63 N_f^{0.321} \quad \text{..................... (8)}$$

Fluid Flow Projects

Advisory Board Meeting, Nov. 3, 2010

Modeling …

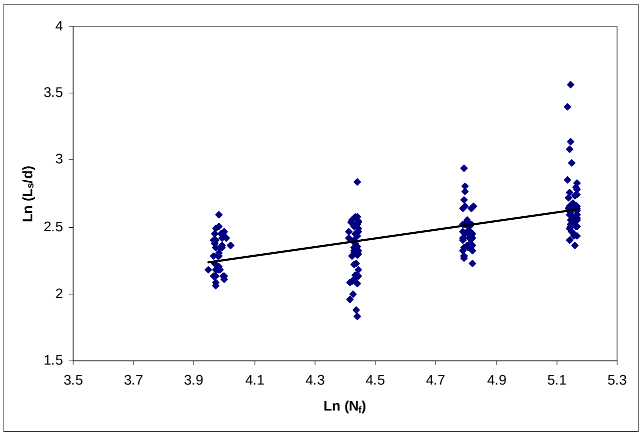

Modeling …

- Model Statistical Evaluation
  - Overall Model Evaluation

Model df	Error df	SSE	MSE	R^2
1	161	6.43	0.200	0.32

  - Model Coefficient Evaluation

Variable	Coef.	Standard Error	t-statistics	p-value	Lower 95% CI	Upper 95% CI
$Ln(\beta_0)$	0.966	0.170	5.800	0.000	0.650	1.310
β_1	0.321	0.036	8.730	0.000	0.246	0.390

Modeling ...

- **Model Validation**
  - **10 data points Selected Randomly and Removed From Model Development Process**
  - **Statistical Error Analysis Results**

Stat. Parameter	Value
APE (%)	1.72
AAPE(%)	9.8
SD(%)	13.6

Modeling …

- **Model Validation …**

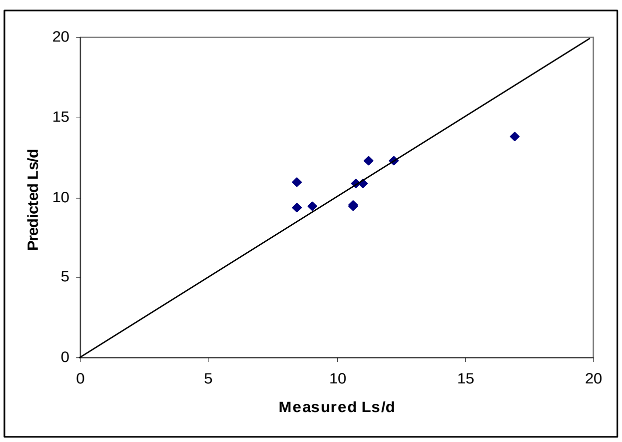

Modeling …

- Model Comparison
  - 10 data points Selected Randomly and Removed From Model Development Process

Correlation	APE (%)	AAPE (%)	SD (%)
Brill *et al*. (1980)	295.2	295.2	78.1
Scott *et al*. (1981)	344.6	344.6	83.3
Norris (1982)	298.9	298.9	74.8
Barnea & Brauner (1985)	203.7	203.7	56.9
Dukler *et al*. (1985)	89.8	89.8	35.6
Present Study	1.7	9.8	13.6

Conclusion

- Slug Structure (Front and Back) in High Viscosity Liquid Condition is Different than Low Viscosity Condition. This Structure Results in Shorter Slugs.
- Average Stable Slug Length is equal 10d and Remains Constant above v_m=0.5 m/s.

Conclusion . . .

- Slug Length Distribution is Truncated and Heavily Skewed to The Right.
- Large Film Thickness and Small Centerline Velocity and Velocity Profile Shorten the Required Slug Length to Reach Stable Slug.
- High Liquid Viscosity Slug Length Empirical Correlation is Proposed, Validated and Compared with Existing Correlations.

Conclusion . . .

- Model Validation Study Show APE=1.7%, AAPE=9.8% and SD=13.6%.
- Comparison Study Show Proposed Model Outperform Large Diameter and Small Diameter Existing Correlations.

High Viscosity Liquid Effect on Two-Phase Slug Length in Horizontal Pipes

Eissa Al-safran

Abstract

Among all the slug flow characteristics, slug length is one of the most critical characteristic for system proper design and safe operation. The recent trends of increasing energy demand, led the industry toward the development of heavy oil unconventional resources. However, the production and transportation of such heavy oil is a challenge due to the lack of understanding of the two-phase flow behavior under the condition of high viscosity liquid phase. The objective of this study is to physically understand and quantify the effect liquid viscosity on slug length and develop two-phase slug length model for high oil viscosity. The developed slug length model can improve the existing two-phase flow models in the development and maintenance of heavy oil fields.

Experimental high viscosity (0.181-0.589 Pa.s) two-phase air/mineral viscous oil slug length data is acquired in a horizontal 0.0508-m ID pipe. Data analysis showed a significant reduction in the average slug length compared to the stable slug length under low viscosity condition. Physical modeling suggests that a thick liquid film in the Taylor bubble zone and short slug mixing zone result in a fully developed velocity profile stabilizing the slug at an average length of 10 diameters. In addition, high speed recorded flow visualization revealed the effect of liquid phase viscosity on the scooping and shedding processes at the front and back of the slug, respectively; which is speculated to reduce the slug length. Statistical analyses showed a significant effect of liquid phase viscosity on slug length distribution including maximum slug length and slug length variation.

Introduction

Gas-liquid two-phase flow in pipes occurs at production and transportation facilities for oil and gas. The most common type of flow patterns in field operation for horizontal and near horizontal pipelines is the slug flow pattern. Slug flow is described by alternating liquid slugs and gas intervals, both of which when combined form what is called slug unit. Among all the slug flow characteristics, slug length is one of the most critical characteristic for system proper design and safe operation. For example, average slug length is important and preferred (over slug frequency) input parameter for mechanistic models to predict liquid holdup and pressure gradient. Furthermore, long slugs often cause operational problems, flooding of downstream facilities, severe pipe corrosion, structural instability of the pipeline, as well as production loss and poor reservoir management due to unpredictable wellhead pressures. Although several investigators studied the average and slug length distribution in pipes for light oil, a recent literature search on high viscosity two-phase slug length revealed no comprehensive study. However, few studies were found on the effect of high viscosity liquid on other two-phase slug flow characteristics such as liquid holdups and frequency, which can be related, implicitly, to slug length.

Nadler and Mewes (1995) experimentally investigated the liquid viscosity effect on liquid holdup in the slug unit, film region and slug zone in the aerated slug flow region. They used three fluid systems, air/light oil (μ_o=17 mPa.s), air/heavy oil systems (μ_o = 34 mPa.s) and air/water systems. In general, their results revealed that by increasing liquid viscosity, a significant increase of liquid holdup in the slug unit and film region is observed, while less significant increase of liquid holdup in the slug zone is observed. The observed directly proportional relationship between film liquid holdup and liquid viscosity is explained by the increase of interfacial and wall shear forces on the liquid film. A significant difference in slug unit and film liquid holdup is observed between air/light oil and air/water systems; which is attributed to the difference in surface tension and densities of the two systems. Abdul-Majeed (2000) developed an empirical correlation for slug liquid holdup as a function of liquid viscosity. He reported that slug liquid holdup is significantly affected by and is directly proportional to liquid viscosity. Brauner and Ullmann (2004) developed a Taylor bubble wake model of gas entrainment from Taylor bubble to slug body to predict the slug liquid holdup in vertical, inclined and horizontal pipes. Their model takes into account the effect of liquid viscosity which predicts that the bubble entrainment decreases (slug liquid holdup increases) with increasing liquid viscosity. Slug frequency was also investigated for the high viscosity two-phase flow. A recent study by Gokcal *et al.* (2009) shows that slug frequency increases with increasing liquid viscosity for which they developed an empirical slug frequency correlation. Comenares *et al.* (2001) slug flow experimental results with a 0.48 Pa.s liquid viscosity revealed an average slug length much sorter than 30d, but they did not report any quantitative value. A recent study by Kora (2010) investigated slug liquid holdup and film height in Taylor bubble region revealed that slug liquid holdup increased with liquid viscosity, while liquid film unchanged with liquid viscosity. Furthermore, proposed a new empirical correlation to predict slug liquid holdup for liquid viscosity range of 0.2-0.6 Pa.s.

The above literature review suggests that under the condition of high liquid viscosity, slugs are less aerated and more frequent. Theoretically, these two characteristics result in short slugs. Furthermore, experimental slug flow data (Kouba (1990), Kokal (1987), Marcano (1996), Rothe (1986), Brandt and Fuchs (1989), and El-Oun (1990)) on light oil showed the inverse relationship between slug frequency and slug length, and between the slug liquid holdup and slug length. Therefore, from the limited literature review on high viscosity oil and the previous knowledge and experimental data on the relationships among slug flow characteristics, one can speculate an inverse relationship between liquid viscosity and slug length. This is what will be discussed in this paper.

Flow Visualization

Flow visualization using high speed camera is presented for different parts of the slug flow, namely slug back and front, slug body, and film region at different viscosities. The purpose of this visualization is to characterize and better understand the slug flow structure under the effect of high liquid viscosity to be able to relate the slug and film structures to slug length.

Slug Body Zone

Figure 1 shows the slug front, slug body and slug tail for two different liquid viscosities, 0.590 Pa.s, and 0.182 Pa.s at v_{Sg}=1.5 m/s and v_{SL}=0.1 m/s. The low liquid viscosity slug (Slug A) shows turbulence and mixing in the slug front due to the high Reynolds number. On the other hand, the high viscosity slug front (slug B) is less turbulent with a top boundary layer moving faster than the slug body and entraining large bubbles. As oppose to the conventional slug front scooping process, this scooping process does not cause bubble fragmentation and entrainment into slug body; instead, it entrains large bubbles into the slugs under a new mechanism. It is evident from the slug front pictures that viscosity affects the scooping process at slug front. The middle pictures of **Fig. 1** illustrate the slug body for the same slug; which shows the impact of gas entrainment in slug front on slug body. Slug B shows a large gas pocket entrained in the slug front which grows further as small bubbles merge in it. This large bubble is a result of the scooping process at the slug front. As the gas pocket grows, it splits the long slug to two shorter slugs, this is one of the mechanism generating short slugs in high liquid viscosity flows. On the other hand, low viscosity slug body shows relatively smaller entrained bubbles due to the high turbulence and mixing in the slug front which causes bubbles fragmentation generating small bubbles. The lower pictures of **Fig. 1** show the slug tail for the same slugs shown previously. The high viscosity slug (Slug A) shows a long bubble nose accelerated by the wake of entrained large gas pocket which leads to short stable slugs. The lower viscosity slug back shows a sharper, less developed and deformed bubble nose. The location of the bubble nose in low viscosity liquid condition with respect to pipe centerline is asymmetric as oppose to the symmetric geometry in the high viscosity condition. In summary, **Fig. 1** shows that liquid viscosity significantly affects the slug structure.

Film (Taylor-bubble) Zone

Similar to the slug zone, high viscosity liquid significantly affects the liquid film characteristics in the Taylor bubble region. Experimental observations, under high liquid viscosity condition, by high speed video recordings show that the film height is significantly large and aerated as oppose to the low liquid viscosity condition. Furthermore, it is observed that the film region has two distinct sub-regions, namely developing and developed regions as shown in **Fig. 2**. The developing region is observed within 5d-10d from the Taylor bubble nose. As **Fig. 2.a** shows, the developed film region is characterized by a relatively thick film at the pipe top wall and a secondary tangential film flow in addition to its axial flow which increases the film height in this developing region. The developed section (**Fig. 2.b**) is far away from the slug zone and can be characterized by a stratified film layer. However, in the case of high liquid viscosity, a thin film layer is observed at the top wall of the pipe similar to annular flow configuration. Under certain condition of high superficial gas velocity, this layer is observed to be wavy with large entrained bubbles. This film characterization under high liquid viscosity may change the conventional modeling approach of the film zone in a slug unit.

Data Analysis

In this section, the average slug length and slug length distributions of high viscosity liquid will be presented and compared with low viscosity liquid slug length. The purpose of this comparison is to illustrate the effect of the liquid viscosity and its magnitude on slug length. **Fig. 3** illustrates the evolution of the dimensionless average slug length with mixture velocity for high and low viscosity liquids which show that under high viscosity liquid condition, average slug length is shorter than that of low viscosity liquid. Figure 3 further shows a decreasing slug length trend at low values mixture velocity followed by a constant average slug length around 10d for a high viscosity liquid. Similar to the low viscosity liquid slug length trend, high viscosity average slug length shows insensitivity to operational conditions. In addition, the critical mixture velocity beyond which average slug length remains constant for high viscosity liquid is in the order of 0.5 m/s, while it is 1 m/s under light oil condition.

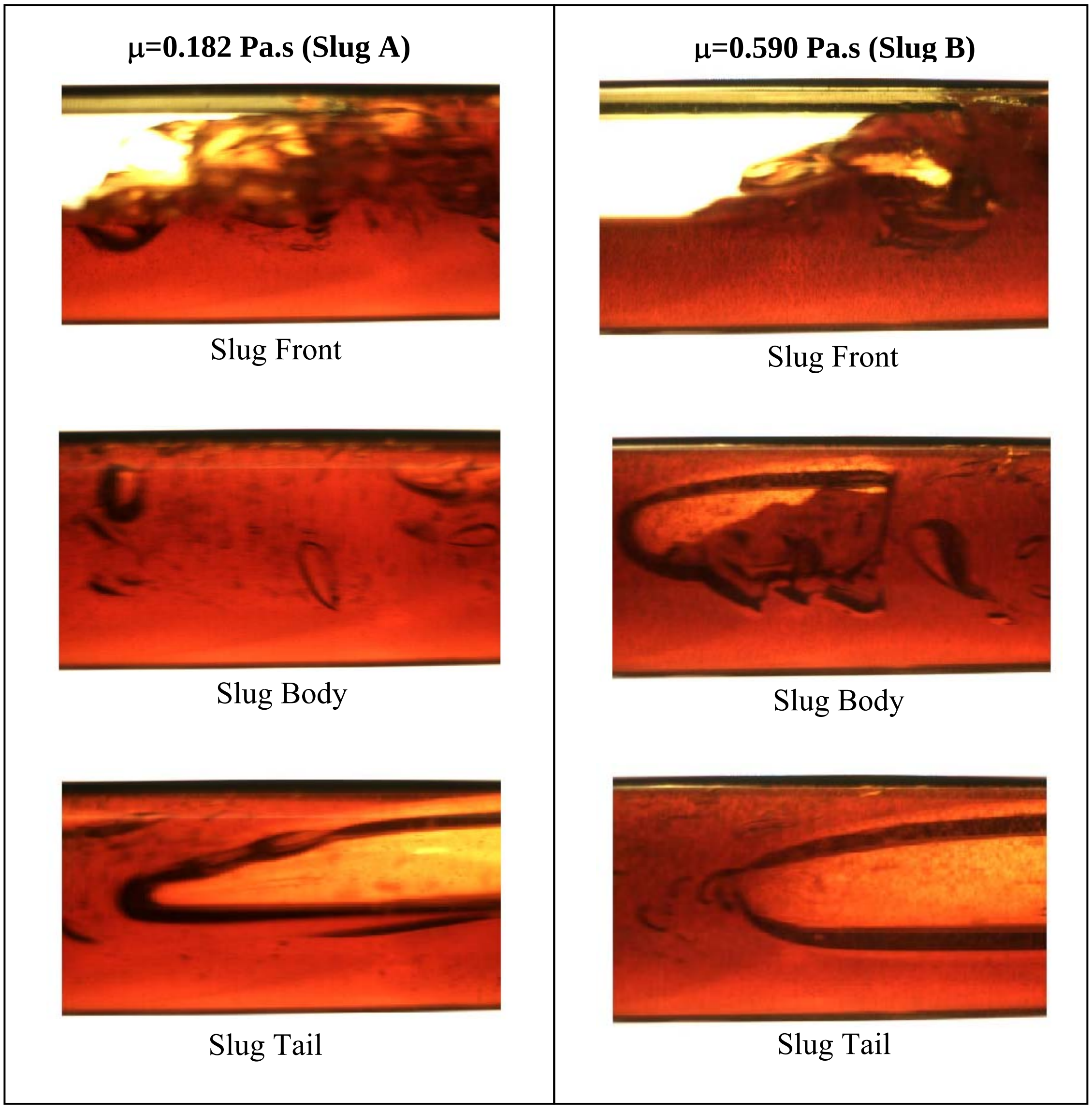

Fig. 1 – Comparison of slug front for different viscosities (v_m=1.51 m/s)

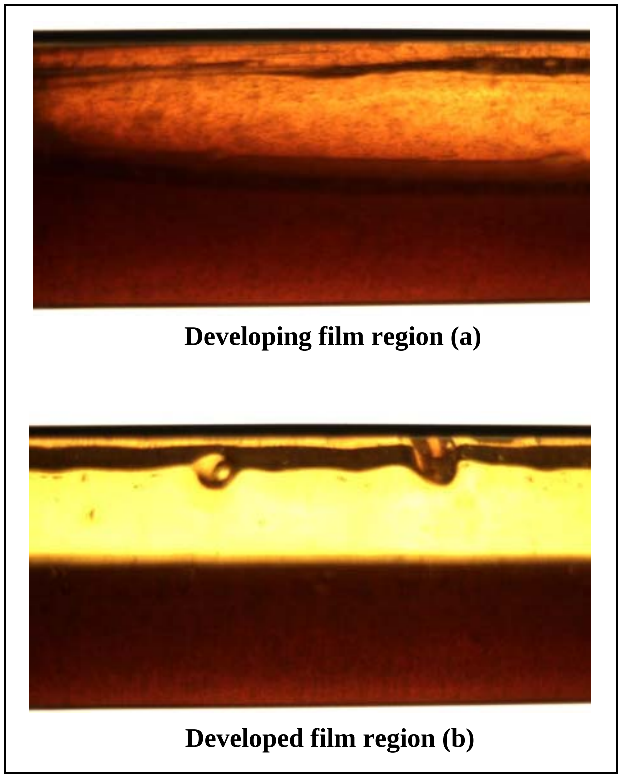

Fig. 2 – Developing and developed film regions
(v_{SL}=0.1 m/s, v_{Sg}=2 m/s, μ=0.26 Pa.s)

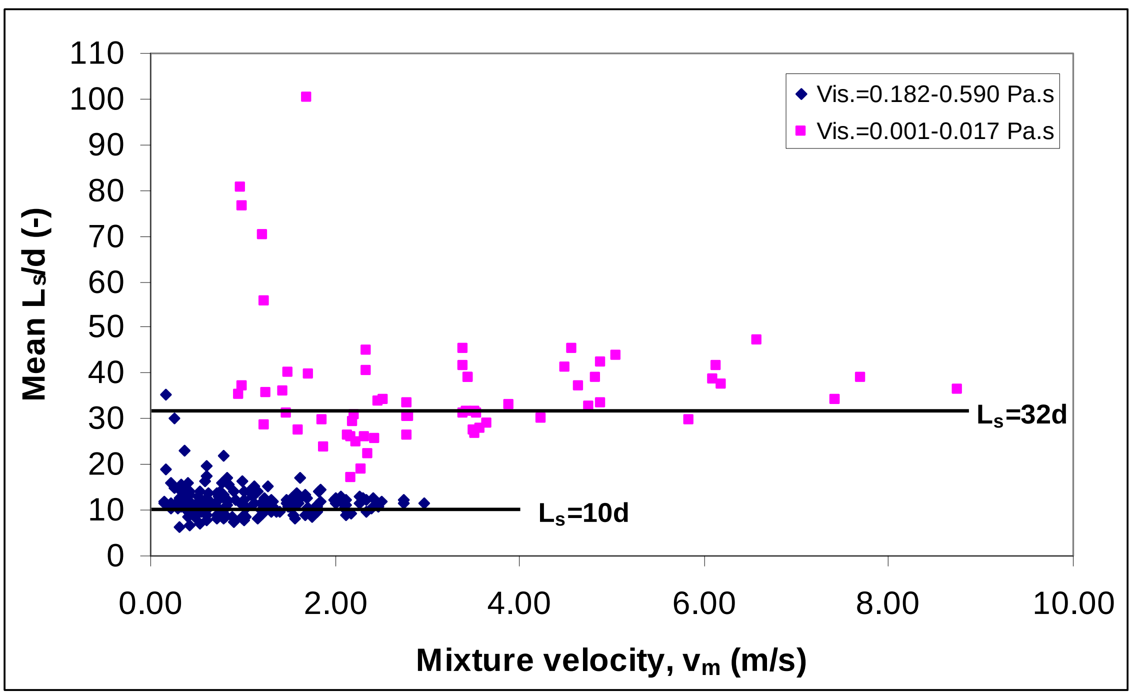

Fig. 3 – Evolution of high and low mean slug length viscosities with mixture velocity

Figures 4-6 investigate the effect of liquid viscosity, superficial gas and superficial liquid velocities on slug length distribution characteristics, namely mean slug length, slug length variation and maximum slug length. As shown in **Fig. 4**, as the liquid viscosity increases approximately ten folds (from 0.017 Pa.s to 0.19 Pa.s) slug length distribution changes in the following aspects. Slug length distribution moves from the conventional Inverse Gaussian or Log Normal to a heavily skewed distribution that can not be modeled by any of these probabilistic models. Consequently, average slug length decreased from approximately 30 to 10 diameters, while the slug length variation increases. As the liquid viscosity further increases by two folds (i.e. 0.580 Pa.s) the central tendency of the data slightly increases moving closer to the average slug length of low viscosity case. In addition, as liquid viscosity increases, distribution skewness severity decreases, while slug length variation increases. The distributions show that maximum slug length increases as liquid viscosity increases; which is counter intuitive and theoretically unjustified. Therefore, it is suspected that long slugs detected by laser props are actually short slugs separated by short gas Taylor bubble. Further investigation is necessary to confirm this observation in the data. To investigate the effect of the superficial gas velocity on slug length statistical parameters, one can inspect the slug length distribution characteristics in **Figs. 4 and 6** for the same liquid viscosity condition. For example, although **Fig. 5** shows a reduction in slug frequency as superficial gas velocity increases, the effect of liquid viscosity on slug length statistical characteristics stay unchanged. The effect of superficial liquid velocity is investigated by comparing **Figs. 5 and 6** for a constant liquid viscosity cases. As superficial liquid velocity decreases, slug frequency is decreases, thus average slug length is increased under all conditions of viscosity. In all of the cases, the effect of liquid viscosity is almost unchanged, indicating insignificant effect of superficial gas and liquid velocities on slug length and on the effect of viscosity of slug length distribution. Conversely, under all different operational conditions, liquid viscosity showed a significant constant effect. These results indicate that liquid viscosity is a significant correlating parameter of slug length, while operational parameters are not.

Although the data analysis is carried out on the sample acquired data in this experimental study, using probability theory, the analysis can be generalized by extending it to a population with a given confidence interval. Analysis of Variance (ANOVA) is carried out to investigate the existence of a significant difference in the mean slug length of light, medium and heavy liquids. ANOVA tests the following null hypothesis: H_0: $\mu_{\text{low vis.}}=\mu_{\text{mid. vis}}=\mu_{\text{high vis.}}$ (μ is the population mean slug length). The null hypothesis will not be rejected unless the sample data provide convincing evidence that it is false. A significance level has to be selected based on which one decides to reject or accept the null hypothesis. The significance level will be compared with the P-value (calculated by ANOVA) and if the P-value is less than the significant level, the null hypothesis will be rejected; otherwise there is no enough evidence to reject the null hypothesis. In this study, we selected a value of 0.1 significance level (α=0.1); meaning that there is 10% probability that Type I error is committed (Type I error is when true hypothesis is rejected). In other words, we will be 90% confident that our statement about the null hypothesis is true. The value of the significance level depends on how much one can tolerate falling in Type I error.

ANOVA separates total variation in the data into two groups, namely variation within groups and variation between groups. Then, ANOVA calculates the two variations and compares them. If the variation between the groups is significantly greater than the variation within groups, then the two population means are significantly (to a level of 10%) unequal. A detailed mathematical formulation of ANOVA may be found in Hethea and Rhinehart (1991). The result of the ANOVA analysis is to reject the null hypothesis, indicating that in a population scale the mean slug length of low, medium and high viscosity liquids are significantly different. This result confirms the effect of liquid viscosity on slug length.

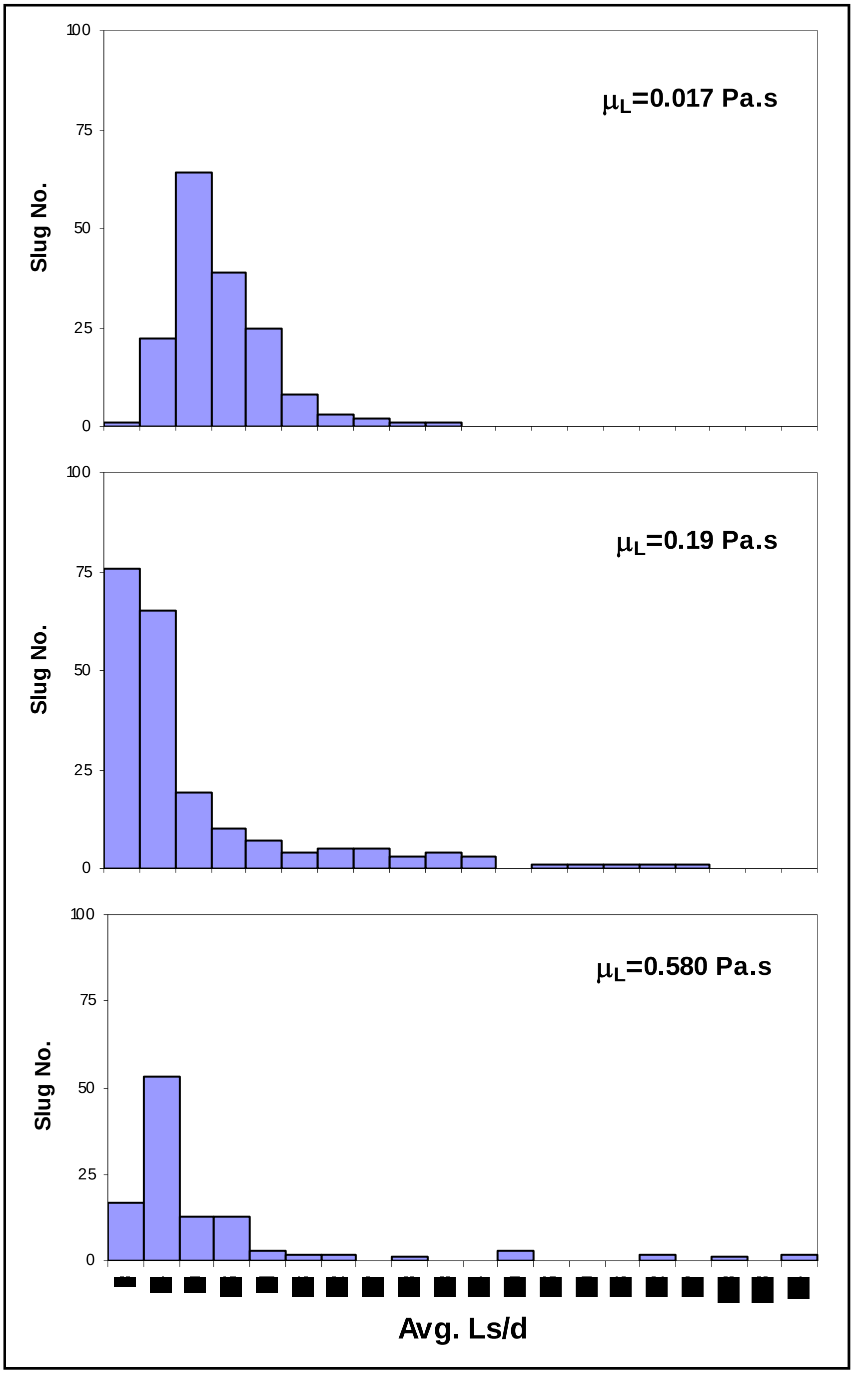

Fig 4 – Effect of liquid viscosity on slug length distribution characteristics (v_{SL}=0.3 m/s, v_{Sg}=1.5 m/s)

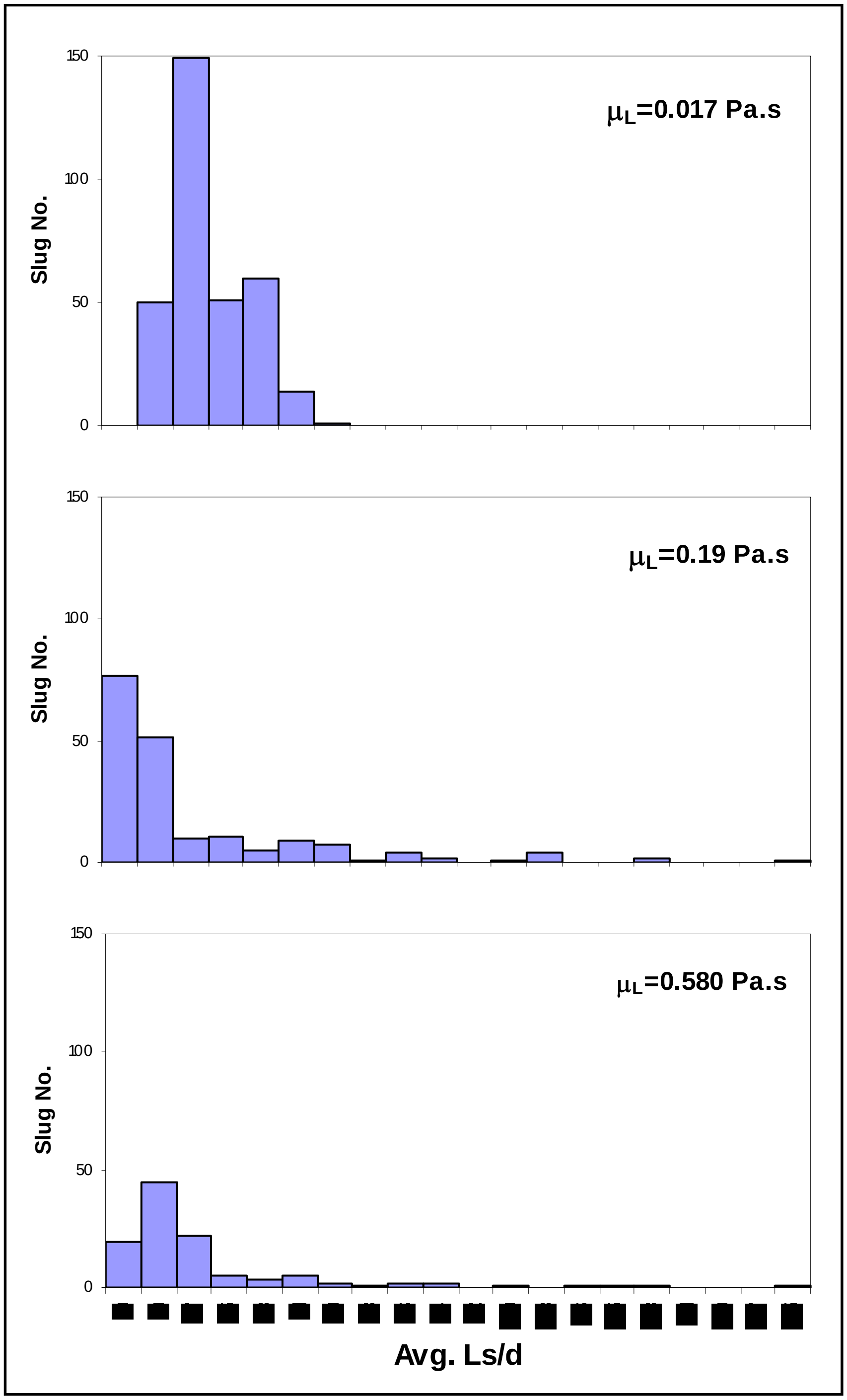

Fig. 5 – Effect of liquid viscosity on slug length distribution characteristics (v_{SL}=0.3 m/s, v_{Sg}=2.1 m/s)

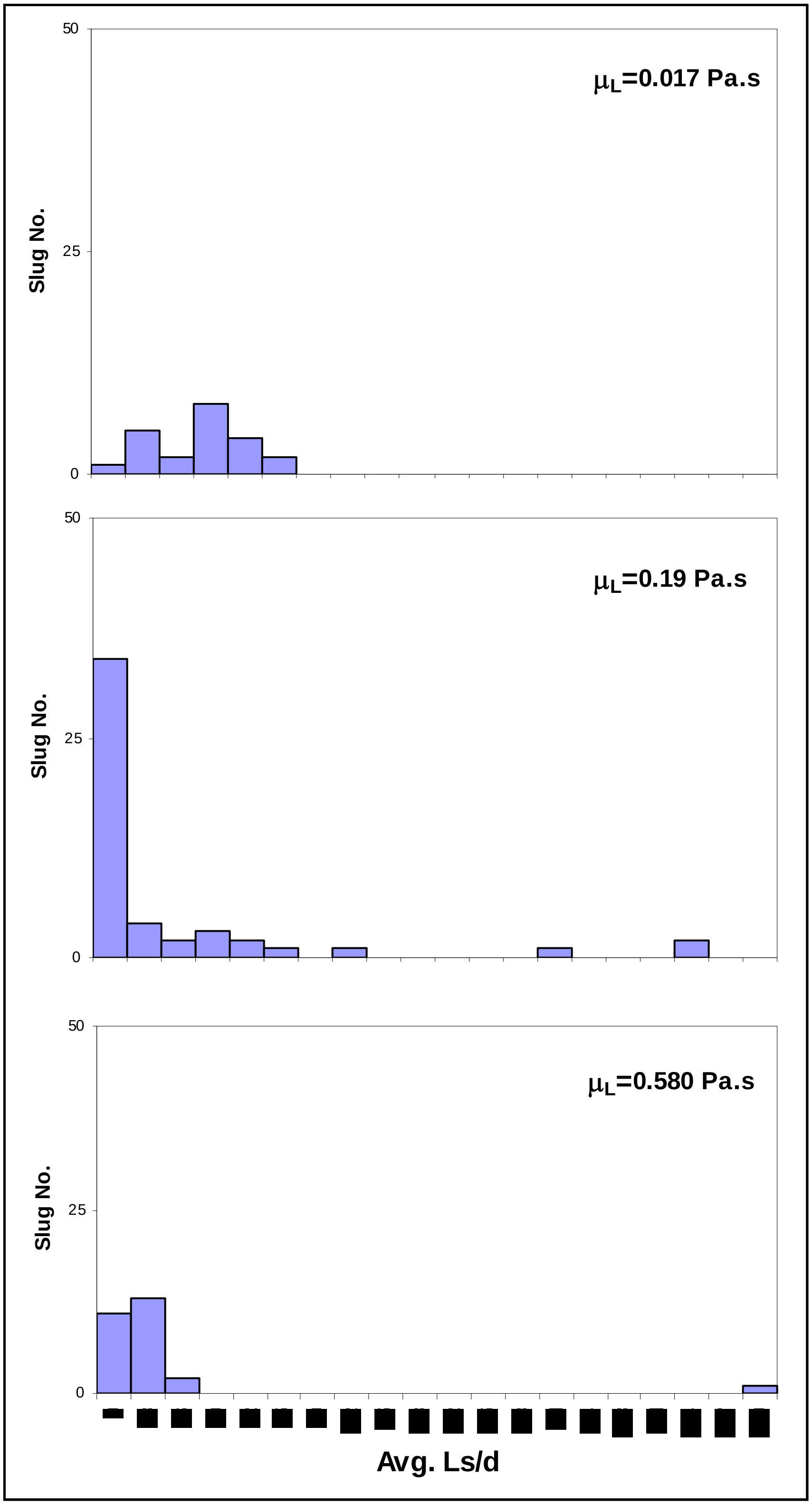

Fig. 6 – Effect of liquid viscosity on slug length distribution characteristics (v_{SL}=0.05 m/s, v_{Sg}=2.1 m/s)

Physical and Theoretical Viscosity Effect

Average slug length of low viscosity liquid two-phase flow is found to be more or less constant, approximately, 30d (Dukler and Hubbard (1975), and Nicholson *et al*. (1978)). A fully developed slug is defined as a stable slug with a constant liquid pickup and shed-back rates. In a stable slug, velocity profile at the tail of slug is fully developed with a maximum velocity close to 1.2 of the slug velocity (Fabre, 1994). Therefore, if a short slug has a developing velocity profile at its back, the trailing bubble velocity will be accelerated to overtake the leading bubble dissipating the short slug in between. This slug dissipation (bubble overtaking) process will continue until all slugs in the pipe are long enough to develop a fully developed velocity profile. This process is the one controls the slug length and establishes stable slug length.

Dukler *et al*. (1985) developed a physical model for minimum slug length in which interaction between film and slug front is simulated as a sudden expansion of a conduit flow into a large reservoir (**Fig. 7**). As liquid separates from film to slug front it goes into a recirculation process, formed between separation point and reattachment point, known as slug mixing zone and characterized by vortices and high local velocity. At reattachment point, a new wall boundary layer is developed ending the turbulence structure region. Downstream of reattachment point, the "memory" of the severe separation effect is vanished and a new developed velocity profile is formed with lower maximum velocity. Dukler *et al*. (1985) found that minimum stable slug length in horizontal pipe is in the order of 20d; however, experimental slug length data were found to be between 20d-40d.

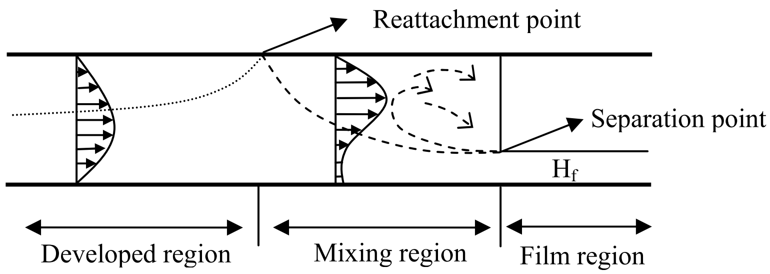

Fig. 7 – Light oil minimum slug length physical model (Dukler *et al.* 1985)

In another work by Taitel *et al*. (1980) and Barnea and Brauner (1985), developed slug length is modeled and found equal to a distance in which a jet is absorbed by liquid and a fully developed velocity profile is established. According to their approach, minimum slug length of 32d was obtained in horizontal flow.

According to the above modeling, two hydrodynamic parameters can be deduced which control minimum stable slug length, namely film height, which controls the sudden expansion or jet velocity into slug front, and time for the redevelopment of fully developed velocity profile, i.e. length of slug mixing region. Liquid viscosity affects both parameters as discussed in the flow visualization section and shown in **Figs. 3 and 4**. **Figure 8** shows a proposed high viscosity liquid slug physical model in which film height in front of slug is thick indicating shorter mixing zone and reattachment distant which shortens slug length to achieve fully developed velocity profile. Furthermore, downstream of reattachment point, velocity profile and centerline maximum velocity are smaller because they are inverse functions of liquid viscosity in laminar flow. This can be shown by laminar velocity profile and maximum velocity in horizontal pipe flow derived from momentum conservation law as follows.

$$v_z = \frac{\Delta P \times R^2}{4\mu L}\left[1-\left(\frac{r}{R}\right)^2\right] \tag{3}$$

$$v_{z,\max} = \frac{\Delta P \times R^2}{4\mu L} \tag{4}$$

The proposed physical model in **Fig. 8** indicates that the change in slug flow characteristics due to high liquid viscosity result in shorter stable slug lengths.

Theoretically, slug length can be derived from mass and momentum conservation laws across slug and film regions (Dukler and Hubbard (1975)) as follows.

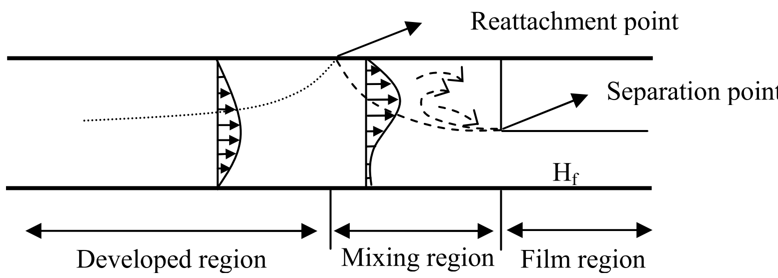

Fig. 8 – Proposed high viscosity oil minimum slug length physical model

$$L_s = \frac{v_s}{\upsilon_s\left(H_{LLS} - H_{LTBe}\right)} \times \left[\left(\frac{W_L}{\rho_L A_p v_s} - H_{LTBe}\right) + c\left(H_{LLS} - H_{LTBe}\right)\right]. \quad (5)$$

From Eq. 5, liquid viscosity can be implicitly related to slug length through slug flow characteristics, namely v_s, υ_s, H_{LLS} and H_{LTBe}. From our experimental observation shown in **Fig. 2**, liquid holdup in Taylor bubble, H_{LTBe}, is promoted as well as slug liquid holdup, H_{LLS}; however, the increase in film holdup is more significant than in slug zone (Nadler and Mewes, 1995). Thus, the effect on their difference (H_{LLS}-H_{LTBe}) is inversely proportional to liquid viscosity. Furthermore, it is experimentally observed and theoretically investigated by Gokcal *et al.* (2009) that slug frequency increases with increasing liquid viscosity. If we look at each term of Eq. 5 and its relationship to the LHS term of slug length as liquid viscosity increases, the following is found.

1st term of Eq. 5:

$$\left[\frac{v_s \downarrow}{\upsilon_s \uparrow \left(H_{LLS} \uparrow - H_{LTBe} \Uparrow\right)\downarrow}\right]\downarrow$$

2nd term of Eq. 5:

$$\left[\left(\frac{W_L \rightarrow}{\rho_L(\rightarrow) A_p(\rightarrow) v_s(\downarrow)}\right)\uparrow - H_{LTBe} \Uparrow\right]\downarrow$$

3rd term of Eq. 5:

$$\left[c(\rightarrow)\left(H_{LLS} \uparrow - H_{LTBe} \Uparrow\right)\right]\downarrow$$

The above analysis, qualitatively, shows the significant inverse effect of liquid viscosity on slug length.

Modeling

Woods and Hanratty (1996) presented relationship between dimensionless slug frequency and the dimensionless slug length as follows.

$$\frac{f_s D}{v_{SL}} = 1.2\left(\frac{L_s}{d}\right)^{-1}. \quad (6)$$

In their study, Woods and Hanratty (1996) derived Eq. 6 from light crude experimental slug flow data; thus the 1.2 constant may not be applicable for high liquid viscosity conditions. Therefore, Eq. 6 is fitted against the high viscosity experimental data acquired in this study as shown in **Fig. 9**.

The data trend in **Fig. 9** can be modeled by a simple linear regression model as follows.

$$\frac{f_s d}{v_{SL}} = 1.94\left(\frac{L_s}{d}\right)^{-1}. \quad (7)$$

Wallis (1969) presented a dimensional analysis for inertia and viscous forces. As a result, two dimensionless numbers were derived, namely Froude number and viscosity number; which can be defined as in Eq. 8 and 9, respectively.

$$Fr_d = \frac{v_d}{(gd)^{0.5}}\sqrt{\frac{\rho_L}{(\rho_L - \rho_G)}}. \quad (8)$$

$$N_\mu = \frac{v_d \mu_L}{gd^2(\rho_L - \rho_G)}. \quad (9)$$

Combining the inertia and viscous forces, a dimensionless inverse viscosity number is found as the ratio of Froude to viscosity numbers as follows.

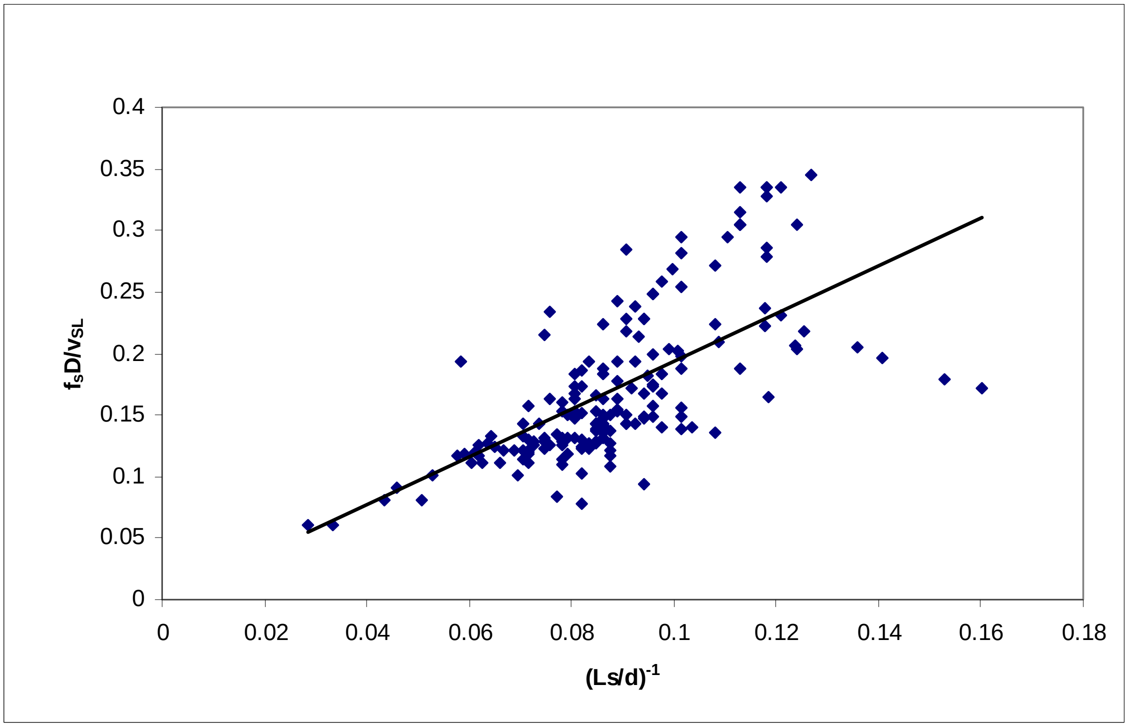

Fig. 9 – Dimensionless slug frequency versus the inverse of average slug length

$$N_f = \frac{Fr_d}{N_\mu} = \frac{d^{3/2}\sqrt{\rho_L(\rho_L-\rho_G)g}}{\mu_L} \tag{10}$$

Eq. 10 combines the inertia and viscous forces; which theoretically affect slug length under high liquid viscosity conditions as shown the previous section. Gokcal *et al.* (2009) showed that slug frequency is correlated to the dimensionless inverse viscosity number as follows.

$$f_s = 2.623\left(\frac{N_f^{-0.612} v_{SL}}{d}\right). \tag{11}$$

Combing Eqs. 7 and 11, the dimensionless inverse viscosity number is related to the dimensionless slug length as follow.

$$\frac{L_s}{d} = \beta_0 N_f^{\beta_1}. \tag{12}$$

Eq. 12 is linearized and fitted against the high liquid viscosity data as illustrated in **Fig. 10**. The two constants, β_0 and β_1, are obtained from simple linear regression model fitted against the data acquired in this study as best linear unbiased estimators as follows.

$$\frac{L_s}{d} = 2.63 N_f^{0.321}. \tag{13}$$

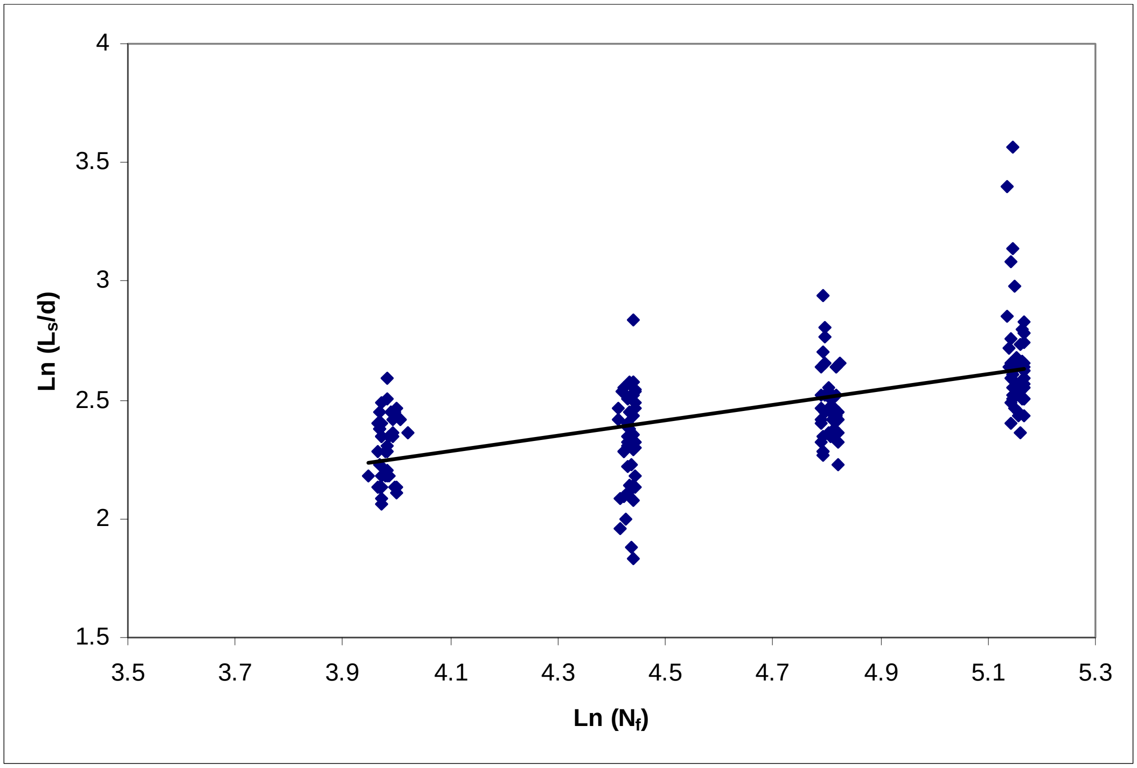

Fig. 10 – Simple linear regression fit of the linearized average slug length model

Model Statistical Evaluation.
Overall and individual coefficient's statistics of developed model in Eq. 13 are calculated and reported in **Tables 1 and 2**, respectively. **Table 1** illustrates the reliability of the regression model and its ability to capture the variability in average slug length. The Sum of Square of Error (SSE) in **Table 1** quantifies the deviation of the predicted data from the actual values by the regression model. The square root of the ratio of SSE to error degrees of freedom (df) is the Mean Squared Error (MSE) which quantifies the degree of scatter of the data around the line. The coefficient of variation, R^2, measures the proportion of the variation in the slug length which is explained by the regression model. An R^2 value of 0.32 indicates the capability of the regression model to capture 32% of the variation in slug length. This is a high percent for average dimensionless slug length which is uncorrelated with any of the flow variables.

Table 1 – Overall Model Evaluation

Model df	Error df	SSE	MSE	R^2
1	161	6.43	0.200	0.32

The second and third columns in **Table 2** report the coefficients and standard errors of the model constants, β_0 ($e^{0.966}$) and β_1. The standard error of each coefficient is the square root of the ratio of model variance to its sum of squares of deviations ($x_i = X_i - \overline{X}$). The coefficient's standard error indicates the scatter of each coefficient value around its mean. When normalized, the estimated regression coefficients follow a t-distribution with model error degrees of freedom. The P-value in the fifth column is area under t-probability curve that is used to test the null hypothesis of whether or not the independent parameter is relevant in predicting the slug length (i.e. H_0: $\hat{\beta}_0 or \hat{\beta}_1 = 0$). Using a 5% significance level, one can reject the null hypothesis (H_0) since the p-value is less than the significance level, confirming that the independent variable is significant. The 95% confidence intervals for each independent variable coefficient are also reported in the last two columns. A 95% confidence interval for a coefficient is ($C.I._{(95\%)} = \hat{\beta}_j \pm t_c s_{\hat{\beta}_j}$), where t_c equals 1.96 and corresponds to two sided 95% of the area under

Normal probability t-distribution curve. $\hat{\beta}_j$ is the coefficient and $s_{\hat{\beta}}$ is its standard error. These confidence intervals give model the flexibility to be tuned when test data is available. Model tuning for a specific flow system will improve the prediction of slug length for that system.

Table 2 – Model Coefficients' Evaluation

Variable	Coef.	Standard Error	t-statistics	p-value	Lower 95% CI	Upper 95% CI
$Ln(\beta_0)$	0.966	0.170	5.800	0.000	0.650	1.310
β_1	0.321	0.036	8.730	0.000	0.246	0.390

Model validation

In this study, a lack of independent high liquid viscosity slug length data in the open domain to validated proposed model against was a challenge. Alternatively, ten data point of this study were randomly selected and eliminated from the process of model development to be used as independent data set for validation. A statistical error analysis is carried out to test the performance of proposed correlation on independent data set. Three statistical parameter are calculated, namely the Average Percent Error (APE), Absolute Average Percent Error (AAPE) and the Standard Deviation (SD), which are summarized in **Table 3**.

Table 3 – Proposed Model Validation

Stat. Parameter	Value
APE (%)	1.72
AAPE(%)	9.8
SD(%)	13.6

Error analysis shows that the model slightly overpredicts experimental data with about 10% absolute error. The analysis further shows that data dispersion around the model represented by standard deviation is low, 13.6%. **Fig. 11** is a cross plot showing model performance against data. Overall model prediction shows a very good performance, yet more independent data is required to further validate the model performance under different conditions.

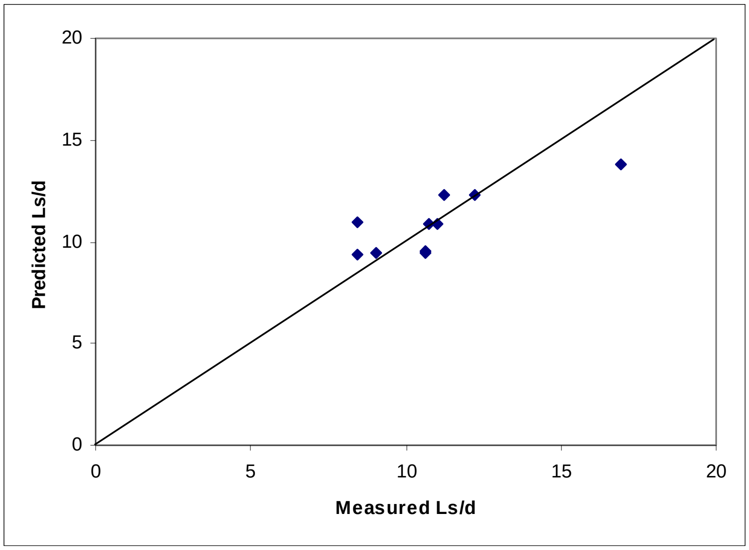

Fig. 11 – Cross plot of model prediction vs. measurement

Model Comparison

Using the ten independent data points, a comparison analysis is carried to compare the prediction of proposed correlation with existing slug length correlations against experimental data. Four correlations were used in the comparison, namely Brill *et al*. (1980), Scott *et al*. (1981), Norris (1982), Branea and Brauner (1985) and Dukler *et al*. (1985). **Table 4** shows the comparison results; which reveals that all existing correlations over-predict average slug length with different magnitudes. The first three correlations are expected to over-predict experimental data with large error because they were developed based on the large diameter Prudhoe Bay pipeline data. In addition, the last two correlations which are based on small diameter data also over-predict experimental data showing the effect of liquid viscosity on average slug length. All in all, comparison analysis shows the need for slug length correlation for high viscosity liquid condition, yet more independent data is required for further comparison.

Table 4 – Proposed and Existing Correlations comparison

Correlation	APE (%)	AAPE (%)	SD (%)
Brill *et al*. (1980)	295.2	295.2	78.1
Scott *et al*. (1981)	344.6	344.6	83.3
Norris (1982)	298.9	298.9	74.8
Barnea & Brauner (1985)	203.7	203.7	56.9
Dukler *et al*. (1985)	89.8	89.8	35.6
Present Study	1.7	9.8	13.6

Conclusions

- Slug front under high liquid viscosity condition is less turbulent with a top boundary layer moving faster than the slug body, entraining large bubbles. This scooping process does not cause bubble fragmentation and entrainment into slug front; instead, it entrains large bubbles/gas pockets leading to slug splitting into shorter slugs.
- Taylor bubble nose at the back of slug under high viscosity liquid is long and accelerated by the wake of entrained gas pockets which leads to short slugs.
- Liquid film height under high liquid viscosity is large and aerated. It has two distinct sub-regions, namely developing region characterized by relatively thick film at pipe top wall and a secondary tangential film flow. A developed region is characterized by a stratified film layer with a thin film layer at the top wall of the pipe.
- Slug length under high liquid viscosity is insensitive to operational conditions with a stable average slug length of 10d. In addition, critical mixture velocity beyond which average slug length remains constant is around 0.5 m/s, as opposed to 1 m/s for low liquid viscosity condition.
- Statistical analysis shows that the slug length distribution under high viscosity liquid conditions is a truncated and right skewed distribution.
- A high viscosity liquid slug length physical model is proposed in this study. The model showed that due to large film thickness in front of slug and small velocity profile and centerline velocity at back of slug body, a shorter mixing zone and reattachment distant are developed. This shortens the required slug length to achieve a fully developed velocity profile resulting in a short minimum stable slug.
- A theoretical analysis on Dukler and Hubbard (1975) slug length mechanistic model coupled with observations of high liquid viscosity slug flow behavior showed the effect of liquid viscosity on slug length.
- A proposed empirical slug length correlation function of liquid viscosity developed based on dimensional analysis. Validation with randomly selected independent data set shows accurate performance of the proposed correlation.
- A comparison study between existing and proposed correlations against experimental data showed the discrepancy of existing correlations predictions under high viscosity oil condition and the need for new high viscosity oil correlation.

Nomenclature

A	=	pipe cross sectional area
c	=	constant
d	=	pipe diameter
H	=	liquid holdup and height
L	=	length
P	=	pressure
R	=	pipe radius
v	=	velocity
W	=	mass rate

Subscripts

f	=	film
L	=	liquid
LS	=	liquid slug
max	=	maximum
o	=	oil
P	=	pipe
S	=	slug
Sg	=	superficial gas
SL	=	superficial liquid
TBe	=	Taylor bubble equil.
z	=	axial direction

Greek

μ	=	viscosity, population mean.
ρ	=	density
υ	=	slug frequency

References

Abdul-Majeed G.: "Liquid Slug Holdup in Horizontal and Slightly Inclined Two-Phase Slug Flow*," J. Pet. Sci. and Eng*. 27, 27-32, (2000).

Barnea, D., and Brauner, N.: "Holdup of the Liquid Slugs in Two Phase intermittent Flow," Int. J. Multiphase Flow 11, 43-49 (1985).

Brandt, I., and Fuchs, P.: "Liquid Holdup in Slugs: Some Experimental Results from the SINTIF Two-Phase Flow Laboratory," BHRG Multiphase Proceedings, Nice, France (1989).

Brauner, N. and Ullmann, A.: "Modeling of Gas Entrainment from Taylor Bubbles. Part A: Slug Flow," *Int. J. of Multiphase Flow*, 30, 239-272, (2004).

Brill, J., Schmidt, Z., Coberly, W., Herring J. and Moore D.: "Analysis of Two-Phase Tests in Large Diameter Prudhoe Bay Field Flowlines," SPE 8305, Presented at SPE ATCE, Las Vegas, September, 1979.

Colmenares,J., Ortega,P., Padino,J., and Trallero, J.L.: "Slug Flow Model for the Prediction of Pressure Drop for High Viscosity Oils in a Horizontal Pipeline," SPE 71111, Presented at SPE International Thermal Operations and Heavy Oil Symposium, Margarita Island, Venezuela, March 12-14 (2001).

Dukler, A.E. and Hubbard, M.G.: "A Model for Gas-Liquid Slug Flow in Horizontal and Near Horizontal Tubes", *I&EC Fundamentals*, 14, pp. 337-347 (1975).

Dukler, A., Moalem-Maron, D., and Brauner, N.: "A Physical Model for Predicting the Minimum Stable Slug Length," Chem. Eng. Sci. 40, 1379-1385 (1985).

El-Oun, Z.: "Gas-Liquid Two-Phase Flow in Pipelines," SPE 20645, Presented at SPE ATCE, New Orleans, LA, (1990).

Fabre, J., Grenier, P. and Gadoin, E.: "Evolution of Slug Flow in Long Pipe," BHRG Production Technology Conference, Cannes, France (1993).

Gokcal, B., Al-Sarkhi, A., Sarica, C. and Al-Safran, E.: "Prediction of Slug Frequency for High-Viscosity Oils in Horizontal Pipes," SPE 124057, Presented in SPE/ATCE, New Orleans, LA, (2009).

Gokcal, B., Wang, Q., Zhang, H. Q., and Sarica, C.: "Effects of High Oil Viscosity on Oil-Gas Flow Behavior in Horizontal Pipes," SPE 102727, *SPE Projects, Facilities & Construction Journal,* June, (2008a).

Gokcal, B.: An Experimental and Theoretical Investigation of Slug Flow for High Oil Viscosity in Horizontal Pipes. Ph.D. Dissertation, The University of Tulsa, Tulsa, Oklahoma, (2008b).

Hethea, R. and Rhinehart, R.: Applied Engineering Statistics, Marcel Dekker Inc., (1991).

Kokal, S.: "An Experimental Study of Two-Phase Flow in Inclined Pipes," Ph.D. Dissertation, The University of Calgary, Calgary, Canada, (1987).

Kora, C.: Effects of High Liquid Viscosity on Slug Liquid Holdup in Horizontal Pipes. M.Sc. Thesis, The University of Tulsa, Tulsa, Oklahoma (2010).

Scott, L. and Kouba, G.: "Advances in Slug Flow Characterization for Horizontal and Slightly Inclined Pipelines," SPE20628, Presented in SPE/ATCE, New Orleans, LA., (1990).

Marcano, R.: "Slug Characteristics for Two-Phase Horizontal Flow," M.S. Thesis, The University of Tulsa, Tulsa, OK, (1996).

Nadler M. and Mewes D.: "Effect of the Liquid Viscosity on the Phase Distribution in Horizontal Gas-Liquid Slug Flow" *Int. J. of Multiphase Flow*, 21, No. 2, 253-266, (1995).

Nicholson, K., Aziz, K., and Gregory, G.: "Intermittent Two Phase Flow in Horizontal Pipes, Predictive Models," *Can. J. Chem. Eng.,* 56, 653-663, (1978).

Norris, L.: " Correlation of Prudhoe Bay Liquid Slug Lengths and Holdups Incluing 1981 Large Diameter Flowline Tests," Internal Report, Exxon Production Research Co., Houston, TX., 1982.

Rothe, P., Crowley, C. and Sam, R.: "Investigation of Two-Phase Flow in Horizontal Pipes at large Pipe Size and High Gas Density," AGA Pipe Research Committee Project, PR-172-507, (1986).

Scott, S., Shoham O. and Brill, J.: "Prediction of Slug Length in Horizontal, Large-Diameter Pipes," *SPE J. Prod. Eng.*, 4, pp. 335-340 (1981).

Taitel, Y., Barnea, D., and Dukler, A.: "Modeling Flow Pattern Transition for Steady Upward Gas-Liquid Flow in Vertical Tube," AIChE J. 26, 345-354 (1980).

Fluid Flow Projects

Executive Summary of Research Activities

Cem Sarica

Advisory Board Meeting, November 3, 2010

Low Liquid Loading Flow

- Significance
  - Wet Gas Transportation
    - Holdup and Pressure Drop Prediction
    - Corrosion Inhibitor Delivery (Top of the Line Corrosion)
- Objectives
  - Develop Better Predictive Tools

Low Liquid Loading Flow …

- Past TUFFP Studies
  - Two-phase, Small Diameter, Low Pressure
    - Air-Water and Air-Oil
    - 2-in. ID Pipe with $\pm 2^{\circ}$ Inclination Angles from Horizontal
  - Two-phase, Large Diameter, Low Pressure
    - Air-Water
    - 6-in. ID and $\pm 2^{\circ}$ Inclination Angles from Horizontal

Low Liquid Loading Flow …

- Past TUFFP Studies …
  - Three-phase, Large Diameter, Low Pressure
    - Air-Mineral Oil-Water
    - 6-in. ID, Horizontal Flow
    - Findings
      - Observed and Described Flow Patterns and Discovered a New Flow Pattern
      - Acquired Significant Amount of Data on Various Parameters, Including Entrainment Fraction
    - Remaining Tasks
      - Development of Improved Closure Relationships

Low Liquid Loading Flow …

- Current Study
  - Three-phase, Large Diameter, Low Pressure Inclined Flow
    - Air-Mineral Oil-Water
    - 6-in. ID and ±2° Inclination Angles from Horizontal
    - Objectives
      - Acquire Similar Data as in Horizontal Flow Study
      - Develop Improved Closure Relationships

Low Liquid Loading Flow …

- Status
  - Ph.D. Student Successfully Passed the Qualifying Exam
  - Additional Tests During This Period
    - Entrainment Fraction Found to Decrease with Superficial Liquid Velocity at a Constant Superficial Gas Velocity
- Future Studies
  - Short Term
    - Low Pressure, Inclined Pipe Study
  - Long Term
    - Two and Three-phase, Large Diameter, High Pressure Horizontal and Inclined Flow
    - Requires New High Pressure Facility

Fluid Flow Projects

Low Liquid Loading Gas-Oil-Water in Pipe Flow

Kiran Gawas

Advisory Board Meeting, November 3, 2010

Outline

- Objectives
- Introduction
- Literature Review
- Experimental Study
- Near Future Tasks

Fluid Flow Projects

Advisory Board Meeting, November 3, 2010

Objectives

- Acquire Experimental Data of Low Liquid Loading Gas-Oil-Water Flow in Horizontal and Near Horizontal Pipes Using Representative Fluids
- Check Suitability of Available Models for Low Liquid Loading Three Phase Flow and Suggest Improvements If Needed

Introduction

- Low Liquid Loading Flows Correspond to Liquid to Gas Ratio ≤ 1100 $m^3/MMsm^3$
- Widely Encountered in Wet Gas Pipelines
- Small Amounts of Liquid Influences Pressure Distribution – Hydrate Formation, Pigging Frequency, Downstream Equipment Design etc.
- Transport of Additives

Literature Review

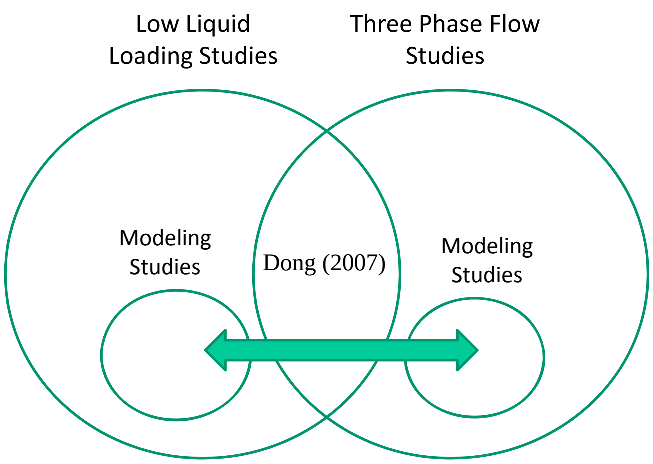

Fluid Flow Projects

Advisory Board Meeting, November 3, 2010

Experimental Study

- Experimental Facility
- Test Section
- Test Fluids
- Instrumentation and Data Acquisition
- Preliminary Tests
- Experimental Program
- Experimental Results

Fluid Flow Projects

Advisory Board Meeting, November 3, 2010

Facility

- 6 in. ID Low Pressure Flow Loop
- Previously Used by Dong (2007)
- Modified to Achieve Higher Gas Flow Rates

Fluid Flow Projects

Advisory Board Meeting, November 3, 2010

Facility …

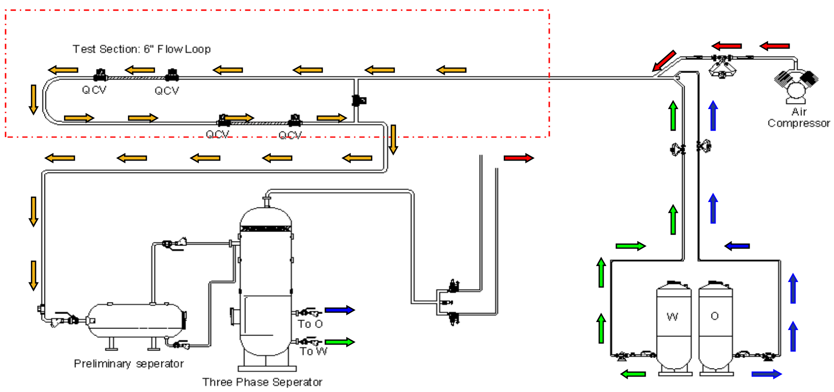

Fluid Flow Projects

Advisory Board Meeting, November 3, 2010

Test Section

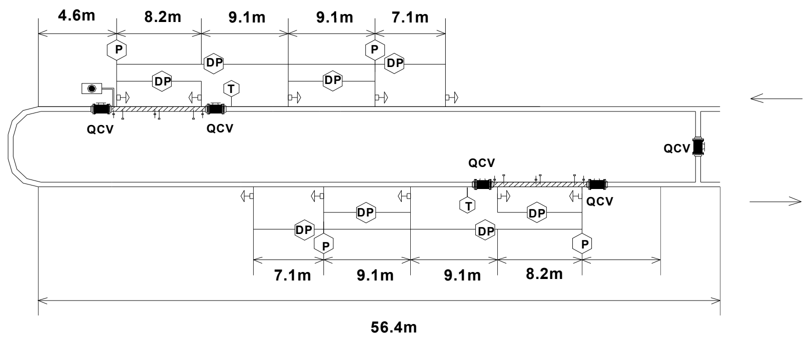

Fluid Flow Projects

Advisory Board Meeting, November 3, 2010

Test Fluids

- Test Fluid
  - Gas – Air
  - Water – Tap Water
  - Oil – Isopar L
- Selection of Test Fluids is Very Important
- Properties Resembling Those of Wet Gas Condensate
  - Low Viscosity and Specific Gravity

Fluid Flow Projects

Advisory Board Meeting, November 3, 2010

Instrumentation/Data Acquisition

- Pressure and Temperature: PTs and DPs and TTs
- Holdup: Quick Closing Valves and Pigging System
- Wetted Wall Perimeter: Scales on Wall
- Liquid Film Thickness: Conductivity Probes
- Liquid Velocity: Cold/Hot Liquid Injection
  - Particle Tracking using High Speed Camera?
- Liquid Entrainment: Iso-kinetic Sampling System
- Fisher Scientific Semi-automatic Model 21 Surface Tensiomat
- Data Acquisition: Delta-V

Liquid Entrainment: Iso-kinetic Probe

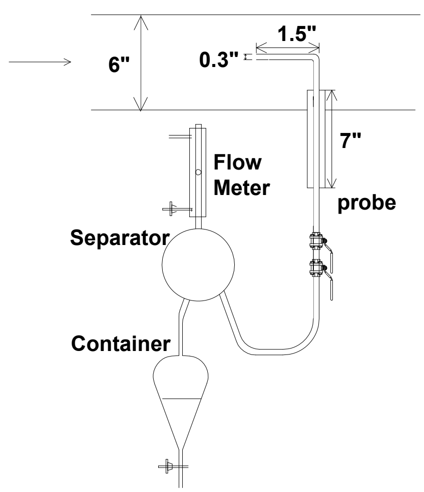

Experimental Program

- Tests at Low Gas Flow Rates
  - Flow Conditions Used by Dong (2007)
- Tests at High Gas Flow Rates
  - Gas-Oil Two-phase Tests
  - Gas-Oil-Water Three-phase Tests

Experimental Program …

- Test Ranges
  - Superficial Gas Velocity:
    5 to 22.5 m/s
  - Liquid Loading Level :
    50 to 1200 $m^3/MMsm^3$
  - Water Cut:
    0 to 0.5
  - Inclination Angles:
    0º, +2º, -2º

Low Gas Flow Rate Studies

- Test Matrix

Superficial Gas Velocity (m/s)	Superficial Liquid Velocity (m/s)			
	Water Cuts : 0, 5%, 10%, 20%, 50%			
5	0.001	0.004	0.007	0.01
10	0.001	0.004	0.007	0.01
15	0.001	0.004	0.007	0.01

High Gas Flow Rate Studies

- Test Matrix

Superficial Gas Velocity (m/s)	Superficial Liquid Velocity (m/s)			
	Water Cuts : 0, 5%, 10%, 20%, 50%			
16.5	0.004	0.01	0.02	0.035
18.5	0.004	0.01	0.02	0.035
22.5	0.004	0.01	0.02	0.035

High Gas Flow Rate Studies …

- Onset of Entrainment
- Vertical Flow – Entrainment Uniform Across the Cross Section
- Entrainment Profile Across the Pipe Cross Section
  - Iso-kinetic Probe at Different Positions Across the Pipe Cross Section

Entrainment Study

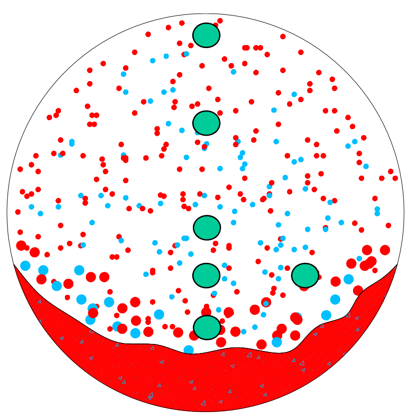

Variation of Liquid Entrainment Flux with Superficial Liquid Velocity (v_{Sg}=16.5 m/s and WC=0 %)

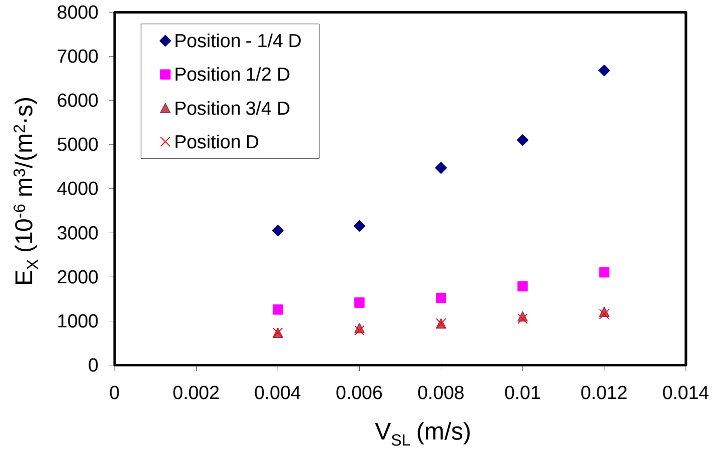

Fluid Flow Projects

Advisory Board Meeting, November 3, 2010

Variation of Liquid Entrainment Flux with Superficial Liquid Velocity (v_{Sg} = 18.5 m/s and WC=0 %)

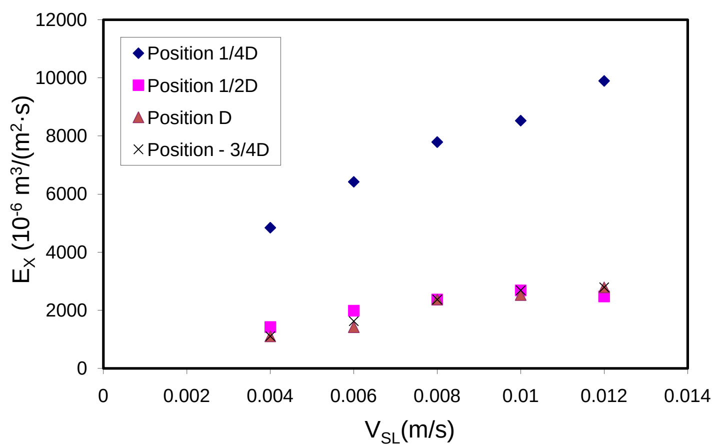

Fluid Flow Projects

Advisory Board Meeting, November 3, 2010

Total Liquid Entrainment flux Profile (v_{Sg} = 16.5 m/s and WC = 0%)

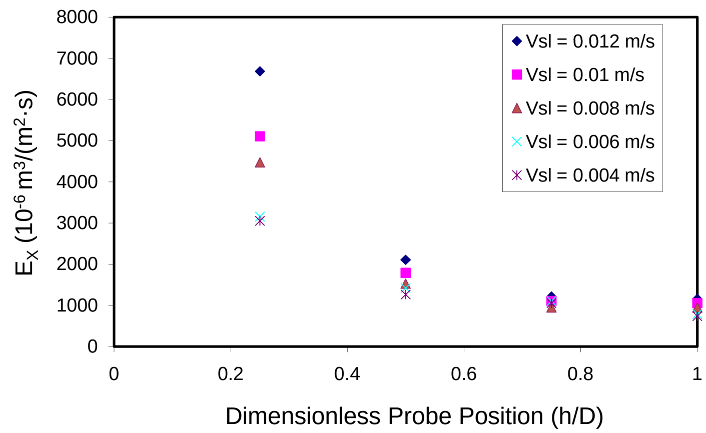

Fluid Flow Projects

Advisory Board Meeting, November 3, 2010

Total Liquid Entrainement flux Profile (v_{Sg} = 18.5 m/s and WC = 0%)

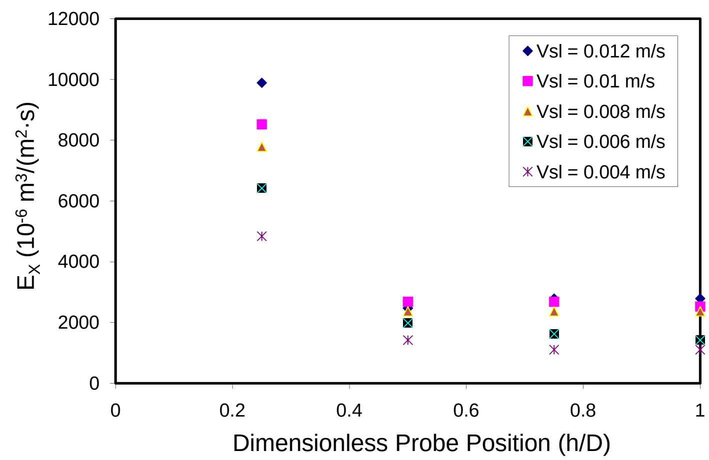

Fluid Flow Projects

Advisory Board Meeting, November 3, 2010

Variation of Liquid Entrainment Flux with Superficial Liquid Velocity (v_{Sg} = 16.5 m/s and WC=5 %)

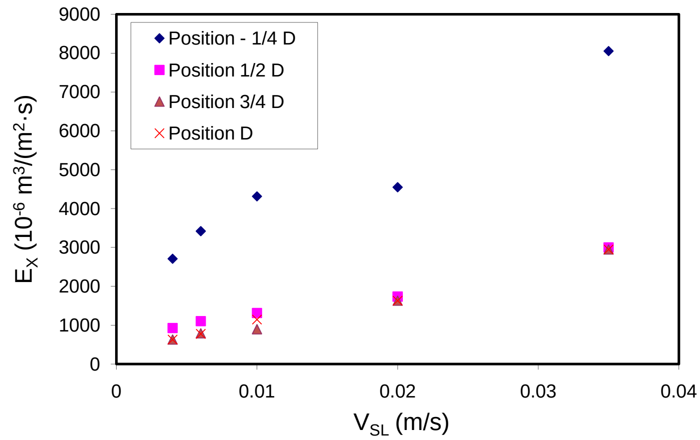

Fluid Flow Projects Advisory Board Meeting, November 3, 2010

Variation of Liquid Entrainment Flux with Superficial Liquid Velocity (v_{Sg} = 22.5 m/s and WC=5 %)

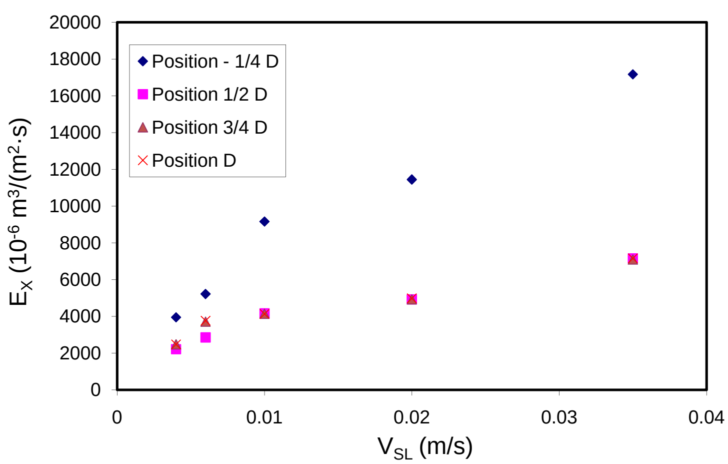

Fluid Flow Projects Advisory Board Meeting, November 3, 2010

Total Liquid Entrainement flux Profile (v_{Sg} = 16.5 m/s and WC = 5 %)

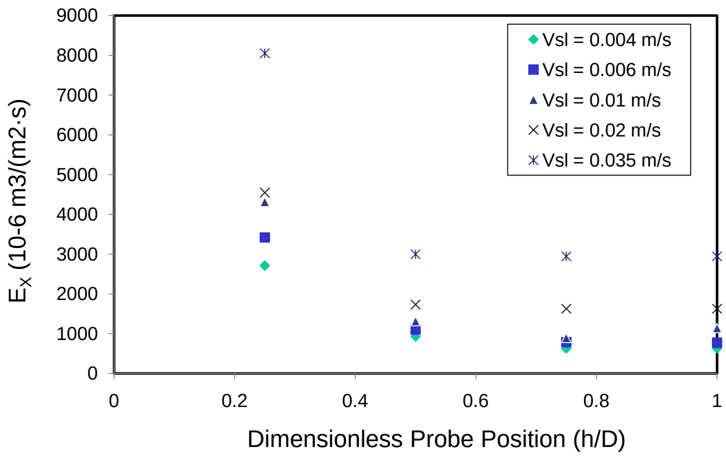

Fluid Flow Projects

Advisory Board Meeting, November 3, 2010

Total Liquid Entrainement flux Profile (v_{Sg} = 22.5 m/s and WC = 5 %)

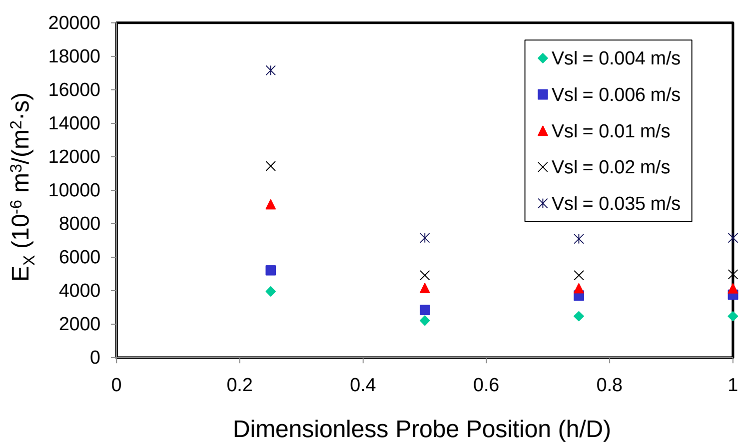

Fluid Flow Projects

Advisory Board Meeting, November 3, 2010

Water Fraction Profile in Total Liquid Entrainment (v_{Sg} = 16.5 m/s and WC = 5 %)

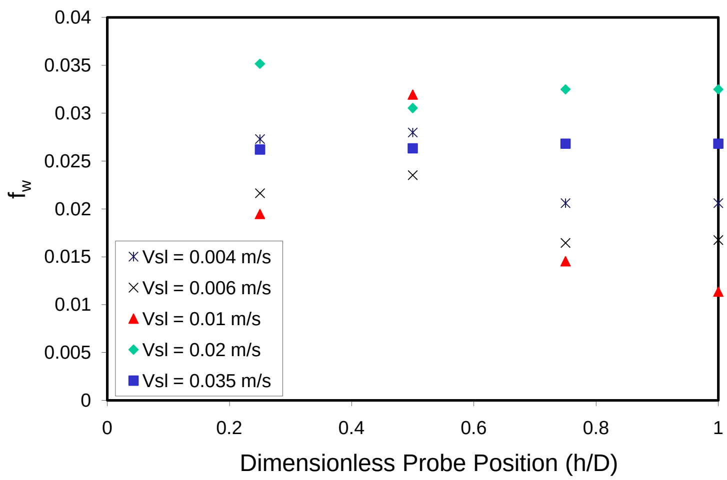

Fluid Flow Projects

Advisory Board Meeting, November 3, 2010

Water Fraction Profile in Total Liquid Entrainment (v_{Sg} = 18.5 m/s and WC = 5 %)

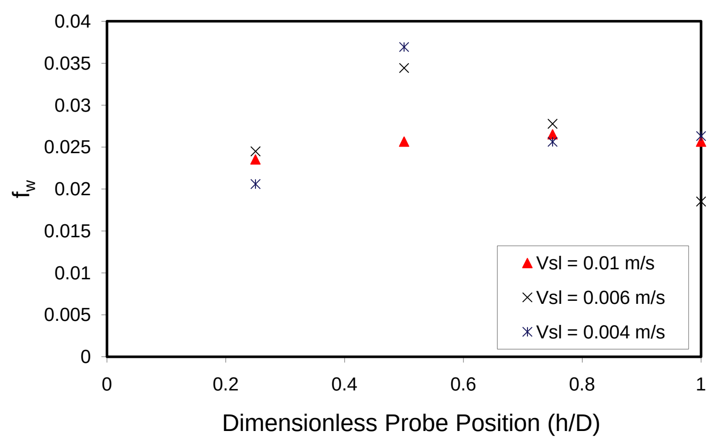

Fluid Flow Projects

Advisory Board Meeting, November 3, 2010

Water Fraction Profile in Total Liquid Entrainment (v_{Sg} = 22.5 m/s and WC = 5 %)

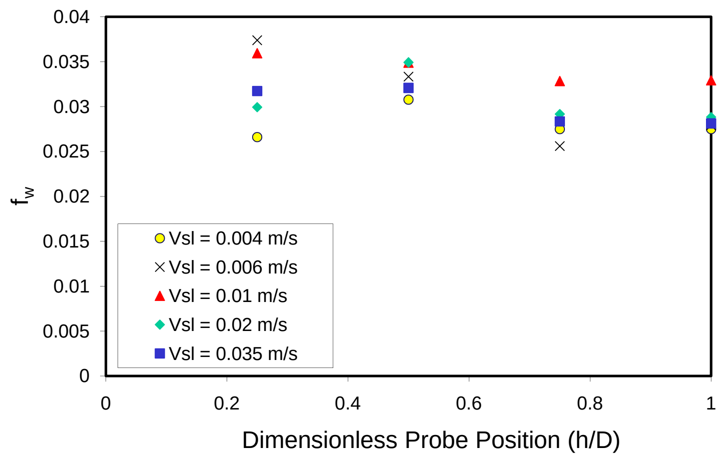

Effect of Water Cut on Liquid Entrainment Flux (V_{Sg} = 16.5 m/s)

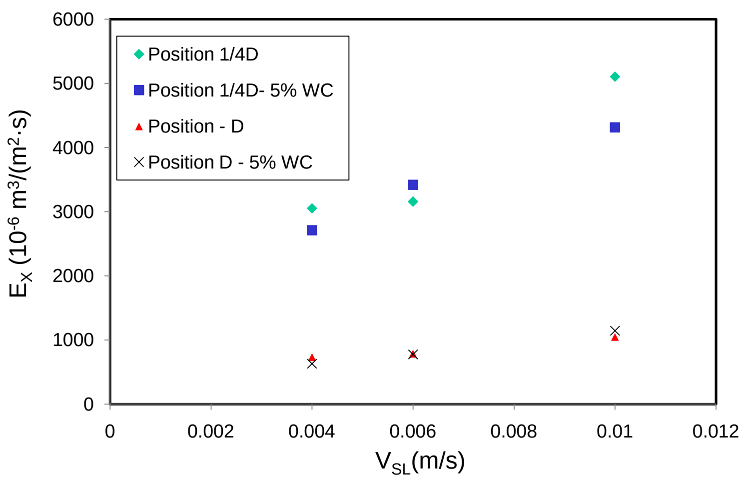

Effect of Water Cut on Liquid Entrainment Flux (V_{Sg} = 18.5 m/s)

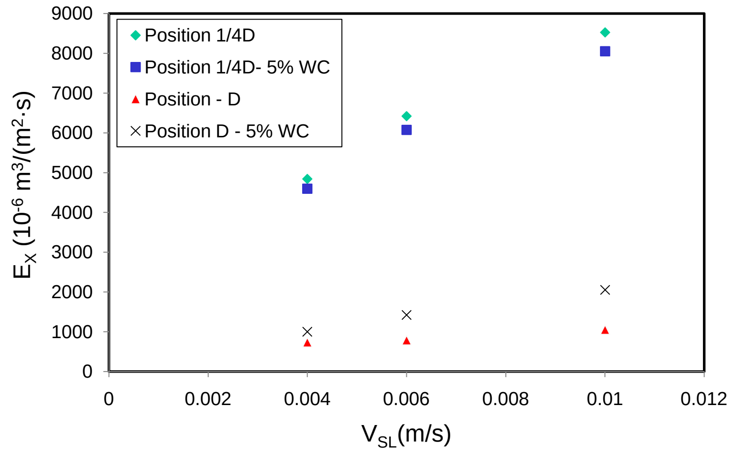

Fluid Flow Projects

Advisory Board Meeting, November 3, 2010

Effect of Superficial Velocity of Liquid and Gas on Entrainment Fraction

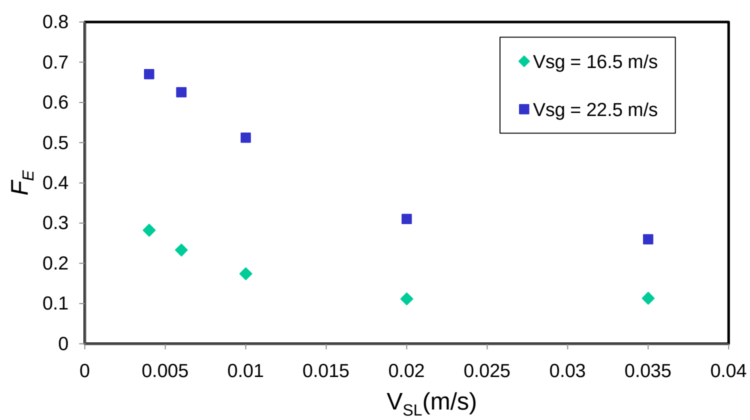

Fluid Flow Projects

Advisory Board Meeting, November 3, 2010

Effect of Superficial Velocity of Liquid and Gas on Entrainment Fraction – Mantilla (2008)

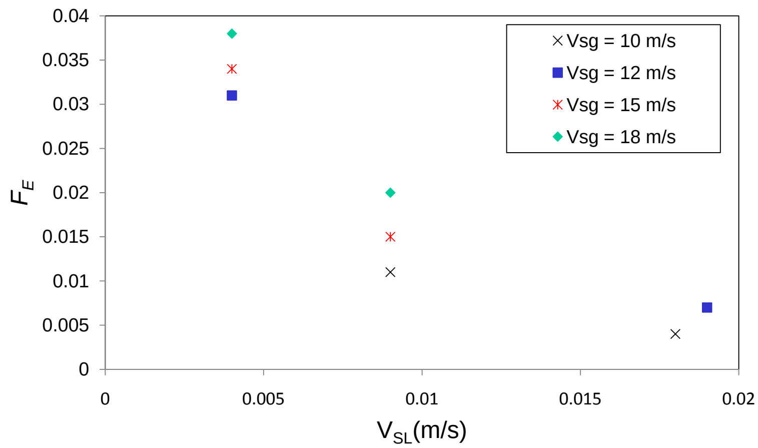

Fluid Flow Projects

Advisory Board Meeting, November 3, 2010

Effect of Superficial Velocity of Liquid and Gas on Entrainment Fraction – Magrini (2009)

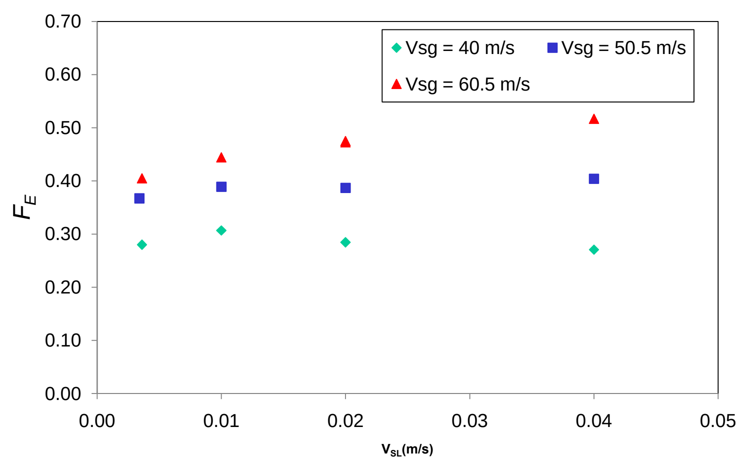

Fluid Flow Projects

Advisory Board Meeting, November 3, 2010

Effect of Superficial Velocity of Liquid and Gas on Entrainment Fraction – Dong (2007)

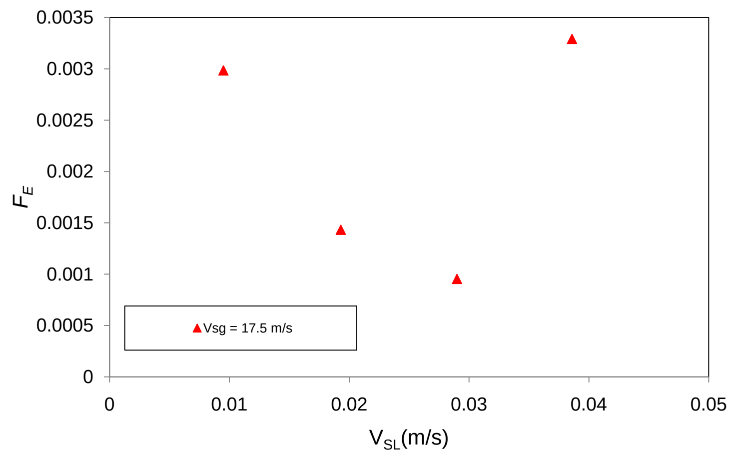

Near Future Tasks

Literature Review	Ongoing
Testing Phase-1	Ongoing
Data Analysis and Model Comparison	December 2010
Testing Phase-2	April 2011
Model Development	December 2011
Final Report	May 2012

Questions

Fluid Flow Projects

Advisory Board Meeting, November 3, 2010

Low Liquid Loading in Gas-Oil-Water Pipe Flow

Kiran Gawas

Project Completion Dates

Literature Review	Ongoing
Testing Phase 1	Completion Date
Data Analysis and Model Comparison	December 2010
Testing Phase 2	April 2011
Model Validation	December 2011
Final Report	May 2012

Introduction

Low liquid loading gas-oil-water flow is widely encountered in wet gas pipelines. Even though the pipeline is fed with single phase gas, the condensation of the gas along with traces of water results in three-phase flow. The presence of these liquids can result in significant changes in pressure distribution. Many issues like hydrate formation, pigging frequency, and downstream facility design dependent on pressure and holdup are thus also affected. Similarly the transport of contaminants and additives such as corrosion inhibitors is of great significance since most of the additives are observed in the liquid phase. Therefore, understanding of the flow characteristics of low liquid loading gas-oil-water flow is of great importance in transportation of wet gas. However, very few studies have been conducted on low liquid loading especially in three-phase flow.

Several authors have published papers on three-phase flow pattern identification and modeling of three-phase flow. However, most of them do not cover the range of low liquid loading flow. In this study, low liquid loading gas-oil-water flow experiments will be conducted in a 6 in. ID flow loop. The flow pattern, pressure drop, volumetric fractions of the three phases, liquid film thickness, wetted wall fractions and entrainment fractions will be observed and measured at different flow rates, liquid loading levels and water cuts.

Literature Review

Although significant research has been conducted in the field of two phase gas liquid flow much fewer studies have been conducted in the domain of low liquid loading. Some of these studies were presented at the previous Advisory Board meetings (2009). The literature review is still an ongoing task.

Experimental Study

Experimental Facility

The experimental facility for this study is the 6 in. flow loop which has been used to conduct research on low liquid loading flow for several years. Due to limitations of the earlier facility tests could only be done up to gas superficial velocity of 18.5 m/s. However, the facility was modified to reduce back pressure of the loop, and higher gas flow rates can now be attained. Moreover, this modification enabled better control over back pressure in the flow loop. Figure 1 shows a schematic of the modified flow loop. The test section consists of two runs of 6 in. ID pipes, each run being 56.4 m in length. Acrylic visualization sections are provided at the end of each run. The inclination angle of the test section can be changed from 0° to 2° in upward and downward directions.

Test Fluids

As shown by Utvik *et al.* (2001) the choice of test fluids play a very important role in the results of the experiments. Since the phenomenon of low liquid loading is observed mainly in wet gas pipelines, the test fluid selected should resemble the gas condensates as much as possible. The selected oil should have low viscosity (comparable to that of water), low specific gravity and high interfacial tension with water. Based on these criteria the test fluids selected are Isopar L, air and water.

Instrumentation and Data Acquisition

The DeltaV^{TM} digital automation system is used as the data acquisition software. Gas flow rate is measured using the micro motion flow meter CMF300 while two micro motion flow meters CMF100 and CMF050 are used to measure oil and water flow rates, respectively. The flow meters are calibrated by the manufacturer and have a mass flow rate uncertainty of ±0.1% and density measurement uncertainty of ±0.5%.

Pressure, temperature and pressure gradients are measured using Rosemount pressure, temperature transmitters and Rosemount differential pressure transducers, respectively.

Liquid holdup is measured by trapping liquid between the two quick-closing valves (QCV) installed on the first run of the test section and then pigging out the entrapped liquid into graduated cylinders.

Wetted wall perimeter is measured using grades on pipe circumference. Liquid entrainment fraction is measured using iso-kinetic sampling system. The working principle of iso-kinetic sampling is shown in Fig. 2.

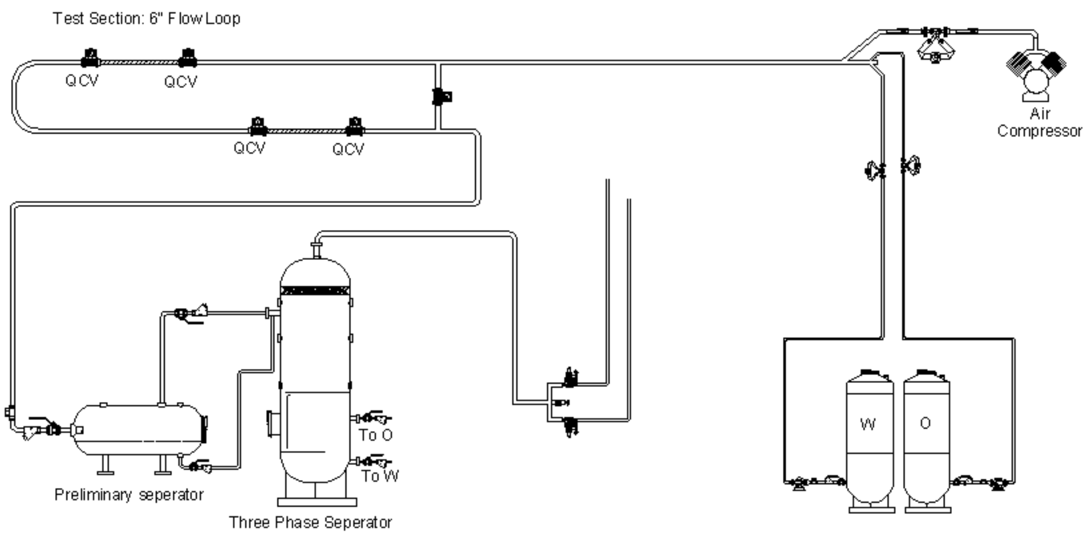

Figure 1: Schematic of Modified Flow Loop

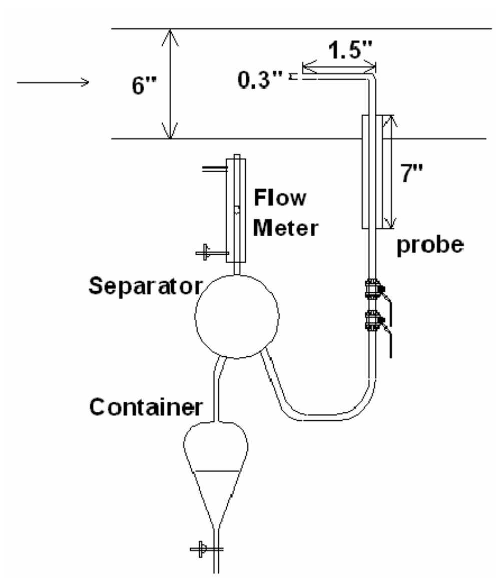

Figure 2: Iso-kinetic Sampling Probe

Liquid entrainment is not uniform in horizontal stratified flow. The entrainment flux is higher near the gas-liquid interface and tends towards a constant value towards the top of the pipe. In the experiments carried out thus far the iso-kinetic sampling probe was inserted into the pipe at four different radial locations (1/4D, 1/D, 3/4D and D; where D is diameter of the pipe). It was found that there was a significant change in entrainment flux from the 1/4D position to 1/2D position. Hence, as suggested in the previous ABM, it has been decided to measure entrainment flux at a location between 1/4D and 1/2D. Also entrainment flux measurement at a position closer to the pipe wall would be done as shown in the Fig. 3. Entrainment flux is calculated using these measurements, and is then integrated over the gas core area to give entrainment fraction.

Liquid film thickness can be measured using conductivity probe. The probe consists of a single wire which traverses across the pipe cross section. The oil water interface is indicated by change in conductance and hence a change in voltage across the probe. This method is time consuming and relies on visual observation and manually traversing the probe which can introduce considerable error in the measurement. The error in measurement is especially higher at higher gas flow rates.

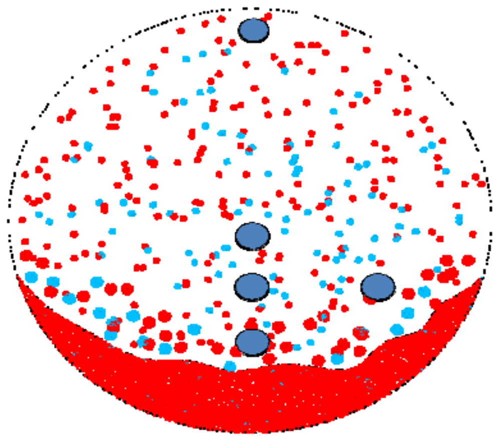

Figure 3: Positions of Iso-kinetic Probe

Cold liquid injection technique is used to determine liquid velocity. A cold liquid injector is placed at a point in the test section to inject cold oil or water into the test section. Two thermal probes are installed 0.5 ft after the injector with a 1 ft interval between them. The time required for the cold liquid to travel between the two probes is measured which gives the velocity of the liquid. This method is effective at lower gas flow rates. However, it was found that at higher gas flow rates the injected liquid quickly disperses into the fast moving flowing fluid so that the thermal probe cannot detect any change in temperature. Hence a new technique for measurement of film velocity is needed. Use of a high speed video camera along with a method to track the moving liquid film is being explored for this purpose.

Fisher Scientific Semi-automatic Model 21 Surface Tensiomat tensiometer is used for measurement of surface tension of oil and water and interfacial tension between oil and water. It employs the Du-Nuoy's ring method for direct determination of the surface tension and interfacial tension.

Experimental Program

Experiments are being performed for oil-gas and oil-water-gas three phase flows. As suggested at the previous ABM, it was decided to expand the test matrix to consider greater range of flow conditions. The proposed test matrix is shown in Table 1 and Table 2. The test matrix is divided into two parts viz. tests at lower gas flow rates and entrainment studies at higher gas flow rates. The flow conditions used for lower gas flow rates are based on the previous studies done by Dong (2007) with Tulco Tech oil.

Table 1- Test Matrix for Low Gas Flow Rate Studies

Superficial Gas Velocity (m/s)	Superficial Liquid Velocity (m/s)			
	Water Cuts : 0, 5%, 10%, 20%, 50%			
5	0.001	0.004	0.007	0.01
10	0.001	0.004	0.007	0.01
15	0.001	0.004	0.007	0.01

Table 2-Test Matrix for High Gas Flow Rate Studies

Superficial Gas Velocity (m/s)	Superficial Liquid Velocity (m/s)			
	Water Cuts : 0, 5%, 10%, 20%, 50%			
16.5	0.004	0.01	0.02	0.035
18.5	0.004	0.01	0.02	0.035
22.5	0.004	0.01	0.02	0.035

Experimental Results

The liquid entrainment onset points were observed visually. Different authors have defined onset point in different ways. For the current study the entrainment onset point is defined as the lowest superficial gas velocity at which droplets can be observed near the top of the pipe. In the previous work by Dong (2007), the entrainment onset point for Tulco Tech 80 (μ=13.5 cP @ 40^0C) was observed at superficial gas velocity of 15 m/s. In the current study the oil used is Isopar L (μ=1.23 cP @ 40^0C) and the onset of entrainment was observed at 12.5 m/s. The entrainment onset point did not vary with superficial liquid velocity.

Entrainment flux is calculated using the following formula

$$E_X = \frac{V_E}{A_{probe} t_s} \quad (1)$$

Where, E_X is the local liquid entrainment flux, V_E is the collected liquid entrainment volume, A_{probe} is the area of probe opening and t_s sampling duration which is 10 minutes in the current study. Though the onset of entrainment occurs at superficial gas velocity of 12.5 m/s, the entrainment flux becomes measurable only above superficial gas velocity above 15.5 m/s. Figures 4 and 5 show the variation of liquid entrainment rate with superficial gas velocities of 16.5 m/s and 18.5 m/s for the case of gas-oil two phase flow.

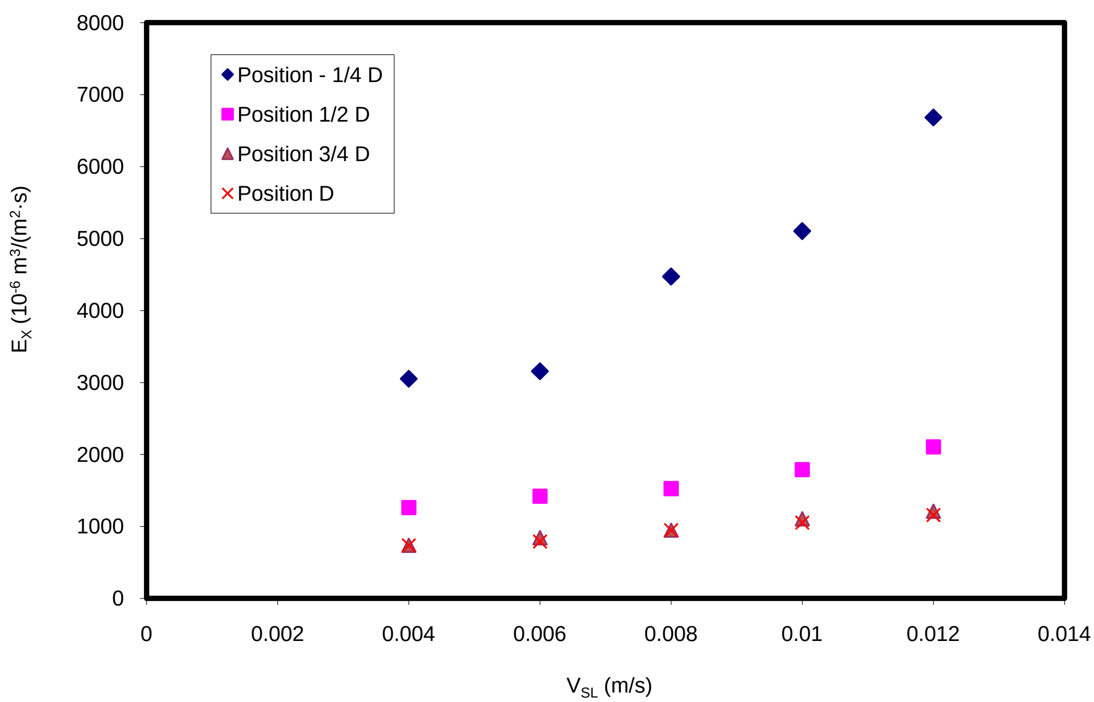

Fig. 4: Variation of Liquid Entrainment Flux with Superficial Liquid Velocity (v_{Sg} = 16.5 m/s and WC=0 %)

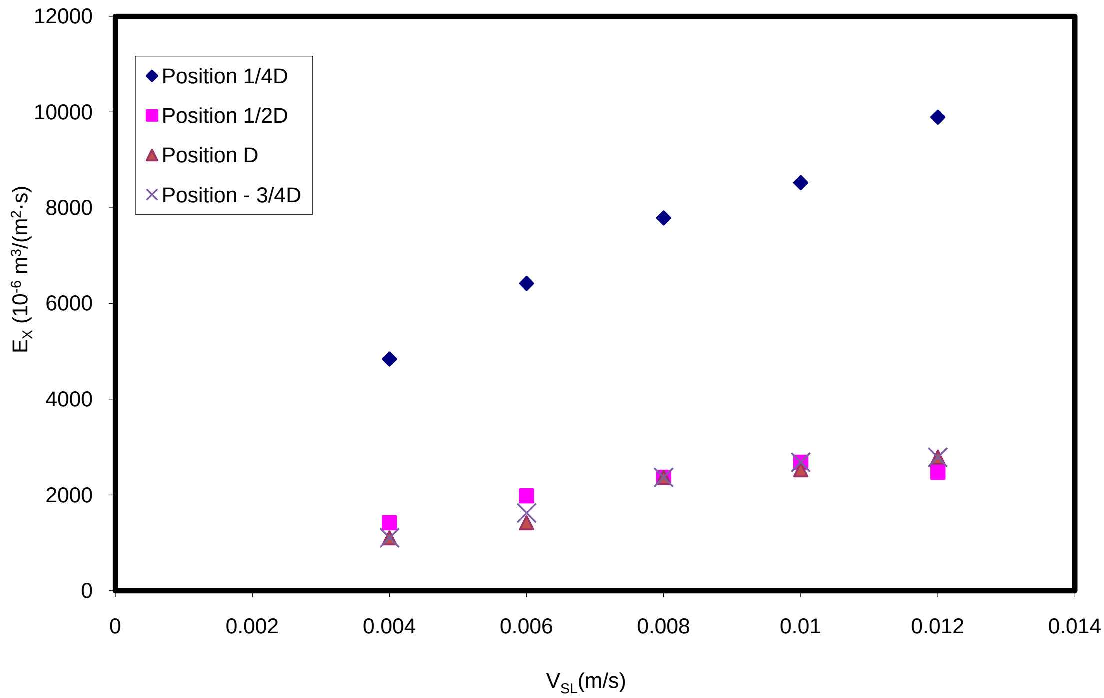

Fig. 5: Variation of Liquid Entrainment Flux with Superficial Liquid Velocity (v_{Sg} = 18.5 m/s and WC=0 %)

It can be seen from these figures that entrainment flux increases with increase in liquid loading levels. Figures 6 and 7 show the variation of the entrainment flux with position of the isokinetic probe for superficial gas velocity of 16.5 m/s and 18.5 m/s, respectively. It can be seen that the entrainment flux is very high near the gas-liquid interface and tends to level off towards the top of the pipe. Similar results are obtained for the case of Gas-oil-water three-phase flows. Figures 8 and 9 show the variation of total liquid entrainment flux with liquid loading level for water cut of 5 %. Also Figs 10 and 11 show the total liquid entrainment flux profile for water cut of 5 %.

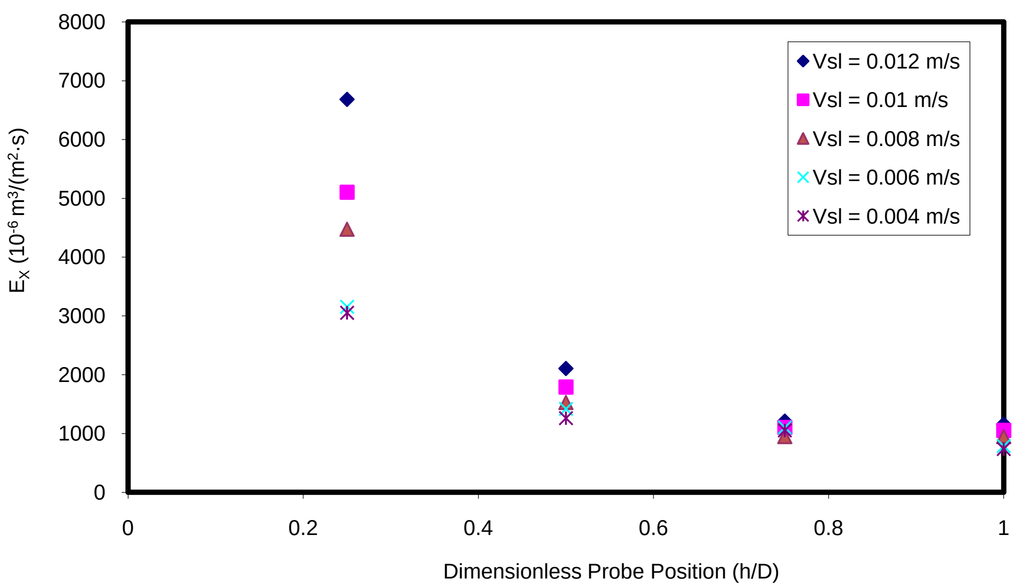

Fig. 6: Total Liquid Entrainment Flux Profile (v_{Sg} = 16.5 m/s and WC = 0%)

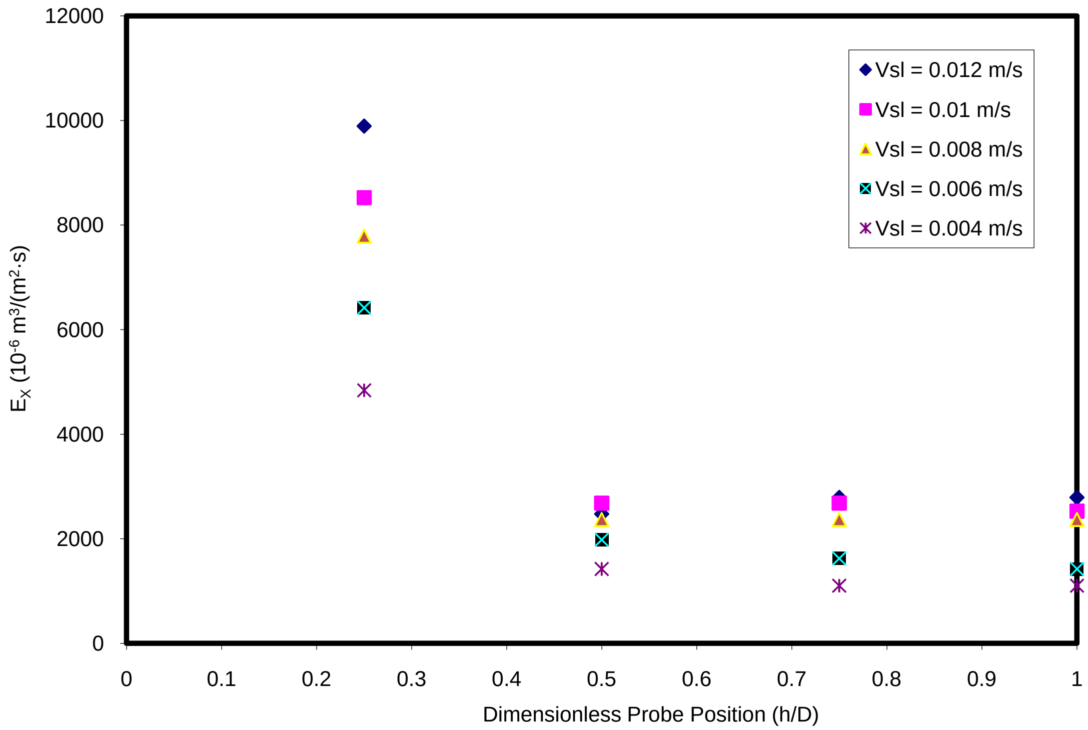

Fig. 7: Total Liquid Entrainement Flux Profile (v_{Sg} = 18.5 m/s and WC = 0%)

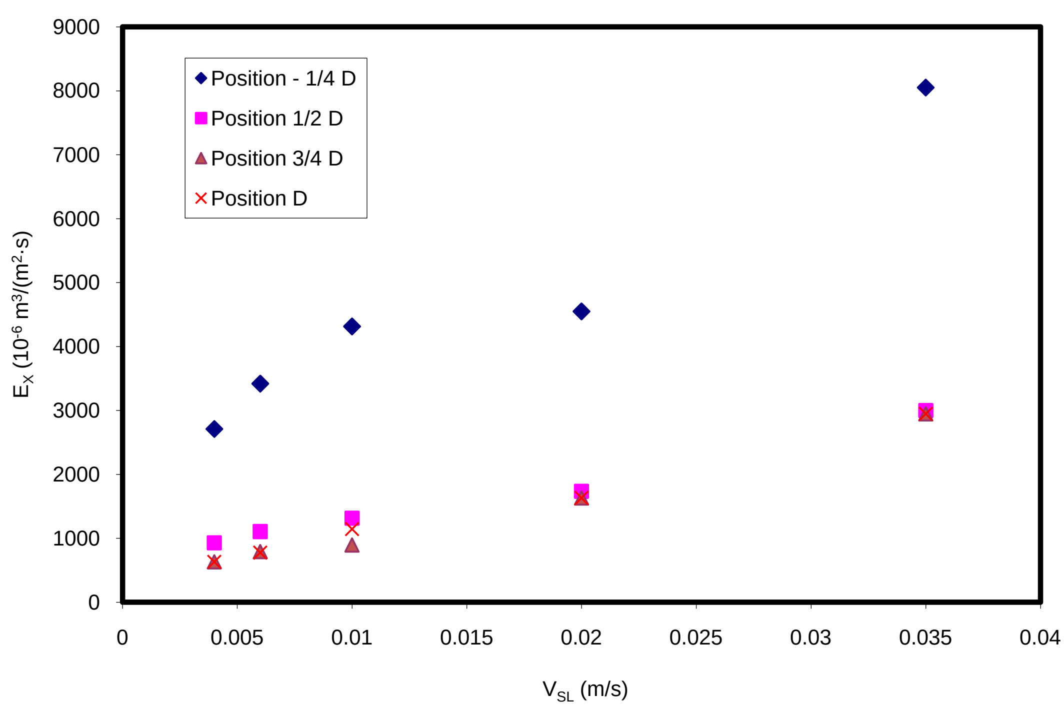

Fig. 8: Variation of Liquid Entrainment Flux with Superficial Liquid Velocity (v_{Sg} = 16.5 m/s and WC=5 %)

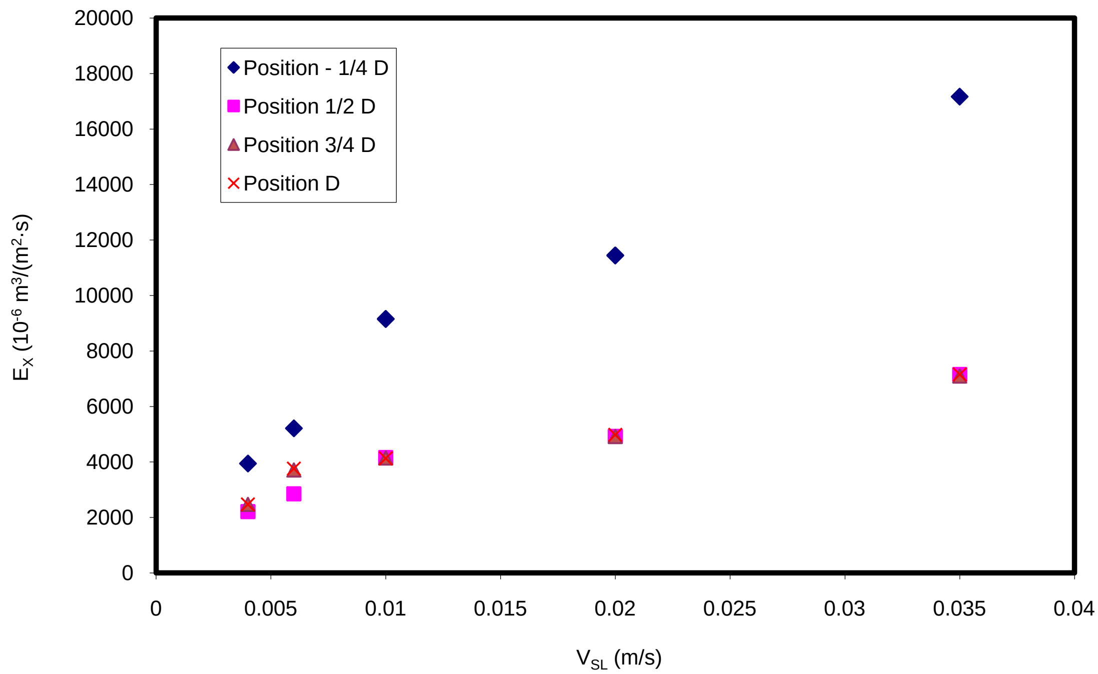

Fig. 9: Variation of Liquid Entrainment Flux with Superficial Liquid Velocity (v_{Sg} = 22.5 m/s and WC=5 %)

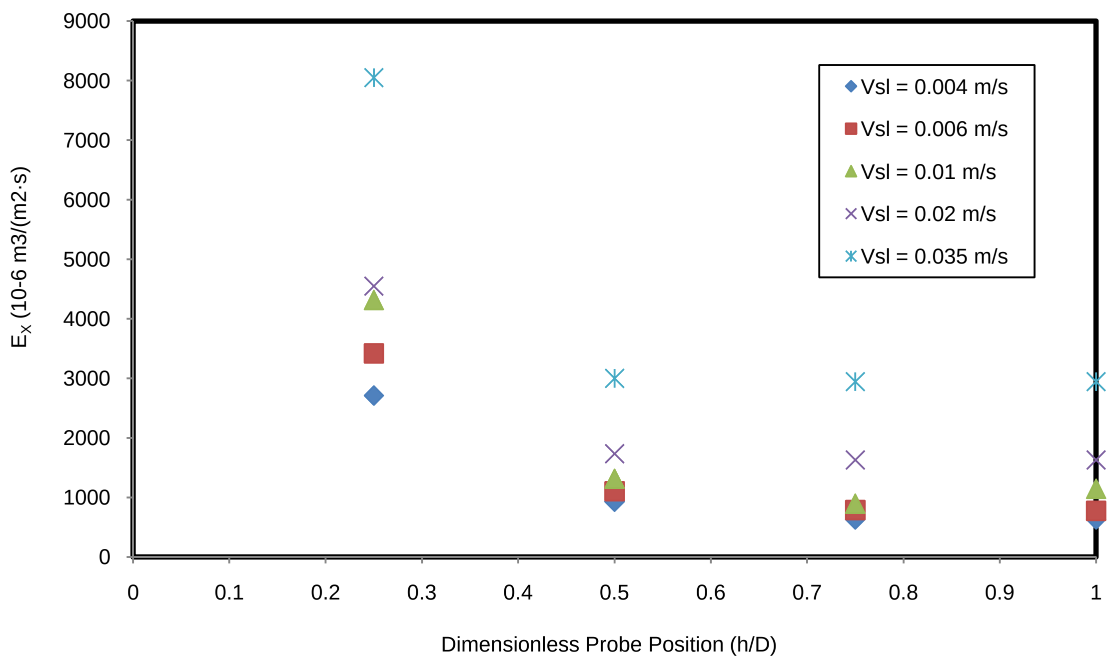

Fig. 10: Total Liquid Entrainement Flux Profile (v_{Sg} = 16.5 m/s and WC = 5 %)

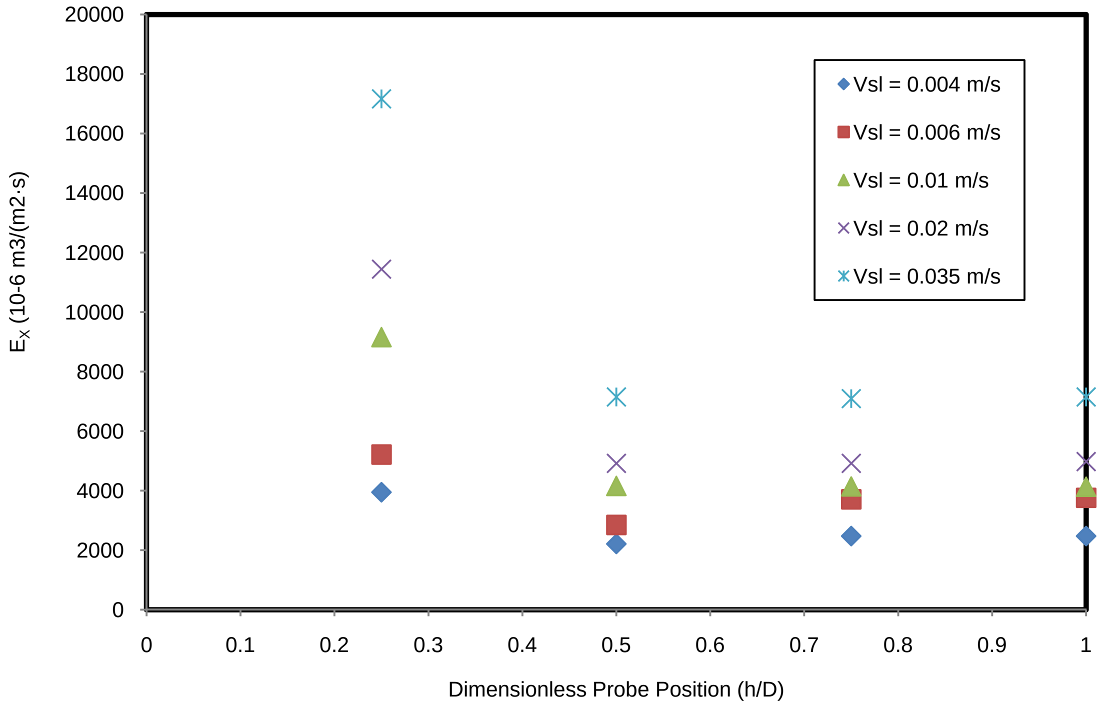

Fig. 11: Total Liquid Entrainement Flux Profile (v_{sg} = 22.5 m/s and WC = 5 %)

Figures 12 to 14 indicate the variation of water fraction in the entrained liquid with position of the iso-kinetic probe. The results indicate that the water fraction in the entrained liquid is less than the inlet water fraction. The fraction of water entrained seems to remain constant with position of the probe. However, more experiments need to be performed at higher water cuts to ascertain the results and draw conclusions.

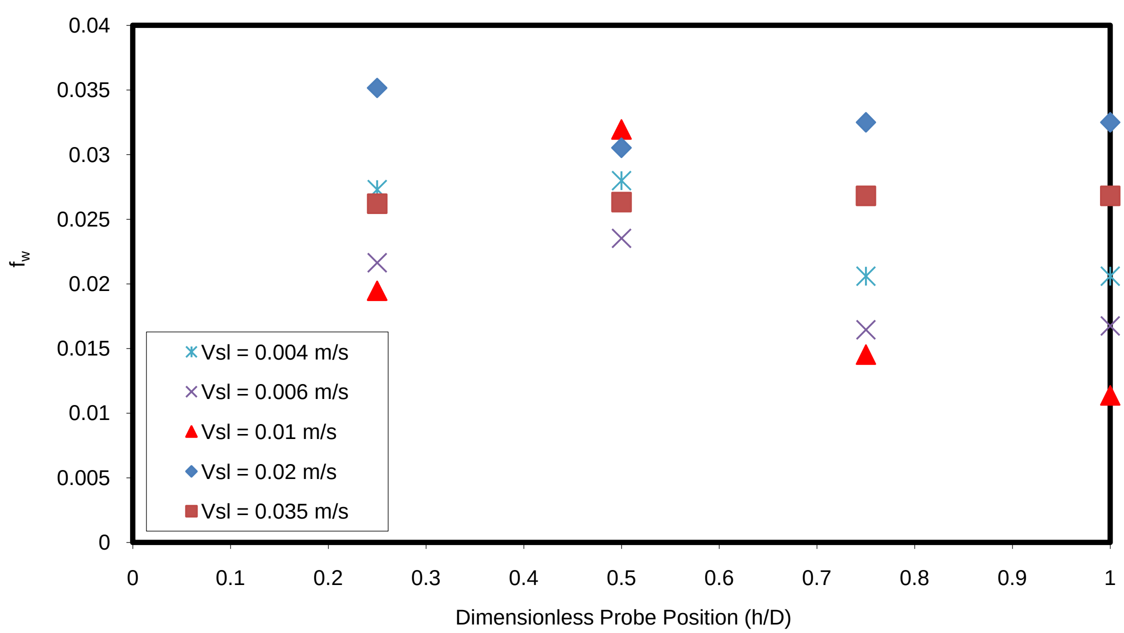

Fig. 12: Water Fraction Profile in Total Liquid Entrainment (v_{sg} = 16.5 m/s and WC = 5 %)

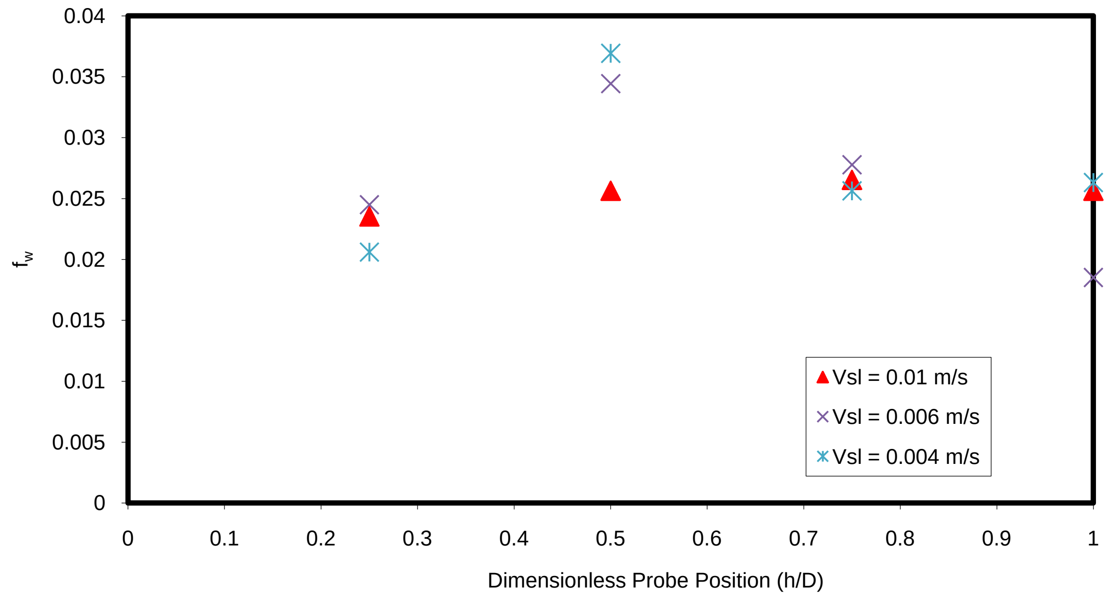

Fig. 13: Water Fraction Profile in Total Liquid Entrainment (v_{Sg} = 18.5 m/s and WC = 5 %)

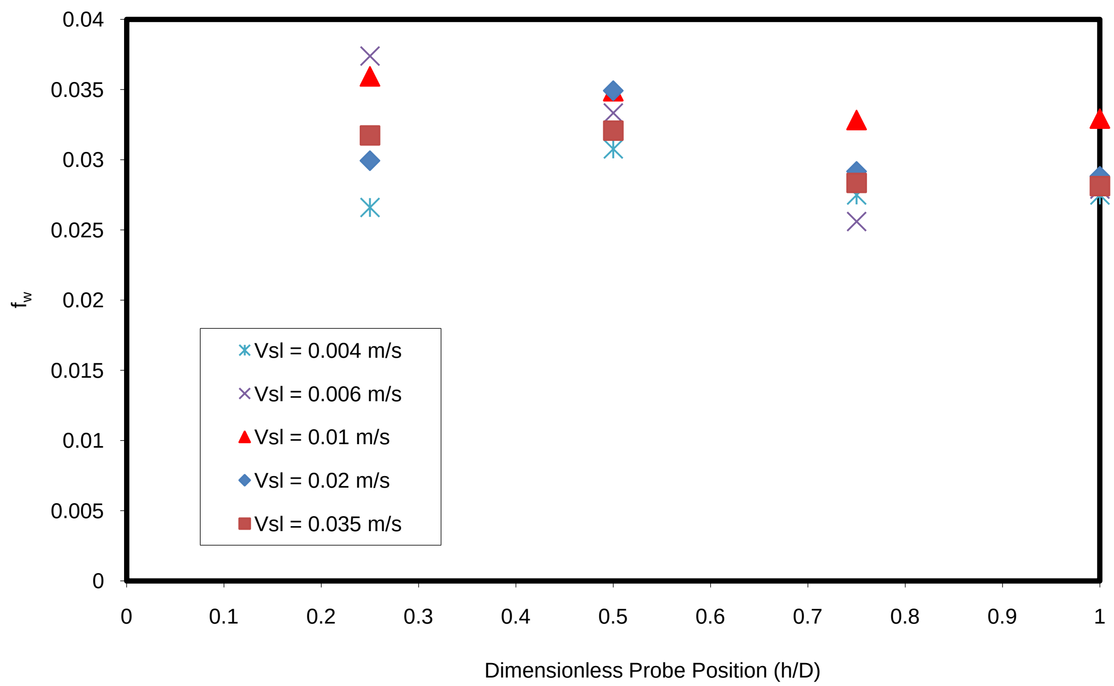

Fig. 14: Water Fraction Profile in Total Liquid Entrainment (v_{Sg} = 22.5 m/s and WC = 5 %)

Figures 15 and 16 indicate that the total liquid entrainment rate decreases with an increase in water cut. This could be due to increase in viscosity of the liquid phase. Moreover, water being heavier would be entrained less than oil which could decrease the liquid entrainment rate.

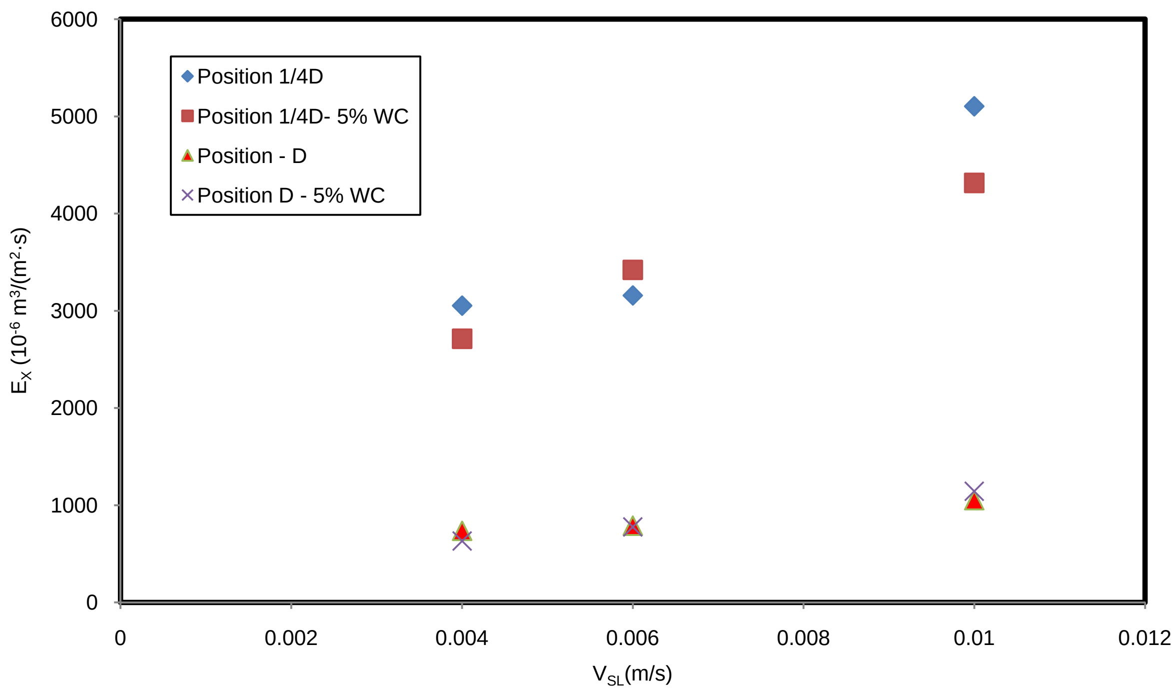

Fig. 15: Effect of Water Cut on Liquid Entrainment Flux (V_{Sg} = 16.5 m/s)

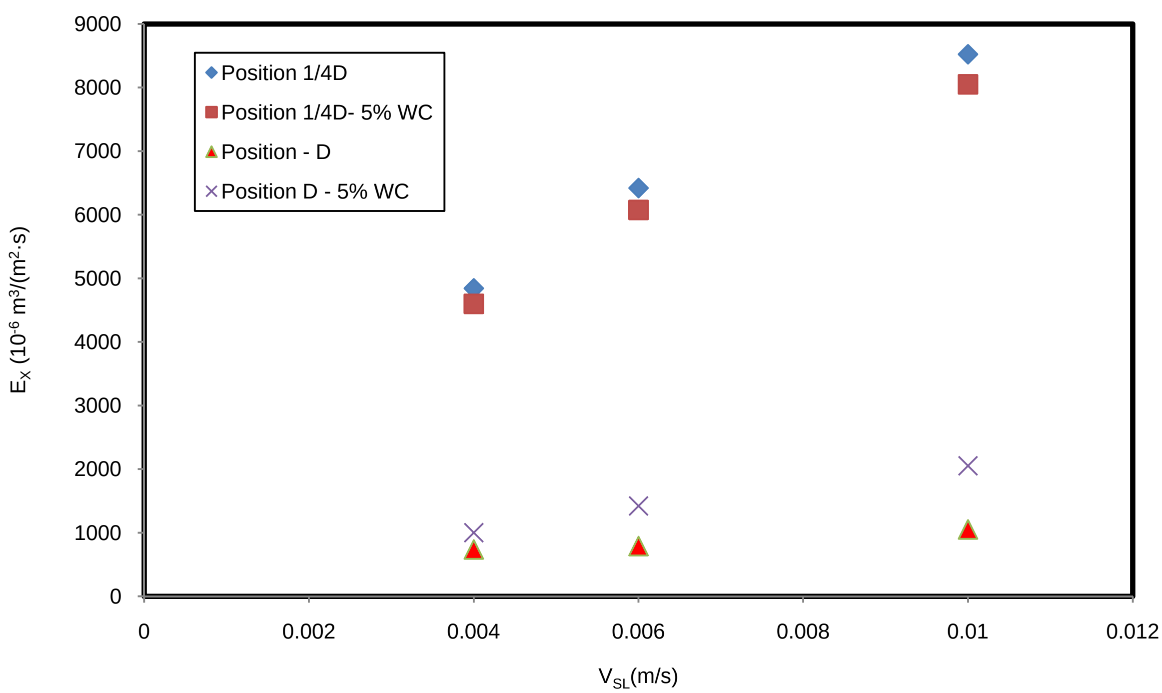

Fig. 16: Effect of Water Cut on Liquid Entrainment Flux (V_{Sg} = 18.5 m/s)

The total amount of liquid entrained in the gas core is obtained by integrating the local entrainment flux over area. Once this is obtained the entrainment fraction, F_E can be obtained as follows:

$$F_E = \int E_X dA / A_{pipe} V_{SL}$$

Figure 17 shows the variation of entrainment fraction with liquid superficial velocity.

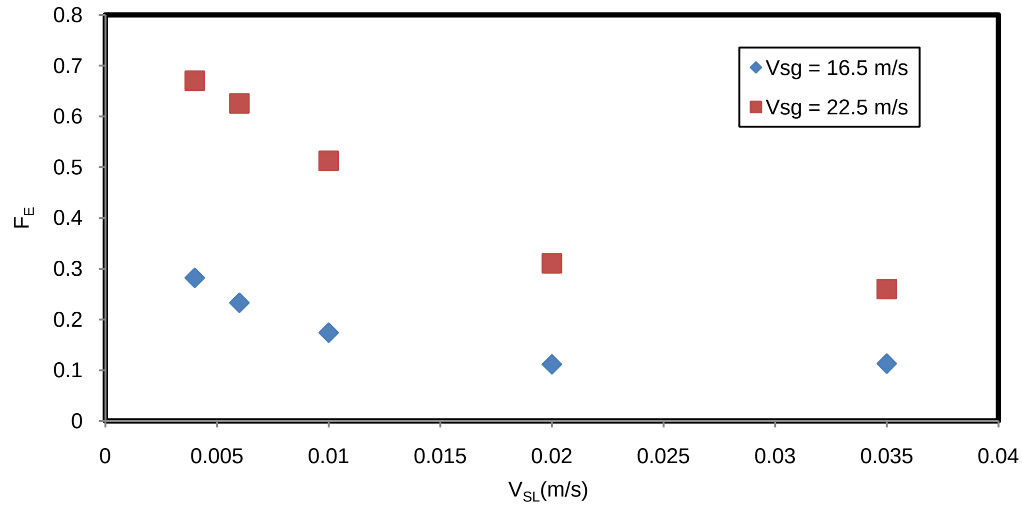

Fig. 17: Effect of Superficial Velocity of Liquid and Gas on Entrainment Fraction

As observed in the graph entrainment fraction increases with increase in gas superficial velocity but tends to decreases with liquid superficial velocity. Similar results were obtained by Mantilla (2008) and Dong (2007) in their studies with air-water flow in 6-IN horizontal pipes as shown in Figs. 18 and 19.

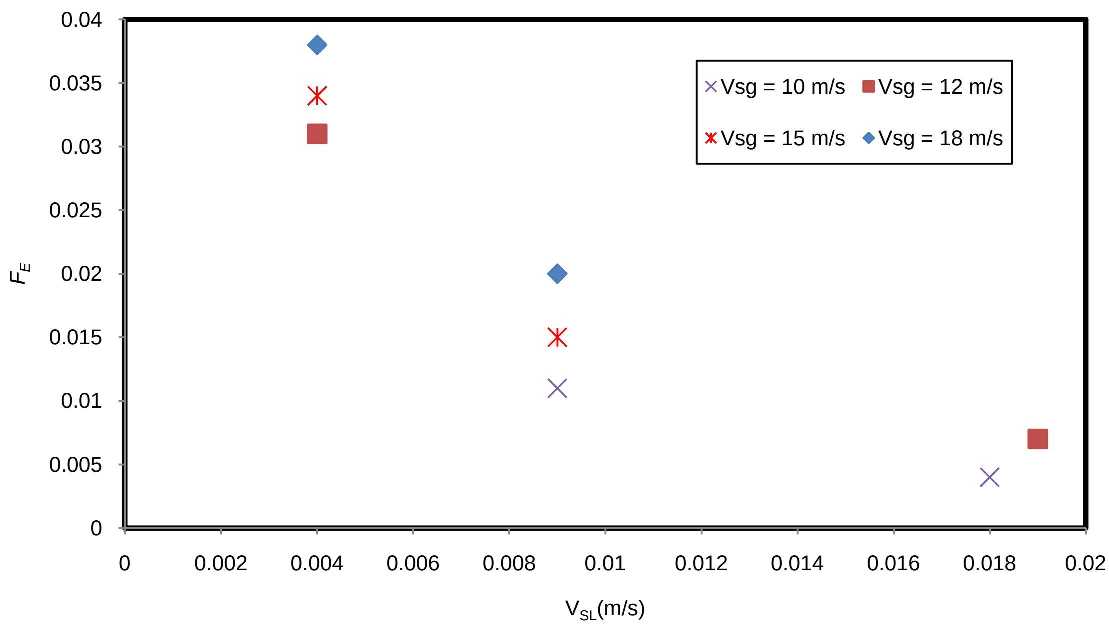

Fig. 18: Effect of Superficial Velocity of Liquid and Gas on Entrainment Fraction – Mantilla (2008)

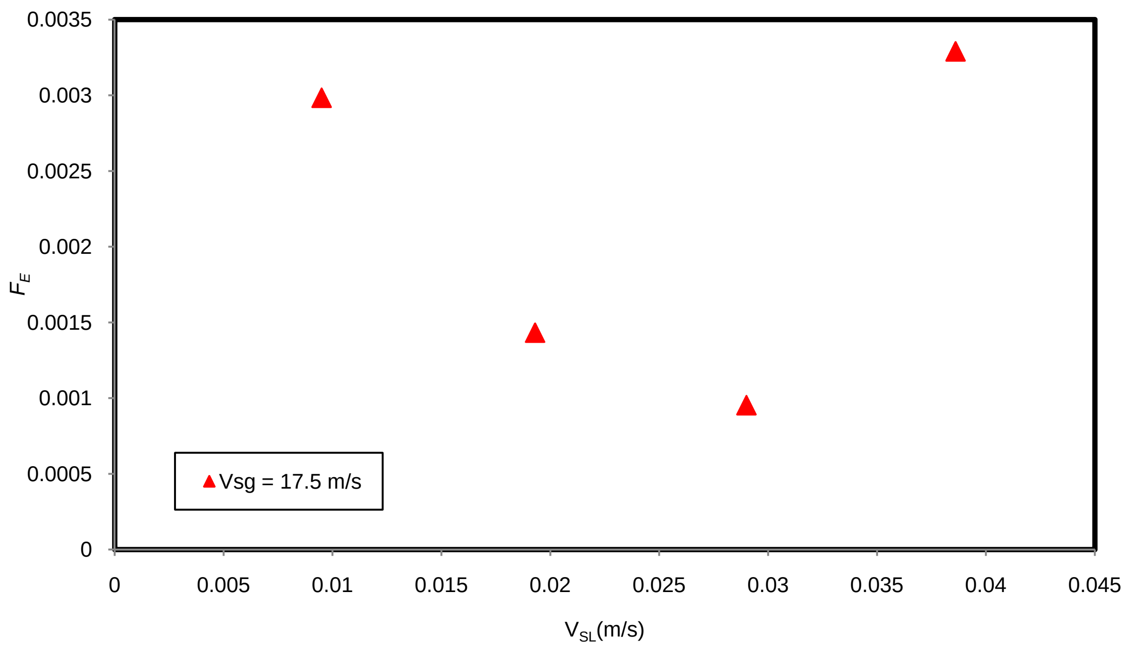

Fig. 19: Effect of Superficial Velocity of Liquid and Gas on Entrainment Fraction – Dong (2007)

However in the studies done for smaller diameter pipes it was found that the entrainment fraction remained constant or slightly increases with increase in superficial liquid velocity. Figure 20 shows the results for air-water flow in 3-IN horizontal pipe done by Magrini (2009).

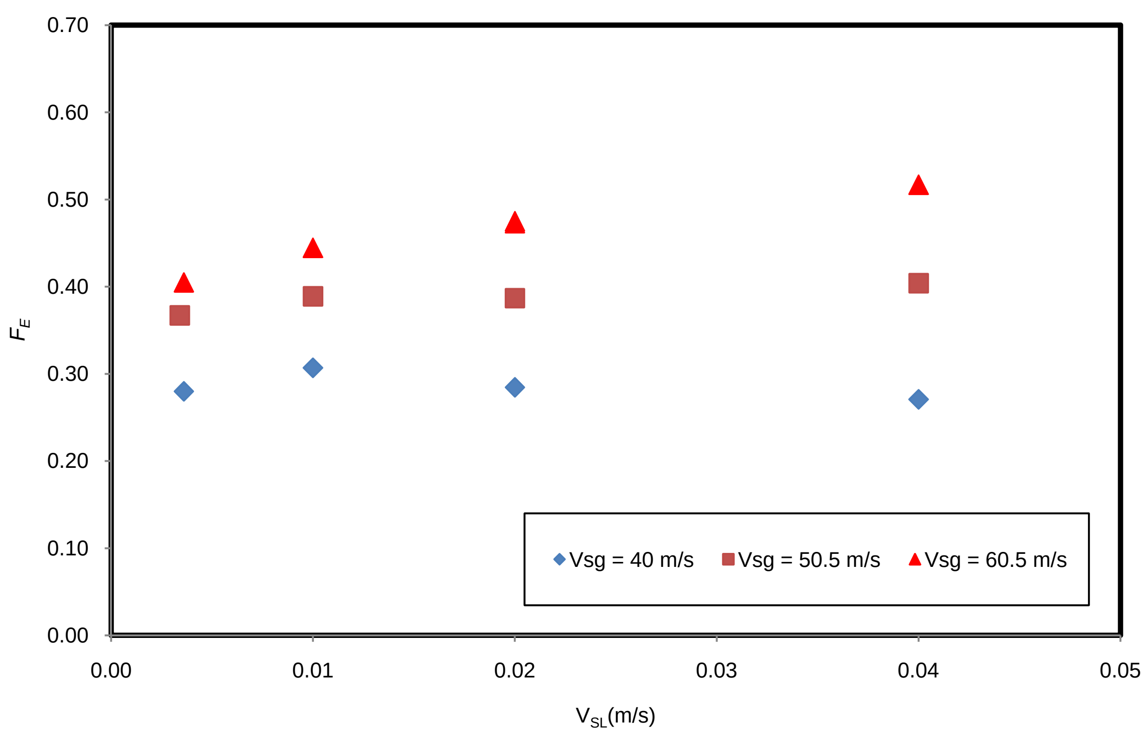

Fig. 20: Effect of Superficial Velocity of Liquid and Gas on Entrainment Fraction – Magrini (2007)

Near Future Tasks

- Complete the proposed test matrix.
- Ph.D. proposal defense.
- Analyze experimental data.
- Carry out comparison with existing models
- Development of new model

Nomenclature

A = area [m^2]
d = pipe diameter [m]
E = entrainment Flux [$m^3/(m^2 \cdot s)$]
V = velocity [m/s]
F_E = Entrainment Fraction [-]

Greek Letters

μ = viscosity [kg/ms]
θ = pipe inclination angle [degree]
ρ = density [kg/m^3]
σ = surface tension [N/m]

Subscripts

E = entrainment
g = gas phase
L = liquid phase
probe = isokinetic probe
s = sampling time
Sg = superficial gas
SL = superficial liquid

References

Chen, X.: "Droplet-Homophase Interaction Studies," TUFFP ABM March 2005, pp. 135-186, (2005).

Dong, H.-K.: "Low Liquid Loading Gas-Oil-Water Flow in Horizontal Pipes," M.S. Thesis, U. Tulsa. Tulsa, OK. (2007).

Magrini, K. L., "Liquid Entrainment in Annular Annular Gas/Liquid Flow in Inclined Pipes", MS Thesis, University of Tulsa, OK., (2009).

Mantilla, I., "Mechanistic Modeling of Liquid Entrainment in Gas in Horizontal Pipes," PhD Dissertation, University of Tulsa, Ok., (2008).

TUFFP ABM September 2009, pp. 325-335, (2009).

TUFFP ABM May 2010, pp. 103-121, (2010).

Utvik, O. H., Rinde, T., and Valle, A.: "An Experimental Comparison Between a Recombined Hydrocarbon-Water Fluid and a Model Fluid System in Three-Phase Pipe Flow," *ASME, J. Energy Res. Tech.*, Vol. 123, pp. 253-259 (2001).

Fluid Flow Projects

Executive Summary of Research Activities

Cem Sarica

Advisory Board Meeting, November 3, 2010

Transient Modeling

- Significance
  - Industry has Capable All Purpose Transient Software
    - OLGA, PLAC, TACITE
  - Next Generation All Purpose Transient Simulators Being Developed
    - Horizon, LEDA
  - Need for a Simple Transient Flow Simulator

Fluid Flow Projects

Advisory Board Meeting, November 3, 2010

Transient Modeling …

- Objective
  - Development and Testing of a Simple and Fast Transient Flow Simulator That Can Be Used as a Screening Tool
- Past Studies
  - TUFFP has Conducted Many Transient Multiphase Studies
    - Scoggins, Sharma, Dutta-Roy, Taitel, Vierkandt, Sarica, Vigneron, Minami, Gokdemir, Zhang, Tengesdal, and Beltran

Transient Modeling …

- Status
  - Significant Progress Since Last ABM
  - Two Models Developed
    - Two-Fluid
    - Drift Flux
  - Compared with TUFFP Transient Flow Data
    - Two-Fluid Model Performed Best for Separated Flow
    - Drift Flux Model Performed Best for Mixed Flow
  - Developed a Driver Routine to Select Proper Model

Fluid Flow Projects

Simplified Transient Two-Phase Flow Modeling

Michelle Li

Advisory Board Meeting, November 3, 2010

Outline

- Objectives
- Significance
- Past Studies
- Current Approach
  - Ways to Simplify
  - Two Fluid Model
  - Drift Flux Model
  - Modified Drift Flux correlation
  - Power Law Correlation
- Further Work

Objectives

- Develop a Simplified Simulator for Gas-Liquid Two-Phase Flow in Pipelines
- Test Model Against Available Experimental Data

Significance

- Oil and Gas Pipelines Rarely Operate under Steady State
- Transient Phenomena can be Induced due to Boundary Conditions, or Geometry of the Pipe
- Currently, Most Two-Phase Flow Pipelines Still Designed Under Steady Condition

Significance …

- All Purpose Transient Software Packages Available: OLGA, PLAC, TACITE
- Further Efforts Underway to Develop Next Generation Transient Simulators: Horizon, LEDA
- Need for a Fast and Simple Transient Simulator

Past Studies

- Scoggins (1977), Drift Flux Model, Horizontal Two-Phase Transient
- Dutta-Roy (1982), Two-Fluid Model for Horizontal Two-Phase Stratified Flow
- Sharma (1986,1993), Two-Fluid Model for Stratified and Slug Flow
- Taitel (1978,1989,1990,1997), Flow Patten Dependant Mechanistic Model
- Minami (1991), Pigging Slug Dynamics, Two-Phase Flow

Past Studies …

- Sarica (1991), Terrain Slugging, Two-Phase Flow
- Zhang (2003), Slug Dissipation and Generation in Two-Phase Hilly-Terrain Pipe Flow
- Tengesdal (2003), Severe Slugging, Gas-Liquid Two-Phase Flow
- Beltran (2006), Severe Slugging, Gas-Oil-Water Three Phase Flow

Ways to Simplify

- Transient Phenomenon Modeled Through Unsteady Mass Conservation Equations
- Momentum Equations Take Steady State Format
- Flow Pattern Free
  - Modify Drift Flux Correlation for Stratified Flow
  - Power Law Correlation

Review of Last Period (Oct 2009 – May 2010)

- Two-Fluid Model for Stratified Flow
- Drift Flux Model for Slug Flow
- Drift Flux Model for Stratified Flow

Model Validation

- Experiments by Vigneron *et al.* (1995)
  - Air and Kerosene
  - Horizontal Pipe L=420 m, d=77.9 mm
  - Two Test Sections
  - Transient Caused By:
    - Liquid flow rate change
    - Gas flow rate change
    - Liquid blow out
    - Start up

Two Fluid Model Summary

- Two-Fluid Model is Developed for Stratified Flow
- For Liquid Flow Rate Change, Model Simulation Gave Good Prediction
- For Gas Flow Rate Change, Current Model Does Not Converge

Drift Flux Model Summary

- Good for Slug Flow
- For Stratified Flow

  Good for Gas Flow Rate Change

  Not Good for Liquid Rate Change

Work in Current Period
(June 2010 – July 2010)

- Modify the Drift Flux Correlation for Stratified Flow
- Power Law Correlation Based Transient Simulator
- Convert Code into Fortran
- Put Together Current Two-Fluid Model and Drift Flux Model

Modified Drift Flux Model

- Modify the Drift Flux Correlation for Stratified Flow

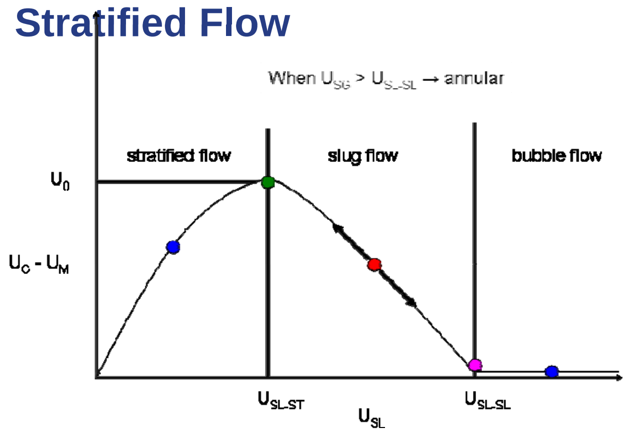

From Danielson and Fan (2010)

Modified Drift Flux Model …

- Drift Velocity

$$v_d = 0.54\sqrt{gd}cos\theta + 0.35\sqrt{gd}sin\theta$$

$$\Downarrow$$

$$v_d = v_d(d, g, \rho_L, \rho_G, \mu_L, \mu_G, \sigma, v_{SL}, v_{SG})$$

Modified Drift Flux Model …

- Use Unified Model to Calculate the $v_d - v_{SL}$ curve;
- Assume Transient Phenomenon a Transition from One Steady State to Another Steady State, We May Get Two Curves with Initial and Final Conditions
- Transient Model Should be Based on the Calculated Drift Velocities

Test 1-C

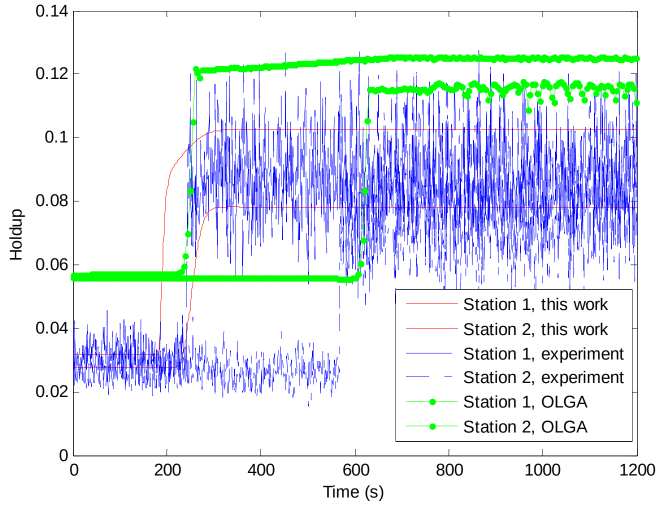

Test 1-C ...

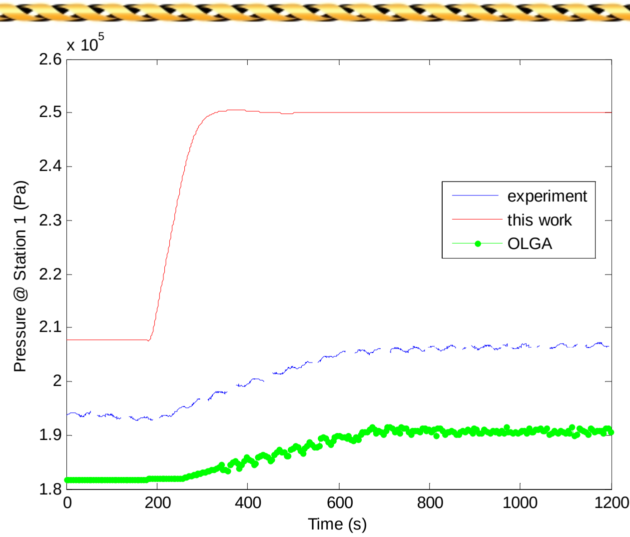

Power Law Model

- **Power Law Correlation**

$$P^* = 0.075 X^{*^{-1.808}}$$

where

$$P^* = \frac{D(-dP/dx)}{{}^1/_2 \rho_L v_{SL}^2}$$

$$X^* = \frac{\dot{m}_L}{\dot{m}_G}\sqrt{\frac{\rho_G}{\rho_L}}$$

Power Law Model …

- **From Power Law Correlation**

$$\dot{m}_{G,i}^{K+1} =$$

$$\left(\frac{0.075}{2}\frac{\Delta x}{DA^2\left(P_i^{K+1} - P_{i+1}^{K+1}\right)}\frac{\left(\dot{m}_{L,i}^{K+1}\right)^{0.192}\left(\rho_{G,i}^{K+1}\right)^{-0.904}}{\rho_L^{0.096}}\right)^{-\frac{1}{1.808}}$$

- **Mass Conservation Equations and Liquid Momentum Equation Used**
- **Solution Procedure Similar as Two-Fluid Model**

Housekeeping

- Convert Code into Fortran
- Put Together Current Two-Fluid Model and Drift Flux Model

Further Work

- Modify the Drift Flux Model for Stratified Flow
- Power Law Correlation Based Transient Simulator
- Terrain/Severe Slugging
- Incorporate a PVT Package
- Incorporate Heat Transfer Model
- More Data for Model Validation

Questions and Comments

?

Fluid Flow Projects Advisory Board Meeting, November 3, 2010

Transient Gas-Liquid Two-Phase Flow Simulation

Michelle Li

Objective

The objective of this study is to develop a simplified simulator for transient gas-liquid two-phase flow in pipelines.

Introduction

Transient phenomena are frequently encountered in pipelines in the oil and gas industry. These phenomena occur when there is a change in inlet and outlet conditions, or when terrain/severe slugging are formed due to the geometry of the pipe. Knowledge of the dynamic behavior is very important to properly design and operate the pipelines, as well as the receiving facilities.

The investigation of transient flow phenomena in petroleum industry started in the late 70's and early 80's. Currently, industry has developed capable all purpose transient simulators such as OLGA, PLAC, TACITE. Further efforts are underway to develop next generation all purpose transient simulators with multidimensional capabilities such as Horizon and LEDA.

These codes normally utilize full set of mass, momentum and energy conservation equations. However, most of the transient phenomena encountered in oil and gas industry are comparatively slow, and the use of full set of equations is probably not necessary. There is a need for a simplified transient flow simulator.

In this study, the transient phenomenon is modeled through unsteady mass conservation equations, while the momentum equation is considered to be in local quasi-steady state.

Apart from the simplification made with momentum equations, we are also trying to simplify it by avoiding the traditional way of flow pattern predictions and flow pattern based simulations. To avoid flow patterns, we need to have the same set of equations and closure relationships applicable to all flow patterns. A model based on this is called flow pattern independent model. Ways to achieve flow pattern independent model are described in power law correlation and modified drift flux correlation sections.

As a starting point, we still tried both two-fluid approach and drift flux approach for each flow pattern, and the results are presented.

Attempt 1: Two Fluid Model

Flow pattern is predicted with steady state models. Hydrodynamic behavior of each flow pattern is modeled separately.

1. Method

Unsteady mass conservation equations are used for both gas and liquid. Momentum equations are considered to be in local equilibrium. Gas is compressible, while liquid is considered to be incompressible.

Governing Equations for Stratified Flow:

The mass conservation equations are:

$$\frac{dm_L}{dt} = \dot{m}_{L,i-1} - \dot{m}_{L,i}, \tag{1}$$

$$\frac{dm_G}{dt} = \dot{m}_{G,i-1} - \dot{m}_{G,i}. \tag{2}$$

The momentum conservation equations are:

$$(P_i - P_{i+1})AH_L = (\tau_L S_L - \tau_I S_I)\Delta x + \rho_L g A H_L \Delta x \sin\theta, \tag{3}$$

$$(P_i - P_{i+1})A(1 - H_L) = (\tau_G S_G + \tau_I S_I)\Delta x + \rho_G g A(1 - H_L)\Delta x \sin\theta. \tag{4}$$

where the shear stresses can be correlated as:

$$\tau_L = f_L \frac{\rho_L v_L^2}{2}, \tag{5}$$

$$\tau_G = f_G \frac{\rho_G v_G^2}{2}, \tag{6}$$

$$\tau_I = f_I \frac{\rho_G (v_G - v_L)^2}{2}. \tag{7}$$

Friction factors f_L and f_G can be approximated by the correlation $f = C\ Re^{-n}$, C=0.046, n=0.2 for turbulent flow, and C=16, n=1 for laminar flow. Interfacial friction factor f_I can be approximated by

$$f_I = f_G\left(1 + 14.3 H_L^{0.5}\left(\frac{v_{SG}}{v_{SG,t}} - 1\right)\right). \tag{8}$$

where $v_{SG,t} = 5\left(\frac{\rho_{GO}}{\rho_G}\right)^{0.5}$, ρ_{GO} is the gas density at atmospheric pressure. The perimeters S_L, S_G, S_I are calculated according to Zhang *et al.* (2003) as follows:

$$S_L = \pi d \Theta, \tag{9}$$

$$S_G = \pi d(1 - \Theta), \tag{10}$$

$$S_I = \frac{S_L(A_{CD} - AH_L) + S_{CD} A H_L}{A_{CD}}, \tag{11}$$

$$S_{CD} = d\sin(\pi\Theta), \tag{12}$$

$$A_{CD} = \frac{d^2}{4}\left(\pi\Theta - \frac{\sin(2\pi\Theta)}{2}\right). \tag{13}$$

The wetted wall fraction Θ is calculated with Grolman correlation,

$$\Theta = \Theta_0\left(\frac{\sigma_{water}}{\sigma}\right)^{0.15} + \frac{\rho_G}{\rho_L-\rho_G}\frac{1}{cos\theta}\left(\frac{\rho_L v_{SL}^2 d}{\sigma}\right)^{0.25}\left(\frac{v_{SG}^2}{(1-H_L)^2 gd}\right)^{0.8}. \quad (14)$$

where Θ_0 is the wetted wall fraction corresponding to a flat gas/liquid interface for a given H_L.

A linear relationship can be obtained from Eq. 3 and Eq. 4 to calculate $\dot{m}_L$ and $\dot{m}_G$ from the pressure difference.

$$\dot{m}_{L,i}^{K+1} = a_{L,i}^{K+1}(P_i^{K+1} - P_{i+1}^{K+1}) + b_{L,i}^{K+1}. \quad (15)$$

$$\dot{m}_{G,i}^{K+1} = a_{G,i}^{K+1}(P_i^{K+1} - P_{i+1}^{K+1}) + b_{G,i}^{K+1}. \quad (16)$$

Where the coefficients $a_{L,i}^{K+1}$, $b_{L,i}^{K+1}$, $a_{G,i}^{K+1}$, $b_{G,i}^{K+1}$ are:

$$a_{L,i}^{K+1} = \frac{1}{\frac{(f_L S_L \rho_L - f_I S_I \rho_G)\Delta x \dot{m}_L}{2\rho_L^2 A^3 H_L^3} + \frac{f_I S_I \Delta x \dot{m}_G}{\rho_L A^3 H_L^2 (1-H_L)}}, \quad (17)$$

$$b_{L,i}^{K+1} = \frac{\frac{f_I S_I \Delta x \dot{m}_G^2}{2\rho_G A^3 H_L (1-H_L)^2} - \rho_L g sin\theta \Delta x}{\frac{(f_L S_L \rho_L - f_I S_I \rho_G)\Delta x \dot{m}_L}{2\rho_L^2 A^3 H_L^3} + \frac{f_I S_I \Delta x \dot{m}_G}{\rho_L A^3 H_L^2 (1-H_L)}}, \quad (18)$$

$$a_{G,i}^{K+1} = \frac{1}{\frac{(f_G S_G + f_I S_I)\Delta x \dot{m}_G}{2\rho_G A^3 (1-H_L)^3} - \frac{f_I S_I \Delta x \dot{m}_L}{\rho_L A^3 H_L (1-H_L)^2}}, \quad (19)$$

$$b_{G,i}^{K+1} = \frac{-\frac{f_I S_I \rho_G \Delta x \dot{m}_L^2}{2\rho_L^2 A^3 H_L^2 (1-H_L)} - \rho_G g sin\theta \Delta x}{\frac{(f_G S_G + f_I S_I)\Delta x \dot{m}_G}{2\rho_G A^3 (1-H_L)^3} - \frac{f_I S_I \Delta x \dot{m}_L}{\rho_L A^3 H_L (1-H_L)^2}}. \quad (20)$$

2. Solution Procedures

Figure 1 shows a flow chart for the two fluid model approach. Detailed descriptions of each step are given below.

1) Initialization: Define pipe geometry, fluid properties, and initial conditions. The pipe is divided into N sections of length Δx. Initial condition at time $t=0$ includes: gas and liquid velocities, liquid holdup, and pressure for each section of the pipe.

2) Specify boundary conditions. Inlet gas and liquid flow rates and outlet pressure at each time step are known.

3) Liquid mass in each section of the pipe at the new time step K+1 is calculated by

$$m_{L,i}^{K+1} = m_{L,i}^{K} + \Delta t\left(\dot{m}_{L,i-1}^{K+1} - \dot{m}_{L,i}^{K+1}\right). \quad (21)$$

4) The new liquid holdup is calculated as

$$H_{L,i}^{K+1} = \frac{m_{L,i}^{K+1}}{\rho_L A_i \Delta x}. \quad (22)$$

5) Gas mass in each section of the pipe at the new time step K+1 is calculated by

$$m_{G,i}^{K+1} = m_{G,i}^{K} + \Delta t(\dot{m}_{G,i-1}^{K+1} - \dot{m}_{G,i}^{K+1}). \quad (23)$$

6) The new gas density is calculated as

$$\rho_{G,i}^{K+1} = \frac{m_{G,i}^{K+1}}{(1-H_{L,i}^{K+1})A_i \Delta x}. \quad (24)$$

7) The new pressure is calculated using the ideal gas equation of state,

$$P_i^{K+1} = \rho_{G,i}^{K+1} RT. \quad (25)$$

8) Calculate wetted wall perimeters S_L, S_G, S_I using Eqs. 9 - 14.

9) Calculate the friction factors f_L, f_G, f_I;

10) Calculate the coefficients $a_{L,i}^{K+1}$, $b_{L,i}^{K+1}$, $a_{G,i}^{K+1}$, $b_{G,i}^{K+1}$ using Eqs. 17 – 20.

11) Given pressure drop, and the coefficients $a_{L,i}^{K+1}$, $b_{L,i}^{K+1}$, $a_{G,i}^{K+1}$, $b_{G,i}^{K+1}$, the new liquid and gas mass flow rate at each section of the pipe are calculated using Eqs. 15 – 16.

12) The new superficial velocities are calculated as

$$v_{SL,i}^{K+1} = \frac{\dot{m}_{L,i}^{K+1}}{\rho_{L,i}^{K+1} A_i}. \quad (26)$$

$$v_{SG,i}^{K+1} = \frac{\dot{m}_{G,i}^{K+1}}{\rho_{G,i}^{K+1} A_i}. \quad (27)$$

13) Compare the newly calculated liquid and gas flow rate with the $\dot{m}_{L,i}^{K+1}$ and $\dot{m}_{G,i}^{K+1}$ calculated from the last iteration, and check the convergence. If converged, change the 'new' variables into 'old' and go to step 3) for the calculation of next time step. If not, go to step 5) for another iteration within the current time step. Convergence criteria are set as

$$\frac{\dot{m}_{L,i}^{K+1,new} - \dot{m}_{L,i}^{K+1}}{\dot{m}_{L,i}^{K+1}} < 1\%. \quad (28)$$

$$\frac{\dot{m}_{G,i}^{K+1,new} - \dot{m}_{G,i}^{K+1}}{\dot{m}_{G,i}^{K+1}} < 1\%. \quad (29)$$

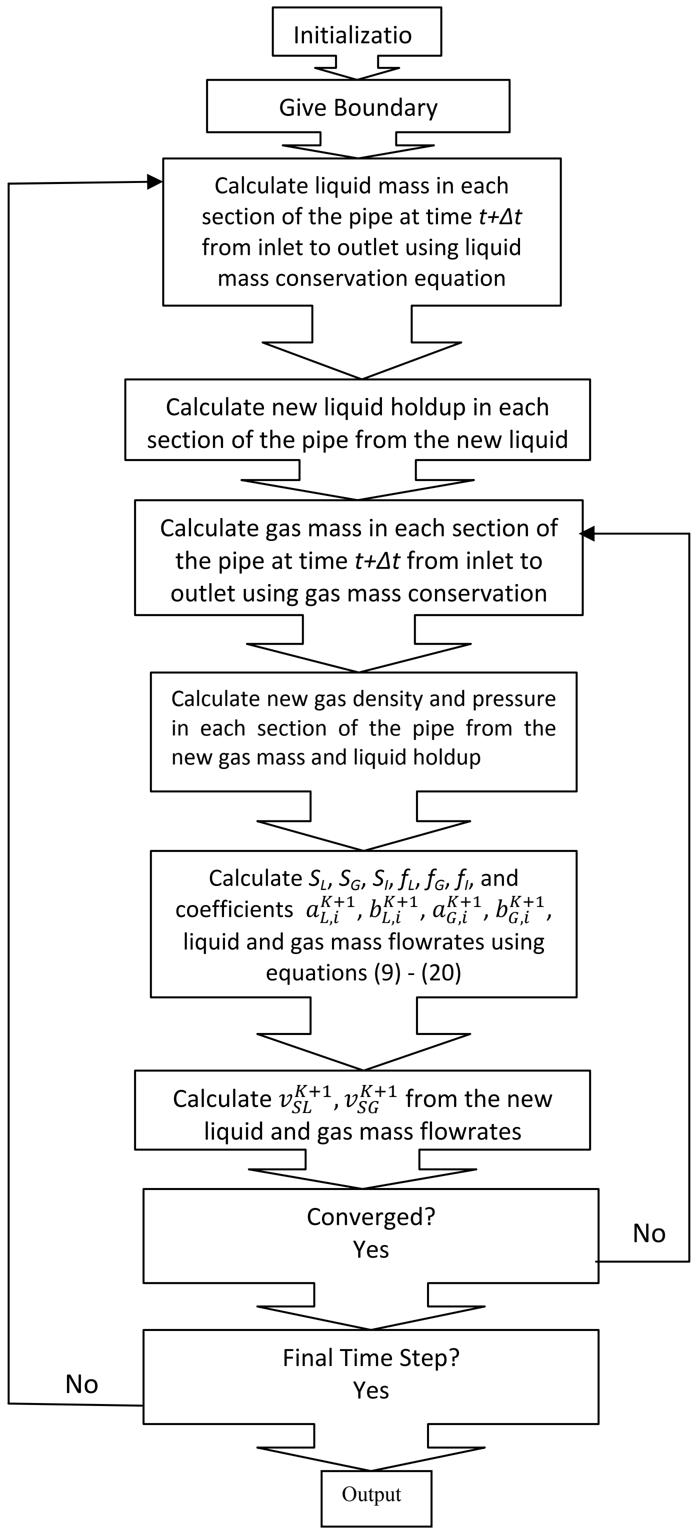

Figure 1: Flow Chart for Two Fluid Model

3. Model Validation

The experimental results from Vigneron *et al.* (1995) are used to validate the model simulation. Vigneron *et al.* used air and kerosene as working fluids. The fluid properties are given as

$$\rho_L = 1006.61 - 0.67167 \times T. \tag{30}$$

$$\mu_L = 0.881377 \times 10^{-4} \times \rho_L \times \exp\left(-0.01277766 \times T\right). \tag{31}$$

$$\rho_G = \frac{P}{287.0 \times T}. \tag{32}$$

$$\mu_G = 0.867886 \times 10^{-5} \times \exp(0.002513 \times T) + 2.9893 \times 10^{-12} \times P. \tag{33}$$

The test facility is a horizontal steel pipe 420 m in length and 77.9 mm in diameter. Two 2.4 m long test sections, made of transparent PVC pipe, were installed along the loop at distances 61.6 m and 396 m, respectively, from the mixing tee. Experiments were carried out within a wide range of operating conditions, and the flow patterns include stratified flow and slug flow. Transient flows caused by changes in liquid and gas flow rates, liquid blow out and startup were tested. A summary of these tests is given in Table 1. Comparisons of these experimental data with simulation results are presented.

Table 1: Summary of Vigneron et al. (1995)

TEST #	INITIAL(I) FINAL(F)	FLOW RATE LIQUID(m^3/d)	GAS(Sm^3/d)	FLOW PATTERN	P_{sep} (Bar)
LIQUID FLOW RATE CHANGE					
1-A	I	32.5	815	Slug	1.67
	F	168.4	815	Slug	
1-B	I	8.4	400	Stratified Smooth	1.67
	F	31.8	400	Stratified Wavy	
1-C	I	8.4	4055	Stratified Wavy	1.76
	F	32.0	4055	Stratified Wavy	
1-D	I	340	880	Slug	1.67
	F	168	880	Slug	
1-E	I	28.1	2590	Stratified Wavy	1.67
	F	294	2590	Slug	
1-F	I	295	7620	Slug	1.74
	F	172	7620	Slug	
1-G	I	32.9	2745	Stratified Wavy	1.67
	F	8.5	2745	Stratified Smooth	
GAS FLOW RATE CHANGE					
2-A	I	8.0	850	Stratified Smooth	1.67
	F	8.0	4520	Stratified Wavy	
2-B	I	20.2	340	Stratified Smooth	1.67
	F	20.2	2530	Stratified Wavy	
2-C	I	203	870	Slug	1.76
	F	203	3690	Slug	
2-D	I	195	1875	Slug	1.67
	F	195	10840	Slug	
2-E	I	323	815	Slug	1.67
	F	323	5000	Slug	
LIQUID BLOW OUT					
3-A	I	48.8	4825	Stratified Wavy	1.69
	F	0.0	4825	Single Phase Gas	
3-B	I	204.0	5880	Slug	1.69
	F	0.0	5880	Single Phase Gas	
STARTUP					
4-A0	I	H_L=0.0			1.68
	F	22.0	2650	Stratified Wavy	
4-A1	I	H_L=1.0			1.68
	F	21.8	2615	Stratified Wavy	
4-B0	I	H_L=0.0			1.66
	F	322.0	1870	Slug	
4-B1	I	H_L=1.0			1.66
	F	322.5	1910	Slug	

Liquid Flow Rate Change

Test 1C

For this test, the inlet gas flow rate was kept at 4055 Sm^3/d. The inlet liquid flow rate was at 8.4 m^3/d initially, and it was raised to 32 m^3/d at time 180 seconds. Separator pressure was 1.76 bar.

Comparison of experimental measurement and simulation results is presented in Fig. 2. Figure 2(a) shows the variation of liquid holdup with time at the two test sections from experimental measurements, and simulation results from both the current model and OLGA. The liquid holdup predictions for both initial and final states are higher than experimental measurements. From the experiments, the liquid holdup is raised from 0.03 to 0.1, while from the current model simulation, the liquid holdup is raised from 0.06 to 0.16, as a result, the propagation of liquid front is slower in the model prediction.

Figure 2(b) shows the variation of pressure with time at the first test section from experimental measurements, and simulation results from both the current model and OLGA. The predicted pressure drop is much lower than the experimental measurement, which again is related to the holdup prediction. Since the holdup is predicted to be larger than experimental measurements, with the same superficial liquid velocity, the on-site liquid velocity is predicted lower, thus gives lower friction loss, and lower pressure drop.

Test 1G

For test 1-G, the inlet gas flow rate was kept at 2745 Sm^3/d. The inlet liquid flow rate was at 32.9 m^3/d initially, and it was decreased to 8.5 m^3/d at time 120 seconds. Separator pressure was 1.67 bar.

Comparison of experimental measurement and simulation results is presented in Fig. 3. Figure 3(a) shows the variation of liquid holdup with time at the two test sections from experimental measurements, and simulation results from both the current model and OLGA. Figure 3(b) shows the variation of pressure with time at the first test section from experimental measurements, and simulation results from both the current model and OLGA.

Liquid Blow Out

Test 3A

The initial condition is a steady state flow with average inlet flow rates of 4825 Sm^3/d for gas and 48.8 m^3/d for liquid. At 120 seconds, the liquid supply is stopped, while gas supply is unchanged. Separator pressure was 1.69 bar.

Comparison of experimental measurement and simulation results is presented in Fig. 4. Figure 4(a) shows the variation of liquid holdup with time at the two test sections from experimental measurements, and simulation results from both the current model and OLGA. Figure 4(b) shows the variation of pressure with time at the first test section from experimental measurements, and simulation results from both the current model and OLGA.

The current model gives a good prediction for both liquid holdup and pressure.

4. Discussion

Two-fluid model is developed for stratified flow. For cases with liquid flow rate change, the model can predict the trend very well. Further improvement on the gas-liquid interfacial friction factor could be able to improve the quantitative agreements.

For tests with gas flow rate change, the current model has not given a converged result yet.

Attempt 2: Drift Flux Model

Develop a simplified transient simulator with drift flux model, ignoring flow pattern and flow pattern transition.

1. Method

Use unsteady mass conservation equations for both gas and liquid. Gas liquid mixture momentum equation is used and considered to be in local equilibrium. Drift flux model is used. Gas is compressible, while liquid is considered to be incompressible.

Gas liquid mixture momentum conservation equation is written as

$$(P_i - P_{i+1})A = \frac{1}{2} f_M \rho_M v_M^2 \pi D \Delta x + \rho_M g A \Delta x sin\theta. \qquad (34)$$

where, v_M is the mixture velocity ($v_M = v_{SL} + v_{SG}$). ρ_M is the mixture density ($\rho_M = H_L\rho_M + (1-H_L)\rho_G$). H_L is the liquid holdup.

Drift flux model is used to obtain the gas velocity,

$$v_G = Cv_M + v_d. \qquad (35)$$

As a starting point, we choose C=1.0, and $v_d = 0.54\sqrt{gd}cos\theta + 0.35\sqrt{gd}sin\theta$ from Bendiksen (1984).

Substituting Eq. (35) into Eq. (34) yields a relationship between gas mass flow rate and pressure difference $P_i - P_{i+1}$. A linear relationship between gas mass flow rate and pressure difference can be obtained as

$$\dot{m}_{G,i}^{K+1} = a_i^{K+1}(P_i^{K+1} - P_{i+1}^{K+1}) + b_i^{K+1}. \qquad (36)$$

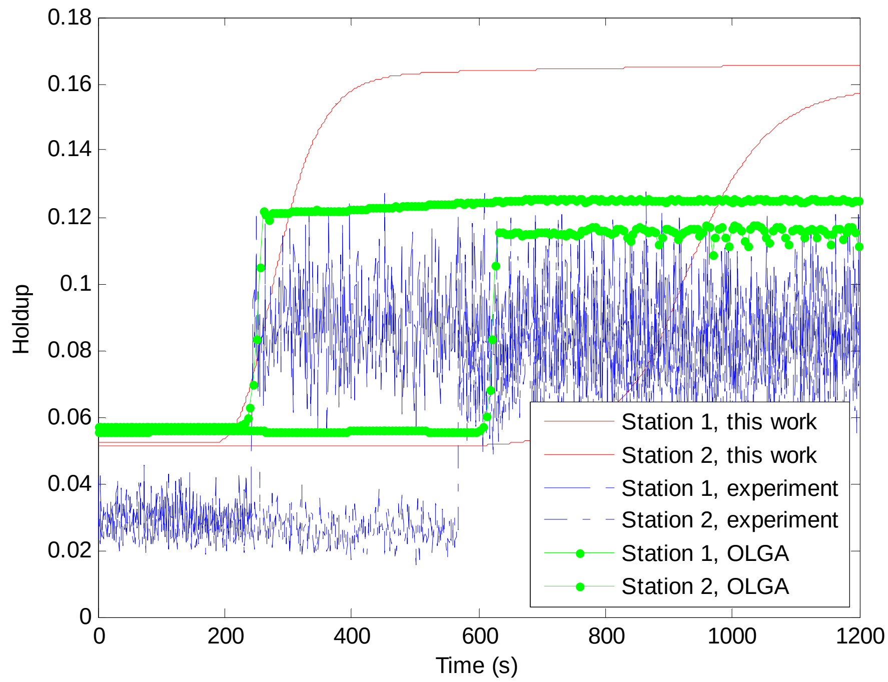

(a) Variation of Liquid Holdup with time at the two test sections.

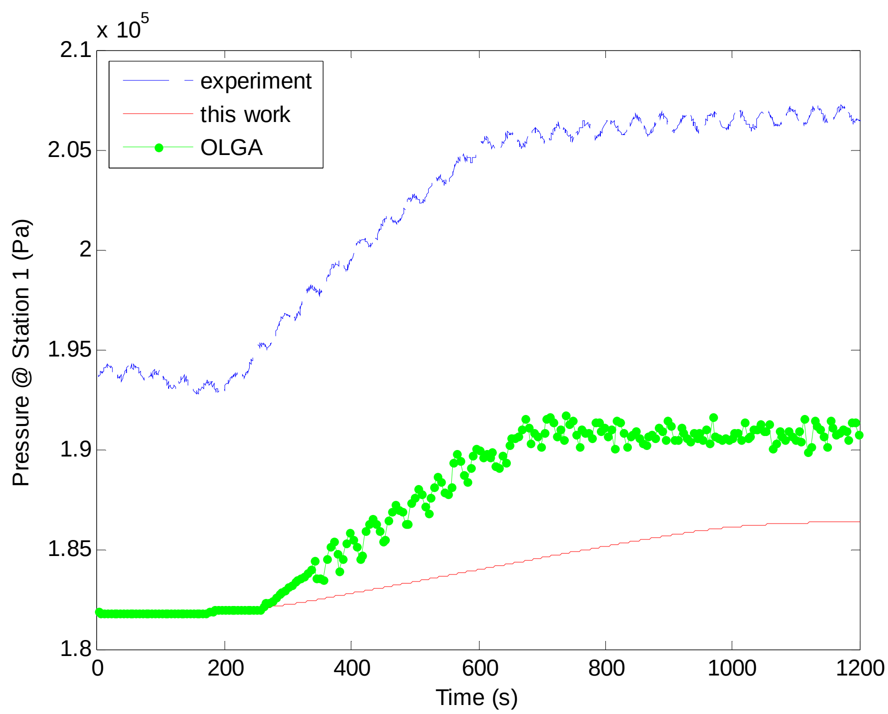

(b) Variation of pressure with time at the first test section.

Figure 2: Results for Test 1-C with two-fluid model

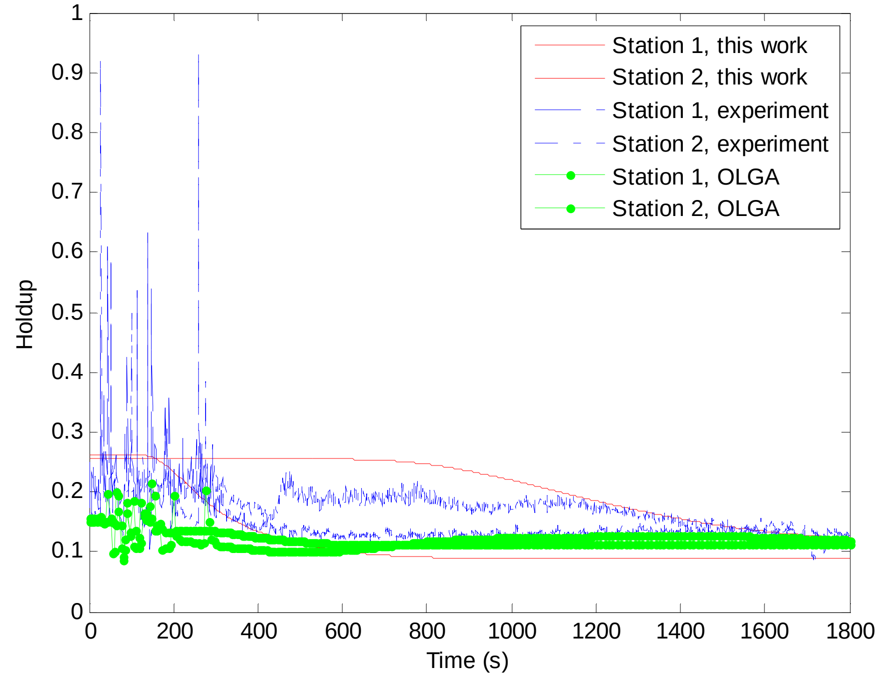

(a) Variation of liquid holdup with time at the two test sections

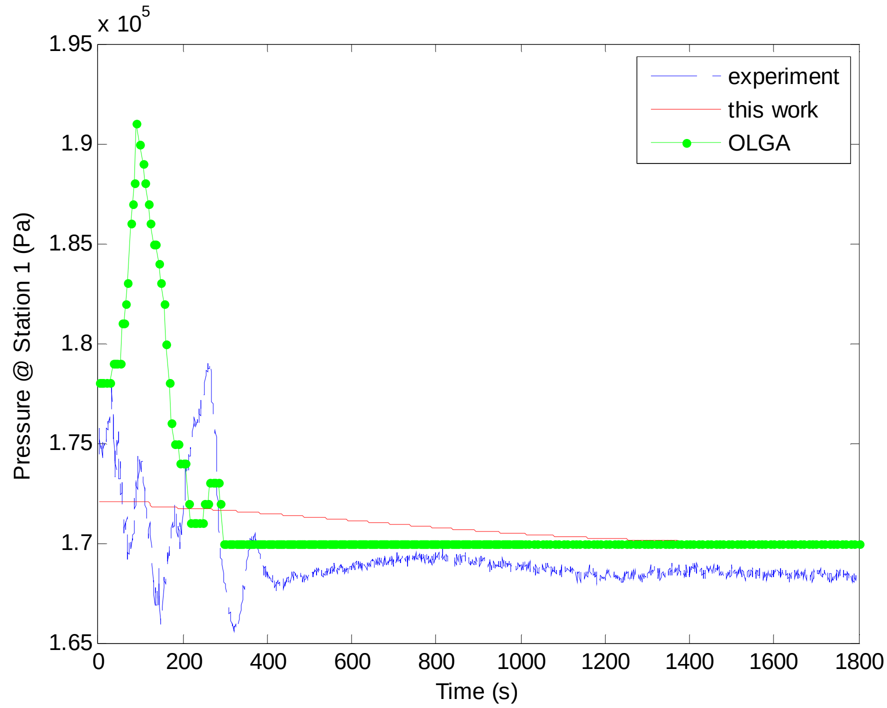

(b) Variation of Pressure with time at the first test section

Figure 3: Results for Test 1-G with two-fluid model

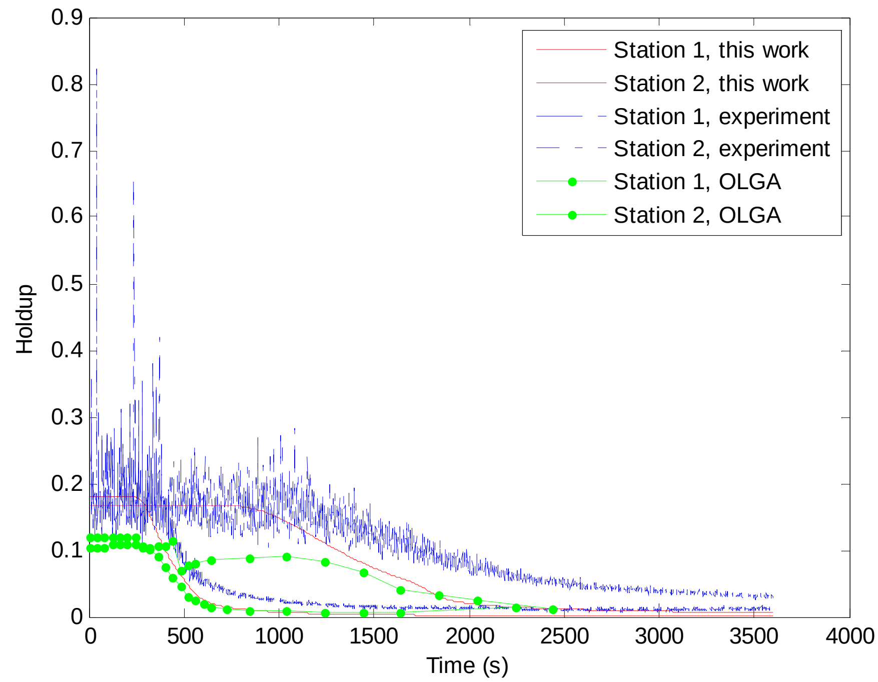

(a) Variation of liquid holdup with time at the two test sections

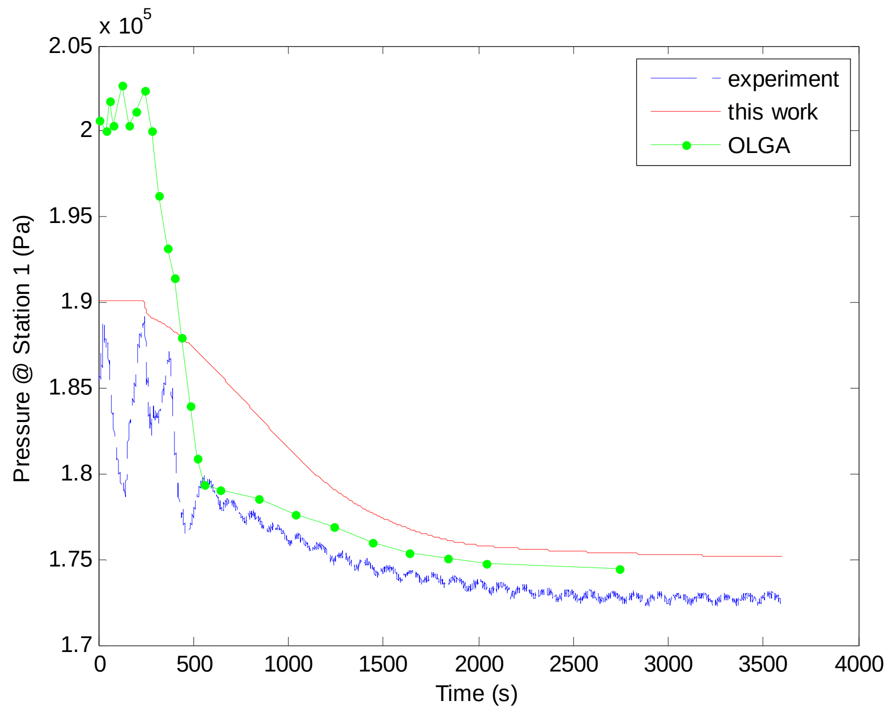

(b) Variation of pressure with time at the first test section

Figure 4: Results for Test 3-A with two-fluid model

Where

$$a_i^{K+1} = \frac{2A^2C^2\rho_g(1-H_L)}{f_M\rho_M\pi D\Delta x(V_G-V_d)}, \quad (37)$$

$$b_i^{K+1} = \frac{-2A^2C^2\rho_g(1-H_L)g\Delta x sin\theta}{f_M\pi D\Delta x(V_G-V_d)}$$
$$+\rho_g A(1-H_L)v_d. \quad (38)$$

2. Solution Procedures

Figure 5 shows a flowchart for the drift flux model approach. Detailed descriptions of each step are given below.

1) Initialization: Define pipe geometry, fluid properties and initial conditions. The pipe is divided into N sections of length Δx. Initial condition at time t=0 includes: gas and liquid velocities, liquid holdup, and pressure for each section of the pipe.

2) Specify boundary conditions: Inlet gas and liquid flow rates and outlet pressure at each time step are given.

3) Liquid mass in each section of the pipe at the new time step K+1 is calculated by

$$m_{L,i}^{K+1} = m_{L,i}^{K} + \Delta t(\dot{m}_{L,i-1}^{K+1} - \dot{m}_{L,i}^{K+1}). \quad (39)$$

4) The new liquid holdup is calculated as

$$H_{L,i}^{K+1} = \frac{m_{L,i}^{K+1}}{\rho_L A_i \Delta x}. \quad (40)$$

5) Gas mass in each section of the pipe at the new time step K+1 is calculated by

$$m_{G,i}^{K+1} = m_{G,i}^{K} + \Delta t(\dot{m}_{G,i-1}^{K+1} - \dot{m}_{G,i}^{K+1}). \quad (41)$$

6) The new gas density is calculated as

$$\rho_{G,i}^{K+1} = \frac{m_{G,i}^{K+1}}{(1-H_{L,i}^{K+1})A_i\Delta x}. \quad (42)$$

7) The new pressure is calculated using the ideal gas equation of state,

$$P_i^{K+1} = \rho_{G,i}^{K+1}RT. \quad (43)$$

8) Calculate the mixture properties ρ_M and μ_M, mixture Reynolds number Re_M, mixture friction factor f_M, and the coefficients a_i^{K+1}, b_i^{K+1}.

9) Given pressure drop, and the coefficients a_i^{K+1}, b_i^{K+1}, the new gas mass flowrate at each section of the pipe is calculated using Eq. (36).

10) The new superficial gas velocity is calculated as

$$v_{SG,i}^{K+1} = \frac{\dot{m}_{G,i}^{K+1}}{\rho_{G,i}^{K+1}A_i}. \quad (44)$$

11) The new superficial liquid velocity is calculated from Eq. (35),

$$v_{SL,i}^{K+1} = \frac{v_{SG,i}^{K+1}}{C(1-H_{L,i}^{K+1})} - \frac{v_d}{C} - v_{SG,i}^{K+1}. \quad (45)$$

12) The new liquid mass flow rate is calculated as

$$\dot{m}_{L,i}^{K+1} = v_{SL,i}^{K+1}\rho_L A_i. \quad (46)$$

13) Compare the newly calculated liquid and gas mass flow rates with $\dot{m}_{L,i}^{K+1}$and $\dot{m}_{G,i}^{K+1}$ calculated from the last iteration, and check the convergence. If converged, change the 'new' variables into 'old' and go to step 3) for the calculation of next time step. If not, go to step 5) for another iteration within the current time step. Convergence criteria are set as

$$\frac{\dot{m}_{L,i}^{K+1,new} - \dot{m}_{L,i}^{K+1}}{\dot{m}_{L,i}^{K+1}} < 1\%, \quad (47)$$

$$\frac{\dot{m}_{G,i}^{K+1,new} - \dot{m}_{G,i}^{K+1}}{\dot{m}_{G,i}^{K+1}} < 1\%. \quad (48)$$

3. Model Validation

The experimental results from Vigneron *et al.* (1995) are used to validate the model simulation. Comparison of experimental data with simulation results is presented in this section.

Liquid Flow Rate Change

Test 1A

The inlet gas flow rate was kept at 815 Sm^3/d. Inlet liquid flow rate increased from 32.5 m^3/d to 168.4 m^3/d at 120 seconds. Separator pressure was kept at 1.67 bar. Both initial and final states are in slug flow regime. Comparison of experimental measurement and simulation results is presented in Fig. 6. Figure 6(a) shows the variation of liquid holdup with time at the two test sections from experimental measurements, and simulation results from both the current model and OLGA. The liquid holdup predictions for both initial and final states are lower than experimental measurements. From the experiments, the liquid holdup is raised from 0.4 to 0.6, while from the current model simulation, the liquid holdup is raised from 0.34 to 0.46.

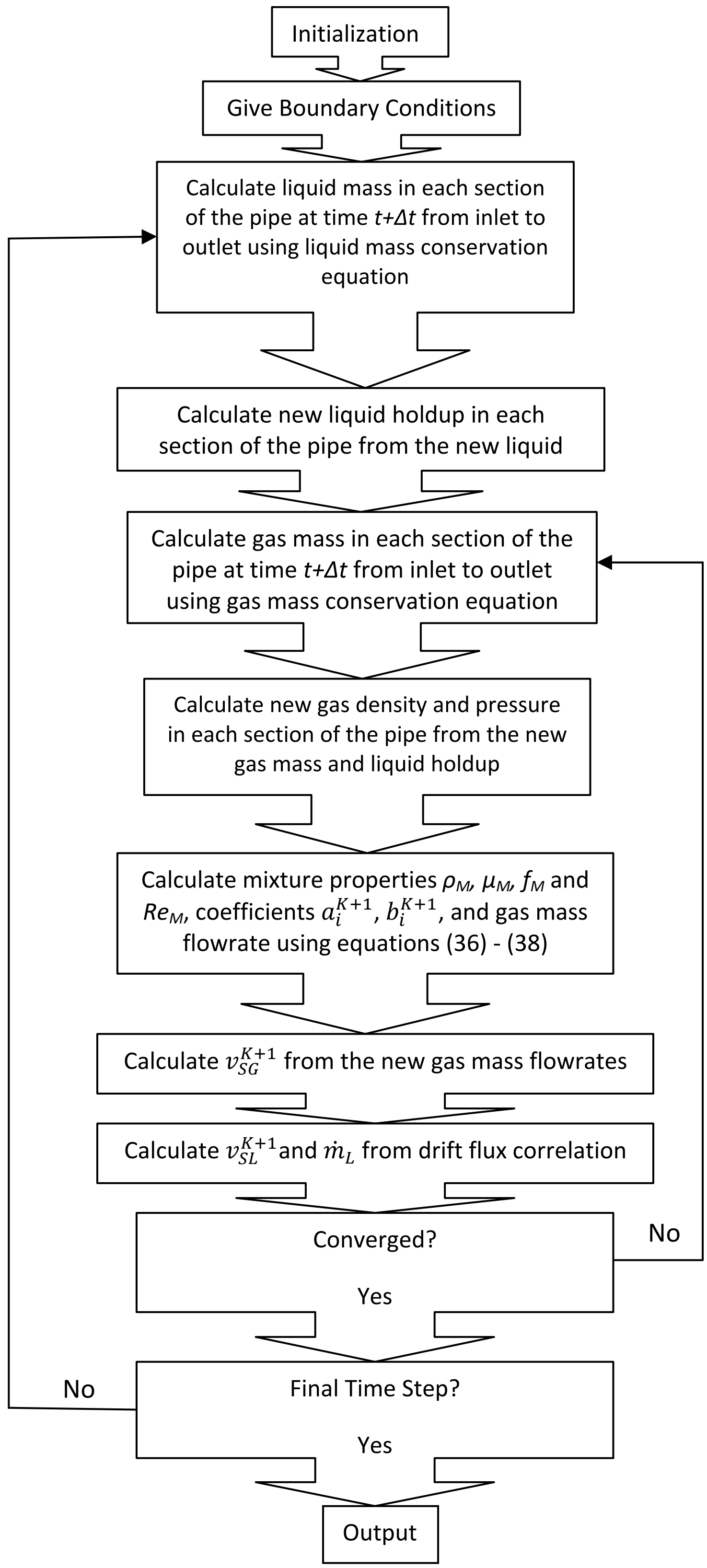

Figure 5: Flow Chart for Drift Flux Model

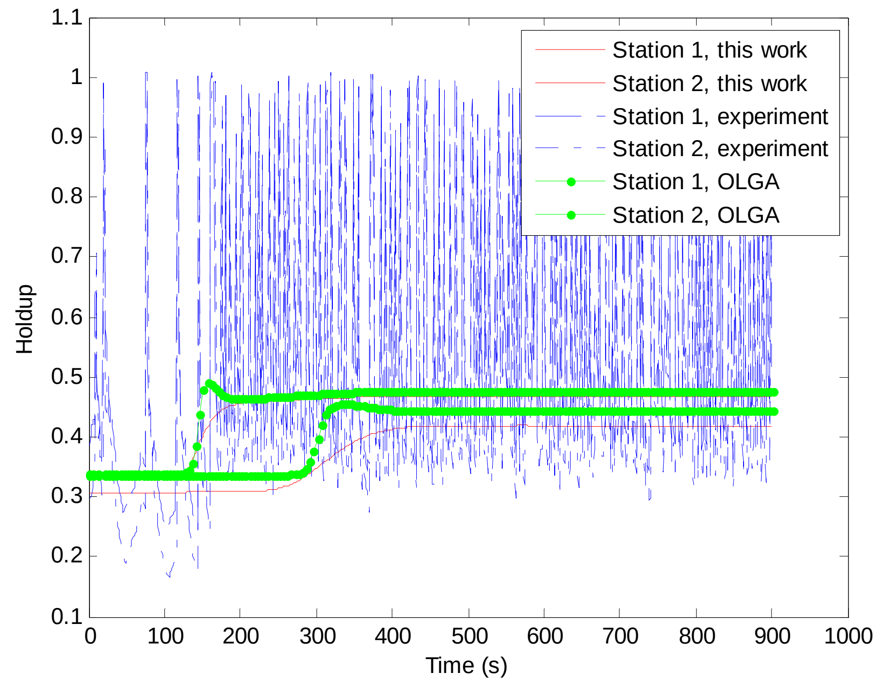

(a) Variation of liquid holdup with time at the two test sections

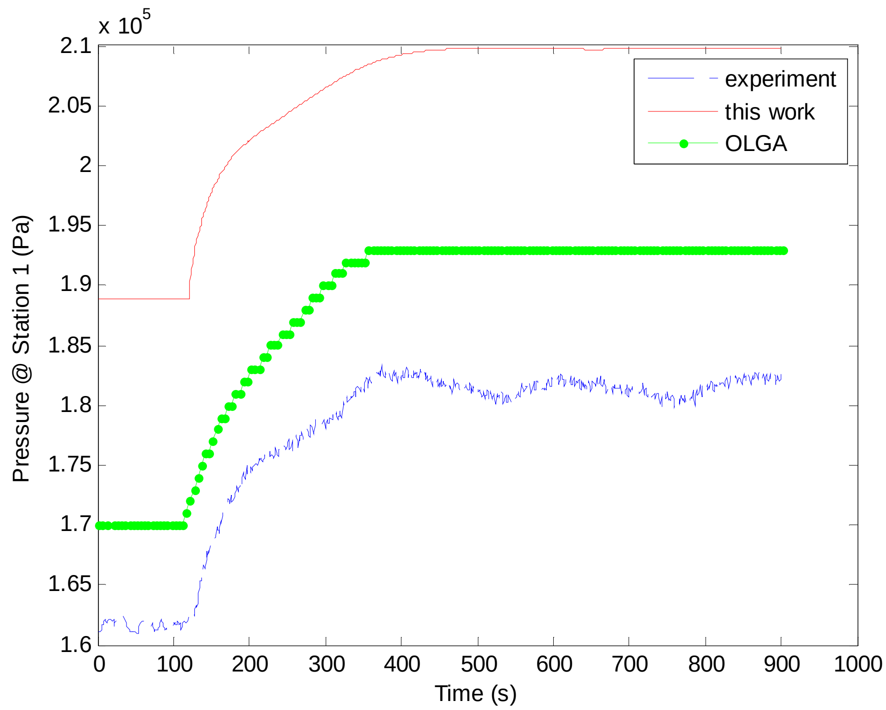

(b) Variation of pressure with time at the first test section

Figure 6: Results for Test 1-A with drift flux model

Figure 6(b) shows the variation of pressure with time at the first test section from experimental measurements, and simulation results from both the current model and OLGA. The current model prediction of pressure drop is much higher than the experimental measurement.

Test 1B

Inlet gas flow rate was kept at 400 Sm^3/d. Inlet liquid flow rate increased from 8.4 m^3/d to 31.8 m^3/d at 190 seconds. Separator pressure was kept at 1.67 bar. Both initial and final states are in slug flow regime. Comparison of experimental measurement and simulation results is presented in Fig. 7. Figure 7(a) shows the variation of liquid holdup with time at the two test sections from experimental measurements, and simulation results from both the current model and OLGA. Figure 7(b) shows the variation of pressure with time at the first test section from experimental measurements, and simulation results from both the current model and OLGA. The liquid holdup predictions for both initial and final states are higher than experimental measurements. Besides, this model is not able to predict the propagation of liquid wave front correctly. The prediction of pressure drop is much higher than the experimental measurement.

Test 1C

For case 1-C, the inlet gas flow rate was kept at 4055 Sm^3/d. The inlet liquid flow rate was at 8.4 m^3/d initially, and it was increased to 32 m^3/d at time 180 seconds. Separator pressure was at 1.76 bar. Both initial and final steady state flow conditions are in the stratified flow regime. After the increase in inlet liquid flow rate, pressure builds up gradually as the liquid front advances through the pipeline. The liquid holdup vs. time plot (Fig. 8(a)) clearly shows the propagation of liquid front. Comparison of experimental measurement and simulation results is presented in Fig. 8. Figure 8(a) shows the variation of liquid holdup with time at the two test sections from experimental measurements, and simulation results from both the current model and OLGA. The liquid holdup predictions for both initial and final states are higher than experimental measurements. The current model is not able to predict the propagation of liquid wave front correctly.

Figure 8(b) shows the variation of pressure with time at the first test section from experimental measurements, and simulation results from both the current model and OLGA. The prediction of pressure drop is much higher than the experimental measurements.

Test 1D

The inlet gas flow rate was kept at 880 Sm^3/d. Inlet liquid flow rate decreased from 340 m^3/d to 168 m^3/d at 120 seconds. Separator pressure was kept at 1.67 bar. Both initial and final states are in slug flow regime.

Comparison of experimental measurement and simulation results is presented in Fig. 9. Figure 9(a) shows the variation of liquid holdup with time at the two test sections from experimental measurements, and simulation results from both the current model and OLGA. The liquid holdup predictions for both initial and final states are slightly lower than experimental measurements. In the experiment, the liquid holdup at station 1 decreased from 0.6 to 0.45, while in the current model simulation, the liquid holdup at station 1 decreases from 0.57 to 0.45. The current model gives good prediction for the liquid wave front movement.

Figure 9(b) shows the variation of pressure with time at the first test section from experimental measurements, and simulation results from both the current model and OLGA. The prediction of pressure drop is higher than the experimental measurements.

Test 1E

The initial condition is a steady state flow with average inlet flow rates of 2590 Sm^3/d for gas phase and 28.1 m^3/d for liquid phase. Inlet liquid flow rate was increased to 294 m^3/d at 125 seconds. Separator pressure was kept at 1.67 bar during the entire process. Flow pattern was stratified wavy initially and then changed to slug flow.

Comparison of experimental measurement and simulation results is presented in Fig. 10. For holdup prediction, the current model agrees very well with OLGA predictions, however, both initial and final holdups are considerably lower than the measured holdups. The predicted initial and final pressures are higher than the measured values.

Test 1F

The inlet gas flow rate was kept at 7620 Sm^3/d. Inlet liquid flow rate decreased from 295 m^3/d to 172 m^3/d at 120 seconds. Separator pressure was kept at 1.74 bar. Both initial and final states were in slug flow regime.

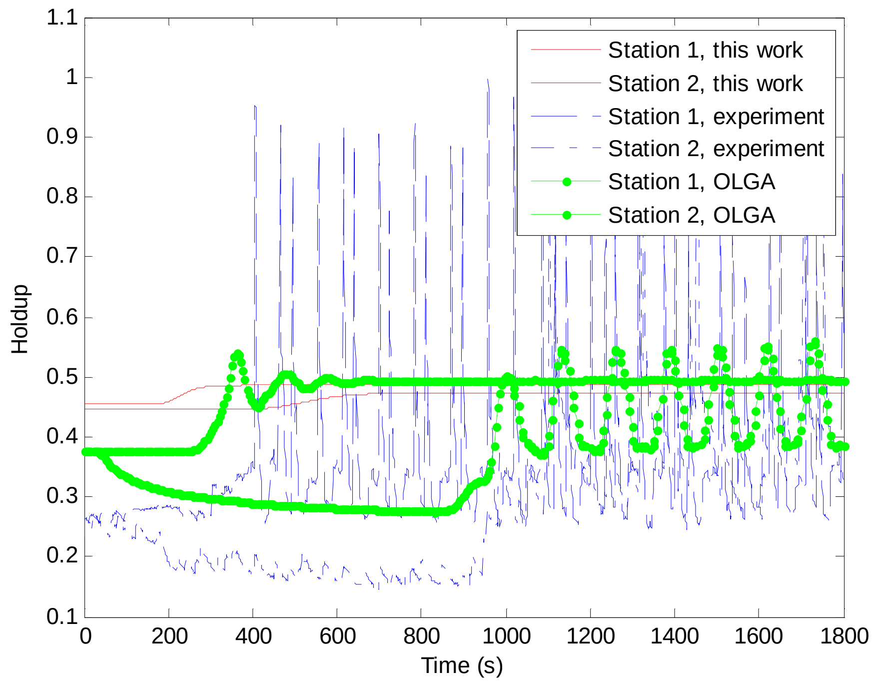

(a) Variation of liquid holdup with time at the two test sections

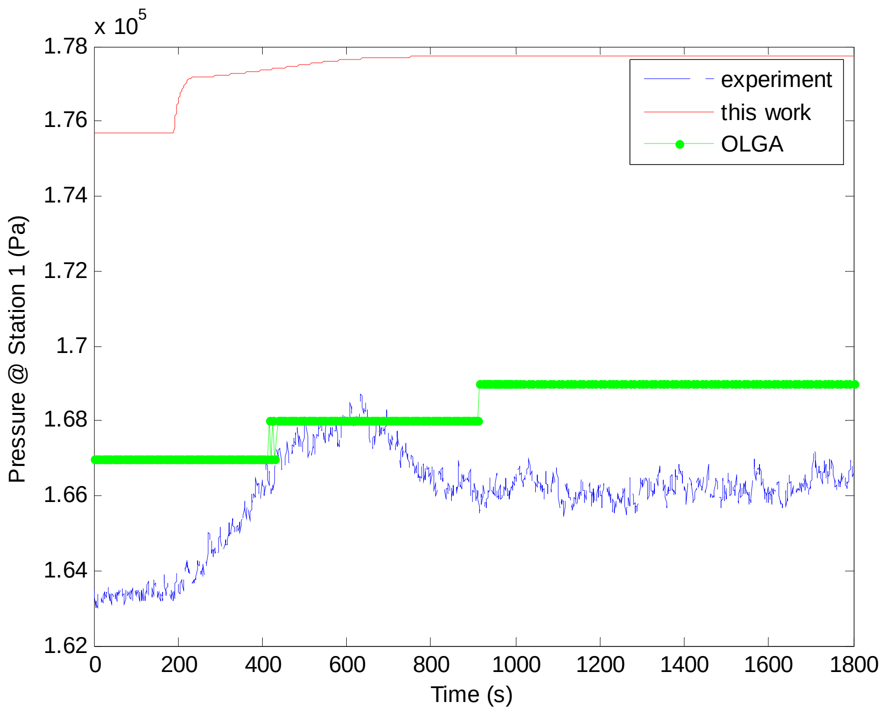

(b) Variation of pressure with time at the first test section

Figure 7: Results for Test 1-B with drift flux model

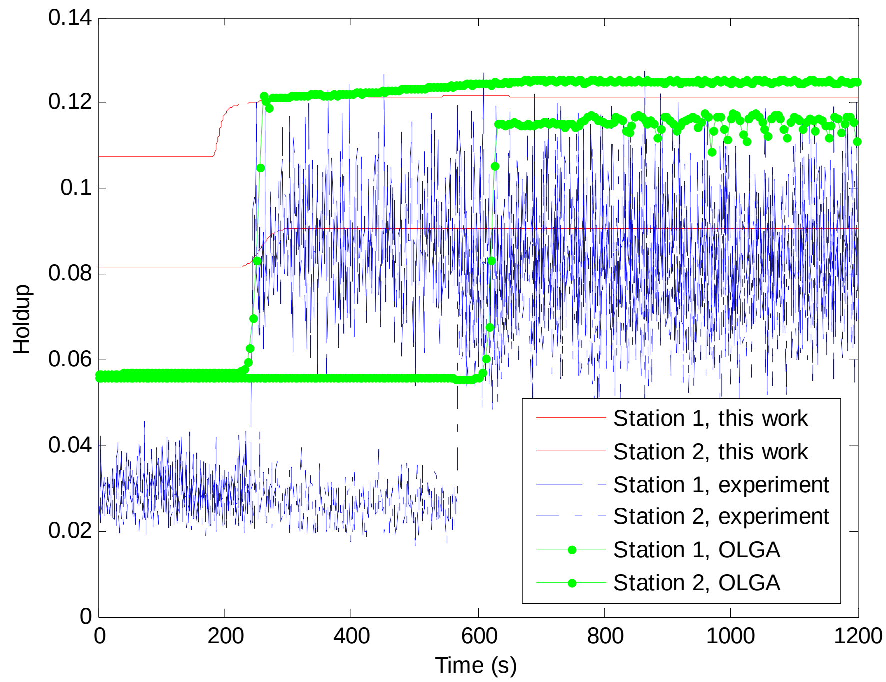

(a) Variation of liquid holdup with time at the two test sections

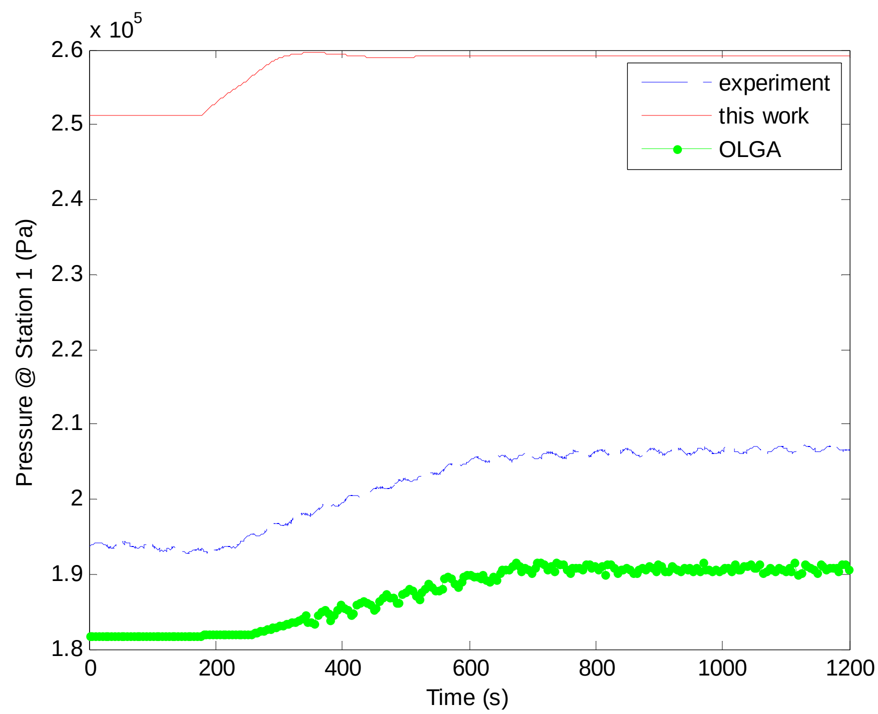

(b) Variation of pressu;re with time at the first test section

Figure 8: Results for Test 1-C with drift flux model

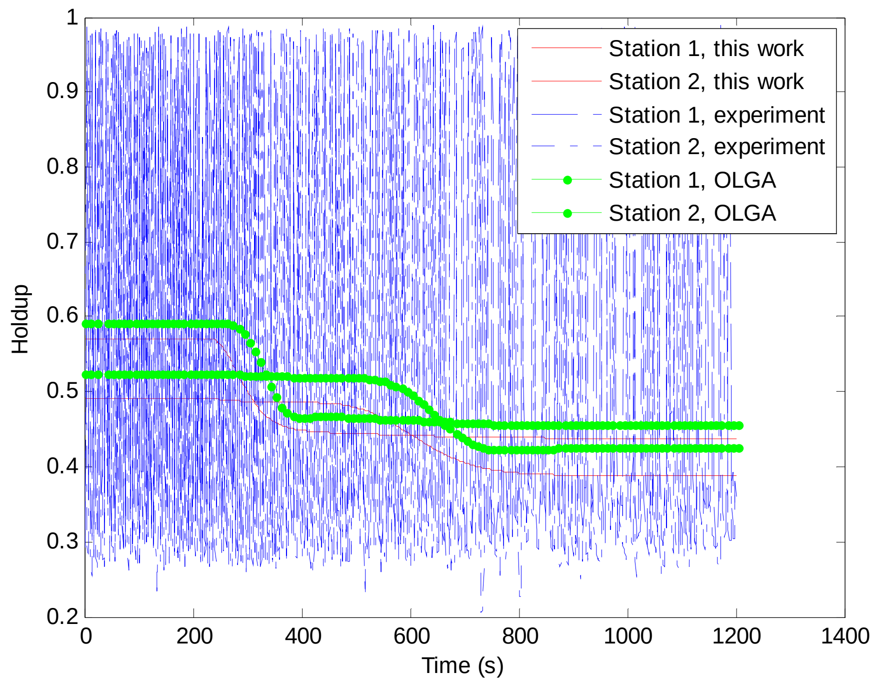

(a) Variation of liquid holdup with time at the two test sections

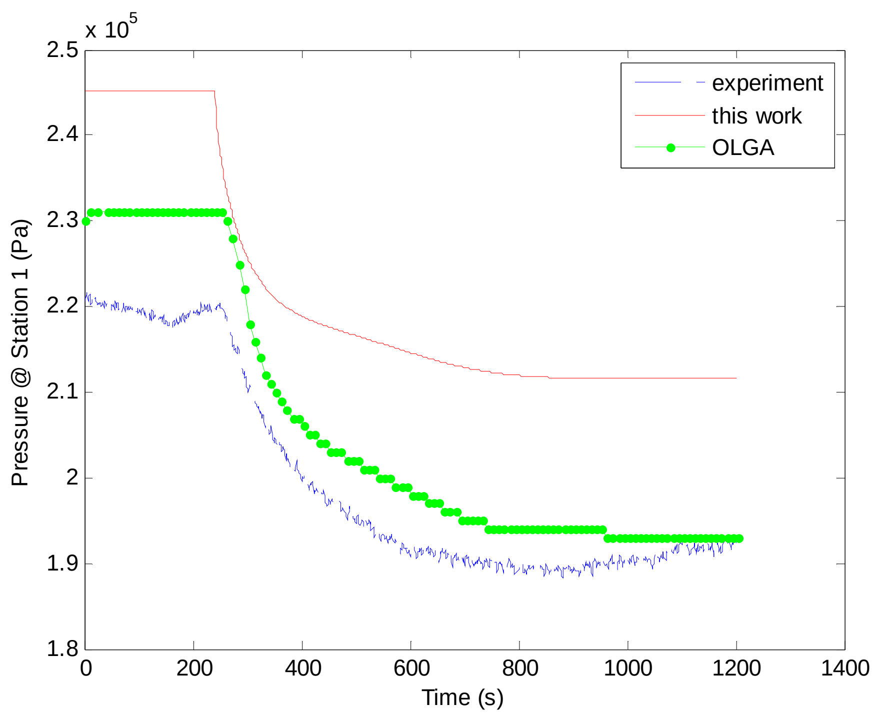

(b) Variation of pressure with time at the first test section

Figure 9: Results for Test 1-D with drift flux model

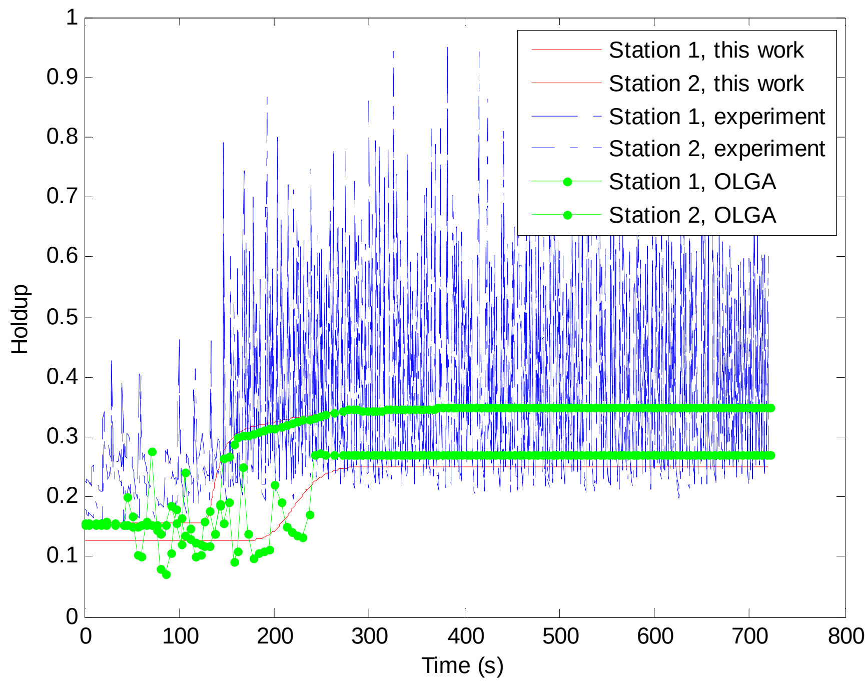

(a) Variation of liquid holdup with time at the two test sections

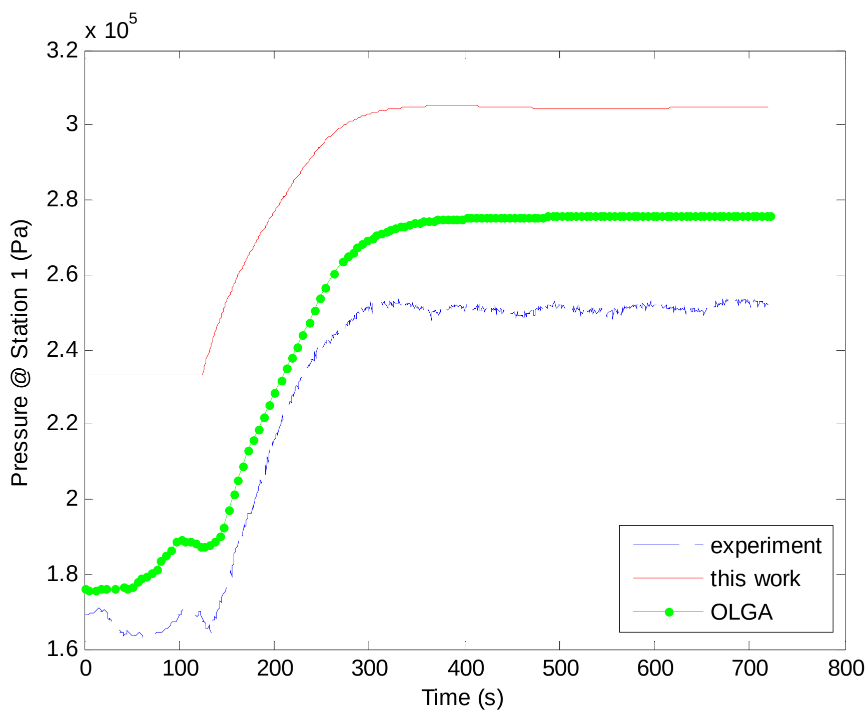

(b) Variation of pressure with time at the first test section

Figure 10: Results for Test 1-E with drift flux model

Comparison of experimental measurement and simulation results is presented in Fig. 11. Figure 11(a) shows the variation of liquid holdup with time at the two test sections from experimental measurements, and simulation results from both the current model and OLGA. The liquid holdup predictions for both initial and final states are lower than experimental measurements. In the experiments, the liquid holdup at station 1 decreased from 0.3 to 0.25, while in the current model simulation, the liquid holdup at station 1 decreased from 0.2 to 0.15.

Figure 11(b) shows the variation of pressure with time at the first test section from experimental measurements, and simulation results from both the current model and OLGA. The prediction of pressure drop is much higher than the experimental measurement.

Test 1G

For case 1-G, the inlet gas flow rate was kept at 2745 Sm^3/d. The inlet liquid flow rate was at 32.9 m^3/d initially, and it was decreased to 8.5 m^3/d at time 120 seconds. Separator pressure was 1.67 bar.

Comparison of experimental measurement and simulation results is presented in Fig. 12. Figure 12(a) shows the variation of liquid holdup with time at the two test sections from experimental measurements, and simulation results from both the current model and OLGA. Figure 12(b) shows the variation of pressure with time at the first test section from experimental measurements, and simulation results from both the current model and OLGA.

Similar as test 1B and test 1C, here the drift flux model is not able to predict the holdup and pressure correctly.

Gas Flow Rate Change

Test 2A

The inlet liquid flow rate was kept at 8.0 m^3/d. Inlet gas flow rate increased from 850 Sm^3/d to 4520 Sm^3/d at 120 seconds. Separator pressure was kept at 1.67 bar. Both initial and final states were in stratified flow regime.

Comparison of experimental measurement and simulation results is presented in Fig. 13. Figure 13(a) shows the variation of liquid holdup with time at the two test sections from experimental measurements, and simulation results from both the current model and OLGA. The liquid holdup predictions for both initial and final states showed good agreements.

The experimental data reveals two different transient phenomena. Immediately after the gas flow rate increase, a compressibility wave moves along the pipe and creates waves throughout the pipe. Some of these waves may form slugs. After the intense slugging, additional time is required to reach the final steady state. The current model is able to predict the first transient phenomenon. However, it failed to predict the second transient phenomenon.

Figure 13(b) shows the variation of pressure with time at the first test section from experimental measurements, and simulation results from both the current model and OLGA. The prediction of pressure drop is higher than the experimental measurement.

Test 2B

The inlet liquid flow rate was kept at 20.2 m^3/d. Inlet gas flow rate increased from 340 Sm^3/d to 2530 Sm^3/d at 130 seconds. Separator pressure was kept at 1.67 bar. Both initial and final states were in stratified flow regime.

Comparison of experimental measurement and simulation results is presented in Fig. 14. Figure 14(a) shows the variation of liquid holdup with time at the two test sections from experimental measurements, and simulation results from both the current model and OLGA. The liquid holdup predictions for both initial and final states showed good agreements.

Similar as in Test 2A, there are two transient phenomena, but the current model is able to predict only the first one.

Figure 14(b) shows the variation of pressure with time at the first test section from experimental measurements, and simulation results from both the current model and OLGA. The prediction of pressure drop is slightly higher than the experimental measurement.

Test 2C

The inlet liquid flow rate was kept at 203 m^3/d. Inlet gas flow rate increased from 870 Sm^3/d to 3690 Sm^3/d at 120 seconds. Separator pressure was kept at 1.76 bar. Both initial and final states were in slug flow regime.

Comparison of experimental measurement and simulation results is presented in Fig. 15. Figure 15(a) shows the variation of liquid holdup with time at the two test sections from experimental measurements, and simulation results from both the current model and OLGA. The current model agrees very well with OLGA predictions.

Figure 15(b) shows the variation of pressure with time at the first test section from experimental measurements, and simulation results from both the current model and OLGA. The prediction of pressure drop is slightly higher than the experimental measurement.

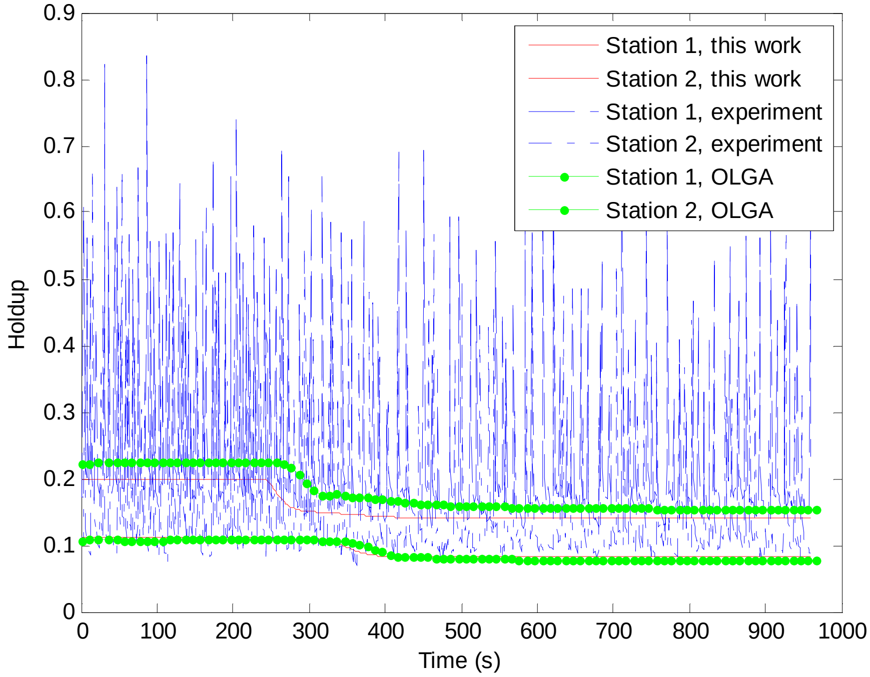

(a) Variation of liquid holdup with time at the two test sections

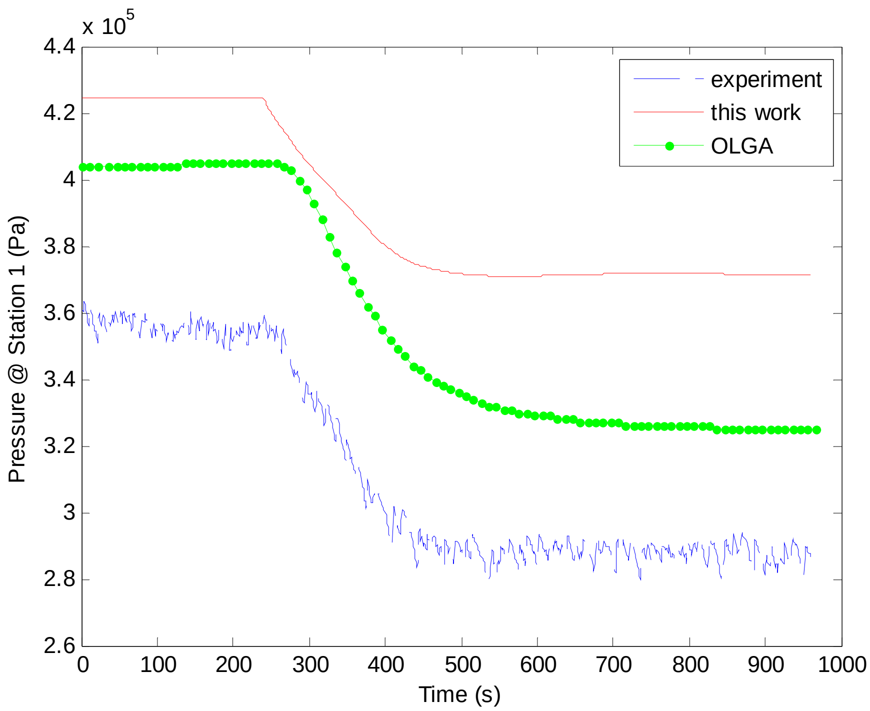

(b) Variation of pressure with time at the first test section

Figure 11: Results for Test 1-F with drift flux model

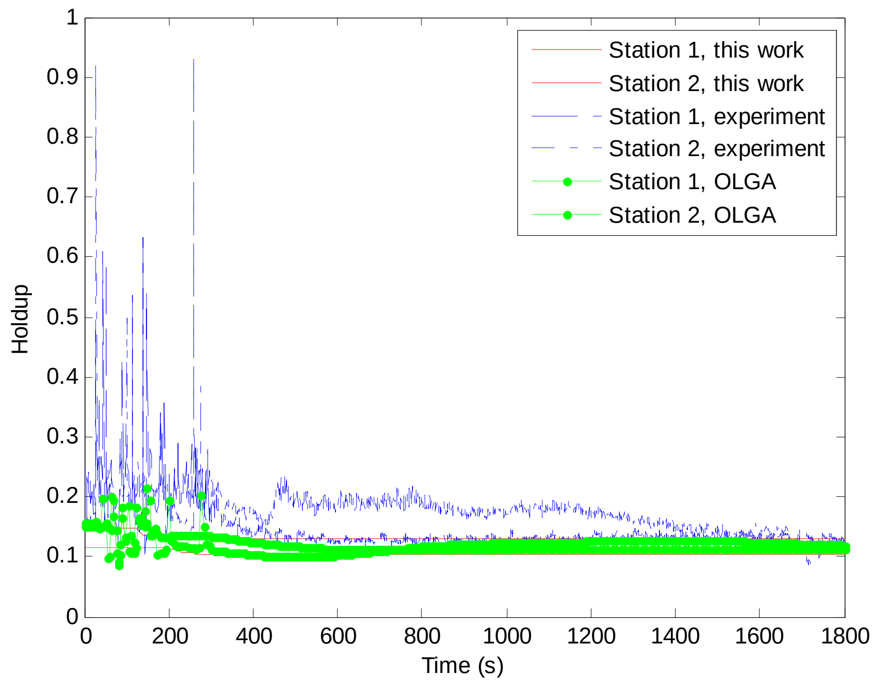

(a) Variation of liquid holdup with time at the two test sections

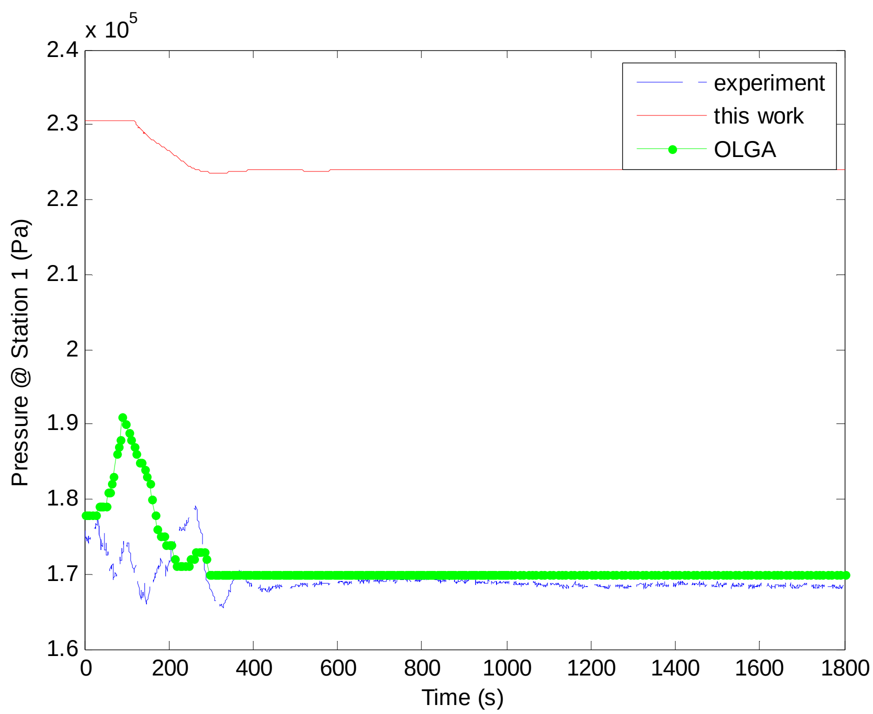

(b) Variation of pressure with time at the first test section

Figure 12: Results for Test 1-G with drift flux model

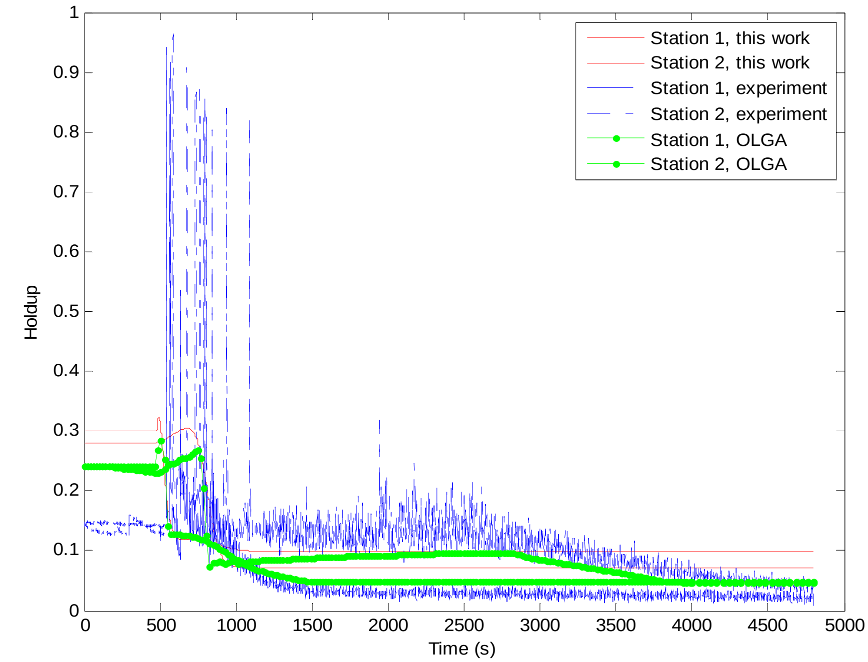

(a) Variation of liquid holdup with time at the two test sections

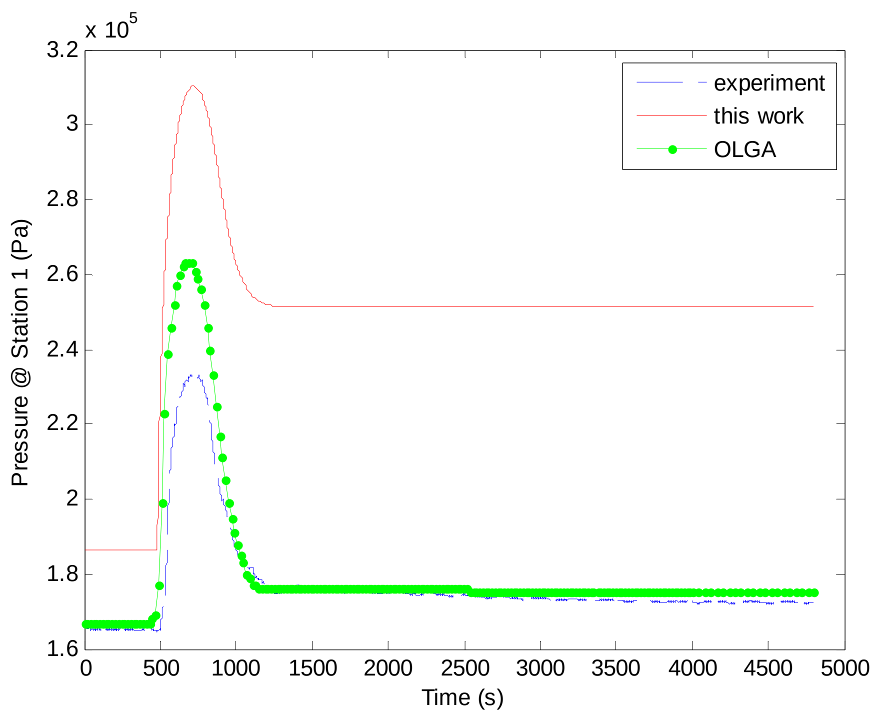

(b) Variation of pressure with time at the first test section

Figure 13: Results for Test 2-A with drift flux model

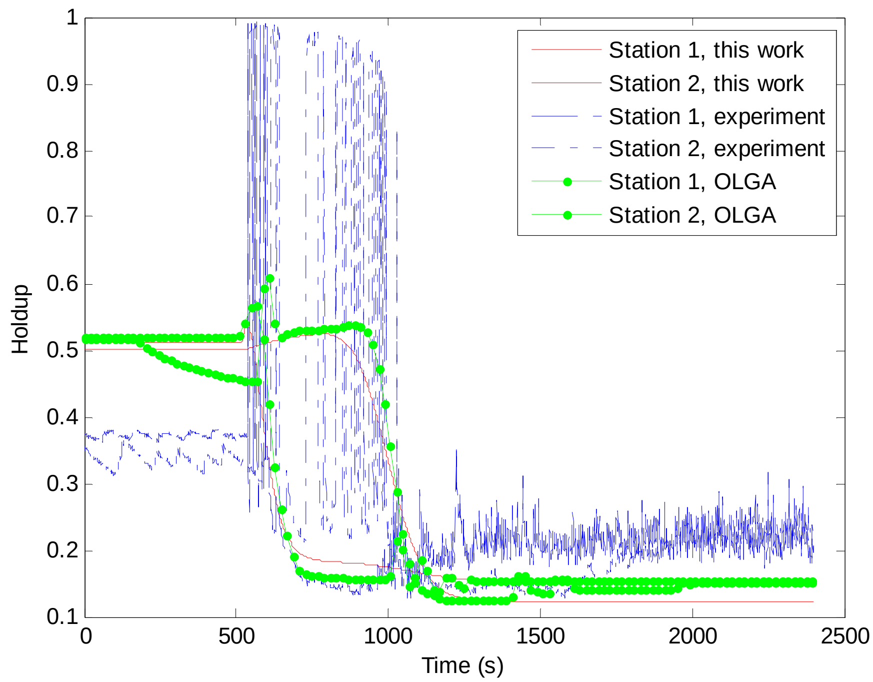

(a) Variation of liquid holdup with time at the two test sections

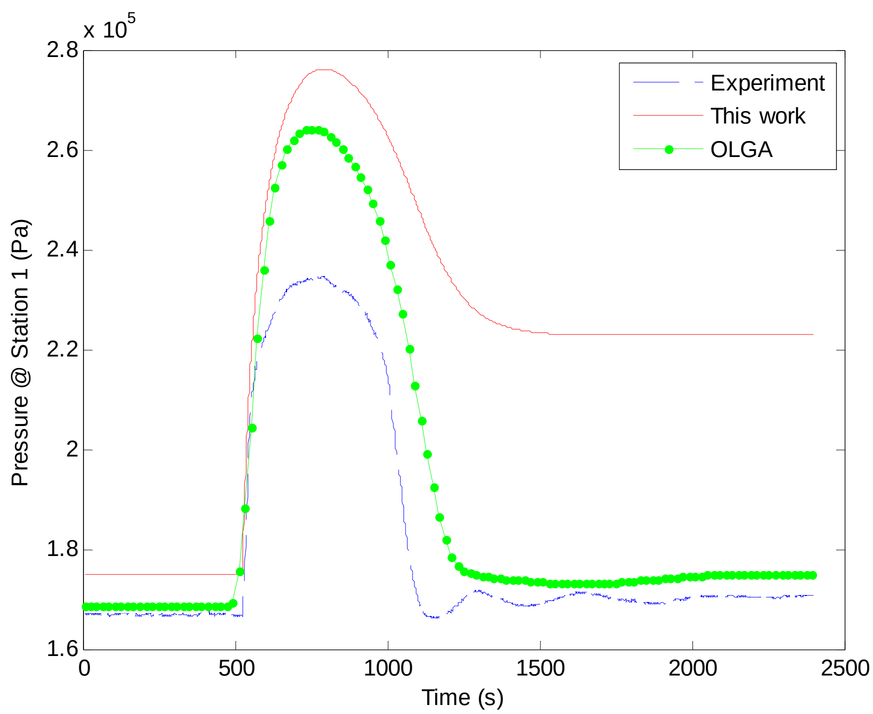

(b) Variation of pressure with time at the first test section

Figure 14: Results for Test 2-B with drift flux model

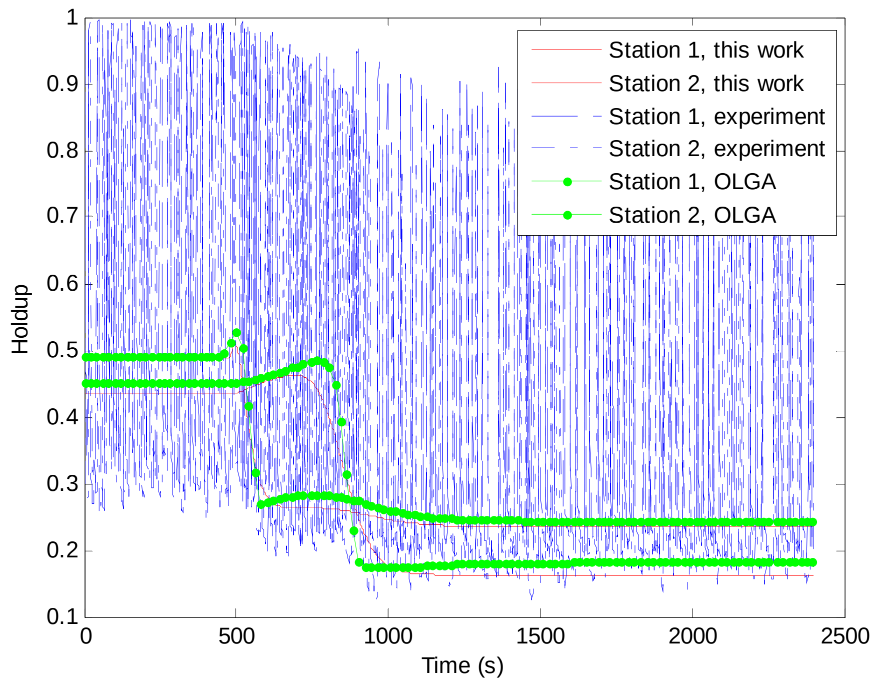

(a) Variation of liquid holdup with time at the two test sections

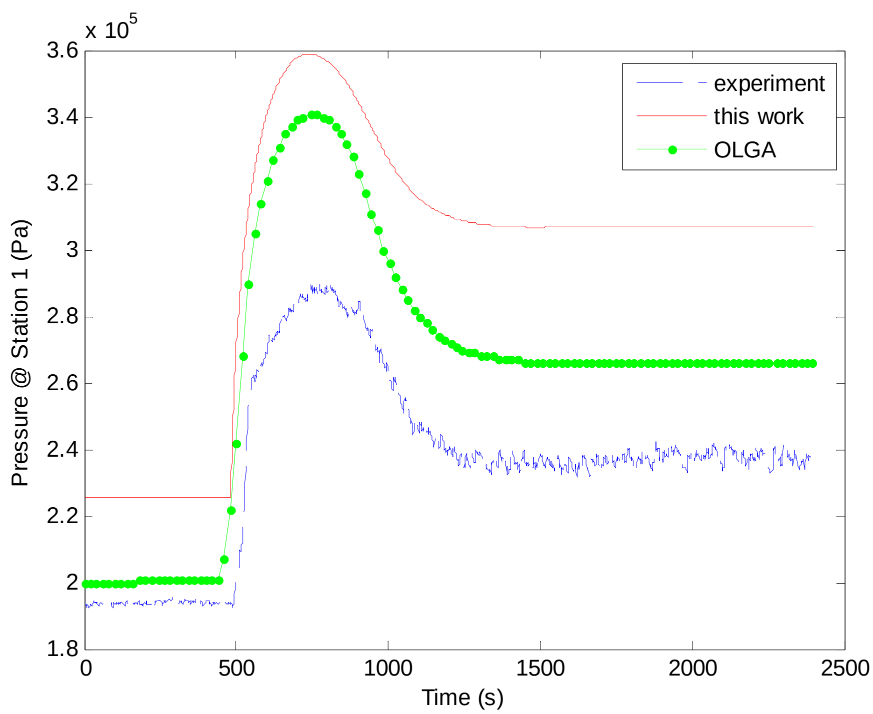

(b) Variation of pressure with time at the first test section

Figure 15: Results for Test 2-C with drift flux model

Test 2D

The inlet liquid flow rate was kept at 195 m^3/d. Inlet gas flow rate increased from 1875 Sm^3/d to 10840 Sm^3/d at 125 seconds. Separator pressure was kept at 1.67 bar. Both initial and final states were in slug flow regime.

Comparison of experimental measurement and simulation results is presented in Fig. 16. Figure 16(a) shows the variation of liquid holdup with time at the two test sections from experimental measurements, and simulation results from both the current model and OLGA. The liquid holdup predictions for both initial and final states are lower than experimental measurements. In the experiments, the liquid holdup at station 1 decreased from 0.4 to 0.2, while in the current model simulation, the liquid holdup at station 1 decreased from 0.32 to 0.13.

Figure 16(b) shows the variation of pressure with time at the first test section from experimental measurements, and simulation results from both the current model and OLGA. The prediction of pressure drop agrees very well with the experimental measurement.

Test 2E

The inlet liquid flow rate was kept at 323 m^3/d. Inlet gas flow rate increased from 815 Sm^3/d to 5000 Sm^3/d at 65 seconds. Separator pressure was kept at 1.67 bar. Both initial and final states were in stratified flow regime.

Comparison of experimental measurement and simulation results is presented in Fig. 17. Figure 17(a) shows the variation of liquid holdup with time at the two test sections from experimental measurements, and simulation results from both the current model and OLGA. Figure 17(b) shows the variation of pressure with time at the first test section from experimental measurements, and simulation results from both the current model and OLGA. Current model gives very good predictions for both holdups and pressure profiles.

Liquid Blow Out

Test 3A

The initial condition was a steady state flow with average inlet flow rates of 4825 Sm^3/d for gas and 48.8 m^3/d for liquid. At 120 seconds, the liquid supply was stopped, while gas supply was unchanged. Separator pressure was kept at 1.69 bar.

Comparison of experimental measurement and simulation results is presented in Fig. 18. Figure 18(a) shows the variation of liquid holdup with time at the two test sections from experimental measurements, and simulation results from both the current model and OLGA. Figure 18(b) shows the variation of pressure with time at the first test section from experimental measurements, and simulation results from both the current model and OLGA.

The current model is not able to predict both holdup and pressure profile well for this case.

Test 3B

The initial condition was a steady state flow with average inlet flow rates of 5880 Sm^3/d for gas and 204 m^3/d for liquid. At 95 seconds, the liquid supply was stopped, while gas supply was unchanged. Separator pressure was kept at 1.69 bar.

Comparison of experimental measurement and simulation results is presented in Fig. 19. Figure 19 (a) shows the variation of liquid holdup with time at the two test sections from experimental measurements, and simulation results from both the current model and OLGA. Figure 19(b) shows the variation of pressure with time at the first test section from experimental measurements, and simulation results from both the current model and OLGA.

Startup

Test 4B0

The pipeline was initially empty. Gas and liquid mixture was fed into the pipe at time 122 seconds. The final condition was a steady state flow with average inlet flow rates of 1870 Sm^3/d for gas and 322 m^3/d for liquid. Separator pressure was kept at 1.66 bar.

Comparison of experimental measurement and simulation results is presented in Fig. 20. Figure 20(a) shows the variation of liquid holdup with time at the two test sections from experimental measurements, and simulation results from both the current model and OLGA. Figure 20(b) shows the variation of pressure with time at the first test section from experimental measurements, and simulation results from both the current model and OLGA.

4. Discussion

A drift flux model is developed to simulate the transient two-phase flow behavior in pipelines. The model is based on drift velocity correlation and is flow pattern independent. The result for slug flow shows good agreement with experimental data as well as OLGA simulations.

When this model is applied to stratified flow, it gives good results only for cases with gas flow rate changes. For transient behavior caused by liquid flow rate change, the current model is not able to simulate it correctly. It seems necessary to modify the drift flux model for stratified flow.

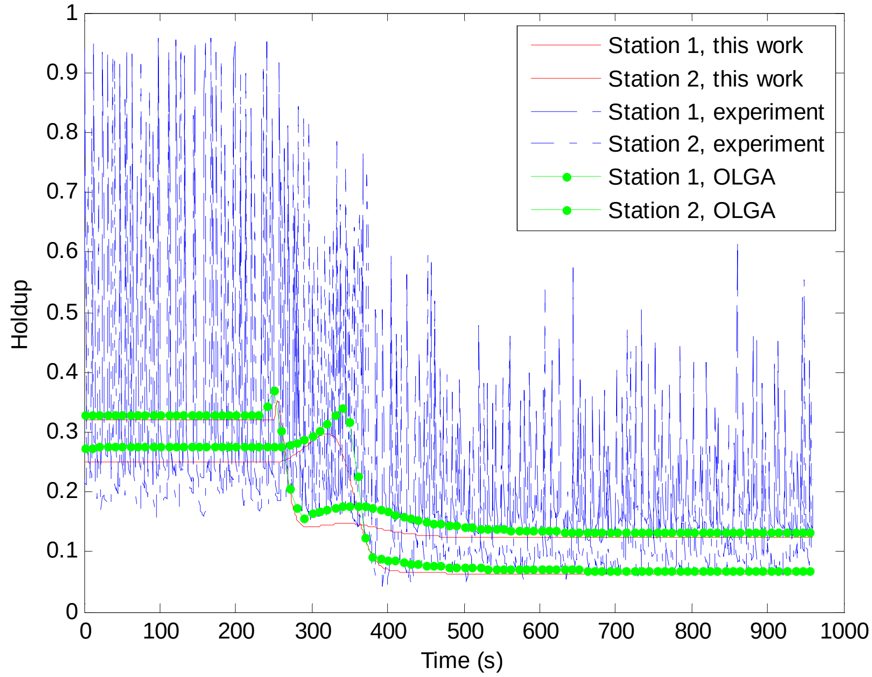

(a) Variation of liquid holdup with time at the two test sections

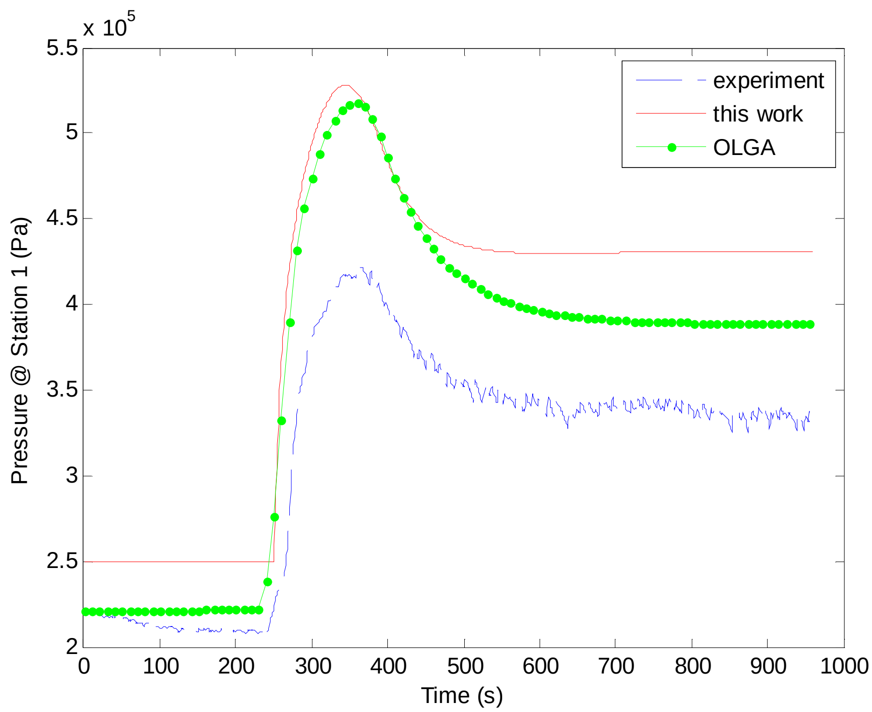

(b) Variation of pressure with time at the first test section

Figure 16: Results for Test 2-D with drift flux model

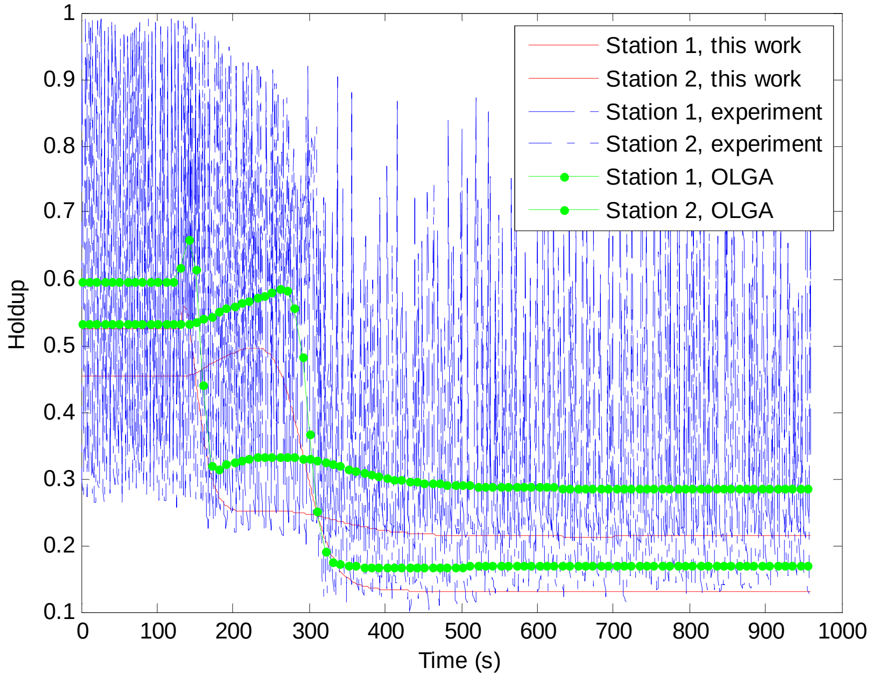

(a) Variation of liquid holdup with time at the two test sections

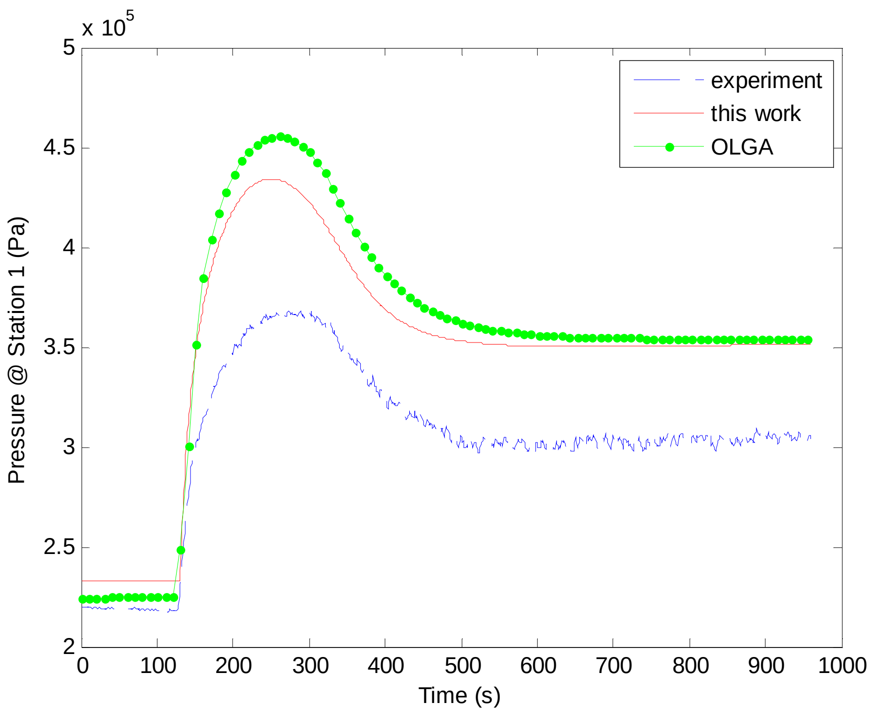

(b) Variation of pressure with time at the first test section

Figure 17: Results for Test 2-E with drift flux model

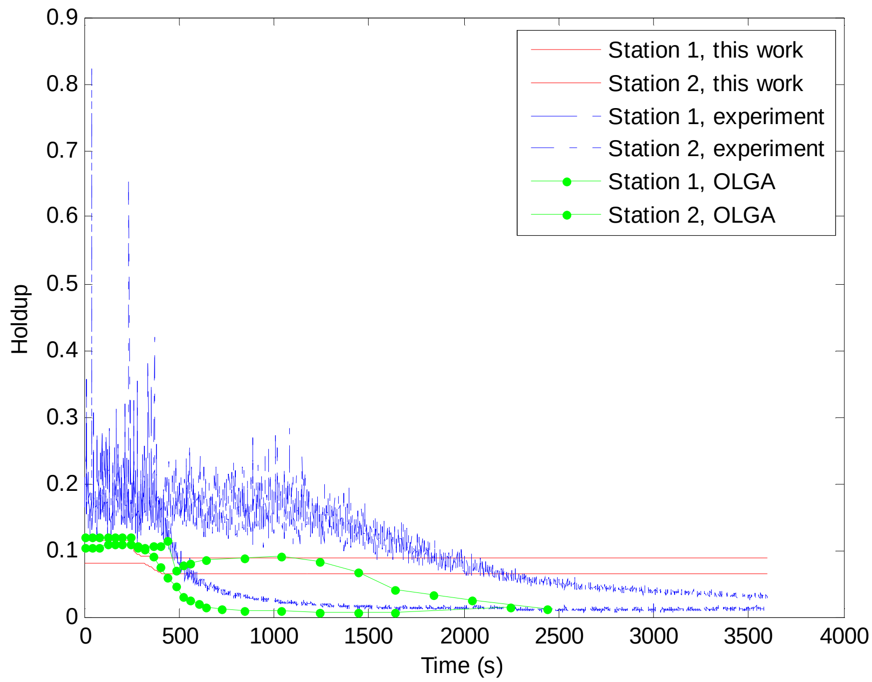

(a) Variation of liquid holdup with time at the two test sections

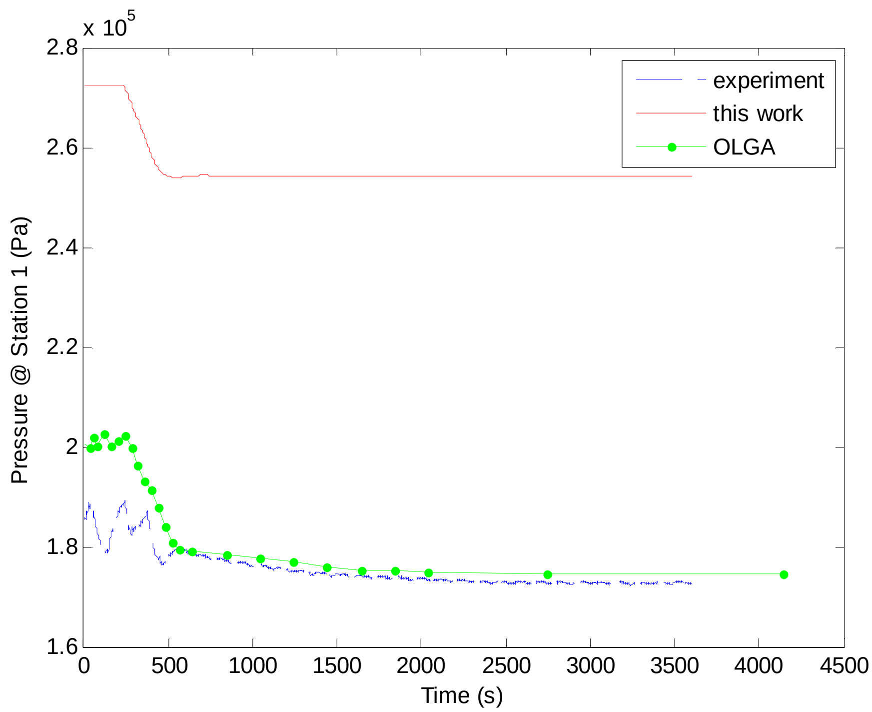

(b) Variation of pressure with time at the first test section

Figure 18: Results for Test 3-A with drift flux model

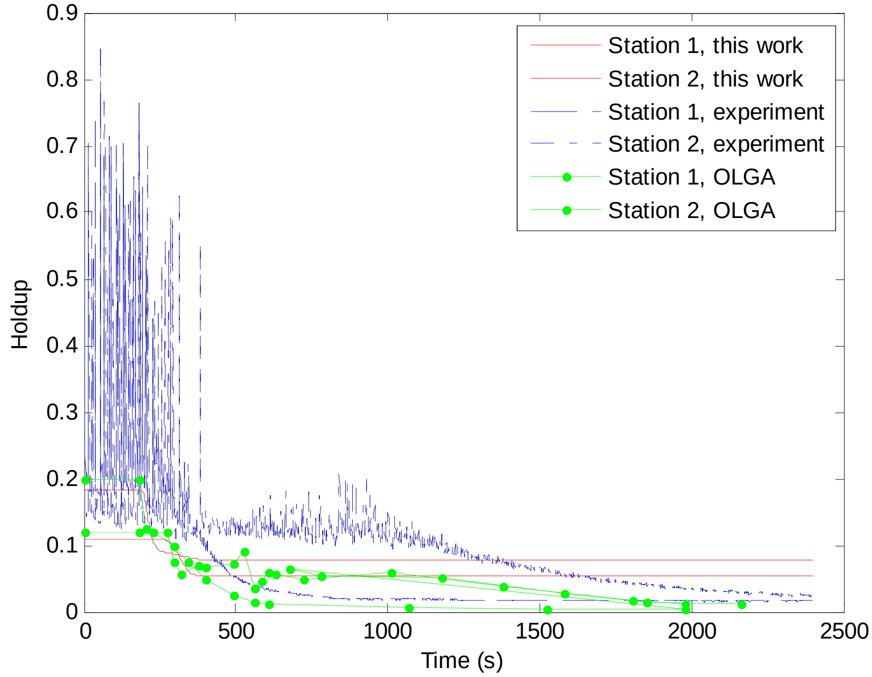

(a) Variation of liquid holdup with time at the two test sections

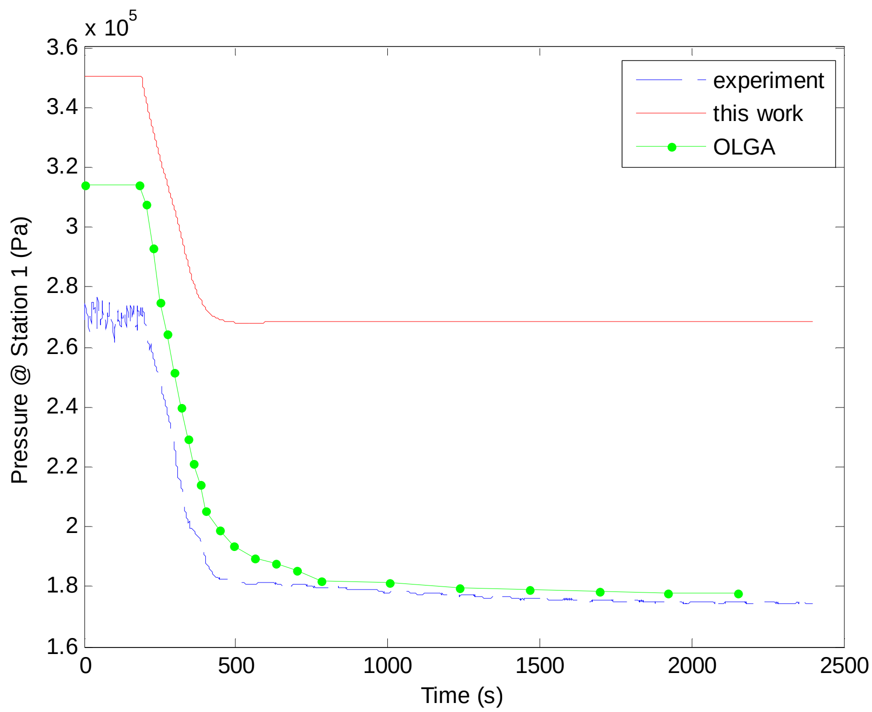

(b) Variation of pressure with time at the first test section

Figure 19: Results for Test 3-B with drift flux model

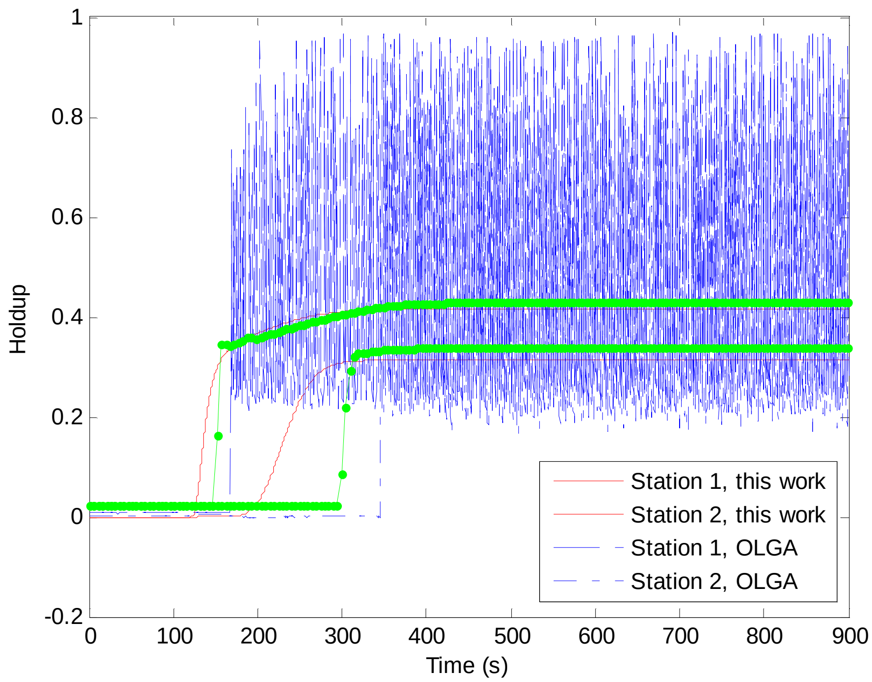

(a) Variation of liquid holdup with time at the two test sections

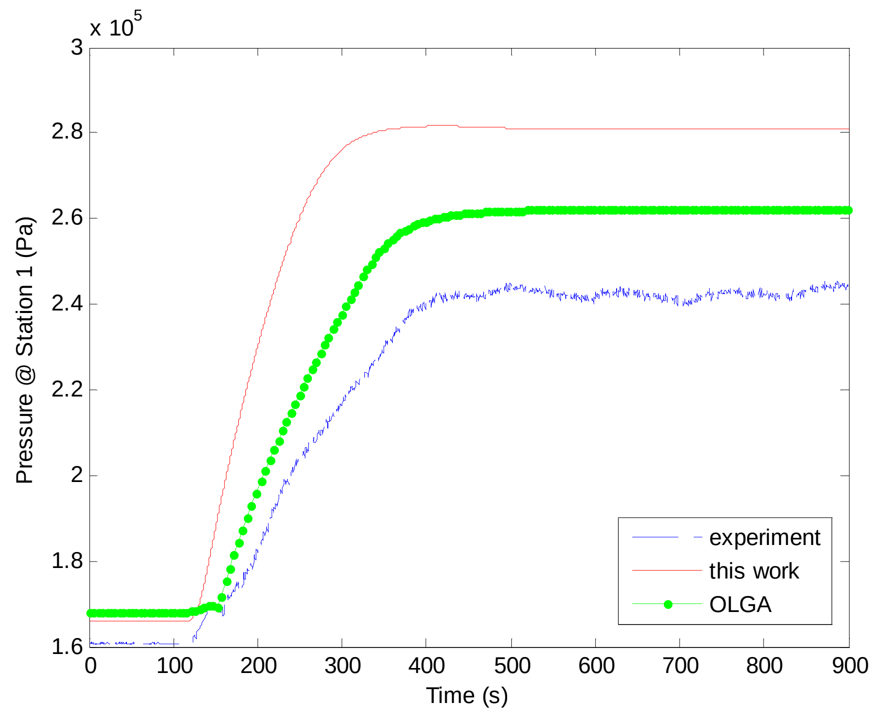

(b) Variation of pressure with time at the first test section

Figure 20: Results for Test 4-B0 with drift flux model

Attempt 3: Power Law Correlation

Develop a simplified transient simulator using power law correlation, ignoring flow pattern and flow pattern transition.

1. Method

Al-Sarkhi and Sarica (2009) developed a closure relationship between pressure gradient and flow rate for stratified gas-liquid two-phase flow in horizontal pipes. Their model performance was tested against more than 1200 published experimental data points and the result showed a good agreement even for flow regimes other than separated flow, and for slightly inclined pipes.

From Al-Sarkhi and Sarica work, the optimized curve which fits the experimental data is expressed as,

$$P^* = 0.075{X^*}^{-1.808} . \tag{49}$$

where

$$P^* = \frac{D(-dP/dx)}{{}^1/_2 \rho_L v_{SL}^2} . \tag{50}$$

$$X^* = \frac{\dot{m}_L}{\dot{m}_G}\sqrt{\frac{\rho_G}{\rho_L}} . \tag{51}$$

Substituting Eq. 50 and 51 into Eq. 49, and discretize it in space and time gives a relationship between $\dot{m}_G$ and pressure difference as,

$$\dot{m}_{G,i}^{K+1} = \left(\frac{0.075}{2}\frac{\Delta x}{DA^2\left(P_i^{K+1} - P_{i+1}^{K+1}\right)}\frac{\left(\dot{m}_{L,i}^{K+1}\right)^{0.192}\left(\rho_{G,i}^{K+1}\right)^{-0.904}}{\rho_L^{0.096}}\right)^{-\frac{1}{1.808}} . \tag{52}$$

Mass conservation equations Eq. 1 and 2, and liquid momentum equation Eq. 3 are used along with the power law correlation Eq. 49 for the simulations.

2. Solution Procedure

The solution procedure is the same as in Attempt 1, except in Step 11, Eq. 52 is used to calculate the new gas mass flow rate.

3. Discussion

Converged result for this approach has not been reached yet.

Attempt 4: Modified Drift Flux Model

Extend the drift flux model to stratified flow, and develop a simplified transient simulator based on the modified drift flux model.

1. Method

Danielson and Fan (2010) presented a work about hydrodynamics slug flow modeling. In that paper, they showed an interesting finding about the relationship between drift velocity and superficial liquid velocity (Fig. 21).

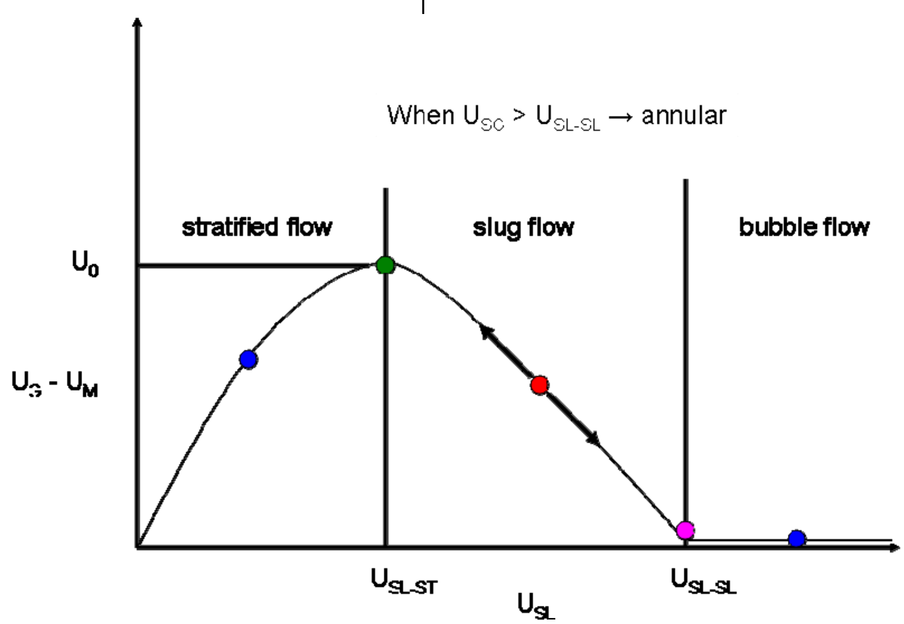

Figure 21: Schematic Diagram about the Relationship Between Drift Velocity and Superficial Liquid Velocity (From Danielson 2010)

Figure 21 shows that for a given v_M, if v_{SL} is increased (v_{SG} has to decrease so that the mixture velocity v_M remains constant), drift velocity v_d falls on a well defined curve. Moreover, the stratified flow pattern lies in the region where the curve has a positive slope, while the slug flow pattern lies in the region where the curve has a negative slope. Bubble flow pattern lies in the region where the curve flattens out.

This finding indicates that the drift flux correlation could be modified to make it applicable for stratified flow. We need to find a way to define the v_d - v_{SL} curve.

From the investigations by Gokcal (2008), we understand that drift velocity could be a function of several parameters including

$$v_d = v_d(d, g, \rho_L, \rho_G, \mu_L, \mu_G, \sigma, v_{SL}, v_{SG}) \qquad (53)$$

An accurate drift flux correlation may not be achievable right now, but we can construct the v_d - v_{SL} curve for any specific case from steady state simulations.

Here we propose to construct the curve by unified model simulations (Zhang, 2003). If we assume the transient phenomenon is a transition from one steady state to another steady state, we will get two curves for initial and final conditions separately. From that we can find the initial and final drift velocities. Then, the transient simulation is carried out based on these newly calculated drift velocities.

2. Solution Procedure

The solution procedure is the same as in Attempt 2, except that the drift velocity is calculated from unified model simulations for each specific case rather than from closure relationships.

3. Discussion

Simulation is underway.

Current Status

Two-fluid model and drift flux model were developed.

Two-fluid model gave good predictions for stratified flow with liquid flow rate change, while drift flux model gave good predictions for slug flow and stratified flow with gas flow rate change. We have combined these two models into one package so that the combined package is able to cover the full range of cases. A driver is developed to determine which model to use. The code was developed in Matlab originally. It is now converted to Fortran and it is running well.

Further Work

- Modify the drift flux model for stratified flow;
- Further study power law correlation based transient simulator;
- Consider terrain/severe slugging;
- Need to incorporate the model with a PVT package;
- Incorporate heat transfer model;
- Compare with more experimental data for validation purpose.

Nomenclature

A	=	cross sectional area [m^2]
d	=	diameter [m]
f	=	friction factor
H	=	holdup
m	=	mass [kg]
$\dot{m}$	=	mass flowrate [kg/s]
P	=	pressure [Pa]
S	=	perimeter over which shear stress acts
v	=	velocity [m/s]
T	=	temperature [°K]

Subscripts

L	=	liquid phase
G	=	gas phase
I	=	interface
M	=	mixture
i	=	the ith section of the pipe

Greek Letters

τ	=	shear stress [Pa]
ρ	=	density [kg/m]
θ	=	inclination angle
Θ	=	wetted wall fraction
σ	=	surface tension [N/m]
μ	=	dynamic viscosity [kg/m·s]

References

Al-sarkhi, A. and Sarica, C.: "New dimensionless parameter and a power law correlation for pressure drop of gas-liquid flows in horizontal pipelines," Proceedings of the BHR Group - 14th International Conference on Multiphase Production Technology , Cannes, France: 17th – 19th June (2009).

Bendiksen, K.: "An experimental investigation of the motion of long bubbles in inclined tubes," *Int. J. Multiphase Flow* 10, 467-483 (1984).

Danielson, T. J. and Fan, Y.: "Hydrodynamic Slug Flow Modeling,"

Vigneron, F., Sarica, C., and Brill, J.P.: "Experimental analysis of imposed two-phase flow transients in horizontal pipelines," Proceedings of the BHR Group 7th international conference, 199-217 (1995).

Zhang, H.Q., Wang, Q., Sarica, C., and Brill, J.P.: "Unified model for gas-liquid pipe flow via slug dynamics – part 1: Model development," ASME *J. Energy Res. Tech.* 125, 266-273 (2003).

Fluid Flow Projects

Executive Summary of Research Activities

Cem Sarica

Advisory Board Meeting, November 3, 2010

Liquid Unloading from Gas Wells

- Objectives
  - Explore Mechanism Controlling Onset of Liquid Loading
  - Investigate Effects of Well Deviation on Liquid Loading

Liquid Unloading from Gas Wells …

- Past Studies
  - Primarily on Droplet Transfer {Turner (1969), Coleman(1991), etc.}
  - Film Reversal {Barnea (1987), Veeken (2009)}
  - No Comprehensive Study on Inclination Angle Effect

Liquid Unloading from Gas Wells …

- Status
  - Literature Review is Complete
  - Experimental Study is Being Planned
    - 3 in. ID Severe Slugging Facility Will be Used

Fluid Flow Projects

Liquid Unloading from Gas Wells

Ge (Max) Yuan

Advisory Board Meeting, November 3, 2010

Outline

- Objectives
- Literature Review
- Experimental Study
- Near Future Tasks
- Project Schedule

Objectives

- Explore Mechanisms Controlling Onset of Liquid Loading
- Investigate Effect of Well Deviation on Liquid Loading

Literature Review

- Influence of Well Deviation on Critical Gas Velocity
  - Belfroid *et al.* (2008) 2 in. ID, Air-water Flow, only 4 Points

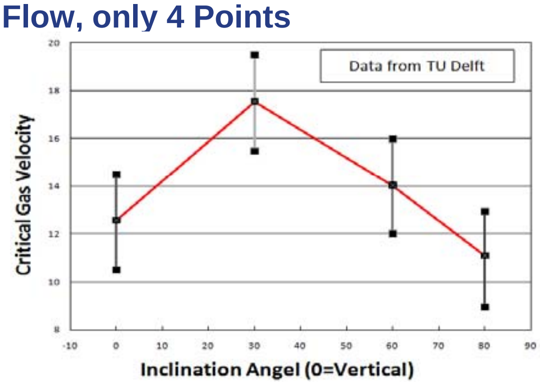

Literature Review …

- Mechanism of Liquid Loading
  - Main Mechanisms (Toma 2007)
    - Film Drainage
    - System Instability
    - Flow Pattern Change
  - Liquid Loading Occurs Due to Liquid Film Flow Reversal Rather than Droplet Flow Reversal
    - Christiansen (2009) - Not Published
    - Veeken (2009) - Simulation Results

Literature Review …

- Modeling of Liquid Loading
  - Turner *et al.* (1969)

$$v_g = \left(\frac{4N_{WE}}{3C_D} \right)^{0.25} \frac{\left[\sigma g \left(\rho_l - \rho_g \right) \right]^{0.25}}{\rho_g^{0.5}}$$

  - Coleman *et al.* (1991)

Literature Summary

- Few Data About Inclination Effect
- No Comprehensive Study on Inclination Effect
- Mechanism In Debate

Experimental Study

- Test Section Design
- Test Fluids
- Testing Range
- Instrumentation

Fluid Flow Projects Advisory Board Meeting, November 3, 2010

Test Section Design

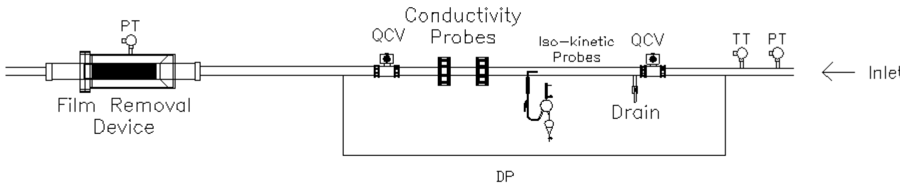

- Diameter of Pipe: 3 in.
- Total Length of Test Section: 17.5 m

Fluid Flow Projects

Advisory Board Meeting, November 3, 2010

Test Section Design…

Section Name	Section Length	
	L/D	L, ft (m)
Pressure Drop Section	50	12.5 (3.8)
Holdup Section	25	6.25 (1.9)
Developing Section	100	25 (7.6)

Fluid Flow Projects

Advisory Board Meeting, November 3, 2010

Test Section Design…

- Pressure and Temperature:
  PT- 6.6 m (distance from inlet)
  TT- 7.6 m
  DP- 9 m and 12.8 m
- Hold Up: QCV
  Valve Type: Knife Type
  Valve: 9.5 m and 11.4 m

Test Fluids

- Test Fluid
  - Gas – Air
  - Water – Tap Water

Testing Range

➢Test Matrix

v_{sg} (m/s)	v_{SL} (m/s) Inclination Angle: 30, 45, 60, 75, 90				
10	0.005	0.01	0.02	0.05	0.1
15	0.005	0.01	0.02	0.05	0.1
20	0.005	0.01	0.02	0.05	0.1
25	0.005	0.01	0.02	0.05	0.1
30	0.005	0.01	0.02	0.05	0.1

Testing Range …

Test Matrix (Vertical)

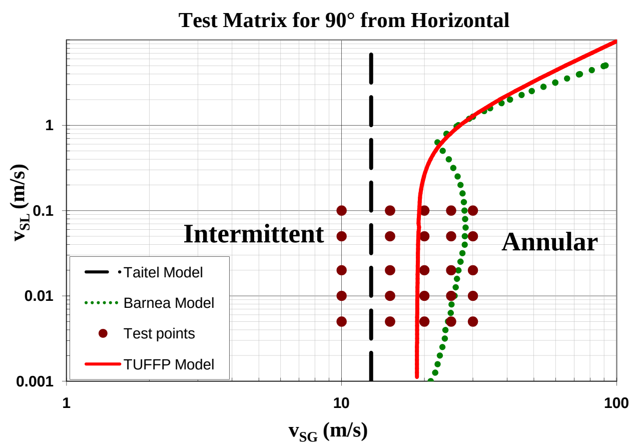

Testing Range …

- Test Matrix (75°)

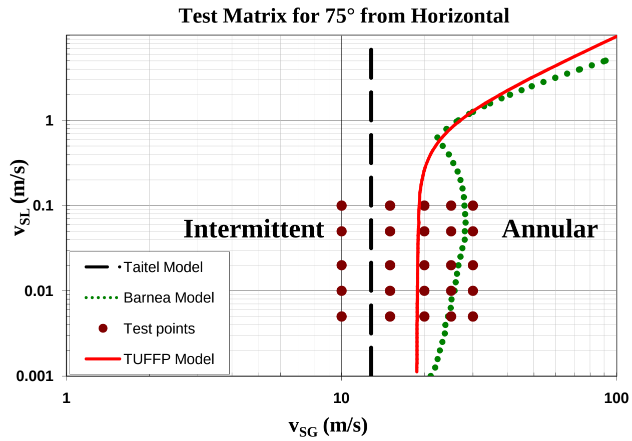

Fluid Flow Projects

Advisory Board Meeting, November 3, 2010

Testing Range …

- Test Matrix (60°)

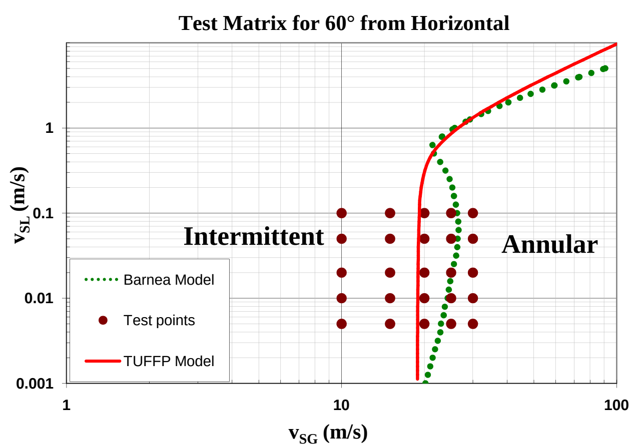

Fluid Flow Projects

Advisory Board Meeting, November 3, 2010

Testing Range …

- Test Matrix (45°)

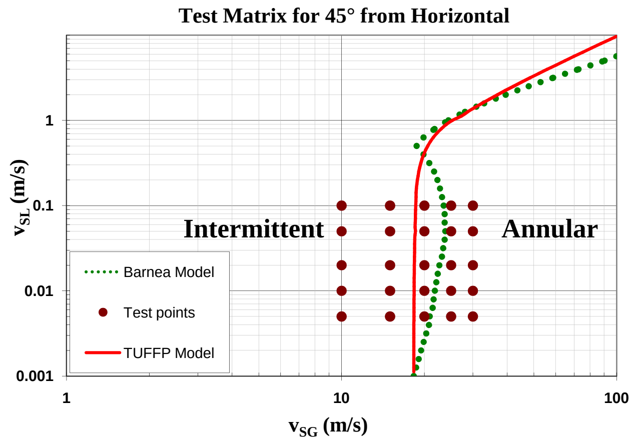

Testing Range …

- Test Matrix (30°)

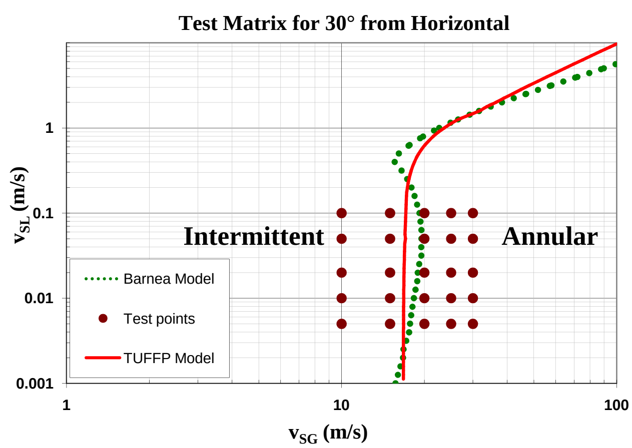

Instrumentation

- Pressure and Temperature: PTs and DPs and TTs
- Holdup: Quick Closing Valves
- Liquid Entrainment Fraction
- Liquid Film Flow Direction
- Liquid Film Thickness
- Liquid Film Velocity
- Potential Available Technology

Liquid Entrainment: Iso-kinetic Probe

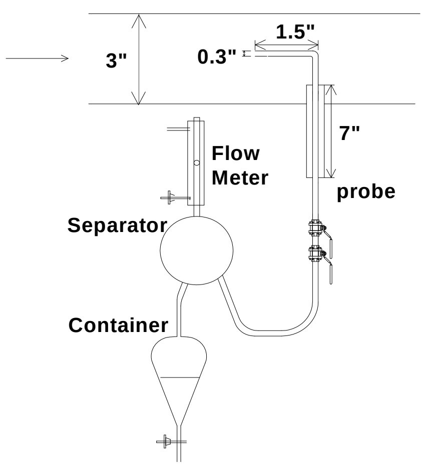

Back Pressure is needed to help get iso-kinetic condition

Film Thickness: Conductivity Probe

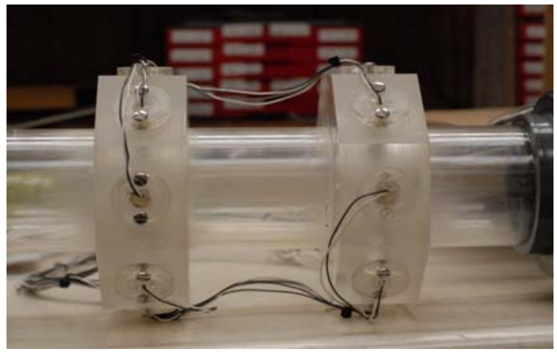

Fluid Flow Projects

Advisory Board Meeting, November 3, 2010

Film Flow Direction

- Silk Attached to Inner Pipe Surface (simple)
- Dye Particle Injection (likely)
- Injecting Hot/Cold Fluid (less likely)
- Thermal Camera (less likely)

Fluid Flow Projects

Advisory Board Meeting, November 3, 2010

Film Velocity

- Film Removal (will work)
- High Speed Camera: Particle Tracking (likely)
- Injecting Hot/Cold Fluid (less likely)
- Thermal Camera (less likely)

Film Removal Device

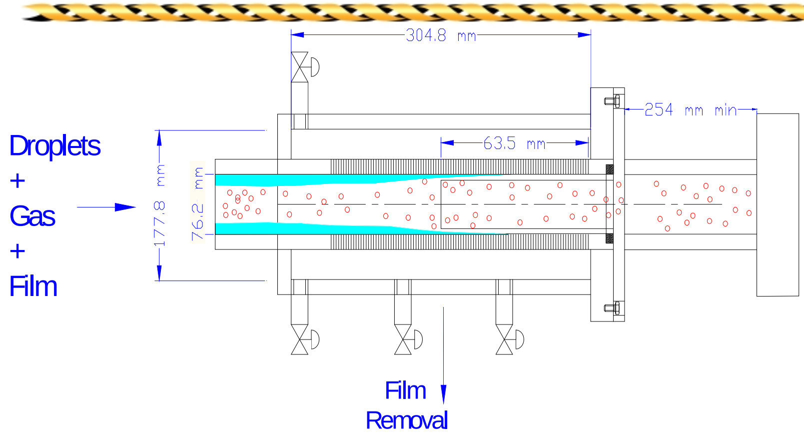

- Can be used to measure film velocity and droplet entrainment

Potential Technology: Thermal Camera

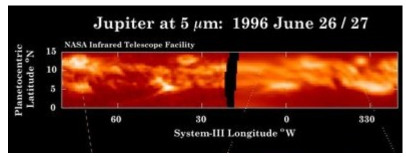

Potential Technology: Thermal Camera

Model	Fluke Ti50/Ti55	Ti 40/Ti45
Resolution	320*240	160*120
Frame Speed	60 Hz	30 Hz
Thermal Sensitivity	0.05 C	0.08 C

- Ti 50/Ti 55 Model is a Good Candidate to Use
- Ti 45 can be Rent for Test from TRSRenTelco

Potential Technology: Bubble Streak Tracking (BST)

- High Speed Camera Capturing Gas Bubbles in Liquid Film

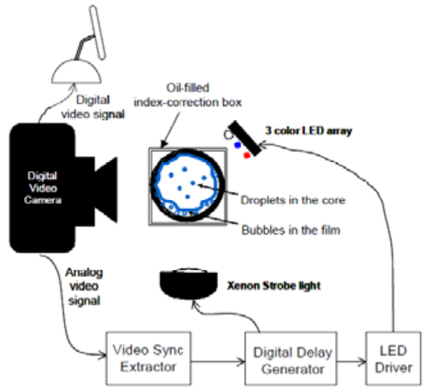

Fluid Flow Projects

Advisory Board Meeting, November 3, 2010

Potential Technology: Thin Film Particle Image Velocimetry

- High Speed Camera Capturing Injected Particle in Liquid Film

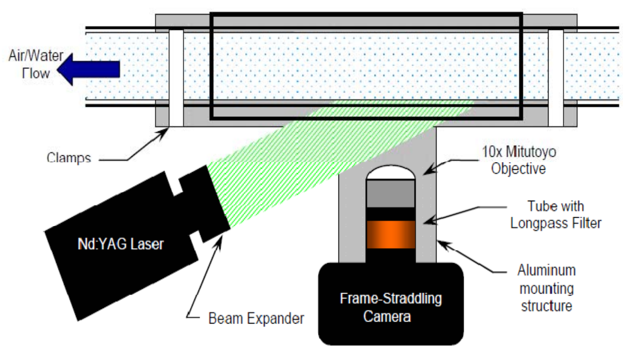

Fluid Flow Projects

Advisory Board Meeting, November 3, 2010

Potential Technology…

- Bubble Streak Tracking (BST) and Thin Film Particle Image Velocimetry (TFPIV)
  - Visualizing film flow direction
  - Measuring film velocity

Near Future Tasks

- Facility Modification
  - Run Simple Test
  - Instrumentation Installation
- Preliminary Testing

Project Schedule

Literature Review	Ongoing
Facility Modification	February 2010
Preliminary Testing	March 2010
Experimental Testing	June 2011
Data Analysis	July 2011
Model Comparison	August 2011
Final Report	September 2011

Questions/Comments

Liquid Unloading from Gas Wells

Ge (Max) Yuan

Project Completion Dates

Literature Review	Ongoing
Facility Modifications	February 2010
Preliminary Testing	March 2011
Experimental Testing	April 2011
Data Analysis	July 2011
Model Comparison	August 2011
Final Report	September 2011

Objectives

The main objectives of this study are to:

- Explore the mechanisms controlling the onset of liquid loading, and
- Investigate the effect of well deviation on liquid loading process.

Introduction

As natural gas is produced from a reservoir, the simultaneous flow of gas with liquid hydrocarbons and/or water is a common occurrence in both onshore and offshore production systems. Liquid loading in the wellbore has been recognized as one of the most challenging problems in gas production. During the early time of the production, natural gas carries liquid in the form of mist. The reservoir pressure is sufficient for the gas wells to transport the liquid phase to the surface along with the gas phase. As the gas well matures, the reservoir pressure decreases and gas flow velocity drops. When the gas velocity becomes lower than a critical value, the liquid falls back and the flow pattern changes from annular flow to slug flow. As liquid loading progresses, the accumulation of liquid increases the bottom-hole pressure and further reduces gas production rate. Then, the flow pattern may change to bubbly flow. Eventually, the well can no longer produce. The process of liquid loading is shown in Fig. 1.

Typical symptoms of liquid loading include sharp drops in the cumulative production decline curve, abrupt changes in the flowing pressure gradient, lower temperature at the wellhead and declining water production or condensate-gas-ratio as shown in Fig. 2.

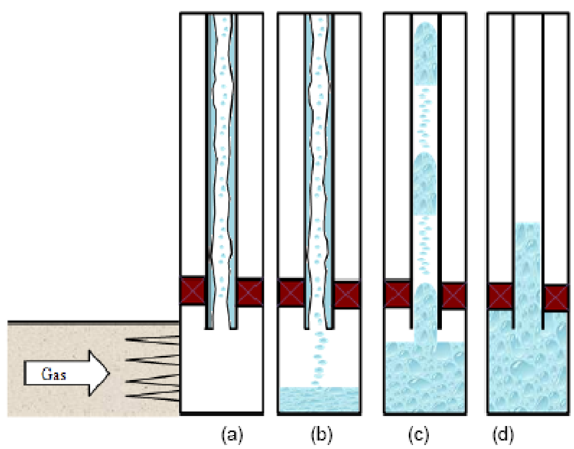

Figure 1: Gas Production Flow Regime Changes from Mist (a) to Annular (b), Slug/Churn Flow (c), and Eventually Loading up (d).

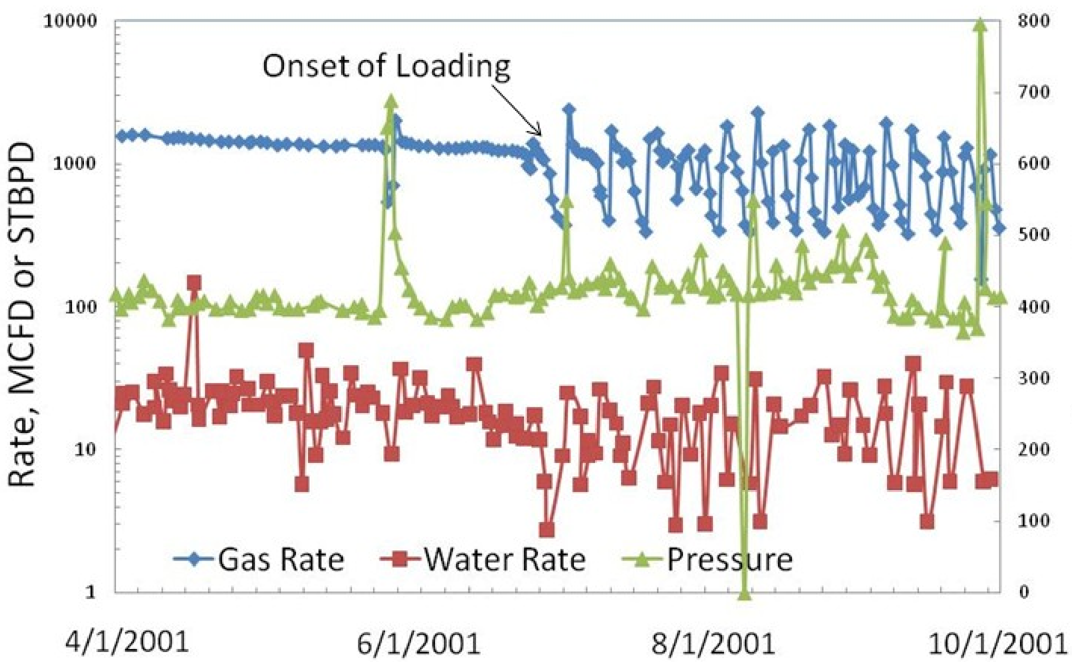

Figure 2: Well Performance Data Indicating Liquid Loading (Sutton *et al.*, 2003)

In the oil and gas industry, several methods have been developed to solve the liquid loading problem; such as using a down-hole pump to produce water, using velocity string, lowering wellhead pressure, and foam assisted lift. Although a lot of efforts have been made to model the liquid loading process of gas wells, experimental data are very limited. Field data from Turner (1969), Coleman (1991) and Veeken (2009) are the only available data to validate the existent models.

Turner *et al.* (1969) derived a method of predicting the critical gas rate by equating the upward drag and downward gravity forces on the largest possible liquid droplet. The maximum Weber number determines the largest possible droplet size. The so-called Turner expression for liquid loading includes a 20% upward adjustment to best-fit field data. The Turner method has been widely used in the industry for decades because it only requires readily measurable wellhead parameters.

Literature Review

Mechanism of liquid loading is still in debate. The flow pattern transition from annular to churn/slug flow plays an important role in the process. In practice some other mechanisms may initiate the liquid loading. The main mechanisms for liquid loading may include (Toma 2007):

- Film drainage,
- System instability,
- Flow regime change.

Recent literature has reported that liquid loading occurs due to liquid film flow reversal rather than droplet flow reversal, which is a challenge to the widely used Turner criterion. Several authors have observed such phenomena in their flow loop experiments. Van't Westende *et al.* (2007) studied liquid transport in a 0.05 m diameter 12 m long air-water pipe. The maximum observed droplet size was about 1 order of magnitude smaller than the maximum droplet size postulated by the Turner expressions, i.e. the droplets should not cause liquid loading.

It was observed that the onset of liquid loading coincides with liquid film flow reversal rather than liquid droplet flow reversal. Christiansen (2009) carried out similar flow loop testing and observed the same film flow reversal. The results of transient flow modeling provided by Veeken *et al.* (2009) also support the flow loop observation.

The Turner's criterion does not consider the influence of well deviation on critical gas velocity. In deviated wells, there may be different mechanisms. Flow loop testing has also been used to investigate the influence of well deviation on liquid loading rate which cannot be predicted by Turner's model. The results for a 2-inch diameter air-water flow loop are presented by Belfroid *et al.* (2008) as four testing points in Fig. 3.

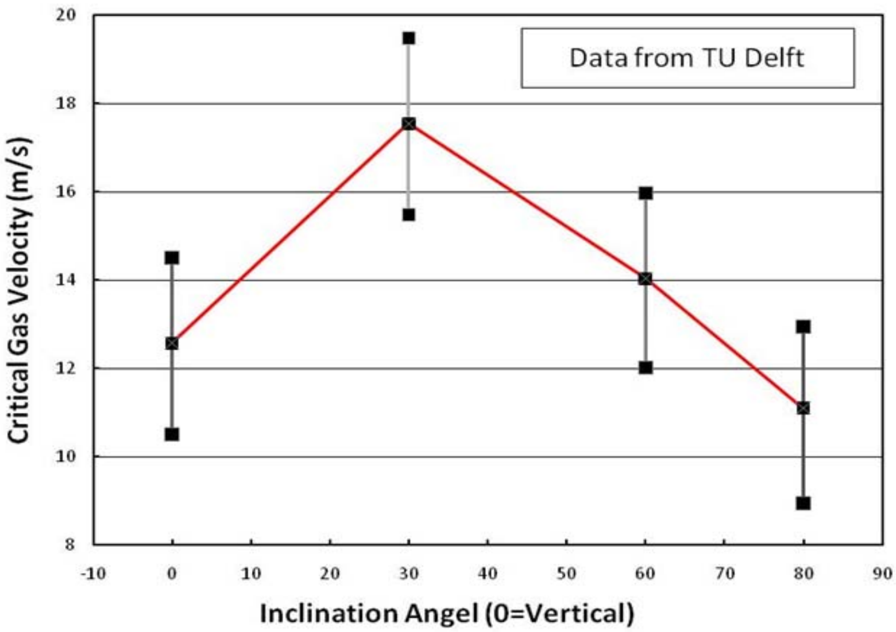

Figure 3: Critical Gas Velocity as Function of Inclination Angle (Belfroid *et al.*, 2008)

Turner *et al.* (1969) proposed the continuous film model and entrained droplet model and concluded that the droplet falling is the controlling mechanism. They adopted the "droplet model" from fluid particle dynamics to calculate the critical gas velocity necessary to lift the liquid droplets in near vertical wells. In this model, the minimum velocity required to keep liquid droplets in suspension is the result of a force balance between the drag exerted by the surrounding gas and the gravity of the droplets. Turner *et al.* (1969) introduced the following expression in oilfield units for the critical gas velocity required to keep liquid droplets in suspension:

$$v_{sg} \approx v_g = 17.6\frac{[\sigma(\rho_l - \rho_g)]^{0.25}}{\rho_g^{\ 0.5}}$$

Coleman *et al.* (1991) adopted the Turner model to analyze the Exxon field data and found out the 20% adjustment was not needed. The major difference between the two sets of field data is the wellhead pressure. The wellhead pressures of most wells in the Turner's field data were higher than 800 psia while those of Coleman's data were less than 500 psia.

The entrained droplet approach is the most widely used in the oil and gas industry to predict the minimum gas flow rate required to prevent the onset of liquid loading. Models based on this approach have been tested against field data, with varying degrees of success reported by each author.

Liquid unloading of gas wells becomes an important issue because there is no satisfactory model to predict the critical velocity for inclined wells. In Grija's (2006) study, a Transitional Annular Flow was observed. In this flow regime, gas flows upward in the central core of the conduit, and a liquid film is on the walls of the conduit. When this regime is observed in the flow loop, it occurs in two zones in the test section. In the lower zone, the liquid film is thick and its direction of flow is changing. In the upper part of the loop, the film is thinner and the direction of flow is downward. The lower zone generates lots of liquid droplets which are lifted to the upper zone in the test section, where they coalesce on the walls and flow downward until they meet the thicker film of the lower zone. Thus, the flow regimes in the loop consist of a lower zone with a gas core and annular film from which droplets are transported upward, and an upper coalescing zone in which droplets strike the wall of the loop and flow downward. There is a distinct interface between the lower zone and the upper zone.

Experimental Study

The 76.2-mm (3 in.) diameter severe slugging facility of the Tulsa University Fluid Flow Projects (TUFFP) will be modified for this project (Fig. 4). The facility is capable of being inclined from horizontal to vertical. Pressure and temperature transducers are placed near the test section to obtain fluid properties and other flowing characteristics.

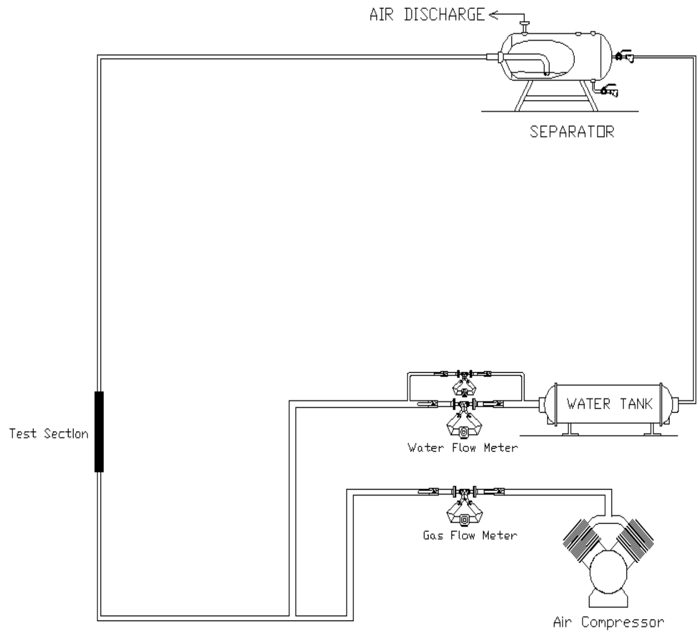

Figure 4: Schematic of Liquid Loading Test Facility of TUFFP

Test Section Design
Test section design is shown in Fig. 5. Main dimensions are listed in Table 1.

Test Fluids
Compressed air and Tulsa city tap water will be used in this study.

Testing Range
In this study, experiments will be conducted at different flow conditions in terms of flow rates and inclination angle. Superficial water velocities range from 0.005 to 0.1 m/s. Superficial gas velocities range from 10 to 30 m/s. The test range should experience the onset of liquid loading in order to get the critical gas velocity. Figures 5 through 9 display the test matrices for experiments to be conducted at inclination angles of 30°, 45°, 60°, 70°, and 90° from horizontal.

Test range is determined based on the simulation results by Taitel Model, Barnea Model and TUFFP Model. In the following figures, the transition from annular flow to intermittent flow is predicted by different models. It is important to point out that Taitel Model adopted Turner's criterion for this transition.

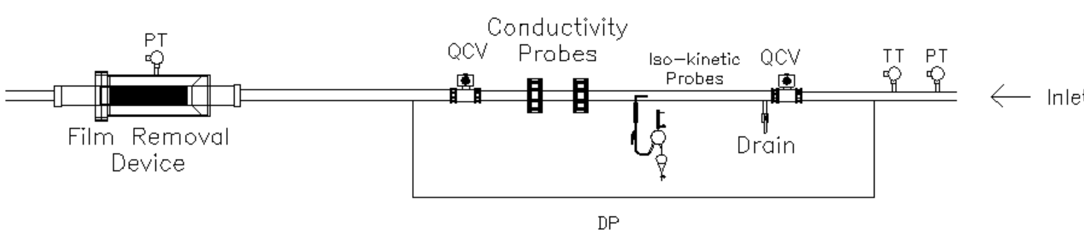

Fig 5: Test Section Design

.

Table 1 - Test section dimensions

Section Name	Section Length	
	L/D	L, ft (m)
Pressure Drop Section	50	12.5 (3.8)
Holdup Section	25	6.25 (1.9)
Developing Section	100	25 (7.6)

Table 2 - Test Matrix

V_{sg} (m/s)	v_{SL} (m/s) Inclination Angle: 30, 45, 60, 75, 90				
10	0.005	0.01	0.02	0.05	0.1
15	0.005	0.01	0.02	0.05	0.1
20	0.005	0.01	0.02	0.05	0.1
25	0.005	0.01	0.02	0.05	0.1
30	0.005	0.01	0.02	0.05	0.1

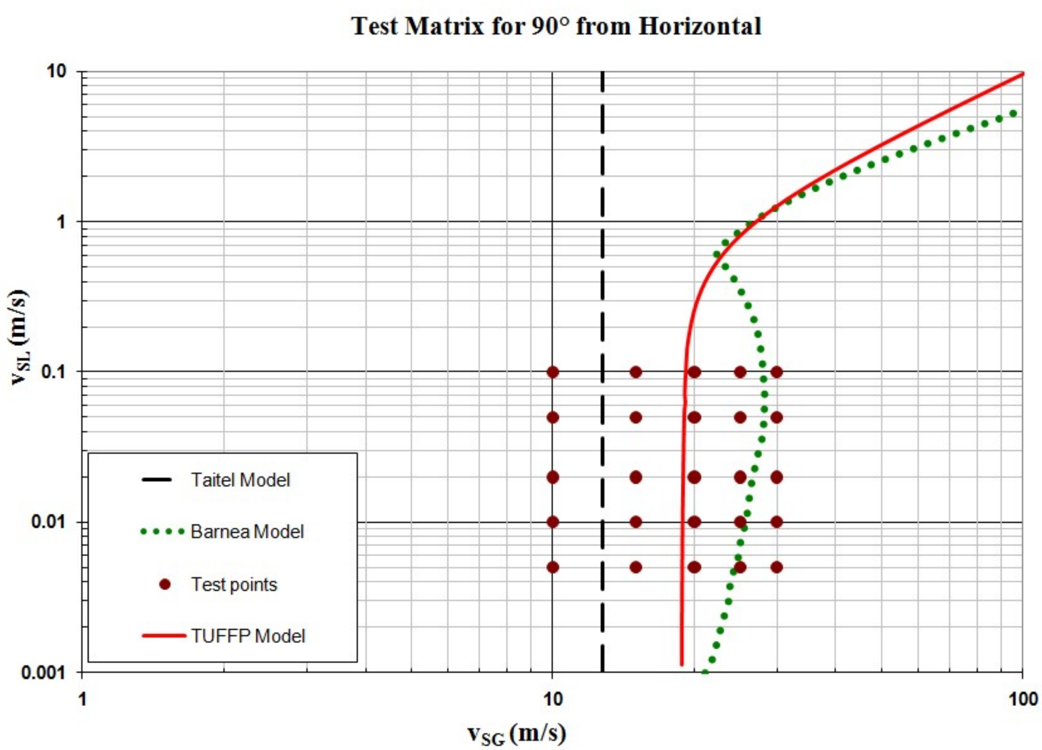

Figure 6: Test Matrix on Annular-Intermittent Transition Map by Different Models (Vertical)

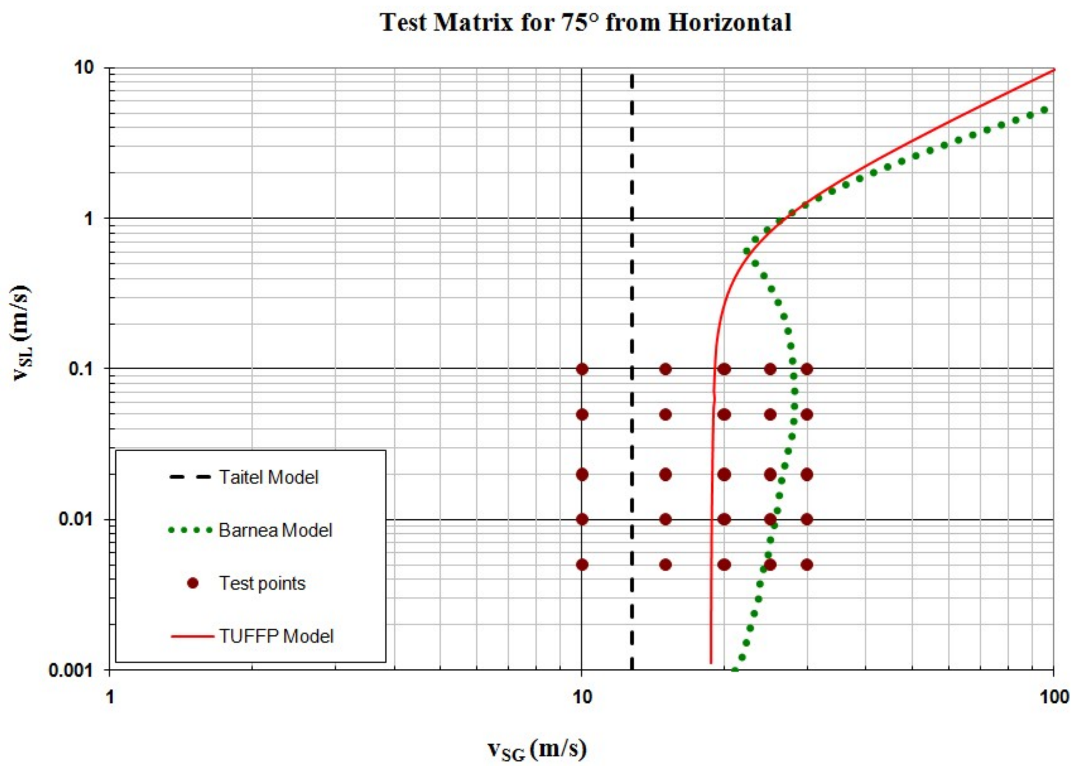

Figure 7: Test Matrix on Annular-Intermittent Transition Map by Different Models (75°)

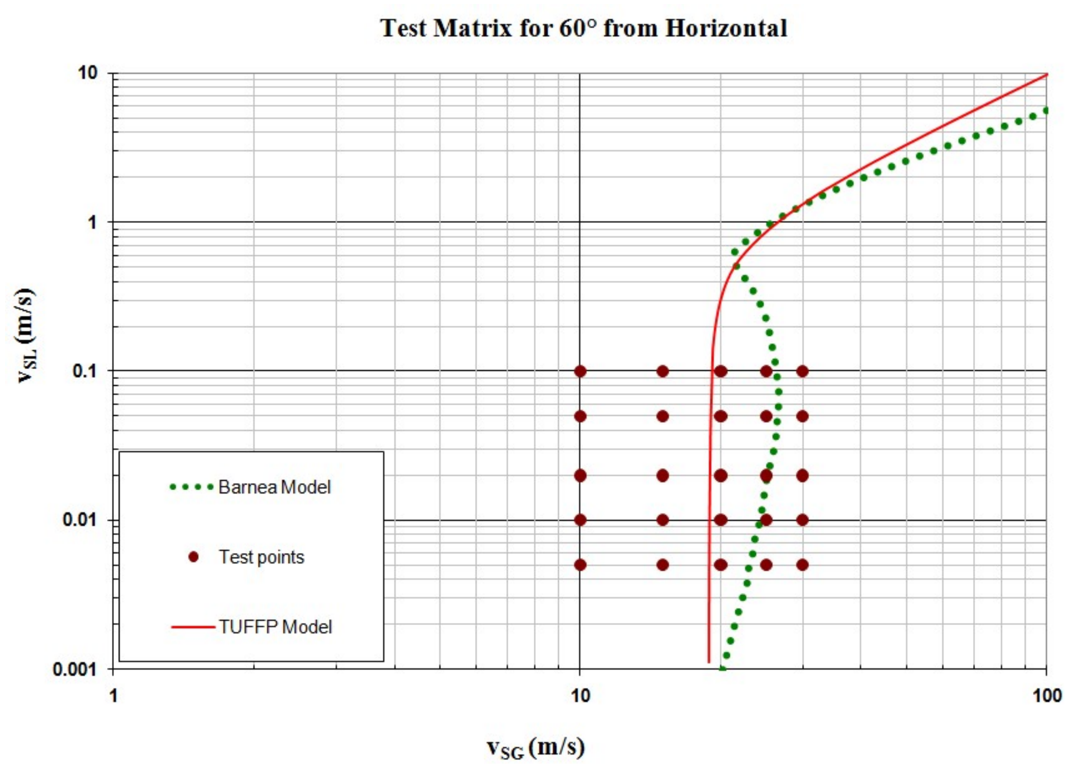

Figure 8: Test Matrix on Annular-Intermittent Transition Map by Different Models (60°)

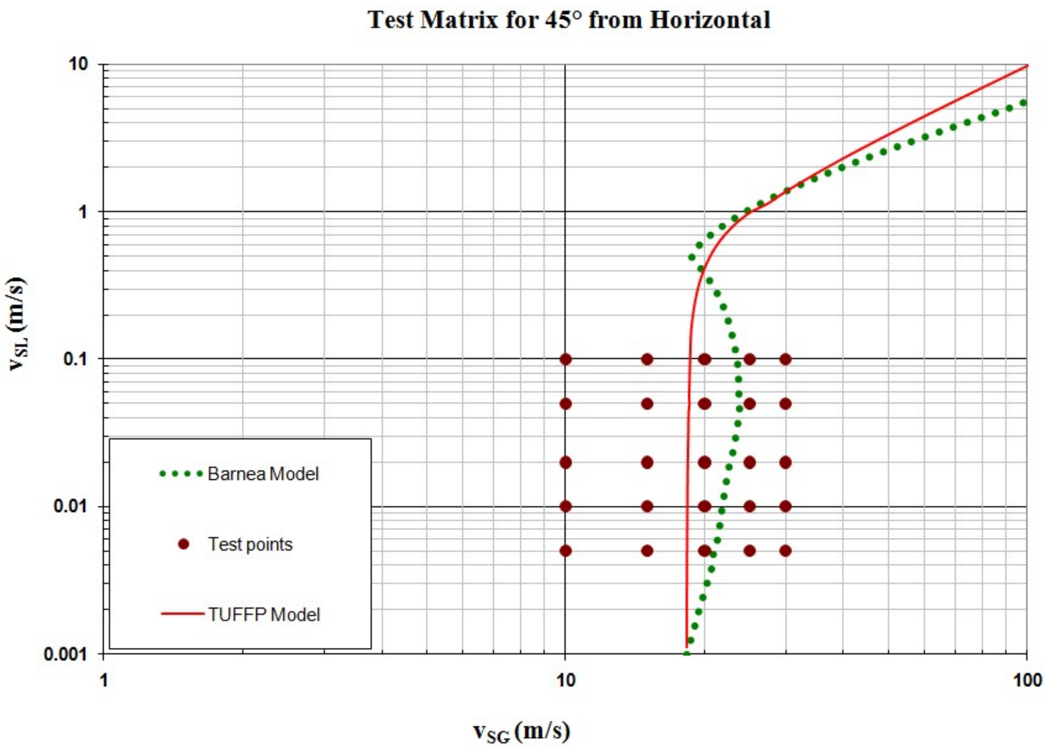

Figure 9: Test Matrix on Annular-Intermittent Transition Map by Different Models (45°)

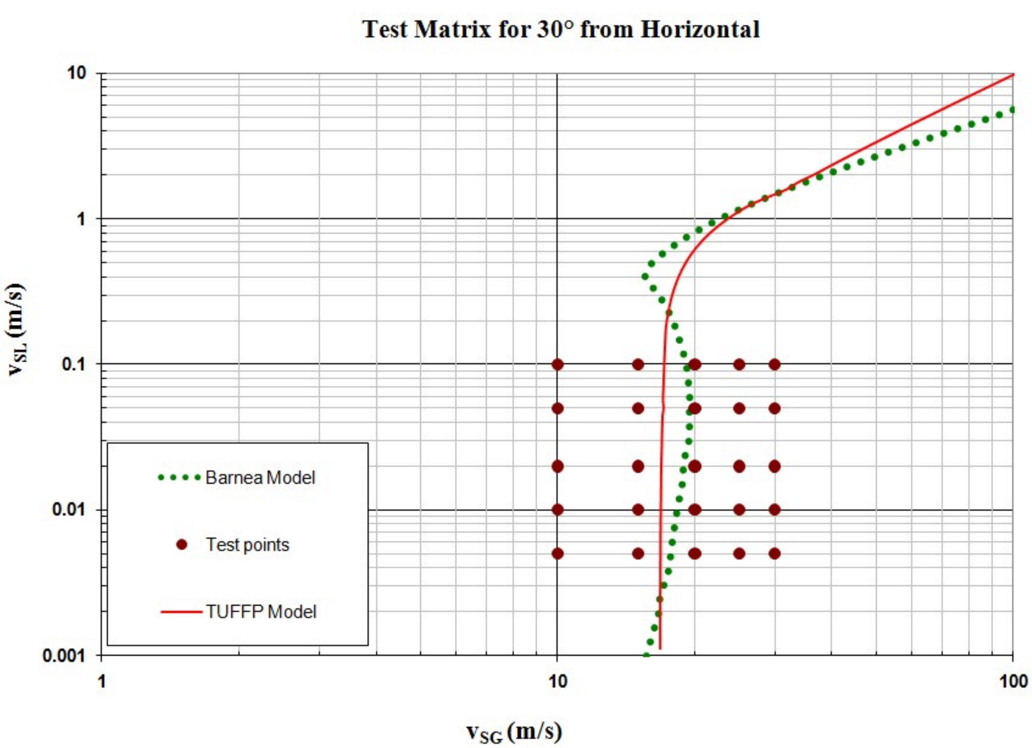

Figure 10: Test Matrix on Annular-Intermittent Transition Map by Different Models (30°)

Measurements and Instrumentation

Liquid Holdup

Quick-closing valves (QCV) will be installed on the test section to measure liquid holdup.

Knife type valves will be used to improve performance. The two valves will be located at 9.5 m and 11.4 m from inlet.

Pressure and Temperature

Pressure transducer is located at 6.6 m and temperature transducer is located at 7.6 m. Two other transducers are located at 9 m and 11.4 m to measure differential pressure.

Liquid Film Thickness

Liquid film thickness can be measured using conductivity probe shown in Fig. 11.

At the transition from annular flow to intermittent flow, a larger film thickness is expected. Since there is an upper limit for the conductivity probe, we may need to use capacitance to measure film thickness at the transition region.

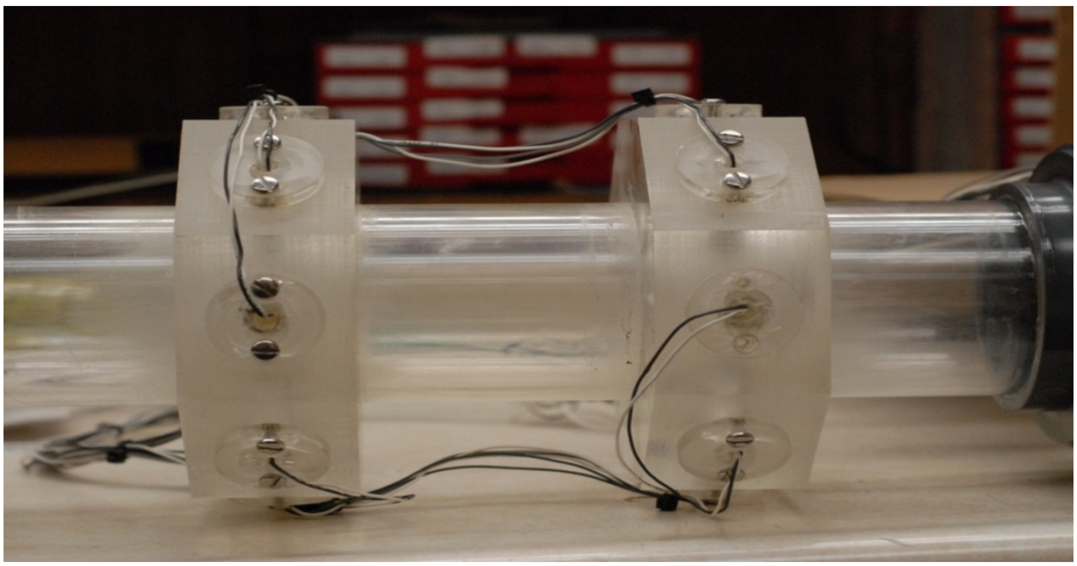

Figure 11: Conductivity Assembly for Film Thickness Measurement

Liquid Entrainment Fraction

An iso-kinetic sampling probe (shown in Fig. 12) will be installed in the facility to measure entrainment fraction. The iso-kinetic sampling probe will be inserted into the pipe at various radial distances. The liquid sampled from the gas core will be separated in a small gas-liquid separator and collected in a graduated cylinder. From these measurements, the droplet entrainment flux profile will be determined. The entrainment fraction can be calculated by integrating this flux profile. Certain back pressure is needed to help reach iso-kinetic flow condition.

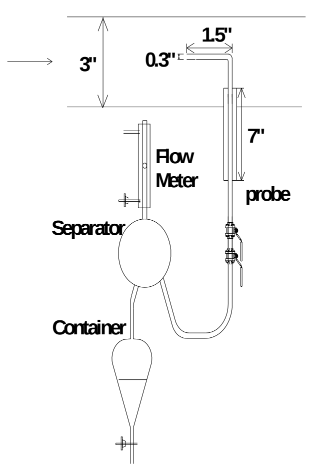

Figure 12: Iso-kinetic Probe for Liquid Entrainment Measurement

Liquid Film Flow Direction

Film flow direction is of great importance in the measurements. Several options are examined for instruments.

- Silk threads attached to inner pipe surface
- Injecting hot/cold fluid
- Dye injection
- Thermal camera

Liquid Film Velocity

Film velocity measurement is another challenge since film flow direction may not be uniform in all cases. It should be noted that film velocity can be back calculated by mass conservation of water using the film removal device.

$$\text{Film velocity} = \frac{\text{Mass from inlet} - \text{Mass of entrainment droplets}}{\text{crossection area of liquid film} * \text{Density of water}}$$

Also, two techniques, Bubble Streak Tracking (BST) and Thin Film Particle Image Velocimetry (TFPIV), have been developed by Kopplin (2004) in horizontal annular flow to measure local film velocity. The BST technique determines the liquid velocity by measuring reflected light streaks from the bubbles within the liquid film. The TFPIV technique applies a typical micro-PIV system to a macroscopic flow with the addition of a non-trivial image processing algorithm. Setups of these two systems are shown below. BST and TFPIV will be evaluated in the near future for film velocity measurement.

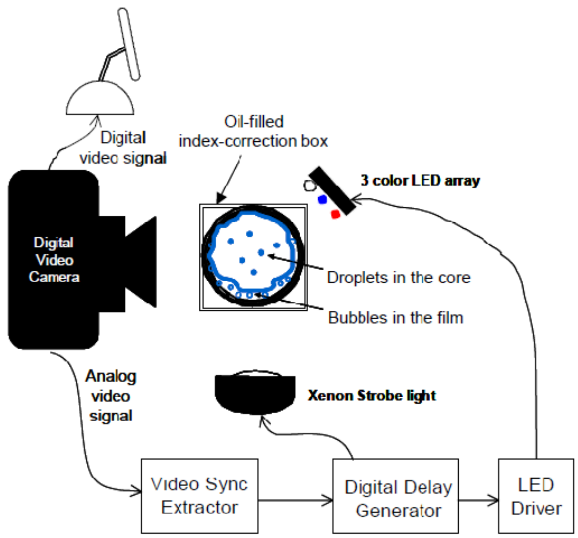

Fig. 13: Schematic of BST Measurement System

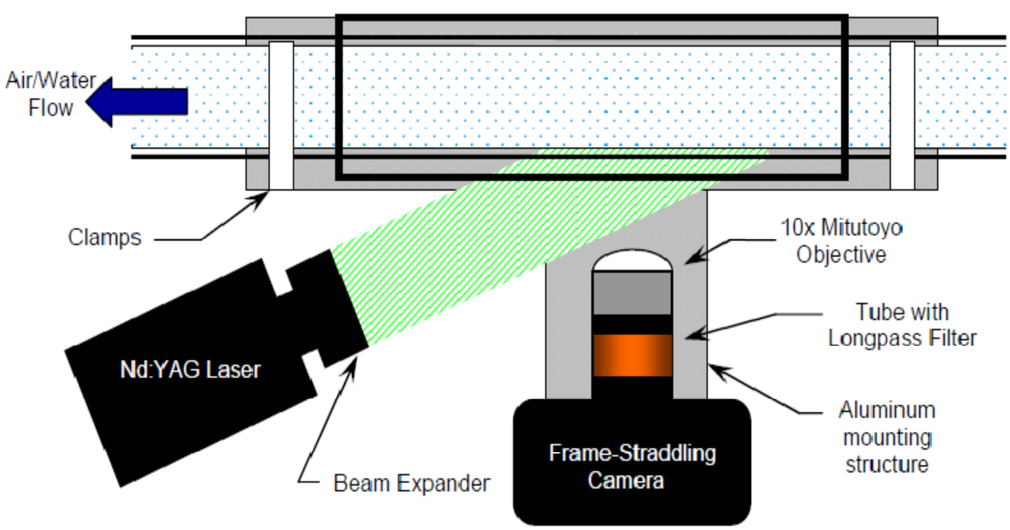

Fig. 14: TFPIV measurement system setup

Near Future Tasks

The main tasks in the near future include:

- Facility modification
  - Run simple test
  - Instrumentation installation
- Preliminary testing

Nomenclature

ID	=	Internal diameter of the pipe
v	=	Velocity [m/s]
C_d	=	Drag coefficient
d_d	=	Droplet diameter [mm]
ρ	=	Density [kg/m^3]
σ	=	Interfacial tension [N/m]
g	=	Gravitational constant [m/s^2]
μ	=	Viscosity [Pa·s]
θ	=	Inclination angle [degree]

Subscripts

g	=	Gas
l	=	Liquid
critical	=	Critical velocity for liquid unloading
SG	=	Superficial gas
SL	=	Superficial liquid

References

Coleman, S.B., Clay, H.B., McCurdy, D.G., and Lee Norris, H. III (1991): "A New Look at Predicting Gas-Well Load Up," J. Pet. Tech., March 1991, 329-333.

Belfroid, S.P.C., Schiferli, W., Alberts, G.J.N., Veeken, C.A.M. and Biezen, E.: "Prediction Onset and Dynamic Behavior of Liquid Loading Gas Wells," SPE paper 115567 presented at 2008 SPE ATCE, Denver, CO, 21-24 September 2008.

Girija, E.G: "Experimental Study of Gas-Liquid Flow through a Tubing-Casing Annulus with Application to Natural Gas Wells," M.S. Thesis, Colorado School of Mines (2006)

Kopplin, C.R.: "Local Liquid Velocity Measurements in Horizontal, Annular Two-Phase Flow," M.S. Thesis, University of Wisconsin-Madison (2004).

Solomon F.A., Falcone G. and Teodoriu C. (2008): "Critical Review of Existing Solutions to Predict and Model Liquid Loading in Gas Wells", SPE paper 115933 presented at SPE ATCE held in Denver, Colorado, USA, 21–24 September 2008.

Toma, P., Vegas E., Kuru E., "Prediction of Slug to Annular Flow Pattern Transition (STA) for Reducing the Risk of Gas-Lift Instabilities and Effective Gas/Liquid Transport for Low-Pressure Reservoirs", SPE Production & Operations November 2007.

Turner, R.G., Hubbard, M.G., and Dukler, A.E. (1969): "Analysis and Prediction of Minimum Flow Rate for the Continuous Removal of Liquids from Gas Wells," J. Pet. Tech., Nov. 1969, 1475-1482.

Van't Westende, J.M.C, Kemp, H.K., Belt, R.J. and Portela, L.M.: "On the Role of Droplets in Cocurrent Annular and Churn-Annular Pipe Flow," International Journal of Multiphase Flow 33 (2007) 595–615.

Veeken K., Hu B. and Schiferli W., (2009): "Transient Multiphase Flow Modeling of Gas Well Liquid Loading," SPE paper 123657 presented at SPE Offshore Europe Oil & Gas Conference & Exhibition held in Aberdeen, UK, 8–11 September 2009.

Fluid Flow Projects

Business Report

Cem Sarica

Advisory Board Meeting, November 3, 2010

Membership and Collaboration Status

- Current Membership Status
  - Membership Stands at 14
    - 13 Industrial and MMS
- Efforts Continue to Increase TUFFP Membership
  - PEMEX Looking for New Funding Mechanism
  - Aspen Tech.
  - Saudi Aramco and BHP is Pursued
- Collaboration with Seoul National University
  - Visiting Research Scholar and Financial Contribution

Personnel Changes

- Dr. Abdel Al-Sarkhi Rejoins TUFFP Team as Visiting Associate Professor
- Dr. Michelle Li Resigns Due to Family Reasons
- Search is Underway for Dr. Li's Replacement
  - Several Applications

Publications and Papers

- Yu, T., Li, M., Zhang, H. Q., and Sarica, C: "A Mechanistic Model for Gas/Liquid Flow in Upward Vertical Annuli," *SPE Production & Operations Journal* August 2010.
- Gokcal, B., Al-Sarkhi, A. S., Sarica, C., and Al-Safran, M. E.: "Prediction of Slug Frequency for High Viscosity Oils in Horizontal Pipes," *SPE Journal Project Facilities & Construction* September 2010.
- Alsarkhi, A. and Sarica, C.: "New Dimensionless Parameters and a Power Law Correlation for Pressure Drop of Gas-Liquid Flows in Horizontal Pipelines," To Be Published in SPE Journal Project Facilities & Construction 2010.

Publications and Papers …

- Ben-Mansour, R., Sharma, A. K., Jeyachandra, B. C., Gokcal, B., Alsarkhi, A., Sarica, C.: "Effect of Pipe Diameter and High Oil Viscosity on Drift Velocity for Horizontal Pipes," 7th North American Conference on Multiphase Technology, June 2 – 4, 2010, Banff, Canada.
- Zhang, H. Q., and Sarica, C.: "A Model for Wetted Wall Fraction and Gravity Center of Liquid Film in Gas-liquid Pipe Flow," 7th North American Conference on Multiphase Technology, June 2 – 4, 2010, Banff, Canada.
- Magrini, K., Alsarkhi, A., Sarica, C., and Zhang, H. Q.: "Liquid Entrainment in Annular Gas/Liquid Flow in Inclined Pipes," SPE 134765, Presented at 2010th SPE Annual Technical Conference and Exhibition, Florence, Italy, September 19-22, 2010.

Next Advisory Board Meetings

- Tentative Schedule
  - April 12, 2011
    - TUHOP Meeting
    - TUFFP Workshop
    - Facility Tour
    - TUHOP/TUHFP/TUFFP Reception
  - April 13, 2011
    - TUFFP Meeting
    - TUFFP/TUPDP Dinner
  - April 14, 2011
    - TUPDP Meeting
- Venue is The University of Tulsa

Financial Report

- Year 2010 Update
  - TUFFP Industrial Account
  - TUFFP MMS Account
- Year 2011 Proposed
  - TUFFP Industrial Account
  - TUFFP MMS Account

2010 Industrial Account Summary

(Prepared October 26, 2010)

Anticipated Reserve Fund Balance on January 1, 2010		**($9,041)**
Income for 2010		
	2010 Anticipated Membership Fees (13 @ $48,000 - exludes MMS)	**624,000**
	Facility Utilization Fee (SNU)	**55,000**
Total Budget		**$ 669,959**

Projected Budget/Expenditures for 2010

		Projected Budget	Revised Budget April 2010	2010 Expenditures
90101 - 90103	Faculty Salaries	29,074.14	918.10	981.10
90600 - 90609	Professional Salaries	47,628.54	53,310.06	52,114.93
90700 - 90703	Staff Salaries	35,262.50	35,291.52	35,434.94
91000	Student Salaries - Monthly	41,550.00	43,725.00	51,150.00
91100	Student Salaries - Hourly	15,000.00	10,000.00	6,987.72
91800	Fringe Benefits	38,068.16	30,986.49	30,602.99
92102	Fringe Benefits (Students)			2,356.00
81801	Tuition & Student Fees	17,898.00	26,637.00	27,296.00
81806	Fellowship			-
92102	Student Fringe		1,762.00	2,356.00
93100	General Supplies	3,000.00	3,000.00	2,000.00
93101	Research Supplies	50,000.00	60,000.00	113,257.46
93102	Copier/Printer Supplies	500.00	500.00	65.00
93104	Computer Software	4,000.00	3,000.00	1,963.11
93106	Office Supplies	2,000.00	2,000.00	1,036.27
93200	Postage and Shipping	500.00	500.00	457.80
93300	Printing and Duplicating	2,000.00	2,000.00	2,087.67
93400	Telecommunications	3,000.00	1,700.00	1,658.66
93500	Membership	1,000.00	1,000.00	204.00
93601	Travel - Domestic	10,000.00	10,000.00	4,199.42
93602	Travel - Foreign	10,000.00	10,000.00	4,247.75
93700	Entertainment	10,000.00	10,000.00	8,917.82
94813	Outside Services	20,000.00	20,000.00	81,549.00
95103	Equipment Rental			18,109.12
95200	F&A (55.6%)	93,694.44	79,679.07	78,801.46
98901	Employee Recruiting	3,000.00		
99001	Equipment	200,000.00	257,868.00	72,192.51
99002	Computers	8,000.00	-	9,118.03
99300	Bank Charges	40.00	40.00	30.00
Total Anticipated Expenditures		**645,215.78**	**663,917.24**	**609,174.76**

Anticipated Reserve as of 12/31/10 **60,783.86**

Salaries are calculated through December 31, 2010

2010 BOEMRE (Formerly MMS) Account Summary

(Prepared October 25, 2010)

Reserve Balance as of 12/31/09			**16,805.82**
2010 Budget			**48,000.00**
Total Budget			**64,805.82**

Projected Budget/Expenditures for 2010

		Budget	2010 Expenditures
91000	Students - Monthly	27,900.00	31,900.00
91202	Student Fringe Benefits		1,160.00
95200	F&A	15,512.40	18,964.27
Total Anticipated Expenditures as of 12/31/10		**43,412.40**	**52,024.27**

Total Anticipated Reserve Fund Balance as of 12/31/10 **12,781.55**

2011 Industrial Account Projections

(Prepared October 26, 2010)

Anticipated Reserve Fund Balance on January 1, 2011		**$60,783.00**
Income for 2011		
	2011 Anticipated Membership Fees (13 @ $55,000 - excludes MMS)	**$715,000.00**
	Facility Utilization Fee (SNU)	**$55,000.00**
	Contract Project Income	**$24,958.00**
Total Income		**$855,741.00**
2011 Anticipated Expenditures		**Projected Budget**
90101-90103	Faculty Salaries	38,481.88
90600-90609	Professional Salaries	71,906.23
90700-90703	Staff Salaries	28,306.09
91000	Graduate Students	43,950.00
91100	Undergraduate Students	15,000.00
91800	Fringe Benefits (35%)	48,542.97
93100	General Supplies	3,000.00
93101	Research Supplies	100,000.00
93102	Copier/Printer Supplies	500.00
93104	Computer Software	4,000.00
93106	Office Supplies	2,000.00
93200	Postage/Shipping	500.00
93300	Printing/Duplicating	2,000.00
93400	Telecommunications	3,000.00
93500	Memberships/Subscriptions	1,000.00
93601	Travel - Domestic	10,000.00
93602	Travel - Foreign	10,000.00
93700	Entertainment (Advisory Board Meetings)	10,000.00
81801	Tuition/Student Fees	0.00
94803	Consultants	0.00
94813	Outside Services	20,000.00
95200	Indirect Costs (52.4%)	103,565.56
98901	Employee Recruiting	3,000.00
99001	Equipment	250,000.00
99002	Computers	8,000.00
99300	Bank Charges	40.00
	Total Expenditures	**$776,792.74**
Anticipated Reserve Fund Balance on December 31, 2011		**$78,948.26**

2011 BOEMRE Account Projections

(Prepared October 26, 2010)

Account Balance - January 1, 2011		**$12,781.55**
Income for 2011		
	2011 Membership Fee	**$48,000.00**
Remaining Balance		**$60,781.55**
2009 Anticipated Expenditures		**Projected Budget**
90101-90103	Faculty Salaries	-
90600-90609	Professional Salaries	-
90700-90703	Staff Salaries	-
91000	Graduate Students	29,000.00
92102	Student Fringe Benefits (8%)	2,320.00
95200	Indirect Costs (52.4%)	15,196.00
	Total Expenditures	**$46,516.00**
Anticipated Reserve Fund Balance on December 31, 2011		**$14,265.55**

History – Membership

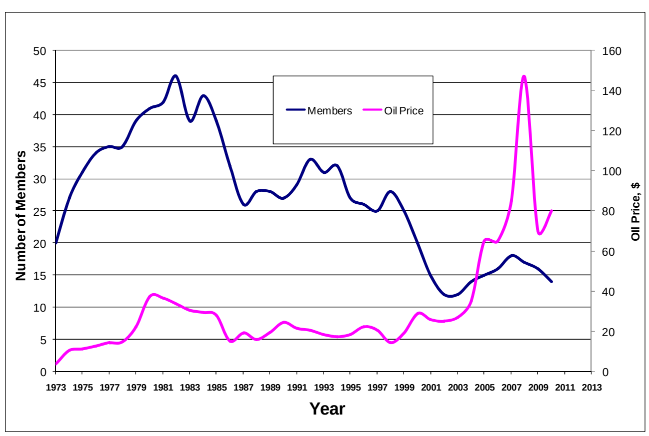

History – Membership Fees

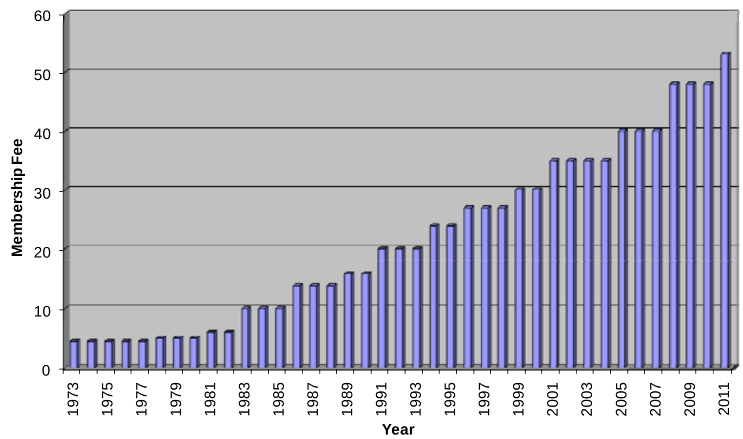

Fluid Flow Projects

Advisory Board Meeting, November 3, 2010

History - Expenditures

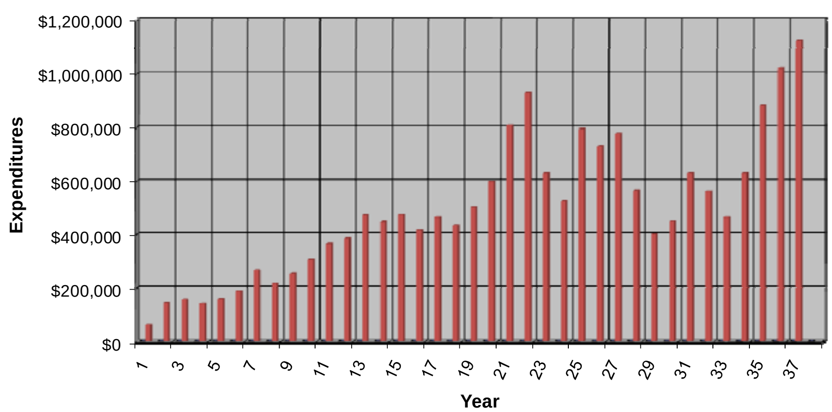

Fluid Flow Projects

Advisory Board Meeting, November 3, 2010

Membership Fees

- 2010 Membership Dues
  - 1 Unpaid (Will be Received Soon)

Fluid Flow Projects

Advisory Board Meeting, November 3, 2010

Introduction

This semi-annual report is submitted to Tulsa University Fluid Flow Projects (TUFFP) members to summarize activities since the May 12, 2010 Advisory Board meeting and to assist in planning for the next six months. It also serves as a basis for reporting progress and generating discussion at the 75th semi-annual Advisory Board meeting to be held in Chouteau Room of Allen Chapman Activity Center (ACAC) of the University of Tulsa Main Campus, ACAC 440 South Gary, Tulsa, Oklahoma on Wednesday, November 3, 2010.

The activities will start with Tulsa University High Viscosity Projects (TUHOP) Advisory Board meeting on November 2, 2010 between 8:15 a.m. and noon in Gallery Room of ACAC. Between 1:00 and 3:00 p.m. on November 2, 2010, there will be TUFFP workshop in the same room. There will be presentations made by TUFFP member companies. A facility tour will be held on November 2, 2010 between 3:30 and 5:30 p.m. Following the tour, there will be a TUHOP/TUHFP/TUFFP reception between 6:00 and 9:30 p.m. in Atrium of ACAC. TUFFP Advisory Board meeting will convene at 8:00 a.m. on November 3rd and will adjourn at approximately 5:00 p.m. Following the meeting, there will be a joint TUFFP/TUPDP dinner between 6:00 and 9:00 p.m. in Atrium of ACAC.

The Tulsa University Paraffin Deposition Projects (TUPDP) Advisory Board meeting will be held on November 4th in Chouteau Room, between 8:00 a.m. and 1:15 p.m.

The reception and the dinner will provide an opportunity for informal discussions among members, guests, and TU staff and students.

Several TUFFP/TUPDP/TUHOP facilities will be operating during the tour. An opportunity will also be available to view the hydrate flow loop.

The following dates have tentatively been established for Spring 2011 Advisory Board meetings. The venue for Spring 2011 Advisory Board meetings is tentatively set to be the University of Tulsa Main Campus.

2011 Spring Meetings

April 12, 2011	Tulsa University High Viscosity Oil Projects (TUHOP) JIP Meeting
	Tulsa University Fluid Flow Projects (TUFFP) Workshop
	Facility Tour
	TUHOP/TUHFP/TUFFP Reception
April 13, 2011	Tulsa University Fluid Flow Projects (TUFFP) Advisory Board Meeting
	TUFFP/TUPDP Reception
April 14, 2011	Tulsa University Paraffin Deposition Projects (TUPDP) Advisory Board Meeting

Personnel

Dr. Cem Sarica, Professor of Petroleum Engineering, continues as Director of TUFFP and TUPDP, and as Co-Principal Investigator of TUHFP and TUHOP.

Dr. Holden Zhang, Associate Professor of Petroleum Engineering, serves as Principal Investigator of TUHOP and Associate Director of TUFFP.

Dr. Brill continues to be involved as the director emeritus on a voluntary basis.

Dr. Abdel Al-Sarkhi of King Fahd University of Petroleum and Minerals, former TUFFP Research Associate, was employed as Research Associate Professor during summer of 2010.

Dr. Mingxiu (Michelle) Li has served as a Research Associate for TUHOP and TUFFP. Dr. Li resigned effective August 2010 due to her family obligations. A search is underway to find her replacement.

Mr. Scott Graham continues to serve as Project Engineer. Scott oversees all of the facility operations and continues to be the senior electronics technician for TUFFP, TUPDP, and TUHOP.

Mr. Craig Waldron continues as Research Technician, addressing our needs in mechanical areas. He also serves as a flow loop operator for TUPDP and Health, Safety, and Environment (HSE) officer for TUFFP, TUPDP and TUHOP.

Mr. Brandon Kelsey serves as an electro-mechanical technician serving TUFFP, TUPDP, and TUHOP projects.

Ms. Linda Jones continues as Project Coordinator of TUFFP, TUPDP and TUHOP projects. She keeps the project accounts in addition to other responsibilities such as external communications, providing computer support for graduate students, publishing and distributing all research reports and deliverables, managing the computer network and web sites, and supervision of part-time office help.

Ms. Lori Watts of Petroleum Engineering is the web master for TUFFP/TUPDP/TUHOP websites.

Table 1 updates the current status of all graduate students conducting research on TUFFP projects for the last six months.

Ms. Ceyda Kora has successfully completed her MS studies with her MS thesis defense titled “Effects of High Oil Viscosity on Liquid Slug Holdup” in September 2010. She is currently employed by Schlumberger in Houston, TX.

Mr. Kiran Gawas, from India, is pursuing his Ph.D. degree in Petroleum Engineering. Kiran has a BS degree in Chemical Engineering from University of Mumbai, Institute of Chemical Technology and a Master of Technology degree from Indian Institute of Technology (IITB). He is studying Low Liquid Loading Three-phase Flow. Kiran has successfully passed his Ph.D. qualifying examinations allowing him to continue his Ph.D. studies. He has received the highest score amongst his peers.

Mr. Benin (Ben) Chelinsky Jeyachandra, from India, is pursuing his MS degree in Petroleum Engineering. Ben has received a BS degree in Chemical Engineering from Birla Institute of Technology and Science University in 2008. Ben is studying the high oil viscosity multiphase flow.

Mr. Ge (Max) Yuan, from Peoples Republic of China (PRC), is pursuing his MS degree in Petroleum Engineering. Max has received a BS degree in Chemical Engineering and Technology from Dalian University of Technology in 2009. Max is studying Liquid Loading in Gas Wells.

Three new graduate students, Ms. Mujgan Guner, from Turkey, Ms. Rosmer Brito from Venezuela, and Ms. Wei Zheng from PRC have recently joined TUFFP team as a Research Assistants.

Ms. Mujgan Guner has dual BS degrees in Petroleum and Mechanical Engineering from Middle East Technical University, Turkey. She is pursuing Ph.D. in Petroleum Engineering. Mujgan is assigned to high pressure effects on multiphase flow project.

Ms. Rosmer Brito has petroleum engineering BS degree from La Universidad del Zulia. She has worked as production technologist for Petroregional del Lago (Joint Venture PDVSA and Shell Venezuela) for over three years before joining TU. Rosmer has received prestigious Fulbright Scholarship to study abroad. Rosmer is pursuing and MS degree in petroleum engineering. She is assigned to high viscosity two-phase flow project.

Ms. Wei Zheng has a BS degree in petroleum engineering from China Petroleum University in Beijing. Wei is currently one of the teaching assistants in Petroleum Engineering Department at TU. She is pursuing her MS degree in Petroleum Engineering. Her research project will be determined after the fall 2010 Advisory Board meeting.

Mr. Jinho Choi and Mr. Hoyoung Lee will participate in two of the TUFFP projects as part of the research collaboration between Seoul National University (SNU) and TUFFP. Mr. Choi and Mr. Lee are Ph.D. candidates in the department of Energy Resources Engineering at SNU.

A list of all telephone numbers and e-mail addresses for TUFFP personnel are given in Appendix D.

Table 1

2010 Fall Research Assistant Status

Name	*Origin*	*Stipend*	*Tuition*	*Degree Pursued*	*TUFFP Project*	*Completion Date*
Ceyda Kora	Turkey	Yes – TUFFP	Waived (BOEMRE)	MS – PE	Effects of High Viscosity Oil on Liquid Slug Holdup	Fall 2010
Kiran Gawas	India	Yes – TUFFP	Waived (TU)	Ph.D. – PE	Three-phase Gas-Oil-Water Low Liquid Loading	Fall 2012
Benin (Ben) Chelinsky Jeyachandra	India	Yes – TUFFP	Waived (BOEMRE)	MS – PE	High Viscosity Oil and Gas Flow in Inclined Pipes	Fall 2011
Ge Yuan	PRC	Yes – TUFFP	Yes – TUFFP	MS – PE	Liquid Unloading from Gas Wells	Fall 2011
Mujgan Guner	Turkey	Yes – TUFFP	Waived – (TU)	Ph.D. – PE	Up-scaling Studies in Two-phase Flow	Spring 2015
Rosmer Brito	Venezuela	No – Fulbright	No – Fulbright	MS – PE	High Viscosity Oil Two-phase Flow	Spring 2012
Wei Zheng	PRC	Partial – TU	Waived – (TU)	MS – PE	TBD	Fall 2012

Membership

The current membership of TUFFP stands at 13 industrial members and Bureau of Ocean Energy Management, Regulation, and Enforcement (BOEMRE) formerly, MMS of Department of Interior (MMS).

Our efforts to increase the TUFFP membership level continues.

Table 2 lists all the current 2010 TUFFP members. A list of all Advisory Board representatives for these members with pertinent contact information appears in Appendix B. A detailed history of TUFFP membership is given in Appendix C.

A collaboration agreement has recently been signed with Seoul National University for a three-year period with possible two-year extension. Through the collaboration TUFFP will receive about $110,000/year and visiting research scholars.

Table 2

2010 Fluid Flow Projects Membership

Baker Atlas	KOC
BOEMRE	Marathon Oil Company
BP Exploration	Petrobras
Chevron	Schlumberger
ConocoPhillips	Shell Global Solutions
Exxon Mobil	SPT
JOGMEG	Total

Equipment and Facilities Status

Test Facilities

The 6 in. ID High Pressure Facility construction is underway. Our aim is to complete the construction within the first quarter of 2011. There has been a significant progress in the construction of the facility. Most of the piping has been completed.

High viscosity oil-gas facility has been inclined for the current high viscosity oil project.

A new capacitance sensor was developed and implemented. The new sensor can cover the entire cross section of the pipe. It has been successfully been tested and will be utilized first in High Viscosity Oil project.

Severe Slugging facility will soon be modified for the liquid unloading project from gas wells. The modifications involve incorporation of proper instruments on the test section.

Low liquid loading facility has also been inclined and readied to conduct upward and downward inclined low liquid loading testing.

Detailed descriptions of these modification efforts appear in a progress presentation given in this brochure. A site plan showing the location of the various TUFFP and TUPDP test facilities on the North Campus is given in Fig. 1.

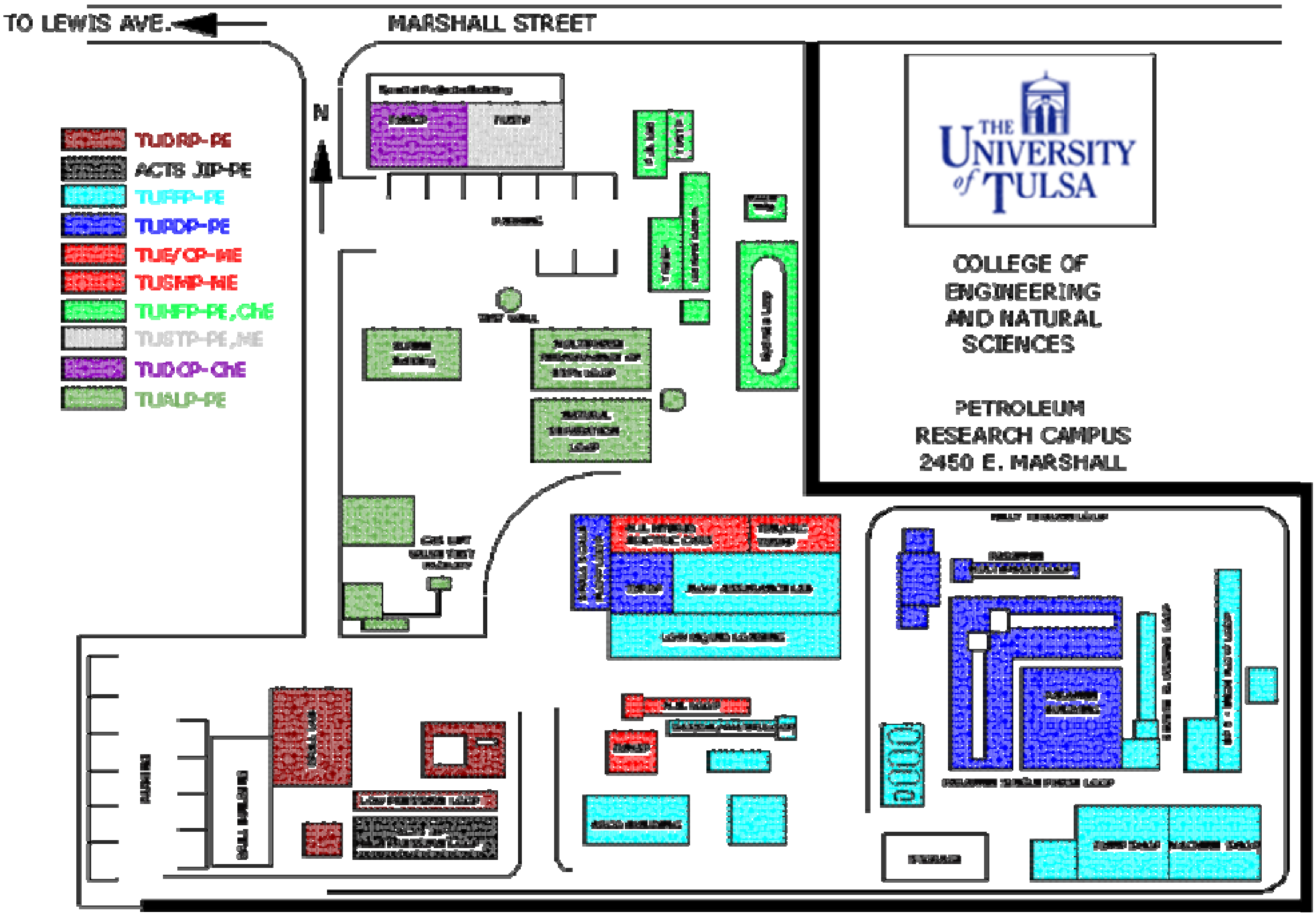

Figure 1 – Site Plan for the North Campus Research Facilities

Financial Status

TUFFP maintains separate accounts for industrial and U.S. government members. Thus, separate accounts are maintained for the Bureau of Ocean Energy Management, Regulation, and Enforcement (BOEMRE) formerly, MMS funds.

As of October 26, 2010, 13 of the 14 TUFFP members had paid their 2010 membership fees. We expect the payment soon.

Table 3 presents a financial analysis of income and expenditures for the 2010 Industrial member account as of October 26, 2010. Also shown are previous 2010 budgets that have been reported to the members. The total industry expenditures for 2010 are estimated to be $609,174.76. This results in an estimated carryover of $60,783.86 to 2011 fiscal year.

Table 4 presents a financial analysis of expenditures and income for the BOEMRE Account for 2010. This account is used primarily for graduate student stipends. A balance of $12,781.55 is anticipated to carry over to 2011.

The University of Tulsa waives up to 19 hours of tuition for each graduate student that is paid a stipend from the United States government, BOEMRE funds. Moreover, The University of Tulsa has granted tuition waiver for one Ph.D. student. A total of 54 hours of tuition (equivalent of $50,000) were waived for 2010.

Tables 5-6 present the proposed budgets and income for the Industrial, and BOEMRE accounts for 2011. The 2011 TUFFP industrial membership is assumed to stay at 13 in this analysis. This will provide $715,000.00 of industrial membership income for 2011. In addition TUFFP receives facility utilization fee from SNU and contract project income totaling $79,958.00. The total of the 2011 income and the reserve account is projected to be $855,741.00. The expenses for the industrial member account are estimated to be $776,792.74 leaving a carryover balance of $78,948.26. The BOEMRE account is expected to have a carryover of $14,265.55 to 2012.

Table 3: TUFFP 2010 Industrial Budget Summary

(Prepared October 26, 2010)

Anticipated Reserve Fund Balance on January 1, 2010					**($9,041)**
Income for 2010					
	2010 Anticipated Membership Fees (13 @ $48,000 - exludes MMS)				**624,000**
	Facility Utilization Fee (SNU)				**55,000**
Total Budget				**$**	**669,959**

Projected Budget/Expenditures for 2010

		Projected Budget	**Revised Budget April 2010**	**2010 Expenditures**
90101 - 90103	Faculty Salaries	29,074.14	918.10	981.10
90600 - 90609	Professional Salaries	47,628.54	53,310.06	52,114.93
90700 - 90703	Staff Salaries	35,262.50	35,291.52	35,434.94
91000	Student Salaries - Monthly	41,550.00	43,725.00	51,150.00
91100	Student Salaries - Hourly	15,000.00	10,000.00	6,987.72
91800	Fringe Benefits	38,068.16	30,986.49	30,602.99
92102	Fringe Benefits (Students)			2,356.00
81801	Tuition & Student Fees	17,898.00	26,637.00	27,296.00
81806	Fellowship			-
92102	Student Fringe		1,762.00	2,356.00
93100	General Supplies	3,000.00	3,000.00	2,000.00
93101	Research Supplies	50,000.00	60,000.00	113,257.46
93102	Copier/Printer Supplies	500.00	500.00	65.00
93104	Computer Software	4,000.00	3,000.00	1,963.11
93106	Office Supplies	2,000.00	2,000.00	1,036.27
93200	Postage and Shipping	500.00	500.00	457.80
93300	Printing and Duplicating	2,000.00	2,000.00	2,087.67
93400	Telecommunications	3,000.00	1,700.00	1,658.66
93500	Membership	1,000.00	1,000.00	204.00
93601	Travel - Domestic	10,000.00	10,000.00	4,199.42
93602	Travel - Foreign	10,000.00	10,000.00	4,247.75
93700	Entertainment	10,000.00	10,000.00	8,917.82
94813	Outside Services	20,000.00	20,000.00	81,549.00
95103	Equipment Rental			18,109.12
95200	F&A (55.6%)	93,694.44	79,679.07	78,801.46
98901	Employee Recruiting	3,000.00		
99001	Equipment	200,000.00	257,868.00	72,192.51
99002	Computers	8,000.00	-	9,118.03
99300	Bank Charges	40.00	40.00	30.00
Total Anticipated Expenditures		**645,215.78**	**663,917.24**	**609,174.76**

Anticipated Reserve as of 12/31/10	**60,783.86**

Salaries are calculated through December 31, 2010

Table 4: TUFFP 2010 BOEMRE Budget Summary

(Prepared October 25, 2010)

Reserve Balance as of 12/31/09				**16,805.82**
2010 Budget				**48,000.00**
Total Budget				**64,805.82**

Projected Budget/Expenditures for 2010

		Budget	**2010 Expenditures**	
91000	Students - Monthly	27,900.00	31,900.00	
91202	Student Fringe Benefits		1,160.00	
95200	F&A	15,512.40	18,964.27	
Total Anticipated Expenditures as of 12/31/10		**43,412.40**	**52,024.27**	
Total Anticipated Reserve Fund Balance as of 12/31/10				**12,781.55**

Table 5: Proposed 2011 TUFFP Industrial Budget

(Prepared October 26, 2010)

Anticipated Reserve Fund Balance on January 1, 2011		**$60,783.00**
Income for 2011		
	2011 Anticipated Membership Fees (13 @ $55,000 - excludes MMS)	**$715,000.00**
	Facility Utilization Fee (SNU)	**$55,000.00**
	Contract Project Income	**$24,958.00**
Total Income		**$855,741.00**
2011 Anticipated Expenditures		**Projected Budget**
90101-90103	Faculty Salaries	38,481.88
90600-90609	Professional Salaries	71,906.23
90700-90703	Staff Salaries	28,306.09
91000	Graduate Students	43,950.00
91100	Undergraduate Students	15,000.00
91800	Fringe Benefits (35%)	48,542.97
93100	General Supplies	3,000.00
93101	Research Supplies	100,000.00
93102	Copier/Printer Supplies	500.00
93104	Computer Software	4,000.00
93106	Office Supplies	2,000.00
93200	Postage/Shipping	500.00
93300	Printing/Duplicating	2,000.00
93400	Telecommunications	3,000.00
93500	Memberships/Subscriptions	1,000.00
93601	Travel - Domestic	10,000.00
93602	Travel - Foreign	10,000.00
93700	Entertainment (Advisory Board Meetings)	10,000.00
81801	Tuition/Student Fees	0.00
94803	Consultants	0.00
94813	Outside Services	20,000.00
95200	Indirect Costs (52.4%)	103,565.56
98901	Employee Recruiting	3,000.00
99001	Equipment	250,000.00
99002	Computers	8,000.00
99300	Bank Charges	40.00
	Total Expenditures	**$776,792.74**
Anticipated Reserve Fund Balance on December 31, 2011		**$78,948.26**

Table 6: Proposed TUFFP 2011 BOEMRE Budget

(Prepared October 26, 2010)

Account Balance - January 1, 2011		**$12,781.55**
Income for 2011		
	2011 Membership Fee	**$48,000.00**
Remaining Balance		**$60,781.55**
2009 Anticipated Expenditures		**Projected Budget**
90101-90103	Faculty Salaries	-
90600-90609	Professional Salaries	-
90700-90703	Staff Salaries	-
91000	Graduate Students	29,000.00
92102	Student Fringe Benefits (8%)	2,320.00
95200	Indirect Costs (52.4%)	15,196.00
	Total Expenditures	**$46,516.00**
Anticipated Reserve Fund Balance on December 31, 2011		**$14,265.55**

Miscellaneous Information

TU Announces Major Gift for Petroleum Engineering

Jeffrey J. McDougall, President and founder of Oklahoma City-based JMA Energy Company, on Oct. 13 announced his strategic investment in the Petroleum Engineering program in the College of Engineering and Natural Science.

McDougall's gift will underwrite a director to lead the school and engage stakeholders. It also will establish the Dr. Kermit Brown Endowment Fund to support faculty through salary supplements, research incentives, and future initiatives to advance the school. To honor his support, the university has renamed the program the McDougall School of Petroleum Engineering.

Fluid Flow Projects Short Course

The 34th TUFFP "Two-Phase Flow in Pipes" short course was taught May 17-21, 2010 for 10 people from 6 different companies.

The 35th TUFFP "Two-Phase Flow in Pipes" short course offering is scheduled for May 16-20, 2011. For this short course to be self sustaining, at least 10 enrollees are needed. We urge our members to let us know soon if they plan to enroll people in the short course.

Cem Sarica Receives SPE 2010 International Production and Operations Award

The Production and Operations Award of the Society of Petroleum Engineers recognizes outstanding achievement or contributions to the advancement of petroleum engineering in the area of production and operations technology. Cem is the third TU petroleum engineering faculty receiving this award after Jim Brill (1994) and Ovadia Shoham (2003). The award presentation was made at the 2010 SPE ATCE.

Dr. Abdel Al-Sarkhi Returns to TUFFP

Dr. Abdel Al-Sarkhi has spend very productive 2 ½ months with TUFFP. During his stay he has helped TUFFP graduate students and worked on the droplet homophase project concentrating on the analysis of the film and entrainment fraction data acquired by Kyle Magrini. We would like to have him spend summers in Tulsa working with TUFFP Research Assistants and Associates in the future.

BHR Group Conference on Multiphase Technology

Since 1991, TUFFP has participated as a co-supporter of BHR Group Conferences on Multiphase Production. TUFFP personnel participate in reviewing papers, serving as session chairs, and advertising the conference to our members. This conference is one of the premier international event providing delegates with opportunities to discuss new research and developments, to consider innovative solutions in multiphase production area.

7th North American Conference on Multiphase Technology, sponsored and supported by Neotechnology Consultants of Calgary, Canada, sponsored by Bornemann Pumps Kongsberg and SPT Group and supported by TUFFP, was held 2-4 of June 2010 in Banff, Canada. Two technical paper presentations based on TUFFP research were made.

15th International Conference on Multiphase Technology, supported by IFP, IFE, NEOTEC and TUFFP, will be held 15-17 of June 2011 in Cannes, France. The conference will benefit anyone engaged in the application, development and research of multiphase technology for the oil and gas industry. Applications in the oil and gas industry will also be of interest to engineers from other industries for which multiphase technology offers a novel solution to their problems. The conference will also be of particular value to designers, facility and operations engineers, consultants and researchers from operating, contracting, consultancy and technology companies. The conference brings together experts from across the American Continents and Worldwide. The detailed information about the conference can be found in BHRg's (www.brhgroup.com).

Publications & Presentations

Since the last Advisory Board meeting, the following publications and presentations are made.

1) Yu, T., Li, M., Zhang, H. Q., and Sarica, C: "A Mechanistic Model for Gas/Liquid Flow in Upward Vertical Annuli," *SPE Production & Operations Journal* August 2010.
2) Gokcal, B., Al-Sarkhi, A. S., Sarica, C., and Al-Safran, M. E.: "Prediction of Slug Frequency for High Viscosity Oils in Horizontal Pipes," *SPE Journal Project Facilities & Construction* September 2010.

3) Alsarkhi, A. and Sarica, C.: "New Dimensionless Parameters and a Power Law Correlation for Pressure Drop of Gas-Liquid Flows in Horizontal Pipelines," To Be Published in SPE Journal Project Facilities & Construction 2010.
4) Ben-Mansour, R., Sharma, A. K., Jeyachandra, B. C., Gokcal, B., Alsarkhi, A., Sarica, C.: "Effect of Pipe Diameter and High Oil Viscosity on Drift Velocity for Horizontal Pipes," 7th North American Conference on Multiphase Technology, June 2 – 4, 2010, Banff, Canada.
5) Zhang, H. Q., and Sarica, C.: "A Model for Wetted Wall Fraction and Gravity Center of Liquid Film in Gas-liquid Pipe Flow," 7th North American Conference on Multiphase Technology, June 2 – 4, 2010, Banff, Canada.
6) Magrini, K., Alsarkhi, A., Sarica, C., and Zhang, H. Q.: "Liquid Entrainment in Annular Gas/Liquid Flow in Inclined Pipes," SPE 134765, Presented at 2010th SPE Annual Technical Conference and Exhibition, Florence, Italy, September 19-22, 2010.

Tulsa University Paraffin Deposition Projects (TUPDP) Activities

The forth three year phase of TUPDP has recently started. The studies concentrate on the paraffin deposition characterization of single-phase turbulent flow with new oils, gas-oil-water paraffin deposition, restart of gelled flow lines and field verification.

Tulsa University Heavy Oil Projects (TUHOP) Activities

TUHOP is an outgrowth of one of the projects initiated through Tulsa University Center of Research Excellence (TUCoRE) initiated by Chevron. Current members of the JIP are BP, Chevron, ConocoPhillips, Petrobras, and Petrochina. The primary objective of the JIP is to investigate the effects of high oil viscosity on multiphase flow behavior.

Tulsa University Foam Flow Conditions (TUFFCP) Joint Industry Project (JIP)

A new JIP is being formed to investigate unloading of vertical gas wells using surfactants for a period of three years. The JIP is funded by Research Partnership to Secure Energy for America (RPSEA), which is an organization managing DOE funds, and various oil and gas operating and service companies. This JIP will utilize some of the TUFFP capabilities. If a member of the JIP is not a member of TUFFP, they will pay a facility utilization fee member equivalent to one year TUFFP membership fee. Current industrial members of the JIP are Chevron, ConocoPhillips, Marathon, and Shell. All are current members of TUFFP.

Two-Phase Flow Calendar

Several technical meetings, seminars, and short courses involving two-phase flow in pipes are scheduled for 2010 and 2011. Table 9 lists meetings that would be of interest to TUFFP members.

Table 9

Meeting and Conference Calendar

2010

November 2	TUHOP Advisory Board Meeting, Tulsa, Oklahoma
	TUFFP Fall Workshop, Tulsa, Oklahoma
	TUHFP Advisory Board Meeting, Tulsa, Oklahoma
November 3	TUFFP Advisory Board Meeting, Tulsa, Oklahoma
November 4	TUPDP Advisory Board Meeting, Tulsa, Oklahoma

2011

March 20 -23	Assuring Flow from Pore to Process (SPE ATW), Langkawi, Malaysia
March 27 – 29	SPE Production and Operations Symposium, Oklahoma City, USA
April 12	TUHOP Advisory Board Meeting, Tulsa, Oklahoma
	TUFFP Fall Workshop, Tulsa, Oklahoma
April 13	TUFFP Advisory Board Meeting, Tulsa, Oklahoma
April 14	TUPDP Advisory Board Meeting, Tulsa, Oklahoma
May 2 - 5	Offshore Technology Conference, Houston, Texas
June 14 – 17	Brasil Offshore Exhibition and Conference, Macae, Brasil
June 15 - 17	BHRg's 15th International Conference on Multiphase Technology, Cannes, France
Sept. 6 – 8	Offshore Europe, Aberdeen UK
Oct. 4 – 6	OTC Brasil, Rio de Janeiro, RJ, Brazil
Oct. 30 – Nov. 2	SPE Annual Technical Conference and Exhibition, Denver, CO, USA

Appendix A

Fluid Flow Projects Deliverables[1]

1. "An Experimental Study of Oil-Water Flowing Mixtures in Horizontal Pipes," by M. S. Malinowsky (1975).

2. "Evaluation of Inclined Pipe Two-Phase Liquid Holdup Correlations Using Experimental Data," by C. M. Palmer (1975).

3. "Experimental Evaluation of Two-Phase Pressure Loss Correlations for Inclined Pipe," by G. A. Payne (1975).

4. "Experimental Study of Gas-Liquid Flow in a Pipeline-Riser Pipe System," by Z. Schmidt (1976).

5. "Two-Phase Flow in an Inclined Pipeline-Riser Pipe System," by S. Juprasert (1976).

6. "Orifice Coefficients for Two-Phase Flow Through Velocity Controlled Subsurface Safety Valves," by J. P. Brill, H. D. Beggs, and N. D. Sylvester (Final Report to American Petroleum Institute Offshore Safety and Anti-Pollution Research Committee, OASPR Project No. 1; September, 1976).

7. "Correlations for Fluid Physical Property Prediction," by M. E. Vasquez A. (1976).

8. "An Empirical Method of Predicting Temperatures in Flowing Wells," by K. J. Shiu (1976).

9. "An Experimental Study on the Effects of Flow Rate, Water Fraction and Gas-Liquid Ratio on Air-Oil-Water Flow in Horizontal Pipes," by G. C. Laflin and K. D. Oglesby (1976).

10. "Study of Pressure Drop and Closure Forces in Velocity- Type Subsurface Safety Valves," by H. D. Beggs and J. P. Brill (Final Report to American Petroleum Institute Offshore Safety and Anti-Pollution Research Committee, OSAPR Project No. 5; July, 1977).

11. "An Experimental Study of Two-Phase Oil-Water Flow in Inclined Pipes," by H. Mukhopadhyay (September 1, 1977).

12. "A Numerical Simulation Model for Transient Two-Phase Flow in a Pipeline," by M. W. Scoggins, Jr. (October 3, 1977).

13. "Experimental Study of Two-Phase Slug Flow in a Pipeline-Riser Pipe System," by Z. Schmidt (1977).

14. "Drag Reduction in Two-Phase Gas-Liquid Flow," (Final Report to American Gas Association Pipeline Research Committee; 1977).

15. "Comparison and Evaluation of Instrumentation for Measuring Multiphase Flow Variables in Pipelines," Final Report to Atlantic Richfield Co. by J. P. Brill and Z. Schmidt (January, 1978).

16. "An Experimental Study of Inclined Two-Phase Flow," by H. Mukherjee (December 30, 1979).

[1] Completed TUFFP Projects – each project consists of three deliverables – report, data and software. Please see the TUFFP website

17. "An Experimental Study on the Effects of Oil Viscosity, Mixture Velocity and Water Fraction on Horizontal Oil-Water Flow," by K. D. Oglesby (1979).

18. "Experimental Study of Gas-Liquid Flow in a Pipe Tee," by S. E. Johansen (1979).

19. "Two Phase Flow in Piping Components," by P. Sookprasong (1980).

20. "Evaluation of Orifice Meter Recorder Measurement Errors in Lower and Upper Capacity Ranges," by J. Fujita (1980).

21. "Two-Phase Metering," by I. B. Akpan (1980).

22. "Development of Methods to Predict Pressure Drop and Closure Conditions for Velocity-Type Subsurface Safety Valves," by H. D. Beggs and J. P. Brill (Final Report to American Petroleum Institute Offshore Safety and Anti-Pollution Research Committee, OSAPR Project No. 10; February, 1980).

23. "Experimental Study of Subcritical Two-Phase Flow Through Wellhead Chokes," by A. A. Pilehvari (April 20, 1981).

24. "Investigation of the Performance of Pressure Loss Correlations for High Capacity Wells," by L. Rossland (1981).

25. "Design Manual: Mukherjee and Brill Inclined Two-Phase Flow Correlations," (April, 1981).

26. "Experimental Study of Critical Two-Phase Flow through Wellhead Chokes," by A. A. Pilehvari (June, 1981).

27. "Experimental Study of Pressure Wave Propagation in Two-Phase Mixtures," by S. Vongvuthipornchai (March 16, 1982).

28. "Determination of Optimum Combination of Pressure Loss and PVT Property Correlations for Predicting Pressure Gradients in Upward Two-Phase Flow," by L. G. Thompson (April 16, 1982).

29. "Hydrodynamic Model for Intermittent Gas Lifting of Viscous Oils," by O. E. Fernandez (April 16, 1982).

30. "A Study of Compositional Two-Phase Flow in Pipelines," by H. Furukawa (May 26, 1982).

31. "Supplementary Data, Calculated Results, and Calculation Programs for TUFFP Well Data Bank," by L. G. Thompson (May 25, 1982).

32. "Measurement of Local Void Fraction and Velocity Profiles for Horizontal Slug Flow," by P. B. Lukong (May 26, 1982).

33. "An Experimental Verification and Modification of the McDonald-Baker Pigging Model for Horizontal Flow," by S. Barua (June 2, 1982).

34. "An Investigation of Transient Phenomena in Two-Phase Flow," by K. Dutta-Roy (October 29, 1982).

35. "A Study of the Heading Phenomenon in Flowing Oil Wells," by A. J. Torre (March 18, 1983).

36. "Liquid Holdup in Wet-Gas Pipelines," by K. Minami (March 15, 1983).

37. "An Experimental Study of Two-Phase Oil-Water Flow in Horizontal Pipes," by S. Arirachakaran (March 31, 1983).

38. "Simulation of Gas-Oil Separator Behavior Under Slug Flow Conditions," by W. F. Giozza (March 31, 1983).

39. "Modeling Transient Two-Phase Flow in Stratified Flow Pattern," by Y. Sharma (July, 1983).

40. "Performance and Calibration of a Constant Temperature Anemometer," by F. Sadeghzadeh (August 25, 1983).

41. "A Study of Plunger Lift Dynamics," by L. Rosina (October 7, 1983).

42. "Evaluation of Two-Phase Flow Pressure Gradient Correlations Using the A.G.A. Gas-Liquid Pipeline Data Bank," by E. Caetano F. (February 1, 1984).

43. "Two-Phase Flow Splitting in a Horizontal Pipe Tee," by O. Shoham (May 2, 1984).

44. "Transient Phenomena in Two-Phase Horizontal Flowlines for the Homogeneous, Stratified and Annular Flow Patterns," by K. Dutta-Roy (May 31, 1984).

45. "Two-Phase Flow in a Vertical Annulus," by E. Caetano F. (July 31, 1984).

46. "Two-Phase Flow in Chokes," by R. Sachdeva (March 15, 1985).

47. "Analysis of Computational Procedures for Multi-Component Flow in Pipelines," by J. Goyon (June 18, 1985).

48. "An Investigation of Two-Phase Flow Through Willis MOV Wellhead Chokes," by D. W. Surbey (August 6, 1985).

49. "Dynamic Simulation of Slug Catcher Behavior," by H. Genceli (November 6, 1985).

50. "Modeling Transient Two-Phase Slug Flow," by Y. Sharma (December 10, 1985).

51. "The Flow of Oil-Water Mixtures in Horizontal Pipes," by A. E. Martinez (April 11, 1986).

52. "Upward Vertical Two-Phase Flow Through An Annulus," by E. Caetano F. (April 28, 1986).

53. "Two-Phase Flow Splitting in a Horizontal Reduced Pipe Tee," by O. Shoham (July 17, 1986).

54. "Horizontal Slug Flow Modeling and Metering," by G. E. Kouba (September 11, 1986).

55. "Modeling Slug Growth in Pipelines," by S. L. Scott (October 30, 1987).

56. "RECENT PUBLICATIONS" - A collection of articles based on previous TUFFP research reports that have been published or are under review for various technical journals (October 31, 1986).

57. "TUFFP <u>CORE</u> Software Users Manual, Version 2.0," by Lorri Jefferson, Florence Kung and Arthur L. Corcoran III (March 1989)

58. "Simplified Modeling and Simulation of Transient Two Phase Flow in Pipelines," by Y. Taitel (April 29, 1988).

59. "RECENT PUBLICATIONS" - A collection of articles based on previous TUFFP research reports that have been published or are under review for various technical journals (April 19, 1988).

60. "Severe Slugging in a Pipeline-Riser System, Experiments and Modeling," by S. J. Vierkandt (November 1988).

61. "A Comprehensive Mechanistic Model for Upward Two-Phase Flow," by A. Ansari (December 1988).

62. "Modeling Slug Growth in Pipelines" Software Users Manual, by S. L. Scott (June 1989).

63. "Prudhoe Bay Large Diameter Slug Flow Experiments and Data Base System" Users Manual, by S. L. Scott (July 1989).

64. "Two-Phase Slug Flow in Upward Inclined Pipes", by G. Zheng (Dec. 1989).

65. "Elimination of Severe Slugging in a Pipeline-Riser System," by F. E. Jansen (May 1990).

66. "A Mechanistic Model for Predicting Annulus Bottomhole Pressures for Zero Net Liquid Flow in Pumping Wells," by D. Papadimitriou (May 1990).

67. "Evaluation of Slug Flow Models in Horizontal Pipes," by C. A. Daza (May 1990).

68. "A Comprehensive Mechanistic Model for Two-Phase Flow in Pipelines," by J. J. Xiao (Aug. 1990).

69. "Two-Phase Flow in Low Velocity Hilly Terrain Pipelines," by C. Sarica (Aug. 1990).

70. "Two-Phase Slug Flow Splitting Phenomenon at a Regular Horizontal Side-Arm Tee," by S. Arirachakaran (Dec. 1990)

71. "RECENT PUBLICATIONS" - A collection of articles based on previous TUFFP research reports that have been published or are under review for various technical journals (May 1991).

72. "Two-Phase Flow in Horizontal Wells," by M. Ihara (October 1991).

73. "Two-Phase Slug Flow in Hilly Terrain Pipelines," by G. Zheng (October 1991).

74. "Slug Flow Phenomena in Inclined Pipes," by I. Alves (October 1991).

75. "Transient Flow and Pigging Dynamics in Two-Phase Pipelines," by K. Minami (October 1991).

76. "Transient Drift Flux Model for Wellbores," by O. Metin Gokdemir (November 1992).

77. "Slug Flow in Extended Reach Directional Wells," by Héctor Felizola (November 1992).

78. "Two-Phase Flow Splitting at a Tee Junction with an Upward Inclined Side Arm," by Peter Ashton (November 1992).

79. "Two-Phase Flow Splitting at a Tee Junction with a Downward Inclined Branch Arm," by Viswanatha Raju Penmatcha (November 1992).

80. "Annular Flow in Extended Reach Directional Wells," by Rafael Jose Paz Gonzalez (May 1994).

81. "An Experimental Study of Downward Slug Flow in Inclined Pipes," by Philippe Roumazeilles (November 1994).

82. "An Analysis of Imposed Two-Phase Flow Transients in Horizontal Pipelines Part-1 Experimental Results," by Fabrice Vigneron (March 1995).

83. "Investigation of Single Phase Liquid Flow Behavior in a Single Perforation Horizontal Well," by Hong Yuan (March 1995).

84. "1995 Data Documentation User's Manual", (October 1995).

85. "Recent Publications" A collection of articles based on previous TUFFP research reports that have been published or are under review for various technical journals (February 1996).

86. "1995 Final Report - Transportation of Liquids in Multiphase Pipelines Under Low Liquid Loading Conditions", Final report submitted to Penn State University for subcontract on GRI Project.

87. "A Unified Model for Stratified-Wavy Two-Phase Flow Splitting at a Reduced Tee Junction with an Inclined Branch Arm", by Srinagesh K. Marti (February 1996).

88. "Oil-Water Flow Patterns in Horizontal Pipes", by José Luis Trallero (February 1996).

89. "A Study of Intermittent Flow in Downward Inclined Pipes" by Jiede Yang (June 1996).

90. "Slug Characteristics for Two-Phase Horizontal Flow", by Robert Marcano (November 1996).

91. "Oil-Water Flow in Vertical and Deviated Wells", by José Gonzalo Flores (October 1997).

92. "1997 Data Documentation and Software User's Manual", by Avni S. Kaya, Gerad Gibson and Cem Sarica (November 1997).

93. "Investigation of Single Phase Liquid Flow Behavior in Horizontal Wells", by Hong Yuan (March 1998).

94. "Comprehensive Mechanistic Modeling of Two-Phase Flow in Deviated Wells" by Avni Serdar Kaya (December 1998).

95. "Low Liquid Loading Gas-Liquid Two-Phase Flow in Near-Horizontal Pipes" by Weihong Meng (August 1999).

96. "An Experimental Study of Two-Phase Flow in a Hilly-Terrain Pipeline" by Eissa Mohammed Al-Safran (August 1999).

97. "Oil-Water Flow Patterns and Pressure Gradients in Slightly Inclined Pipes" by Banu Alkaya (May 2000).

98. "Slug Dissipation in Downward Flow – Final Report" by Hong-Quan Zhang, Jasmine Yuan and James P. Brill (October 2000).

99. "Unified Model for Gas-Liquid Pipe Flow – Model Development and Validation" by Hong-Quan Zhang (January 2002).

100. "A Comprehensive Mechanistic Heat Transfer Model for Two-Phase Flow with High-Pressure Flow Pattern Validation" Ph.D. Dissertation by Ryo Manabe (December 2001).

101. "Revised Heat Transfer Model for Two-Phase Flow" Final Report by Qian Wang (March 2003).

102. "An Experimental and Theoretical Investigation of Slug Flow Characteristics in the Valley of a Hilly-Terrain Pipeline" Ph.D. Dissertation by Eissa Mohammed Al-safran (May 2003).

103. "An Investigation of Low Liquid Loading Gas-Liquid Stratified Flow in Near-Horizontal Pipes" Ph.D. Dissertation by Yongqian Fan.

104. “Severe Slugging Prediction for Gas-Oil-Water Flow in Pipeline-Riser Systems,” M.S. Thesis by Carlos Andrés Beltrán Romero (2005)

105. “Droplet-Homophase Interaction Study (Development of an Entrainment Fraction Model) – Final Report,” Xianghui Chen (2005)

106. “Effects of High Oil Viscosity on Two-Phase Oil-Gas Flow Behavior in Horizontal Pipes” M.S. Thesis by Bahadir Gokcal (2005)

107. “Characterization of Oil-Water Flows in Horizontal Pipes” M.S. Thesis by Maria Andreina Vielma Paredes (2006)

108. “Characterization of Oil-Water Flows in Inclined Pipes” M.S. Thesis by Serdar Atmaca (2007).

109. “An Experimental Study of Low Liquid Loading Gas-Oil-Water Flow in Horizontal Pipes” M.S. Thesis by Hongkun Dong (2007).

110. “An Experimental and Theoretical Investigation of Slug Flow for High Oil Viscosity in Horizontal Pipes” Ph.D. Dissertation by Bahadir Gokcal (2008).

111. “Modeling of Gas-Liquid Flow in Upward Vertical Annuli” M.S. Thesis by Tingting Yu (2009).

112. “Modeling of Hydrodynamics of Oil-Water Pipe Flow using Energy Minimization Concept” M.S. Thesis by Anoop Kumar Sharma (2009).

113. “Liquid Entrainment in Annular Gas-Liquid Flow in Inclined Pipes” M.S. Thesis by Kyle L. Magrini (2009).

114. "Effects of High Oil Viscosity on Slug Liquid Holdup in Horizontal Pipes" M.S. Thesis by Ceyda Kora (2010).

Appendix B

2010 Fluid Flow Projects Advisory Board Representatives

Baker Atlas

Michael R. Wells
Director of Research
Baker Hughes
Phone: (281) 363-6769
Fax: (281) 363-6099
Email Mike.Wells@bakerhughes.com

Dan Georgi
Baker Atlas
2001 Rankin Road
Houston, Texas 77073
Phone: (713) 625-5841
Fax: (713) 625-6795
Email: dan.georgi@bakeratlas.com

Datong Sun
Baker Atlas
2001 Rankin Road
Houston, Texas 77073
Phone: (713) 625-5791
Fax: (713) 625-6795
Email: datong.sun@bakeratlas.com

Bureau of Ocean Energy Management, Regulation, and Enforcement (BOEMRE)

Timothy Steffek
BOEMRE
381 Elden Street, MS-4021
Herndon, VA 20170-4817
Phone: (703) 787-1562
Email: Timothy.Steffek@boemre.gov

Sharon Buffington
Minerals Management Services
Technology Research Assessment Branch
381 Elden Street
Mail Stop 2500
Herndon, VA 20170-4817
Phone: (703) 787-1147
Fax: (703) 787-1555
Email: sharon.buffington@boemre.gov

Kurt Stein
Program Analyst
Minerals Management Services
Engineering and Research Branch
Mail Stop 4021
381 Eldon Street
Herndon, VA 20170-4817
Phone: (703) 787-1687
Fax: (703) 767-1549
Email: Kurt.Stein@boemre.gov

BP

Official Representative & UK Contact
Paul Fairhurst
BP
Flow Assurance Engineering – UTG
Building H
Chertsey Road
Sunbury on Thames, Middlesex TW16 7LN
England
Phone: (44 1 932) 774818
Fax: (44 7 787) 105183
Email: fairhucp@bp.com

Alternate UK Contact
Andrew Hall
BP
Pipeline Transportation Team, EPT
1H-54 Dyce
Aberdeen, AB21 7PB
United Kingdom
Phone: (44 1224) 8335807
Fax:
Email: halla9@bp.com

Alternate UK Contact
Trevor Hill
BP
E&P Engineering Technical Authority – Flow Assurance
Chertsey Road
Sunbury on Thames, Middlesex TW16 7BP
United Kingdom
Phone: (44) 7879 486974
Fax:
Email: trevor.hill@uk.bp.com

US Contact
Taras Makogon
BP
501 Westlake Park Blvd.
Houston, Texas 77079
Phone: (281) 366-8638
Fax:
Email: taras.makogon@bp.com

US Contact
George Shoup
BP
501 Westlake Park Blvd.
Houston, Texas 77079
Phone: (281) 366-7238
Fax:
Email: shoupgj@bp.com

US Contact
Oris Hernandez
Flow Assurance Engineer
BP
501 Westlake Park Blvd.
Houston, Texas 77079
Phone: (281) 366-5649
Fax:
Email: oris.hernandez@bp.com

Chevron

Lee Rhyne
Chevron
Flow Assurance Team
1400 Smith Street, Room 23188
Houston, Texas 77002
Phone: (713) 372-2674
Fax: (713) 372-5991
Email: lee.rhyne@chevron.com

Sam Kashou
Chevron
1500 Louisiana Street
Houston, Texas 77002
Phone: (832) 854-3917
Fax: (832) 854-6425
Email: samkashou@chevron.com

Jeff Creek
Chevron
Flow Assurance Team
1600 Smith Street
Houston, Texas 77002
Phone: (713) 754-7347
Fax: (713) 754-7300
Email: lcre@chevron.com

Hariprasad Subramani
Chevron
Flow Assurance
1400 Smith Street, Room 23192
Phone: (713) 372-2657
Fax: (713) 372-5991
Email: hjsubramani@chevron.com

ConocoPhillips, Inc.

Tom Danielson
ConocoPhillips, Inc.
600 N. Dairy Ashford
1036 Offshore Building
Houston, Texas 77079
Phone: (281) 293-6120
Fax: (281) 293-6504
Email: tom.j.danielson@conocophillips.com

Kris Bansal
ConocoPhillips, Inc.
1034 Offshore Building
600 N. Dairy Ashford
Houston, Texas 77079
Phone: (281) 293-1223
Fax: (281) 293-3424
Email: kris.m.bansal@conocophillips.com

Yongqian Fan
ConocoPhillips, Inc.
600 N. Dairy Ashford
1052 Offshore Building
Houston, Texas 77079
Phone: (281) 293-4730
Fax: (281) 293-6504
Email: yongqian.fan@conocophillips.com

ExxonMobil

Don Shatto
ExxonMobil
P. O. Box 2189
Houston, Texas 77252-2189
Phone: (713) 431-6911
Fax: (713) 431-6387
Email: don.p.shatto@exxonmobil.com

Jiyong Cai
ExxonMobil
P. O. Box 2189
Houston, Texas 77252-2189
Phone: (713) 431-7608
Fax: (713) 431-6387
Email: jiyong.cai@exxonmobil.com

Nader Berchane
ExxonMobil Upstream Research Company
Gas & Facilities Division
P. O. Box 2189
Houston, Texas 77252-2189
Phone: (713) 431-6059
Fax: (713) 431-6322
Email: nader.berchane@exxonmobil.com

JOGMEC

Tomoko Watanabe
JOGMEC
1-2-2, Hamada, Mihama-ku
Chiba, 261-0025 Japan
Phone: (81 43) 2769281
Fax: (81 43) 2764063
Email: watanabe-tomoko@jogmec.go.jp

Masaru Nakamizu
JOGMEC
One Riverway, Suite 450
Houston, Texas 77056
Phone: (713) 622-0204
Fax: (713) 622-1330
Email: nakamizu-masaru@jogmec.go.jp

Kuwait Oil Company

Eissa Alsafran
Kuwait University
College of Engineering and Petroleum
Petroleum Engineering Department
P. O. Box 5969
Safat – 13060 – Kuwait
Phone: (965) 4987699
Fax: (965) 4849558
Email: eisa@kuniv.edu.kw
dr_ealsafran@yahoo.com

Adel Al-Abbasi
Manager, Research and Technology
Kuwait Oil Company (K.S.C.)
P. O. Box 9758
Ahmadi – Kuwait 61008
Phone: (965) 398-8158
Fax: (965) 398-2557
Email: aabbasi@kockw.com

Ahmad K. Al-Jasmi
Team Leader R & T (Surface)
Research and Technology Group
Industrial Area
Kuwait Oil Company
P. O. Box 9758
Ahmadi – Kuwait 61008
Phone: (965) 3984126
(965) 3866771
Fax: (965) 3989414
Email: ajasmi@kockw.com

Bader S. Al-Matar
Snr. Reservoir Engineer
R & T Subsurface Team
Kuwait Oil Company
P. O. Box 9758
Ahmadi – Kuwait 61008
Phone: (965) 398-9111 ext. 67708
Email: bmatar@kockw.com

Marathon Oil Company

Rob Sutton
Marathon Oil Company
P. O. Box 3128
Room 3343
Houston, Texas 77253
Phone: (713) 296-3360
Fax: (713) 296-4259
Email: rpsutton@marathonoil.com

Petrobras

Rafael Mendes
Petrobras
Cidade Universitaria – Quadra 7 – Ilha do Fundao
CENPES/PDEP/TEEA
Rio de Janeiro 21949-900
Brazil
Phone: (5521) 38652008
Fax:
Email: rafael.mendes@petrobras.com.br

Marcelo Goncalves
Petrobras
Cidade Universitaria – Quadra 7 – Ilha do Fundao
CENPES/PDEP/TEEA
Rio de Janeiro 21949-900
Brazil
Phone: (5521) 38656712
Fax: (5521) 38656796
Email: marcelog@petrobras.com.br

Kazuoishi Minami
Petrobras
Av. Republica do Chile
65 – 17° Andar – Sala 1703
Rio de Janerio 20035-900
Brazil
Phone: (55 21) 5346020
Fax: (55 21) 5341128
Email: minami@petrobras.com.br

Ibere Alves
Petrobras
Phone: (55 21) 5343720
Email: ibere@petrobras.com.br

Schlumberger

Mack Shippen
Schlumberger
5599 San Felipe
Suite 1700
Houston, Texas 77056
Phone: (713) 513-2532
Fax: (713) 513-2042
Email: mshippen@slb.com

Maria Vielma
Production Engineer
Schlumberger Information Solutions
1625 Broadway, Suite 1300
Denver, Colorado 80202
Phone: (303) 389-4438
Fax: (303) 595-00667
Email: mvielma@denver.oilfield.slb.com

Sammy Haddad
GFM Reservoir Domain Champion & Res. Eng. Advisor
Schlumberger Middle East S.A.
Mussafah
P. O. Box 21
Abu Dhabi, UAE
Phone: (971 2) 5025212
Fax:
Email: shaddad@abu-dhabi.oilfield.slb.com

William Bailey
Principal
Schlumberger – Doll Research
1 Hampshire Street, MD-B213
Cambridge, MA 02139
Phone: (617) 768-2075
Fax:
Email: wbailey@slb.com

Shell Global Solutions

Rusty Lacy
Fluid Flow (OGUF)
Shell Global Solutions (US) Inc.
Westhollow Technology Center
3333 Hwy 6 South
Houston, Texas 77082-3101
Phone: (281) 544-7309
Fax: (281) 544-8427
Email: rusty.lacy@shell.com

Ulf Andresen
Fluid Flow Engineer
Shell Global Solutions (US) Inc.
Westhollow Technology Center
3333 Hwy 6 South
Houston, Texas 77082
Phone: (281) 544-6424
Fax:
Email: ulf.andresen@shell.com

SPT

Richard Shea
SPT
11490 Westheimer, Suite 720
Houston, Texas 77077
Phone: (281) 496-9898 ext. 11
Fax: (281) 496-9950
Email: richard.shea@sptgroup.com

Yordanka Gomez-Markovich
SPT
Flow Assurance
DEV-GP6-1438
Phone: (281) 654-7549
Fax: (281) 654-6202
Email: yordanka.e.gomez@exxonmobil.com

Lee Norris
SPT
11490 Westheimer, Suite 720
Houston, Texas 77077
Phone: (281) 496-9898 ext. 14
Fax: (281) 496-9950
Email: hln@sptgroup.com

Gunnar Staff
SPT Group A/S
P. O. Boks 113, Instituttveien 10
N-2027 Kjeller, Norway
Phone: 47 63 89 04 94
Fax: 47 64 84 45 00
Email: gunnar.staff@sptgroup.com

TOTAL

Fabien Papot
TOTAL Exploration & Production
DGEP/SCR/ED/ECP
2, place Jean Millier – La Defense 6
92078 Paris la Defense Cedex - France
Phone: (33) 1 47 44 82 78
Email: fabien.papot@total.com

Benjamin Brocart
Research Engineer
Rheology and Disperse Systems
TOTAL Petrochemicals France
Research & Development Centre Mont/Lacq
B. P. 47 – F – 64170
Lacq, France
Phone: (33 559) 926611
Fax: (33 559) 926765
Email: Benjamin.brocart@total.com

Emmanuel Duret
TOTAL Exploration & Production
DGEP/SCR/ED/ECP
2, place Jean Millier – La Defense 6
92078 Paris la Defense Cedex - France
Phone: (33) 1 47 44 35 03
Fax:
Email: emmanuel-denis.duret@total.com

Appendix C

History of Fluid Flow Projects Membership

		1973	
1.	TRW Reda Pump	12 Jun. '72	T: 21 Oct. '77
2.	Pemex	15 Jun. '72	T: 30 Sept. '96 R: Dec '97 T: 2010
3.	Getty Oil Co.	19 Jun. '72	T: 11 Oct. '84 with sale to Texaco
4.	Union Oil Co. of California	7 Jul. '72	T: for 2001
5.	Intevep	3 Aug. '72	TR: from CVP in '77; T: 21 Jan '05 for 2006
6.	Marathon Oil Co.	3 Aug. '72	T: 17 May '85 R: 25 June '90 T: 14 Sept. '94 R: 3 June '97 **Current**
7.	Arco Oil and Gas Co.	7 Aug. '72	T: 08 Dec. '97
8.	AGIP	6 Sep. '72	T: 18 Dec. '74
9.	Otis Engineering Corp.	4 Oct. '72	T: 15 Oct. '82
10.	ConocoPhillips, Inc.	5 Oct. '72	T: Aug. '85 R: 5 Dec. '86 **Current**
11.	Mobil Research and Development Corp.	13 Oct. '72	T: 27 Sep. 2000
12.	Camco, Inc.	23 Oct. '72	T: 15 Jan. '76 R: 14 Mar. '79 T: 5 Jan. '84
13.	Crest Engineering, Inc.	27 Oct. '72	T: 14 Nov. '78 R: 19 Nov. '79 T: 1 Jun. '84
14.	Chevron	3 Nov. '72	**Current**
15.	Aminoil	9 Nov. '72	T: 1 Feb. '77

16.	Compagnie Francaise des Petroles (TOTAL)	6 Dec. '72	T: 22 Mar. '85 R: 23 Oct. '90 T: 18 Sep. '01 for 2002 R: 18 Nov. '02 **Current**
17.	Oil Service Co. of Iran	19 Dec. '72	T: 20 Dec. '79
18.	Sun Exploration and Production Co.	4 Jan. '73	T: 25 Oct. '79 R: 13 Apr. '82 T: 6 Sep. '85
19.	Amoco Production Co. (now as BP Amoco)	18 May '73	
20.	Williams Brothers Engrg. Co.	25 May '73	T: 24 Jan. '83
	1974		
21.	Gulf Research and Development Co.	20 Nov. '73	T: Nov. '84 with sale to Chevron
22.	El Paso Natural Gas Co.	17 Dec. '73	T: 28 Oct. '77
23.	Arabian Gulf Exploration Co.	27 Mar. '74	T: 24 Oct. '82
24.	ExxonMobil Upstream Research	27 Mar. '74	T: 16 Sep. '86 R: 1 Jan. '88 T: 27 Sep. 2000 R: 2007 **Current**
25.	Bechtel, Inc.	29 May '74	T: 14 Dec. '76 R: 7 Dec. '78 T: 17 Dec. '84
26.	Saudi Arabian Oil Co.	11 Jun. '74	T: for 1999
27.	Petrobras	6 Aug. '74	T: for 2000 R: for 2005 **Current**
	1975		
28.	ELF Exploration Production (now as TotalFina Elf)	24 Jul. '74	T: 24 Feb. '76 Tr. from Aquitaine Co. of Canada 19 Mar. '81 T: 29 Jan. '87 R: 17 Dec. '91
29.	Cities Service Oil and Gas Corp.	21 Oct. '74	T: 25 Oct. '82 R: 27 Jun. '84 T: 22 Sep. '86

30.	Texas Eastern Transmission Corp.	19 Nov. '74	T: 23 Aug. '82
31.	Aquitaine Co. of Canada, Ltd.	12 Dec. '74	T: 6 Nov. '80
32.	Texas Gas Transmission Corp.	4 Mar. '75	T: 7 Dec. '89
	1976		
33.	Panhandle Eastern Pipe Line Co.	15 Oct. '75	T: 7 Aug. '85
34.	Phillips Petroleum Co.	10 May '76	T: Aug. 94 R: Mar 98 T: 2002
	1977		
35.	N. V. Nederlandse Gasunie	11 Aug. '76	T: 26 Aug. '85
36.	Columbia Gas System Service Corp.	6 Oct. '76	T: 15 Oct. '85
37.	Consumers Power Co.	11 Apr. '77	T: 14 Dec. '83
38.	ANR Pipeline Co.	13 Apr. '77	TR: from Michigan- Wisconsin Pipeline Co. in 1984 T: 26 Sep. '84
39.	Scientific Software-Intercomp	28 Apr. '77	TR: to Kaneb from Intercomp 16 Nov. '77 TR: to SSI in June '83 T: 23 Sep. '86
40.	Flopetrol/Johnston-Schlumberger	5 May '77	T: 8 Aug. '86
	1978		
41.	Norsk Hydro a.s	13 Dec. '77	T: 5 Nov. '82 R: 1 Aug. '84 T: 8 May '96
42.	Dresser Industries Inc.	7 Jun. '78	T: 5 Nov. '82
	1979		
43.	Sohio Petroleum Co.	17 Nov. '78	T: 1 Oct. '86
44.	Esso Standard Libya	27 Nov. '78	T: 2 Jun. '82
45.	Shell Internationale Petroleum MIJ B.V. (SIPM)	30 Jan. '79	T: Sept. 98 for 1999
	1980		
46.	Fluor Ocean Services, Inc.	23 Oct. '79	T: 16 Sep. '82
47.	Texaco	30 Apr. '80	T: 20 Sep. '01 for 2002
48.	BG Technology (Advantica)	15 Sep. '80	T: 2003

		1981	
49.	Det Norske Veritas	15 Aug. '80	T: 16 Nov. '82
		1982	
50.	Arabian Oil Co. Ltd.	11 May '82	T: Oct.'01 for 2002
51.	Petro Canada	25 May '82	T:28 Oct. '86
52.	Chiyoda	3 Jun. '82	T: 4 Apr '94
53.	BP	7 Oct. '81	**Current**
		1983	
54.	Pertamina	10 Jan. '83	T: for 2000 R: March 2006
		1984	
55.	Nippon Kokan K. K.	28 Jun. '83	T: 5 Sept. '94
56.	Britoil	20 Sep. '83	T: 1 Oct. '88
57.	TransCanada Pipelines	17 Nov. '83	T:30 Sep. '85
58.	Natural Gas Pipeline Co. of America (Midcon Corp.)	13 Feb. '84	T:16 Sep. '87
59.	JGC Corp.	12 Mar. '84	T: 22 Aug. '94
		1985	
60.	STATOIL	23 Oct. '85	T:16 Mar. '89
		1986	
61.	JOGMEC (formerly Japan National Oil Corp.)	3 Oct. '86	T: 2003 R: 2007 **Current**
		1988	
62.	China National Oil and Gas Exploration and Development Corporation	29 Aug. '87	T:17 Jul. '89
63.	Kerr McGee Corp.	8 Jul. '88	T:17 Sept. '92
		1989	
64.	Simulation Sciences, Inc.	19 Dec. '88	T: for 2001
		1991	
65.	Advanced Multiphase Technology	7 Nov. '90	T:28 Dec. '92

66.	Petronas	1 Apr. ‘91	T: 02 Mar. 98 R: 1 Jan 2001 T: Nov. 2008 for 2009
	1992		
67.	Instituto Colombiano Del Petroleo	19 July ‘91	T: 3 Sep. ’01 for 2002
68.	Institut Francais Du Petrole	16 July. '91	T: 8 June 2000
69.	Oil & Natural Gas Commission of India	27 Feb. '92	T: Sept. 97 for 1998
	1994		
70.	Baker Jardine & Associates	Dec. ‘93	T: 22 Sept. ‘95 for 1996
	1998		
71.	Baker Atlas	Dec. 97	**Current**
72.	Bureau of Ocean Energy Management, Regulation, and Enforcement (BOEMRE)	May. 98	**Current**
	2002		
73.	Schlumberger Overseas S.A.	Aug. 02	**Current**
74.	Saudi Aramco	Mar. 03	T: for 2007
	2004		
75.	YUKOS	Dec. ‘03	T: 2005
76.	Landmark Graphics	Oct. ‘04	T: 2008
	2005		
77.	Rosneft	July ‘05	T: 2010
	2006		
78.	Tenaris		T: Sept 2008 – for 2009
79.	Shell Global		**Current**
80.	Kuwait Oil Company		**Current**
	2009		
81.	SPT		**Current**

Note: T = Terminated; R = Rejoined; and TR = Transferred

Appendix D

Contact Information

Director

Cem Sarica | (918) 631-5154
cem-sarica@utulsa.edu

Associate Director

Holden Zhang | (918) 631-5142
hong-quan-zhang@utulsa.edu

Director Emeritus

James P. Brill | (918) 631-5114
brill@utulsa.edu

Project Coordinator

Linda M. Jones | (918) 631-5110
jones@utulsa.edu

Project Engineer

Scott Graham | (918) 631-5147
sdgraham@utulsa.edu

Research Technicians

Brandon Kelsey | (918) 631-5133
brandon-kelsey@utulsa.edu

Craig Waldron | (918) 631-5131
craig-waldron@utulsa.edu

Research Assistants

Rosmer Brito | (918) 631-5119
rosmer-brito@utulsa.edu

Kiran Gawas | (918) 631-5138
kiran-gawas@utulsa.edu

Mujgan Guner | (918) 631-5117
mujgan-guner@utulsa.edu

Benin Jeyachandra | (918) 631-5119
bjeyachandra@utulsa.edu

Ceyda Kora | (918) 631-5117
ceyda-kora@utulsa.edu

Anton Skopich | (918) 631-5117
anton-skopich@utulsa.edu

Ge Yuan | (918) 631-5124
ge-yuan@utulsa.edu

Wei Zheng | (918) 631-5124
wei-zheng@utulsa.edu

Web Administrator

Lori Watts | (918) 631-2979
lori-watts@utulsa.edu

Fax Number:	**(918) 631-5112**
Web Sites:	**www.tuffp.utulsa.edu**